

# **SCIENTIFIC PROGRAMME**



**KEYNOTE**



# ADVANCED PROCESS CONTROL THE OPPORTUNITIES, BENEFITS AND BARRIERS

Hans H. Eder  
ACT, Brussels office  
B 3080, Tervuren,  
Belgium  
E-mail: [actgmbh@compuserve.com](mailto:actgmbh@compuserve.com)

Keywords: Advanced control, control performance, service factor, economics,

## ABSTRACT

Advanced Process Control (APC) has been around for more than 35 years, yet is still very much underutilized: Only a few companies have recognized the tremendous potential and realized enormous credits. APC is still perceived often as too difficult, too expensive and without really hard 'incentives'. As a consequence, the industry is by far not exploiting the possible benefits. To help improve this situation is the overall intent of this paper. The first objective is to promote the use of APC by raising the awareness of its many benefits and opportunities, by describing the mechanism why and how APC can deliver these credits and how to estimate the economics. The second objective is to show the key factors for successful implementation and use.

## INTRODUCTION

Despite its many benefits, only a small percentage of the possible APC applications have been implemented in industry to date. Also, APC is often used in a sporadic way rather than as integral part of a complete operations and control strategy. This calls for improvement. As far as a more widespread use of the most powerful control technology is concerned, two obstacles stand in the way:

- Technical staff often lacks the knowledge where APC could bring extra credits and how to apply it in practice
- Management is typically not aware of the benefits and thus reluctant to support the required effort.

The second fact is only partly the fault of management, since many technical experts are unable to quantify the credits. The objective of the first part of this presentation is therefore to raise the awareness of the benefits of APC and to give guidance on when to use and how to justify it.

The second objective of this paper is to help establish a solid basis which enables that maximum benefits are achieved from the use of this powerful technology.

## DEFINITION

To start, let us see what APC means. Unfortunately, already the name "Advanced Control" gives rise to many different perceptions, most of them being too narrow as they relate just to the technological aspects. Therefore I would like to present here a more complete definition:

**"Advanced Control is the intelligent, well managed use of process control technology, systems and tools, based on sound process knowledge, with the objective to enable and benefit from operations improvements in a most cost and time effective way".**

Let us briefly expand on two of the keywords:

- 'Intelligent' means here that we are aware of the currently available technologies, that we have a suitable subset, a Technology Set, readily available on our control systems and that we know when and how to use them.
- 'Well managed' means here that all APC activities are well planned, monitored and continuously improved, that they are in line with the overall plant operations objectives and based on sound standards and rules.

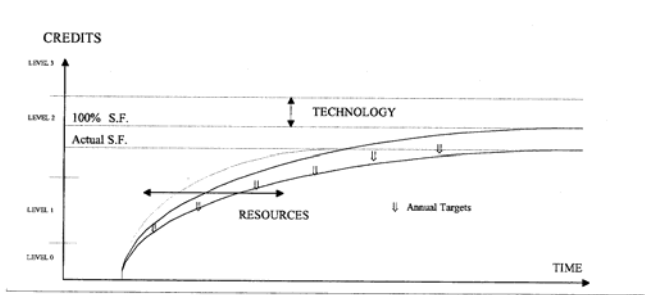
Form this definition we can already derive that APC has in fact three main dimensions:

- Technology
- Economics
- Organization

## EXPECTATIONS FROM APC

Process control is a service to plant operations, assisting them to reach the operating objectives. The goal of APC in particular is to maximize the contributions of process control, its "credits", over time. This has again two dimensions:

- a) The maximum achievable credits (the "gain") when all possible advanced controls are implemented and used. The economical gain is mainly influenced by the technology used. Superior technology can deliver higher performance, resulting in additional credits and thus will raise this gain.
- b) The time needed to reach the maximum gain (the "time constant"). The speed of the approach of the maximum gain is mainly influenced by manpower, skills, planning and the use of suitable productivity tools.



Picture 1: "Credits over time"

## WHAT IS 'CONTROL PERFORMANCE'?

To be able to improve operations, APC must deliver higher performance. Lets us briefly look at what this means:

To be able to produce the products with the right properties, the process must follow certain targets as closely as possible. These targets are seen as the optimal values, every deviation from such target results therefore in some kind of economical loss (or safety hazard). If the process was always stable and without any influences then this would be quite easy: Once the target conditions are reached no further interactions were necessary. But the opposite is the case, the process is permanently undergoing disturbing influences, dynamic effects, which must be compensated. The challenge here is therefore to manage the process dynamics. And "performance" means in this context in general terms how well we are able to master these dynamics.

The above implies of course that the targets are set correct or optimal. But they are typically calculated based on static calculations and not taking the process dynamics and the variations into account: If the process has a highly non-linear behavior and we must accept large variations in the variable under consideration then we need to adjust even the target.

To illustrate this let us look at the following example: For Claus plants, which produce sulfur out of H<sub>2</sub>S containing "sour" gas, the maximum theoretical conversion is achieved at a H<sub>2</sub>S / SO<sub>2</sub> ratio of 2.8. But the conversion degrades with different slopes on both sides of the optimum. With a mean value of the H<sub>2</sub>S / SO<sub>2</sub> ratio of exactly 2.8 but a certain variance, the actual conversion will, however, be much less than the maximum value. And because of the different slopes in the vicinity of the optimum, we can achieve higher conversion by reducing the variance and by moving the target ratio to a value **higher** than the theoretical one.

Looking at the situation the other way round we can state: The more we can reduce the variations of that process variable, the smaller are the overall deviations from the setpoint and therefore the economical losses and also the closer we will operate to the true (static) optimal value.

## WHERE CAN APC HELP THE MOST?

APC does not aim to replace every simple flow controller, but should be used where the standard PID controllers is overwhelmed and where operators need extra help. In general, APC shall be used where we face

- difficult process behavior
- high performance and operability requirements.

Typical examples for difficult process behavior are:

**Long deadtime** is known as a major difficulty for control. This is a key reason why relatively few product qualities are controlled in closed loop, even where stream analyzers exist, since analysis time is often quite long.

**High controllability ratio CR** (the ratio deadtime to time constant), which is another key indicator for the degree of difficulty: Generally, up to a ratio of 2 the PID will deliver a fine job, for values between 2 and 3, PID tuning becomes more difficult and time consuming and beyond 3 the PID is not recommended any more. Using the CR to choose the right controller, of course, requires at least some quantitative knowledge of the process dynamics.

**Inverse response and overshoot:** For processes with inverse response any reactive controller will apply initially the wrong action on the process. This can be avoided with approaches like Model Based Control (MBC). And for systems with overshoot much smoother yet tight control can be achieved.

**Strong interactions:** Dynamic decoupling can be performed also with PID's but is quite difficult and thus confined to small (2x2) systems. And there is the risk of instability when the decouplers are not active. Thus the controllers cannot be tuned tightly. MBC e.g. is much easier to tune, delivers better performance and has practically no limitation in size.

Despite the common belief that APC mainly is justified in large oil refineries, successful applications have proven that it has its value in the food industry as well: Applications exist in the production of cookies, in batch freezing of ice cream, in meat production etc. In dairy production, increased product yield can be realized by targeting upper specification limit. Other benefits are increased productivity because more product is produced and 'Right Time First' energy savings by not over-drying, reduction in waste/scrap, increased product quality. In beer production, temperature control of brew kettle, fermenter, wort cooling, bottle washer can yield significant energy savings and also water reduction in the bottle washer. In the canning production, temperature control of blanching sections and of retorts have similar results. In sugar industry higher extraction rate, less energy and water consumption and reduction of environmental issues are key achievements.

## WHAT ARE THE RESULTING BENEFITS?

APC aims at reducing the variance of the controlled variable and / or of the manipulated variable(s). Reducing the variance of the controlled variable will yield the following effects:

1) If the controlled variable must be pushed against a limit, then reducing the variance allows moving the average value closer to this limit. In other words: We can **squeeze** the variance and **shift** the mean! This effect is very important, since about 60 to 70% of the total credits from APC come from operation closer to limiting constraints. An example: A reactor shall be operated at maximum conversion. Conversion increases with increasing inlet temperature, which may, however, be constrained by the maximum tube metal temperature of the preheat furnace. Therefore, tighter control allows to push the average furnace temperature closer to its constraint, achieves higher conversion and thus higher profits. It should be noted that in this example (like in many other cases) the final effect is not directly but indirectly related to the variable we have to control. Tighter temperature control itself does not make the money – but its effect on product yield, qualities etc.!

2) Often the “money making” variable stands in a non-linear relationship with the controlled variable. If e.g. a temperature would have zero variance then this would result in a certain product quality. However, the larger the temperature variance the more the actual quality will differ from the ideal value.

**The average value of the dependent variable – here the product quality – is a function of both the average value of the independent variable – here the temperature – and the variance of the independent variable.**

This means that we are forced to run at a “non-ideal” temperature setpoint in order to stay on the target quality. The typical consequence is a lower product yield. However, at the end the product is on spec, there is no apparent problem and therefore the loss of yield is often overlooked.

Having succeeded in minimizing the variance of the controlled variable, we have reached our first performance goal. But we have also to look at the manipulated variable, basically addressing the question: How have we achieved this performance – with minimum, reasonable or excessive effort?

**Smooth action on the process is the second objective.** This should be stressed especially since it is easily overlooked. Good performance of the controlled variable can be often achieved with quite simple controllers, even on-off switches, but at the price of drastic action on the process and thus over-utilization (“consumption”) of the resource, the manipulated variable. A typical example is again temperature control. Many controllers deliver good temperature behavior but at the expense of excessive consumption of the heating or cooling medium. Smooth action is especially important in integrated plants where any corrective action at one place means a disturbance for another variable.

## HOW CAN THE CREDITS BE DETERMINED?

The economics of the effects described above can be relatively easily quantified, given the process mechanisms are known and the economic data and some calculation tools are available. Several steps are required:

Steps 1: Determine the current performance like the variance, distance of the mean value from limiting constraints, etc., also the overall consumption of the resource over time.

Step 2: Determine how much the variance can be reduced. This is more difficult if no prior experience values exist. Several methods exist which cannot be discussed here further. One easy way is to monitor the performance of the variable in question and to compare its average performance with the best demonstrated performance. This gives at least a conservative indication of the potential improvements. More realistic figures are, of course, obtained by using suitable simulation tools that allow to compare different techniques.

Step 3: What is / are the effect(s) of the reduced variance? Again, a variety of methods exist but one simple case shall be described here to illustrate the procedure: Where several products are produced in a unit typically these products have different prices and market outlets. Thus the product for which a market exists and which yields the highest profit margin shall be maximized. We call it the marginal product.

Next, we need to know the mechanisms, the effects, quantitatively. Example: Increasing the reflux of a splitter tower will increase the fractionation and thus reduce the impurities in both products. This allows in turn to change the cutpoint and to raise the impurity of the marginal product back to the original value - which results in a higher yield of the marginal product and thus higher overall profits.

## WHAT STANDS IN THE WAY OF APC?

Despite its merits, APC is typically not aggressively applied in industry, the contrary is the case, a main reason being the lack of knowledge of the economical and operational benefits of APC by both technical staff and management.

Because of this deficiency, we hear many defensive and often destructive arguments against APC: We will just take the two very common ones and see if they hold at all.

*“My process is too simple.”*

This is a very destructive statement. The process may be simple but it still may carry a tremendous improvement potential. By simply ignoring all simple processes by principle, tremendous credits can be lost: A typical example is liquid level control: A drum or vessel is a very simple piece of equipment and to control the level within a band is in principle an extremely simple request. Yet, up to 80% of all level controllers perform poorly, many of them causing substantial problems downstream because of the permanent

swings in the manipulated flow. Using an error squared PID instead of the standard PID is a very simple yet effective 'advanced' alternative, but is hardly known and used by control professionals. The answer: The right attitude is to look at the cost of non-conformance – rather than at the complexity of the process.

*“My process is too complex.”*

Even for simple processes we see typically quite some differences in the performance from operator to operator and from shift to shift. The objective should be clearly to run the plant permanently at least as good as the best operator or shift. One advantage of automatic control is to ensure this. And we see that with increasing complexity the spread in the performance between different operators and shifts is clearly increasing. Thus - in contrary to the statement - increasing complexity demands even more intense use of APC.

## SUCCESSFUL APC DEVELOPMENT AND USE

Once we have convinced ourselves and management to apply higher levels of control, then the next step is to plan for its most effective use. Before we go on let us re-state: The main objective of process control is to improve operations with controllers and applications that deliver top performance and are operating whenever needed. It is important to keep in mind that the latter – a high service factor – does by no means come automatically together with top performance, we have to take separate, special measures.

But first of, to be able to fully exploit the APC capabilities a several changes are required. Of all the requirements for solid performance there is one factor that stands out: **Process knowledge**. Therefore we will address it up-front.

### Success factor 1: Process knowledge

This is by far the most important factor. It is often stated that one of its strongest advantages of the PID is that it can be tuned without solid process knowledge. In my opinion, it one of its strongest **disadvantages**. Even during studies to locate improvement opportunities the process knowledge was always significantly increased and has lead in many cases to changes in targets and constraints. The consequence: Quite often the development effort has been already paid out **before** the first application was commissioned! For closed loop control itself the most important success factors are known as the 4 T's: Technology, Training, Tools and Tactics.

### Success factor 2. Technology:

Successful exploitation of advanced control demands the establishment of a Technology Set. This is the “arsenal” that allows the control engineer to find the right “weapon” for every task. Many different approaches exist and it is very important to select the ones which are not only best suited for the tasks but also matches the company's situation with respect to manpower, skills and available infrastructure. Small, yet powerful, DCS based approaches are available as

well as large scale control and optimization packages that require extra computing platforms.

Technical selection criteria shall be: Performance, ability to handle a wide range of process types (integrating processes!), robustness against model errors, expandability (multivariable, control, feedforward), built-in constraint handling, ease of use (implementation, tuning, maintenance and updating) and the computing requirements.

Important is also the vendors' philosophy: Some supply not only control algos and applications but also transfer their know-how. This puts the user in full command and enables him to maintain the application later himself. Others provide only turn-key solutions, without any know how transfer at all, which can bring the user in some dilemma at a later stage.

A key consideration is to use the most simple approach possible (Einstein: “All models shall be as simple as possible - but no simpler”). Most of the unsuccessful APC applications for example failed because of their unnecessary complexity.

### Success factor 3. Training

Since the user has to choose the technology for a certain application, he must be in a position to make a conscious decision, he must have had adequate education **before**. Most have theoretical education and system specific knowledge. Yet the know-how to turn theory into working and lasting control applications is rather scarce and so is the ability to locate improvement opportunities and to quantify the credits. Therefore **additional** practice and profitability oriented education of the control engineers comes first and is in fact the second most important factor after process knowledge.

### Success factor 4: Tools

Not only the maximum achievable credits are of concern but also the speed by which they can be realized. This demands for productivity tools, may it be for incentive calculation, performance measurement, model development, comparison of different techniques - but also for training and refresher. Measuring the performance plays a key role: Implementing a Performance Monitoring System is neither difficult nor work-intensive yet it is a key instrument in application development and follow-up. It helps to detect under-performing controls, documents the base case situation and shows in quantitative, indisputable terms the achieved improvement. To stress this point I would like to use two citations, one from the US and one from The Netherlands:

*“What I cannot measure I cannot manage” - “Meten is weten, gissen is missen”* (measuring means knowing, guessing means missing)

### Success factor 5: Tactics

By “tactics” I mean all the organizational means and measures needed to steer process control to maximum success. This includes standards - from tag and display

naming conventions to standard control elements (e.g. feedforwards, analyzer controls,...), as well as careful design of human and also system interfaces: Higher level control also crosses sometimes the boundary between target setting (planning/scheduling) and execution of the targets.

Giving the operator the right information is the key to high application service factors. The operator decides over the use of the application, thus we must make sure he has all the required information and that it is properly presented.

Furthermore, there must be an overall “business plan” describing how and when the identified applications will be developed, what skills, training, human and system resources and tools are required and when. Only with such a sound plan we will be able to realize the full economical success.

#### **Success factor 6: Management involvement and support**

Last but by no means least, this is another crucial non-technical success factor. Unfortunately, in most companies management is hardly aware of the potential contributions and benefits of process control, seems often just concerned with average and not so much with optimal execution of the operating targets. The key to get management agreement and support is to explain the reasons for applying APC, for hiring and training engineers **in the language of management**, in economical, in business terms! But this, again, calls for a plan and it calls for knowledge of the economics.

#### **PLANNING FOR SUCCESS**

The steps towards a successful plan are not all that difficult: The best start is to begin measuring the current performance of key variables with a suitable Performance Measurement System. The next step is the conduct of an operations improvement (“incentive”) study. The goal is to assess the current controls and to pinpoint areas for improvement and to locate and evaluate further opportunities - besides known operational problems. Untapped, overlooked opportunities are more difficult to locate and the exploitation strategies more difficult to “sell”. Therefore it is typically advisable to seek help from outside experts, provided that they have strong experience in operations and esp. in economics. It is helpful to start always with the business drivers, with question like:

- What would it be worth to run 1 m<sup>3</sup>/hr more throughput?
- What would it be worth to increase product yield by 1 %?
- What would it be worth to decrease the giveaway in product quality by 1%?
- What would it be worth to reduce the consumption of energy or additives etc. by one unit?

Once the necessary improvements on the existing controls and the future applications, their objectives, the current and the targeted performance are defined then, just as for any project, we have to determine the potential incentives. Once they are known we can easily calculate how much we are

allowed to spend using standard techniques like DCF or IRR. When the economics speak for the project then we can go ahead and select the technology and put this into our overall process control business plan and start developing the applications according to this plan.

#### **CONCLUSIONS**

The APC technology is mature, the computing platforms are in most cases available, today there are no serious technical hurdles any more that prevent us from harvesting the benefits. And once the incentives are determined, the remaining barriers are typically breaking down. To achieve the maximum benefits, however, we must plan carefully and observe the key success factors – just as for any other project. Its certainly means extra effort, but the rewards have proven absolutely to be worth it - in many different industries, on many different processes, in many different locations.

The key in any case is to undertake the first step and to start measuring the current **dynamic** performance and to take a serious, unbiased look at the improvement potential in the plant. To benefit the most on a long term basis, also all future conventional **and** advanced controls should be defined **before** a new DCS system is purchased: Then the best suitable platform is available and applications development can go on without running into capacity of functional limitations.

Were a suitable DCS was already in place, APC has proven to be the most cost and time effective way to improve plant operations and profitability.

#### **AUTHOR BIOGRAPHY**

**HANS HEINZ EDER** was born in Vienna, Austria. He spent over 20 years with EXXON in various European countries and the USA. As APC engineer he has implemented MBC applications already in 1979. Later he was APC manager and CIM Advisor. Today he heads ACT, a company providing consulting and know-how transfer in process control and esp. APC. A major recent achievement is the development of a complete model based batch-reactor control scheme in just one day. Hr. Eder is also a registered expert with European Commission and helping projects in the field of eLearning, Knowledge Management and Virtual Enterprises.



# **METHODOLOGY**



# HYBRID MODELING FOR DEVELOPMENT AND OPTIMIZATION OF FOOD PRODUCTION CHAINS INCLUDING COSTS AND FOOD QUALITY

Peter de Jong, Maykel Verschueren, Marc M.M. Vissers, Han Straatsma and Erik Smit  
Department of Processing, Quality & Safety  
NIZO food research  
PO Box 20, 6710 BA Ede,  
Netherlands  
E-mail: pdejong@nizo.nl

## KEYWORDS

Hybrid modeling, Model design, Agricultural, Global, Industrial processes

## ABSTRACT

The need for predictive models of food quality aspects is increasing. To shorten the time of model development more and more black box modeling techniques are applied. However, the predictive capabilities of these models are not sufficient for food product and process development. On the other hand, the industry has no time enough to wait until all process-product interactions are covered by mechanistic white box models. Thus, the solution is to use both model types: white box models for all the known and well mathematical described phenomena and black box models for the complex and fuzzy phenomena. This approach is called hybrid modeling and has been applied for some applications in the dairy industry: (1) modeling of the raw milk quality at the farm, (2) modeling of the cheese ripening process and (3) modeling of powder properties. The results show that by the hybrid modeling approach complex phenomena such as bacterial load in raw milk and the taste of Gouda cheese can be predicted.

## INTRODUCTION

The production of high quality, safe foods becomes more and more important. The question is how to predict and to guarantee the product properties based on specifications of the raw material for different types of processes. Therefore, mathematical models to predict product properties would largely benefit the food industry. Especially, if it is possible to optimise the process operation in relation to the desired product quality and safety.

In general, three types of obstructions for full industrial use of models can be recognised:

1. The extensive effort needed for model development. Development of white box models is too time-consuming and black box models have very limited predictive capabilities.
2. Many models are focused on specific unit-operations, the impact on the production chain is ignored.
3. Many models are either focused on certain food quality aspects or on production costs, while for marketing

purposes the industry wants to compare both quality and costs.

To shorten the time of model development more and more black box modeling techniques are applied. However, the predictive capabilities of these models are not sufficient for food product and process development. On the other hand, the industry has no time enough to wait until all process-product interactions are covered by mechanistic white box models.

New developments in modeling are both market-driven and encouraged by advancing modelling techniques and increasing computer resources. Different modelling techniques can be combined to obtain so-called hybrid models. For example, white box models representing physical or chemical processes taking place can be combined with black box models (e.g. fuzzy logic, neural networks) representing classifications by a sensory panel. Models describing food properties can also be combined with advanced 3D calculations by Computational Fluid Dynamics (CFD) representing complex processing events. Hybrid modeling is a new approach in the food industry. Examples of hybrid modeling are found in majority in fermentation technology (Alves et al. 1998, Silva-Henriques et al. 1999, Beluhan and Beluhan 2000). Energy and mass balances as the most basic form of white box models are combined with neural network modeling. More recently Nantawan and Weibiao (2002) published a hybrid neural network model to predict the electrical conductivity of recombined milk.

In this paper the hybrid modeling approach is described for prediction of food properties in production chains. Some examples of applications for the food industry are given.

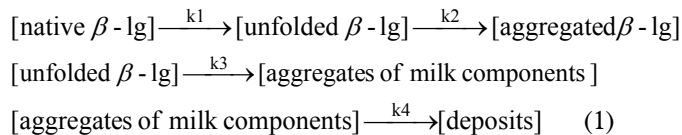
## PREDICTIVE PRODUCT MODELS

### Mechanistic models (white box)

Traditionally (food) science is focused on white box modeling, mostly represented as a hypothesis. The most basic form of white box models are mass and energy balances based on the conservation laws (e.g. CFD). To describe the transformation of food products during processing, good results are obtained with reaction kinetic modeling techniques. The model consists of a set of reaction rate equations based on a reaction scheme that implies a mechanistic hypothesis. Depending on the

application this set might be very simple or very complex. Examples of more complex mechanistic models are the polymerization model for prediction of heat-induced protein denaturation and viscosity changes in milk (De Jong and Van der Linden 1998) and reaction models of the Maillard process (Brands 2002).

Reaction kinetic modeling can also be used for product-process interaction such as fouling. De Jong et al. (1992) developed a predictive fouling model based on the following reaction scheme:



where  $\beta\text{-lg}$  stands for  $\beta$ -lactoglobulin, a reactive protein in milk and  $k_1 \dots k_4$  are reaction rate constants depending on temperature. The protein denaturation affects the product texture while the amount of deposits affects the heat transfer and indirectly the process economics. This model has been used for optimizing dairy production plants by related the amount of deposits to operating costs (De Jong 1996).

White box models are excellent for doing process and product development. The model constants have a physical meaning and are not depending on process design. The main disadvantage of white box models is the time of development but an increasing number of white box models become available.

### Neural network and fuzzy logic models (black box)

Black box models such as neural network and fuzzy logic models are data-driven. In principal, physical laws are ignored. These black box models have no mechanistic basis and are very specific for the process and product trained for. Training is performed by use of fitting the (numerous) model constants with a huge data set of measured process and product data. In the case of fuzzy logic models it is possible to translate qualitative relations (expert knowledge) into linguistic rules. These rules avoid the model to produce unrealistic numbers just outside the model training area. For example: if *temperature is high* than *bacterial product load is high*.

The main advantage of black box models is their simplicity to develop them, even for complex phenomena such taste development. Once there is enough data computer tools, with some expert help, can make a model within minutes. However, one small change in de process equipment or the composition of the raw materials the model must be trained again. In most cases this makes black box models only interesting for control of processes and bulk products that show no variation in requirements.

### Hybrid modeling

Hybrid modeling combines the advantages of white and black box modeling. In Figure 1 the hybrid modeling

approach for food production chains is presented. To model the effect of processing and composition on the food properties recognized by the consumer three levels of relevant knowledge are described.

1. Phenomena that can be modeled by mechanistic white box models (energy balances, mass balances, reaction kinetic models).
2. Phenomena that can be modeled by linguistic rules based on expert experience.
3. Phenomena that have uncertain effects on the food properties but appear to be relevant.

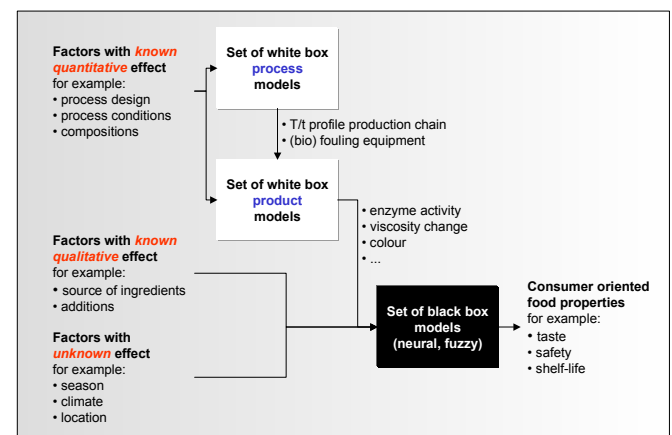


Figure 1: The Hybrid Modeling Approach for Food Production

It is important to realize that factors which have a clear effect (white box model) on food property  $x$  may have an uncertain effect on food property  $y$ . The main advantage of this approach is that all the knowledge available is incorporated into the hybrid model.

Summarizing, make first a long list of all the factors that may affect the food properties. Then, collect all the available white box models that describe the relation between these factors and the food properties. Fill the 'white spots' in the quantitative knowledge with black box models such as neural network and fuzzy logic models.

## EXAMPLES

### Bacterial load of raw milk

One of the major quality issues in the dairy industry is the contamination of raw milk arriving at the processing plant with micro-organisms, such as *Bacillus cereus*. This bacteria is one of the major spoilage causing bacteria in dairy products. The origin of *B. cereus* is at the farm and is transported from cow and milking equipment to the dairy factory, see Figure 2. In order to control and reduce the levels of microorganisms, a predictive model has been developed. The model, *FarmQ*, describes the contamination and outgrowth of *Bacillus cereus* in raw milk at the farm environment. Special attention is given to the effects of non-controlled factors such as the weather conditions and hygiene at the farm (black box). Further more adherence of vegetative cells and spores of *Bacillus cereus* to surfaces

and insufficient cleaning procedures of equipment are taken into account (De Jong et al. 2002a). The model can be extended to other micro-organisms, viruses, enzymes and milk contaminants.

As shown in Figure 3, the model distinguishes four “unit-operations”:

1. The cow
2. Milking equipment
3. Milk bulk tank at the farm
4. Milk collection tanker

Each step is influenced by different factors and therefore various calculation modules are used. The modules can be connected flexible in different ways to describe each possible situation.

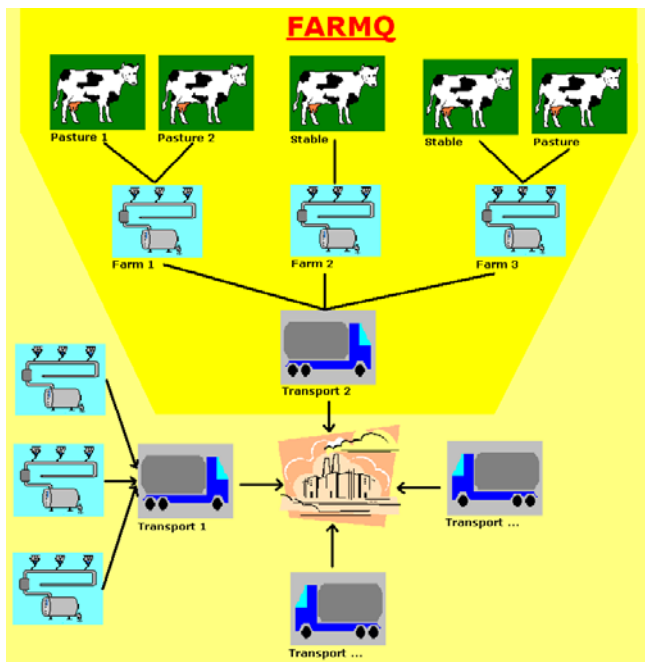


Figure 2: The Hybrid FARMQ Model to Predict the Occurrence of *Bacillus cereus* at the farm

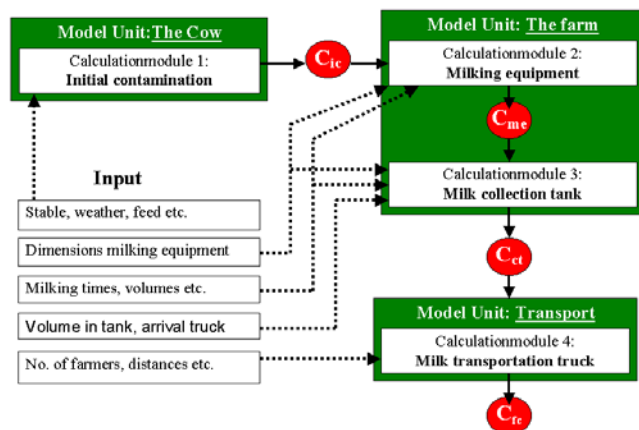


Figure 3: The Combination of White (module 2-4) and Black Box (module 1) Modeling in FARMQ

The initial contamination of raw milk is of major importance and is affected by various controllable (e.g. farm hygiene) and non-controllable factors, (e.g. weather

conditions). Because it is very complex to quantify these effects fuzzy logic is used to model the initial contamination.

To calculate the initial contamination the fuzzy logic model follows three steps (see Figure 4 )

1. Fuzzyfication: translation of numerical input into fuzzy values.
2. Rule evaluation: fuzzy output values are computed using the rule base.
3. Defuzzification: fuzzy output values are translated into a numerical value.

The developed model for initial contamination can be applied for example to simulate temperature effects and to classify the farm’s hygiene. In Figure 4 an example is given of a fuzzy logic modeling approach. The bacterial load of the raw milk is modeled as a function of the outside temperature and humidity (%RAH). A temperature of 23 °C is for 70% warm and 40% hot resulting in 70% medium and 30% high bacterial load which is equivalent to 4.1 colony forming units of *B. cereus* per ml.

The model-units that describe the milking equipment, collection tank and contamination during transport take growth characteristics into account and have a white box nature. To optimise milk handling at the farm and during transport dimensions, the cooling capacity and interval times can be changed. Cleaning efficiency is also a variable.

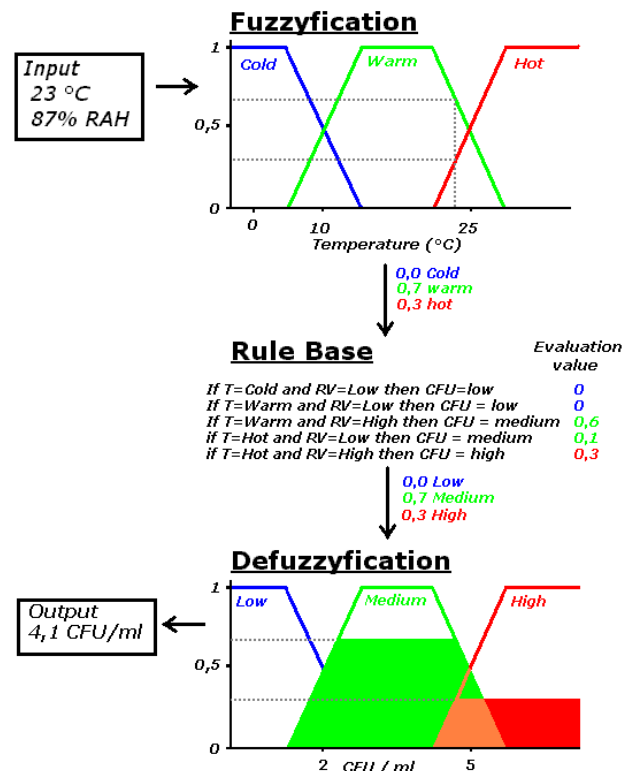


Figure 4: The Fuzzy Inference System (example)

It can be concluded that the uncontrollable factors and qualitative relations can be modeled using fuzzy logic. The hybrid FarmQ model allows a stepwise description of the milk proces and can be used for identification of critical control points at the farm (HACCP approach). Simulations

can be performed to determine the effectiveness of measures to reduce the contamination level of raw milk.

### Taste of cheese

Research on cheese manufacturing has resulted in collection of white box models focused on different processes and operations taking place during cheese manufacturing (e.g. pasteurisation, renneting, acidification, pressing, brining and storage). These models can be used to evaluate the process of cheese manufacturing from cheese milk storage tanks to storage in warehouses and at retailers as a function of various process parameters such as concentration of milk constituents, amount of rennet, heat load, cheese geometry, storage conditions etc. Predicted values are cheese yield, renneting time, the degree of denaturation of whey proteins, inactivation of enzymes, moisture and salt content, pH of the cheese.

Variations in processing conditions during the manufacturing of cheese often also have an effect on the taste of the cheese. Taste parameters are often quantified by means of sensory evaluations. White-box approaches can not be used to include the sensory data in the model. In this case black-box approaches can be used (e.g. neural networks, fuzzy logic). Most of the white models are also relevant for the modelling of taste development. The effect of changes in processing conditions on taste parameters can therefore be described most accurately by a hybrid model, consisting of both white- and black-box elements.

To be able to predict the taste development of cheese during ripening as a function of processing and storage conditions, a hybrid model was developed based on white-box model related to cheese-making. First, the key parameters for taste development and the relevant processing and storage conditions were identified. Based on the results of this investigation the database on which the white box models are based was extended with the relevant experimental results (e.g. protein breakdown, enzyme activities, sensory panel evaluations etc.). A large database based on the evaluations of about 400 cheeses (Gouda) was used.

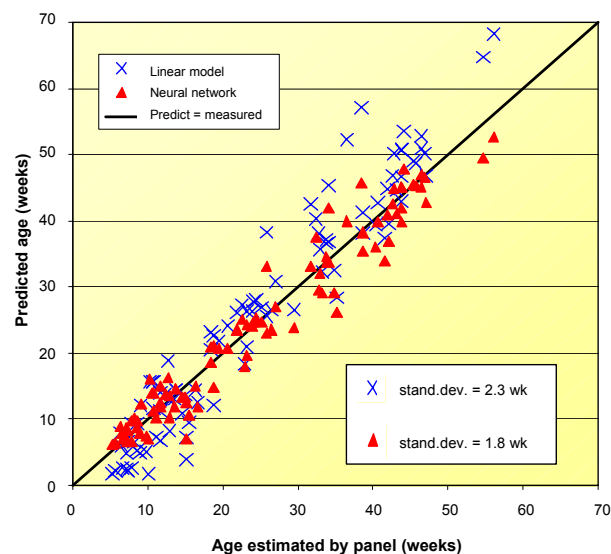


Figure 5: Results of Hybrid Cheese Ripening Model: Age

The hybrid model firstly relates the relevant processing conditions to the relevant parameters (e.g. moisture, salt, pH, enzyme activities) in the cheese at the end of the manufacturing process. After that the fermentation process during ripening is modelled by considering protein breakdown as a function of the storage conditions (e.g. temperature, relative humidity) and the relevant (time-dependent) parameters (e.g. salt, moisture, enzyme activities). Finally, the sensory evaluations are related to the relevant parameters in the cheese (e.g. concentration of small proteins and peptides, pH).

The hybrid model accurately predicts the effect of variations in the processing and storage conditions on the relevant parameters in the cheese during ripening and the sensory evaluations. The sensory evaluations are related to the salt concentration, the moisture content, the pH and the parameters representing protein breakdown. By using white-box elements in the hybrid global model the predictive capacities of the model increase. Moreover, hybrid modeling allows for an optimal use of the available data and knowledge since white-box models that were developed in the past can be integrated.

In Figure 5 and Figure 6 some preliminary results are given of the hybrid modeling approach of cheese-ripening. In Figure 5 the model outcomes are shown with respect to the estimated age of the cheese by an expert panel. In comparison with a linear black box model the used neural network model shows a better prediction of about 20%. In Figure 6 the hybrid model predicts the panel score of a typical off-flavour in cheese. The results show that in approximately 80 % of the cheeses the panel score could be predicted on forehand.

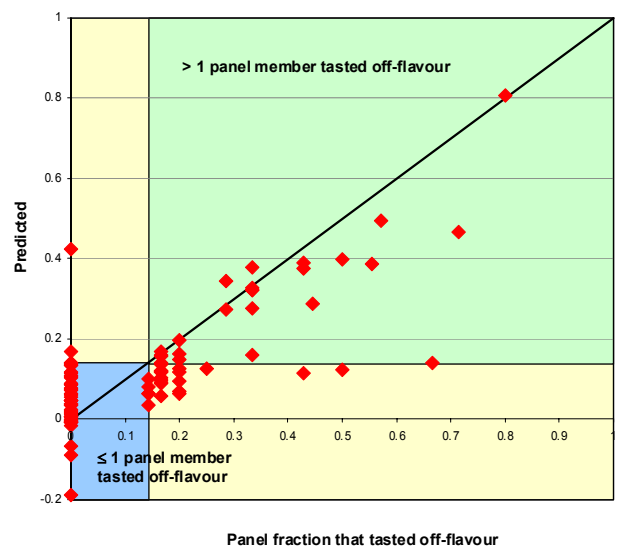


Figure 6: Results of Hybrid Cheese Ripening Model: Flavour attributes

## INDUSTRIAL USE

### NIZO *Premia*

In order to combine hybrid models with other predictive models or to construct a new hybrid model a software system has been developed called *Premia* (Predictive Models ready for Industrial Application). *Premia* consists of a database of (white box) models covering a wide range of phenomena, which are often encountered in food processing, such as predictive models for reduction of fouling, reduction of contamination, loss of nutritional value, rheological properties, powder solubility and flavour development. Functionality is available to connect these models with each other and with process models. For example, Figure 7 shows a screenshot of the cheese ripening model design ('Chermo') within NIZO *Premia*.

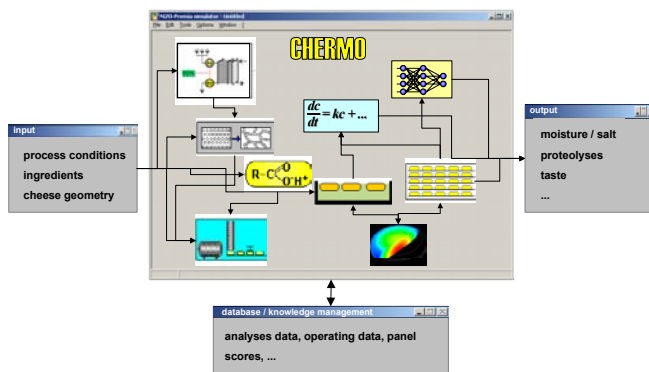


Figure 7: Cheese Ripening Model within NIZO *Premia*

### Cost minimization

The operating costs of many food production chains primarily depend on microbial and physical fouling of the equipment. In general, process operating times at relatively low temperatures ( $< 70\text{ }^{\circ}\text{C}$ ) are due to adherence and growth of bacteria. The operating time of equipment at temperatures above  $80\text{ }^{\circ}\text{C}$  is determined largely by the deposition of protein and minerals. The amount of (bio)fouling directly influences the costs for cleaning, product losses, pollution and production efficiency. Studies show that fouling is responsible for 80 % of the operating costs in the dairy industry (De Jong 1996).

Within NIZO *Premia* it is relatively simple to connect cost models to (hybrid) predictive models. These means that at a given set of desired product specifications the operating costs can be minimized (De Jong et al. 2002b).

### CONCLUSIONS

Hybrid modeling offers great opportunities in the food industry. First of all, hybrid modeling makes it possible to predict complex food properties such as taste and even consumer panel scores. These properties are essential for

product development activities of the industry. Besides, the proposed combination of white and black models decrease the time for model development of predictive models. And, finally, hybrid models have predictive capabilities with respect to black box models.

### REFERENCES

- Alves, T.L.M.; A.C. da Costa; A.W. da Silva-Henriques and E.L. Lima. 1998. "Adaptive optimal control of fed-batch alcoholic fermentation". *Applied Biochemistry and Biotechnology* 70-72, 463-478.
- Beluhan, D. and S. Beluhan. 2000. "Hybrid modeling approach to on-line estimation of yeast biomass concentration in industrial bioreactor". *Biotechnology Letters* 22, 631-635.
- Brands, C. 2002. "Kinetic modelling of the Maillard reaction between proteins and sugar". Ph.D. thesis, Wageningen University.
- De Jong, P.; S. Bouman and H.J.L.J. van der Linden. 1992. "Fouling of heat treatment equipment in relation to the denaturation of  $\beta$ -lactoglobulin." *Journal of the Society of Dairy Technology* 45, 3-8.
- De Jong, P. 1996. "Modelling and optimization of thermal processes in the dairy industry". ISBN 90-9009034-7, Montfoort, the Netherlands.
- De Jong, P. and H.J.L.J. van der Linden. 1998. "Polymerisation model for prediction of heat-induced protein denaturation and viscosity changes in milk". *Journal of Agricultural and Food Chemistry* 46, 2136-2142.
- De Jong, P.; M.C. te Giffel and E.A. Kiezebrink. 2002a. "Prediction of the adherence, growth and release of microorganisms in production chains". *International Journal of Food Microbiology* 74, 13-25.
- De Jong, P.; M.C. te Giffel; H. Straatsma and M.M.M. Vissers. 2002b. "Reduction of fouling and contamination by predictive kinetic models". *International Dairy Journal* 12, 285-292
- Nantawan, T. 2002. "Hybrid neural modeling". *International Journal of Food Properties* 5, 49-61.
- Silva-Henriques, A.W. da; A.C. da Costa; T.L.M. Alves and E.L. Lima. 1999. "A hybrid neural model of ethanol production by *Zymomonas mobilis*". *Applied Biochemistry and Biotechnology* 77-79, 277-291.

### ACKNOWLEDGEMENT

A part of this work (modeling cheese ripening) was supported by the J. Mesdag Foundation.

### BIOGRAPHY

**PETER DE JONG** was born in Utrecht, the Netherlands and studied chemical engineering (B.Sc.) in The Hague and obtained his Ph.D. degree at the University of Delft on modeling and optimization of thermal processes in the dairy industry. In 1986 he went to the R&D department of Campina, a major international dairy company. In 1987 he started to work at NIZO food research as a process engineer. In the nineties together with Han Straatsma he initiated a modeling group for applications in the food industry. At this moment he is responsible for all the research activities on processing, modeling and control within NIZO food research and is the head of a group of 13 scientific workers.

# A PRELIMINARY QUANTITATIVE RISK ASSESSMENT OF *E. COLI* 0157:H7 IN IRISH MINCED BEEF

E. Cummins  
P. Nally  
F. Butler

Department of Agricultural and Food Engineering  
University College Dublin  
Earlsfort Terrace  
Dublin 2  
Ireland

E-mail: [Enda.Cummins@UCD.ie](mailto:Enda.Cummins@UCD.ie)

G. Duffy  
E. Carney  
J. Sheridan  
S. O'Brien

The National Food Centre  
Teagasc  
Dunsinea  
Castleknock  
Dublin 15  
Ireland

## KEYWORDS

Risk assessment, Simulation, *E. coli* 0157:H7, Minced beef.

## ABSTRACT

This study looks at the development of a quantitative risk assessment model for *Escherichia coli* (*E. coli*) 0157:H7 in beef products. A deterministic simulation was developed to assess the prevalence and counts of *E. coli* 0157:H7 on beef trimmings. Beef trimmings are cuts of meat taken from an animal carcass at the time of slaughter and are later processed into saleable products such as beef burgers. The mean calculated prevalence of *E. coli* 0157:H7 on trimmings was 6% and the calculated mean number of counts on contaminated trimmings was 2.26 log<sub>10</sub> CFU/g. The model developed here is one module of a quantitative risk assessment investigating the risks of *E. coli* 0157:H7 contamination to humans and highlights the need for further quantitative risk assessments in the Irish food industry.

## INTRODUCTION

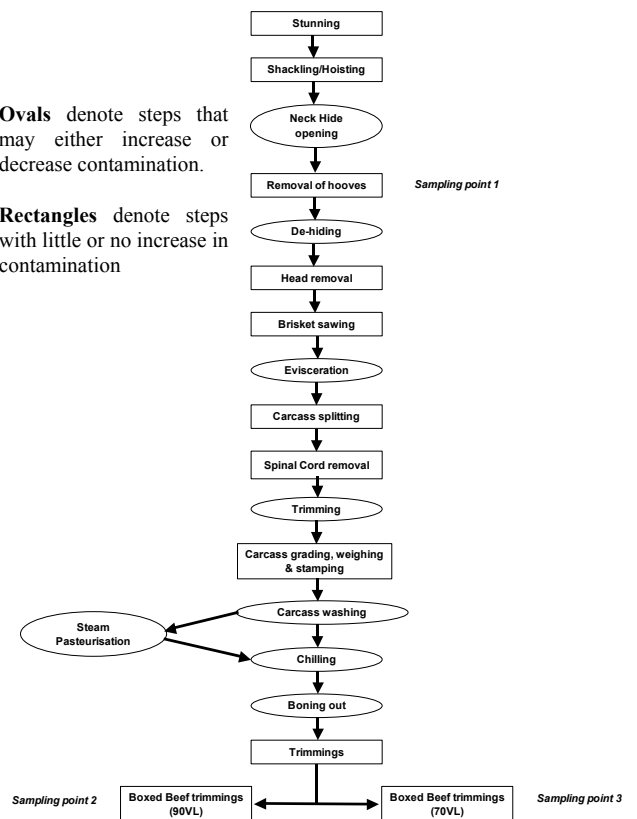
Verocytotoxigenic *Escherichia coli*, in particular serogroup 0157, has emerged as a pathogen of major public concern. High profile outbreaks have focused attention on outbreaks connected to food products, in particular minced beef and beef burgers (CDC 1993). The bacterium is present in faeces and the intestines of healthy bovines (prevalence in Ireland of approx. 2-4%, McEvoy et al. 1998) and can contaminate meat during the slaughter process (Chapman 2000). Over 25 confirmed cases of *E. coli* 0157:H7 poisoning were confirmed in Ireland during 2001. Consequences can vary from severe illness to kidney failure, central nervous system damage and death. A quantitative risk assessment (QRA) is a methodology that can help to identify those stages in the manufacture, distribution, retail and consumption of Irish minced beef products, which can contribute to food borne risks. A quantitative risk assessment currently in progress in Ireland aims to tackle this issue. This quantitative risk assessment is broken into 3 main modules: 1. production of boxed beef trimmings; 2. processing of trimmings and burger formation 3. retail and consumer behaviour. These modules are modelled separately with each preceding module acting as an input into the next. A preliminary risk assessment model of *E. coli* 0157:H7 in Irish minced beef has been developed for the first module and is presented

here. The module aims to assess the prevalence and counts of *E. coli* 0157:H7 in Irish beef trimmings destined for beef burger production.

## MATERIALS AND METHODS

### Model Development

The primary focus of this module was within the slaughterhouse. The prevalence and numbers of *E. coli* 0157:H7 bacteria was modelled at various stages along the slaughter line. A flow diagram of the process is given in Figure 1. The model was created in Excel with the add-on package @Risk (Pallisade Corporation, New York, USA).



Figures 1: Flow diagram of beef trimmings production from the time of slaughter

### Model Inputs

The occurrence of *E. coli* 0157:H7 in live cattle in Ireland was estimated from studies conducted by McEvoy et al. (1998) in which 6 of 250 cattle tested were shedding detectable levels of the pathogen in their feces. Bacon et al. (2000) evaluated microbial populations on animal hides and changes in carcass microbial population at various stages in the slaughtering process in the USA. Sponge swab samples yielded mean generic *E. coli* on the exterior hide of 5.5-7.5 log cfu/100cm<sup>2</sup> with corresponding concentration levels on the carcass (after hide removal but before any decontamination intervention) of 2.6-5.3 log cfu/100cm<sup>2</sup>. The concentration on the hide was obtained by fitting a continuous empirical distribution to the data using a cumulative distribution. The dehiding stage can contaminate the carcass in many ways including direct contact between a carcass and a contaminated hide or cross contamination via worker handling. Elder et al. (2000) performed a survey in the USA to estimate the frequency of enterohemorrhagic *Escherichia coli* 0157:H7 in feces and on hides within groups of cattle from single lots presented for slaughter at meat processing plants. The frequency of carcass contamination during processing from cattle was also surveyed. A cross contamination factor from hide to carcass can be created from data supplied by Elder et al. (2000). From a sample of 355 hides 38 were *E. coli* positive. From a sample of 341 carcasses, 148 carcasses were positive (pre-evisceration). The two beta distributions were combined to create a cross-contamination factor.

Evisceration represents another opportunity for contamination of the carcass to occur. If the gut of an animal is positive for *E. coli* 0157:H7 and the gut is inadvertently nicked during the evisceration process gross contamination of the carcass may occur due to spilling of the gut contents. The prevalence of *E. coli* 0157:H7 in the gut of Irish cattle was determined from McEvoy et al. (1998) where it was discovered that two animals from a sample of 250 were positive for the bacteria. The prevalence in the gut was thus modeled using a beta distribution. The number of times evisceration resulted in a nicked gut was determined to be relatively small (between 1 in 100 to 1 in 1000, personal communication, meat plant production manager). Thus the probability of gut contents spilling and contaminating the carcass during evisceration was modeled as a uniform distribution with a minimum of 0.001 and a maximum 0.01. After carcass splitting and spinal cord removal there is some knife trimming to remove visible spots of fecal contamination. The effectiveness of knife trimming is highly variable (Prasai et al. 1995) in particular work by Sheridan et al. (1992) and Smeltzer et al. (1998) have shown that equipment such as knives, gloves and aprons can act as reservoirs for bacteria.

Carcass washing can have the effect of reducing numbers of bacteria (Reagan et al. 1996). There is also evidence that some washing procedures may redistribute bacteria to other parts of the carcass (McEvoy et al. 1997). In this preliminary analysis a reduction of between 1 and 2.5 fold was assumed as suggested by Cassin et al. (1998) and is incorporated in the model by means of a uniform distribution. Steam pasteurization is used in a small number of meat plants in Ireland. Its efficiency was assessed by Phebus et al. (1997).

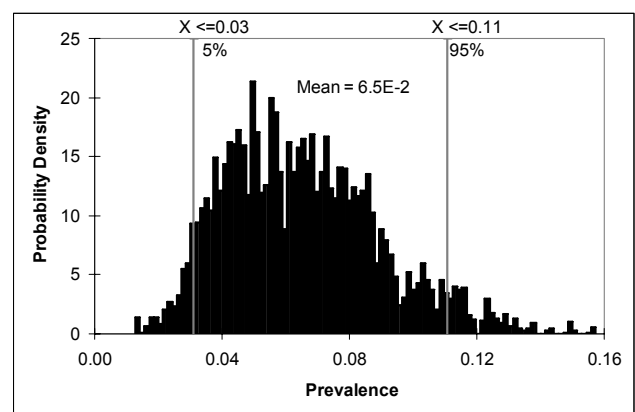
Reductions of *E. coli* 0157:H7 was found to be approximately 3.53 ( $\pm$  0.49) log CFU/cm<sup>2</sup>. In this preliminary analysis the model considers production in a plant which does not have steam pasteurization in place. The most likely effect from chilling is that there is no effect (Cassin et al. 1998). Growth or decline is assumed to occur only on carcasses which are contaminated on entering the chiller. The potential growth was modelled using a triangular distribution with minimum growth -2, a mode of 0 and a maximum of 5 generations. This factor and further inputs and calculations used in the model are detailed in Table 1.

### Second order modelling

There is increasing emphasis being placed on quantifying the impact of uncertainty and variability in risk assessments (Kelly and Campbell 2000) Variability and uncertainty in the input parameters was incorporated in the construction of a second order model by means of probabilistic distributions. As @Risk does not facilitate the separation of variability and uncertainty a macro was developed in visual basic to deal with this task. 100,000 iterations were performed using Latin Hypercube sampling with @Risk software. After 1000 iterations the macro was designed to change the uncertainty parameters, i.e. both uncertainty and variability were simulated with 1000 iterations performed for 100 uncertainty values (giving the required total of 100000 iterations). The results are presented in Figures 2-4.

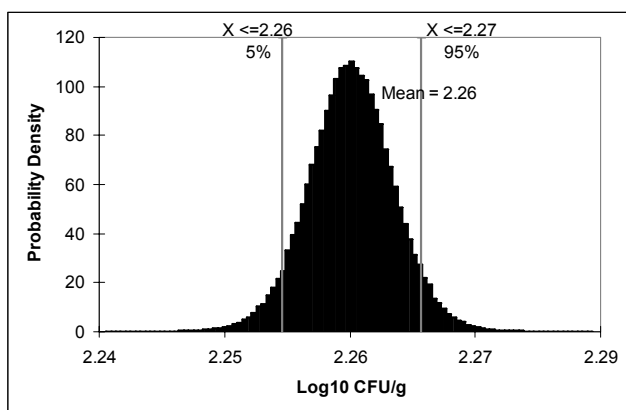
## RESULTS AND DISCUSSION

A plot of the prevalence of *E. coli* 0157:H7 in Irish beef trimmings is given in Figure 2.



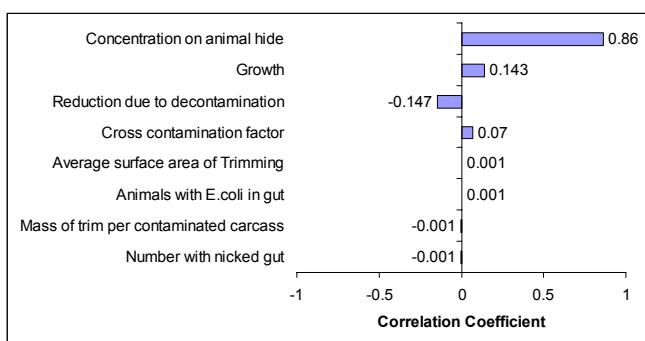
Figures 2: Prevalence of *E. coli* 0157:H7 in beef trimmings

The mean calculated prevalence of contaminated trimmings is 6% with 90 percentile range between 0.03 and 0.11%. The calculated mean number of counts of *E. coli* 0157:H7 on contaminated trimmings was 2.26 log<sub>10</sub> CFU/g (Figure 3). Given the estimated small dose required to cause illness resulting from the ingestion of *E. coli* 0157:H7 (Cassin et al. 1998) these predictions may be a cause for concern. Results from this module will be validated by ongoing sampling work currently being carried out at a major Irish beef processing plant.



Figures 3: Counts of *E. coli* 0157:H7 on contaminated beef trimmings

The sensitivity of the number of counts of *E. coli* 0157:H7 on contaminated trimmings to input values was measured by rank correlation. The results of the sensitivity analysis can be seen in Figure 4. The input having greatest impact on model results was the concentration of *E. coli* 0157:H7 on the animal hide (correlation coefficient 0.86). This highlights the importance of having animals as clean as possible when presented for slaughter.



Figures 4: Sensitivity of counts of *E. coli* 0157:H7 to model inputs

## CONCLUSIONS

The model described in this paper predicted the prevalence and counts of *E. coli* 0157:H7 in Irish beef trimmings. With the addition of further modules the model should encompass available information about the processing, treatment and use of beef trimmings. The health risks posed to humans by potential *E. coli* 0157:H7 contamination can therefore be quantitatively assessed. The model results indicate there may be cause for concern if *E. coli* counts are not reduced at a later stage in the processing process. The fact that *E. coli* concentration on the hide is having the largest effect on *E. coli* counts highlights the importance clean animal policies may be having on reducing *E. coli* numbers. The model can provide an appropriate decision support tool aiding risk mitigation strategies in an effort to protect human health.

## ACKNOWLEDGEMENTS

The authors wish to acknowledge the Department of Agriculture for their funding of this project under the Food Institute Research Measure.

## REFERENCES

- Bacon, R.T.; K.E. Belk; J.N. Sofos; and G.C. Smith. 2000. "Incidence of Escherichia Coli 0157:H7 on hide, carcass and beef trimmings samples collected from United States packing plants". Presented at *FSIS public meeting on E.coli 0157:H7*, February 29, 2000, Arlington, VA.
- Cassin, M.H.; A.M. Lammerding; E.C.D. Todd; W. Ross; R.S. McColl. 1998. "Quantitative risk assessment for Escherichia coli O157 : H7 in ground beef hamburgers". *International Journal of Food Microbiology*. 41 (1): 21-44.
- Chapman, P.A. 2000. "Sources of Escherichia coli 0157 and experiences over the past 15 years in Sheffield, UK". *Journal of Applied Microbiology Symposium Supplement*. 88: 51S-60S.
- CDC, 1993. Centre for Disease Control. "Updata: multistate outbreak of Escherichia coli 0157:H7 infections from hamburgers- western United States, 1992-1993". *Morbid. Mortal. Weekly Report* 42:258-263.
- Elder R.O.; J.E. Keen; G.R. Saragusa; G.A. Barkocy-Gallagher; M. Koomaraie; and W.W. Laegreid. 2000. "Correlation of enterohemorrhagic E.coli 0157 prevalence in feces, hides and carcasses of beef cattle during processing". In *Proceedings of the National Academy of Science*. 7: 2999-3003.
- Kelly, E. and K. Campbell. 2000. "Seperating variability and uncertainty- making choices". In *Human and Ecological Risk assessment*. 6, (1) 1-13.
- McEvoy, J.M.; A.M. Doherty; J.J. Sheridan; F.M. Thomson-Carter; P. Garvey; L. McGuire; I.S. Blair; and D.A. McDowell. 1998. "The incidence and spread of Escherichia coli 0157:H7 at a commercial beef abattoir. Epidemiology of verocytotoxigenic E.coli." In *Proceedings of Concerted action, CT98-3935*, hosted by Teagasc, The National Food centre, Malihide, Dublin, Ireland 8-10th February 2001.
- McEvoy, J., J.J. Sheridan; L. McGuire. 1997. "The effect of cold water washing on beef carcass contamination." Unpublished data. The National Food Centre Dublin.
- Phebus R.K.; A.L. Nutsch; D.E. Schafer; R.C. Wilson; M.J. Riemann; J.D. Leising; C.L. Kastner; J.R. Wolf; and R.K. Prasai. 1997. "Comparison of steam pasteurization and other methods for reduction of pathogens on surfaces of freshly slaughtered beef." *Journal of Food Protection*, 60: 476:484.
- Prasai R.; R.K. Phebus; C.M. Garcia Zepeda; C.C. Kastner; A.E. Boyle; and D.Y.C. Fung. 1995. "Effectiveness of trimming and/or washing on microbial quality of beef carcasses." *Journal of Food Protection*, 58: 1114-1177
- Reagan J.O; GR. Acuff; D.R. Buege; M.J. Buyck; J.S. Dickson; C.L. Kastner; J.L. Marsden; J.B. Morgan; R. Nickelson; G.C. Smith; J.N. Sofos. 1996. "Trimming and washing of beef carcasses as a method of improving the microbiological quality of meat." *Journal of Food Protection*. 59 (7): 751-756.
- Sheridan, J.; B. Lynch; and D. Harrington. 1992. "The effect of boning plant cleaning on the contamination of beef cuts in commercial boning hall." *Meat Science*, 32: 155-164.
- Smeltzer, T.; B. Peel; and G. Collins. 1998. "The role of equipment that has direct contact with the carcass in the spread of Salmonella in beef abattoir." *Australian Veterinary Journal*, 55: 275-277.

Table 1: Model input details

Variable	Description	Distribution/model	Units
S	Slaughterings	2000000	animals/year
Ph	Prevalence of <i>E. coli</i> on hide	Beta(6+1,250-6+1)	
Nh	No. Animals with <i>E. coli</i> on hide	Poisson(S*Ph)	animals
Pg	Prevalence of <i>E. coli</i> in gut	Beta(2+1,250-6+1)	
Ng	No. Animals with <i>E. coli</i> in gut	Poisson(S*Pg)	animals
Ch	Conc of <i>E. coli</i> on hide	Cumulative	log <sub>10</sub> CFU/cm <sup>2</sup>
Cm	Mean	4.533	
Cstd	Standard deviation	1.1915	
Cha	Average Conc. of <i>E. coli</i> on all contaminated hides	Normal(Cm, Cstd/SQRT(Nh))	log <sub>10</sub> CFU/cm <sup>2</sup>
Fcc	Factor for cross-contamination	Beta(148+1,341-148+1)/Beta(38+1,355-38+1)	
Fccm	Mean	4.5333	
Fccstd	Standard deviation	1.1915	
Tcc	Total contaminated carcasses	Normal(Nh*Fccm, SQRT(Nh)*Fccstd)	Carcasses
Pe	Probability of evisceration	Uniform(0.001, 0.01)	
Ngc	Number Animals cut at evisceration with gut infection	Poisson(Pe*Ng)	Animals
Fei	Factor for evisceration increase	2	
CCF	Factor for increase/decrease from hide to carcass	Cumulative	
CCFm	Mean	0.53586	
CCFstd	Standard deviation	0.2166	
CCFav	Average factor increase/decrease from hide to carcass	Normal(CCFm, CCFstd/SQRT(Tcc))	
Wr	Washing reduction	Uniform(1,2.5)	
G	Growth	Triang(-2,0,5)	Generations
Cctc	Concentration on contaminated carcass	Ch+CCFm-Wr+LOG(2^G)	log <sub>10</sub> CFU/cm <sup>2</sup>
Cctcg	Concentration on contam. carcass if gut nicked	Ch+CCFm+Fei-Wr+LOG(2^G)	log <sub>10</sub> CFU/cm <sup>3</sup>
St	Surface area of trimmings	RiskUniform(0.25,1)	cm <sup>2</sup> /g
Stm	Mean	0.625	
Ststd	Standard deviation	0.21651	
Stct	Average surface area of contaminated trim	Normal(Stm, Ststd/SQRT(Tcc))	
Mt	Mass of 90VL trimmings	Normal(12000, 1000, Truncate(50, ))	grams
Mtm	Mean	12000	
Mtstd	Standard deviation	993.61	
TMcc	Total mass of trim from contaminated carcasses	Normal(Tcc*Mtm, SQRT(Tcc)*Mtstd)	grams
TMcg	Total mass of trim from contam. carcasses when gut cut	Normal(Ngc*Mtm, SQRT(Ngc)*Mtstd)	grams
Nct	Number of contaminated trimmings	TMcc/Mtm	
Nctg	Number of contam. trimmings when gut nicked	TMch/Mtm	
Tt	Total Number of trimmings produced	S*2	
Ptrim	Prevalence of contaminated trimmings	Nct+Nctg/Tt	
Ccta	Average concentration for each contaminated trimming	Stct*Cctc	CFU/g
Cctag	Average concentration for each contam. trimming if gut nicked	Stct*Cctcg	CFU/g

# COMBINING LATENT CLASS ANALYSIS AND TREE-BASED MODELLING TO SIMULATE THE DECISION PROCESS OF EXPERTS DURING VISUAL QUALITY CLASSIFICATION

Schrevens Eddie and Coppenolle Hans  
K.U.Leuven  
Faculty of Agricultural and Biological Sciences  
Research Unit for Quality Management  
W. De Croylaan 42  
B-3001 Heverlee, Belgium  
Email: eddie.schrevens@agr.kuleuven.ac.be

## KEYWORDS

Image processing, chicory, quality, classification, variability, simulation.

## ABSTRACT

Study of uncertainty and enclosed subjectivity in expert quality decision processes is a first step towards a structural comprehension of fuzzy classification concepts and the definition of optimal quality criteria. This paper relates to visual quality classification of chicory by auction experts in a measurement space of quality descriptors length and width, in accordance with the traditional grading mechanism. A uniform sample of products was optimally selected in the bivariate measurement space based on digital imaging techniques. Image sequences of the selected products, were classified by five experts based on length and width in accordance with the traditional auction system. The image sequences were visualized using a computer based image system.

Between-expert variability is analysed by latent class analysis. This statistical technique reveals latent clusters of homogeneous chicory products based on the observed mixture of expert classification scores. The contingency-based approach of latent class analysis simultaneously explains how the identified consensus structure relates to the quality scoring of individual experts. The latent classes of chicory products are thereafter related to the perceptual space of product quality descriptors using tree-based modelling to simulate the variability construct inherent in expert quality classification.

## INTRODUCTION

The definition of quality is often subjective and/or difficult to interpret. The uncertain nature of quality gives rise to the typical variability in quality decision between different experts. This work specifically concerns the quality classification of chicory (*Cichorium intybus* L. var. *Foliosum Helgi*) by auction experts. At the auction, the quality of a perishable heterogeneous commodity of chicory products is controlled based on a set of visual quality

descriptors. The grading process of chicory follows a dual grading mechanism. The dual system includes:

- Classification based on intrinsic product characteristics: shape, freshness, colour, openness of the top, length of the kernel, ...
- Classification based on the size of the product: length and width

Present-day classification rules for chicory include overlapping regions on the classification measurement scale between quality classes. The fuzzy nature of the grading system as well as the typical subjectivity in visual quality classification contributes to uncertainty of the decision process. Differences in interpretation of classification rules, handling of different classification schemes and limitations of the human perceptive system, result in inter- and intra-individual variability of the quality decision. However, optimal quality classification of horticultural products at the auction is necessary for an optimal management of the distribution channel.

Structural approaches that optimally recognize expert variability, are a pre-requisite for an objective comprehension of the probabilistic nature of human decision processes. In this paper, a transparent statistical approach to simulate the typical between-expert variability inherent in human quality classification is proposed. A combination of latent class analysis and tree-based modelling is used to optimally detect uncertainty patterns in the quality classification of chicory by auction experts.

## MATERIAL AND METHODS

### Extraction of quality descriptors by quantitative imaging techniques

The study of visual quality evaluation of the fresh product requires primarily an objective measurement method to define quality. The visual character of quality evaluation makes horticultural products very suitable for investigation by quantitative imaging techniques. Extraction of quality descriptors, as size, shape and colour, from digital video images of a product, results in a quantitative, objective description of external product features. Quality descriptors of different varieties of chicory were objectively measured during the season to compile a database of product features,

corresponding images and full-sized images sequences. This resulted in database of 1000 chicory crops. In this experiment, only the quality parameters length and width are involved. The length of a chicory crop is defined as the mean of the length of the head on four different images, the product respectively rotated over 0, 90, 180 and 270 degrees. Width is calculated similarly.

### Sampling strategy

In this experiment, only classification based on the size of the product is studied. The dual grading mechanism for chicory justifies the assumption of independence between classification based on quality descriptors as shape, colour, top openness, etc. and classification based on the size of the product.

Chicory is selected in the 2-dimensional measurement space of length and width by use of a 2-dimensional grid. The distance between successive grid-points is determined as 5 percent of the range of both quality descriptors. Eliminating biologically impossible grid-points and selecting products as close as possible to the remaining grid-points in the measurement space, results in a collection of experimental subjects that are uniformly distributed over the product space. The method resulted in 214 products selected from the constructed database of 1000 chicory crops (Figure 1). The sampling strategy assumes each part of the bivariate space of quality descriptors to be equally important. In this way, the experimental design protocol enables an optimal exploration of the classification activities of auction experts with respect to the entire range of the length and the width of commercial chicory products.

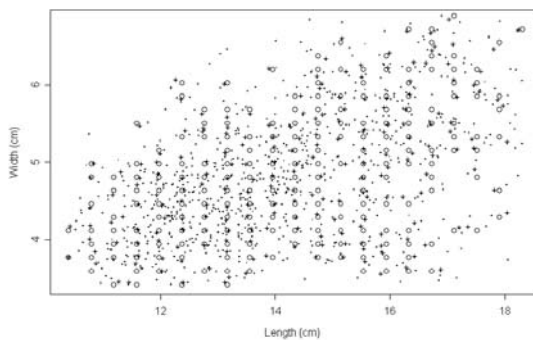


Figure 1: Selection of products in a 2-dimensional space length-width (. = product, o = gridpoint, + = selected product)

### Experiment by use of a computer based image system

Full-sized image sequences of the 214 selected products, uniformly distributed over length and width, were evaluated by five experts (A1, B1, C1, D1, E1) using a computer based image system (Figure 2). The use of a computer visualisation system eliminated seasonal effects and deterioration as influencing factors in the sampling strategy.

The full-sized image sequences were shown in the same order to all experts. This limited positional effects by controlling the influence of preceding image sequences on quality judgement.



Figure 2: Computer based image system

Experts scored the products on a categorical five-point scale, corresponding to the auction grading system. The classes represent very short (quality class 1), short thin (quality class 2), short thick (quality class 3), thick (quality class 4) and long chicory (quality class 5). The classification scheme imposed on the quality experts is graphically represented in Figure 3. The auction experts involved in the experiment were all familiar with the imposed classification scheme. Figure 3 clearly shows the extensive overlap between the quality classes. Thus, variability between auction experts arises in this experimental context from the existing overlap between quality classes as well as from subjectivity of auction experts in quality classification. The defined five-point categorical response scale exhibits a partially ordinal character. The longer and thicker the product, the higher the correspondence with a higher quality class. Quality evaluation of selected chicory was not repeated within experts.

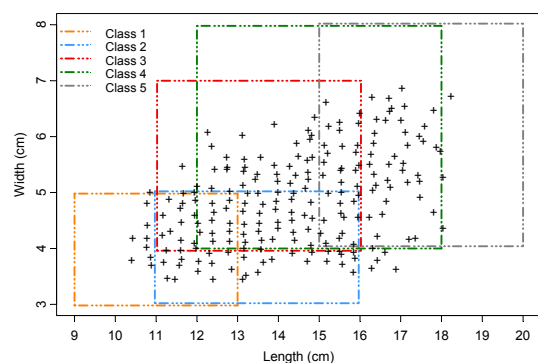


Figure 3: Auction grading criteria for chicory based on length and width, superimposed on the selected chicory crops (indicated as +)

## Latent class analysis

Latent class analysis is proposed as a statistical technique that is able to define a consensus structure over auction experts. Quality classification typically results in a multi-way contingency table with the quality decision by different auction experts as classification criteria. The psychometric concept of latent class analysis relies on an additive decomposition of the observed frequencies for the expert response patterns in a multi-way contingency table by an unmeasured latent categorical variable  $x$  based on an optimality criterion (McCutcheon 1987). The decomposition by  $x$  is such that the classification by the experts in each of the resulting equidimensional contingency table components, or latent classes, is statistically independent. A latent class can be considered as a group of homogeneous chicory crops based on the mixture of expert classification scores. In this way, latent class analysis results in the definition of a consensus model over auction experts. The contingency-based approach of latent class analysis simultaneously explains how the latent classes relate to the quality scoring of individual experts.

Let the five experts judge products on the five-point categorical scale. The experiment implies five categorical variables  $a, b, c, d, e$  for the five experts, with corresponding quality class levels indexed by  $j, k, l, m, n$  respectively. Categorical values  $j, k, l, m, n$  vary from 1 to 5. The levels for the latent variable  $x$ , referred to as its latent classes, are indexed by  $i$  and assumed to vary from 1 to  $y$ . The associated latent class model is formalised as

$$P_{ijklmn}^{xabcde} = P_i^x P_{ji}^{a|x} P_{ki}^{b|x} P_{li}^{c|x} P_{mi}^{d|x} P_{ni}^{e|x}$$

with

$$P_{ijklmn}^{xabcde}$$

the expected joint probability of level  $i$  of the latent variable  $x$  and response pattern  $ijklmn$  given by the experts.

$$P_i^x$$

is the latent class probability of falling into latent class  $i$ , and

$$P_{ji}^{a|x}, P_{ki}^{b|x}, P_{li}^{c|x}, P_{mi}^{d|x}, P_{ni}^{e|x}$$

are conditional probabilities of falling into levels  $j, k, l, m$  and  $n$  respectively, given latent class  $i$ . The model parameters are restricted as

$$\sum_i P_i^x = \sum_j P_{ji}^{a|x} = \sum_k P_{ki}^{b|x} = \sum_l P_{li}^{c|x} = \sum_m P_{mi}^{d|x} = \sum_n P_{ni}^{e|x} = 1$$

The expected probabilities  $P_{ijklmn}^{xabcde}$  are related to the expected probabilities  $P_{ijklmn}^{abcde}$  for a response pattern  $ijklmn$  in the original observed multi-way contingency table by

$$P_{ijklmn}^{abcde} = \sum_i P_{ijklmn}^{xabcde}$$

Posterior probabilities

$$P_{i|ijklmn}^{xabcde} = \frac{P_{ijklmn}^{xabcde}}{\sum_i P_{ijklmn}^{xabcde}}$$

can be derived to assign each product having response pattern  $ijklmn$  to that latent class  $i$  for which  $P_{i|ijklmn}^{xabcde}$  is highest (McCutcheon 1987; McLachlan and Basford 1988).

Maximum likelihood estimates for the latent class model are obtained by the Expectation-Maximisation (EM) algorithm (Goodman 1974; Goodman 1979; McLachlan and Thriyambakam 1997). The iterative procedure proceeds by successively updating the initially random parameter values using a maximum likelihood approach for the assumed model concept.

The formulation of the latent class model agrees with a conditional independence loglinear model where the quality classification by the different experts is independent given the unobserved latent class  $i$  (Agresti 1990; Haberman 1979, Hagenars 1993). In the specific context of quality classification, theoretical independence between experts given a latent class corresponds to the intuitive assumption of homogeneity of scored products within a latent class.

## Tree-based modeling

The method of classification and regression trees (CART) is an approach to model the relationship between a categorical- or numeric response variable with independent variables possibly measured on different scales (Breiman et al. 1984). In a statistical framework it can be considered as a non-parametric discriminant analysis. Tree based modelling generates decision trees as a succession of decision rules derived from an existing classified data set or training set. For each binary split, an impurity function is minimised over the set of all possible univariate decision rules. The rule resulting in minimal impurity is retained. The splitting procedure is stopped when a terminal node receives less than 5 observations. From this point on, the decision tree is pruned by minimising a cost-complexity function, compromising between minimal cross-validated deviance and minimal number of terminal nodes.

A mixture model consensus structure over experts is obtained by means of latent class analysis. Once the latent distribution known, probabilistic clustering assigns each product to the latent class to which it has the highest estimated posterior probability of belonging. This step enables to explain the relationship between the consensus configuration represented by the latent classes with the measurement space of product quality descriptors using tree-based modelling.

## RESULTS

In the context of the classification experiment with chicory, a latent class can be interpreted as a group of homogeneous chicory crops. Based on the mixture of expert classification data, we searched for optimal groups of homogeneous chicory crops that reflected the best possible consensus agreement among quality experts. Different latent class models were run for an increasing sequence of latent classes. A latent class model with a higher number of latent classes implies a better goodness of fit for the conditional independence structure or more homogeneous

chicory per latent class. Hence, an optimality criterion is necessary to select an optimal latent class model compromising between model complexity and model bias. Model selection was based on minimisation of Akaike's information criterion (AIC). This parameter integrates information about model bias with a penalty for the number of estimated model parameters (Akaike 1974).

A latent class analysis was performed based on the observed classification data of the five experts. The marginal frequency distribution of the classification pattern for the five experts is represented in Table 1. Expert E classified many chicory crops in quality class 5 with respect to other experts, expert B didn't use quality class 5 at all when classifying chicory crops.

Table 1: Marginal probabilities for the five experts

Expert	Class 1	Class 2	Class 3	Class 4	Class 5
A1	29	70	55	55	5
B1	48	79	61	26	0
C1	40	63	95	15	1
D1	29	84	67	26	8
E1	25	54	69	41	25

As expert B did not use quality class five when classifying chicory crops, the initial conditional probabilities  $P_{s_{ji}^{b|x}}$  of expert B classifying chicory in quality class 5 were restricted to 0 in the latent class initialisation phase for all levels of latent variable  $x$ . Latent class models for an assumed number of latent classes ranging from two to eight were estimated. Each latent class model was estimated five times to circumvent the eventual occurrence of local maxima in the estimation procedure. The values for the log-likelihood and Akaike's information criterion (AIC) of the fitted models are represented in Figure 4. The figure shows the log-likelihood as monotonously increasing with an increasing number of latent classes. This essentially agrees with the idea that a higher number of latent classes implies either a better fit for the conditional independence structure or the identification of groups of more homogeneous chicory crops.

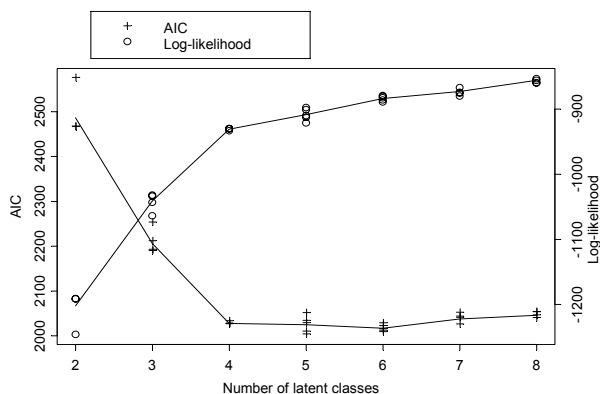


Figure 4: Log-likelihood and Akaike's information criterion (AIC) of the fitted models

The latent class model with six latent classes, showing the minimal AIC value of 2008.64 was selected. Conditional and latent class probabilities of the selected model are represented in Table 2. From the conditional probabilities follows that latent class 1 mainly agrees with chicory classified as quality class 1 (very short), latent class 2 with chicory classified as quality class 2 (short thin) or 3 (short thick), latent class 3 with chicory classified as quality class 3 (short thick) or 4 (thick), latent class 4 with chicory classified as quality class 2 (short thin), latent class 5 with chicory classified as quality class 5 (long) by expert E1, latent class 6 with chicory classified as quality class 3 (short thick). As a latent class includes homogeneous chicory, uncertainty exists for particular chicory crops to classify them as quality class 2 (short thin) or 3 (short thick), for other crops to classify them as quality class 3 (short thick) or 4 (thick). This supposes uncertainty nearby the boundaries of adjacent quality classes, which agrees with the existing overlapping regions between adjacent quality classes in the commercial grading system for chicory. Other latent classes (latent class 1, 4 and 6) reveal evidence that some basic understanding of the appearance of chicory typical for quality class 1, 2 and 3 exists. The latent class probabilities reported in Table 2 indicate the relative magnitude of the different latent classes.

Table 2: Latent and conditional probabilities of the selected latent class model with six latent classes

Latent class probability	Latent class	Quality class	Expert	Expert	Expert	Expert	Expert
			A1	B1	C1	D1	E1
0.183	1	1	0.719	0.946	0.917	0.712	0.637
	1	2	0.201	0.054	0.026	0.173	0.199
	1	3	0.080	0.000	0.057	0.115	0.164
	1	4	0.000	0.000	0.000	0.000	0.000
	1	5	0.000	0.000	0.000	0.000	0.000
0.111	2	1	0.000	0.000	0.039	0.000	0.000
	2	2	0.501	0.576	0.186	0.738	0.064
	2	3	0.378	0.424	0.775	0.262	0.936
	2	4	0.121	0.000	0.000	0.000	0.000
	2	5	0.000	0.000	0.000	0.000	0.000
0.181	3	1	0.000	0.000	0.000	0.000	0.000
	3	2	0.000	0.027	0.000	0.079	0.000
	3	3	0.120	0.506	0.772	0.428	0.000
	3	4	0.880	0.467	0.228	0.493	0.911
	3	5	0.000	0.000	0.000	0.000	0.089
0.274	4	1	0.000	0.089	0.021	0.000	0.000
	4	2	0.856	0.911	0.897	0.965	0.761
	4	3	0.000	0.000	0.082	0.017	0.068
	4	4	0.144	0.000	0.000	0.000	0.017
	4	5	0.000	0.000	0.000	0.018	0.154
0.065	5	1	0.000	0.000	0.000	0.000	0.000
	5	2	0.000	0.428	0.357	0.000	0.000
	5	3	0.000	0.000	0.217	0.000	0.000
	5	4	0.639	0.572	0.354	0.499	0.093
	5	5	0.361	0.000	0.072	0.501	0.907
0.186	6	1	0.020	0.141	0.046	0.026	0.000
	6	2	0.000	0.070	0.000	0.000	0.000
	6	3	0.961	0.789	0.922	0.974	0.914
	6	4	0.019	0.000	0.032	0.000	0.086
	6	5	0.000	0.000	0.000	0.000	0.000

Once the latent distribution is known, the defined latent classes are linked with the from images extracted quality descriptors length and width using tree-based modelling. Based on the cost-complexity measure, an optimal pruned tree-based model with 6 terminal nodes and 21.5 % misclassification error was selected. The pruned tree-based model which links the latent classes with the quality measurement space is represented in Figure 5. The branches connecting the nodes, are labelled by the left and the right splitting rules. Ellipses denote interior nodes, while rectangles represent terminal leaves. The predicted value of the quality classification response is centred in each node. The predicted value corresponds to the quality class to which the majority of the chicory crops arriving at a node are assigned. The number under each node denotes the misclassification.

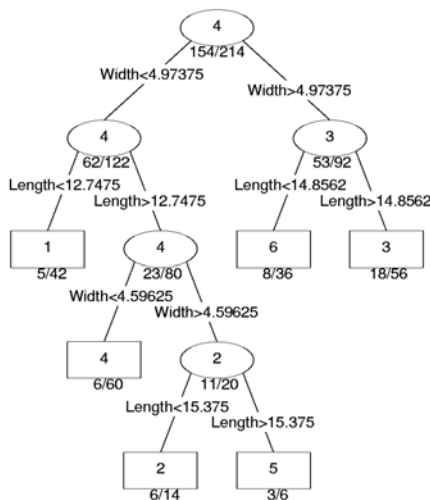


Figure 5: Optimal, pruned tree-based model that links the latent classes with the quality descriptors length and width

Figure 6 shows the same tree-based model, represented as predictor versus fitted values, superimposed on Figure 3. The location of the latent classes in the measurement space of length and width and their relation with the imposed grading rules can easily be read from the graphical display.

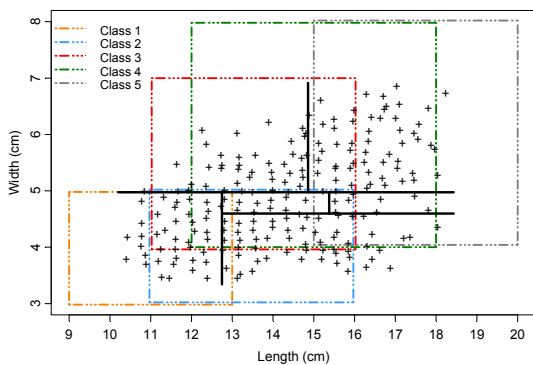


Figure 6: Latent class structure (black lines) in relation to the auction classification scheme imposed on the experts, chicory crops are indicated as +

## CONCLUSIONS

The beneficial use of combining latent class analysis and tree-based modelling to define a consensus model based on expert quality classification data has been demonstrated. Latent class analysis results in a consensus structure underlying the decision process while simultaneously explaining its interaction with individual expert information. The latent class analysis simply clusters products with homogeneous uncertainty patterns in an optimal way. In this way, the groups of homogeneous chicory crops detected based on the observed classification scores, reflect the quality perception of an average expert. Conditional probabilities resulting from latent class analysis relate the latent classes of homogeneous chicory products with the classification of individual experts. The consensus structure is finally linked with explanatory quality descriptors using tree-based modelling.

By summarising all facets in the quality decision process efficiently, the technique provides an informative construct for redefinition of fuzzy classification systems. The technique allows an elegant specification of between-expert variability in model formulation. The integration of this essential information in one single model defines a statistical approach to the analysis of classification data with a broad range of applicability.

## REFERENCES

- Agresti, A. 1990. *Categorical data analysis*. John Wiley & Sons, New York.
- Akaike, H. 1974. "A new look at the statistical model identification." *IEEE Transactions On Automatic Control* 19, 716-723.
- Breiman, L.; J. Friedman; R. Olshen; and C. Stone. 1984. *Classification and regression trees*. Wadsworth International Group, Belmont.
- Goodman, L.A. 1974. "Exploratory latent structure analysis using both identifiable and unidentifiable models." *Biometrika* 61, 215-231.
- Goodman, L.A. 1979. "On the estimation of parameters in latent structure analysis." *Psychometrika* 44, 123-128.
- Hagenaars, J.A. 1993. *Loglinear models with latent variables*. Sage Publications, London.
- McCutcheon, A.L. 1987. *Latent class analysis*. Sage Publications, London.
- McLachlan, G.J.; and K.E. Basford. 1988. *Mixture models: inference and applications to clustering*. Marcel Dekker Inc., New York.
- McLachlan, G.J.; and K. Thriyambakam. 1997. *The EM algorithm and extensions*. Wiley, New York.

# SYSTEMIC AND INTERPRETATION OF FOOD TEXTURE TESTS

Alain-Claude ROUDOT  
ESMISAB, Université de Bretagne Occidentale  
Laboratoire de Microbiologie et Sécurité Alimentaire  
Technopole Brest-Iroise  
F-29280 Plouzané  
France  
E-mail: Alain-Claude.Roudot@univ-brest.fr

## KEYWORDS

Food texture, tissue organisation, histological modelling, systemic.

## ABSTRACT

Food texture analysis is a method of testing agricultural product which is actually well known. However, interpretation of the results obtained usually uses continuous theories which are not able to give good mechanical interpretations. Different examples are given showing the limits of such theories. In order to solve this problem one can "mentally" interpret the results as global results of a particulate medium. This paper shows that it may be possible to model food tissue and apply a mechanical theory of cellular medium, which gives far more better results. That theory is based on complexity theories taking into account tissue organisation as well as static and dynamic relations between its components.

## INTRODUCTION

A cellular food product such as vegetable or fruit, is constituted of various elements, each one having its own physical behaviour. A cellular tissue has a behaviour in itself which is linked to its cells properties and cells organisation. Classical methods of interpretation and/or testing are based on a continuous paradigm whose advantage is simplicity. However its drawback is that it is impossible to link tests results to physical characteristics of the products. Another theoretical approach only takes into account the individuals cells behaviour. Unfortunately, intercellular links are forgotten and then interpretation, when possible, is truncated. So, neither the macroscopic method, nor the microscopic one is sufficient to understand cell tissue responses to external physical stresses. Nowadays systemics and complexity theories (Le Moigne, 1991) seem to be the best approaches to explain cell tissue behaviour and find the links between physical structure and texture of this kind of food products (Roudot, 2002b). This can be shown by studying different tests results and

comparing the interpretation's possibilities of these methods.

## COMPLEXITY THEORY APPLIED TO FOOD STRUCTURE

A cellular tissue is assumed to be a complex system in which we can find different parts: the individual cells, the physical organisation of these cells and the intrinsic functions of the cells as parts of the tissue.

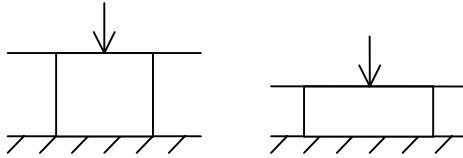
These different elements exist in all complex systems and need to be taken into account in a modelling process if further simulations have to be close to actual experimentations.

Here, we will only consider two independent domains: the domain of operation of the structural components of the tissue (*i.e.* of the cells), and the domain in which they will be considered as a whole (Maturana, 1987). The first one will be used during creation of the model, and the second one during the simulations using this created tissue. In this case, what we can call the tissue organisation is the configuration of both static and dynamic relations between its components which specify its identity as a whole. So, tissue organisation takes place partly in the first domain and partly in the second one. In fact it is the link between the two domains. During physical tests on the created tissue, interactions occur between external elements, the tissue as a whole and individual cells. It follows that interactions can modify both the first and second domains. Relations between external events and constitutive elements are directed by classical physical laws, all relations with tissue as a whole being directed by structure organisation, and hence its own internal laws.

Finally, what appears, is that tissue behaviour is not determined by tissue structure or external medium, but by interactions inside the tissue itself and between that tissue and this external medium. This is the reason why theories which consider that tissue behaviour comes from cells' physical characteristics are not sufficient, as they forget the interactions inside the tissue itself and the high degree of recursivity in such a system.

### Example of a compressed cellular tissue

A cellular tissue is made of numerous cells placed together, each one in contact with some others. If a load is applied on this tissue (Fig. 1), one can see some global geometrical deformations.



$$\sigma = \frac{F}{S}; \varepsilon = \frac{\Delta h}{h}; E = \frac{\sigma}{\varepsilon}$$

Figure 1: Continuous model of a tissue under load. One uses calculates global stress and strain.

But if the strain is supposed to be quasi-static, and if one looks at a cellular level, the deformation is far more complex (Fig. 2). First the contact cell is compressed and then is deformed because of its elastic wall. This cell strain creates strains and stresses on the local other cells whose inner pressure grows and so on. Added to this first effect another one appears which is geometrical modifications of the tissue, due to the void spaces and the moving possibilities of the cells.

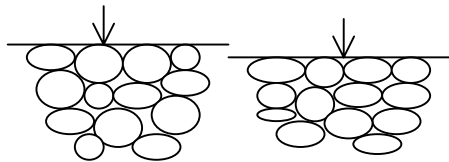


Figure 2: Tissue analysis of the same test as on figure 1. One can note structural (physical and geometrical) modifications, and has to take into account local stress and strain analysis.

Porosity of cells occurs too between their inner part and void spaces. When the local stress has a high value, destruction of cell(s) can occur, creating large heterogeneities with their own consequences such as variations of stress, strain and position of other cells, possibility of a failure process and so on. So a very simple test from a macroscopic point of view is clearly a complex one from a microscopic point of view. A good analysis of such a phenomenon needs a specific method using complex theories and not a simple macroscopic interpretation. A microscopic analysis (Gao and Pitt, 1991) is no more a good method because dynamic relations between cells (strain and stress transfer), between cells and voids (mass transfer) or between cells and tissue (geometrical changes) cannot be taken into account. Then this last interpretation cannot be an actual one in order to

understand the test effects. So, a macroscopic load creates a macroscopic strain, but the only way of explaining this last one is looking at the microscopic level and then generalise the results. In fact, microscopic analysis of an isolated cell may be of interest in order to better understand its modification procedures in terms of stresses and strains. But one can see that without a generalising process, this point of view is only a reductionist one which is absolutely insufficient in explaining the external effects on a whole tissue.

### SOME EFFECTS EXPLAINED BY SYSTEMIC

#### Tissue breakdown under mechanical stresses

When submitted to a mechanical stress, a cellular tissue first accommodates, then fractures. This fracture is very different from the result obtained on a continuous medium and is generally not explained: with a continuous theory the explanation is impossible, with a microscopic theory the explanation is insufficient. In this last case one speaks of cell wall rupture, cell debonding and tissue rupture, but gives no explanation on the localisation of these problems. Actually, this strain phenomenon is only explainable at the tissue level using systemic tools. The first tool is the percolation theory, which explains that the external stress progresses chaotically because of the cell conglomerate (Cundall and Strack, 1979). Because of that structure, the stress may attain very high values from place to place (Travers *et al.*, 1987) (Fig. 3).

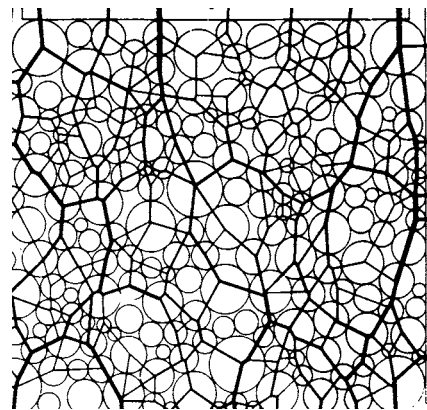


Figure 3: Lines of principal stresses for a granular assembly under vertical load. Analysis of such effect uses percolation theory. (from Cundall and Strack, 1979)

Another tool is the geometrical analysis of the structure allowing detection of unstable areas where cells and voids organisation creates some local pre-stressed areas (Lee, 1989). Another important point usable with complexity theories is the time constant which is different for one cell, a cell tissue or a continuous medium (Subhash, 1991). This time

constant is for instance the main factor to use in order to differentiate impact and compression tests. It is also linked with tissue accommodation. So these different tools are necessary in the explanation of the strains obtained on cellular tissue during these mechanical tests.

### Energy transfer

Some tests on texture analysis use energy transfer such as near infrared or mechanical vibration like ultrasound. The problem is to catch a signal resulting from its transmission inside a sample, or its inner reflection on the different tissue interfaces. In these cases the most important fact in order to obtain good results is to have a constant acoustical impedance over the sample. Variations in this parameter attenuate the signal and can suppress it and one has to understand the reasons of this attenuation or has to determine the depth attained by the input signal before its reflection (Birth, 1978). Most of the impedance variations come from cell-voids interfaces (Fig. 4).

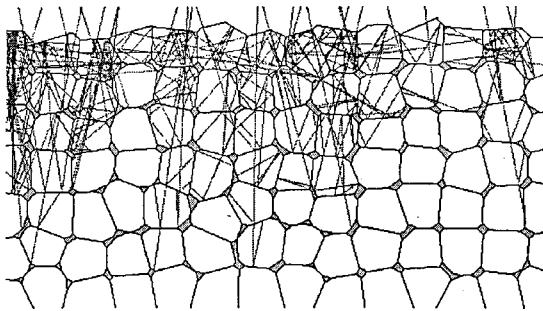


Figure 4: Simulation of electromagnetic waves transfer through a cellular tissue. The waves can go through the cell walls, reflect or vanish.

It seems clear that continuous theories cannot explain the attenuation effects. In that case too, microscopic theories seem an actual progress but they are quite limited because each element is analysed separately from others. The only theoretical solution is given by systemic. The tools necessary in this explanation are the same as before except that the time constant problem is changed in a wavelength problem.

This kind of problem also occurs in food processing with heat transfer. In that case, heat transfer is due to two independent facts: conduction along the cell wall (and then percolation theory appears), and convection inside each cell (Gibson and Ashby, 1988).

### Warner-Bratzler test

This test is essentially used on meat and fish products. It is a shearing test made in order to evaluate the sample tenderness. In its ideal

interpretation it is a cutting test with a knife perpendicular to the sample fibres (Fig. 5). However, the classical interpretation considers that the sample is undeformable and continuous. In fact this tests is an assembly of different deformations occurring altogether: shearing, extension, compression, and so on (Roudot, 2002a).

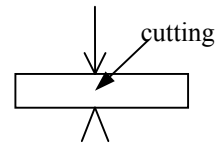


Figure 5: Classical macroscopic analysis of the test

An actual analysis of this test has to take into account this fact (which is macroscopic) but also the actual structure of the product which is fibrous. So the deformations occurring at a global level also occurs at the fibre level, with some particularities such as large deformations before failure, differences in elasticity between the fibres or local tissue collapses (Fig. 6). These effects necessitate a local analysis before a globalisation process, if a complete interpretation of the failure process is needed. Nevertheless, this test is rarely fully analysed, and lack of knowledge on its interpretation does not seem to be a problem for users.

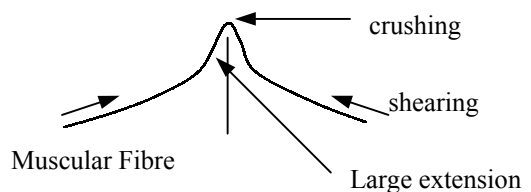


Figure 6: Different phenomena occurring during the test at the fibre level.

### Mechanical heterogeneity of plant food

It is well known that plant tissues are heterogeneous, from a mechanical point of view. This is a direct consequence of the cellular structure, but also of the agronomic growing conditions. What is less studied is the influence of the growing phenomenon itself: cell division, tissue organisation, intercellular stresses, and so on. In fact, this last point is classically forgotten because it cannot be studied with classical method, but only using systemic ones. The main consequence of this fact is that lots of things concerning tissue structure and relations between the different kinds of cells are unknown. Results from such a science as histology cannot be verified numerically using simulation because physical theories of such tissue are not developed enough in a usable way. However, when used these new methods show that the growing phenomenon is probably the

main parameter responsible for this mechanical heterogeneity (Roudot *et al.*, 1994).

## CONCLUSION

The various examples described permit to conclude that systemic analyses are the best solutions in order to understand strains and stresses in food texture analysis tests. In fact, if classical methods (microscopic and macroscopic) are currently used in modelling these tests, their actual interpretations are very often empirically based on systemic. For instance, the researcher uses classical mechanics in order to analyse the consequences of a loading process such as the first described in this paper. Looking at the differences between the experimental results and its continuous theory (shearing bands for instance), he tries to explain them by the cellular structure of the tissue. However, though this empirical explanation is a good one, it does not give a clear answer to the reasons why a cellular structure gives shear bands under loading. The solution will only come from the definition of a theory of cellular tissue. The next point is the capacity of model cellular tissue and simulate the loading test. As different theories begin to appear ( Niklas, 1989; Ouwerkerk, 1991; Roudot, 2002b)(all based on complexity theories), the main problem now encountered is to define a systemic numerical model able to verify empirical interpretation. For that, different methods can be used (Roudot, 2000) but none is still sufficiently universal and easy to use, to be largely used by food technologists.

## REFERENCES

- Birth, G.S. 1978. "The light scattering properties of food". *J. Food Sci.*, **43**, 916-925
- Cundall, P.A. and O.D.L. Strack. 1979. "A discrete numerical model for granular assemblies". *Géotechnique*, **29** (1), 47-65
- Gao Q. and R.E. Pitt. 1991. "Mechanics of parenchyma tissue based on cell orientation and microstructure" *Trans. ASAE*, **34** (1) : 232-238.
- Gibson L.J. and M.F. Ashby. 1998. "Cellular solids, structure and properties", Pergamon Press, Oxford, England, 212-240
- Le Moigne, J.L.1991."La modélisation des systèmes complexes" Gauthier-Villars, Paris
- Lee, Y.K. 1989. "Conditions for shear banding and material instability in finite elastoplastic deformation" *Int. J. Plasticity*, **5**, 197-226
- Maturana, H.R. 1987. "The biological foundation of self consciousness and the physical domain of existence". *In: Physics of cognitive processes*. Caianello E.R. (Ed.) World scientific, Singapore, 324-379
- Niklas, K. 1989. "The cellular mechanics of plants". *American Scientist* **77**, 344-349
- Ouwerkerk, C.E.D. 1991 "A micromechanical connection between the single-particle strength and the bulk strength of random packings of spherical particles" *Powder Technol.* **65**, 125-138
- Roudot, A-C., Studman, C.J. and F. Duprat. 1994. "Morphogénèse et fermeté de la pomme". Plant Biomechanics International Symposium, Montpellier, 1994/09/05-09. Elsevier, Paris, 151-152
- Roudot, A-C. 2000. "Histological modelling, a new paradigm for food texture analysis". 1<sup>st</sup> International Conference on Simulation in Food and Bio Industries (FOODSIM'2000), Nantes, 2000/06/26-27 *In: D. Thiel* (Ed.), Society for Computer Simulation International, Delft, Pays-Bas, 200-204
- Roudot, A-C., 2002a. "Rhéologie et analyse de texture des aliments" *Tec&Doc*, Paris, 76-77
- Roudot, A-C. 2002b. "Theory of plant tissue mechanics". *J. Theoret. Biol.* (submitted for publication)
- Subhash, G., Nemat-Nasser, S., Mehrabadi, M.M. and H.M. Shodja.1991. "Experimental investigation of fabric-stress relations in granular materials". *Mech. Mat.* **11**, 87-106
- Travers, T., Ammi, M., Bideau, A., Gervois, A., Messager J.C. and J.P. Troadec. 1987. "Uniaxial compression of 2d packings of cylinders. Effects of weak disorder". *Europhys. Lett.*, **4** (3), 329-332

## BIOGRAPHY

A-C Roudot received his PhD in mechanics in 1985. Then he worked as a researcher at the National Institute of Agronomic Research on the texture analysis of vegetables and tissue structure modelling. Since 1993, he has been senior lecturer at the School of Microbiology and Food Safety in Brest (France). His interests include image analysis in bacteriology and toxicology and studies on biological cells organisation.

# SIMULATION-BASED ENVIRONMENTS FOR PRACTICING DATA-COLLECTION SKILLS

Paul L. Darius  
Goële Massonnet  
Eddie Schrevens

Katholieke Universiteit Leuven  
Kasteelpark Arenberg 30  
B3001 Leuven Belgium

Henk C.M. van der Knaap

Unilever Research Vlaardingen  
O. van Noortlaan 120  
3133 AT Vlaardingen, The  
Netherlands

Kenneth M. Portier

University of Florida  
Gainesville, FL 32611-0339,  
USA

## KEYWORDS

Data collection, design of experiments, statistical analysis, web based training, VIRTEX applet library.

## ABSTRACT

A set of web based simulation applets (called VIRTEX) is described. Each applet mimics a real situation of interest, and invites the user to collect data to answer a research question. The data are noisy and generated by an underlying realistic model, invisible to the user. Once the data are collected, they can be transferred to a standard statistical package. The user can train his/her data collection skills by relating the quality of the statistical results obtained to the data collection strategy used.

## INTRODUCTION

Engineers often have to make decisions based on noisy data. Sometimes the data are already available (e.g. routinely measured production or quality data), sometimes they have to be collected first (e.g. problem solving in a research lab, fine-tuning of a pilot plant). In the latter case, there is a vast range of situations about which data could be collected, but only time and money to explore a few. Efficient data collection (i.e. experimental design) is an important skill, but there is typically little opportunity to get experience. Textbooks introduce standard general-purpose designs, and then proceed with the analysis of data already collected.

Here we explore another approach: for some situations of practical interest, software environments were developed that mimic a real situation of interest. Data can be easily collected, but this can be done in so many ways that before doing so, many nontrivial decisions must be taken. Once the data are collected, they can be transferred to a statistical software package, and the user can relate the quality of the analysis results to the data collection strategy used.

## THE VIRTEX LIBRARY

Some simulation-based environments have been developed, others are still in development. The collection is called VIRTEX (VIRtual EXperiments), and is a companion to the

VESTAC collection, previously developed for other statistical purposes (Darius et al. 2000). The environments are all realized in the form of JAVA applets, and are freely available on the web at

<http://www.kuleuven.ac.be/ucs/virtex/>. They can be run on any computer with a web browser that supports JAVA. Due to the safety requirements of applets, they cannot read or write data from or to the user's hard disk. Yet data can be exchanged with other programs through cut and paste. This paper describes some applets that are already available. Their level ranges from fairly simple to quite complicated. The description given here is short and introductory. A detailed description can be found in each applet's help menu.

## SOME SAMPLING APPLETS

The first applet introduces some relatively simple sampling problems. There are three versions, which preferably should be used in sequence. The user sees a window, showing part of a large (50x100) array of candies with different colors. The purpose is to get an idea of the percentage of candies that are colored red (fig 1).

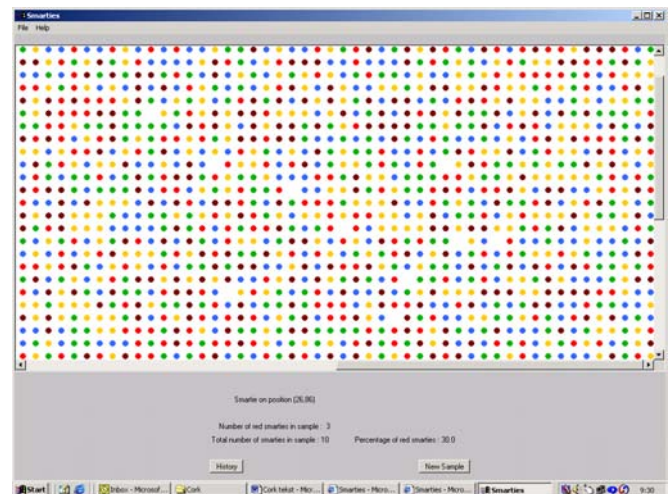


Fig 1. The candy applet, version 1.

When the user moves the mouse over a candy, its coordinates appear. With a left click, a candy is selected and

the counters for the number of candies selected and the number of red candies are incremented.

In the first version, the colors are (at first sight) evenly distributed over the window. In the second version however, patches are clearly visible where one color occurs more frequently.

Since there are so many candies, simply counting the number of reds is not an option. The user will have to use some form of sampling. Hence he/she will have to decide on a sample size and a sampling scheme. In the first version, the colors are distributed randomly and any form of selection will do. In the second version the sampling must be done much more carefully. The user can then choose for random or stratified sampling, but will discover that each of those requires careful planning before it becomes operational.

In the third version, the candies are wrapped in black and the color of a candy is only revealed after it has been included in the sample.

The second applet represents an environmental sampling problem. The user sees an aerial photograph of a section of a railway track (fig 2). It is explained that for many years a diesel train uses this place to take a halt. Hence diesel pollution of the site is suspected, and should be investigated.



Fig 2. The environmental sampling applet.

The user is invited to take a set of soil samples (by clicking the mouse on the selected spot). Since there is a limited budget and analysis is expensive, at most 20 samples can be taken. The results of the analyses are shown in a separate window, from where they can be cut and pasted into e.g. a spreadsheet or a statistical package.

Again the user is confronted with a sampling problem, but now simple random sampling will not work. The user will have to set up a sampling strategy that takes the context (the layout of the site, the fact that part of it is covered by water and hence cannot be sampled,..) is taken into account.

## THE FACTORY APPLET

In the factory applet, the user has to experiment with a pilot plant in order to find optimized settings for the parameters of a production process. The experiment runs in “real” time: when the start button is hit, time starts to run as shown in the top portion of the screen (fig 3). The user has 39 “weeks”

(one “week” is about 3 minutes of real time) to complete the experiment. Each experimental run takes a number of “days” before the results are visible.

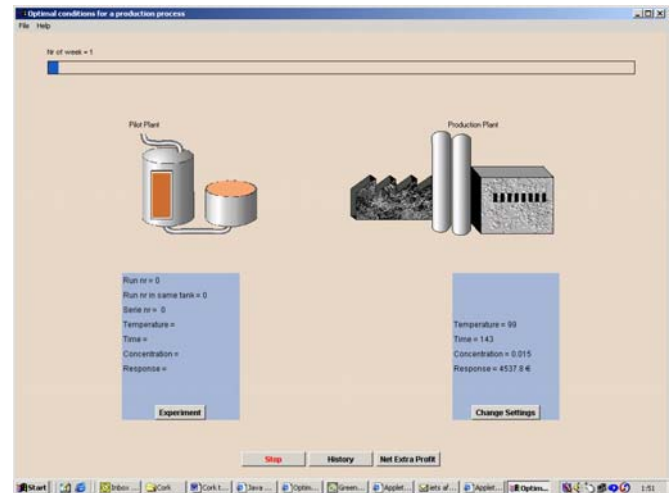


Fig 3. The factory applet.

The production plant appears at the right hand side. The current settings for the parameters temperature, time and concentration are shown, as well as the current mean yield per batch (averaged over a large number of batches). The left hand side shows the pilot plant. This is a scaled down version of the production process with (hopefully) similar characteristics. The raw material for the pilot plant is stored in a tank, which can contain enough material for 10 trials. When the tank is empty (or upon request of the user) it will be refilled, but the new raw material may have slightly different characteristics.

The user sets up an experiment by clicking on the “Experiment” button, which opens a new window. He/she can fill in the parameter settings for any number of runs (as well as instructions for handling the tank), or use an external package to generate a design and paste it in. After hitting the “Perform” button and waiting an appropriate amount of “time”, the results become available in the “History” window. This also shows the results of all previous experiments. Data from this window can be copied and pasted into an external program for statistical analysis.

The user now has to decide whether sufficiently promising new parameter settings have been found. If there are, the production plant can be halted and the new parameter settings installed. The resulting new average yield becomes available after 6 “weeks”.

The “Profit” window gives an overview of the current situation of costs and benefits. There are initial costs, a fixed cost per experimental run with the pilot plant, and a fixed cost each time the production plant is halted to change the settings. Benefits are computed from the change in yield in the production plant, multiplied by the number of weeks these changed settings were operational. At the end of the 39 weeks, the balance should be positive and as large as possible.

This applet allows the user to get some hands on experience with several important concepts. All types of designs discussed in Response Surface Methodology courses can be tried out. The tank-to-tank variability has to be dealt with.

Moreover the user is confronted with two other problems, for which textbooks offer no immediate solution. The first problem is: when are the pilot plant results sufficiently convincing to justify the cost for the production plant settings? The second problem deals with the overall strategy: should one perform one large experiment and then decide, do many very small experiments with a possibility to make an adjustment each time, or do something in between ?

## THE GREENHOUSE APPLET

The greenhouse applet requires the user to set up an experiment with (tomato) plants in a greenhouse. To succeed, the user has to deal with the problem of selecting appropriate levels for a treatment variable, and with the many problems caused by diversity in raw material and experimental circumstances.

The purpose of the experiment is to find the optimal dose of a new fertilizer. At the start, a set of 144 young tomato plants is available (12 trays of 3x4 plants). These are the green circles on the right hand side in fig 4. The young plants are not all the same: the initial weight of each is shown on the green circle. The user has to select some (or all) of the plants for the experiment and place them on the greenhouse tablet in the middle. The tablet is bordered on the left and the right with central heating devices (the thick black vertical lines). The tablet is also lighted by four special light bulbs. The resulting pattern can be seen on the screen. Consequently the positions on the tablet are not identical, and the differences in light and heat can be expected to have an effect on the growth.

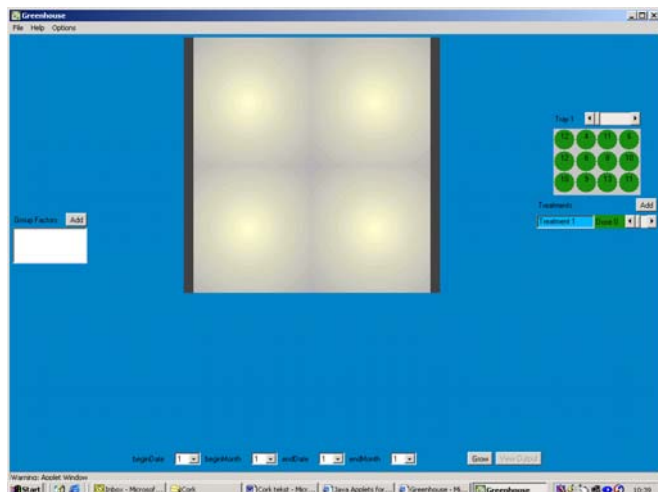


Fig 4. The greenhouse applet: initial view

The user also has to decide which plant gets which amount of fertilizer. Defining and selecting doses, and applying doses to plants is done with simple mouse operations.

To account for the difference in locations and initial weights, “grouping” factors can be defined. This is done on the left side of the screen. Defining levels and assigning them to plants is similar to the dose assignment mechanism.

Fig 5 shows a simple example of an experimental setup. 9 plants were selected and placed on the tablet in 3 rows of 3. Here, only plants with initial weight 10 were selected and the light effect was ignored. Three doses (control, 4 and 8) were selected, and the plants grouped in 3 blocks (the

columns) to account for the heat gradient. The color of a circle shows which treatment was applied, the color of the pie-part to which group (column) it belongs. A copy/paste mechanism is available to save a current setup to disk and to restore a saved setup.

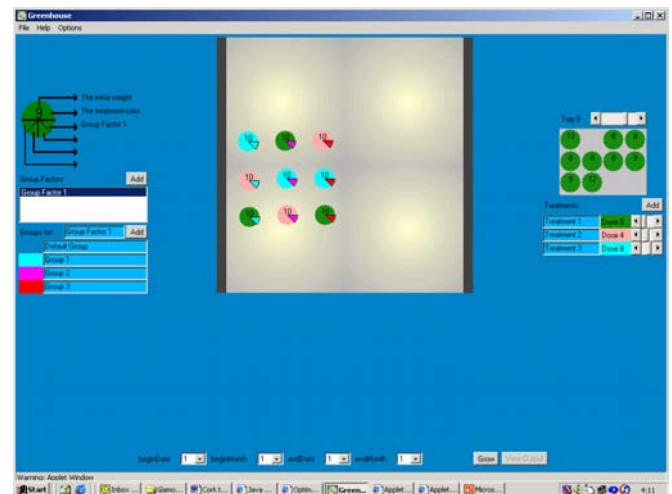


Fig 5. The greenhouse applet: a simple experimental setup

When the plants have been properly placed, the user should select the time period for the plants to grow with the buttons at the bottom. When the “Grow” button is hit, the growth of each plant is simulated on an hour-to-hour basis, and the final weight (along with all the other variables) is available in the “Output” window, from where it can be copied and pasted into an external program for statistical analysis. The growth simulation uses an adapted version of TOMGRO, a well-known growth model for tomatoes (Jones et al. 1991), as well as standard climatic data for the time period selected. This applet allows the user to get comparative experience with almost all classical designs (Box et al. 1978, Montgomery 1997): completely randomized, complete or incomplete block, Latin Square, etc. There is also ample opportunity to invent and use new setups, made to accommodate the specific features of the greenhouse situation.

## CONCLUSION

Since the applets were only recently developed, we have little user experience to report on. However, the applets show that current computer technology allows the creation of special purpose, accessible and rich environments that have, in the area of data collection and analysis, the potential to give learning experiences well beyond those of traditional textbook exercises.

## REFERENCES

- Box, G.E.P., W.G. Hunter, and J.S. Hunter. 1978. *Statistics for Experimenters*. Wiley, New York.
- Darius, P.L., J-P. Ottoy, A. Solomin, O. Thas, B. Raeymaekers, S. Michiels. “A Collection of Applets for Visualizing Statistical Concepts“ In *Proceedings in Computational Statistics 2000*, Bethlehem, J.G. and P.G.M. van der Heijden (eds). Physica Verlag.
- Montgomery, D.C. 1997. *Design and Analysis of Experiments*. Wiley, New York.

Jones, J., Dayan E., Allen L.H., Van Keulen, H. And Challa, H.  
1991. A dynamic tomato growth and yield model (TOMGRO).  
Trans ASAE. 34(2), 663-672

# MODELLING FOOD PRODUCTS VARIABILITY USING NON-LINEAR MIXED EFFECTS MODELS

Julio C. Montañez  
Fernanda A.R. Oliveira  
Department of Process Engineering  
University College Cork, Ireland  
E-mail: j.montanezsaenz@mars.ucc.ie;  
faroliveira@ucc.ie

Jesús M. Frías  
School of Food Science & Environmental Health  
Dublin Institute of Technology, Cathal Brugha St.  
Dublin 1, Ireland  
E-mail: Jesus.Frias@dit.ie

Susana C. Fonseca  
Escola Superior de Biotecnologia  
Universidade Católica Portuguesa  
Rua Dr. António Bernardino de Almeida  
4200-072 Porto, Portugal  
E-mail: suscal@esb.ucp.pt

Jeffrey K. Brecht  
Department of Horticultural Sciences  
University of Florida, 1217 Fifield Hall  
Gainesville FL 32611-0690, USA  
E-mail: jkb@mail.ifas.ufl.edu

Rocio Luna  
Centro Tecnológico Nacional de la Conserva y Alimentación  
(C.T.C.), c/ Concordia s/n 30500 Molina de Segura  
Murcia, España  
E-mail: ctcrocio@ctnc.es

Pablo Fernandez  
Universidad Politécnica de Cartagena, E.T.S.I. Agronomía,  
Dpto. de Ingeniería de Alimentos y del Equipamiento Agrícola,  
Área de Tecnología de Alimentos, Pº Alfonso XIII Nº 48  
30203 Cartagena, España  
E-mail: pablo.fernandez@upct.es

## KEYWORDS

*C. sporogenes*, modified atmosphere packaging, microbial thermal death kinetics, non-linear mixed effects, respiration rate, variability.

## ABSTRACT

Food processes are largely influenced by the natural variability of the raw products. This variability constitutes a major constraint in process design, control and optimisation. The development and building of mathematical models from experimental data that describe not only the particular process kinetics but also estimate different components of variance with known precision can help to establish more precise product and processing tolerances. Non-linear mixed effects models are a modelling technique widely used in the Agricultural and Pharmaceutical research fields that can aid to estimate model parameters and associated variances from experimental data. The objective of this paper is to illustrate the potential of non-linear mixed effects models in food processing. Two cases are presented: analysis of the effect of batch-to-batch variation of respiration rate of Galega kale on the atmosphere reached inside a modified atmosphere package, and assessment of variability in thermal death kinetics of *C. sporogenes*.

## INTRODUCTION

Non-linear mixed effects models have an intuitive appeal: the notion that individuals' responses all follow a similar functional form, despite the inter-individual variability, with parameters that vary among individuals, seems to be appropriate in many situations (Pinheiro and Bates 2000). Also, this model framework may be viewed as an extension of the standard non-linear modelling techniques, with the addition of inferential procedures to accommodate the different components of the variance (within individuals and among individuals) (Davidian and Giltinan 1996).

The simplest case where a mixed effects model might be considered is when there are two stages at sampling. In the first stage units are selected at random from a population, and in the second stage a number of measurements is made on each unit sampled in the first stage (Pinheiro and Bates 2000).

Non linear mixed-effects models have recently received a great deal of attention in the statistical literature because they are flexible and adequate for unbalanced repeated measurement data that occur in pharmacokinetics (e.g. drug intake), health sciences (study of human and animal medical experiments), economics, biology, and other areas. In these models, some of the levels could be set as fixed effects (e.g. level of drug concentration in the individual) but the individual variability is considered to be influential (Lindstrom and Bates 1988).

Model building techniques for mixed-effects models involve issues that do not have a parallel with conventional fixed effects linear and non-linear models, such as: (i) use of structured random effects variance-covariance matrices (e.g. diagonal matrices) to model variability associated to the parameters in the model; (ii) use of covariates to explain inter-individual parameter variability; (iii) identification via maximum likelihood tests of effects with an associated random component. Using these tools mixed models can be built from experimental data in a parsimonious way (Pinheiro and Bates 1995). The modelling framework in pharmaceutical and agricultural experiments, where mixed effect models have been successfully applied to estimate parameters and model variances, resembles the case of kinetic modelling in food preservation and processing, where different random effects may be relevant, often due to raw product variability.

One example is Modified Atmosphere Packaging (MAP) of fresh fruits and vegetables. This packaging technique consists on the use of packaging materials with selective permeability

to O<sub>2</sub> and CO<sub>2</sub> that interplays with the natural product respiration rate to create a low O<sub>2</sub>/high CO<sub>2</sub> atmosphere inside the package, which extends the product shelf life. Engineering design of MAP is based on predictive models that include the gas transfer through the package and the O<sub>2</sub> consumption/CO<sub>2</sub> production due to respiration. Respiration rate often depends on batch and also varies between individual plants. For this reason, it is important to estimate the variability of the product respiration rate from experimental data, and determine its influence on the variability of gas composition inside the package (Hertog 2002).

Another example is the determination of microbial death rates, which provides the basis for the calculation of sterilisation values associated with a certain thermal process and/or for process design and optimisation. In this case, it would be important to investigate if stochasticity due to batch-to-batch variation can be significant, and if this variability can be associated with a particular sterility parameter (D or z-values) in order to design thermal processes that maximise safety.

The main objective of this paper is to illustrate the potential of non-linear mixed effects models in food processing and preservation, addressing in particular the two examples above mentioned.

## MATERIALS AND METHODS

### Case Study I - Design of MAP for Shredded Galega Kale

Our study is based on data earlier reported in literature (Fonseca *et al.* 2002). Shredded Galega kale is a traditional fresh-cut vegetable in Portugal. It is thinly shredded and consumed in a soup. O<sub>2</sub> consumption and CO<sub>2</sub> production rates of shredded Galega kale were determined in the reported work. The storage temperatures used were 1, 5, 10, 15 and 20°C. The atmospheres tested were all combinations of 1, 5 and 10% v/v O<sub>2</sub> plus 0, 10 and 20% v/v CO<sub>2</sub> with the balance being N<sub>2</sub>, as well as ambient air.

### Case Study II – Thermal Degradation of *C. Sporogenes* Spores

Microorganisms were obtained from the National Culture type Collection (Spain). Sporulation, synchronisation, and collection of spores is detailed in Fernandez *et al.* (1996). 0.5 ml of the mother suspension were placed in a sterile tube, heat shocked at 83 °C during 13 min in a thermostatic bath (Polistat CC2, Huber, Germany) and cooled in an ice bath. The suspension was then diluted to 350 ml using phosphate buffer (pH=7.0) and placed in 10 µl glass capillaries where they were subjected to a thermal treatment at the desired temperature using a thermostatic bath (Stern and Proctor 1954). The temperatures tested were 110, 113, 115, 118 and 121°C, with sampling times between 24 minutes and 30 seconds depending on the temperature. Experiments were replicated with 6 different batches at least. Enumeration of the cfu/mL was performed using the media from Grischy *et al.* (1983).

The R software (R 1.1.1, A Language and Environment Copyright 2000) was used for statistical analysis. In particular, the nlme library was used for building the non-linear mixed effects models (Pinheiro and Bates 2000).

## RESULTS AND DISCUSION

### Case Study I - Design of MAP for Shredded Galega Kale

O<sub>2</sub> consumption and CO<sub>2</sub> production rates were modelled using a Michaelis-Menten type equation, with uncompetitive CO<sub>2</sub> inhibition and model constants increasing exponentially with temperature (Fonseca *et al.* 2002). The respiratory quotient (RQ) was considered to be constant in the range of temperature and gas composition tested. To describe the variability among different product batches, the following assumptions were made: (i) intra-batch variance is described by a power variance model; (ii) inter-batch variance is due to a mixed additive effect with a normal distribution of the model constants on the respiration rate; (iii) the effect of season, harvest, etc. on variance is negligible. The first assumption was confirmed by preliminary analysis of the data and agrees with the hypothesis of proportional errors in the experimental measurements.

The respiration rate of a particular sample from batch *i* taken at time *j*, based on the above assumptions, is given by:

$$R_{O_{2y}} = \frac{e^{\ln(\alpha_i)} \cdot O_{2y}}{e^{\ln(\phi)} + O_{2y} \left(1 + \frac{CO_{2y}}{e^{\ln(\gamma_i)}}\right)} + \varepsilon_{ij} \text{ where } \varepsilon_{ij} \sim \mathcal{N}(0, \sigma^2 | R_{O_{2y}} |^{2\delta}) \quad (1)$$

$$R_{CO_2} = RQ_{ij} \cdot R_{O_{2y}} \quad (2)$$

where:

$$\begin{aligned} \ln(\alpha_i) &= \ln(\alpha_0) + \alpha_1 T + b_{\ln(\alpha_i)} & b_{\ln(\alpha_i)} &\sim \mathcal{N}(0, \sigma_{\ln(\alpha)}) \\ \ln(\phi_i) &= \ln(\phi_0) + \phi_1 T + b_{\ln(\phi_i)} & b_{\ln(\phi_i)} &\sim \mathcal{N}(0, \sigma_{\ln(\phi)}) \\ \ln(\gamma_i) &= \ln(\gamma_0) + \gamma_1 T + b_{\ln(\gamma_i)} & b_{\ln(\gamma_i)} &\sim \mathcal{N}(0, \sigma_{\ln(\gamma)}) \\ RQ_i &= RQ + b_{RQ_i} & b_{RQ_i} &\sim \mathcal{N}(0, \sigma_{RQ}^2) \end{aligned}$$

The average population constants (RQ, ln(α<sub>0</sub>), ln(φ<sub>0</sub>), ln(γ<sub>0</sub>), α<sub>1</sub>, φ<sub>1</sub> and γ<sub>1</sub>) were estimated together with the inter-batch variability parameters (σ<sub>RQ</sub>, σ<sub>ln(α)</sub>, σ<sub>ln(φ)</sub> and σ<sub>ln(γ)</sub>) and with the intra-batch variability parameters (σ and δ). In order to build a parsimonious model, the following procedure was followed: (i) a model with all the mixed effects σ<sub>RQ</sub>, σ<sub>α</sub>, σ<sub>φ</sub>, σ<sub>γ</sub> was built; (ii) nested models with all the combinations of three, two and one mixed effects were built; (iii) the likelihood ratio test was applied to all the models in order to select the nested model with a minimum set of effects that would be statistically different from the full model accounting for all mixed effects. This procedure led to the rejection of the random effect associated to the ln(α) parameter (σ<sub>ln(α)</sub>), as shown in Table 1. The estimates of the constants of the best performing model are presented in Tables 2 and 3. Figure 1 shows an example of the fit of the model to the experimental data.

Table 1: Information Criteria Parameters for Selection of a Non-Linear Mixed Effects Model to Predict Respiration Rate of Shredded Galega Kale

Model	df	LogLik	Test	p-value
1 - No inter-batch variability	9	-2676		
2 - Nested model neglecting the effect in $\ln(\alpha)$	12	-2654	1vs.2	<0.001
3 - Full model	13	-2654	2vs.3	0.97

Table 2: Estimates of the Michaelis-Menten Model Constants for the Non-Linear Mixed Effects Model with Three Random Effects

Parameter	Estimate $\pm$ 95% CI
RQ	0.97 $\pm$ 0.05
$\ln(\alpha_0)$	2.74 $\pm$ 0.09
$\alpha_1$	0.132 $\pm$ 0.007
$\ln(\phi_0)$	-1.6 $\pm$ 0.5
$\phi_1$	0.16 $\pm$ 0.03
$\ln(\gamma_0)$	2.7 $\pm$ 0.4
$\gamma_1$	0.04 $\pm$ 0.02

Table 3: Estimates of the Parameters Accounting for Variability for the Non-linear Mixed Effects Model with Three Random Effects

Parameter	Low 95% CI	Estimate	High 95% CI
$\sigma_{RQ}$	0.05	0.09	0.145
$\sigma_{\ln(\gamma)}$	0.27	0.42	0.67
$\sigma_{\ln(\phi)}$	0.03	0.11	0.46
$\delta$	0.62	0.69	0.75
$\sigma$	0.6	0.7	0.9

A perforation-mediated MA package was designed, using the average population constants (Table 1) in the following set of equations, which describe the gas mass balance at equilibrium (Fonseca *et al.* 1999):

$$y_{O_2}^{eq} - y_{O_2}^e = -\frac{R_{O_2}^{eq}}{3.6 \times 10^7} \times \frac{M}{N \times a \times D^b \times L^c} \quad (3)$$

$$y_{CO_2}^{eq} - y_{CO_2}^e = \frac{R_{CO_2}^{eq}}{3.6 \times 10^7} \times \frac{M}{N \times a \times D^b \times L^c} \times \frac{RQ}{\beta} \quad (4)$$

The design target was to reach a steady state gas composition corresponding to the central point of the recommended gas composition for extending the shelf life of Galega kale:  $5\% < CO_2 < 20\%$  and  $1\% < CO_2 < 2\%$  (Fonseca *et al.* 1999). Then, following the approach of Talasila and Cameron (1995) and using the estimated inter-variability of the constants of the respiration rate model ( $\sigma_{RQ}$ ,  $\sigma_{\ln(\phi)}$  and  $\sigma_{\ln(\gamma)}$  – Table 2), a Monte Carlo simulation was performed to estimate the steady state gas composition inside 3,000 packages. The results are shown in Figure 2.

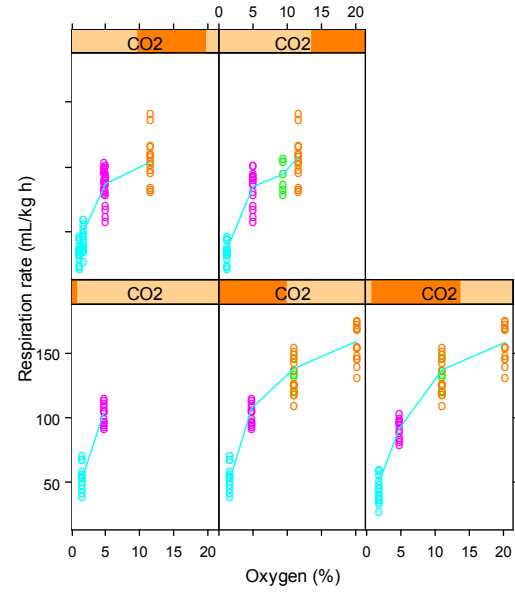


Figure 1: Fit of the Non-Linear Michaelis-Menten Mixed Effects Model with Three Random Effects to the Experimental Data at 20 °C (different colours refer to different batches)

It can be observed that the distribution in terms of  $CO_2$  composition is close to normal, with 5.5% of the packages reaching a steady state gas composition outside the recommended range. Regarding  $O_2$ , the distribution curve is skewed to the right but only 0.3% of the packages show a concentration above the maximum recommended value (2%).

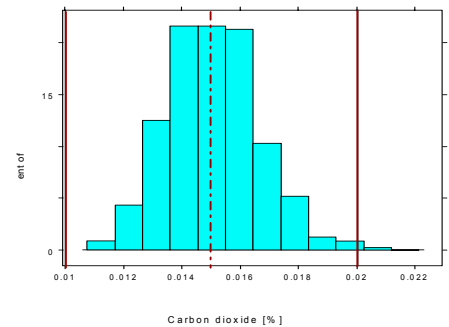
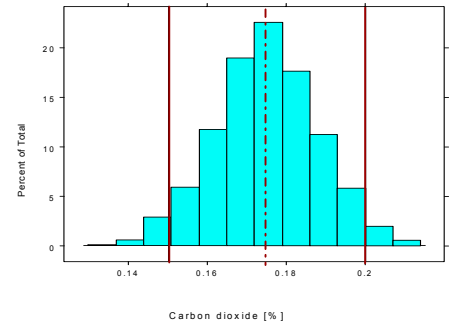


Figure 2: Effect of Batch-to-Batch Respiration Rate Variability on the Gas Concentration Inside a MAP Containing Shredded Galega Kale (the full vertical lines represent the limits of recommended gas composition and the vertical broken lines represent the target gas concentration)

## Case Study II – Thermal Degradation of *C. Sporogenes* Spores

The thermal death kinetics of *C. Sporogenes* spores was described by the Bigelow model, coupled to a mixed additive effect with a normal distribution of the model constants,  $D_r$  and  $z$ . For batch  $i$  at time  $j$ :

$$\log \frac{n_{ij}}{n_{o_i}} = -\frac{t_{ij}}{D_{r_i}} 10^{\frac{T-T_r}{z_i}} + \varepsilon_{ij} \quad (5)$$

where:

$$D_{r_i} = D_r + b_{D_{r_i}} \quad b_{D_{r_i}} \sim \mathcal{N}(0, \sigma_{D_r})$$

$$z_i = z + b_{z_i} \quad b_{z_i} \sim \mathcal{N}(0, \sigma_z)$$

The average population constants were estimated together with the inter-batch variability parameters ( $\sigma_{D_r}$ ,  $\sigma_z$ ). Different models were tested, considering no random effects and random effects in  $D_r$  and/or  $z$ . The information criteria parameters (Table 4) show that mixed effects clearly improve the model, particularly when the random effect in  $D_r$  is considered. Actually, when random effects in  $D_r$  and  $z$  are estimated simultaneously, the latter is negligible (or unidentifiable with the experimental design used). Thus, the model that best fits the data with the least number of parameters is the one that accounts for random effects in  $D_r$  only.

Table 4: Information Criteria Parameters for Selection of a Non-Linear Mixed Effects Model to Predict Thermal Degradation of *C. Sporogenes* Spores

Model	df	AIC	logLik	Test	L Ratio	p-value
1 - No inter batch variability	1	219	-108			
2 - Random effect in $z$	4	212	-102	1vs2	13.	0.0041
3 - Random effect in $D_r$	4	162	-77.			
4 - Random effect in $D_r$ and $z$	5	164	-77.	3vs4	0.003	0.96

This finding may support the hypothesis often assumed in literature that microbial thermal degradation rate (measured by the constant  $D_r$ ) is quite dependent on endogenous and exogenous conditions, whereas its sensitivity to temperature changes (measured by the constant  $z$ ) is characteristic of the particular specie, genus and strain of the bacteria. Thus, the  $z$  parameter could therefore be considered as a “fingerprint” of the microorganism in question. The constants of this model are summarised in Table 5 and an example of the fit of the model to the experimental data is shown in Figure 3.

Table 5: Estimates of the Bigelow Model Constants for the Non-Linear Mixed Effects Model with Random Effects in  $D_r$

Parameter	Low 95% CI	Estimate	High 95% CI
$D_r$	0.85	0.94	1.03
$z$	10.84	11.95	13.06
$\sigma_{D_r}$	0.12	0.16	0.22
$\sigma$	0.28	0.31	0.34

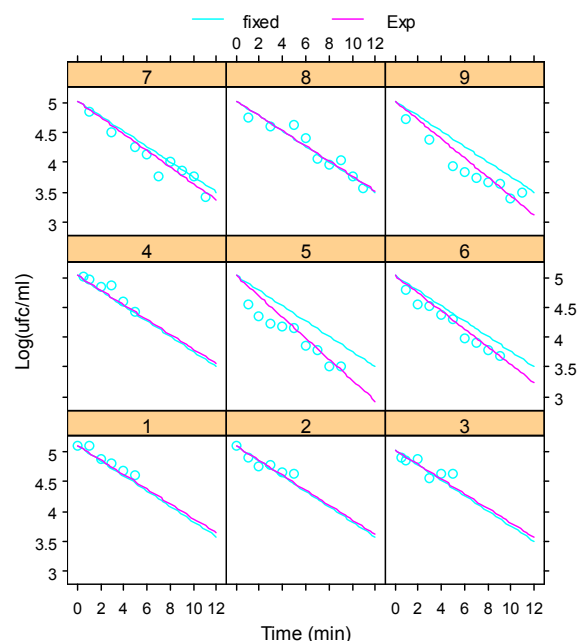


Figure 3: Fit of the Non-Linear Mixed Effects Bigelow Model with Random Effects in  $D_r$  to the Experimental Data at 100 °C (the blue line represents the fit prediction using the average population parameters and the purple line represents best individual predictions considering a random effect in  $D_r$ ; the numbers in each plot refer to different experiments)

## CONCLUSIONS

The two case studies presented in this work show that non-linear mixed effects modelling is a statistical tool that can be applied in food studies, to build stochastic models that account for product variability. These models may then be used to assess the impact of the raw materials variability on the final product and to identify sources of variability, and eventually the processes may be optimised to yield maximum product quality whilst minimising variability.

## ACKNOWLEDGEMENTS

Author J.C. Montañez is grateful to CONACyT (Mexico) for financial support.

## NOMENCLATURE

$a$	gas exchange model constant ( $6.42 \times 10^{-6} \text{ m}^{-2.148} \text{ s}^{-1}$ )
$b$	additive mixed effect or gas exchange model constant (1.45)
$c$	gas exchange model constant (-0.598)
$D$	perforation diameter (m)
$D_r$	time required for a 90% reduction at $T_r$ (min)
$L$	perforation length (m)
$M$	product mass (kg)
$N$	number of perforations
$n$	number of cell of <i>C. sporogenes</i> ( $\log \text{CFU ml}^{-1}$ )
$n_o$	initial cell number of <i>C. sporogenes</i> ( $\log \text{CFU ml}^{-1}$ )
$R_{\text{CO}_2}$	$\text{CO}_2$ production rate ( $\text{ml kg}^{-1} \text{ h}^{-1}$ )
$R_{\text{CO}_2}^{eq}$	$\text{CO}_2$ production rate at equilibrium ( $\text{ml kg}^{-1} \text{ h}^{-1}$ )

$R_{O_2}$	$O_2$ consumption rate ( $ml\ kg^{-1}\ h^{-1}$ )
$R_{O_2}^{eq}$	$O_2$ consumption rate at equilibrium ( $ml\ kg^{-1}\ h^{-1}$ )
$RQ$	respiratory quotient (dimensionless)
$T$	temperature ( $^{\circ}C$ )
$t$	time (s)
$T_r$	reference temperature ( $121^{\circ}C$ )
$y_{CO_2}^{eq}$	$CO_2$ concentration at equilibrium (% v/v)
$y_{CO_2}^e$	$CO_2$ external concentration (% v/v)
$y_{O_2}^{eq}$	$O_2$ concentration at equilibrium (% v/v)
$y_{O_2}^e$	$O_2$ external concentration (% v/v)
$z$	slope of the Thermal Death Time graphic ( $^{\circ}C$ )
$\mathcal{N}$	Normal distribution function
$\alpha, \alpha_1$	Michaelis-Menten equation constant ( $ml\ kg^{-1}\ hr^{-1}$ )
$\alpha_2, \phi_2, \gamma_2$	Michaelis-Menten equation constant ( $^{\circ}C^{-1}$ )
$\phi, \phi_1, \gamma, \gamma_1$	Michaelis-Menten equation constant (%v/v)
$\beta$	permeability ratio (0.81)
$\delta$	power index of intra-individual variance model
$\sigma$	standard deviation
$\varepsilon$	within-subject error term

## REFERENCES

- Davidian, M. and Giltinan, D. M. 1996. Nonlinear models for repeated measurement data. Chapman and Hall, London, UK.
- Fonseca, S.C.; Oliveira, F.A.R.; Brecht, J. K and Chau, K.V. 1999. "Development of perforated-mediated modified atmosphere packaging for fresh-cut vegetables". In: Processing Foods: Quality Optimisation and Process Assessment. F.A.R. Oliveira and J.C. Oliveira (eds.). CRC Press, United States.
- Fonseca, S.C.; Oliveira, F.A.R.; Frias, J.; Brecht, J.K. and Chau, K.V. 2002. "Modelling respiration rate of shredded Galega kale for development of modified atmosphere packaging". *Journal of Food Engineering*. In press.
- Hertog, M.L.A.T.M. 2002. "The impact of biological variation on postharvest population dynamics". *Postharvest Biology and Technology*. In press.
- Lindstrom, J. J. and Bates, D. M. 1988. "Nonlinear mixed effects models for repeated measures data". *Biometrics* 46, 673-687.
- Pinheiro, J. C. and Bates, D. M. 1995. Model Building for Nonlinear Mixed-Effects Models *Technical Report 91*, Department of Biostatistics, University of Wisconsin - Madison
- Pinheiro, J.J. and Bates, D.M. 2000. *Mixed-Effects models in S and S-PLUS*. Statistics and Computing Series, Springer-Verlag, New York, NY.
- Stern, J.A. and Proctor, B.E. 1954. "A micro-method and apparatus for the multiple determination of rates of destruction of bacteria and bacterial spores subjected to heat". *Food Technology*, 8: 139-143
- Talasila, P.C. and Cameron, A.C. 1995. "Modelling frequency distribution of steady-state  $O_2$  partial pressures in modified-atmosphere packages". *Journal of Food Process Engineering*. 18:199.
- Fernandez, P.S.; Ocio, M.J.; Rodrigo, F.; Rodrigo, M.; Martinez, A. 1996. "Mathematical model for the combined effect of temperature and pH on the thermal resistance of *Bacillus stearothermophilus* and *Clostridium sporogenes* spores". *International-Journal-of-Food-Microbiology*, 32 (1/2) 225-233.
- Grischy, R.O.; Speck, R.V. and Adams, D.M. 1983. "New media for enumeration and detection of *Clostridium sporogenes* (PA 3679) spores". *Journal of Food Science*, 48(5): 1466-1469.

## AUTHORS BIOGRAPHY

**JULIO CESAR MONTAÑEZ** was born in Chihuahua, Mexico, and obtained his undergraduate degree in Chemical Engineering at the University of Coahuila, Mexico. Currently he is a Ph.D. student at the Department of Process Engineering, University College Cork, under the supervision of Prof. Fernanda Oliveira and Dr. Jesús Frias. His research work focuses on the engineering design of MAP systems for fresh-cut produce.  
<http://www.ucc.ie/acad/departments/processeng/postgrad/montanezj.html>

**FERNANDA OLIVEIRA** was born in Viana do Castelo, Portugal, and obtained an undergraduate degree in Chemical Engineering in 1985 at the Faculty of Engineering, University of Porto, Portugal, and a PhD degree in Food Engineering in 1989 at University of Leeds, UK. She worked as Associate Professor and Associate Director at the College of Biotechnology, Catholic University of Portugal, as Associate Professor and Vice-President of the Inter-University Institute of Macau, China, and as Senior Consultant and Director of the Portuguese Society for Innovation (Porto, Portugal) before moving to Ireland, where she is currently Professor and Head of the Department of Process Engineering, at University College Cork.  
<http://www.ucc.ie/acad/departments/processeng/staff/oliveiraf.html>

**JESUS FRIAS** was born in Tolosa (Spain) and obtained a degree in Food Science and Technology in 1992 at Basque Country University and a PhD. Degree in Biotechnology at the Catholic University of Portugal in 1998. He worked as Research Assistant at the ENSIA-INRA (France) and at the Department of Process Engineering at University College Cork before joining the Dublin Institute of Technology (Ireland), where he currently is Lecturer of Food Chemical Analysis.

**SUSANA FONSECA** was born in Porto, Portugal, and obtained an undergraduate degree (in 1993) and a PhD degree (in 2002) in Food Engineering at the College of Biotechnology, Catholic University of Portugal. She has worked as a teaching assistant at the College of Biotechnology, Catholic University of Portugal, where she currently a postdoctoral research fellow.

**JEFFREY BRECHT** obtained an undergraduate degree in Biology in 1979 at Whittier College, California, USA and a PhD degree in Plant Physiology in 1984 at University of California, Davis, USA. He worked as Research Assistant at Tri-Valley Growers, California, and as Graduate Research Assistant at the Department of Pomology, University of California, Davis, before moving to the Horticultural Sciences Department at the University of Florida where is currently Professor of Postharvest Physiology and Horticulture.  
<http://www.hos.ufl.edu/jkbweb/>

**ROCIO LUNA** was born in Jerez de la Frontera (Spain) and obtained an undergraduate degree in Veterinary in 1997 at the University of Cordoba (Spain). She has been working since 1998 as analyst at the National Canning Technology Centre (Murcia, Spain) and started a PhD. Programme in 1999, under the supervision of Prof. Pablo Fernandez and Prof. Antonio Martinez (Univ. de Cartagena, Spain).

**PABLO FERNANDEZ** is a lecturer at the Department of Food Engineering and Agricultural Equipment of the Universidad Politecnica de Cartagena (Spain). He has published extensively in the area of microbial thermal destruction and mathematical modelling of spore inactivation.



# **FOOD ENGINEERING**



**CONTROL**



# A NEW PROCESS CONTROL SYSTEM BASED ON PREDICTIVE KINETIC MODELS FOR FOOD QUALITY AND OPERATING COSTS

Peter de Jong\*, Erik Smit, Marc M.M. Vissers, Han Straatsma,  
Maykel Verschueren  
Department of Processing, Quality & Safety  
NIZO food research  
PO Box 20, 6710 BA Ede,  
Netherlands  
E-mail: [pdejong@nizo.nl](mailto:pdejong@nizo.nl)

Jan van de Wiel  
Department of Industrial Automation & Control  
Honeywell  
Laarderhoogtweg 18, 1101 EA Amsterdam,  
Netherlands

## KEYWORDS

Control systems, Agriculture, Global, Industrial Control, Computer Integrated Manufacturing.

## ABSTRACT

A new process control system for the food industry has been developed, called PREMIC (PREdictive Models ready for Industrial Control). The system is focused on predictable optimal product quality and minimal operating costs. Majority of the models used are have a white box nature and are based on reaction kinetics. The models predict the food properties (e.g. stability, shelf-life, nutritional value, texture, color) and the operation costs of production chains. An optimization algorithm converts this information together with actual process information (SCADA) to optimal set-points. The estimated savings amount up to 10 – 50 % of the production costs.

## INTRODUCTION

A substantial amount of the knowledge and experience of research institutes and universities never reach the food industry. The main bottleneck is the interpretation of the scientific results. Thus the objective is to find a way to benefit the food industry by application of these results in practice. Experience with industrial projects shows that predictive kinetic models are an effective tool to apply state-of-the-art knowledge in the factory (De Jong 1996, De Jong et al. 1999, De Jong et al. 2002a,b). Examples of these models are:

1. Models to predict the concentration of micro-organisms in final products as a result of growth, adherence, release and inactivation in process equipment;
2. Kinetic models that predict the transformation of food components related to the food properties recognised by the consumer (e.g. viscosity, colour, shelf-life);
3. Predictive models to estimate the costs related to process operation.

A number of these models (e.g. the kinetic models) are mechanistic models based on reaction schemes describing the product changes during processing.

In order to increase the application of scientific results for food production it is important that the models developed

are implemented in the industrial R&D and production plants. A powerful method to realise this objective is integration of these models into the process control equipment. This ensures a continuous optimization of the production plant.

In recent studies some applications of model based applications are reported. Most of the models are of a black box nature and increasingly based on neural networks. The model-based control procedures are used for single unit-operations such as beer fermentation (Kurz et al. 2002, Corrieu et al. 2001), cane sugar evaporation (Benne et al. 2001) and extrusion (Haley and Mulvaney 2000). Trelea et al. (1998) used a more white box modeling approach and developed a physical model for optimal control of a batch refrigeration process. Six years earlier Straatsma et al. (1992) already developed a control system for spray drying of dairy products based on physical models (mass and energy balances and sorption isotherms). However, non of these control procedures applies a combination of physical models and mechanistic (kinetic) models for prediction of product properties such as protein denaturation degree, enzyme activity and microbial contamination. In contradiction with black box models, mechanistic kinetic models have good predictive capabilities. In the case of black box models such as neural networks every change in process configuration or product composition means a renewed necessary model training. Effects of food composition and small changes in process operation (e.g. changed piping, plate configuration heat exchangers) on the product properties are not included. Thus, for robust control of food production plants it is essential to use a mechanistic models.

In this paper a new process control system based on predictive mechanistic (kinetic) models for food quality and operating costs is presented. The system is called PREMIC (PREdictive Models for Industrial Control) and developed in co-operation with Honeywell. The fundamentals of the PREMIC system are described and some applications are given.

## PREDICTIVE MODELS

### Contamination models

The concentration of micro-organisms in food largely depends on the adherence of micro-organisms to equipment walls (Bouman et al. 1982, De Jong et al. 2002a). In many unit operations no contamination problems would occur if bacteria would not adhere to equipment surfaces. The increase in the levels of bacteria in the product during process operation is partly the result of growth in the product, but the release of bacteria that have grown on the walls of the equipment also plays a significant role. Growth of micro-organisms in consumer food products leads to spoilage and defects, e.g. excessive openness in cheese or taste deviations of milk.

To model the contamination due to both adherence and growth of bacteria the following approach has been applied. A production chain can be considered as a cascade of model reactors (process model). In each reactor, growth, adherence and/or destruction of bacteria can occur (transformation model). The basis of the proposed model is formed by two mass balances: one balance for the wall on which bacteria may adhere and one for the liquid bulk phase. The bacterial growth as a function of the operating time  $t$  at position  $x$  at the wall in a tubular plug flow reactor is defined by the transfer equation as:

$$\frac{dn_w}{dt} = \mu_T n_w (1 - \beta) + k_a C \quad (1)$$

where  $n_w$  is the wall coverage in  $\text{cfu m}^{-2}$ ,  $\mu_T$  is the bacterial growth rate at temperature  $T$  in  $\text{s}^{-1}$ ,  $\beta$  is the fraction of generated bacteria which is released into the bulk and  $k_a$  is the adhesion constant in  $\text{m s}^{-1}$ . The local bulk concentration  $C$  in  $\text{cfu m}^{-3}$  at operating time  $t$  follows from the component (bacteria) balance:

$$\frac{dC}{dx} = \frac{\pi D}{\phi} (\beta \mu_T n_w - k_a C) + \frac{\pi D^2}{4\phi} (\mu_T - k_{d,T}) C \quad (2)$$

where  $\phi$  is the milk flow in  $\text{m}^3 \text{s}^{-1}$ ,  $k_a$  the inactivation (destruction) constant at temperature  $T$  in  $\text{s}^{-1}$  and  $D$  the hydraulic diameter of the reactor in m. In the case of a tank reactor the concentration is independent of position  $x$ :

$$\frac{dC}{dt} = \frac{4\phi}{\pi D^2 L} (C_{in} - C) + \frac{4}{D} (\beta \mu_T n_w - k_a C) + C (\mu_T - k_{d,T}) \quad (3)$$

where  $L$  is the liquid level in the tank in m. Since the wall temperature is a function of the position in the heat exchanger ( $x$ ) the differential equations 1, 2 and 3 have to be solved numerically in parallel.

In Figure 1 the effect of adherence and growth of micro-organisms on product contamination (industrial conditions) is demonstrated. The lines represent the model calculations after determination of the process configuration and main process conditions in the factory and before taking the samples. It is obvious that in the case that no bacteria would adhere to the equipment walls, the contamination would be governed by growth in the liquid phase. The downstream processing of whey consists of equipment (e.g. vessels) with sufficient residence time in which the bacteria can grow in the liquid phase ( $> 10^4$  cfu

$\text{mL}^{-1}$ ). However, the real contamination problems ( $10^8$  cfu  $\text{mL}^{-1}$ ) are due to adherence and growth on equipment walls.

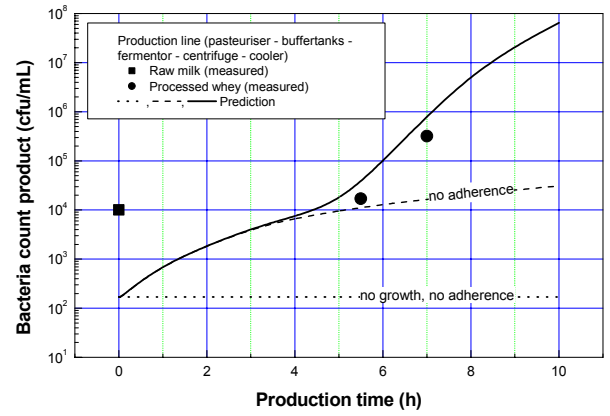


Figure 1: Concentration of *Streptococcus thermophilus* in Product related to the Operating Time of Downstream Processing of Whey: Effect of the Local Adherence and Growth in the Processing Equipment

## Transformation of food components

During processing, food behaves like a complex reaction system. A large number of chemical, physical and biochemical reactions take place. Some of these transformations are important because they change those product characteristics that are easily recognized by a consumer. Examples are: inactivation of enzymes, denaturation of proteins, loss of nutrients and formation of new components. In general, most of these reactions can be described by  $n^{\text{th}}$  order reactions (single or consecutive):

$$\frac{dC_1}{dt} = k_n C_1^n, \quad \frac{dC_1}{dt} = k_n C_1^n - k_m C_2^m, \quad \text{etc.} \quad (4)$$

A large amount of kinetic data of several food components has been collected. Models available (De Jong 1996) are the protein fouling model, models for bacterial spores (quality related), models for vitamins and Maillard products (flavour related), models for enzyme inactivation (shelf-life related), models for protein denaturation and aggregation (texture related) and models for protein breakdown.

## Operating costs

The operating costs of many food production chains primarily depend on microbial and physical fouling of the equipment. In general, process operating times at relatively low temperatures ( $< 70$  °C) are due to adherence and growth of bacteria. The operating time of equipment at temperatures above 80 °C is determined largely by the

deposition of protein and minerals. Physical fouling due to deposition of proteins and minerals can be described by an adsorption reaction (De Jong et al. 1992):

$$J_{x,t} = k'' C_{x,t}^{1.2} \quad (5)$$

where  $J_{x,t}$  is the local flux ( $\text{kg m}^{-2} \text{s}^{-1}$ ) of food components to the wall,  $k''$  the adsorption rate constant of proteins ( $\text{m}^{1.6} \text{kg}^{-0.2} \text{s}^{-1}$ ) and  $C_{x,t}$  the local bulk concentration of the key component related to fouling (e.g. whey proteins). The amount of fouling is obtained by integrating the flux over operating time and surface area of the equipment walls. This amount can be related to the costs due to cleaning, change-over (rinsing losses), depreciation, energy, operator, pollution and product losses (De Jong 1996).

As an example, in Figure 2 the operating costs (energy, emission, product losses) of a sterilisation plant as a function of heating rate and heating temperature are shown. In the case of heating rates higher than  $10 \text{ }^\circ\text{C s}^{-1}$  the operating costs increase with heating temperature, mainly due to increased fouling rates. At extreme heating rates ( $> 100 \text{ }^\circ\text{C s}^{-1}$ ) the operating costs become lower due to the fact that the residence time is very short. This results in a lower concentration of the key component for fouling (e.g. denatured proteins) and according to equation (5) in less fouling.

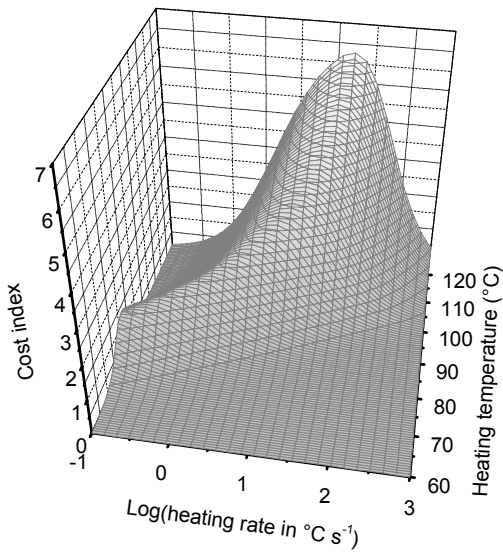


Figure 2: Operating Costs (energy, emission, product losses) of a Sterilisation Plant as a function of Heating Rate and Heating Temperature

## CONTROL APPROACH

### General description of PREMIC

Predictive models as described turn out to be an effective tool to translate scientific knowledge to the food factories. The most effective way to ensure the benefits of using predictive models would be to integrate them into process control systems. Based on actual process data and the

composition of the raw materials the models can predict the state of the process (e.g. amount of fouling, biofilm thickness, energy usage) and the state of product (degree of contamination, stability, texture). This means that the process can be controlled on product specifications instead of process conditions. By adding cost related models the system can continuously optimize the production process with respect to the product quality and the production costs. The PREMIC system aims to provide this control approach. In Figure 3 the PREMIC system is shown in general terms. Based on process design (e.g. dimensions, apparatus configuration, in-line measured process conditions) the temperature time history of the product is calculated with the process model. Together with the given composition this information is used to predict the product properties using the kinetic product models. Besides the operating costs per ton product are estimated based on the fouling and contamination models. The predicted product properties are compared with the given desired product properties. In the optimization module the production process set points are optimized to meet the desired product properties as close as possible with minimum operating costs.

In the ideal situation the process is controlled based on the desired product specifications and minimum operating costs. The system corrects itself automatically when:

- Fouling changes the temperature-time history the product
- The product specifications change
- The composition of the raw materials change
- Disturbances occur (temperature changes, flow instabilities)

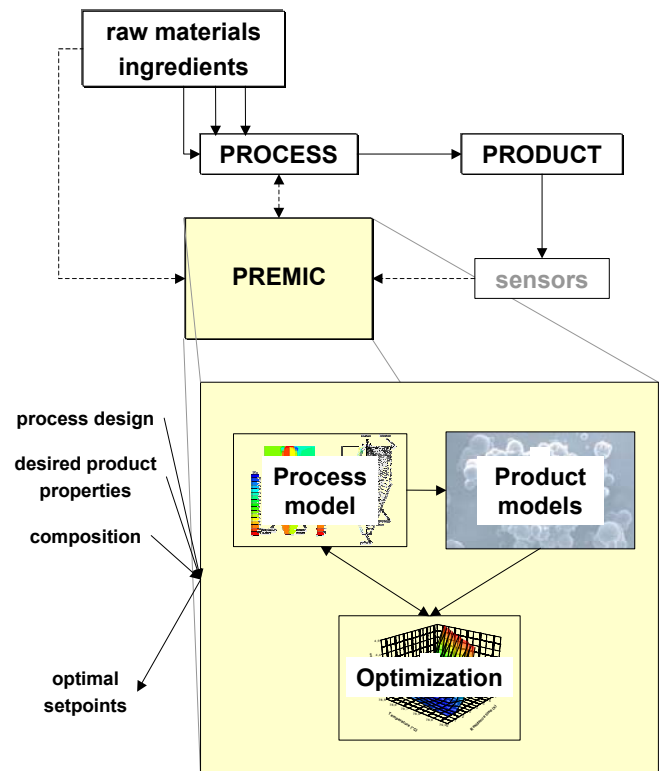


Figure 3: Schematic Representation of the PREMIC Control System

### Optimization algorithm

An essential part of the PREMIC system is the optimization module. The main control factors for product and process optimization are the temperature-time relationship and the configuration of the processing equipment. In order to determine the optimal values of the control variables, a general objective function is used:

$$F(u, x) = \alpha c_{quality}(u, x) + \beta c_{operation}(u) \quad (6)$$

where  $u$  is a vector of process control variables (e.g. temperature, flow) and  $x$  is a vector of desired product properties related to food quality and safety. The value of  $c_{quality}$  depends on the outcomes of the predictive models for contamination and transformation of food components.  $c_{operation}$  is related to the operating costs. The optimal configuration and operation of a production chain is achieved by minimization of the objective function. To avoid trivial and undesired solutions, the weight factors  $\alpha$  and  $\beta$  are introduced. These weight factors give the relative importance of each term of the objective function. For example, too high a value of  $\beta$  may result in a very clean and cheap production process but an inferior product quality.

### Example

To illustrate the application of the described procedure for optimizing food production chains the following case study has been performed. A heating process with a capacity of 40 tons skim milk per hour, consists of a regenerative section, a heating section and 2 holders sections and a cooler. In Figure 4 the scheme of the process is shown with some preliminary temperatures and residence times. In order to have a process model the equipment is transformed to a cascade of model reactors. The objective function is defined as:

$$F(u, x) = \sum_{i=1}^3 \alpha_i \left( \frac{x_{i,des} - x_i(u)}{x_{i,des}} \right)^2 + F_{cost} \quad (7)$$

where

$$F_{cost} = \frac{c_{operation} \cdot t_{operation} + c_{solids} \cdot t_{production} \cdot \iint_{x,t} J_{x,t} dt dx}{t_{production} \cdot \phi} \quad (8)$$

where  $\alpha$  is weight factor for the relative importance of product property  $x_i$ ,  $x_{i,des}$  is the desired product property,  $u$  is the set of control variables,  $c$  are costs,  $t$  is time and the integral term is the total amount of deposits after 1 h of production and  $\phi$  is the capacity of the process in tons per hour and:

$$t_{production} = \frac{t_{operation} \cdot t_{run}}{t_{run} + t_{cleaning}} \quad (9)$$

and the production time per run:

$$t_{run} = t \quad \text{if } (C_{S.thermophilus} > 0.0001 \text{ cfu mL}^{-1}) \quad (10)$$

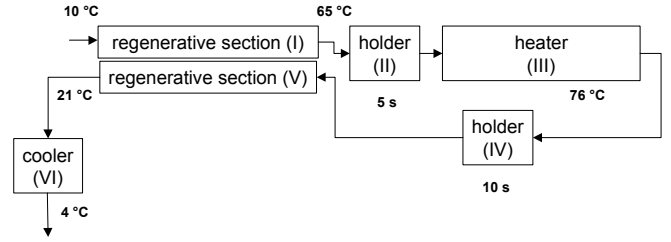


Figure 4: Example Process

The weight factor  $\alpha$  is introduced to avoid trivial and undesired solutions. The chosen values of the weight factors are determined by the relative importance of the different product properties. However, since the relationship between the weight factor values and the optimization results are not clear on forehand, the determination of the weight factor value is an iterative process in consultation with industrial experts.

In this case the control variables ( $u$ ) are limited to two, the heating temperature and the residence time at this temperature in the second holder section. With two control variables surface plots can present the results of the computer model simulations. Figure 5 shows the results of the objective function evaluations. The optimal setpoints are a heating temperature of 78.7 °C and a residence time of 3 seconds. Compared to the initial preliminary design (10 s, 76 °C) the operating costs could be decreased by 14 %. At an annual production of 4700 h this means an estimated cost saving of Euro 58,000. More details are given by De Jong et al. (2002b). Detailed studies show that cost reduction of more than 50 % are feasible (De Jong 1996).

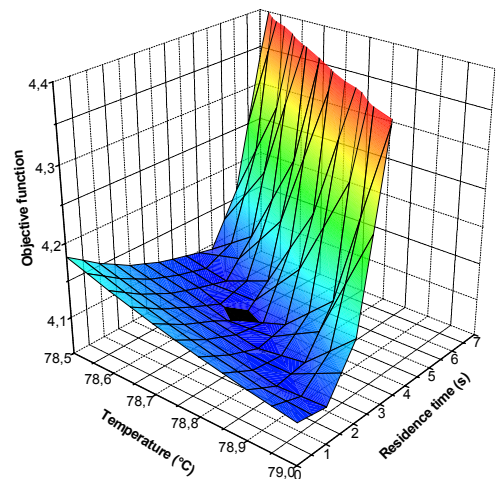


Figure 5: Evaluation of the Objective Function

The PREMIC system using this optimization procedure for the determination of the optimal set-points. Already with a PC it is possible to repeat this procedure every 10 seconds.

## CONCLUSIONS

The ultimate solution for the transfer of (scientific) research results towards industrial practice is the application of model-based control approaches. These models should be based on mechanistic (kinetic) modeling approaches as much as possible and include an adequate process description (model). With the development of the PREMIC control system and the availability of a relatively large number of product models this advanced type of model-based control will be realized in the food industry. As a consequence the cleaning times will be shortened, the product quality will be more constant and process development time will be minimized. Detailed studies show that the savings in operating costs are estimated at more than 10-50 % .

## REFERENCES

- Benne, M.; B. Grondin-Perez; J.P. Chabriat and P. Herve. 2001. "Artificial neural networks for modelling and predictive control of an industrial evaporation process". *Journal of Food Engineering* 46, 227-234
- Bouman, S.; D.B. Lund; F.M. Driessen and D.G. Schmidt. 1982. "Growth of thermoresistant streptococci and deposition of milk constituents on plates of heat exchangers during long operating times". *Journal of Food Protection* 45, 806-812.
- Corrieu, G.; I.C. Trelea and B. Perret. 2001. "On-line estimation and prediction of density and ethanol evolution in the brewery". *Technical Quarterly of Masters Brewers' Association of the Americas* 37, 173-181.
- De Jong, P.; S. Bouman and H.J.L.J. van der Linden. 1992. "Fouling of heat treatment equipment in relation to the denaturation of  $\beta$ -lactoglobulin." *Journal of the Society of Dairy Technology* 45, 3-8.
- De Jong, P. 1996. "Modelling and optimization of thermal processes in the dairy industry". ISBN 90-9009034-7, Montfoort, the Netherlands.
- De Jong, P.; H.C. van der Horst and R. Waalewijn. 1999. "Reduction of protein and mineral fouling". In *Fouling and cleaning in food processing '98*, D.I. Wilson; P.J. Fryer and A.P.M. Hasting (Eds.). EUR 18804, Cambridge, 39-46.
- De Jong, P.; M.C. te Giffel and E.A. Kiezebrink. 2002a. "Prediction of the adherence, growth and release of microorganisms in production chains". *International Journal of Food Microbiology* 74, 13-25.
- De Jong, P.; M.C. te Giffel; H. Straatsma and M.M.M. Vissers. 2002b. "Reduction of fouling and contamination by predictive kinetic models". *International Dairy Journal* 12, 285-292.
- Haley, T.A. and S.J. Mulvaney. 2000. "On-line system identification and control design of an extrusion cooking process". *Food Control* 11, 121-129.
- Kurz, T.; M. Fellner; T. Becker and A. Delgado. 2002. "Observation and control of the beer fermentation using cognitive methods". *Journal of the Institute of Brewing* 107, 241-252.
- Straatsma, J; G. van Houwelingen; A.P. Meulman; A.E. Steenbergen. 1992. "Dryspec2: a computer model of a two-stage dryer". *Journal of the Society of Dairy Technology* 44, 107-111.
- Trelea, I.C.; G. Alvarez and G. Trystram. 1998. "Nonlinear predictive optimal control of a batch refrigeration process". *Journal of Food Process Engineering* 21, 1-32.

## ACKNOWLEDGEMENT

This work has been supported by Senter, the Netherlands.

## BIOGRAPHY

**PETER DE JONG** was born in Utrecht, the Netherlands and studied chemical engineering (B.Sc.) in The Hague and obtained his Ph.D. degree at the University of Delft on modeling and optimization of thermal processes in the dairy industry. In 1986 he went to R&D department of Campina, a major international dairy company. In 1987 he started to work at NIZO food research as a process engineer. In the nineties together with Han Straatsma he initiated a modeling group for applications in the food industry. At this moment he is responsible for all the research activities on processing, modeling and control within NIZO food research and is the head of a group of 13 scientific workers.

# TRACKING IN GENERALISED PREDICTIVE CONTROL USING THE P TRANSFER FUNCTION

Ben Griffin\* and Conor Downing  
Department of Electronic Engineering  
Cork Institute of Technology  
Cork, Ireland  
\*E-mail: bgriffin@cit.ie

## KEYWORDS

GPC, Model-following control, servo response, tuning.

## ABSTRACT

One of the techniques cited in the literature on tracking specifications in Generalised Predictive Control is the use of the so-called  $P$  polynomial, to shape the closed-loop transient response.  $P(q^{-1})$  was originally defined as a transfer function written as  $P(q^{-1}) = P_n(q^{-1})/P_d(q^{-1})$ . However,  $P_d$  is normally selected as a scalar equal to  $P_n(1)$ . The authors observed that there is no analysis in the literature for any case other than scalar  $P_d$ . This paper analyses the case where  $P(q^{-1})$  is used to achieve model-following control. It is shown that the use of a polynomial  $P_d$ , with roots in the left-half of the  $z$ -plane unit circle, reduce the magnitude and ringing of the control signal in the exact and detuned model-following tuning strategy. However, when the  $T$  polynomial, associated with robustness and disturbance rejection, was included in the design, the presence of the polynomial form of  $P_d(q^{-1})$  severely degrades the disturbance rejection performance and sensitivity to measurement noise. The poor performance observed when using  $P$  to achieve model-following suggests that an alternative tuning strategy would be more appropriate in a practical application.

## INTRODUCTION

An important feature of any control loop is the response to a setpoint change, called the transient, tracking or servo response. For example, the plant engineer has to specify how fast or slow it should take to fill a tank to a particular level or how fast a product is brought up to a particular temperature. This paper analyses some of the issues related to the specification of the desired transient response in Generalised Predictive Control (GPC) (Clarke *et al.* 1987, Clarke and Mohtadi 1989). One of the techniques cited in the literature to achieve a particular closed-loop transient response is model-following control using the  $P$  polynomial, (McIntosh *et al.* 1991).  $P$  was originally defined as a unity gain transfer function as follows:

$$P(q^{-1}) = P_n(q^{-1})/P_d(q^{-1})$$

However,  $P_d$  is normally selected as a scalar equal to  $P_n(1)$ , hence the reason why it is usually referred to as the  $P$  polynomial. This paper examines the case when  $P_d$  is

specified as a polynomial when used in model-following control for second order processes. It will be shown that there are advantages in selecting  $P_d$  as a polynomial, for example, reduced controller ringing and closer tracking of the specified continuous time dynamics. However, the polynomial form of  $P_d$  has an adverse effect on the sensitivity of the controller to measurement noise and the disturbance rejection properties of the closed-loop. The sensitivity and disturbance rejection was worsened by the inclusion of the  $T$  polynomial, which is normally associated with improving the robustness of the closed loop.

The layout of the paper is as follows. A brief introduction to GPC is given, followed by a discussion on model-following using  $P(q^{-1})$ . Following this the equivalent linear form of GPC is presented so that the closed loop can be analysed. An example is then given illustrating the undesirable problems associated with model-following using  $P$  and the advantages and disadvantages of the inclusion of the polynomial form of  $P_d$ . Finally, an alternative method for achieving model-following control, which does not suffer from the poor performance associated with using  $P$ , is briefly discussed.

## GENERALISED PREDICTIVE CONTROL

The GPC algorithm belongs to the family of Model Based Predictive Controllers (MBPC). A locally linearised CARIMA (Controlled Autoregressive and Integrated Moving Average) model of the process to be controlled is required:

$$y(t) = \frac{B(q^{-1})}{A(q^{-1})}u(t-1) + \frac{C(q^{-1})}{A(q^{-1})\Delta}\xi(t) \quad (1)$$

where  $A$ ,  $B$  and  $C$  are polynomials in the backward shift operator  $q^{-1}$  of order  $na$ ,  $nb$  and  $nc$  respectively.  $u(t)$  is the process input (control signal) and  $y(t)$  is the process output.  $\xi(t)$  is zero mean white noise and  $\Delta$  is the differencing operator  $(1 - q^{-1})$ . The  $C$  polynomial in the noise term is rarely estimated in practice, but instead replaced by a *design polynomial*  $T(q^{-1})$ . A  $j$ -step ahead predictor,  $\hat{y}(t+j)$ , is derived from the model in Equation (1) so that the future process outputs can be predicted. In order to calculate the control signal a quadratic cost function is used to minimise the sum of squared errors between the predicted and desired outputs with an additional term weighting projected control increments as follows:

$$J = \sum_{j=N_1}^{N_2} [P(q^{-1})\hat{y}(t+j) - w(t+j)]^2 + \sum_{j=1}^{NU} \lambda_c [\Delta u(t+j-1)]^2 \quad (2)$$

subject to :  $\Delta u(t+j-1) = 0$ ;  $NU < j \leq N_2$ .

In Equation (2),  $N_1$  is the initial prediction horizon,  $N_2$  is the final prediction horizon and  $NU$  is the control horizon.  $\lambda_c$  is the control weighting factor used to penalise control increments.  $P(q^{-1})$  is the  $P$  polynomial introduced to broaden the range of control objectives available in GPC, for example, model-following control.  $w(t+j)$  is referred to as the *reference trajectory* and defines the desired trajectory that the output,  $\hat{y}(t+j)$ , or auxiliary output,  $P(q^{-1})\hat{y}(t+j)$ , should follow. Future setpoint changes are generally not considered in which case the reference trajectory is set equal to the current setpoint value i.e.  $w(t+j) = r(t)$ .

The tuning of the GPC controller involves setting the various parameters ( $N_1$ ,  $N_2$ ,  $NU$ ,  $\lambda_c$ ,  $P$ ,  $T$ ). To make the tuning process easier, various tuning strategies have been developed. In (McIntosh *et al.* 1991), McIntosh presents three tuning strategies utilising these parameters, where at the time of commissioning, a single tuning parameter (either  $N_2$ ,  $\lambda_c$  or  $P$ ) is used to vary the servo response while the remaining parameters are set to default values. The  $T$  polynomial may then be used to improve the robustness and regulation without influencing the servo response (that is, if there is no plant-model mismatch). Furthermore, particular settings of the GPC parameters lead to some standard control laws such as minimum variance, dead-beat and mean-level control.

## MODEL-FOLLOWING CONTROL

Model-following control involves specifying a *reference or closed loop model*,  $H_M(q^{-1})$ , that describes the desired closed loop response. A good way of selecting this reference model is to consider an appropriate continuous time model and transform this to the discrete domain. The continuous time model is usually derived from specifications such as the rise time, settling time, percentage overshoot, time constant etc.

GPC can be set up to follow the closed loop model  $H_M$  exactly. In this case  $P$  is set equal the inverse of the desired closed loop model, i.e.  $P = 1/H_M$  and the horizons are set to minimum variance (MV) settings. However, in this case the process zeros are cancelled, in which case if they are outside the unit circle will lead to an unstable closed loop. In order to have a practical control scheme for plants with arbitrary zeros the model-following capabilities must be detuned. This can be achieved by either increasing the output horizon relative to the control horizon or by adding control weighting, i.e.  $\lambda_c > 0$ . The former method is used in the "Detuned Model-Following" tuning strategy (McIntosh *et al.* 1991) and is achieved by commissioning GPC with:

$$NU = na + 1, \quad N_1 = 1, \quad N_2 > d + NU, \quad \lambda_c = 0$$

and using the inverse closed-loop model,  $P = 1/H_M(q^{-1})$ , as the active tuning parameter ( $d$  is the process dead-time in

sample intervals). Note that  $N_2 = d + NU$  would yield exact model-following.

If the desired closed loop model is first order than the standard  $P$  polynomial can be easily used to represent the desired dynamics, since in this case  $P_d$  is a scalar, i.e.  $P = 1/H_M = (1 - aq^{-1})/(1 - a)$ . However, a first order closed loop model is primarily applicable to plants that exhibit first order characteristics only, because excessive control action is required to make higher order processes to respond in a first order manner.

The z-transform of second and higher order continuous time models including zero order hold (ZOH) results in the discrete model having zero (numerator) as well as pole (denominator) dynamics. For example, the following second order continuous time model has a 2% settling time of 10s and a damping ratio  $\zeta = 1$ :

$$H_M(s) = 0.3318/(s^2 + 1.152s + 0.3318)$$

Transforming this to the discrete domain including ZOH and ignoring the unit delay, yields

$$H_M(q^{-1}) = 0.114(1 + 0.68q^{-1})/(1 - 1.124q^{-1} + 0.316q^{-2}) \quad (3)$$

In (McIntosh *et al.* 1991) only the poles of the reference model in Equation (3) are used to specify the  $P$  polynomial and the zero dynamics are ignored. McIntosh states that ignoring the numerator dynamics makes little difference since the closed loop model is not followed precisely when using detuned model-following. However, as will be seen in the example, when  $P$  is specified using only the poles of the discrete reference model, the result is a very active ringing control signal. However, a small value of  $\lambda_c$  can be found, on a trial and error basis, which removes this ringing and has little effect on the servo response. Furthermore, the step response of a second order discrete model without a zero in the left-half plane has a sharper initial response similar to a first order plant. Thus, larger control signal excursions will be required to track this faster response. In light of this and the requirement of finding a suitable value of  $\lambda_c$  to remove the ringing control, the author was motivated to investigate the specification of  $P_d$  as a polynomial rather than a scalar. The next section shows how the GPC control law can be reformulated as an equivalent linear controller, see Figure 1, which will be used to perform closed-loop analysis.

## EQUIVALENT LINEAR FORM OF GPC

Minimising the cost function in Equation (2) with respect to the vector of future control increments,  $\Delta u(t+j-1)$ , yields the GPC control law, (Clarke *et al.* 1987). For the purpose of carrying out closed loop analysis, the control law can be rearranged in the general linear form (Griffin 2002):

$$S(q^{-1})\Delta u(t) = hT(q^{-1})r(t) - \frac{R(q^{-1})}{P_d(q^{-1})}y(t)$$

where the scalar  $h$  and polynomials  $R(q^{-1})$  and  $S(q^{-1})$  are functions of the GPC parameters and of the specified

process model. The influence of  $P_d(q^{-1})$  on the closed loop is not only its appearance in the denominator of the feedback term, but it also influences the  $R$  and  $S$  polynomials (a step in the calculation of the control law involves the division of  $P_n T$  by  $A \Delta P_d$ ). Figure 1 illustrates the block diagram for the general linear form of GPC, along with the various sources of disturbances that can affect the closed-loop. The derivation of equivalent three-term linear control law obtained when  $P_d$  is a scalar and incorporated into  $P_n$ , such that  $P = P_n$  where  $P(1) = 1$ , can be found in (McIntosh *et al.* 1991).

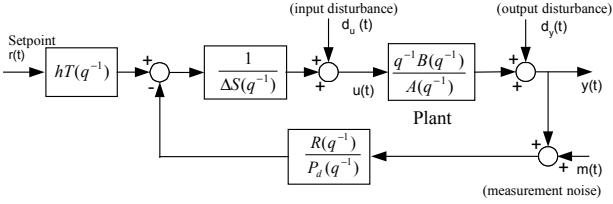


Figure 1: Block Diagram for the General Linear Form of GPC.

From Figure 1, the transfer function between the output  $y(t)$  and the setpoint  $r(t)$  (servo response) and the transfer function between output and the output disturbance  $d_y(t)$  (output sensitivity function) are as follows:

$$y(t) = \frac{q^{-1} h T B P_d}{P_{clpd}} r(t) + \frac{P_d \Delta S A}{P_{clpd}} d_y(t) \quad (4)$$

where  $P_{clpd}$  defines the closed-loop poles:

$$P_{clpd} = P_d(q^{-1}) \Delta S(q^{-1}) A(q^{-1}) + q^{-1} B(q^{-1}) R(q^{-1})$$

The transfer function between the output disturbance  $d_y(t)$  (or measurement noise  $m(t)$ ) and the control signal  $u(t)$  (input sensitivity function) is given by:

$$S_{udy}(q^{-1}) = \frac{u(t)}{d_y(t)} = \frac{-AR}{P_{clpd}} \quad (5)$$

This transfer function defines the influence of the output disturbance and measurement noise on the control signal, for example, how active the control signal will be in response to high frequency measurement noise.

### Closed Loop Analysis for Exact Model-Following

For an exact model-following configuration, i.e. when minimum variance horizon settings are used ( $N_1 = 1$ ,  $N_2 = NU + d$  and  $\lambda_c = 0$ ) and when there is no plant-model mismatch,  $P_{clpd}$  becomes:

$$P_{clpd} = h P_n(q^{-1}) B(q^{-1}) T(q^{-1}) \quad (6)$$

Note that, with MV horizon settings,  $S = B(q^{-1})/b_1$ , where  $b_1$  is the first element of the  $B$  polynomial (this applies for plants with no dead-time). Substituting Equation (6) into Equation (4) and (5) yields:

$$y(t) = \frac{q^{-1} P_d}{P_n} r(t) + \frac{P_d \Delta A}{b_1 h T P_n} d_y(t) \quad (7)$$

and the input sensitivity function becomes:

$$S_{udy}(q^{-1}) = \frac{u(t)}{d_y(t)} = \frac{-AR}{h T P_n B} \quad (8)$$

Equation 7 shows that exact model-following is achieved, i.e. the servo transfer function is  $q^{-1} P_d / P_n = 1/P(q^{-1})$ . This means that the output will track exactly the specified closed loop model. Furthermore,  $T$  is present in the regulatory transfer function but not in the servo transfer function. Therefore,  $T$  can be used to vary the regulatory response and sensitivity of the controller without affecting the servo response. Equation (8) shows that  $S_{udy}$  has poles at the roots of  $B$ , now if the roots of  $B$  are in the left half of the unit circle, this can lead to a ringing control signal during the rejection of an output step disturbance.

To examine the control signal with respect to a setpoint change, note that from Eq. (1) (ignoring the noise term):

$$u(t) = \frac{A}{q^{-1} B} y(t) \quad (9)$$

Replacing  $y(t)$  by the servo response from Equation (7), yields:

$$u(t) = \frac{A}{B} \cdot \frac{P_d}{P_n} r(t) \quad (10)$$

Note, if the process numerator  $B$  contains roots in the left-half of the unit circle, the presence of these roots in the denominator of Equation (10) will result in a ringing control signal in response to a setpoint change. For control strategies that do not cancel the process zeros, for example, pole-placement, the servo response is (ignoring a prefilter)  $y(t) = q^{-1} B r(t) / P_{cl}$ , where  $P_{cl}$  defines the desired closed loop servo poles. Replacing  $y(t)$  in Equation (9) with this servo response, results in  $u(t) = A r(t) / P_{cl}$ , a transfer function independent of  $B$ . However, examining Equation (10), note that if  $P_d(q^{-1})$  is selected so that its roots are in the left-half plane, then  $P_d$  will reduce the ringing due to  $B$ . For the case  $P_d = B$ , (assuming  $B$  is inverse stable) no ringing in the control signal will take place during a setpoint change and the servo response will be  $y(t) = q^{-1} h B r(t) / P_n$ , similar to a pole-placement strategy. This similarity however, is in relation to the servo response only since the process zeros are cancelled by the minimum variance control law, whereas they are not cancelled in a pole-placement strategy. Transforming a second order continuous time model to the discrete domain results in a zero in the left-half of the unit circle, see Equation (3). Therefore, specifying this zero for  $P_d$  will reduce the magnitude and ringing of the control signal.

### Closed Loop Analysis of Detuned Model following

The above analysis was for exact model-following strategy using MV horizon settings. Similar results are established here for the more practical detuned model-following

configuration. In detuned model-following the closed loop poles are defined by the polynomial  $T\tilde{P}_nQ$ . In this case  $\tilde{P}_n \approx P_n$  and if  $B$  has roots in the left half of the unit circle then  $Q$  generally contains roots in the left-half plane in order to minimise the effect of the process zeros on the specified servo response,  $1/P(q^{-1})$ . The value of  $Q$  depends mainly on  $B$  and  $P$ . The servo transfer function in this case is:

$$y(t) = \frac{q^{-1}hBP_d}{\tilde{P}_nQ} r(t)$$

which is similar to the servo response in Equation (7) except that  $B$  is not cancelled. An exception to this is when  $P_d = B$ , (assuming the roots of  $B$  are inside the unit circle), in which case  $Q = B$ , and the servo transfer function becomes  $q^{-1}hB/\tilde{P}_n$ . The input sensitivity function will be similar to that in Equation (8) but with  $P_nB$  replaced by  $\tilde{P}_nQ$ , thus the possibility of a ringing control signal in response to an output disturbance. The control signal in response to a setpoint change becomes:

$$u(t) = \frac{A}{q^{-1}B} \cdot \frac{q^{-1}hBP_d}{\tilde{P}_nQ} r(t) = \frac{hAP_d}{\tilde{P}_nQ} r(t) \quad (11)$$

As in the exact model-following case, specifying  $P_d$  as a polynomial can be used to reduce the ringing during a setpoint change, caused by the roots of  $Q$  in Equation (11).

### EXAMPLE

In this example the process is second order with a settling time of 23s given by

$$G_p(s) = 0.09/(s^2 + 0.66s + 0.09)$$

With a sampling interval of 1s the discrete time model is

$$G_p(q^{-1}) = \frac{q^{-1}B}{A} = \frac{0.03628q^{-1}(1+0.8026q^{-1})}{1-1.451q^{-1}+0.517q^{-2}}$$

Note the left half plane zero at  $z = -0.8026$ . To achieve detuned model-following the horizons are set to  $N_1 = 1$ ,  $N_2 = 6$  and  $NU = 3$ . The reference model with a settling time of 10s defined in Equation (3) will be used to specify  $P$ . Figures 2 and 3 shows the response when  $P_d$  is specified as a scalar, in which case  $P$  is specified as follows:

$$P(q^{-1}) = P_n/P_n(1) = (1-1.124q^{-1}+0.316q^{-2})/0.192$$

In each case,  $T = [1 - 0.8q^{-1}]$ , was used to improve the robustness and reduce the sensitivity of the controller to the measurement noise. Figure 2 shows the servo response when  $\lambda_c = 0$ . Note that the servo response is very close to the ideal,  $1/P$ , however, at the expense of a very active ringing control signal as expected from the previous closed-loop analysis. Note also the undesirable ringing control in response to the output step disturbance. Figure 3 shows the servo response when  $\lambda_c = 0.01$ . In this case the servo response is not as close to  $1/P$ , however, it is closer to the

specified continuous time model. The effect of  $\lambda_c$  is to push the left-half plane closed loop pole, introduced by  $Q$ , towards the origin. This results in a much improved control signal during both the setpoint change and the disturbance. Note also, the control signal is also less active in response to the measurement noise.

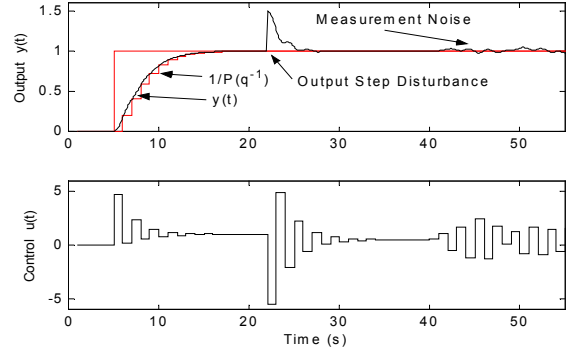


Figure 2: Detuned Model-Following with  $P_d$  a Scalar,  $\lambda_c = 0$  and  $T = [1 - 0.8q^{-1}]$ .

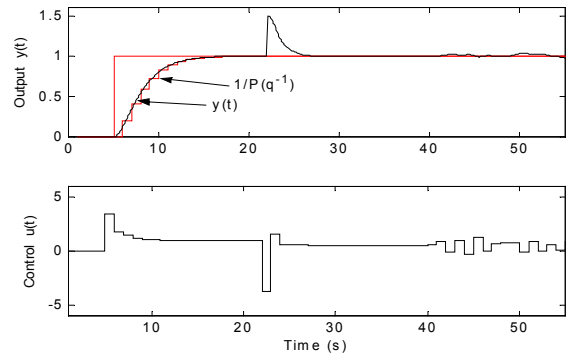


Figure 3: Detuned Model-Following with  $P_d$  a Scalar,  $\lambda_c = 0.01$  and  $T = [1 - 0.8q^{-1}]$ .

The influence of specifying  $P_d$  as a polynomial will now be examined. In this case  $P$  is specified to include the zeros as well as the poles of the reference model as follows:

$$P(q^{-1}) = \frac{1}{H_M} = \frac{P_n}{P_d} = \frac{1-1.124q^{-1}+0.316q^{-2}}{0.114(1+0.68q^{-1})}$$

The closed loop response in this case is shown in Figures 4 and 5. The same horizon settings were used and  $\lambda_c = 0$  was used in both cases. Examining the servo response, the expected reduction in the initial control excursion and control signal ringing can be seen, in compared to Figure 1. Furthermore, very accurate tracking of the specified model is achieved, which in this case is equivalent to the originally specified continuous time reference model.

However, the inclusion of  $P_d$  as a polynomial has an unexpected adverse effect on the disturbance rejection and the sensitivity of the controller to measurement noise. Figure 4 shows the response when  $T = 1$ . The ringing control in response to an output step disturbance and the very active control signal in response to measurement noise can be seen. In an attempt to improve this, Figure 5 shows the response when  $T = [1 - 0.8q^{-1}]$ , which is the same as that used in Figures 2 and 3. However, this has made the

sensitivity and disturbance rejection of the controller even worse. Note, in Figure 5 the initial control signal, in response to the step disturbance, is in the same direction as the disturbance, i.e. the  $S_{udy}$  transfer function has an inverse response characteristic. This has the effect of amplifying the disturbance before removing it, and greatly amplification of the measurement noise. Specifying a slower  $T$  polynomial, while it may improve the gain, phase and delay margins, made this high amplification of the noise and inverse response of  $S_{udy}$  even worse. Furthermore, increasing the order of  $T$  also worsened the situation while not in general improving the robustness margins.

This inverse response characteristic of  $S_{udy}$  was also seen to occur for the case when  $P_d$  was a scalar, when much slower  $T$  polynomials were specified, more so in the case when  $\lambda_c = 0$ . Interestingly, if this occurs and  $P_d$  is specified with a root in the right half of the unit circle (e.g. at  $z = 0.2$ ) then this removed the inverse response of  $S_{udy}$  and greatly reduced the high frequency gain of  $S_{udy}$ . However, a right half plane zero will increase the ringing during a setpoint change.

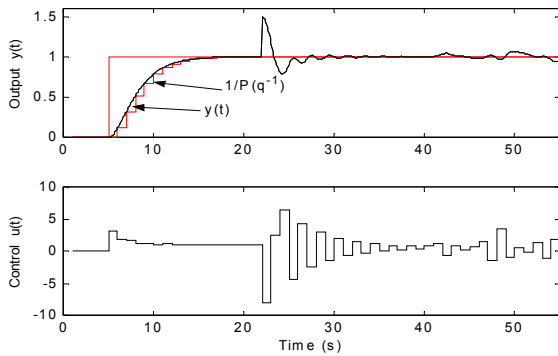


Figure 4: Detuned Model-Following with  $P_d$  as a Polynomial and  $T = 1$ .

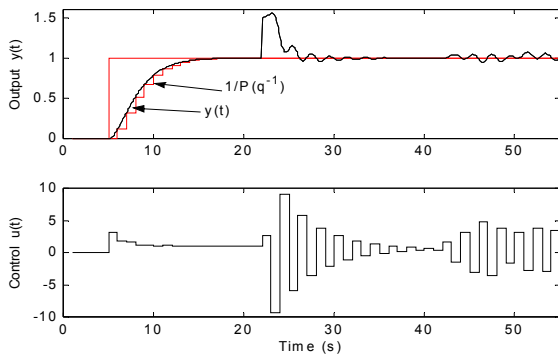


Figure 5: Detuned Model-Following with  $P_d$  as Polynomial and  $T = [1 - 0.8q^{-1}]$ .

## ALTERNATIVE TUNNING STRATEGIES

The two other tuning strategies presented in (McIntosh *et al.* 1991), involving the output horizon  $N_2$  and the control weighting factor  $\lambda_c$ , cannot in general be used to specify a specific response time, for example, a settling time of 20s. However, they do allow the speed of the closed loop to be adjusted in a predictable manner over a wide range. Furthermore, the inclusion of the  $T$  polynomial with these

tuning strategies gives more predictable results than with model-following using the  $P$  polynomial.

## Model-Following Using the $M$ Setpoint Prefilter

The  $M$  setpoint prefilter (Griffin and Downing 2002, Soeterboek 1992) offers superior model-following capabilities over using the  $P$  polynomial. In this case the reference trajectory values,  $w(t+j)$ , that appear in the cost function of Eq. (2), are generated by filtering the setpoint  $r(t)$  with the reference model,  $M(q^{-1}) = M_n(q^{-1})/M_d(q^{-1})$ , i.e.

$$w(t+j) = M(q^{-1})r(t); j = 1, \dots, N_2$$

In this case the reference model can be either a FIR or IIR filter. Furthermore, the  $M$  setpoint prefilter has no influence on the closed loop dynamics and acts only on the setpoint, therefore complete independent tracking and regulation is achieved.

## CONCLUSIONS

Using the detuned model-following configuration to control a process with zeros in the left-half of the unit circle results in a ringing control signal during a setpoint change when  $P_d$  is a scalar. The ringing can be removed by including a 'small' value of  $\lambda_c$ . The use of  $P_d$  as a polynomial with roots in the left-half of the unit circle also reduced the magnitude and ringing of the control signal during a setpoint change. However, when the  $T$  polynomial was included in the design, it led to greatly compromised disturbance rejection, sensitivity and robustness properties. These problems associated with using detuned model-following, with either  $P_d$  as a scalar or a polynomial more so, suggests that the other tuning strategies presented in the final section are more applicable to a practical application.

## REFERENCES

- Clarke, D.W., C. Mohtadi, and P.S. Tuffs. 1987. "Generalised Predictive Control – Part I & Part II", *Automatica*, Vol. 23, No. 2, 137-160.
- Clarke, D.W. and C. Mohtadi. 1989. "Properties of Generalised Predictive Control", *Automatica*, Vol. 25, No. 6, 859-875.
- Griffin, B. and C.J Downing. 2002. "Servo Response Specification Using Setpoint Prefiltering in GPC", *Proceedings of 2002 Irish Signals and Systems Conference*, Cork, Ireland.
- Griffin, B. 2002. "Servo Response and Modelling Issues in Generalised Predictive Control". *M. Eng. Thesis*, Cork Institute of Technology, Cork, Ireland.
- McIntosh, A.R, S.L. Shah, D.G. Fisher. 1991. "Analysis and Tuning of Adaptive Generalised Predictive Control", *The Canadian Journal of Chemical Engineering.*, Vol. 69 (Feb), 97-110.
- Soeterboek, R. 1992. *Predictive Control: A Unified Approach*, Prentice Hall, 92-97

**Acknowledgements:** The Authors wish to acknowledge the support of Enterprise Ireland under the Food Factory of the Future Program.

# AN AUTOTUNED ROBUST GENERALISED PREDICTIVE CONTROLLER

Tom O'Mahony & Conor J. Downing  
Advanced Control Group,  
Department of Electronics Engineering,  
Cork Institute of Technology,  
Cork, IRELAND.  
E-mail: [tomahony@cit.ie](mailto:tomahony@cit.ie)

## KEYWORDS

Computer Aided Design, Genetic Algorithms, GPC, Robust Control, Optimisation, System Identification

## ABSTRACT

The contribution of this paper is the development of a systematic tuning technique for the GPC such that an optimal trade-off between robustness and performance is achieved. This trade-off is achieved by selecting the GPC parameters to minimise a mixed  $H_2/H_\infty$  design problem. A number of simulation studies demonstrate the usefulness of this tool.

## INTRODUCTION

*Model predictive control* (MPC), also referred to as *model based predictive control* (MBPC), is now regarded, by many, as one of the most important developments in process control since the development of the PID controller over 50 years ago. The technique now enjoys a large installed base in the process industry in general (Qin & Badgwell, 1996) and the refining, petrochemical and chemical industries in particular. In terms of the food industry, recent MPC applications include riboflavin production (Kovarova-Kovar *et al.*, 2000); melter units and evaporators in the sugar industry (Zamarreno & Vega, 1997, Lissane-Elhaq & Giri, 1998); crossflow grain dryers (Liu & Bakker-Arkema, 2001); drying towers (Clarke, 1998) and greenhouse climate control (Gonzalez & Leyris, 1996).

The acclaim associated with MPC, both in industry and academia, is due to its unique combination of simplicity and control acumen. Unlike  $H_\infty$  control (Kwakernaak 1993) the tuning parameters associated with MBPC are based in the time-domain and hence MPCs are considerably simpler to tune and more intuitive to commission. More importantly, perhaps, MPCs have a unique predictive capacity and constraint handling capability. The former endows the strategy with the ability to surmount the time-delay problem while the latter facility is considered essential in most industrial implementations. Notwithstanding these advantages, most MPCs do not adequately address the design trade-off between robustness and performance. Hence the focus in this paper has been to address this problem and develop a design technique that encompasses the trade-off alluded to above.

In particular, the *generalised predictive control* (GPC) law, (Clarke *et al.*, 1987) was considered for the control versatility it allows and because of its combined academic and industrial success. Since the late 1980's considerable effort has been

expended on the development of tuning guidelines to simplify the task of commissioning the GPC. Initially this research focused on the GPC servo-parameters  $\{N_1, N_2, N_U, \lambda\}$  and subsequently on the selection of the so-called  $T$ -polynomial. Research into the latter is of considerable importance, since this polynomial has a significant effect on the closed-loop robustness and disturbance rejection properties. The difficulty in choosing this polynomial is partly associated with the robustness/performance trade-off and partly due to the fact that its influence is not monotonic. Since the existing tuning rules do not adequately address this trade-off, many practitioners resort to the use of an iterative trial-and-error design (Demirioglu & Karasu, 2000) or neglect to implement this parameter altogether (Wu *et al.*, 1998; Liu & Daley, 1999). As a result sub-optimal performance is likely, particularly in the latter case where it is necessary to detune the tracking performance in order to achieve sufficient robustness.

The procedure advocated in this paper differs considerably from previously published works, in that, while the latter have invariably concentrated on the development of empirical tuning guidelines, this paper has concentrated on the development of a generalised systematic tuning mechanism which achieves a realistic trade-off between performance and robustness. Thus to simplify the tuning process, an auto-tuning tool was devised, which successfully negotiates a practical trade-off between performance and robustness. This trade-off is achieved by selecting the GPC parameters to minimise a mixed  $H_2/H_\infty$  design problem. Simulations demonstrate the usefulness of this tool where the results are compared with previously published tuning techniques. The excellent results obtained support the belief that the advocated design is of practical significance and is the principal contribution of this paper.

## GPC ALGORITHM

Since the literature abounds with extensive derivations of the GPC algorithm, (Clarke *et al.*, 1987; Soeterboek, 1992) such a derivation will be avoided here. Suffice it to say that in its formulation, the GPC algorithm utilises a CARIMA model of the process to predict the process output,  $y(t)$ , over a finite horizon, e.g. it generates the predictions  $\{\hat{y}(t+N_1|t), \dots, \hat{y}(t+N_2|t)\}$ ;  $N_1, N_2 \in \mathbb{Z}^+$ ;  $N_2 \geq N_1$ , based on the postulation that the future control sequence remains unchanged (i.e. open-loop prediction). Using these predictions a set of control increments,  $\Delta \hat{u}(t+j)$ ;  $0 \leq j \leq N_2 - N_1$ ;  $\Delta = (I - z^{-1})$ , are calculated by minimising a quadratic cost comprising the predicted errors plus some weighting,  $\lambda$ , on the future control

signal increments. This philosophy yields a trajectory of future control increments and therefore constitutes an open-loop strategy. To close the loop, only the first element,  $\Delta \hat{u}(t)$  is applied to the system and the optimisation recomputed at time instant  $t+1$ . This strategy is called the *receding horizon principle* and is one of the key features of *model based predictive control* in general and GPC in particular. In the absence of constraints on, for example, the process output, input or states, the GPC algorithm may be re-arranged as a general linear causal 2DoF control law of the form

$$R(z^{-1})\Delta u(t) = T_1(z^{-1})w(t) + S(z^{-1})y(t) \quad (1)$$

where  $u(t)$  is the process input,  $y(t)$  the process output and  $w(t)$  the reference trajectory or set-point sequence. The polynomials  $R(z^{-1})$ ,  $T_1(z^{-1})$ , and  $S(z^{-1})$  are polynomials in  $z^{-1}$  defined through the choice of model and GPC design parameters namely the prediction horizons and  $T(q^{-1})$  polynomial (McIntosh *et al.*, 1991).

## ROBUST GPC

Regardless of the design technique used, controllers are always designed based on (necessarily incomplete) information about the dynamic behaviour of the process. In the context of linear time invariant models, the most significant source of model uncertainty may be attributed to the non-linear nature of real processes. Thus if the process model is obtained via linearisation, then it is accurate only in the neighbourhood of the reference chosen for linearisation and different operating conditions generally lead to changes in the parameters of the linear model. For example, increased throughput and flowrates usually result in smaller dead-times and time constants. Furthermore process models are usually simplified by neglecting fast dynamic phenomena, and additional parametric uncertainty arises as a result of system identification experiments. Neglecting the uncertainty between the model and the process is not advisable as the resulting controller tends to be too "tight" and is likely to become unstable in the real operating environment.

A basic mechanism for dealing with model uncertainty is illustrated via the Nyquist plot, Figure 1. Denoting the true open-loop transfer function  $L(z^{-1}) = C(z^{-1})G(z^{-1})$  where  $C(z^{-1})$  represents the compensator and  $G(z^{-1})$  the plant. The nominal loop transfer function is designated  $L_o(z^{-1}) = C(z^{-1})G_o(z^{-1})$  and assume, for simplicity, that both  $L$  and  $L_o$  are stable. In order to ensure the stability of the closed-loop system for an open-loop transfer function  $L_o$  which differs from the actual one  $L$ , the Nyquist plot of  $L$  should leave the critical point  $[-1, j0]$  on the left when traversed in the sense of growing frequencies. Thus a sufficient condition for stability is, that at each frequency, the distance between  $L$  and  $L_o$  be less than the distance between the nominal open-loop transfer function and the critical point. This may be expressed mathematically as

$$|L(j\omega) - L_o(j\omega)| < |1 + L_o(j\omega)| \quad \forall \omega \in \mathfrak{R} \quad (2)$$

and is equivalent to

$$\frac{|L(j\omega) - L_o(j\omega)|}{|L_o(j\omega)|} \cdot \frac{|L_o(j\omega)|}{|1 + L_o(j\omega)|} < 1 \quad \forall \omega \in \mathfrak{R} \quad (3)$$

It follows that if

$$\frac{|L(j\omega) - L_o(j\omega)|}{|L_o(j\omega)|} \cdot |\mathcal{T}(j\omega)| < 1 \quad \forall \omega \in \mathfrak{R} \quad (4)$$

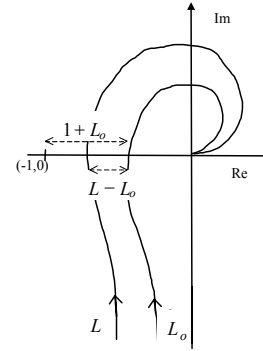


Figure 1: Nyquist plot of real and nominal loop transfer functions

then the perturbed closed-loop system is stable. In expression (4)  $\mathcal{T}(j\omega)$  is the nominal complementary sensitivity function and the factor  $|L(j\omega) - L_o(j\omega)| / |L_o(j\omega)|$  is the *relative size* of the perturbation of the loop gain  $L$  from its nominal value  $L_o$  and denoted  $\Delta_M$ . Thus the relation (4) shows that the closed-loop system is guaranteed to be stable as long as the loop perturbations satisfies

$$|\Delta_M| \cdot |\mathcal{T}(j\omega)| < 1 \quad \forall \omega \in \mathfrak{R} \quad (5)$$

Hence the complementary sensitivity function represents an upper bound on the allowable magnitude of the proportional loop perturbation - in other words, it defines the maximum amount of mismodelling that the closed-loop will tolerate prior to instability. The larger the magnitude of the complementary sensitivity function, the smaller the allowable uncertainty. Hence it is desirable that  $\mathcal{T}$  be small, particularly at the frequencies where it is anticipated that the modelling errors may be severe.

More formally, the inequality (5) is written as  $\|W \mathcal{T}\|_\infty < 1$  where  $W$  represents an upper bound on the uncertainty i.e.  $W = \bar{\Delta}_M$  and the notation  $\|\cdot\|_\infty$  represents the  $H_\infty$  norm defined as  $\|H\|_\infty = \sup_{\omega \in \mathfrak{R}} |H(j\omega)|$ . The  $H_\infty$  norm may be interpreted as the maximum amplitude of the frequency response of the transfer function. In the context of control system design, the minimum requirement of robust stability is achieved by satisfying  $\|W \mathcal{T}\|_\infty < 1$ . An effective method of seeking a compensator that satisfies this is to minimise  $\|W \mathcal{T}\|_\infty$  with respect to all compensators  $C$  that stabilise the system. This problem is one version of the general  $H_\infty$ -optimisation problem (Kwakernaak, 1993). In terms of the GPC, robust stability may be achieved by minimising the following  $H_\infty$ -norm with respect to the  $T$ -polynomial

$$\min_T \|W \mathcal{T}\|_\infty = \min_T \sup_\omega |W(e^{-j\omega}) \mathcal{T}(e^{-j\omega})| \quad (6)$$

The difficulty associated with this optimisation may readily be appreciated by developing an expression for the complementary sensitivity function,  $\mathcal{T}$ . From the equivalent linear control law of equation (1), this transfer function is:  $\mathcal{T} = z^{-1}SB/P_c$  where  $P_c$  is the closed-loop characteristic polynomial. It can readily be shown that the  $T$ -polynomial is a factor of the closed-loop characteristic equation hence  $P_c$  may be expressed as  $P_c = T \cdot P_c'$  and the robust stability requirement becomes:  $|W_2| < \frac{1}{|\mathcal{T}|} = \left| \frac{P_c' T}{SB} \right|$ . It is clearly

evident that the  $T$ -polynomial may be manipulated to satisfy this. A difficulty arises due to the fact that the polynomial  $S$  depends on  $T$ . Due to the complex non-linear relationship between  $T$  and  $S$  an analytical solution to the optimisation problem (6) is not feasible and numerical techniques must be employed.

To minimise the inequality (6) an optimisation technique known as *genetic algorithms* (GAs) was utilised. Inherently GAs are very different from conventional optimisation techniques. By dealing with several independent points, the GA samples the solution space in parallel and hence is less susceptible to lingering in or converging to local optima. GAs do not utilise gradient techniques and hence the search space need not be differentiable or continuous. The optimisation only requires objective information so that GAs can utilise various kinds of objective function, even non-linear, multi-objective or knowledge-based ones and are theoretically and empirically proven to provide robust searches (Goldberg, 1989). Thus, with their robust features, simple structure and the ability to attain global optimisation, GAs are now regarded as important mathematical tools for complex optimisation problems and are ideally suited for searching discrete, noisy, multi-modal or complex spaces.

The salient characteristics of the GA utilised for the optimisation of the  $T$ -polynomial may be described as follows

1) **Parameter Encoding:** Similar to their biological counterparts GAs utilise binary strings called chromosomes to represent the parameters of an optimisation problem. In this problem the optimisation amounts to the determination of the optimum location of the roots of the  $T$ -polynomial such that the criterion (6) is minimised. Experience suggests that there are few applications that require a high-order  $T$ -polynomial therefore a fifth-order  $T$ -polynomial was selected i.e.

$$T(z^{-1}) = \prod_{i=1}^5 (1 - t_i z^{-1}); \quad -1 < t_i < 1 \quad (7)$$

The translation from real parameters to binary strings may utilise any desired coding scheme e.g. standard binary, Gray code, etc.

2) **Initial population:** In a GA the population is the set of possible solutions and is characterised by the binary chromosomes. The GA commences by randomly generating an initial population consisting of  $N$  binary strings or chromosomes, each of which is of length  $m$ . In this application a population size of  $N = 30$  was selected, based on the principle that every possible point in the search space should be *reachable* from the initial population (Reeves, 1995).

3) **Evaluate fitness:** Each individual of the initial and subsequent generations must be evaluated to determine their fitness. This is accomplished by firstly decoding each individual in the current population to obtain the parameters  $\{t_1, t_2, t_3, t_4, t_5\}$ . The  $T$ -polynomial is formed from these roots and the controller polynomials  $S$  and  $R$  calculated. Finally the complementary sensitivity function is computed and the  $H_\infty$ -norm (6) determined. This norm is evaluated for the entire population, the population is ranked by assigning a fitness value of one to the solution(s) that minimise (6), and a fitness value of zero to the solution that maximises it. The intermediate solutions are appropriately scaled between zero and one.

4) **Evaluate fitness:** To generate a population of offspring, a set of individuals, taken from the current population, is selected as parents. Individuals with higher fitness values (i.e. those that are closer to the optimum solution) have an increased probability of survival. In this strategy the probability of an individual,  $x_i$ , being selected,  $P(x_i)$ , is defined by

$$P(x_i) = \frac{f(x_i)}{\sum_{i=1}^N f(x_i)} \quad (8)$$

where  $f(x_i)$  is the fitness value of an individual and  $N$  is the population size. The selected individuals are placed in a *mating pool*, to await the application of other GA operators e.g. crossover and mutation.

5) **Crossover:** The crossover operator is applied after selection and produces a two new chromosomes or offspring by combining information extracted from the two parent chromosomes. The parents are randomly selected from the mating pool and *single-point crossover*, with a *crossover probability*,  $P_c = 0.95$ , is employed.

6) **Mutation:** Mutation is the last genetic operator applied in a simple genetic algorithm. It operates on each individual by altering the value of a randomly selected bit position. Again the success of the mutation operator depends on the *mutation probability*,  $P_m$ , which is usually very low. The combined use of the crossover and mutation operators ensures against total loss of any genes in the population by their ability to introduce any gene which may not have existed initially, or, may subsequently have been lost.

7) **Iteration:** The GA runs iteratively and the evolution strategy ensures the search converges to a highly fit population representing optimal or near-optimal solutions to the considered problem. The GA terminates when some user-prescribed criterion is reached. This may be a predetermined number i.e. the GA is to stop after 50 generations, or a prescribed degree of convergence.

## AUTOTUNED GPC

In the previous section the GA tuning considered a single closed-loop design criterion; robust stability. In contrast a practical design requires a successful trade-off between performance and stability. To achieve this it is necessary to extend the cost function utilised in the GA optimisation to incorporate tracking and disturbance rejection performance metrics, in addition to the stability criterion previously discussed. In this section the new GA cost is defined to be

$$\begin{aligned} & \min_{\{T, N_1, N_2, \lambda\}} \{J_{GA}\} \\ & = \min_{\{T, N_1, N_2, \lambda\}} \{\eta \cdot J_{stability} + J_{servo} + J_{reg} + J_{noise}\} \end{aligned} \quad (9)$$

where  $J_{stability}$  represents that component of the cost that accounts for robust stability,  $J_{servo}$  specifications on the tracking performance and the latter two represent specifications on the disturbance rejection performance. In general good disturbance rejection implies that low-frequency or deterministic disturbances are rejected with suitably rapid transients and also that high-frequency noise is appropriately attenuated. In the robust control literature the effect of high-frequency or measurement noise is frequently tackled by restricting the amplitude of the input sensitivity function i.e. by minimising the norm

$$J_{noise} = \|U\|_{\infty} \quad (10)$$

The input sensitivity function, defined as  $U = C/(I+GC)$  relates measurement noise to the control signal and hence is a suitable metric in that it will also tend to ensure a smooth control signal. The disturbance metric is defined as

$$J_{reg} = \int_0^{\tau} |e(t)| dt \quad (11)$$

where  $\tau$  represents the duration of the simulation and assuming a pure regulatory problem  $e(t)$  is defined as  $e(t) = -y(t)$ . Hence  $J_{reg}$  represents the *integral of absolute error* (IAE) of the load disturbance response. In the problem definition (9) the servo tracking criterion was simply defined using the *integral of squared error* (ISE) criterion i.e.

$$J_{servo} = \int_0^{\tau} \{r(t) - y(t)\}^2 dt \quad (12)$$

though more complex definitions are possible. Finally  $J_{stability}$  represents the robust stability constraint, defined by the norm

$$J_{stability} = \|W T\|_{\infty} \quad (13)$$

while the term  $\eta$  represents a weighting factor that may be used to heavily penalise the robust stability criterion i.e. increase the importance of this component. In this context, the problem (9) may be interpreted as optimising the closed-loop performance subject to the constraint of robust stability.

Since both performance and stability criteria are now included in the optimisation problem the parameter search space is extended to incorporate all of the significant GPC parameters. The exception is the parameter  $N_u$  as this generally has a very restricted range -  $1 \leq N_u \leq 5$ ,  $N_u \in \mathbb{Z}^+$  - and typically is set to the number of unstable or badly damped open-loop poles. Thus the search is focused on the parameter subset  $\{T, N_1, N_2, \lambda\}$ . Since the  $T$ -polynomial was chosen as fifth-order the GA optimisation is accomplished over, effectively, eight parameters.

Note that performance is automatically dictated by the ISE criterion on the servo tracking error and the IAE on the regulator error. Hence the user is not required to either specify performance or select the GPC tuning parameters. What is required of the user is a rather significant modelling effort to determine  $W = \bar{\Delta}_M = |G(j\omega) - G_o(j\omega)|/|G_o(j\omega)|$ . In a typical industrial scenario the process is non-linear and  $G_o$  therefore represents a low-order nominal model and  $G$  selected as the model corresponding to the operating point furthest from the nominal. Thence  $W = \bar{\Delta}_M$  can be calculated. With  $W$  specified, equation (9) is optimised via the GA and the optimal GPC parameters identified. In this context, optimal implies that the joint IAE/ISE performance criterion is minimised subject to the robust stability constraint, eqn. (13).

## EVALUATION VIA SIMULATION EXAMPLES

Many researchers, McIntosh *et al.* (1991), Soeterboek (1992), Yoon & Clarke (1994) have examined the problem of designing a robust GPC control law in the presence of model uncertainty. In each of these studies the selection of the  $T$ -polynomial was the key element in enhancing robustness. Many of these researchers suggested design guidelines to aid the selection of the  $T$ -polynomial. These proposals are quite similar and the recommendation is to choose either  $T = (I - \mu z^{-1})^n$ ,  $T = A$ , or a combination of these two expressions;  $A$

being the model denominator polynomial. For example the most recent offering, Yoon & Clarke (1994), suggests setting:

$$T = A(1 - \beta z^{-1})^n \quad (14)$$

with  $n = N_l$ . The parameter  $\beta$  has a value  $\in (0, 1)$  and a rule-of-thumb is to place  $\beta$  in the neighbourhood of the dominant root of the model denominator polynomial. To evaluate the autotuning design advocated in this paper, a number of simulation examples will be taken from the recent GPC literature. For each example a GPC is designed based on (i) the advocated autotuning procedure and (ii) equation 5.1.

## Simulation Example 1

To evaluate the proposed tuning strategy the following example, taken from Normey-Rico & Camacho (1999), was utilised. This example, representing a typical industrial process, is modelled by

$$G_p(s) = \frac{k}{s+p} e^{-t_d s} \quad (15)$$

where the nominal values of the parameters are  $t_d = 0.5$ ,  $k=1$  and  $p=1$ . This process is subject to considerable parametric uncertainty where the uncertainties are defined as  $\pm 30\%$  in the delay and  $\pm 25\%$  in the other two parameters. Sampling at 0.1second intervals yields the following discrete-time nominal model:

$$G_o(z^{-1}) = z^{-5} \frac{0.1z^{-1}}{1 - 0.9z^{-1}} \quad (16)$$

The uncertainty was defined as

$$\Delta_M(z^{-1}) = \left( \frac{G_p(z^{-1})}{G_o(z^{-1})} - 1 \right) \quad (17)$$

where  $G_p(z^{-1})$  represents the discrete equivalent of one of the plant extremes. Selecting various possible models for  $G_p$  and examining the corresponding uncertainty model  $|\Delta_M(j\omega)|$  revealed that the worst case scenario occurred for the process model  $G_p(s) = 1.25e^{-0.65s}/(1+0.75s)$ . This uncertainty model was used to characterise the upper bound for the uncertainty  $W = \bar{\Delta}_M$ .

The GPC servo parameters are defined as

$$N_1 = 1; \quad N_2 = 70; \quad N_u = 1; \quad \lambda = 0; \quad P = 1 \quad (18)$$

and from the sampled plant transfer function (16) and with reference to (14) a reasonable parameterisation for the  $T$ -polynomial is  $T = (I - 0.9z^{-1})(1 - 0.7z^{-1})$ . Applying the autotuning procedure of the previous section yielded the parameter set

$$N_1 = 6; \quad N_2 = 45; \quad \lambda = 0.89 \quad (19)$$

$$T = (1 - 0.85z^{-1})(1 - 0.51z^{-1})(1 + 0.42z^{-1})$$

Interestingly, this choice of servo parameters closely parallels those of equation (18); the effect of making  $N_2$  somewhat smaller is counteracted by the increase in  $\lambda$ . Also the value of  $N_l$  selected by the GA corresponds to the standard recommendation, i.e.  $N_l = d + 1$ ; where  $d$  is the value of the delay in sampling periods. The resulting performance is illustrated in Figure 2. This comparison highlights a limitation that is common to all the proposed recommendations for the  $T$ -polynomial. When developing these tuning rules, the respective authors have tended to focus on a single criterion - that of robust stability and the rules have been developed

from this perspective only. As noted previously however any practical design inherently involves a trade-off and focusing

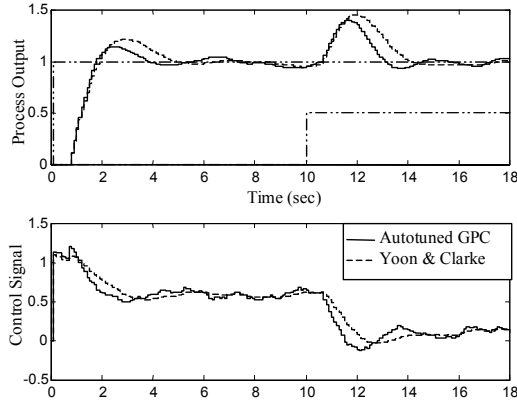


Figure 2: Closed-loop GPC responses for worst case uncertainty

exclusively on one design criterion, such as robustness, is not conducive to a balanced design process. Thus Yoon & Clarke's recommendations result in a conservative control law, for the given model uncertainty, and hence performance is impinged upon. In contrast, the design based on the GA, which combines several criteria, results in a better trade-off between performance and robustness.

### Simulation Example 2

This example, also taken from Normey-Rico & Camacho (1999), considers the following high-order plant process

$$G_p(s) = \frac{(1+0.2)e^{-s}}{(1+0.45s)(1+0.1s)(1+0.6s)(1+0.125s)} \quad (20)$$

This system can be approximated by a first-order model with time-delay where the model is defined by

$$G_m(s) = \frac{e^{-1.2s}}{1+0.7s} \quad (21)$$

A sampling time of 0.12 seconds was used to obtain  $G_m(z^{-1})$ . Based on this model, Normey-Rico & Camacho (1999), recommend setting the servo parameters as  $N = 15$ ,  $\lambda = 1$ , where the parameter  $N$  is the prediction horizon i.e.  $N = N_2 - N_1 + 1$ . Choosing the initial prediction horizon equal to the model time-delay yields following servo parameters –

$$N_1 = 10; \quad N_2 = 25; \quad N_u = 1; \quad \lambda = 1; \quad P = 1 \quad (22)$$

In this case, due to the large value of  $N_1$  it is unreasonable to utilise equation (14) to define the  $T$ -polynomial. Instead  $T$  was simply chosen as  $T = A = (1 - 0.84z^{-1})$ . Applying the GA to autotune the GPC yielded –

$$N_1 = 3; \quad N_2 = 19; \quad \lambda = 0 \quad (23)$$

$$T = (1 - 0.79z^{-1})(1 - 0.57z^{-1})(1 + 0.34z^{-1})$$

In this case identical performance resulted from both designs. Thus the autotuner again negotiated a successful trade-off between the various performance objectives, and considerably simplifies the commissioning process for the user. Note that considering the relatively large time delay (10 samples), neglected high-order dynamics and mismodelling of the time-delay parameter, admirable performance was obtained from the GPC.

### CONCLUSION

A difficulty with any controller design is the selection of tuning parameters, intrinsic in which is the performance/robustness trade-off. This paper reports on an initial attempt to solve this problem by developing an autotuning tool, which automatically determines the tuning parameters for the GPC, based on a nominal process model and the estimated model uncertainty. The parameters are selected by optimising the performance (ISE/IAE criterion) subject to a robust stability constraint being satisfied. Future work includes investigation of a multi-objective cost function, alternative optimisation techniques and practical applications.

### REFERENCES

- Ansary, P. & V. Wertz, (1997), 'Model uncertainties in GPC: A systematic two-step design', *European Control Conf., ECC'97*, Bruxelles, Belgium
- Clarke, D.W., C. Mohtadi, and P.S. Tuffs, (1987), 'Generalised predictive control – Part 1. The basic algorithm, - Part II. Extensions and interpretations', *Automatica*, 23, (2), pp 137-160
- Demirioglu, H. & E. Karasu, (2000), 'Generalised predictive control', *IEEE Control Systems Mag.*, October 2000, pp 36-47
- Goldberg, D.E., (1989), *Genetic Algorithms in Search, Optimisation and Machine Learning*, Addison-Wesley, Reading, Mass.
- Gonzalez, A. & J.P. Leyris, (1996), 'Application of GPC in MIMO systems to greenhouse climate regulation', *Int. J. System Science*, Vol. 27, No. 1, pp. 27
- Kovarova-Kovar, K., S. Gehlen, A. Kunze & A.P. Van Loon, (2000), 'application of model-predictive control based on artificial neural networks to optimise the fed-batch process for riboflavin production', *J. Biotechnology*, 79, (1), pp 39-52.
- Kwakernaak, H., (1993), 'Robust control and  $H_\infty$ -optimisation - Tutorial paper', *Automatica*, Vol. 29, No. 2, pp. 255-273
- Lissane-Elhaq, S. & F. Giri, (1998), 'Modelling, identification and control of sugar evaporation - Theoretical design and experimental evaluation', *IFAC Adapt. Sys. Ctrl. & Signal Process.*, Glasgow, Scotland.
- Liu, G.P. & S. Daley, (1999), 'Design and implementation of an adaptive predictive controller for combustor  $\text{NO}_x$  emissions', *J. of Process Control*, Vol. 9, pp. 485-491
- Liu, Q. & F.W. Bakker-Arkema, (2001), 'A model-predictive controller for grain drying', *J. Food Eng.*, Vol. 49, pp. 321-326
- McIntosh, A.R., S.L. Shah & D.G. Fisher, (1991), 'Analysis and tuning of adaptive generalised predictive control', *Canadian J. Chem. Eng.*, Vol. 69, pp 97-110
- Normey-Rico, J.E. & E.F. Camacho, (1999), 'Robustness effects of a pre-filter in a Smith predictor-based generalised predictive controller', *IEE Proc.*, Vol. 146, No. 2, Pt. D, pp. 179-185
- Qin, S.J., & T.A. Badgwell, (1996), 'An overview of industrial model predictive control technology', *Chemical Process Control V*, Tahoe City, California, 1996
- Reeves, C.R., (1995), 'Using genetic algorithms with small populations', *Proc. 5<sup>th</sup> Int. Conf. on GAs*, pp. 92-99
- Soeterboek, R., (1992), *Predictive Control - A Unified Approach*, Prentice Hall Int.
- Wu, G., N. Sepehri & K. Ziaei, (1998), 'Design of a hydraulic force control system using a generalised predictive control algorithm', *IEE Proc.* Vol. 145, No. 5, Pt. D, pp. 428-436
- Yoon, T., & D.W. Clarke, (1994), 'Observer design in receding horizon predictive control', *Int. J. Control*, 61, (1), pp 171-191
- Zamarreno, J.M. & P. Vega, (1997), 'Identification and predictive control of a melter unit used in the sugar industry', *Artificial Intelligence Eng.*, Vol. 11, No. 4, pp 365-373

### ACKNOWLEDGEMENT

Funding for this research was provided the HEAPRTL program, 2000-2003. The authors wish to gratefully acknowledge this support.

# A SURVEY OF PID CONTROLLER TUNING METHODS FOR PROCESSES WITH TIME DELAY PROPOSED SINCE 1998

Aidan O'Dwyer  
School of Control Systems and Electrical Engineering,  
Dublin Institute of Technology, Kevin St., Dublin 8, Ireland  
E-mail: [aidan.odwyer@dit.ie](mailto:aidan.odwyer@dit.ie)

## KEYWORDS

Time delay, compensation, PID

## ABSTRACT

A time delay may be defined as the time interval between the start of an event at one point in a system and its resulting action at another point in the system. Delays are also known as transport lags or dead times; they arise in physical, chemical, biological and economic systems, as well as in the process of measurement and computation. In the food processing industry, for example, time delays arise in steam heated dryers used to regulate moisture content in a food product. Methods for the compensation of time delayed processes may be broadly divided into proportional integral derivative (PID) based controllers, in which the controller parameters are adapted to the controller structure, and structurally optimised controllers, in which the controller structure and parameters are adapted optimally to the structure and parameters of the process model. The purpose of this paper is to extract the essence of the developments in design, tuning and implementation of PID controllers for delayed processes over the past few years, concentrating on journal publications. The paper will provide a framework against which the literature may be viewed.

## INTRODUCTION

The use of the PID controller is ubiquitous in industry; it has been stated, for example, that in process control applications, more than 95% of the controllers are of PID type (Astrom and Hagglund 1995). Despite the development of a large number of alternative control algorithms over the past four decades, and the fact that PID controllers have been used widely in industry for almost sixty years, their popularity is growing; eighty-three publications on the control of delayed processes using PID controllers have been recorded by the author in the year 2000, for example (O'Dwyer 2002). However, Ender (1993) maintains that, in his testing of thousands of control loops in hundreds of plants, it has been found that more than 30% of installed controllers are operating in manual mode and 65% of loops operating in automatic mode produce less variance in manual than in automatic (i.e. the automatic controllers are poorly tuned); this is rather sobering, considering the wealth of information available in the literature for determining controller parameters. The following table is instructive in this regard:

Table 1: Control of delayed processes using PID controllers: publications by date (O'Dwyer, 2002)

Year	Journal articles	Total publications
1942-1951	3	3
1952-1961	5	6
1962-1971	11	14
1972-1981	8	13
1982-1991	48	87
1992-date	217	380
1992-1997	112	183
1998-date	105	197

Due to space considerations, this paper will provide an overview of PID compensation techniques, proposed since 1998, for processes with time delay.

The PID controller may be implemented in continuous or discrete time, in a number of controller structures. The ideal continuous time PID controller is expressed in Laplace form as follows:

$$G_c(s) = K_c \left( 1 + \frac{1}{T_i s} + T_d s \right) \quad (1)$$

with  $K_c$  = proportional gain,  $T_i$  = integral time constant and  $T_d$  = derivative time constant. If  $T_i = \infty$  and  $T_d = 0$  (i.e. P control), then the closed loop measured value will always be less than the desired value for processes without an integrator term, as a positive error is necessary to keep the measured value constant, and less than the desired value. The introduction of integral action facilitates the achievement of equality between the measured value and the desired value, as a constant error produces an increasing controller output. The introduction of derivative action means that changes in the desired value may be anticipated, and thus an appropriate correction may be added prior to the actual change. Thus, in simplified terms, the PID controller allows contributions from present, past and future controller inputs.

In many cases, the design of PID controllers for delayed processes are based on methods that were originally used for the controller design of delay-free processes. However, there is general agreement that PID controllers are not well suited for the control of dominant delay processes. It has been suggested that the PID implementation is recommended for the control of processes of low to medium order, with small delays, when controller parameter setting must be done using tuning

rules and when controller synthesis may be performed a number of times (Isermann 1989).

## THE SPECIFICATION OF PI OR PID CONTROLLER PARAMETERS

### Iterative Methods

The choice of appropriate compensator parameters may be achieved experimentally e.g. by manual tuning. However, such an approach is time consuming and the process typically has to be driven to its stability limit. Alternatively, a graphical or analytical approach to controller tuning may be done in either the time or frequency domains. The time domain design is done using root locus diagrams; it is, however, questionable that a delayed process would be sufficiently well modelled by the necessary second order model. The frequency domain design is typically done using Bode plots to achieve a desired phase margin. Iterative methods for controller design provide a first approximation to desirable controller parameters.

### Tuning Rules

Process reaction curve tuning rules are based on calculating the controller parameters, from the model parameters determined from the open loop process step response. This method was originally suggested by Ziegler and Nichols (1942), who modelled the SISO process by a first order lag plus delay (FOLPD) model, estimated the model parameters using a tangent and point method and defined tuning parameters for P, PI and PID controllers. Other process reaction curve tuning rules of this type are also described, sometimes in graphical form, to control processes modelled by a FOLPD model (Shinsky 2001) or an integral plus delay (IPD) model (Hay 1998). The advantages of such tuning strategies are that only a single experimental test is necessary, a trial and error procedure is not required and the controller settings are easily calculated; however, it is difficult to calculate an accurate and parsimonious process model, load changes may occur during the test which may distort the test results and a large step input may be necessary to achieve a good signal to noise ratio.

Performance (or optimisation) criteria, such as the minimisation of the integral of absolute error in a closed loop environment, may be used to determine a unique set of controller parameter values. Tuning rules have been described, sometimes in graphical form, to optimise either the regulator response or the servo response, of a compensated SISO process, modelled in stable or unstable FOLPD form (Wilton 1999; Majhi and Atherton 2000; Visioli 2001a), IPD form (Visioli 2001a), or stable or unstable second order system plus delay (SOSPD) form (Wilton 1999; Kwak et al. 2000). Tuning rules to achieve specified servo and regulator responses simultaneously are also described (Tan et al. 1998; Yang and Shao 2000a).

Ultimate cycle tuning rules are calculated from the controller gain and oscillation period recorded at the ultimate frequency (i.e. the frequency at which marginal

stability of the closed loop control system occurs). The first such tuning method was defined by Ziegler and Nichols (1942) for the tuning of P, PI and PID controller parameters of a process that may or may not include a delay. The tuning rules implicitly build an adequate frequency domain stability margin into the compensated system. Such tuning rules, to compensate delayed processes by either minimising a performance criterion, or achieving a specified gain and/or phase margin, are discussed when the SISO process is modelled in IPD form (Kookos et al. 1999), or stable or unstable SOSPD form (Luyben 2000). Alternatively, ultimate cycle tuning rules, and modifications of the rules in which the proportional gain is set up to give a closed loop transient response decay ratio of 0.25, or a phase lag of  $135^\circ$ , may compensate general, possibly delayed, stable or unstable processes (Hay 1998; Tan et al. 1999; Yu 1999; Prashanti and Chidambaram 2000; Tan et al. 2001; Robbins, 2002), sometimes to achieve either a specified gain and/or phase margin (Prashanti and Chidambaram 2000; Tan et al. 2001) or a specified closed loop response (Vrancic et al. 1999, 2001). The controller settings are easily calculated; however, the system must generally be destabilised under proportional control, the empirical nature of the method means that uniform performance is not achieved in general, several trials must typically be made to determine the ultimate gain, the resulting process upsets may be detrimental to product quality, there is a danger of misinterpreting a limit cycle as representing the stability limit and the amplitude of the process variable signal may be so great that the experiment may not be carried out for cost or safety considerations.

Direct synthesis tuning rules result in a controller that facilitates a specified closed loop response. These methods include pole placement strategies and frequency domain techniques, such as gain margin and/or phase margin specification methods. Pole placement strategies are described to compensate SISO processes modelled in stable or unstable FOLPD form (Bi et al. 1999; Chien et al. 1999; Huang et al. 2000; Zhang and Xu 2000; Mann et al. 2001b), IPD form (Chen et al. 1999; Chien et al. 1999a) or SOSPD form (Wang et al. 1999a; Bi et al. 2000). Frequency domain based tuning rules are also described, for processes modelled in stable or unstable FOLPD form (Ho et al. 1998; Ho and Xu 1998; Chen et al. 1999a), stable or unstable SOSPD form (Ho and Xu 1998; Huang et al. 2000; Wang et al. 2001a), IPD form (Poulin and Pomerleau 1999; Cheng and Yu 2000), or more general form (Yang and Shao 2000b).

The presence of unmodelled process dynamics demands a robust design approach. The Internal Model Control (IMC) design procedure, which allows uncertainty on the process parameters to be specified, may be used to design appropriate PI and PID controllers for the compensation of SISO processes modelled in stable or unstable FOLPD form (Alvarez-Ramirez et al. 1998; Lee et al. 1998; Chen et al. 1999b; Chun et al. 1999; Isaksson and Graebe 1999; Lee et al. 2000; Leva and Colombo 2000; Rivera and Jun 2000; Marchetti and Scali 2000; Ho et al. 2001), IPD form (Alvarez-Ramirez et al. 1998; Zhang et al. 1999; Rivera and Jun 2000) or stable and

unstable SOSPD form (Lee et al. 1998; Chen et al. 1999b; Rivera and Jun 2000).

Tuning rules are easy to use, even in the absence of an accurate process model. These design methods are suitable for the achievement of a simple performance specification, for a compensated process with a non-dominant delay. Comprehensive summaries of the tuning rule formulae are available (O'Dwyer 2001). A summary of tuning rules published by year and medium is provided in Table 2; as this table shows, interest in the development of tuning rules is growing.

Table 2: Tuning rules - publications by date (O'Dwyer, 2001)

Year	Journal articles	Total publications
1942-1951	3	3
1952-1961	5	6
1962-1971	5	8
1972-1981	7	9
1982-1991	20	36
1992-date	86	146
1992-1997	46	73
1998-date	40	73

### Analytical Techniques

Controller parameters may be determined using analytical techniques. Some methods minimise an appropriate performance index (Astrom et al. 1998; Ham and Kim 1998; Kookos et al. 1999; Liu and Daley 1999; Leva and Colombo 1999; He et al. 2000; Howell and Best 2000; Tan et al. 2000; Wang and Cluett 2000; Leva and Colombo 2001). Alternatively, a direct synthesis strategy may be used to determine the controller parameters. Such strategies may be defined in the time domain, possibly by using pole placement (Atherton 1999; Daley and Liu 1999; Jung et al. 1999a, 1999b; Majhi and Atherton 1999) or in the frequency domain, possibly by specifying a desired gain and/or phase margin (Fung et al. 1998; Wang et al. 1999b, 1999c; Grassi et al. 2001).

Robust methods may be used to design analytically an appropriate PID controller (Huang and Wang 2001; Wang et al. 2001b; Ge et al. 2002). Finally, alternative design methods may be used to determine the controller parameters, such as fuzzy logic (Bandyopadhyay and Patranabis 1998, 2001; Blanchett et al. 2000; Xu et al. 1998, 2000; Li and Tso 1999, 2000; Mudi et al. 1999; Visioli 1999, 2001b; Wang et al. 1999d; Tao and Taur 2000; Mann et al. 2001a), genetic algorithms (Cheng and Hwang 1998; Mudi and Pal 1999) or neural networks (Huang et al. 1999; Sbarbaro et al. 2000; Shu and Pi 2000).

Analytical methods are suitable for the design of PI/PID controllers for non-dominant delay processes where there are well-defined performance requirements to be achieved.

### CONCLUSIONS

Control academics and practitioners remain interested in the use of the PID controller to compensate processes with time delay. This paper provides a comprehensive summary of such compensation techniques that have appeared in relevant journals since 1998. It is the hope of the author that the paper will provide a convenient reference for application work. The work demonstrates that new design techniques have been accumulating, each claiming that it is the best suited for the application. In general, there is a lack of comparative analysis with other design techniques; associated with this is the lack of benchmark examples for testing the different methods. The main priority for future research should be a critical analysis of available design techniques.

### REFERENCES

- Alvarez-Ramirez, J., A. Morales, and I. Cervantes. 1998. "Robust proportional-integral control", *Industrial Engineering Chemistry Research*, 37, 4740-4747.
- Astrom, K.J., H. Panagopoulos, and T. Hagglund. 1998. "Design of PI controllers based on non-convex optimisation", *Automatica*, 34, 1998, pp. 585-601.
- Astrom, K.J. and T. Hagglund. 1995. *PID controllers: theory, design and tuning*, Second Edition, Instrument Society of America.
- Atherton, D.P. 1999. "PID controller tuning", *IEE Computing and Control Engineering Journal*, April, 44-50.
- Bandyopadhyay, R. and D. Patranabis. 1998. "A fuzzy logic based PI autotuner", *ISA Transactions*, Vol. 37, 227-235.
- Bandyopadhyay, R. and D. Patranabis. 2001. "A new autotuning algorithm for PID controllers using dead-beat format", *ISA Transactions*, 40, 255-266.
- Bi, Q., W.-J. Cai, E.-L. Lee, Q.-G. Wang, C.-C. Hang and Y. Zhang. 1999. "Robust identification of first-order plus dead-time model from step response", *Control Engineering Practice*, 7, No. 1, 71-77.
- Bi, Q., W.-J. Cai, Q.-G. Wang, C.-C. Hang, E.-L. Lee, Y. Sun, K.-D. Liu, Y. Zhang and B. Zou 2000. "Advanced controller auto-tuning and its application in HVAC systems", *Control Engineering Practice*, 8, No. 6, 633-644.
- Blanchett, T.P., G.C. Kember and R. Dubay. 2000. "PID gain scheduling using fuzzy logic", *ISA Transactions*, 39, No. 2, 317-325.
- Chen, C.-L., S.-H. Hsu and H.-P. Huang. 1999a. "Tuning PI/PD controllers based on gain/phase margins and maximum closed loop magnitude", *Journal of the Chinese Institute of Chemical Engineers*, 30, No. 1, 23-29.
- Chen, C.-L., H.-P. Huang and C.-T. Hsieh. 1999b. "Tuning of PI/PID controllers based on specification of maximum closed-loop amplitude ratio", *Journal of Chemical Engineering of Japan*, 32, No. 6, 783-788.
- Cheng, S.-L. and C. Hwang. 1998. "Designing PID controllers with a minimum IAE criterion by a differential evolution algorithm", *Chemical Engineering Communications*, 170, 83-115.
- Cheng, Y.-C. and C.-C. Yu. 2000. "Nonlinear process control using multiple models: relay feedback approach", *Industrial Engineering Chemistry Research*, 39, No. 2, 420-431.
- Chien, I.-L., H.-P. Huang and J.-C. Yang. 1999. "A simple multiloop tuning method for PID controllers with no proportional kick", *Industrial Engineering Chemistry Research*, 38, No. 4, 1456-1468.
- Chun, D., J.Y. Choi and J. Lee. 1999. "Parallel compensation with a secondary measurement", *Industrial Engineering Chemistry Research*, 38, No. 4, 1575-1579.
- Daley, S. and G.P. Liu. 1999. "Optimal PID tuning using direct

- search algorithms”, *IEE Computing and Control Engineering Journal*, April, 51-56.
- Ender, D.B. 1993. “Process control performance: not as good as you think”, *Control Engineering*, September, 180-190.
- Fung, H.-W., Q.-G. Wang and T.-H. Lee. 1998. “PI tuning in terms of gain and phase margins”, *Automatica*, 34, 1145-1149.
- Ge, M., M.-S. Chiu and Q.-G. Wang. 2002. “Robust PID controller design via LMI approach”, *Journal of Process Control*, 12, 3-13.
- Grassi, E., K.S. Tsakalis, S. Dash, S.V. Gaikwad, W. MacArthur and G. Stein. 2001. “Integrated system identification and PID controller tuning by frequency loop-shaping”, *IEEE Transactions on Control Systems Technology*, 9, No. 2, 285-293.
- Ham, T.W. and Y.H. Kim. 1998. “Process identification using pulse response and proportional-integral-derivative controller tuning with combined guidelines”, *Industrial Engineering Chemistry Research*, 37, 482-488.
- Hay, J. 1998. *Regeltechnik 1*, Die Keure n.v., Brugge, Belgium, 197-198.
- He, J.-B., Q.-G. Wang and T.-H. Lee. 2000. “PI/PID controller tuning via LQR approach”, *Chemical Engineering Science*, 55, 2429-2439.
- Ho, W.K., K.W. Lim and W. Xu. 1998. “Optimal gain and phase margin tuning for PID controllers”, *Automatica*, 34, No. 8, 1009-1014.
- Ho, W.K. and W. Xu. 1998. “PID tuning for unstable processes based on gain and phase-margin specifications”, *IEE Proceedings - Control Theory and Applications*, 145, No. 5, 392-396.
- Ho, W.K., T.H. Lee, H.P. Han and Y. Hong. 2001. “Self-tuning IMC-PID control with interval gain and phase margins assignment”, *IEEE Transactions on Control Systems Technology*, 9, No. 3, 535-541.
- Howell, M.N. and M.C. Best. 2000. “On-line PID tuning for engine idle-speed control using continuous action reinforcement learning automata”, *Control Engineering Practice*, 8, 147-154.
- Huang, C.-T., M.-Y. Lin and M.-C. Huang. 1999. “Tuning PID controllers for processes with inverse response using artificial neural networks”, *Journal of the Chinese Institute of Chemical Engineers*, 30, No. 3, 223-232.
- Huang, H.-P., M.-W. Lee and C.-L. Chen. 2000. “Inverse-based design for a modified PID controller”, *Journal of the Chinese Institute of Chemical Engineers*, 31, No. 3, 225-236.
- Huang, Y.J. and Y.-J. Wang. 2001. “Robust PID controller design for non-minimum phase time delay systems”, *ISA Transactions*, 40, 31-39.
- Isaksson, A.J. and S.F. Graebe. 1999. “Analytical PID parameter expressions for higher order systems”, *Automatica*, 35, 1121-1130.
- Isermann, R., *Digital control systems Volume 1. Fundamentals, deterministic control*, 2nd Revised Edition, Springer-Verlag, 1989.
- Jung, C.L., H.K. Song and J.C. Hyun. 1999a. “A new direct-synthesis tuning method for PI-controllers”, *The Canadian Journal of Chemical Engineering*, 77, 180-185.
- Jung, C.L., H.K. Song and J.C. Hyun. 1999b. “A direct synthesis tuning method of unstable first-order-plus-time-delay processes”, *Journal of Process Control*, 9, No. 3, 265-269.
- Kookos, I.K., A.I. Lygeros and K.G. Arvanitis. 1999. “On-line PI controller tuning for integrator/dead time processes”, *European Journal of Control*, 5, 19-31.
- Kwak, H.J., S.W. Sung and I.-B. Lee. 2000. “Stabilizability conditions and controller design for unstable processes”, *Transactions of the Institute of Chemical Engineers*, 78, Part A, 549-556.
- Lee, Y., S. Park, M. Lee and C. Brosilow. 1998. “PID controller tuning to obtain desired closed-loop responses for SI/SO systems”, *AIChE Journal*, 44, 106-115.
- Lee, Y., J. Lee and S. Park. 2000. “PID tuning for integrating and unstable processes with time delay”, *Chemical Engineering Science*, 55, 3481-3493.
- Leva, A. and A.M. Colombo. 1999. “Method for optimising set-point weights in ISA-PID autotuners”, *IEE Proceedings – Control Theory and Applications*, 146, No. 2, 137-146.
- Leva, A. and A.M. Colombo. 2000. “Estimating model mismatch overbounds for the robust autotuning of industrial regulators”, *Automatica*, 26, 1855-1861.
- Leva, A. and A.M. Colombo. 2001. “Implementation of a robust PID autotuner in a control design environment”, *Transactions of the Institute of Measurement and Control*, 23, No. 1, 1-20.
- Li, H.-X. and S.K. Tso. 1999. “Higher order fuzzy control structure for higher order or time-delay systems”, *IEEE Transactions on Fuzzy Systems*, 7, No. 5, 540-552.
- Li, H.-X. and S.K. Tso. 2000. “Quantitative design and analysis of fuzzy proportional-integral-derivative control – a step towards autotuning”, *International Journal of Systems Science*, 31, No. 5, 545-553.
- Liu, G.P. and S. Daley. 1999. “Optimal tuning PID controller design in the frequency domain with application to a rotary hydraulic system”, *Control Engineering Practice*, 7, 821-830.
- Luyben, W.L. 2000. “Tuning proportional-integral controllers for processes with both inverse response and deadtime”, *Industrial Engineering Chemistry Research*, 39, No. 4, 973-976.
- Majhi, S. and D.P. Atherton. 1999. “Autotuning and controller design for processes with small time delays”, *IEE Proceedings – Control Theory and Applications*, 146, No. 5, 415-425.
- Majhi, S. and D.P. Atherton. 2000. “Online tuning of controllers for an unstable FOPDT process”, *IEE Proceedings – Control Theory and Applications*, 147, No. 4, 421-427.
- Mann, G.K.I., B.-G. Hu and R.G. Gosine. 2001a. “Two-level tuning of fuzzy PID controllers”, *IEEE Transactions on Systems, Man and Cybernetics – Part B: Cybernetics*, 31, No. 2, 263-269.
- Mann, G.K.I., B.-G. Hu and R.G. Gosine. 2001b. “Time-domain based design and analysis of new PID tuning rules”, *IEE Proceedings – Control Theory and Applications*, 148, No. 3, 251-261.
- Marchetti, G. and C. Scali. 2000. “Use of modified relay techniques for the design of model-based controllers for chemical processes”, *Industrial Engineering Chemistry Research*, 39, 3325-3334.
- Mudi, R.K. and N.R. Pal. 1999. “A robust self-tuning scheme for PI- and PD-type fuzzy controllers”, *IEEE Transactions on Fuzzy Systems*, 7, No. 1, 2-16.
- O’Dwyer, A. 2001. “PI and PID controller tuning rules for time delay processes: a summary”, *Technical Report AOD-00-01*, Version 2, School of Control Systems, Dublin Institute of Technology, Ireland (Dec).
- O’Dwyer, A. 2002. “PID compensation of time delayed processes: a full survey”, *Technical Report AOD-00-05*, Version 3, School of Control Systems, Dublin Institute of Technology, Ireland (Feb).
- Poulin, E. and A. Pomerleau. 1999. “PI settings for integrating processes based on ultimate cycle information”, *IEEE Transactions on Control Systems Technology*, 7, No. 4, 509-511.
- Prashanti, G. and M. Chidambaram. 2000. “Set-point weighted PID controllers for unstable systems”, *Journal of the Franklin Institute*, 337, No. 2-3, 201-215.
- Rivera, D.E. and K.S. Jun. 2000. “An integrated identification

- and control design methodology for multivariable process system applications”, *IEEE Control Systems Magazine*, June, 25-37.
- Robbins, L.A. 2002. “Tune control loops for minimum variability”, *Chemical Engineering Progress*, January, 68-70.
- Sbarbaro, D., J.P. Segovia, S. Alcozer and J. Gonzales. 2000. “Applications of radial basis network technology to process control”, *IEEE Transactions on Control Systems Technology*, 8, No. 1, 14-22.
- Shinsky, F.G. 2001. “PID-deadtime control of distributed processes”, *Control Engineering Practice*, 9, 1177-1183.
- Shu, H. and Y. Pi. 2000. “PID neural networks for time-delay systems”, *Computers and Chemical Engineering*, Vol. 24, 859-862.
- Tan, K.K., Q.G. Wang, C.C. Hang and T.J. Hagglund. 1999. *Advances in PID control*, Advances in Industrial Control Series, Springer-Verlag London.
- Tan, K.K., T.H. Lee and X. Jiang. 2000. “Robust on-line relay automatic tuning of PID control systems”, *ISA Transactions*, 39, No. 2, 219-232.
- Tan, K.K., T.H. Lee and X. Jiang. 2001. “On-line relay identification, assessment and tuning of PID controller”, *Journal of Process Control*, 11, pp. 483-496.
- Tan, W., J. Liu and P.K.S. Tam. 1998. “PID tuning based on loop-shaping  $H_\infty$  control”, *IEE Proceedings - Control Theory and Applications*, 145, No. 6, 485-490.
- Tao, C.W. and J.S. Taur. 2000. “Flexible complexity reduced PID-like fuzzy controllers”, *IEEE Transactions on Systems, Man and Cybernetics - Part B: Cybernetics*, 30, No. 4, 510-516.
- Visioli, A. 1999. “Fuzzy logic based set-point weight tuning of PID controllers”, *IEEE Transactions on Systems, Man and Cybernetics - Part A: Systems and Humans*, 29, No. 6, 587-592.
- Visioli, A. 2001a. “Optimal tuning of PID controllers for integral and unstable processes”, *IEE Proceedings - Control Theory and Applications*, 148, No. 2, 180-184.
- Visioli, A. 2001b. “Tuning of PID controllers with fuzzy logic”, *IEE Proceedings - Control Theory and Applications*, 148, No. 1, 1-8.
- Vrancic, D., Y. Peng and S. Strmcnik. 1999. “A new PID controller tuning method based on multiple integrations”, *Control Engineering Practice*, 7, No. 5, 623-633.
- Vrancic, D., S. Strmcnik and D. Juricic. 2001. “A magnitude optimum multiple integration tuning method for filtered PID controller”, *Automatica*, 37, 1473-1479.
- Wang, L. and W.R. Cluett. 2000. *From plant data to process control*, Taylor and Francis Ltd.
- Wang, Q.-G., T.-H. Lee, H.-W. Fung, Q. Bi and Y. Zhang. 1999a. “PID tuning for improved performance”, *IEEE Transactions on Control Systems Technology*, 7, No. 4, 457-465.
- Wang, Q.-G., H.-W. Fung and Y. Zhang. 1999b. “PID tuning with exact gain and phase margins”, *ISA Transactions*, 38, 243-249.
- Wang, Q.-G., C.-C. Hang, S.-A. Zhu and Q. Bi. 1999c. “Implementation and testing of an advanced relay auto-tuner”, *Journal of Process Control*, 9, No. 4, 291-300.
- Wang, L., M.L. Desarmo and W.R. Cluett. 1999d. “Real-time estimation of process frequency response and step response from relay feedback experiments”, *Automatica*, 35, 1427-1436.
- Wang, Q.-G., Y. Zhang and X. Guo. 2001a. “Robust closed-loop identification with application to auto-tuning”, *Journal of Process Control*, 11, 519-530.
- Wang, Q.-G., C.C. Hang and X.-P. Yang. 2001b. “Single-loop controller design via IMC principles”, *Automatica*, 37, 2041-2048.
- Wilton, S.R. 1999. “Controller tuning”, *ISA Transactions*, 38, 157-170.
- Xu, J.-X., Y.-M. Pok, C. Liu and C.-C. Hang. 1998. “Tuning and analysis of a fuzzy PI controller based on gain and phase margins”, *IEEE Transactions on Systems, Man and Cybernetics - Part A: Systems and Humans*, 28, 685-691.
- Xu, J.-X., C.-C. Hang and C. Liu. 2000. “Parallel structure and tuning of a fuzzy PID controller”, *Automatica*, 36, 673-684.
- Yang, Y.G. and Shao, H.-H. 2000a. “PID auto-tuner based on sensitivity specification”, *Transactions of the Institute of Chemical Engineers*, 75, Part A, 312-316.
- Yang, Y.-G. and Shao, H.-H. 2000b. “Optimal tuning for PI controller”, *Automatica*, 36, 147-152.
- Yu, C.-C. 1999. *Autotuning of PID controllers*, Advances in Industrial Control Series, Springer-Verlag London Ltd.
- Zhang, W., X. Xu and Y. Sun. 1999. “Quantitative performance design for integrating processes with time delay”, *Automatica*, 35, 719-723.
- Zhang, W. and X. Xu. 2000. “On the model reference method for unstable time delay systems”. *Computers and Chemical Engineering*, 24, 2765-2766.
- Ziegler, J.G. and N.B. Nichols. 1942. “Optimum settings for automatic controllers”, *Transactions of the ASME*, 64, 759-768.

## AUTHOR BIOGRAPHY

**AIDAN O'DWYER** was born in Portumna, Co. Galway, Ireland and was educated at Portumna College, University College Galway, and Dublin City University, from which he received B.E., M.Eng. and Ph.D. degrees in 1984, 1992 and 1996, respectively. Since 1990, he has been a lecturer in electrical engineering at Dublin Institute of Technology. His research interests are the identification and control of time delay systems. He is the author or co-author of thirty-four published papers on these topics.

# A COMPARISON BETWEEN A SELF-TUNING FLC AND A FLC WITH GAIN SCHEDULER FOR VARIABLE GAIN

Denis Herlihy & Dr. Barry O'Connor  
AMT Ireland  
University College Cork  
d.herlihy@student.ucc.ie  
jboc@ucc.ie

## ABSTRACT

Ebrahim Mamdani constructed the first Fuzzy Logic Controller (FLC) in 1973 and since then FLC's are becoming increasingly popular in process industries. This paper proposes the design of two different FLC's to control the liquid level in a tank that possesses variable deadtime. An attractive feature of this closed loop system would be to minimise the deadtime. It will be shown that this can be achieved in FLC's by scaling the control signal of the controller, by means of a controller gain. Two designs are proposed in this paper to attain minimisation of variable deadtime, namely a Self-tuning FLC and a FLC with Gain Scheduler. The Self-tuning FLC consists of two FLC's, the first FLC outputs the control signal for the process and the second FLC outputs a value ( $\alpha$ ), which further scales the control signal. This value of  $\alpha$  is determined from a rule-base defined on both error ( $e$ ) and gradient of liquid level ( $\Delta e$ ) of the controlled variable. The FLC can be tuned by dynamically adjusting the controller gain in each sampling instance by a scaling factor  $\alpha$ . For the second FLC (with Gain Scheduler) design, it will be shown that the effect of deadtime is minimised using an automatic procedure. Which estimates the deadtime on start-up and an appropriate gain is then selected from the gain scheduler to minimise the effect of this deadtime. This paper presents the design of both FLC's followed by a performance comparison between them. Several performance criteria such as, rise time, settling time, disturbance rejection and Integral Absolute Error will be employed.

## INTRODUCTION

Fuzzy control denotes the field in control engineering in which fuzzy set theory and fuzzy inference are used to derive control laws. In 1973, Ebrahim Mamdani constructed the first Fuzzy Controller to control a steam engine and since then FLC's have been rapidly gaining popularity among practicing engineers. This increased popularity can be attributed to the fact that fuzzy logic provides a powerful vehicle that allows engineers to incorporate human reasoning in the control algorithm. This characteristic of FLC's is further utilized in process industries where it is sometimes difficult to obtain an accurate plant model.

In this paper, the problem of variable deadtime in a process is addressed. Two FLC's are designed to minimise this problem followed by a performance comparison between both techniques. Consider a liquid level control application shown in block diagram form in Figure 1.

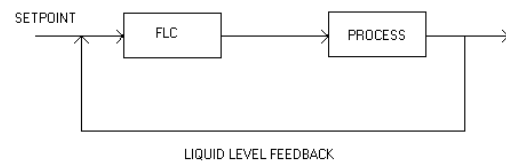


Figure 1

A suitable sensor is used to measure the actual liquid level in the process (tank) and it is then compared to the setpoint. The error is evaluated and fed to the controller, which calculates the appropriate control signal to the processes pump. This forces it to increase or decrease its flow rate depending on the error magnitude, maintaining liquid level at its desired value.

It can be easily shown that a simple PD-type FLC will sufficiently control this process. However, the presence of deadtime causes serious performance degradation. These include longer rise and settling times, larger overshoot and even the possibility of unwanted oscillation. Varying deadtime causes a greater problem still, which occurs from manufacturing discrepancies, new product development and physical constraints placed on sensors at different locations. Several control design methods for systems with varying deadtime have appeared in recent literature including forms of self-tuning and self-organising FLC's (HE 1993; Maeda and Murakami 1992; Procyk and Mamdani 1979; Shao 1988). Further research employed neural networks and genetic algorithms to design such controllers, to achieve more improved performance and increased robustness (Chen and Chen 1994; Homaifar and McCormick 1995; Karr and Gentry 1993; Li 1997). Also MathWorks have a function in their Fuzzy Logic Toolbox called ANFIS, which tunes the membership functions of the controller off-line using input/output training data.

One method of minimising deadtime is to adjust the magnitude of the control signal, by varying the controller gain. In practice a skilled human operator manipulates this controller gain in an ad hoc fashion based on the current process state to achieve optimal control (Mudi and Pal 2000). However, this paper proposes two automated

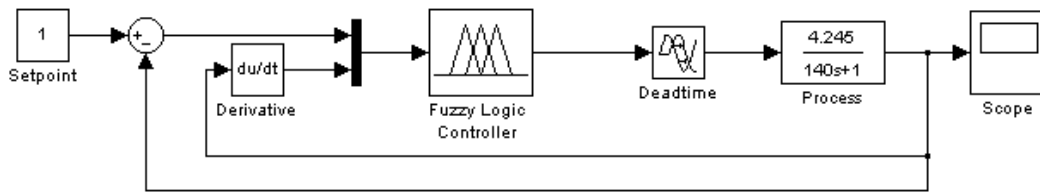


Figure 2: PD-Type FLC Block Diagram

procedures to tune the controller gain on-line, listed as

1. A FLC with Gain Scheduler (FLCGS)
2. A Self-tuning PD-type FLC (STFLC)

The FLCGS system consists of a PD-type FLC and an automatic procedure. That measures the deadtime on start-up followed by a gain scheduler that selects the appropriate gain for the measured deadtime. On the other hand, the STFLC system is slightly more complex. The controller gain is adjusted on each sampling instant using a scaling factor ( $\alpha$ ), the value of which is determined by a second FLC.

Both controllers are simulated using a mathematical model of the CE105 Coupled Tank Apparatus from TecEquipment Inc., which mimics liquid level control.

This paper is organised as follows: Section 2 shows the controller design procedure and performance evaluation of the FLCGS with different values of deadtime. Design and testing of the STFLC is seen in Section 3, again with different values of deadtime. Following this, Section 4 compares the performance of both controllers. Finally, conclusions are presented in Section 5.

## FLCGS DESIGN

The FLCGS is designed using the Fuzzy Logic Toolbox in MATLAB and is simulated using Simulink, a software package for modelling, simulating, and analysing dynamical systems. However a mathematical model of the CE105 Coupled Tank Apparatus is obligatory when simulating the designed FLCGS. Using classical system identification techniques outlined in (Ljung 1987) the mathematical model for the process (ignoring deadtime) was found to be,

$$G(s) = \frac{4.245}{140s + 1}$$

In order to design the FLCGS, a PD-type FLC must be designed initially to control the process without deadtime, Figure 2 shows the block diagram of the PD-type FLC. In a fuzzy control system, both input and output data are represented by linguistic variables, which are intuitively expressed by natural language words (Ross 1995; Jamshidi et al. 1993). In this system the FLC has two inputs, *ERROR*

(*e*), difference between desired and actual liquid height and *RATE* ( $\Delta y$ ) rate of change of process output. Furthermore, one output referred to as *VOLTAGE* ( $u(k)$ ), corresponds to the input voltage to the pump. The linguistic terms decided for the input and output variables were:

Error = {large\_neg, med\_neg, okay, med\_pos, large\_pos}

Rate = {neg\_fast, negative, okay, positive, pos\_fast}

Voltage = {very\_small, small, no\_change, high, very\_high}

Fuzzy sets must now be associated with each of these linguistic terms, whereupon the designer selects the size and shape of these fuzzy sets based on apriori or heuristic knowledge of the plant. Figures 4, 5 and 6 show the fuzzy sets for the inputs and output. The above linguistic terms then use a set of If-Then rules (rule-base) that are specified to emulate the designer's knowledge of the process and its appropriate control. In this case, nine rules are required to efficiently track the setpoint, which state the output actions to be performed depending on the status of the input variables. These rules can be specified as follows:

If error is large\_pos Then voltage is very\_high  
 If error is med\_pos Then voltage is very\_fast  
 If error is okay Then voltage is no\_change  
 If error is med\_neg Then voltage is very\_small  
 If error is large\_neg Then voltage very\_small  
 If error is okay and rate is positive Then voltage is small  
 If error is okay and rate is negative Then voltage is high  
 If error is okay and rate is pos\_fast Then voltage is small  
 If error is okay and rate is neg\_fast Then voltage is high

With these rules designed, the PD-type FLC is now implemented and tested using the mathematical model of the process. The resultant process response of the closed loop system is depicted in Figure 7. It can be seen that good setpoint tracking is achieved after a rise time of approximately 60 seconds. However, such a satisfactory performance with the PD-type FLC requires a good understanding of the physics of the underlying system.

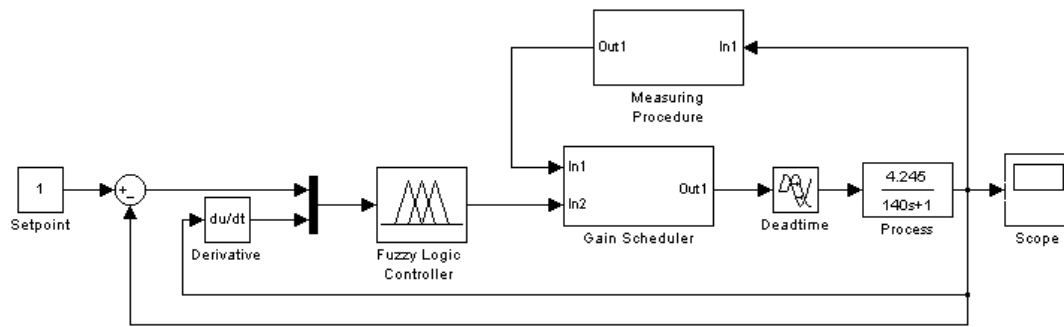


Figure 3: FLCGS Block Diagram

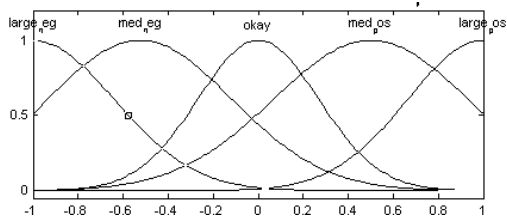


Figure 4: Input variable Error

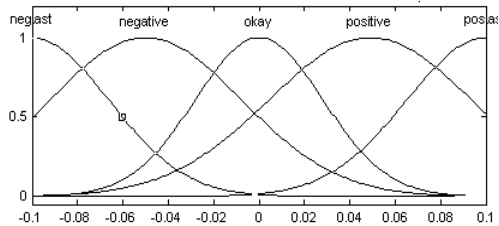


Figure 5: Input variable Rate

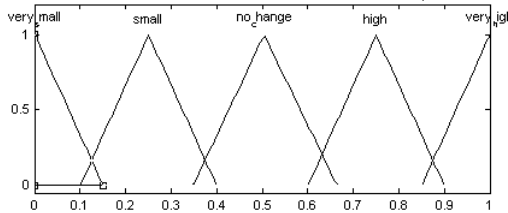


Figure 6: Output variable Voltage

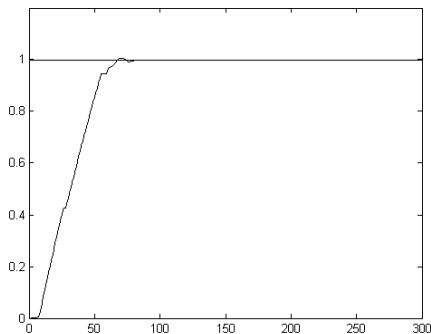


Figure 7: Response of PD-type FLC

In processes where the deadtime is known apriori a controller gain (scaling factor) can be placed after the controller and can be tuned off-line to minimise this deadtime. However, this gives poor performance in the case where the deadtime varies.

Here, an automatic procedure will be used to measure the variable deadtime on start-up and is then requested to minimise the measured deadtime using a gain scheduler.

A simple If-Then procedure is used to measure the deadtime. The process output is monitored on commencement of the process and the deadtime is estimated. The If-Then procedure to perform such estimation is as follows,

```

Count = 0
If (process output = 0) then
    Count = Count + 1
Endif
Deadtime = Count
  
```

This value of deadtime is then fed to the gain scheduler, which switches to the appropriate gain for that specific deadtime. Table 1 contains the appropriate gains for their respective deadtime. The values of these gains are found through trial and error.

Table 1

Deadtime	Gain
0	1
1	0.8
2	0.6
3	0.29
4	0.22
5	0.19
6	0.17
7	0.165

Simulated output responses for the process with deadtimes of 1 and 3 seconds can be seen in Figures 8 and 9 respectively.

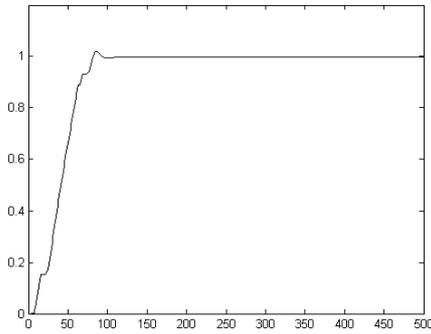


Figure 8: Response of FLCGS, deadtime = 1s

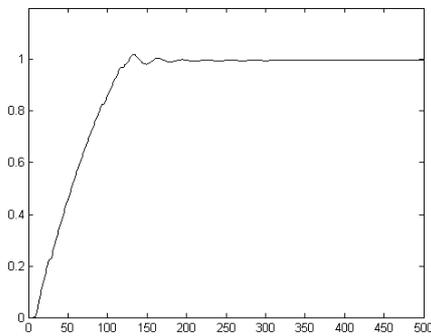


Figure 9: Response of FLCGS, deadtime = 3s

## STFLC DESIGN

Similar to the pervious FLC technique, the STFLC system is designed using MATLAB and Simulink. Two FLC's are required for the STFLC system, a PD-type FLC as the main control strategy and a FLC ( $\alpha$ -FLC) to compute the value of the scaling factor  $\alpha$ . The PD-type FLC used is identical to the one designed in Section 2, same input and output membership functions and rules apply.

Designing the  $\alpha$  FLC is similar to that of the PD-type FLC, in that it has the same two inputs,  $e$  and  $\Delta y$  but a different output  $\alpha$ . The shape and domain of the  $e$  and  $\Delta y$  membership functions are the same as the PD-type FLC but their size differs slightly, as can be seen from Figures 10 and 11. The membership functions for the output  $\alpha$  are symmetric triangles with equal base and 50% overlap with neighbouring membership functions, with a domain of  $[0, 1]$  as shown in Figure 12. The linguistic terms associated with the input variables are the same as that of the PD-type FLC but the linguistic terms for the output variable  $\alpha$  are:

$$\alpha = \{ze, \text{very\_small}, \text{small}, \text{small\_big}, \text{med\_big}, \text{big}, \text{very\_big}\}$$

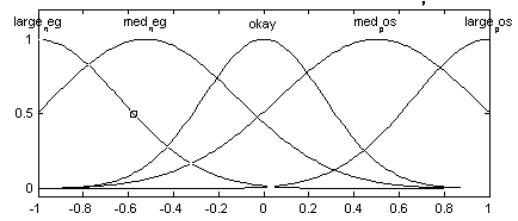


Figure 10: Input variable Error

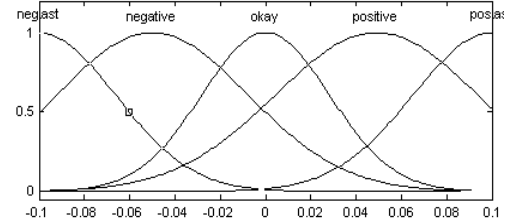


Figure 11: Input variable Rate

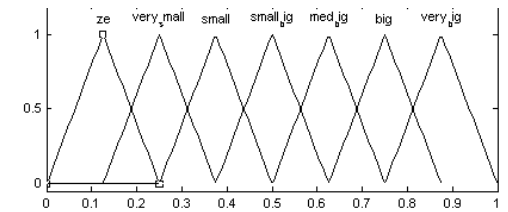


Figure 12: Output variable  $\alpha$

As can be seen from Figure 13, there are three gains (scaling factors) in the STFLC system, two input and one output. Determination of suitable values for these gains is made based on designer's knowledge of the workings of the process and sometimes through trial and error. The relationship between the gains and the input and output variables of the STFLC are as follows:

$$\begin{aligned} E_n &= G_e \cdot e \\ Y_n &= G_y \cdot \Delta y \\ U_n &= (\phi U_n \cdot G_u) \cdot \alpha \end{aligned}$$

The controller output for the STFLC is derived using the actual scaling factor ( $\alpha \cdot G_u$ ). The value of  $\alpha$  is determined from a rule-base, whose inputs are ERROR and RATE and its output is  $\alpha$  as described in the previous section.

When designing this rule-base, it is important to consider the classical closed loop performance trade-off. For example, setting the controller gain at a small value when the error is very big achieves a reduced overshoot and settling time, but must be coupled with an increase in rise time. In this situation the fuzzy rule will be as follows,

If error is *large\_pos* and rate is *negative* then  $\alpha$  is *VS*

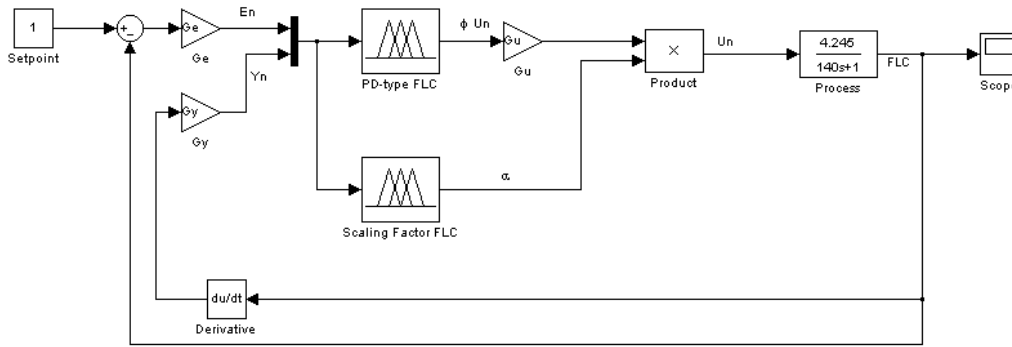


Figure 13: STFLC Block Diagram

### Tuning the Controller

The tuning of the STFLC requires a number of design steps given by,

1. The scaling factors of the STFLC must be tuned first. This is achieved by disconnecting the self-tuning FLC and adjusting the three scaling factors to yield a satisfactory output response.
2. The self-tuning FLC is then reconnected and the value of  $G_u$  scaling factor is increased to three times its value in step 1, keeping the values of the other two scaling factors the same. This value of  $G_u$  may be slightly adjusted to improve the performance of the controller at this point. At the end of this step a STFLC has been designed and tuned.
3. Depending on the response required, changes could be made to the rule base to achieve the output response needed. For example, if reduced overshoot is required, the value of  $\alpha$  should be kept very small up to the medium values of  $\alpha$ .

The fully designed STFLC was then tested using the mathematical model of the Tank Apparatus described in section 1. Figures 14, 15 and 16 show the output responses of the process with deadtimes of 0s, 0.5s and 1.5s respectively. These figures illustrate the effectiveness of the STFLC to efficiently track the setpoint. It was decided for these simulations to design the rules to keep the percentage overshoot as minimum as possible. However, this had the adverse effect of increasing the rise times.

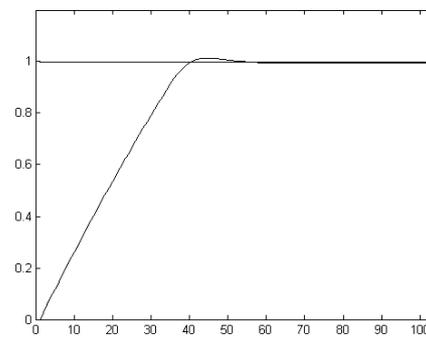


Figure 14: Response of STFLC, deadtime = 0s

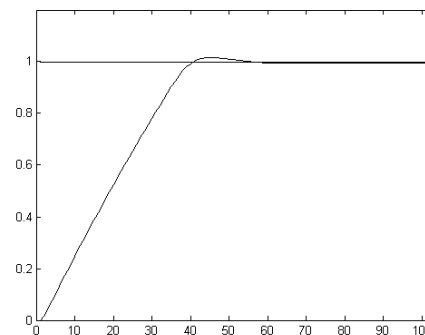


Figure 15: Response of STFLC, deadtime = 0.5s

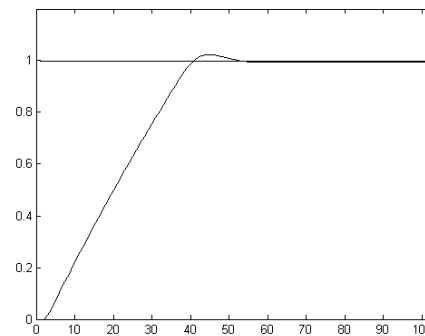


Figure 16: Response of STFLC, deadtime = 1.5s

### PERFORMANCE COMPARISON

The performance of the FLCGS is compared with the STFLC for the tank apparatus process. Several performance metrics such as, rise time, settling time, disturbance rejection and integral absolute error (IAE) are used to illustrate the difference between both controllers. The results of each metric will be tabulated for both controllers simulated with different values of deadtime. The performance of both controllers will then further compared with load disturbances.

The controllers were tested with three values of deadtime, i.e. 1s, 2s & 3s, a constant input and a load step disturbance of magnitude 0.3 at 150s. In Figures 17, 18 & 19 the solid curves represent the responses due to the STFLC while the dashed curves depict the responses due to the FLCGS. Table 2 illustrates the resulting performance metrics of both controllers with each value of deadtime. The performance of the STFLC exceeds that of the FLCGS for all operating conditions. One of the main differences to be observed is that the rise times of the STFLC did not vary with deadtime. However, the rise times of the FLCGS degraded with increasing deadtimes.

Table 2: Performance Analysis of the STFLC & FLCGS

FLC	Deadtime (s)	Rise Time (s)	Settling Time (s)	Time to Reject Disturbances (s)	IAE
FLCGS	1	41	54	33	31.41
STFLC	1	30	43	29	23.4
FLCGS	2	41	70	35	32.58
STFLC	2	30	45	30	24.78
FLCGS	3	83	125	66	57.75
STFLC	3	30	55	41	26.64

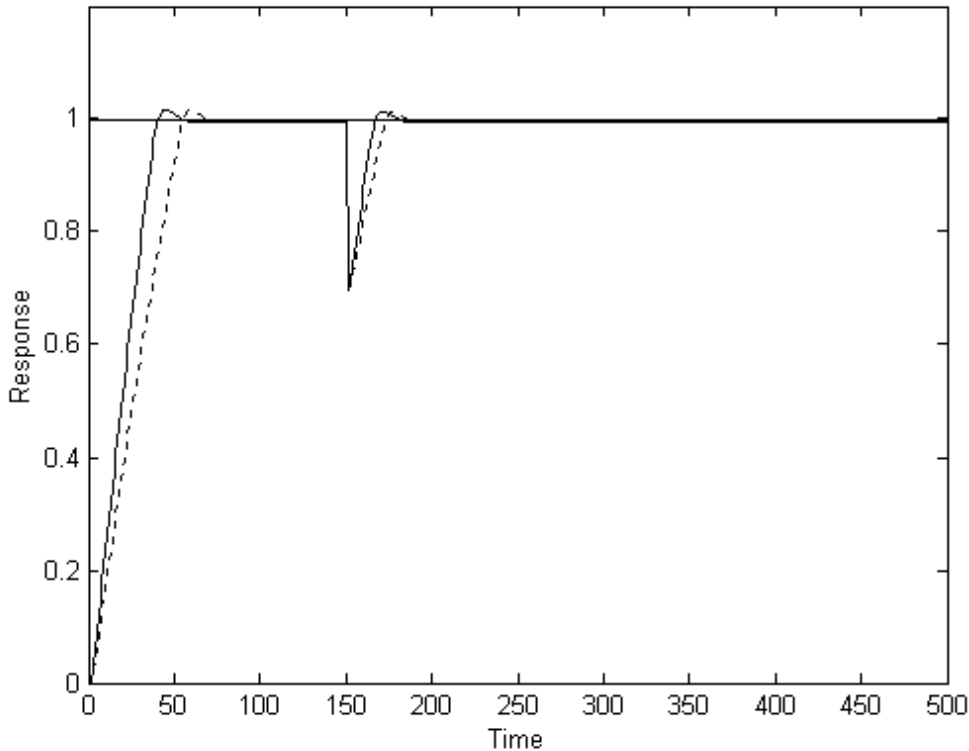


Figure 17: Response of the STFLC & FLCGS, deadtime = 1s

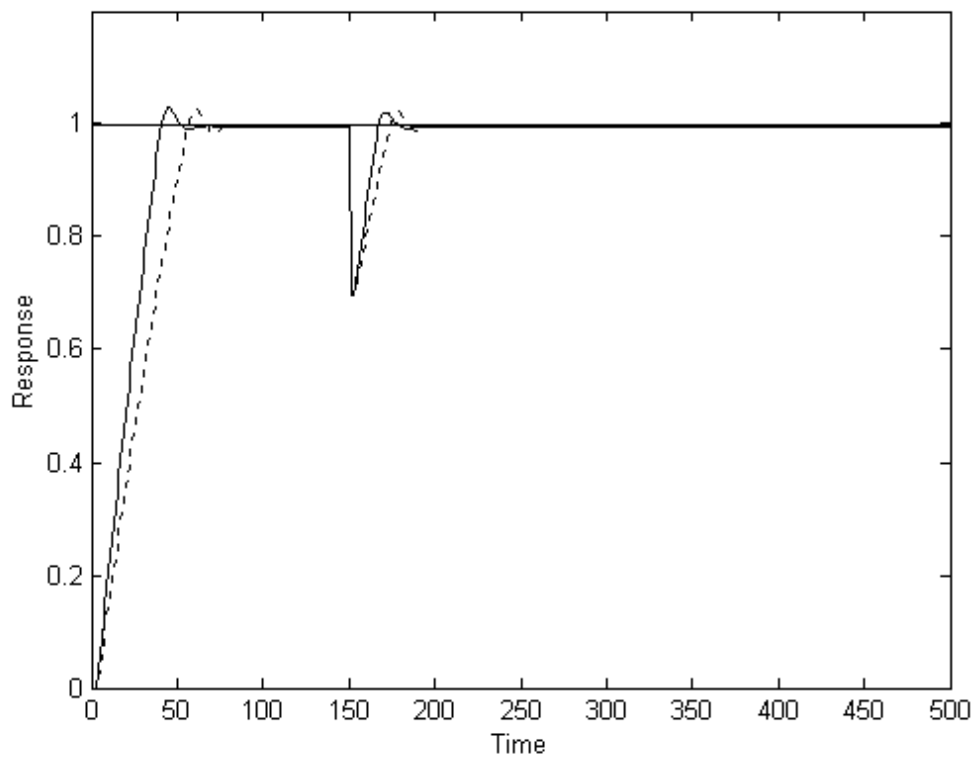


Figure 18: Response of the STFLC & FLCGS, deadtime = 2s

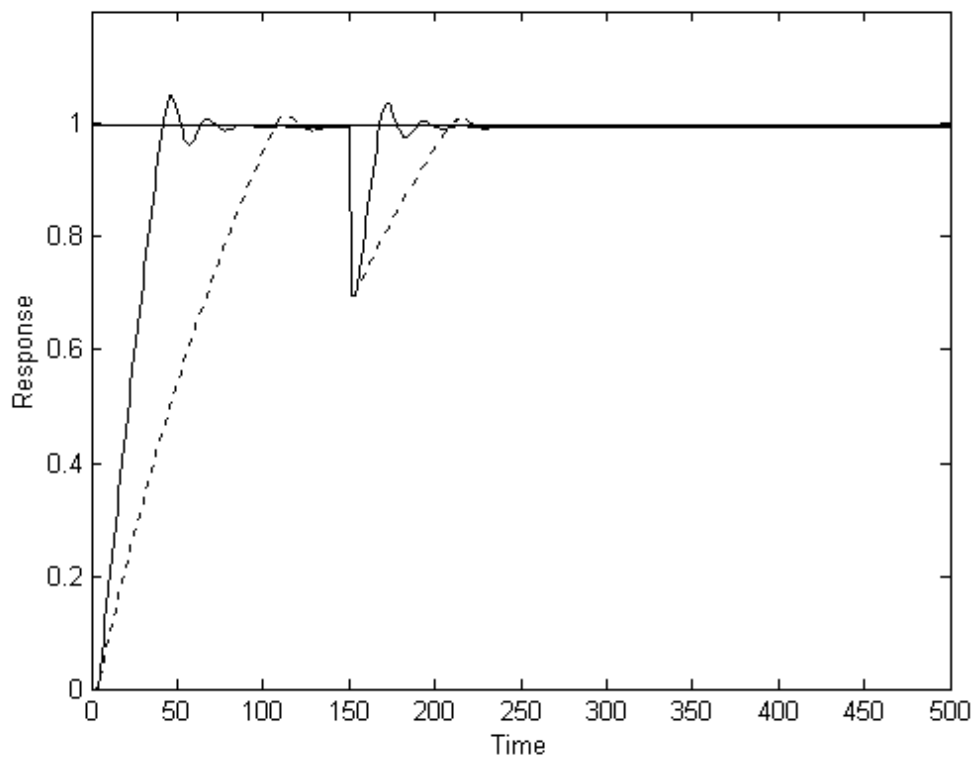


Figure 19: Response of the STFLC & FLCGS, deadtime = 3s

## CONCLUSIONS

This paper proposed the design of two different FLC's, the FLCGS and the STFLC, to minimise the effect of variable deadtime on a process. Minimisation of deadtime can be achieved in FLC's by scaling the control signal of the controller, by means of a controller gain. The two designs proposed use this technique, but the attractiveness of both designs is that they tune the controller gain on-line. The FLCGS measures the deadtime on process start-up and selects the appropriate gain to yield minimisation of the measured deadtime. On the other hand, the STFLC uses two FLC's, the first produces the control signal, while the other outputs a value of  $\alpha$ , which scales the control signal on each sampling instant. Both the controllers successively controlled the process for different values of deadtime. Results from a performance comparison between both controllers indicated that the STFLC exhibited better quality performance than that of the FLCGS.

## REFERENCES

- Chen, C.L. and Chen, W.C. 1994. "Fuzzy controller design by using neural network techniques." *IEEE Trans. Fuzzy Systems* 2, (3), 235-244.
- He, S.Z. Tan, S. Xu, F.L. Wang, P.Z. 1993. "Fuzzy self-tuning of PID controller." *Fuzzy Sets and Systems*, 56, 37-46.
- Homaifar, A. and McCormick, E. 1995. "Simultaneous design of membership functions and rule sets for fuzzy controllers using genetic algorithms." *IEEE Trans. Fuzzy Systems* 3, (2), 129-139.
- Jamshidi, M. et al. 1993. "Fuzzy Logic And Control." Prentice-Hall, Inc., NJ.
- Karr, C.L. and Gentry, E.J. 1993. "Fuzzy control of PH using genetic algorithm." *IEEE Trans. Fuzzy Systems* 1, (1), 46-53.
- Li, W. 1997. "A method for design of a hybrid neuro-fuzzy control system based on behaviour modelling." *IEEE Trans. Fuzzy Systems* 5, (1), 791-797.
- Ljung, L. 1987. "System Identification." Prentice-Hall, Inc., NJ.
- Maeda, M and Murakami, S. 1992. "A self-tuning fuzzy controller." *Fuzzy Sets and Systems* 51, 29-40.
- Mudi, R.K and Pal, N.R. 2000. "A self-tuning PI controller." *Fuzzy Sets and Systems*, 115, 327-338.
- Procyk, T.J. and Mamdani, E.H. 1979. "A linguistic self-organising process controller." *Automatica* 15, (1), 53-65.
- Ross, T. J. 1995. "Fuzzy Logic with Engineering Applications." Mc Graw Hill, E. U.
- Shao, S. 1988. "Fuzzy self-organising control and its application for dynamical systems." *Fuzzy Sets and Systems*, 26, 151-164.

# **MODELLING**



# MODELLING THE HYDRATION OF FOODSTUFFS

A.H. Weerts<sup>1</sup>, D.R. Martin<sup>1</sup>, G. Lian<sup>1\*</sup>, J.R. Melrose<sup>1</sup>

<sup>1</sup>Unilever R&D Colworth  
Sharnbrook, Bedford  
MK44 1LQ Bedfordshire  
United Kingdom

\*Corresponding author: guoping.lian@unilever.com

## KEYWORDS

rehydration, porous media, mass transfer, NMR measurements, biomaterials

## ABSTRACT

The rehydration kinetics of dried foodstuffs is of critical importance to their sensory properties and delivery of flavour and functional molecules. Based on the dynamics of capillary flow in partially saturated porous media, a finite element model is developed to predict the infiltration of water into dried food products taking into account temperature effects. The finite element model is based on the mixed form of the mass conservation equation. The constitutive relationships of water retention and hydraulic conductivity are adopted from the fields of hydrology and soil science. The transfer properties of water in the porous medium depend on the moisture content and the microstructure. This is contrast to the constant transfer properties often used in the heat and mass transfer models developed for foods. Rehydration of green tea as a function of Temperature has been simulated and results are compared with NMR measurements. There is good agreement.

## INTRODUCTION

Dried foodstuffs often need to be rehydrated before they are consumed. It is desirable that these foodstuffs hydrate as fast as possible and show adequate structural and chemical characteristics. Information about water absorption as a function of temperature of those food materials is critically important to their shelf life and product usage. Rehydration of food materials also has an important impact on their nutritional and sensorial properties.

A number of studies have been reported to model the hydration kinetics of foodstuffs and different types of models have been used. Two main approaches can be identified. One approach uses the empirical and semi-empirical models like for instance the Peleg and the Weibull equation (Machado et al., 1999; Machado et al., 1998; Lim et al., 1995; Sopade et al., 1992; Sopade and Obekpa, 1990; Peleg, 1988). The other approach employs diffusive models based on Fick's second law of diffusion (Sanjuan et al., 1999; Sanjuan et al., 2001; Thorvaldsson and Janestad, 1999; Simal et al., 2000; Hsu, 1983). Despite numerous studies using Fick's law to model liquid water transport in porous

foodstuffs, the liquid water movement cannot be simply defined as a diffusion process. Hydration occurs by capillary flow, driven by an energy potential gradient, rather than by diffusion. Some studies using capillary flow approach to model hydration and/or drying of foodstuffs have been reported recently (Ni et al., 1999; Feng et al., 2001; Irudayaraj and Wu, 1999; Turner and Jolly, 1991; Lian et al., 1997). However, the capillary flow approach is still not widely used.

The objective of this work is to show the feasibility of modelling the rehydration process of foodstuffs using the capillary flow approach applying constitutive relationships often used in soil science and hydrology. In particular, the effect of temperature is modelled. We first demonstrate that the effect of temperature on hydration can be directly taken into account in the constitutive properties. A finite element model is then proposed. As a model system of porous foodstuff, we use dried green tea leaf material (Sencha). Hydration behavior of green tea at various temperatures is investigated using time domain NMR. Consequently we compare our model predictions with the experimental data of green leaf tea hydration. For a range of temperatures studied, we find good agreement between the model prediction and the experimental data. More details of this work can be found in Weerts et al. (2002ab).

## THEORY

### *Capillary flow model*

We use the following mixed form of the unsaturated flow equations derived from the

mass conservation equation (Celia et al. 1991; Weerts et al., 2002ab)

$$\frac{\partial \theta}{\partial t} = \nabla \cdot (K \nabla h) - \nabla \cdot (K \sin \varphi) \quad (1)$$

where  $K$  (m/s)

$$K = \frac{k k_r \rho_w g}{\mu_w} \quad (2)$$

where  $k$  is the intrinsic permeability ( $\text{m}^2$ ),  $k_r$  is the relative water permeability, where  $\rho_w$  is the density of water ( $1000 \text{ kg/m}^3$ ),  $g$  is gravity ( $-9.81 \text{ m}^2/\text{s}$ ) and  $\mu_w$  (Pa.s) is the viscosity of water,  $h$  is the pressure head (m), or pressure in equivalent water column and  $\varphi$  is the angle away from the horizontal.

### *Constitutive Relationships*

To solve the equation of water transfer in partially-saturated porous media, constitutive relationships describing the relative water permeability and capillary potential are needed. Heat and mass transfer models developed for foods often assume simple Fick's diffusion theory applies. As a result, empirically-fitted weak constitutive relationships are often used. Here, the constitutive relationships adopted are physically-based and characteristic to porous media. We first introduce the water retention curves most often used in soil physics and hydrology. The water retention curve describes capillary potential of a porous medium as a function of moisture content and temperature. One of the commonly used equations in soil science is given by van Genuchten et al. (1980)

$$\frac{\theta}{\theta_s} = \frac{1}{[1 + |ah|^n]^m} \quad (3)$$

where  $h$  is the pressure head (m),  $\theta$  is the volumetric water content ( $\text{m}^3/\text{m}^3$ ),  $\theta_s$  ( $\text{m}^3/\text{m}^3$ ) is the saturated water content assumed to be equal to the porosity  $\phi$ ,  $\alpha$  ( $\text{m}^{-1}$ ) and  $n$  ( $>1$ ) are two parameters defining the shape of the water activity curve, and  $m=1-1/n$ . The water retention curve can be related to the water activity curve (Campbell et al., 1993; Gee et al., 1992) by using the Kelvin Equation:

$$h = \frac{RT}{\rho_w g M_w} \ln(A_w) \quad (4)$$

where  $A_w$  is the water activity,  $R$  is the gas constant and  $M_w$  is the molecular mass of water. The value of  $R/M_w$  is 0.461 MPa/K.

According to Mualem (1976), the relative permeability may be modelled by the following relationship as a function of water content and porosity

$$k_r = \left( \frac{\theta}{\theta_s} \right)^{0.5} \left( 1 - \left( 1 - \left( \frac{\theta}{\theta_s} \right)^{1/m} \right)^m \right)^2 \quad (5)$$

The viscosity of water depends on temperature. The relationship may be approximately described as follows (Thomas and King, 1992)

$$\mu_w = 661.2 (T - 229)^{-1.562} \times 10^{-3} \quad (6)$$

where  $T$  is the temperature in Kelvin.

## MATERIAL AND METHODS

### *Leaf tea hydration data*

Isothermal hydration experiments have been performed on green tea using Time Domain NMR. which is a well established technique for the measurement of rehydration kinetics of porous systems such as dried foods (Hills, 1998).

### *Tea leaf model*

The hydration of green tea was measured at different temperatures (288, 298, 308, 318, 328,338,348 K). Computer simulations of hydration have been also performed at these temperatures. The tea leaf is modelled as a two dimensional block of 0.0002 m by 0.0025 m, representing the average thickness and size of tea leaves.

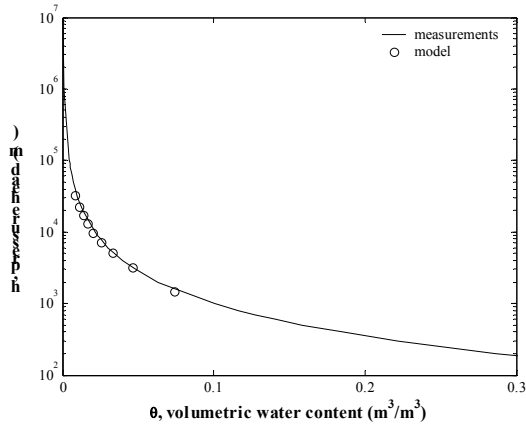
### *Water activity model parameters*

Water activity curves of tea were taken from Panchariya et al. (2001). Using the least square method, the data were fitted to equation (3) to obtain the values of  $\alpha$  and  $n$ . Extrapolation and interpolation between these water retention parameters as a function of temperature yielded the water retention curves at the temperatures of the hydration data.

### *Hydraulic conductivity*

From our study on the hydration of black tea as a function of tea leaf size (Weerts et al., 2002b), we know that the hydraulic conductivity in the horizontal direction (from the cut edges of the leaf) is much greater than that in the vertical direction (top-bottom), about 100-250 times. Here we assumed that the hydraulic conductivity in the horizontal directions is 125 times greater than that in the vertical direction. The hydraulic conductivity at saturation is calibrated on the hydration data obtained at 25 °C, the only temperature at which the water activity curve was also measured. Hydraulic conductivity at other

temperatures was directly predicted by substituting the viscosity equation (6) into (2).



## RESULTS AND DISCUSSION

Figure 1. Measured water activity data (Panchariya et al., 2001) and fitted water retention function as a function of water content at T=298 K.

Figure 1 shows the measured water activity data compared with the fitted water retention equation proposed by van Genuchten et al. (1980) at T=298K. The model fits the data well. Results at the other temperatures are similar. Figure 2 shows a comparison of the modelled and measured rehydration data at T=298K. The data at this temperature was used to calibrate the values of the hydraulic conductivity. The modelled hydration curve compares well with the measured data. The calibrated value of the hydraulic conductivity at saturation is  $10^{-11}$  m/s. This value of hydraulic conductivity is comparable to the value obtained by Weerts et al. (2002b) for black tea.

Figure 3 shows the predicted hydration of green tea at T=288 and T=308, 318, 328, 338, and 348 K. The measured data are also given in the figure for comparison. The predicted hydration curves agree well with the

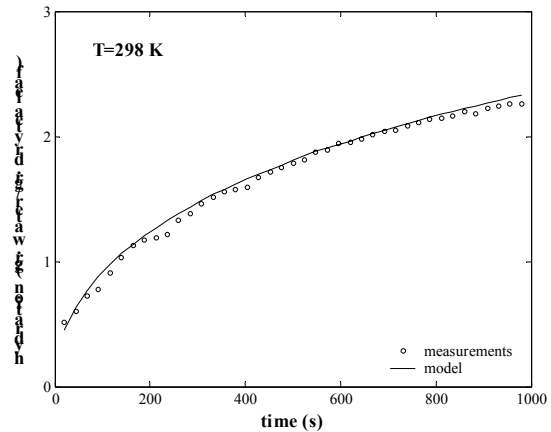


Figure 2. Comparison of the modelled (dots) and measured (circles) rehydration data on green tea at T=298 K as a function of time Temperature is indicated in the graph.

experimental measurements, suggesting that, by using the physically-based constitutive relationships, the effect of temperature can be directly predicted with good accuracy. The only model parameters that varied with temperature are the viscosity and activity (i.e. surface tension) of water. Their variations with temperature are well documented and are given by simple equations.

The experimental data of leaf tea hydration showed moderate variations in the equilibrium moisture content. There is no clear trend in terms of temperature effect. In the model, we assumed that the equilibrium moisture content was constant for all temperatures. This has resulted in some under and over predictions in the equilibrium moisture uptake at some temperatures. However, the differences are very small (<10%). Experimental studies on other foods stuffs showed that the equilibrium moisture content varied (decreased) as a function of temperature (Abu-Ghannam, 1998; Lim et al., 1995; Sanjuan et al., 1999). From the current hydration data of leaf tea, the effect of temperature on the equilibrium water uptake is not clear.

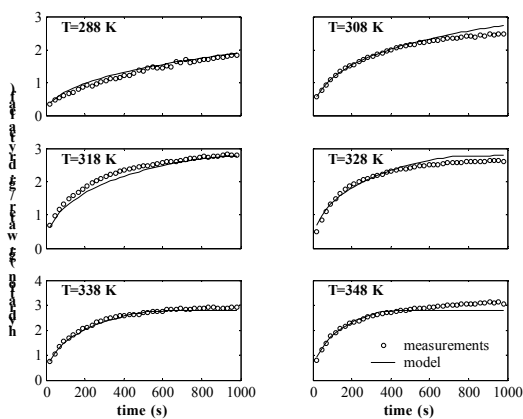


Figure 3 Comparison of the model predicted (dots) and measured (circles) rehydration data on green tea at T=288 and T=308-348 K as a function of time.

## CONCLUSIONS

Hydration of foods and biomaterials is greatly influenced by temperature. Presented in this paper is a mixed form of the unsaturated flow equation based on the capillary flow in porous media. Using this approach, the hydration of green tea at a range of temperatures has been successfully modelled. The predicted hydration curves agree well with the experimental data of NMR. The hydraulic conductivity of green tea was estimated to be  $10^{-11}$  m/s at 298 K in the horizontal direction (from the cut edges of the leaves). The hydraulic conductivity in the vertical direction is  $8.0 \times 10^{-14}$  m/s.

The mixed form capillary flow model presented in this paper directly predicts the effect of temperature on hydration. Increase in the hydration rate with temperature is due to mainly viscosity and surface tension of water contained in the physically-based constitutive relationships. The current model is apparently advantageous over the models based on so-called Fick's second law of diffusion. The

current model can easily be applied to model the hydration and dehydration of foodstuffs. Moreover, this approach can easily be extended to include the coupling with heat and solute transport

## LITERATURE CITED

- Abu-Ghannam, N., Modelling textural changes in the hydration process of red beans, *Journal of Food Engineering*, 38, 341-352 (1998).
- Campbell, G.S., J.D. Jungbauer, S. Shiozawa and R.D. Hungerford, A one-parameter equation for water sorption isotherms of soils, *Soil Sci.*, 156, 302-305 (1993).
- Celia, M.A. and P. Binning, A mass conservative numerical-solution for 2-phase flow in porous-media with application to unsaturated flow, *Water Resour. Res.*, 28, 2819-2828 (1992).
- Celia, M.A., E.T. Bouloutas and R.L. Zarba, A general mass-conservative numerical-solution for the unsaturated flow equation, *Water Resour. Res.*, 26, 1483-1496 (1990).
- Chen, P.S. and D.C.T. Pei, A mathematical-model of drying processes, *Int. J. Heat Mass Transfer*, 32, 297-310 (1989).
- Feng, H., J. Tang, R.P. Cavalieri and O.A. Plumb, Heat and mass transport in microwave drying of porous materials in a spouted bed, *AIChE J.*, 47, 1499-1512 (2001).
- Gee, G.W., M.D. Campbell, G.S. Campbell and J.H. Campbell, Rapid measurement of low soil-water potentials using a water activity meter, *Soil Sci. Soc. Am. J.*, 56, 1068-1070 (1992).
- Hills, B. *Magnetic resonance in food science*, J. Wiley and Sons, New York (1998).
- Hsu, K.H., A diffusion-model with a concentration-dependent diffusion-coefficient for describing water-movement in legumes during soaking, *J. Food Sci.*, 48, 618-624 (1983).
- Irudayaraj, J. and Y. Wu, Finite-element analysis of coupled heat, mass, and pressure transfer in porous biomaterials, *Numerical Heat Transfer Part A-Applications*, 26, 337-350 (1994).
- Irudayaraj, J. and Y. Wu, Heat and mass transfer coefficients in drying of starch based food systems, *J. Food Sci.*, 64, 323-327 (1999).
- Lian, G., C.S. Harris, R. Evans and M. Warboys, Coupled heat and moisture transfer during microwave vacuum drying, *Journal of Microwave Power and Electromagnetic Energy*, 32, 34-44 (1997).
- Lim, L.T., J.M. Tang and J.S. He, Moisture sorption characteristics of freeze-dried blueberries, *J. Food Sci.*, 60, 810-814 (1995).
- Lin, T.M., T.D. Duran and C.D. Scaman, Characterization of vacuum microwave, air and freeze dried carrot slices, *Food Res. Int.*, 31, 111-117 (1998).
- Machado, M.D., F.A.R. Oliveira, V. Gekas and R.P. Singh, Kinetics of moisture uptake and soluble-solids loss by puffed breakfast cereals

- immersed in water, *International Journal of Food Science and Technology*, 33, 225-237 (1998).
- Machado, M.F., F.A.R.Oliveira and L.M.Cunha, Effect of milk fat and total solids concentration on the kinetics of moisture uptake by ready-to-eat breakfast cereal, *International Journal of Food Science and Technology*, 34, 47-57 (1999).
- Mualem, Y., New model for predicting hydraulic conductivity of unsaturated porous-media, *Water Resour.Res.*, 12, 513-522 (1976).
- Ni, H., A.K.Datta and K.E.Torrance, Moisture transport in intensive microwave heating of biomaterials: a multiphase porous media model, *Int.J.Heat Mass Transfer*, 42, 1501-1512 (1999).
- Panchariya, P.C., D.Popovic and A.L.Sharma, Modeling of desorption isotherm of black tea, *Drying Technology*, 19, 1177-1188 (2001).
- Peleg, M., An empirical-model for the description of moisture sorption curves, *J.Food Sci.*, 53, 1216-&(1988).
- Sanjuan, N., J.A.Carcel, G.Clemente and A.Mulet, Modelling of the rehydration process of broccolli florets, *European Food Research and Technology*, 212, 449-453 (2001).
- Sanjuan, N., S.Simal and A.Mulet, Modelling of broccolli stems rehydration process, *J.Food Eng.*, 42, 27-31 (1999).
- Simal, S., A.Femenia, P.Llull and C.Rossello, Dehydration of aloe vera: simulation of drying curves and evaluation of functional properties, *Journal of Food Engineering*, 43, 109-114 (2000).
- Simunek, J., T. Vogel and M.Th. van Genuchten, The SWMS\_2D code for simulating water flow and solute transport in two-dimensional variably saturated media, *USSR, ARS, US Dept. of Agric., Riverside, USA, Research Report No 132*, (1994).
- Sopade, P.A., E.S.Ajisehiri and M.H.Badau, The use of pelegs equation to model water-absorption in some cereal-grains during soaking, *Journal of Food Engineering*, 15, 269-283 (1992).
- Sopade, P.A. and J.A.Obekpa, Modeling water-absorption in soybean, cowpea and peanuts at 3 temperatures using peleg equation, *J.Food Sci.*, 55, 1084-1087 (1990).
- Thomas, H.R. and S.D.King, Coupled heat and mass-transfer in unsaturated soil - a potential-based solution, *International Journal for Numerical and Analytical Methods in Geomechanics*, 16, 757-773 (1992).
- Thorvaldsson, K. and H.Janestad, A model for simultaneous heat, water and vapour diffusion, *Journal of Food Engineering*, 40, 167-172 (1999).
- Tiktak, A. and W.Bouten, Modeling soil-water dynamics in a forested ecosystem .3. model description and evaluation of discretization, *Hydrological Processes*, 6, 455-465 (1992).
- Turner, I.W. and P.G.Jolly, Combined microwave and convective drying of a porous material, *Drying Technology*, 9, 1209-1269 (1991).
- Van Genuchten, M.T., A closed-form equation for predicting the hydraulic conductivity of unsaturated soils, *Soil Sci.Soc.Am.J.*, 44, 892-898 (1980).
- Weerts, A.H., G. Lian, D. Martin, Modelling of hydration of foodstuffs: Temperature effects, Submitted to AIChE. (2002a)
- Weerts, A.H., G. Lian, D. Martin, Modelling of rehydration of porous biomaterials: Anisotropy effects, Submitted to *J. of Food Sci.* (2002b)

# MODELLING THE KINETICS OF TEXTURAL CHANGES IN HAZELNUTS DURING ROASTING

Ali Doğan Demir

Kevin Cronin

Department of Process Engineering

University College, Cork

Ireland

E-mail: a.demir@mars.ucc.ie

## KEYWORDS

Hazelnut roasting, Texture kinetics, Exponential Integral function.

## ABSTRACT

The texture changes in hazelnuts that were dry roasted at four temperatures (120, 140, 160 and 180 °C), for times ranging from 5 up to 60 minutes were studied using instrumental analysis. Textural changes were determined from the force deformation curves obtained from compression tests. The first break point of the maximum force (Newtons) was used as a measure of texture. The magnitudes of the parameters for a corresponding texture change model were determined using linear regression. Statistical analysis of the data showed that the change in texture with roasting time was represented by a first-order reaction. The reaction rate constants were assumed to have an Arrhenius-type dependence on temperature. The activation energy,  $E_a$  and the frequency (pre-exponential) factor,  $k_\infty$  were determined as 22.5 kJ mol<sup>-1</sup> and 0.338 s<sup>-1</sup> respectively. Theoretical equations, based on the Exponential Integral function ( $E_i$ ), to predict texture changes when product temperature is varying exponentially were developed. These equations were validated by comparison with the experimental data. The results of this study showed that both time and temperature effects were significant ( $p < 0.001$ ) on the textural changes in hazelnuts. The Exponential Integral prediction of texture change when product temperature varies during roasting was superior to the isothermal prediction throughout the process.

## INTRODUCTION

The most common form of nuts used in the food-processing sector are shelled nuts which undergo processes including blanching, dicing, roasting and grinding to fit product formulation needs or add consumer appeal. Roasting is one of the most important processes giving necessary alterations to the product. Currently, 17.5 % of commercially produced nuts throughout the world is hazelnut (*Corylus avellana L.*) production (Somogyi et al. 1996). One of the several objectives to hazelnut roasting is to alter and significantly enhance the flavour, texture, colour and appearance of the product. Roasting gives hazelnut a variety of texture and colours increasing the crispness and crunchiness (Özdemir and Devres 1999; Özdemir et al. 2001; Saklar et al. 1999). Roasted hazelnuts are widely consumed as an appetizer and as raw materials in sweets, confectionary, chocolate and biscuits. For the processing

industry and the catering business it is important to predict the roasting behaviour and the quality of hazelnuts.

During hazelnut roasting, the time-temperature relationship affects the resulting texture strongly, as well as other quality factors. In industry, hazelnuts are generally roasted at temperatures between 100 and 180 °C from 5 to 60 minutes (Özdemir and Devres 2000; Perren and Escher 1997). Low temperature roasting for long times can be considered as an iso-thermal process because for the majority of the process, the nut temperature is asymptotically equal to the air temperature after the short initial period. For this schedule, most of the quality changes that occur during roasting will take place during this 'iso-thermal' period. In high temperature roasting, as the required process time is much shorter and air temperature considerably higher, hazelnut temperature exponentially rises throughout the process and quality changes occur over the entire temperature range. Thus, a complementary model is required for systems in which the quality change occurs during both exponentially increasing temperature period and iso-thermal temperature period.

Force deformation curves have been widely used to measure textural changes in food products. Initial slope, maximum force, energy, fracture points or other curve-related parameters have been analysed and correlated with these textural parameters. In literature, the fracture points on force deformation curves have been named as maximum force, peak force or first peak of break (Saklar et al. 1999). First-order reaction kinetics and Arrhenius temperature dependence have been commonly used in evaluating the textural quality changes of thermally processed foods (Abu-Ghannam 1998; Verlinden and Baerdemaeker 1997). Califano et al. (1997) evaluated the hardness of cooked beef with a first-order kinetics equation to describe the textural changes during the cooking process. The texture changes of dry peas in long time cooking followed first-order reaction kinetics (Xie et al. 1998). Lau et al. (2000) showed that the thermal softening of green asparagus followed a first-order kinetic reaction. The texture change of potatoes during cooking was described using a first-order model (Verlinden et al. 1995).

In this study the textural changes occurring in hazelnuts during roasting were instrumentally measured using compression tests. The objective of this study is to determine the reaction kinetics to characterise textural changes defined by force deformation curves and to apply a theoretical formula using Exponential Integral function that can predict

the texture changes at both high temperature-short time (where hazelnut temperature exponentially increases) and low temperature-long time (where the temperature is isothermal) processes.

## THEORY

### Temperature Model

The thermal geometry of hazelnuts is regarded as a solid sphere placed at the centre of a fan oven. Heat transfer is by convection from the air and by radiation from the oven wall to the hazelnut. Mass transfer and shrinkage effects have been shown to be negligible on sun-dried hazelnuts. The temperature model consists of first term of the infinite series solution to the Fourier field equation for a sphere undergoing unsteady state heat conduction. Average hazelnut texture is the parameter of interest in the analysis of product quality and hence average temperature through the nut is required. The average temperature, of the hazelnut can thus be defined as (Ilicali 1989):

$$\bar{T} = (T_0 - T_\infty)A_1 e^{-r_c t} + T_\infty \quad (1)$$

where  $T_0$  is the initial hazelnut temperature and  $T_\infty$  is the air temperature in the oven. The thermal rate constant,  $r_c$  can be defined as:

$$r_c = \frac{\lambda_1^2 k}{\rho C_p r_0^2} \quad (2)$$

The equation constant  $A_1$  for the average temperature is:

$$A_1 = \frac{12(\text{Sin} \lambda_1 - \lambda_1 \text{Cos} \lambda_1)^2}{\lambda_1^3 (2\lambda_1 - \text{Sin} 2\lambda_1)} \quad (3)$$

where  $\lambda_1$  is the function of Biot number:

$$1 - \lambda_1 \text{Cot} \lambda_1 = Bi \quad (4)$$

and the Biot Number for the spherical geometry is:

$$Bi = \frac{h r_0}{k} \quad (5)$$

The heat transfer to the hazelnuts in the oven is a combination of both convective and radiative heating and thus the overall heat transfer coefficient,  $h$  is the sum of the convective and radiative heat transfer coefficients. Restricting the solution to the first term of the infinite series expansion of the Fourier equation places a lower limit of about 90 seconds on solution validity for these conditions (Çengel 1997).

### Texture Kinetics

The texture change of hazelnuts during roasting can be described using an  $n^{\text{th}}$  order model:

$$\frac{dF}{dt} = -k_R F^n \quad (6)$$

where  $F$  is the texture parameter (maximum force at the first fracture point) and  $k_R$  is the reaction rate constant. The effect of temperature on the reaction rate constant can be expressed using an Arrhenius type relationship:

$$k_R = k_\infty \exp\left(-\frac{E_a}{RT_\infty}\right) \quad (7)$$

where  $k_\infty$  is the frequency factor,  $E_a$  is the activation energy,  $R$  is the universal gas constant and  $T_\infty$  is the absolute oven temperature. For first-order reactions ( $n = 1$ ), Equation (6) can be solved introducing Equation (7):

$$F = F_0 \exp\left[-k_\infty \exp\left(-\frac{E_a}{RT_\infty}\right)t\right] \quad (8)$$

where  $F_0$  is the initial texture. The first-order model in Equation (8) can be linearized into the following form:

$$\ln\left(\frac{F}{F_0}\right) = -k_R t \quad (9)$$

### Non-isothermal Texture Change Model

Equation (8) predicts the texture change versus time once the product temperature is constant. For a non-isothermal process, replacing  $T_\infty$  with Equation (1) in Equation (7), and solving Equation (6) for a first-order process, the texture change can be predicted when the temperature is exponentially varying by Equation (10) (Demir et al. 2001):

$$F = F_0 \frac{\exp\left\{\frac{k_\infty}{r_c} \left[ E_1\left(\frac{E_a}{RT}\right) - \exp\left(-\frac{E_a}{RT_\infty}\right) E_1\left(\frac{E_a}{RT} - \frac{E_a}{RT_\infty}\right) \right]\right\}}{\exp\left\{\frac{k_\infty}{r_c} \left[ E_1\left(\frac{E_a}{R[(T_0 - T_\infty)A_1 + T_\infty]}\right) - \exp\left(-\frac{E_a}{RT_\infty}\right) E_1\left(\frac{E_a}{R[(T_0 - T_\infty)A_1 + T_\infty]} - \frac{E_a}{RT_\infty}\right) \right]\right\}} \quad (10)$$

The solutions of Equation (10) is valid for times where Fourier number is greater than 0.2. The function  $E_1$  is the Exponential Integral, which can be defined by:

$$E_1(x) = \int_x^\infty \frac{e^{-u}}{u} du \quad (11)$$

where  $x$  is a positive number. The Exponential Integral can be directly evaluated in packages such as MATLAB or MATHEMATICA and a large number of different approximations, based on simple polynomial and exponential functions, are available for different ranges of the argument (Abramowitz and Stegun 1970).

## MATERIALS AND METHODS

### Experimental Roasting Procedure

Sun-dried raw hazelnuts with skin were supplied. The skins of the hazelnuts were removed by applying hot glycerine-sodium carbonate solution before roasting. A digital vernier and a digital analytical balance (Bosch SAE 200) were used to measure hazelnuts radius and mass respectively. The average density value for hazelnuts was found by mass to volume ratio. The thermal properties of the hazelnuts were experimentally measured by a thermal properties meter (Thermolink Sensor Model TL-1) before the roasting process. Hazelnuts were placed in an incubator to guarantee an initial temperature of 20 °C. A Memmert ULP 600 conventional fan oven was used to carry out the roasting trials. Airflow in the oven was kept constant at 0.3 m s<sup>-1</sup> at the centre of the oven by a fan operating throughout

the experiments. The aim of the experiments was to obtain experimental hazelnut texture versus time curves at four different oven temperatures of 120, 140, 160 and 180 °C. These oven temperatures cover the commonly used temperatures in the hazelnut industry for roasting. From an initial batch of hazelnuts, sets consisting of five randomly selected hazelnuts were assembled. Each set was placed on a small table located at the centre of the oven. Each of the five hazelnuts was placed apart with no contact between each other to prevent any shielding effect on the nuts during roasting. A 1.5 mm diameter hole was drilled through one side of one of the five hazelnuts and a thermocouple inserted and sealed in there to measure the centre temperature and data-log by a computer. The reason for forming sets with five hazelnuts was to be able to eliminate any unexpected texture formation that could result. The roasting times were ranging from 5 min up to 60 min. As it was not possible to measure texture change on-line, the roasting trials were repeated with 5 min increments for each set. Each set was roasted at four different temperatures and same time combination to enable the texture versus time curves to be assembled. At the end of each experiment, the roasted hazelnuts were removed from the oven and placed in a freezer at 0 °C to prevent any further roasting and thus any textural changes after removing from the oven. They were cooled to room temperature and kept in an incubator at 4 °C until the texture analysis was undertaken off-line.

### Texture Measurements

The texture of the raw and roasted hazelnuts were measured using a computer interfaced JJ Lloyd Tensile Testing Machine (model T5K). A load cell of 500 N was mounted on the moving head of the tester. Each hazelnut kernel was placed on a small table in the longitudinal position. The same position was applied to all hazelnuts. Hazelnuts, which were not able to stand in that position, were slightly flattened on the bottom surface with sandpaper. The samples were compressed individually at a constant deformation speed of 10 mm min<sup>-1</sup>. The force deformation curves were recorded by a computer. Recorded data represents 260 hazelnuts. The force deformation curves were analysed for the first fracture point in Newtons and deformation in millimetres. The maximum force ( $F$ ) at the first peak of the break was used as the measure of texture.

### Statistical Analysis

The force ( $F$ ) data obtained from the experiments were analysed by analysis of variance technique (ANOVA) to find out the effect of time and temperature on those responses. From the two-way ANOVA technique, the sensitivity of  $F$  response was determined to time and temperature change (Devore and Farnum 1999). Hazelnut force versus time curves were available at four different temperatures. The fit of data to first-order model given by Equation (8) was assessed at each temperature by determining the coefficient of determination values using one-step regression in MATLAB. The slopes obtained from Equation (9) yield the reaction rate constants,  $k_R$  for each case. Having decided the order of reaction to represent the texture changes satisfactorily, the reaction rate constants were checked for the Arrhenius temperature dependence. In order to calculate the activation energy,  $E_a$  and the frequency

term,  $k_\infty$  two-step linear regression analysis was performed using the package MATLAB. The activation energy and the frequency factor were obtained from the slope and intercept defined by the Arrhenius equation.

## RESULTS AND DISCUSSIONS

### Physical And Thermal Properties

The average hazelnut radius,  $r_0$  was measured as 7.07 mm. The mean density,  $\rho$  value for hazelnuts was found as 875 kg m<sup>-3</sup>. Thermal conductivity,  $k$  of hazelnuts was measured as 0.204 W m<sup>-1</sup> K<sup>-1</sup>. Specific heat capacity,  $C_p$  was found to be 1994 J kg<sup>-1</sup> K<sup>-1</sup> (giving a thermal diffusivity,  $\alpha$  of 1.17\*10<sup>-7</sup> m<sup>2</sup> s<sup>-1</sup>). The overall heat transfer coefficient for hazelnuts in the oven was experimentally evaluated as 33.3 W m<sup>-2</sup> K<sup>-1</sup>. Using this data, the Biot Number for heat transfer to the hazelnut was evaluated as 1.15 meaning that the constants  $A_l$  and  $\lambda_l$  were 0.981 and 1.66 respectively. The thermal rate constant,  $r_c$  was calculated as 6.52\*10<sup>-3</sup> s<sup>-1</sup>.

### Texture Data Analysis And Reaction Order

Table (1) gives the results obtained from two-way analysis of variance (ANOVA). As can be seen from the values of temperature and time effects, the effect of temperature on the texture response force,  $F$  is greater than the time effect. The analysis showed that both time and temperature effects are significant ( $p < 0.001$ ) on the textural changes in hazelnuts. The texture response  $F$  demonstrated the highest sensitivity to temperature change.

Table 1: F-Statistics of the Time and Temperature Effects on the Texture Response,  $F$  from two-way ANOVA.

Texture Response	Force ( $F$ )
F-Statistics of temperature effect	48.97
F- Statistics of time effect	4.66
df (temperature - time)	3 - 11
Standard deviation, $\sigma$	13.35
Range	77.97
Coefficient of variation, $c_v$	0.45

The goodness-of-fit of first-order model with the experimental data was assessed from the coefficient of determination,  $R^2$  values at each temperature. The average  $R^2$  value was found to be 0.6912 indicating that the overall fit of the first-order reaction to  $F$  response was satisfactory at the temperatures applied. Hence the first-order reaction was selected to be the model representing the  $F$  response. The main reason for low  $R^2$  values was found to be the high variation between nuts at the roasting times and relatively small textural changes that occurs at the temperatures applied. The high variations in the experimental texture responses were due to the size, shape and ripeness of hazelnuts. There were other factors, which affect the variation in hazelnut texture. First of all, hazelnuts were not perfectly spherical and they did not have exactly the same shape and size. There was an internal cavity at the core of each nut, which is independent of the size and the shape of the hazelnut. The size of this cavity also varied between nuts. The first break point was dependent on this cavity, as a larger internal gap leads to a lower force whereas a smaller gap requires a greater force to break the hazelnut.

## Arrhenius Temperature Dependence

The Arrhenius temperature dependence of the reaction rate constants was checked with the plot of  $\ln(k_R)$  versus  $1/T$ . Figure (1) shows that the reaction rate constants obtained from the first-order model follows the Arrhenius equation well giving a coefficient of determination value of 0.9925. From the slope and intercept of the straight line described by the Arrhenius equation, the activation energy,  $E_a$  and the frequency term,  $k_\infty$  were determined as  $22.5 \text{ kJ mol}^{-1}$  and  $0.338 \text{ s}^{-1}$  respectively.

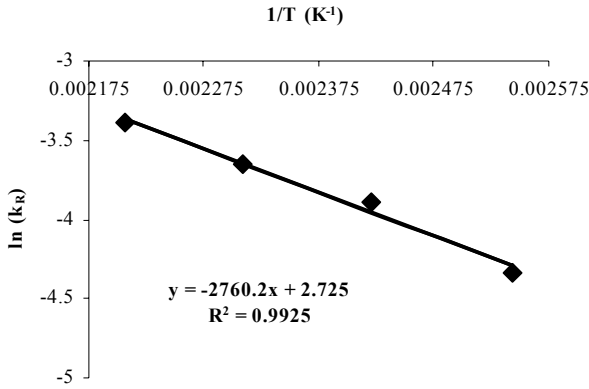


Figure 1: Arrhenius Temperature Dependence of Reaction Rate Constants.

## Validation Of Non-Isothermal Texture Change Model

Figure (2) shows the non-isothermal predictions of texture change versus time by Equation (10) with the experimentally measured ( $F$ ) values. The theoretical profile is given for times greater than 90 seconds corresponding to the lower limit on solution validity. The initial value of  $F$  was measured as  $66.35 \text{ N}$ . As can be seen from the figure, there is a good agreement between the experimental results and theoretical predictions of Equation (10).

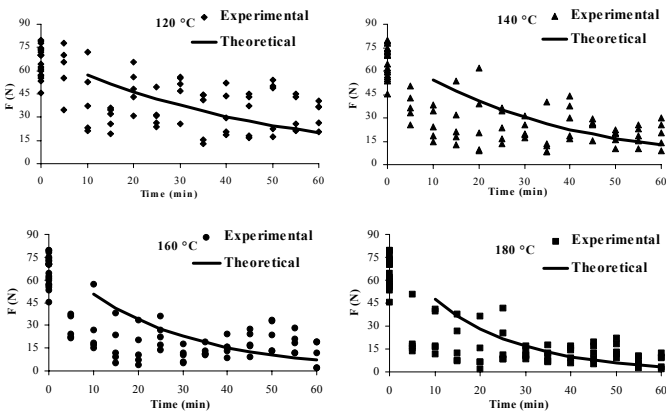


Figure 2: Non-isothermal Prediction of Texture Changes ( $F$ ) together with the Experimental Data.

Table (2) gives the one-way ANOVA results performed between the experimental data and theoretical predictions of Equation (10) at the times and temperatures studied. As it is seen in the table, the low mean square error values indicated that the theoretical prediction of the textural changes in hazelnuts was satisfactory. The p-values, which are different

than zero, showed that the mean values of experimental data were in good agreement with the predicted values.

Table 2: One-way ANOVA Results of the Experimental and Predicted Values of the Texture Response,  $F$ .

Texture	Force ( $F$ )			
	Temperature ( $^{\circ}\text{C}$ )	120	140	160
p-value	0.859	0.552	0.777	0.381
MSE	98.38	66.19	46.13	48.62
SS (interaction)	3475	4244	5940	5081
F-Statistics	3.21	5.83	11.71	9.5
df (temp. - time)	1-11	1-11	1-11	1-11

## CONCLUSIONS

The results of this study showed that the effect of both roasting air temperature and roasting times were significant on the textural changes in hazelnuts. The maximum force at the first fracture point was used to monitor the textural changes in hazelnuts during roasting. The texture response,  $F$  had higher sensitivity for temperature than the time change. Textural change represented by the maximum fracture force was a first-order reaction where the fit of the first-order model was found to be satisfactory. The reaction kinetic sensitivity to temperature was described well by the Arrhenius equation. The theoretical formula to predict the textural changes during the non-isothermal part of the roasting resulted in good agreement with the experimental data. The validation of Equation (10) using the Exponential Integral function showed that the theoretically predicted texture changes during the heating up (non-isothermal) part of the process was superior to the isothermal prediction.

Further research is required on the high temperature short time roasting of hazelnuts in order to obtain more information on the texture changes occurring in the non-isothermal part of the process that can be modelled by the application of the Exponential Integral function. The development of a validated texture model over a large roasting temperature range allows optimisation studies to be performed to determine the best roasting schedule in terms of delivering required product texture.

## NOMENCLATURE

$A_I$	Equation constant
$Bi$	Biot number
$c_v$	Coefficient of variation
$C_p$	Specific heat capacity ( $\text{J kg}^{-1} \text{K}^{-1}$ )
$E_a$	Activation energy ( $\text{kJ mol}^{-1}$ )
$E_I$	Exponential Integral function
$F$	Fracture force (Newton)
$h$	Overall heat transfer coefficient ( $\text{W m}^{-2} \text{K}^{-1}$ )
$k_\infty$	Frequency factor ( $\text{s}^{-1}$ )
$k$	Thermal conductivity ( $\text{W m}^{-1} \text{K}^{-1}$ )
$k_R$	Reaction rate constant ( $\text{s}^{-1}$ )
$n$	Reaction order
$r_0$	Radius (m)
$r_c$	Thermal rate constant ( $\text{s}^{-1}$ )
$R$	Universal gas constant ( $8.314 \cdot 10^{-3} \text{ kJ mol}^{-1} \text{K}^{-1}$ )
$R^2$	Coefficient of determination
$t$	time (s, min)
$T$	Temperature ( $^{\circ}\text{C}$ , K)

$\bar{T}$	Average Temperature ( $^{\circ}\text{C}$ , $\text{K}$ )
$u$	Exponential Integral function parameter
$x$	Exponential Integral function parameter

### Greek Symbols

$\rho$	Density ( $\text{kg m}^{-3}$ )
$\lambda_1$	Thermal model constant
$\sigma$	Standard deviation

### Subscripts

$\infty$	Asymptotic value
$0$	Initial value

### REFERENCES

- Abramowitz, M. and I. Stegun. 1970. *Handbook of Mathematical Functions*. Dover Publications, New York.
- Abu-Ghannam, N. 1998. "Modelling Textural Changes During the Hydration Process of Red Beans." *Journal of Food Engineering*, 38, 341-352.
- Çengel, Y.A. 1997. *Introduction to Thermodynamics and Heat Transfer*. McGraw-Hill, New York.
- Califano, A.N.; N.C. Bertola; A.E. Bevilacqua and N.E. Zaritzky. 1997. "Effect of Processing Conditions on the Hardness of Cooked Beef." *Journal of Food Engineering*, 34, 41-54.
- Demir, A.D.; J.M. Frias; K. Abodayeh; K. Cronin and F.A.R. Oliveira. 2001. "Modelling of the Thermal Kinetics of Colour Change in Hazelnuts During Roasting." In *Proceedings of the International Symposium on Applications of Modelling as an Innovative Technology in the Agri-Food-Chain* (Palmerston North, New Zealand, Dec. 9-13). Model-IT, Acta Horticulturæ, 566, 317-322.
- Devore, J.L. and N.R. Farnum. 1999. *Applied Statistics for Engineers and Scientists*. Duxbury Press ITP, Pacific Grove, USA.
- Ilicali, C. 1989. "A Simplified Analytical Model for Thawing Time Calculation in Foods." *Journal of Food Science*, 54 (4), 1031-1039.
- Lau, M.H.; J. Tang and B.G. Swanson. 2000. "Kinetics of Textural and Colour Changes in Green Asparagus during Thermal Treatments." *Journal of Food Engineering*, 45, 231-236.
- Özdemir, M. and O. Devres. 1999. "The Thin Layer Drying Characteristics of Hazelnuts during Roasting." *Journal of Food Engineering*, 42, 225-233.
- Özdemir, M. and O. Devres. 2000. "Kinetics of Colour Changes of Hazelnuts during Roasting." *Journal of Food Engineering*, 44, 31-38.
- Özdemir, M.; F.G. Seyhan; A.K. Bakan; G.Ö. İltter and O. Devres. 2001. "Analysis of Internal Browning of Roasted Hazelnuts." *Food Chemistry*, 73, 191-196.
- Perren, R. and F.E. Escher. 1997. "Investigations on the Hot Air Roasting of Nuts." *The Manufacturing Confectioner*, June, 123-127.
- Saklar, S.; S. Urgan and S. Katnas. 1999. "Instrumental Crispness and Crunchiness of Roasted Hazelnuts and Correlations with Sensory Assessment." *Journal of Food Science*, 64, (6), 1015-1019.
- Somogyi, L.P.; D.M. Barrett and Y.H. Hui. 1996. *Major Processed Products*. Technomic Publishing, Pennsylvania.
- Verlinden, B.E.; B.M. Nicolai and J.D. Baerdemaeker. 1995. "The Starch Gelatinisation in Potatoes during Cooking in Relation to the Modelling of Texture Kinetics." *Journal of Food Engineering*, 24, 165-179.
- Verlinden, B.E. and J.D. Baerdemaeker. 1997. "Modelling Low Temperature Blanched Carrot Based on Heat Induced Processes and Enzyme Activity." *Journal of Food Science*, 62, (2), 213-229.
- Xie, G.; R. Xiong and I. Church. 1998. "Modelling of Texture Changes of Dry Peas in Long Time Cooking." *Food Control*, 9, (4), 233-241.

### AUTHOR BIOGRAPHY

**ALI DOĞAN DEMİR** was born in 1974 in Turkey. He went to Middle East Technical University, Ankara, where he studied and obtained his B.E. degree in Food Engineering between 1993 and 1998. He has studied for a year in the Department of Environmental Science and Engineering, Technical University of Denmark. He started his Ph.D. degree in 1999 in the Department of Food Engineering, University College Cork, Ireland. Currently he is doing his PhD and working in the Department of Process Engineering, University College, Cork. Further information can be obtained from his e-mail address, a.demir@mars.ucc.ie or from the web address, which is <http://www.ucc.ie/acad/departments/foodeng/postgrad/dogandemir.html>.

**KEVIN CRONIN** was born in 1963 in Ireland. He went to University College Dublin where he studied and obtained his B.E. (Mech.) degree between 1980 and 1984. He got his Master of Engineering Science (M.Eng.Sc) degree in University College Dublin in 1984 and 1986. He obtained his Ph.D. (Mechanical Engineering) degree in 1988 and 1991 in Brunel University, UK. He worked in SKF, Engineering and Research Centre in Holland from 1986 to 1987. Between 1991 and 1994, he worked as a research officer in University of Ulster. Currently he is working as a lecturer in the Department of Process Engineering, University College, Cork. Further information can be obtained from his e-mail address, k.cronin@ucc.ie or from the web address in <http://www.ucc.ie/acad/departments/foodeng/staff/cronink.html>.

# MODELLING AND OPTIMISATION APPROACHES IN INDUSTRIAL FERMENTATION PROCESSES

T. Kurz  
S. Arnold  
M. Fellner  
E. Murnleitner  
M. Mitzscherling  
T. Becker  
A. Delgado

TU München / Weihenstephan  
Chair for Fluid Mechanics and Process Automation  
85350 Freising / Germany  
Phone: + 49 (0)8161 / 71-3247  
Facsimile: + 49 (0)8161 / 71-4510  
Mail: [T.Kurz@wzw.tum.de](mailto:T.Kurz@wzw.tum.de)

## KEYWORDS

Metabolic modelling, fuzzy logic, artificial neural network, software sensor

## ABSTRACT

In this paper different approaches for process modelling and control of industrial fermentations are presented. A method for the online determination of diacetyl is depicted. The concentration of diacetyl, a key component during the fermentation of beer, is estimated using an artificial neural network model (ANN). A metabolic kinetic modelling approach was used to describe the yeast propagation of brewing yeasts under industrial conditions. A similar approach was used for the description of the process behaviour of an industrial anaerobic wastewater treatment plant. Here, it served to evaluate the state detection and process control based on an adaptive fuzzy logic system. State detection and adaptive process control based on fuzzy logic was also applied in the beer fermentation. In another application fuzzy logic was used to adapt microorganisms to extreme conditions in the industrial vinegar fermentation to improve the acid yield.

## INTRODUCTION

In order to reach a precise, economic, and homogenous production in food and biotechnological industry an active process control is obligatory. Prerequisites of an active process control and process optimisation are the observability of the process and a comprehensive knowledge about the influence of manipulated variables upon the process behaviour or process variables. Observability here is defined as the possibility to receive relevant information from the process in order to describe the process behaviour comprehensively at every time. Particularly of interest in food and biotechnology is the online determination of biochemical substances, which normally are only measurable after a sample preparation using gas- or liquid-chromatographical methods.

Usually, biotechnology - and in particular food technology - is characterised by a high complexity of the matrix as well as dynamic and non-linear processes. Therefore, most of the processes and the matrix are not describable with mathematical methods in an effective way. However a lot of technological knowledge or large quantities of data exist, which can be used for cognitive approaches e.g. based on fuzzy-logic or artificial neural networks.

## THE COGNITIVE ESTIMATOR FOR DIACETYL

Diacetyl, an indirect by-product of yeast metabolism, is a key component in beer. It causes an off-flavour if its concentration exceeds a threshold of about 0.1 mg/L. Diacetyl and its precursors are present in beer during fermentation and maturation. The concentration of diacetyl is considered to be the most important criterion in the shortening of the maturation process, making its online determination of special economic interest. The current state of the art in diacetyl measurement technology is the off-line laboratory analysis using specially adopted headspace gas chromatography. The major disadvantages of this method are the high cost of the laboratory equipment, the required manual sample handling and pre-treatment and the delay of several hours before results are available. These disadvantages make this method unsuited for an on-line fermentation control. To date there are no alternative methods available.

There are, however, readily measurable process parameters which provide indirect information about the diacetyl concentration in the fermenting beer. The main physical and chemical process parameters used in our studies are temperature, specific gravity, pressure, turbidity and pH. In order to facilitate the estimation of the diacetyl concentration the cognitive estimator needs a model of the dynamic properties of the process and their dependence on the changes in diacetyl. Dynamic artificial neural networks were used in this project to deduce these properties from the available measurements. Since it was not sufficient to only use the current set of measurements, a measurement

history was used in order to internally reconstruct parts of the unknown process dynamics.

In the present problem a multilayer feed forward network was applied. A special neuron with a FIR filter was inserted at each connection (tapped delay line). A supervised method using the sum of the squared errors as the cost function was used to train the neural network. Gradient information was obtained using the IC-1 algorithm (instantaneous cost, instantaneous gradient), weight updates were calculated with different learning algorithms such as Rprop, SuperSAB and Quickprop. Reliable results, in terms of training time and convergence stability have been obtained in the prediction phase using these configurations. In Fig. 1 and 2 results of the “Cognitive Estimator” are presented. Fig. 1 shows the online estimation of diacetyl during the maturation exemplarily for two fermentations (line). Additionally the reference values are shown (points). It is obvious, that the ANN represents the reference values very well. Fig. 2 shows a parity plot of online and offline diacetyl determination. The “Cognitive Estimator” works not only during the maturation phase, but, as can be seen, over the whole range of possible diacetyl contents. Almost all points are within the marked tolerance range of 0.05 ppm, which is required from the online estimation to be used as an input for a closed loop control.

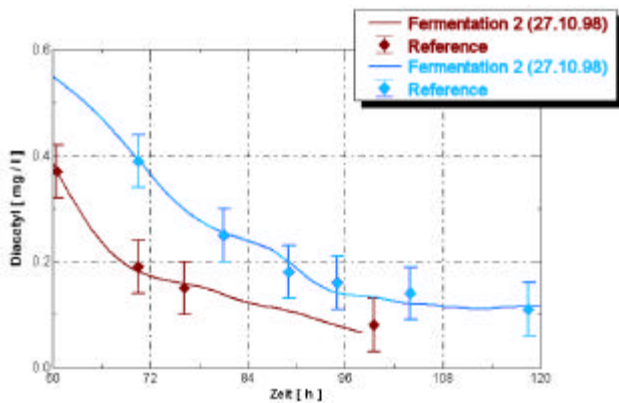


Figure 1: Online estimation of diacetyl

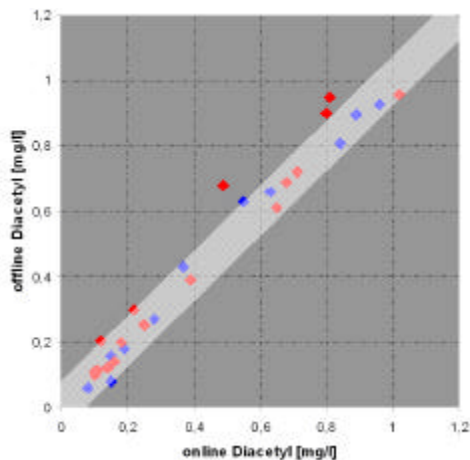


Figure 2: Parity plot of online and offline diacetyl determination

The system was adapted to online determination of diacetyl for an industrial beer fermentation. Based on the results obtained, it can be said that the accuracy and reliability of the software sensor is sufficient for practical applications.

## METABOLIC MODELLING OF BREWING YEAST PROPAGATION

For industrial yeast fermentations, e.g. brewing or baker’s yeast fermentations, it is essential to provide the inoculum at the right time in a desired quantity with a high fermentation activity, in order to guarantee an efficient fermentation process and high quality fermentation products. Therefore, in this work a comprehensive modelling approach of the fed-batch-wise yeast propagation is introduced. Also physiological data of a cell cycle analysis are correlated to experimental data. Both approaches represent the basis for a control strategy aiming at the provision of an optimal inoculum at the starting time of subsequent fermentations. In the presented metabolic modelling approach (formulated with the software tool ‘Aquisim’) respiratory metabolism on sugars and ethanol and fermentative metabolism respectively, are included. Occurring limitations, due to specific nutritional data of the beer-wort, were taken into account for sugars, nitrogen, ethanol and oxygen. Correspondingly, inhibitions of the metabolism by ethanol and high sugar concentrations were formulated. Especially the Crabtree-effect is represented by the model. For model identification, literature data were used and selected experiments out of the relevant range of manipulated variables (temperature, dissolved oxygen) were carried out. Model based simulations matched these data with an accuracy of 2-8% with standard deviations of 5% after an adaptation of three variable parameters, which were extracted in a sensitivity analysis before. A relation between the temperature and the variable parameters could be formulated. The influence of oxygen, in particular at low concentrations (oxygen limitation) could be quantified too. So, predictive simulations of the yeast propagation process using non isothermic trajectories were possible. Figure 3 presents a case scenario for a brewery, where the yeast propagation process has to be delayed for several hours.

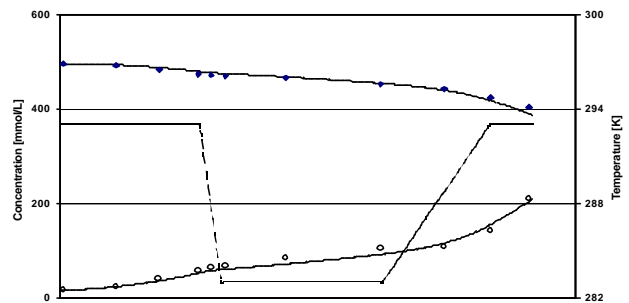


Figure 3: Application of a temperature scenario for the yeast propagation process.

A temperature profile (20-10-20°C) was applied (dotted line). Reference values for the progressions of biomass (○) and substrate (◆) and the model based predictive

simulations (lines) of the concentrations of biomass and substrate (as glucose equivalents) for the given temperature profile are presented. The change of temperature caused a deceleration and acceleration respectively of the propagation process, which can be found in the progressions of the reference values as well as in the belonging predictive simulation runs. The accuracy of the simulation was about 8% with standard deviations of 7%. Also in other scenarios applying temperature and dissolved oxygen profiles it could be shown, that with a precise adjustment of trajectories the crop time of the inoculum could be varied within a period of 7 to 50 hours while maintaining a high fermentation activity for the subsequent anaerobic fermentation. In the same way the actual physiological state could be comprehended by evaluation of cell cycle analysis and correlation to experimental data. So, a basis for a reliable process optimisation could be established, which takes into account biomass growth as well as information on the physiological state of the biomass.

### THE FUZZY-LOGIC FERMENTATION CONTROL

The main topic of interest was to realise an active process control for the fermentation of beer. As a lot of technological knowledge exists, the use of fuzzy logic for a process control suggested itself. The implemented system combined a process state (fermentation phase) detection module and a process control module based on fuzzy logic. In addition to the online measurement of physical or chemical values it was necessary to record information about biochemical values by integrating the described "Cognitive Estimator".

The gained values of online measurement and estimation are used as input for the fuzzy logic fermentation phase detection. The result is the actual fermentation phase like "main-fermentation" or "maturation". The well known coherences between input data and the fermentation phase are described in rules.

A second fuzzy logic system for the control of the fermentation uses the absolute deviation of the measured data from given set curves of defined partial processes as the input. Dependent on the input data and the detected fermentation phase the manipulated variables (temperature, pressure) can be adjusted.

In Fig. 4 the scheme of the fuzzy system is presented. Data from online measurement is used to determine the fermentation phase. A superimposed control system uses the detected phase and the deviation of the online values from given set curves. The systems tries to steer the process towards the set curves by manipulating temperature and/or pressure.

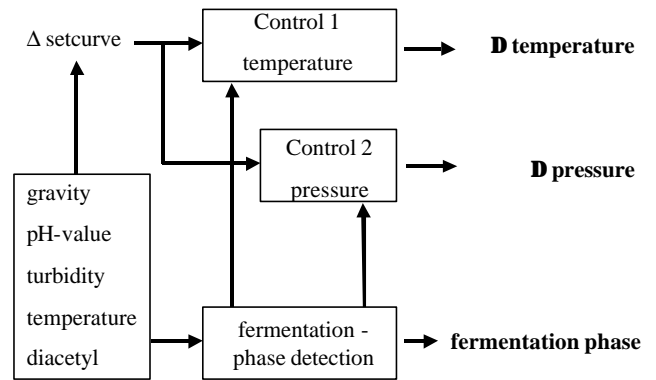


Figure 4: Scheme of the fuzzy system

The fuzzy logic fermentation phase detection worked very robust and reliable. Even trials with simulated failures of measurement values produced sufficient results. By using this fuzzy system it was possible to reduce the complete fermentation time up to 25%, by an automatic change between the fermentation phases in the sequential control. The superimposed closed loop control resulted in an increased process homogeneity. The process spread of gravity could be reduced to 50%.

### ANAEROBIC WASTEWATER TREATMENT WITH FUZZY LOGIC

For an efficient anaerobic wastewater treatment, supervision by highly qualified staff or a proper process control is required, particularly if the volumetric loading or the substrate composition is variable or if toxic inhibition can occur.

However, anaerobic treatment is difficult to control, because a system overload can halt the process, whereby a system restart can take up to weeks. Fuzzy logic was used to model and control the process, because qualitative or semi-quantitative expert knowledge is available. Moreover, states like "hydrogen is normal" and "hydrogen is high", which cannot be distinguished sharply because the transition from "high" to "normal" is not well known (it is fuzzy), are handled with the Fuzzy logic's concept of partial truth. Hydrogen was chosen as the key parameter for the detection of an overload, as its concentration increases sharply after an overload. Not only the hydrogen concentration, but also pH, the first derivative of pH, the concentration of methane, the gas production rate, and – if necessary - also the concentration of organic compounds (TOC, COD, or BOD) are used as input variables.

With these variables, the state of the reactors, like "shortage", "normal", "overload", "toxic" is estimated. Using these biological states together with the current reactor conditions (e. g. acidification buffer tank is full), the conditions are altered or the feed rate is changed. The conditions are influenced by changing temperature, pH, velocity of circulation and the recirculation rate.

In Fig. 5 data from a two stage anaerobic treatment of potato processing waste water are shown. The first graph shows the feed rate into the acidification buffer tank (divided by the methane reactor volume) and its fuel level.

The latter is the result of the feed and the control action. Gas concentrations in the methane reactor are depicted in the second graph (% methane, ppm hydrogen, and the gas flow normalised by the volume of the methane reactor). The third graph shows truth values (membership value) of the sets from the state of the methane reactor (--- shortage, — normal, — overload). As shown in the third graph, the states could be predicted well, so proper control actions could be taken, too. Additionally a kinetic modelling approach was developed to allow simulation runs and to evaluate the process state detection and control.

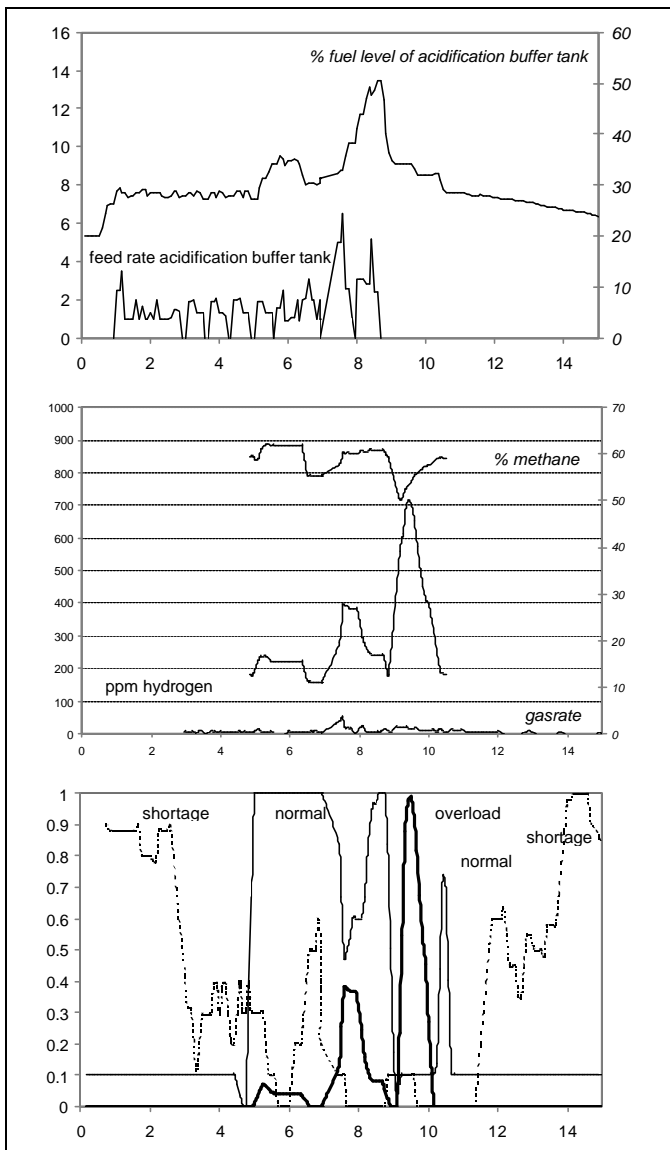


Figure 5: Data from a two stage anaerobic treatment of potato processing waste water

### FUZZY-LOGIC CONTROL STRATEGIES FOR THE “VIRTUAL VINEGAR BREWER”

In this fuzzy logic approach process data from a two-stage vinegar fermentation, prepared or directly measured, provide the input values for an expert knowledge based fuzzy control system. This "virtual vinegar brewer" allows

the consideration of available know-how for situational set point management. The fuzzy module as the cognitive core of the computational system was adapted to the acetic acid fermentation by setting up a specific structure of input variables, rule bases and output variables. This structure (Fig. 6) bases on expert knowledge collected in reports and interviews, combined with experimental data.

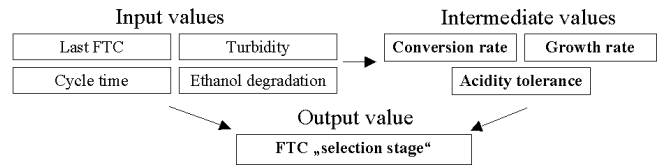


Figure 6: Structure of the fuzzy system

The final total concentration (FTC) was considered as the manipulated variable. This value can be regarded as a measure for the maximum stress conditions or selection acid concentration. As input information for the fuzzy system physical measurement data of two bygone fermentation cycles were logged and prepared (FTC, cycle time, degradation rate, turbidity development). This input information is processed in a multilevel rulebase, where intermediate variables are calculated. The intermediate variables enable a “fuzzy” grading of the two bygone cycles by respecting the conversion rate, the growth rate and the not directly measurable value “acidity tolerance” of the bacteria. Finally from these intermediate variables it is decided, whether “selective conditions” or “recovering conditions” should be chosen for the culture in the following cycle. This is done by setting the FTC value for the following cycle. Preliminary fermentation tests and the results of expert questionnaires showed clear limits. It is not possible to choose too much acidity stress, especially after several cycles, without losing average productivity.

After refining the parameters of the fuzzy system in respect to further fermentation experiments, both focused factors - a better conversion rate and a higher product concentration - could be improved.

Conventional process strategies are able to reach about 18,5% product concentration in a two stage configuration. As illustrated in Fig. 7a, immediately after a first selection cycle by forcing up the FTC, the final concentration in the second stage could be risen to 19,2%. Instanting the fuzzy managed fermentation serial given in Fig. 7b, two selection cycles with a higher FTC were determined. In this case the fermentation temperature was not kept on a constant level. It was lowered with the increasing inhibition of the microorganisms, respectively with decreasing conversion rate. After three cycles with situational inhibition of the biological material, an increase in the fourth cycle from 19,6% to nearly 20% final acetic acid concentration indicated an improvement by selection effects. In the 5th cycle, the final acidity could be lifted to more than 20,3%, combined with a shortened cycle time. These improvements could be reproduced in all cases after selection cycles with a calculated FTC in the first stage.

According to practical experience, the productivity of a vinegar plant can decrease seriously, if the FTC is forced up

merely 0,2% and is kept for several cycles. With respect to this, the performed increase of 2% in the maximum product concentration with the same given apparatuses is remarkable.

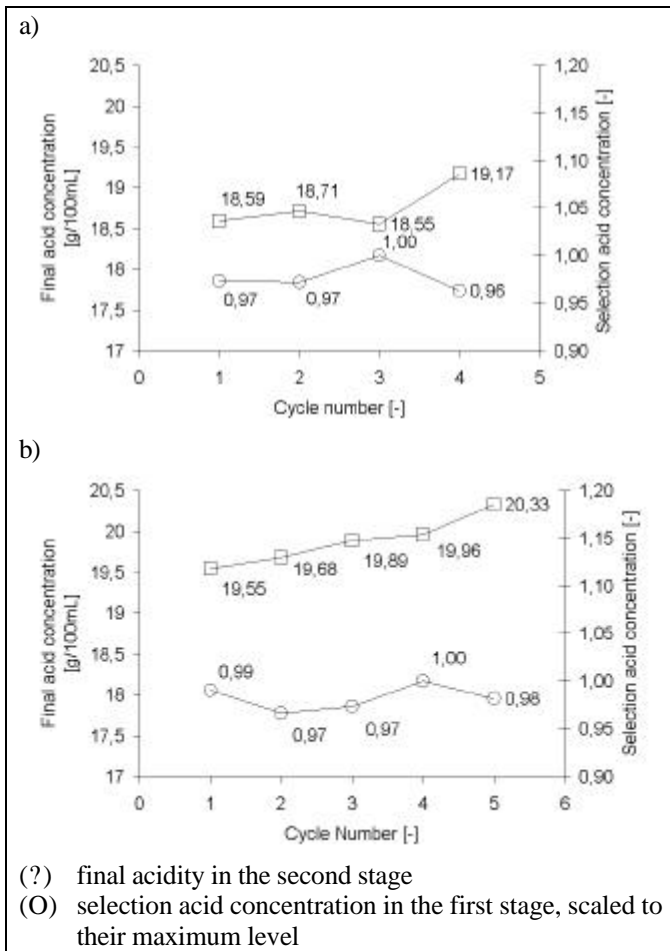


Figure 7: Effect of fuzzy moderated selection acidity in the first stage on finally reached acid concentration in the second stage

## CONCLUSION

The paper shows that mathematical and cognitive approaches can be used in many fields of biotechnology and food-technology. Main topic in the future will be the

development of hybrid approaches. Especially the integration of mathematical or technological knowledge in the learning process of ANN is suggested. This allows to improve the accuracy of process predictions. On the other hand fuzzy logic systems should be developed or adapted which use self generating methods for rules or sets. With these methods it would be possible to obtain technological knowledge about processes, which was not accessible so far, since most of the considered processes could only be modelled by black box approaches. In particular, the description of the actual physiological state based on knowledge based expert systems is a main topic in current research. Hence, it can be stated that there is still a high potential of implementing modelling and optimisation algorithms in various problems of food technology.

## REFERENCES

- Arnold, S.; R. Schmidt and T. Becker. 2001. "Online determination of Acetic acid during an aerobic acetobacter cultivation." *Anal. Chim. Acta*, submitted.
- Murnleitner, E.; T. Becker and A. Delgado. 2001. "State Detection and Control of Overloads in the Anaerobic Wastewater Treatment using Fuzzy Logic." *Water Research*. accepted.
- Kurz, T.; T. Becker and A. Delgado. 2002. "Model based control of the metabolism of saccharomyces cerevisiae under growth limiting conditions." *Journal of Biotechnology*. submitted.
- Fellner, M.; A. Delgado and T. Becker. 2001. "Functional neurons in dynamic neural networks for bioprocess modelling." *Bioprocess and Biosystems Engineering*. submitted.
- Murnleitner, E.; A. Delgado and T. Becker. 2001. "Simulation and optimisation of a two stage anaerobic digestion using knowledge based methods." *Journal of Hydroinformatics*. submitted.
- Arnold, S.; T. Becker; A. Delgado; F. Emde and A. Enenkel. 2001. "Optimizing high strength acetic acid bioprocess by cognitive methods in an unsteady state cultivation." *Journal of Biotechnology*. submitted.
- Murnleitner, E.; A. Delgado; T. Becker: 2001. "Optimisation and validation of a fuzzy-based closed-loop control strategy using a dynamic simulation model." *Biotechnology and Bioengineering*. submitted.
- Kurz, T.; M. Fellner; T. Becker; A. Delgado. 2001. "Observation and control of the beer fermentation using cognitive methods" *Journal of the Institute of Brewing* 107, No. 4, 241-252.

# MODELING OF THE COOKING LOSSES DURING THE COOKING OF BEEF PATTIES USING FAR INFRARED RADIATION

Nicholas Shilton<sup>1</sup>, P. Mallikarjunan<sup>2</sup>, P. Sheridan<sup>3</sup>

<sup>1</sup> Department of Agricultural and Food Engineering, University College Dublin, Earlsfort Terrace, Dublin 2, Ireland. <sup>2</sup> Department of Biological Systems Engineering, Virginia Polytechnic Institute and State University, Blacksburg, VA, 24061. <sup>3</sup> Waterford Institute of Technology, Waterford, Ireland

## KEYWORDS

Food, Biology, Differential equation solvers, Model testing.

## ABSTRACT

During the cooking of beef patties, material is lost from the patty by two mechanisms. The first is evaporation of water, which can easily be described by standard drying theory, while the second mechanism is the expression of juices from the patty during cooking. These 'juices' will contain a significant amount of fat and moisture in addition to proteins, and can be characterized as 'cook losses'. The objective of this study is to investigate the moisture and fat losses from beef patties during cooking by far infrared radiation and to develop a model to describe these cooking losses. Fresh minced beef patties were prepared at 2 different fat levels, (15% & 22 % fat). These were cooked using a far infrared radiation heat source for 20 minutes. The resulting data was modelled using a coupled finite difference model to predict heat transfer, moisture losses and fat losses. Results showed heat and mass transfer profiles similar to those found in similar studies. Good agreement was found in the prediction of heat transfer, moisture losses and fat losses. The model also showed that internal movement of the fat through the beef patty influences heat transfer through the beef patty. This paper describes a simple model that is suitable for the prediction of heat and mass transfer during the cooking of beef patties.

## NOMENCLATURE

$C$	Moisture content (kg moisture / kg solid)
$D_{eff}$	Mass diffusivity ( $m^2.s^{-1}$ )
$D_x, D_T, D_C$	Constants in Equation 12
$h$	Heat transfer coefficient ( $W.m^{-2}.K^{-1}$ )
$h_{eff1}, h_{eff2}$	Constants in Equation 8
$k$	Thermal conductivity ( $W.m^{-1}.K^{-1}$ )
$k_1, k_2, k_3$	Constants in Equation 6
$Km$	Mass transfer coefficient ( $m.s^{-1}$ )
$r_1, r_2, r_3$	Constants in Equation 7
$t$	Time (s)
$T$	Temperature (K)
$T_\infty$	Infinite temperature (K)
$x$	Thickness of beef patty (m)

## Greek Letters

$\alpha$	Thermal diffusivity ( $m^2.s^{-1}$ )
$\rho$	Density ( $kg.m^{-3}$ )
$\sigma$	Stefan Boltzmann constant ( $W.m^{-2}.K^{-4}$ )

## Subscripts

f	Final
s	Surface

## INTRODUCTION

During the cooking of beef patties, material is lost from the patty by two mechanisms. The first is by evaporation of water, which can easily be described by standard drying theory. The second mechanism is the expression of juices from the patty during cooking. These 'juices' will contain a significant amount of fat and moisture in addition to proteins, and can be characterized as 'cook losses'. The total amount of product remaining can be viewed as the 'cooking yield'. Some researchers will refer to the 'cook loss' as being a combination of vaporized losses and juices.

Previous papers, (Sheridan and Shilton, 2002a; Shilton *et al.*, 2002) have described moisture losses due to evaporation and the simulation of these losses, in this paper the cook losses in terms of total moisture loss and the fat loss will be described and simulated. Sheridan (2000) found that as fat content of beef patties increased, so did the amount of fat in the cook losses. A number of different researchers have examined the affect of increasing fat content on the fat losses from beef patties during cooking by a variety of methods including grilling (Troutt *et al.*, 1992; Sheard *et al.*, 1998; Kirchner *et al.*, 2000). These researchers were mainly examining the affects of the cooking process on the chemical and sensory properties of the beef patties, no modelling of the cooking process was included. The fat contents examined ranged from 0% to 50% added fat. The affect of using far infrared radiation was not examined by any of the above researchers. Andersson *et al.*, (2000) report that loss of fat during the frying of beef patties increases linearly with fat content.

Due to the risk of food poisoning by *E. coli* O157:H7 from undercooked beef patties it is important to heat such products so that they are

cooked thoroughly. There have been a number of models proposed for the cooking of beef patties that account for heat transfer (Pan *et al.*, 2000; Shilton *et al.*, 2002). The Food Safety Authority of Ireland recommends that the internal temperature exceed 70 °C for 2 minutes (Food Safety Authority of Ireland, 1999) to ensure adequate cooking and thermal destruction of micro-organisms. It has also been postulated that heat transfer in beef patties is influenced by the movement of fat during cooking (Shilton *et al.*, 2002), thus the model developed in this paper will account for this.

The objective of this study is to investigate the moisture and fat losses from beef patties during cooking by far infra red radiation and to develop a model to describe these cooking losses, while also accounting for heat transfer.

## MATERIALS AND METHODS

Minced meat (fat content 15% & 22%) was obtained from a local supermarket. Beef patties were prepared by pressing the minced beef into round stainless steel sample holders, (50 mm internal diameter, 20 mm depth). The sample holder was placed on a wide mesh (5 mm), and was allowed to sit on a drip tray to collect cooking losses. Holes at 8 and 12 mm were drilled in the side of the sample holder, to allow for the radial insertion of thermocouples. The temperature was recorded using type T thermocouples, with data being collected by a datalogger (Campbell Scientific 21X; Campbell Scientific Inc., Logan , Utah) every 30 s.

Samples were cooked for 5, 10, 15 and 20 minutes using a far infrared heater. Once the cooking cycle was complete the cook losses were measured.

The cooked samples were sliced into 3 samples along the longitudinal axis on cooling, representing the top, middle and bottom of the beef patty. The top slice represents the portion of the beef patty closest to the far infrared heat source, whereas the bottom slice represents the portion of the beef patty furthest away from the heat source during cooking. Proximate analysis was carried out in order to determine the moisture and fat profiles in the different slices during cooking. The moisture and fat content of the sliced beef patties was determined using AOAC methods (AOAC, 1990).

### Far infrared heater

Samples were cooked in a far infra oven, with internal dimensions; height 330 mm, width 330 mm and depth 340 mm. The heating element consisted of a far infrared gas catalytic heater (Bruest Flameless Catalytic Heater S12-12FM; Catalytic

Industrial Group, Independence, Kansas) mounted in the roof of the oven. Samples were placed 75 mm below the heating element for the duration of the cooking time.

### Mathematical Model

The beef patty was assumed to be homogeneous and isotropic as a result of the mixing during preparation. As heating was from one side only, the beef patty was assumed to be an infinite slab, due to the sample geometry, thus heat and mass transfer could be considered in one dimension only. It was assumed that the change in moisture content can be used to account for both evaporative and drip losses of moisture from the beef patty, and that no fat was lost as a result of vaporisation, but mainly as drip. The model described here was developed in Shilton *et al.*, (2002) for prediction of heat transfer and moisture vapour losses. It has now been modified to account for total moisture lost as well as fat losses by drip.

### HEAT TRANSFER

Unsteady state one dimensional heat transfer in a slab can be described by:

$$\frac{\partial T}{\partial t} = \alpha \frac{\partial^2 T}{\partial x^2} \quad (1)$$

where  $T$  is the temperature of the beef patty,  $\alpha$  is the thermal diffusivity and  $x$  is the thickness of the beef patty. The initial conditions are  $T=T_i$  for all locations and the boundary conditions are given by:

$$k \frac{dT}{dx} = h \cdot (T_\infty - T_s) \text{ at } x = X, \quad 0 < t \leq t_f, \quad (2)$$

$$\frac{\partial T}{\partial x} = 0 \text{ at } x = 0 \quad (3)$$

where  $k$  ( $\text{W}\cdot\text{m}^{-1}\cdot\text{K}^{-1}$ ) is the thermal conductivity of the beef patty and  $h$  is the heat transfer coefficient ( $\text{W}\cdot\text{m}^{-1}\cdot\text{K}^{-1}$ ). The heat transfer coefficient was calculated by:

$$h = \sigma (T_\infty - T_s)^3 \quad (4)$$

where  $\sigma$  is the Stefan-Boltzman constant ( $5.669 \times 10^{-8} \text{ m}^2\cdot\text{K}^{-4}$ ). This allows for the absorption of the far infra-red radiation by the beef patty, and enables the temperature of the infra red source to be used as an initial boundary condition. Physical property data for the beef patties at the different fat contents will vary with increasing temperature. Data was calculated using the expressions of Choi & Okos (1985) for thermal conductivity and density, as follows;

$$k = k_1 + k_2 \cdot T - k_3 \cdot T^2 \quad (5)$$

$$\rho = r_1 - r_2 \cdot T - r_3 \cdot T^2 \quad (6)$$

where  $k_1$ ,  $k_2$ ,  $k_3$ ,  $r_1$ ,  $r_2$  and  $r_3$  are constants. Results for the heat transfer in higher content beef patties indicated that heat transfer was not occurring by convection alone, but that movement of moisture and fat contributed to heat transfer by internal convection. Thus equation 6 was modified to include a convection term, designated an effective heat transfer coefficient, as follows;

$$k = (k_1 + k_2 \cdot T - k_3 \cdot T^2) + (heff_1 + heff_2 \cdot T) \quad (7)$$

where  $heff_1$  and  $heff_2$  are constants.

## MASS TRANSFER

In a previous paper (Shilton *et al.*, 2002) the evaporative moisture loss from beef patties was predicted. In this paper the total moisture loss is being considered by the following equations. The same equation set could be used in the prediction of fat loss from the beef patties. When predicting moisture loss,  $C$  represents moisture content (d.w.b.), when predicting fat loss,  $C$  represents fat content (d.w.b.). Unsteady state one dimensional mass transfer in a slab can be described by:

$$\frac{\partial C}{\partial t} = \alpha \frac{\partial^2 C}{\partial x^2} \quad (8)$$

where  $C$  is the concentration of the moisture in the beef patty (kg moisture / kg solid). The initial conditions are  $C=C_i$  for all locations and the boundary conditions are given by:

$$D_{eff} \frac{dT}{dx} = K_m \cdot (C_\infty - C_s) \text{ at } x = X, \quad 0 < t \leq t_f \quad (9)$$

$$\frac{\partial C}{\partial x} = 0 \text{ at } x = 0 \quad (10)$$

where  $D_{eff}$  is the mass diffusion coefficient ( $m^2 \cdot s^{-1}$ ) and  $K_m$  is the mass transfer coefficient ( $m \cdot s^{-1}$ ). The mass diffusion coefficient for both moisture and fat loss predictions was calculated using the following expression (Maroulis *et al.*, 1998);

$$D_{eff} = D_x \cdot \exp\left(\frac{D_T}{T}\right) \cdot \exp\left(\frac{D_c}{C}\right) \quad (11)$$

where  $D_x$ ,  $D_T$  and  $D_c$  are constants. Maroulis *et al.* originally derived this expression for calculating mass diffusivities during air drying processes.

Moisture loss during cooking can be considered analogous to moisture loss during drying, thus use of the equation here is justified.

The equations were solved in a discretised finite difference domain, using the differential equation solver, DESIRE™. The beef patty was divided into 10 nodes of equal thickness.

## RESULTS AND DISCUSSION

### HEAT TRANSFER

The results for the temperature penetration into the beef patties during cooking can be seen in Figures 2 and 3 for the 15 and 22 % fat beef patties respectively. The time temperature profiles were found to be very similar to those found previously by Sheridan & Shilton (2002b). This data was modelled using the model developed in Shilton *et al.*, (2002), the results are shown in Figures 1 and 2. There is an excellent agreement between the experimental and predicted data, the mean square deviation is in the range 1.91 to 3.51 °C for the two fat contents. From Figures 1 and 2 it can be seen that after 600 s (10 minutes) the temperature in the centre of the beef patty has risen above 80 °C for both the 15 and 22% fat beef patties. If this were a thinner patty, then it could be considered cooked at this point, as the temperature has been exceeded 70 °C for 2 minutes (Food Safety Authority, 1999).

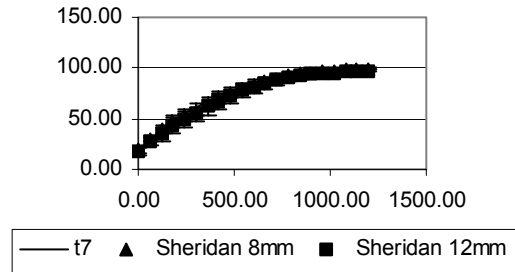


Figure 1: A comparison between experimentally derived data and the finite difference model of the heat transfer in beef patties containing 15% fat during cooking by far-infra red radiation.

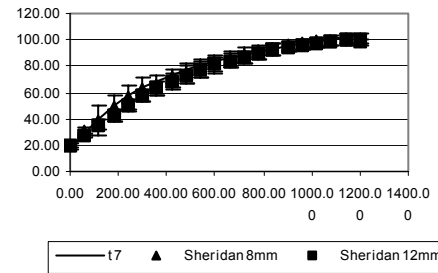


Figure 2: A comparison between experimentally derived data and the finite difference model of the heat transfer in beef patties containing 22% fat during cooking by far-infra red radiation.

## MASS TRANSFER

### Change in moisture content

From Figures 3 & 4 it can be seen that during the cooking process the middle portion of the beef patty of both fat contents maintains a higher moisture content than the top or bottom portions. The top portion initially is the source of most of the moisture loss, by evaporation from the surface. Once heat has penetrated sufficiently into the beef patty, the bottom portion loses moisture more rapidly, and moisture loss is occurring from both surfaces. This was confirmed by the presence of water in the drip fraction, however it is postulated that evaporation will also be occurring during the latter stages of the cooking process. Formation of a surface crust on top of the beef patty may well provide a barrier for mass transfer.

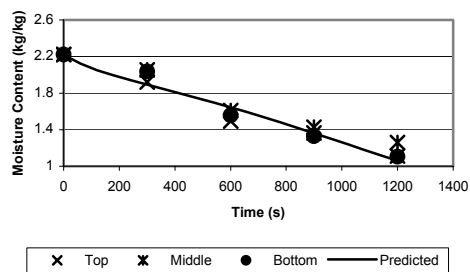


Figure 3: Change in the moisture content of slices of 15% beef patties during cooking by far infra red radiation compared against an average moisture content predicted using the model.

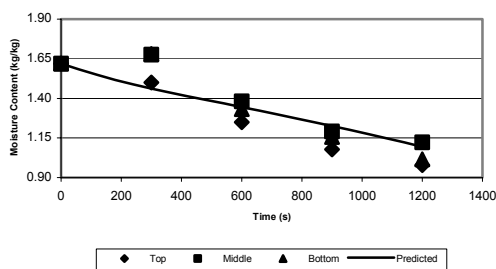


Figure 4: Change in the moisture content of slices of 22% beef patties during cooking by far infra red radiation compared against an average moisture content predicted using the model.

The average predicted moisture loss is also shown in Figures 3 & 4. It can be seen that in both cases there is very good prediction of the loss of total moisture from the beef patties during drying. The mean square deviations are 0.08 and 0.08 kg/kg for the 15% and 22 % fat contents respectively. These moisture loss profiles have a similar profile to that observed by Pan *et al.*, (2000) for 24 % fat content beef patties cooked using a contact heating process.

### Change in fat content

Figures 5 & 6 show the change in fat composition of the three layers in the beef patties for the two different fat compositions. In both cases the bottom layer undergoes the largest decrease in fat composition during the initial stages of the cooking process. However by the end of the cooking process this bottom layer can be seen to have the highest fat content of the three layers, this is pronounced in the lower (15%) fat content beef patty. Thus fat is moving from the top and middle layers into the bottom layers as a result of diffusion. This process is probably accelerated as the temperature of the beef patty increases. The hot fat is being driven downwards through the beef patty. It can be seen that the change in fat content is much greater in the higher (22%) fat samples than with the lower (15%) samples, this is in agreement with the results of Andersson *et al.* (2000).

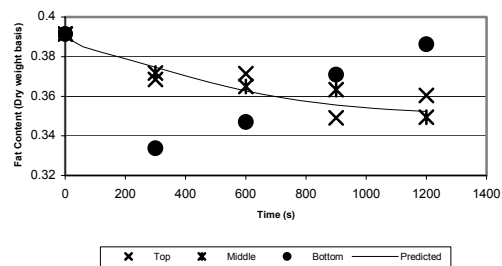


Figure 5: Change in the fat content of slices of 15% beef patties during cooking by far infra red radiation compared against an average fat content predicted using the model.

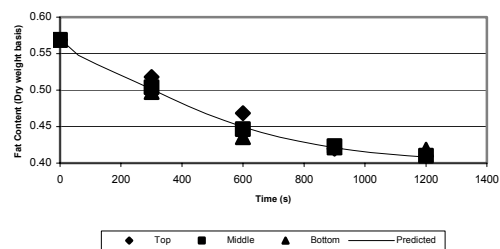


Figure 6: Change in the fat content of slices of 22% beef patties during cooking by far infra red radiation compared against an average fat content predicted using the model.

All of the layers tend towards the same final fat content towards the end of the cooking process, regardless of the initial fat content. This would imply that there is an equilibrium fat content for products such as beef patties. In this case it would appear to be around 0.35 (d.w.b.). Goihl *et al.* (1992) monitored the fat loss from beef steaks during contact grilling. Most fat is lost from the bottom of the beef steak, in this case in contact with the heating surface. The researchers also found that

untrimmed beef steaks experienced a high degree of fat penetration from the external fat during cooking, with the fat content inside the meat rising to over 100% of the original fat content. Olsson & Tornberg (1991) found that the protein matrix played an important role in regulating fat losses from beef patties during cooking. They also found that fat migration from the inner to the outer portions of beef patty are significant in influencing fat losses during cooking.

Figure 5 shows the prediction of the change in fat content from the lower (15%) fat beef patty. The predicted fat content is an average value for the entire beef patty. It can be seen that there is an excellent agreement between the predicted data and that observed for the top and middle portions, but the observed results for the bottom portion do not allow for prediction by the model. Analysis of the predicted results for the top and middle portions, gives a similar profile with the bottom portion still giving an anomalous result. It is postulated that surface tension on the bottom of the beef patty did not allow the fat to fall as drip, thus this extra fat was retained in the portion during analysis. This is despite the fact that the patty was placed on a paper towel during recording of the cooked weight.

Figure 6 shows the prediction of the change in the average fat content from the higher (22%) fat beef patty as compared to the observed fat contents of the 3 layers. In this case it can be seen that there is an excellent agreement between the model and experimental data, with a mean square deviation of 0.01 kg/kg between the predicted data and the observed mean fat content.

## CONCLUSIONS

A model was developed that successfully described heat transfer, moisture losses and fat losses during cooking by far infrared radiation. Moisture is lost from the top surface as a result of evaporation, and from the bottom of the beef patty as a result of drip. The results showed that fat is lost primarily from the bottom of the patty as a result of drip, and that fat moves from the top to the bottom of the beef patty during the cooking process.

## REFERENCES

Andersson A, K. Andersson & E. Tornberg, (2000), A comparison of fat-holding between beefburgers and emulsion sausages, *Journal of the Science of Food and Agriculture*, **80**, 555-560.

AOAC, (1990), *Official Methods of Analysis*, 15<sup>th</sup> ed., Association of Official Analytical Chemists, Washington, DC.

Choi Y & Okos M, (1985), Effects of temperature and composition on the thermal properties of foods, In: *Food Engineering and Process Applications*,

*Transport Phenomena*, (M. Le Maguer & P. Jelen Eds.), Volume 1, p.p. 93-101, Elsevier Science, London.

Food Safety Authority of Ireland, (1999), *E. coli* O157: Preventing the Spread of Infection in Catering and Retailing, Food Safety Authority of Ireland, Dublin.

Goihl DM, KB Harris, JW Savell & HR Cross, (1992), Location of fat migration during cooking of beef loin steaks with external fat still attached, *Journal of Food Composition and Analysis*, **5**, 246-251.

Kirchner JM, LC Beasley, KB Harris, JW Savell, 2000, Evaluating the cooking and chemical characteristics of low fat ground beef patties, *Journal of Food Composition and Analysis*, **13**, 253-264

Maroulis ZB, Kiranoudis CT & D. Marinos-Kouris, 1998, Heat and mass transfer modeling in air drying foods, *Journal of Food Engineering*, **26**, 113-130.

Olsson A & E Tornberg, 1991, Fat-holding in hamburgers as influenced by the different constituents of beef adipose tissue, *Food Structure*, **10**, 333-344.

Pan Z., R.P. Singh & T.R. Rumsey, (2000), Predictive modeling of contact heating process for cooking of a hamburger patty, *Journal of Food Engineering*, **46**, 9-19.

Sheard, PR, GR Nute & AG Chappell, 1998, The effect of cooking on the chemical composition of meat products with special reference to fat loss, *Meat Science*, **49** (2), 175-191

Sheridan P., (2000), Heat and mass transfer aspects of cooking beefburger patties in a range of fat contents, with mid and far infra red, ceramic and catalytic gas radiant sources, Ph.D., National University of Ireland, Dublin.

Sheridan P.S. & Shilton N.C., (2002a), Analysis of yield while cooking beefburger patties using far infrared radiation, *Journal of Food Engineering*, **51**, (1), 3-11.

Sheridan P.S. & N.C. Shilton, (2002b) Determination of the thermal diffusivity of ground beef patties under infrared radiation oven-shelf cooking, *Journal of Food Engineering*, In press.

Shilton N., P. Mallikarjunan & P. Sheridan, (2002), Modeling of heat transfer and evaporative mass losses during the cooking of beef patties using far infrared radiation, *Journal of Food Engineering*, In review.

Troutt ES, MC Hunt, DE Johnson, JR Claus, CL Kastner, DH Kropf & S Stroda, 1992, Chemical, physical and sensory characterization of ground beef containing 5 to 30 % fat, *Journal of Food Science*, **25** (1), 25-29



# **FUZZY CONTROL**



# A FUZZY SYMBOLIC APPROACH TO ESTIMATE THE SENSORY STATE OF A FOOD PRODUCT : APPLICATION TO CHEESE RIPENING

Nathalie Perrot, Laure Agioux, Irina Ioannou, Vincent Chevallereau, Gilles Trystram

UMR Génie Industriel Alimentaire – Equipe Automatique et Qualité Alimentaire ( Cemagref), 24, Avenue des Landais, BP 50085, 63172 Aubière cedex, tel: (33) 473-44-06-69 – fax: (33) 473-44-06-97 email : nathalie.perrot@cemagref.fr

Gilles Mauris

LAMII Université de Savoie 74000 Annecy  
gilles.Mauris@esia.univ-savoie.fr

Georges Corrieu

UMR Génie et microbiologie des procédés alimentaires INRA,  
INA-PG,78850 Thiverval Grignon, 330 130 815 488  
corrieu@platon.grignon.inra.fr

## INTRODUCTION

In the food industry, end-products must conform to precise specifications. Among the latter, sensory properties are essential because they influence the choice and preferences of consumers. These properties depend on the choice and combination of “raw materials” and on an appropriate feedback control of the process. The capacity to manage these properties right from the fabrication stage in an automatic framework constitutes a key issue for companies. Little research has been done in this area thus leaving the field open to study.

Managing sensory properties with the aim of controlling them is no easy task. This is due to different factors:

Firstly, from the point of view of automation, human sensory perception of, for example, the texture of a biscuit or the aspect of a sausage slice, cannot simply be manipulated on line using existing sensors (Perrot and al. 2000). On the one hand, few suitable sensors are available to carry out such measurement (Trystram and Courtois 1996; Wide 1999); on the other hand, it is difficult to develop a classical automated approach due in part to the many dimensions that must be taken into account in parallel and in part to the non linearity and coupling between the variables involved in the system.

Secondly, on another level these sensory properties are in practice evaluated on line by the operators who use their evaluation in combination with existing sensors to adjust the process (Perrot and al. 2000). Product properties that contribute to quality and process productivity depend mainly on the accuracy of their evaluation and reaction. The integration of such knowledge in a control frame is a relevant direction (Davidson 1994; Trystram and al. 1998). Nevertheless, this type of measurement is specific and the conventional methods of descriptive sensory analysis that have been developed are ill-adapted (Curt and al. à paraître) for acquiring these evaluations on line and a specific format for variables must be used. Last but not least, the operator's measurements are not on the same scale as sensor data. They are expressed on a discontinuous graduated scale, such as classes of color defined to characterize the degree of cooking of a biscuit during the baking process (Perrot and al. 1996).

An interpolation is applied by the operators between these classes in a control context.

Different ways can be developed to solve this problem, including:

Development of new sensors.

Estimation of the sensory measurements of the operators using an adapted mathematical framework.

We focus our study on the second point. If lot of mathematical methods can be used to estimate numerical data (Valet and al. 2000) from linear regressions to more elaborated one like statistical methods (Bayesian for example), theory of evidence, neural networks, theory of fuzzy sets and theory of possibilities, few are adapted to treat the data at the linguistic level manipulated by the experts. The fuzzy set theory (Zadeh 1971; Davidson 1996; Wide 1999) is one interesting method adapted to treat numeric and linguistic format of data at a symbolic level which can be the linguistic level manipulated by the operators.

## PROBLEMATIC

The aim of our study is to present an application of this approach to estimate the symbolic state of a cheese during ripening, in view to help the operator in his task. This study was developed in accordance with a research program concerning the application of the ESTimation to the SENSory evaluation with the application on an operation of cheese ripening (ESSENS supported by MENRT and in collaboration between the UMR GENIAL, the LGMPA of INA-PG and a factory H. Mons).

Cheese ripening still remind a process where the operators evaluation and reasoning keep a major role (Lemoine 2001). Some studies have developed (i) methods to follow in line some sensory properties of the product like texture using sensors (O'Callahan and al. 2000) or (ii) methods to characterize in laboratory the sensory properties of a cheese (Lesage and al. 1992; Martin and al. 1999). Few studies are focus on the estimation versus time of the sensory trajectory and standard deviation trajectory of the product during processing. Nevertheless, it is a pertinent way to help the operator in his task, and as a consequence improve the

productivity. The example treated is focus on the ripening of a soft mould cheese so called “rogeret” (figure 1).



Figure 1 : a cheese called “rogeret”

### THE SYMBOLIC MODEL TO ESTIMATE THE SENSORY STATE OF THE CHEESE DURING RIPENING

The rogeret is ripened in 1 month. The evolution of the product which is strongly linked to complex microbiological reactions (Eck and Gillis 1997) is evaluated on line by the operators through 7 different sensory characteristics that have been formalized upon the concept of sensory indicators (Curt and al. 2001). Sensory measurements are made on a structured ratio scale between [0,6]. Tests of reproducibility of their measurements have been achieved (A level of at mean 92% on the point tested).

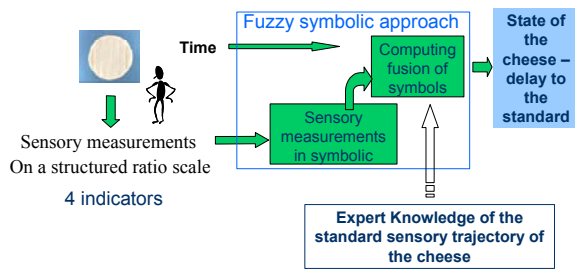


Figure 2 : the fuzzy symbolic approach built to estimate the sensory state of the cheese

The fuzzy symbolic approach was built to inform an operator on the potential derive of the sensory trajectory of the cheese at t time as to help him to control the process. The configuration of the symbolic approach in this case is presented figure 2.

On the basis of 4 of the 7 indicators of the cheese quality (humidity, *Geotrichum candidum* coat, cheese consistency, color) and the expert knowledge, an information on the state of the product is extract : cheese “in advance”, “standard” or

“late” and a quantification of this state is calculate. For example at t = 10 days of ripening, a cheese is supposed to be in a state B called “little ripened” or “state 3.5 weeks”. Suppose a cheese evaluate to have a ripening delay of two days : the answer of the system would be B-2days.

Our approach implements two levels of the experts' knowledge: (i) their knowledge of the standard sensory behavior of the cheese, and (ii) their knowledge of the different possible trajectories around this standard behavior stemming from experience. By hypothesis, a standard behavior is associated to the mean trajectory of the cheese in standard conditions of ripening.

#### knowledge of the symbolic standard sensory behavior



Figure 3 : example of the standard symbolic behavior of the cheese at stage 4 and 3.5

Experts have memorized the standard sensory behavior of their specific cheese in terms of symbols like : at a stage called “3.5 weeks” a cheese in a standard behavior should be “middle” in term of humidity, “little” in term of *Geotrichum Candidum* coat” and “few” in term of cheese consistency. We express this symbolic knowledge using the theory of fuzzy sets. Logical AND and OR functions are respectively associated to product and bounded sum. Fuzzy membership functions of each sensory measurements ensure the link between symbols manipulate by the experts and the scale of the sensory measurements. Figure 3 presents an example of implemented knowledge for the two state in the beginning of the cheese ripening figure 3. It involves at this stage three indicators on four : humidity, *Geotrichum candidum* coat and cheese consistency.

#### Global symbolic sensory behavior of the cheese

Around the standard behavior of the cheese, other characteristics trajectories are also memorized and expressed in the symbolic model implemented with an example for one of this corresponding period of ripening (state “B” or “3.5 weeks”) presented table 1. Fusion between symbols are

calculated upon the fuzzy formalism presented below. Equations (1) and (2) express the calculus applied to table 1.

Ripening state at time t=RS(t)

$$RS(t) = \text{standard}(RS)(t) - RFR(t) \quad (1)$$

$$RFR(t) = \sum_n^{i=1} \mu Ri * (\text{delay}(Ri)) \quad (2)$$

$\mu Ri$  = activation degree of each rule  $Ri$

standard(RS)(t) = standard ripening state of the corresponding period t : for example 3.5 weeks for 4 < t < 6 days

Table 1 : example of knowledge implemented at Stage B – « 3.5 weeks »

Gc coat Humidity	few	little	middle	coat
low	late delay = -0.5 with drying default	Normal with drying default	In advance delay = +0.5 for a cheese consistency middle	
middle	late delay = -0.2	Standard Delay=0	In advance delay = +0.5 for a cheese consistency middle	
high	Late delay = -0.5	Late delay = -0.5		

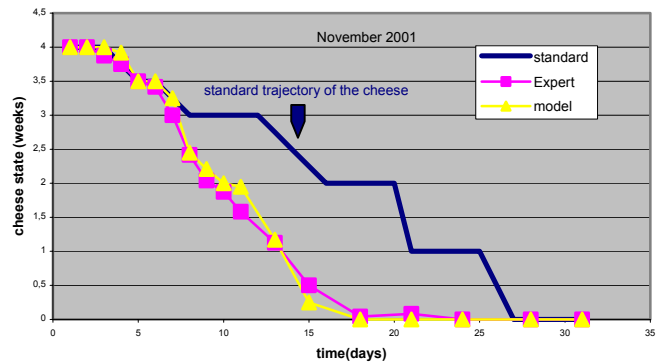
## METHOD OF VALIDATION

A basis of 54 data is acquired in a pilot and processed to validate our approach. The kinetics of cheese ripening are measured in the pilot unit at four constant relative air moistures and air temperatures representative of different trajectories of the cheese ([15°C, 98%], [9°C, 92%], [9°C, 96%], [12°C, 94%]) in the experimental domain of [9°C, 15°C] for temperature and [92%, 98%] for relative humidity.

## RESULTS

The results obtained show the ability of the approach to follow the sensory trajectory of a cheese during ripening and help the operator to diagnosis a derive of it. On an example of a kinetic at 9°C and 92 % of relative humidity of the air (figure 4), we can see the estimation of the symbolic approach by comparison to the operator evaluation. 96% on 54 of the tested points were compatible at a grade of 0.5.

This level of compatibility is defined upon the sensibility of



the operator measurement.

Figure 4 : Comparison between the evaluation of the operator and the model on estimation of the state of the cheese during an experiment at 9°C and 92% of relative humidity of the air

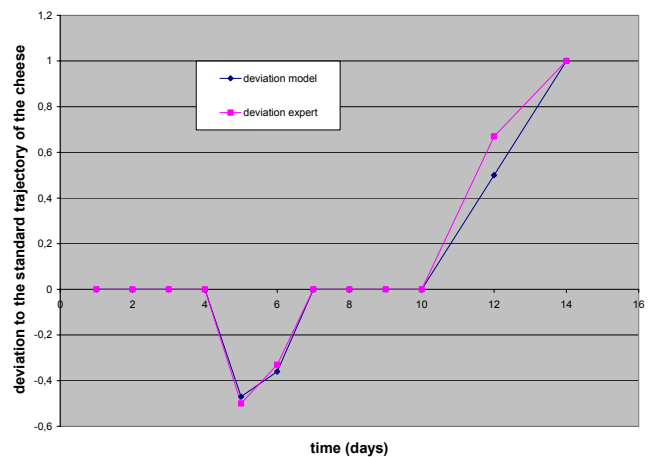


Figure 5 : estimation of the derive to the standard symbolic sensory kinetic by the model and the operator during an experiment lead at 15°C and 98% of relative humidity

The result is treated in the form of an evaluation of the trajectory of the considered cheese by comparison to its traditional standard behavior registered by the experts from experience and during experiments. An example of such an answer of the model is presented figure 5 for a kinetic at 15°C and 98% of relative humidity. We can see that at 10 days, the symbolic model point out an important and constant derive of the trajectory of the cheese which is validated by the expert and is linked to the experimental conditions of ripening. Such an approach, combined with a model of kinetics of some indicators could be used to predict some derive of the quality of the cheese before it appears and thus help the operator in its task.

## CONCLUSIONS

A fuzzy symbolic approach has been implemented and validated on 54 data to estimate the sensory state of a cheese during ripening.

The results are relevant with regard to the objective of controlling the sensory properties of the products at the fabrication stage. These first examples are encouraging for different reasons :

- This approach is a simple way to integrate operator reasoning whenever the operator is involved in measurement diagnosis or control of the process.
- It allows treating the measurements from the sensors and operators at the same level.
- It introduces interpolation between symbols manipulated by the operators that provides robustness but which should be quantified more precisely and linked to processing uncertainty.

## REFERENCES

- Curt, C., L. Agioux, et al. 2001. "Formalisation of at line human evaluations". 4th symposium Rose Marie Pangborn, 22-26 July, Dijon: 97.
- Curt, C., G. Trystram, et al. (à paraître). "Formalisation of at line human evaluations. Integration of human decision in the dry sausage ripening process." *Science des aliments*.
- Davidson, V. 1994. "Expert systems in process control." *Food Research International* 27: 121-128.
- Davidson, V. 1996. Fuzzy control of food processes. *Computerized Control Systems in the Food Industry*. G. Mittal. New York, Basel, Hong Kong, Marcel Dekker Inc.: 179-205.
- Eck, A. and J. Gillis 1997. "Le Fromage", Lavoisier Tec et Doc.
- Lemoine, R. 2001. "L'affinage, une étape décisive pour la qualité du fromage." *Revue Laitière Française*(614): 16-19.
- Lesage, L., F. Sauvageot, et al. 1992. "Influence de la teneur en NaCl et de la durée d'affinage sur les caractéristiques sensorielles d'un fromage type camembert enrichi en magnésium." *Lait* (72): 73-85.
- Martin, N., S. Savonitto, et al. 1999. "Flavor generation in cheese curd by coculturing with selected yeast, mold and bacteria." *Journal of Dairy Sciences* (82): 1072-1080.
- O'Callahan, D., C. O'Donnell, et al. 2000. "On-line sensing techniques for coagulum setting in renneted milks." *Journal of food engineering* 43: 155-165.
- Perrot, N., G. Mauris, et al. 2000. "Modeling of the expert sensory evaluation of the sausage crusting using fuzzy symbolic approach". 1st International Conference on Simulation in Food and Bio Industries - FoodSim, Nantes, 26-27 June, France: 36-40.
- Perrot, N., G. Trystram, et al. 2000. "Feed-back quality control in the baking industry using fuzzy sets." *Journal of Food Process Engineering* 23: 249-279.
- Perrot, N., G. Trystram, et al. 1996. "Sensor fusion for real time quality evaluation of biscuit during baking. Comparison between Bayesian and Fuzzy approaches." *Journal of Food Engineering* 29: 301-315.
- Trystram, G. and F. Courtois 1996. *Food process modeling and simulation. Computerized Control Systems in the Food Industry*. G. Mittal. New York, Basel, Hong Kong, Marcel Dekker Inc.: 55-85.
- Trystram, G., J. Hossenlopp, et al. 1998. "Experiences about man/technology cooperation through decision systems for the control of food unit operations". *Biodecision'98*, Montpellier (France).
- Valet, L., G. Mauris, et al. 2000. "A statistical overview of recent literature in information fusion". ISIF, Paris.
- Wide, P. 1999. "The human decision making in the dough mixing process estimated in an artificial sensor system." *Journal of food engineering* 39: 39-46.
- Zadeh, L. 1971. "Quantitative fuzzy semantics." *Inf. Sci.* 3: 159-176.

# ADAPTIVE FUZZY CONTROL AS ADVANCED CONTROL TECHNIQUE IN MILK PASTEURISATION.

C. Riverol and B. O' Connor

Advanced Process Technology Group, Food and Science Building, University  
College Cork, Cork, Ireland.

email: c.riverol@ucc.ie, b.oconnor@ucc.ie

Control into new areas of application  
as described here.

## KEYWORDS

Process control, milk, adaptive,  
robustness.

## ABSTRACT

This short communication outlines the use of an adaptive fuzzy control system as an alternative method for milk pasteurisation. A comparison with respect to PID classic system is made.

## INTRODUCTION

This appeal is primarily motivated by the desire to maintain a high degree of product quality while operating at the highest possible production rates (Edan, 1992). Advanced process control techniques have been successfully used to improve productivity in other process industries, such as the petrol-chemical industries. This fact suggests that the food industry can also realise similar benefits from advanced control technology. There are, however, a number of obstacles, which mitigate against the transfer of this technology into the food/bio

sector. These include issues concerning lack/unavailability of product and process data and knowledge, economic factors and the traditional conservatism of the sector. Advances in hardware speed and capacity, communications and supporting software resulting in increased presence of factory 'shop-floor' information systems have made possible the extension of Adaptive

## MATHEMATICAL MODELLING OF THE PLATE HEAT EXCHANGER

Plate heat exchanger (PHEs) exhibit excellent heat transfer characteristics which allow more compact designs than are achievable with conventional shell-and-tube heat exchangers. Along with their easy maintenance and other advantages, this factor has made PHEs the prime choice for many engineering applications, involving liquid-liquid heat transfer duties. They are most commonly used in the dairy, beverage, general food processing and pharmaceutical industries due to their ease of cleaning and their thermal control characteristics. The fundamental energy conservation laws lead to equations that describe the heat transfer between any channel and its neighbouring plates. These are typically of the following form:

Channel  $j$ :

$$\rho C_p A_x \left( \frac{\partial T_j}{\partial t} - v_j \frac{\partial T_j}{\partial z} \right) = U_j A_j (T_{pj-1} - T_j) + U_j A_j (T_{pj} - T_j)$$

Plate  $j$ :

$$\rho_p C_{pp} A_{xp} \left( \frac{\partial T_{pj}}{\partial t} - v_j \frac{\partial T_j}{\partial z} \right) = U_j A_j (T_{pj-1} - T_{pj}) + U_j A_j (T_{j+1} - T_{pj})$$

where  $t$  denote time and  $z$  axial position with a channel,  $T_j(z, t)$  is the temperature of the milk in channel  $j$  and  $T_{pj}(t)$  the temperature of the metal in plate  $j$ . The quantity  $n_j$  takes a value of +1 or -1, depending on the direction of the flow in channel  $j$ . This general model can be used to simulate

the transient behaviour of several types of PHEs, including counter-current, co-current, multi-channel etc.

### ADAPTIVE FUZZY SYSTEM CONTROL DESIGN

The adaptive control used in this paper is depicted in the Figure 1. In this approach the “adaptation mechanism” observes the signals from the control system and adapt the parameters of the controller to maintain performance even if there changes in the plant. The desired performance is characterised with a “reference model” as the described above, and the controller then seeks to make the closed-loop system behave as the reference model would even if the plant changes. This is called “model reference adaptive control “ (MRAC) (Sanchez, 1997).

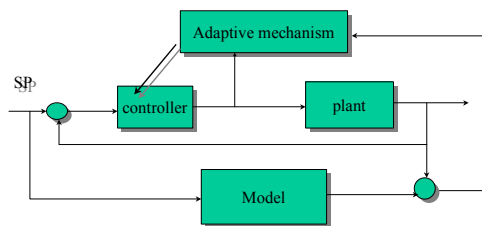


Figure 1. MRAC model

The learning mechanism tunes the rule-base of direct fuzzy controller so that the closed-loop system behaves like the reference model. These rule-base modifications are made by observing data from the controlled process, reference model and fuzzy controller. The learning mechanism consists in two parts: “fuzzy inverse model” and a “knowledge-base modifier”. The fuzzy inverse model performs the function of mapping (representing the deviation from desired behaviour), to change in the process inputs that are necessary to force to zero. The knowledge-base modifier performs the function of modifying the fuzzy controller’s rule-base to affect the needed changes in the process inputs.

### RESULTS AND CONCLUSIONS

The adaptive control system achieves process regulation by specifying the desired plant output (set point 72.3 °C). The system gets the settling time shortly without overshoot as depicted the Figure 2.

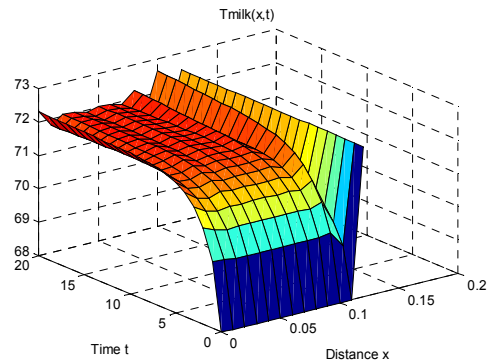


Figure 2. Milk temperature as function of time and axial position (z)

The temperature of the hot water was simulated as well as depicted the Figure 3 where the input temperature was 73.8 °C (very closed to the setpoint) for avoid over pasteurisation.

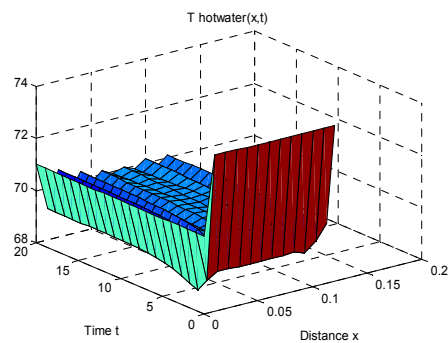


Figure 3. Hotwater temperature as function of the time and axial position

The model was used with a PID controller. The loop turning was made using the traditional Ziegler-Nichols Method. The result is depicted in the Figure 4.

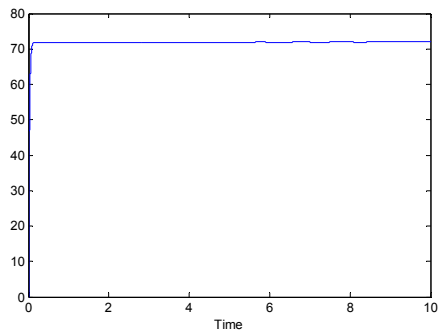


Figure 4. Milk temperature using PID controller.

The system did not show overshoot with a quick settling time but the offset is 2.4°C in consequence the quality of the product would be seriously affected.

A glance for three figures allows to conclude that the MRAC method used in this work guarantee the quality of the milk avoid overheating and quick changes in the profile of temperature.

## REFERENCES

Edan Y, P. Grinspen and H. Kahn (1992). "Fuzzy logic applications in dairy industry", International Winter Meeting of ASAE, Nashville, Tennessee, (Dec), 1-15.

Sanchez R. and J. Rubio (1997) "Control adaptivo y Robusto", Universidad de Sevilla, Spain, 55-66.



# **NUTRITION**



# FREEZING IN POROUS MEDIA

Jean-Yves Monteau

Nasser Hamdami

Alain Le Bail

GEPEA – ENITIAA

Laboratoire de Génie des Procédés Alimentaires

Rue de la Géraudière, BP82225

44322 Nantes Cedex 3, France

E-mail: [monteau@enitiaa-nantes.fr](mailto:monteau@enitiaa-nantes.fr)

## KEYWORDS

Freezing, porous media, heat and mass transfer, modeling.

## ABSTRACT

Heat and mass transfers are important phenomena involved in the freezing of porous media; this is especially valid for product with strong porosity. However, few studies are available in the case of foodstuffs. In this paper a model is proposed for the freezing of bread. The dominating physical phenomena are conduction for the heat transfer inside the product and diffusion for the mass transfer. However, evaporation-condensation and capillarity play an important role in both heat and mass transfer. On the external surface heat transfer is driven by convection, radiation and evaporation or sublimation. Mass transfer is driven by evaporation or sublimation. The model presented in this work formalizes these exchanges by introducing an effective thermal conductivity which accommodates evaporation-condensation phenomena. Mass transfer is modeled by the Fick's law. Thermal conductivity is modeled by using a Maxwell type model with four components: ice, liquid water, dry matter and air. The resolution is achieved by a hybrid method which uses an enthalpic formulation and an apparent specific heat. Temperature changes and mass loss are compared with experimental results obtained with a sponge which was used as a model product. Experimental and numerical results are satisfactory, but show that the thermal conductivity model has to be improved.

## INTRODUCTION

Heat and mass transfers are important phenomena involved in the freezing of porous media.

Porosity permits to quantify the void fraction of a porous medium. Freezing of porous media has been studied quite extensively for low porosity media (i.e. rock, sand, soil...) whereas few studies are available for high porosity media (i.e. bread, ...). For example, studies on phase front propagation in soils are proposed by (Bronfenbrener and

Korin 1997; Miyata 1998; Bronfenbrener and Korin 1999), others on the frost damage of concrete by threeze-thaw cycles are presented by (Chatterji 1999a; Chatterji 1999b). Besides, freezing of porous food material are not numerous. Immersion freezing is presented and modeled by (Lucas et al. 1999; Lucas et al. 2000). These works are related to heat and mass transfer in a non-porous biological matrix. Most of these articles are general and consider the problem as a theoretical one with minimal concern on the application (Weaver and Viskanta 1986; Sasaki 2000; Song and Viskanta 2001).

According to the problem which is considered, equations describing the phenomena are more or less complex. For example, very often for foodstuffs, the mass transfer has a minimal influence on the heat transfer, especially for low porosity media. By the way, mass transfer is often neglected or modeled in a simple approach. In the case of high porosity products such as bakery products, mass transfer can't be neglected. Mass transfer, which is mainly related to water diffusion in the case of porous biological substances, is proportional to the gradient of partial pressure of water in the product. Water has a very high latent heat and a quite moderate specific heat. Water diffusion by evaporation-condensation can be taken into account thanks to an effective thermal conductivity which accommodates conductivity of the matrix and water diffusion. This concept can be used to model coupled heat and mass transfer (Pham 2001).

In some simple cases, an analytical solution can be obtained (Mikhailov 1976; Marcus and Tarzia 2000). Generally a computational solution is necessary (Campañone et al. 1998). Specific software can be developed such as "Baktix" for the simulation of cooling and freezing of bakery products (van der Sluis 1993).

This work is presenting a model developed for bread freezing. The industrial application concerns part baked frozen bread. Transport phenomena involved in the case of bread freezing are first presented and the model used is presented. Results obtained with this model are then discussed.

## TRANSPORT PHENOMENA DURING THE FREEZING

Transfer takes place on the surface by convection, radiation, and evaporation. Evaporation results in water loss, which can interact with the final quality of the product such as crust flaking.

A temperature gradient is established between surface and center of the bread. The water vapor pressure is higher for higher temperature. Thus, water diffuses through the crumb from the warmer zones towards the cooler zones, i.e. from center towards the periphery. Condensation might occur if the temperature of the crumb reaches the dew point of the humid air contained in the bread. This evaporation-condensation mechanism plays a significant part in the heat transfer inside the product (de Vries 1958). Heat and mass transfer also occurs by capillarity inside the wall of the porous matrix (van der Sluis 1993).

Radford et al. (Radford et al. 1976), while working on the meat chilling, indicated that at the beginning of chilling, evaporation is higher than the diffusion of water in the product, and thus the surface dries out rapidly. Then a balance settles between the diffusion and evaporation. In a third phase, the difference in water vapor pressure between the product surface and the ambient air decreases. The diffusion becomes the governing phenomena compared to evaporation, and the surface re-wets.

Freezing starts when the surface temperature is sufficiently low. A phase front travels through the product while frozenable water turns to ice. The freezing of water does not prevent a transfer of water in vapor form (Campañone, Salvadori et al. 1998). At the same time, the frozen zone dries out by sublimation of the ice, from a front receding into the product much more slowly than the phase front of freezing (Pham and Willix 1984). The thermal transfer is done mainly by conduction in the dehydrated zone.

## MODELING

The model was developed for a slab (1D) of thickness  $2l$  and of infinite length and width.

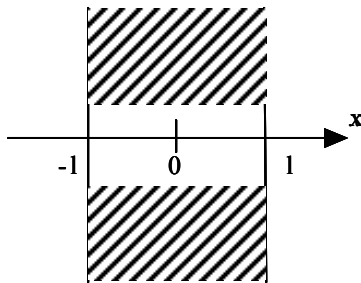


Figure 1: Slab of Infinite Length

## Governing Equations

The equation describing the temperature change can either use the temperature as primary variable, or use the enthalpy. In the first case a variable called apparent specific heat is defined. The apparent specific heat includes the heat capacity and the enthalpy of fusion of ice. The equation is

$$c(W, T) \frac{\partial T}{\partial t} = \lambda(W, T) \frac{\partial^2 T}{\partial x^2} \quad (1)$$

The drawback of this method is that the apparent specific heat traced versus the temperature presents a peak, which can lead to numerical non-stability.

An enthalpy formulation such as the equation (2) permits to avoid these problems and was used for the model.

$$\frac{\partial H}{\partial t} = \lambda(W, T) \left( \frac{\partial^2 T}{\partial x^2} \right) \quad (2)$$

The thermal conductivity used in this model was an effective thermal conductivity that includes evaporation-condensation and capillarity phenomena. It is modeled with a Maxwell type model, which considers a dispersed phase in a continuous one. The effective thermal conductivity of Maxwell model is written

$$\lambda = \lambda_c \left[ \frac{\lambda_d + 2\lambda_c - 2\varepsilon_d(\lambda_c - \lambda_d)}{\lambda_d + 2\lambda_c - 2\varepsilon_d(\lambda_c - \lambda_d)} \right]$$

where  $\lambda_c$  stands for the continuous phase,  $\lambda_d$  for the dispersed, and  $\varepsilon_d$  for the occupation ratio (by volume) of the dispersed phase.

Four constituents were considered in our case: ice, liquid water, dry matter and air. In a first stage ice is the dispersed phase, and water the continuous one. In a second stage this system constitutes the dispersed phase, and the continuous one is dry matter. In a third and last stage the continuous phase is formed by the previous part, and the dispersed phase is air. Thermal conductivity expressions for ice and water are from (Singh 1992), and for air from (Özişik 1985). Thermal conductivity of dry matter has been previously measured with a transient hot source method. Air conductivity is modified to take into account evaporation-condensation (Sakiyama et al. 1999).

$$\lambda_{air}^* = \lambda_{air} + \frac{D_{wa}}{RT} \frac{P_{air}}{P_{air} - a_w P_{sat}(T)} L a_w \frac{dP_{sat}}{dT}$$

The mass transfer is modeled by the Fick's law amended with a source term to express the ice formation.

$$\frac{\partial W}{\partial t} = D(T_a) \left( \frac{\partial^2 W}{\partial x^2} \right) - \frac{\partial X_i}{\partial t}$$

where

$$X_i = (W + 1) \frac{x_i}{1 - x_i}$$

The mass diffusivity  $D$  was modeled by the Arrhenius's law.

The change of mass fraction of ice was modeled by the conventional equation below where  $x_b$  is calculated according to the Pham's method (Pham 1987).

$$x_i = (x_{tw} - x_b) \left( 1 - \frac{T_f - 273,15}{T - 273,15} \right) \quad \text{if } T < T_f$$

$$x_i = 0 \quad \text{if } T \geq T_f$$

The method of resolution used requires the knowledge of a table T-H. This table is calculated using the apparent specific heat

$$Cp_{app} = Cp_s(T)x_s + Cp_w(T)x_w + Cp_i(T)x_i(x, T) - L \frac{dx_i}{dt}$$

with L, latent heat of fusion.

Polynomial expressions for the Cp functions are drawn from (Singh 1992).

H(T) is then calculated by integration of Cp since  $-40$  °C. H or T is calculated by interpolating from the values of this table.

### Boundary Conditions

Forced convection, radiation and evaporation or sublimation were considered for the heat balance at the external surface of the product.

$$-\lambda(W, T) \frac{\partial T}{\partial x}(l, t) = h_m (T_s - T_a) + \varepsilon \sigma (T_s^4 - T_a^4) + k_g L (P_s - P_a)$$

L is the latent heat of water vaporization if  $T \geq T_f$  and of water sublimation if  $T < T_f$ .

$h_m$  is given in experiments.  $k_g$  is calculated by (Özişik 1985):

$$\frac{h_m}{k_g} = \frac{M_a}{M_w} P_{atm} Cp_a (Le)^{\frac{2}{3}}$$

$P_s$  and  $P_a$  are calculated by

$$P_s = a_w P_{sat}(T_s)$$

and

$$P_a = H_a P_{sat}(T_a)$$

where  $a_w$  is water activity on surface calculated according to the sorption curves.

On surface, the mass transfer is driven by evaporation or sublimation.

$$-D(T_a) \rho_s \frac{\partial W}{\partial x}(l, t) = k_g (P_s - P_a)$$

A null heat flux and mass transfer conditions were assumed at center of the slab.

### Initial Conditions

Temperature and moisture were supposed constant and uniform in the product at time zero.

### SIMULATOR

The method of resolution used is a hybrid temperature-enthalpy method suggested by Pham in (Pham 1985). This method is unconditionally stable. It is based on a finite differences scheme. The equation (2) enables the enthalpy change estimation on two time-steps, from  $H^m$  to  $H^{m+2}$

for example. The enthalpy change / temperature change ratio gives an estimate of voluminal heat at time step  $m+1$ ,  $c^{m+1}$ . The use of the three time-steps Lees's scheme (Lees 1966) enables to solve the temperature heat equation (1) at the time step  $m+2$ . To not jump the peak of phase change, the temperature is corrected according to the following method: enthalpy at time-step  $m+2$  is calculated for every space-step with

$$H^{m+2} = H(T^m) + c^{m+1} (T^{m+2} - T^m)$$

$H(T^m)$  is calculated by interpolation in table H-T. Then

$T^{m+2}$  is calculated in the same way by  $T(H^{m+2})$ .

### EXPERIMENTS

A vegetable sponge Cello G, reference F44110 (Euréponge – France) was chosen as a model product. The size of the sample was 10 cm×10 cm×4 cm. After washing and rinsing, the sponge was humidified to obtain a water content of 0.6 kg water/kg product. Four K-thermocouples were placed on the surface, at 1 cm, 1.7 cm and 2.6 cm below the surface respectively. The sample was installed in a polystyrene box to insulate the side walls and the lower face. The system (sponge in the polystyrene box) was placed in a freezing tunnel at  $-40$  °C. The relative humidity of air was logged throughout the experiment. Air flowed parallel to the product surface at a velocity of 1 m/s. Sample mass was measured before and after the experiment. Thermocouples temperatures were logged on a data acquisition system every 4 s.

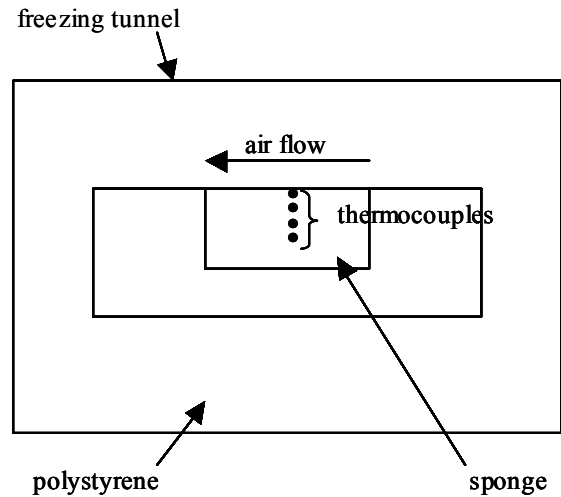


Figure 2: Experimental Assembly

### RESULTS AND DISCUSSION

Experimental and computed temperature profiles are presented in figures (3) to (6). For the curves at 1 mm below the surface, some oscillations of the computed temperature profile were observed until 500 s. After this limit, the agreement was acceptable, the computed temperature being 2 K lower than the measured one. This difference vanishes with time. For the 1.1 cm position, the

computed temperature starts above the measured one because the real initial temperature was not strictly uniform in the sample. Then, up to 1700 s, the two curves were superposed, although the computed one exhibited some oscillations during phase change (time 1000 s). Then the two curves diverge after the phase change plateau. At 1.8 cm the curves evolve in the same way, but phase change was delayed. The two curves for the 2.6 cm position are the same except at the beginning, but are distinct at the phase change time, at 3200 s.

The experimental mass loss during freezing was 1.23 % of the total mass whereas the model indicated only 0.5 %. This difference can be explained by the fact that the computed surface temperature decreased much faster than the real temperature. This yielded in a lower vapor pressure difference between the surface and the ambient air in the simulation in comparison with experiments.

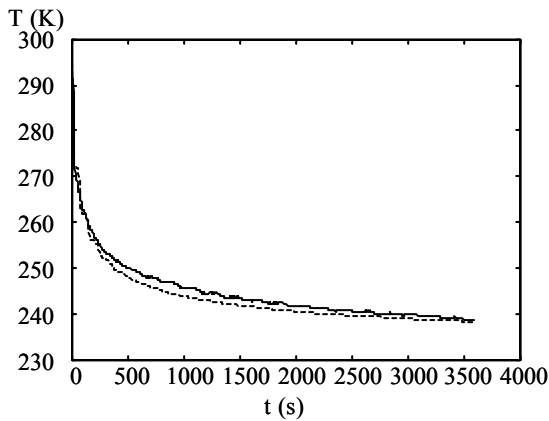


Figure 3: Temperature Profile at 0.1 cm below the Surface

— experimental  
 - - - - - computed

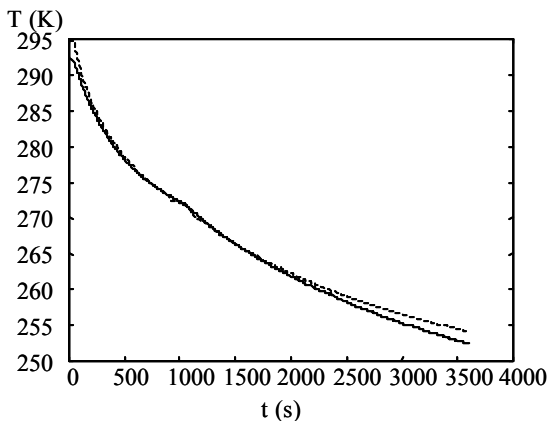


Figure 4: Temperature Profile at 1.1 cm below the Surface

— experimental  
 - - - - - computed

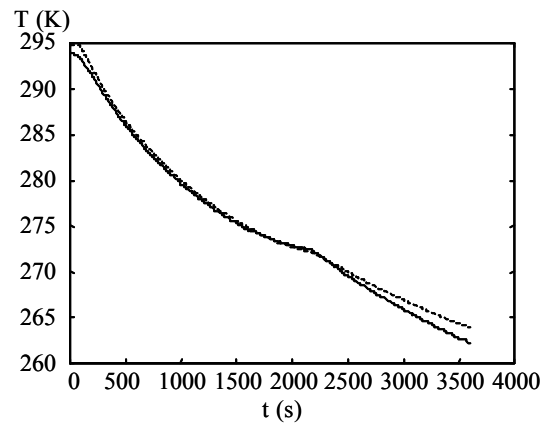


Figure 5: Temperature Profile at 1.8 cm below the Surface

— experimental  
 - - - - - computed

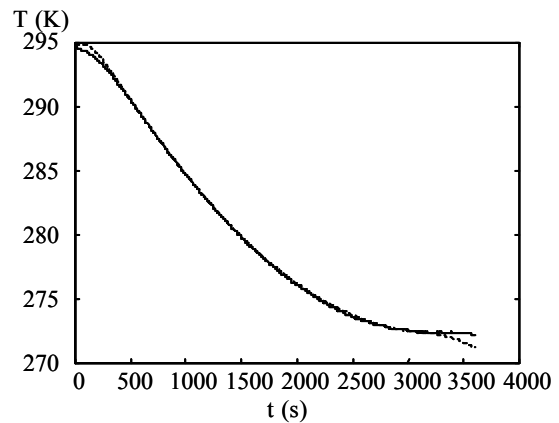


Figure 6: Temperature Profile at 2.6 cm below the Surface

— experimental  
 - - - - - computed

## CONCLUSION

The simulator developed in this study gave satisfactory results. A good agreement was observed between experimental and computed temperature profiles whereas a larger difference was obtained for the water loss. The differences observed can be explained by an under estimation of the evaporation-condensation phenomena in the thermal conductivity. The continuation of this work will consist in developing more realistic models of thermal conductivity.

## NOMENCLATURE

$a_w$	water activity
$c$	voluminal heat, $J/(m^3.K)$
$C_p$	specific heat, $J/(kg.K)$
$D$	mass diffusivity, $m^2/s$
$D_{wa}$	diffusivity of water vapor in air, $m^2/s$
$h_m$	thermal convection coefficient, $W/(m^2.K)$

H	voluminal enthalpy, J/m <sup>3</sup>
H <sub>a</sub>	relative humidity
k <sub>g</sub>	mass convection coefficient, s/m
L	latent heat or fusion or sublimation, J/kg
Le	Lewis number
M	molecular mass, kg
P	pressure, Pa
R	molar gas constant, 8.314510 J/(mol.K)
t	time, s
T	temperature, K
W	humidity, kg liquid water/kg dry matter
x	spatial coordinate, m
x	mass fraction, kg/kg product
X <sub>i</sub>	local ice content, kg ice/kg dry matter

### Greek letters

ε	product emissivity
ε <sub>d</sub>	voluminal ratio of the dispersed phase
λ	thermal conductivity, W/(m.K)
ρ	density, kg/m <sup>3</sup>
σ	Stefan-Boltzmann constant, 5.67051 10 <sup>-8</sup> W/(m <sup>2</sup> .K <sup>4</sup> )

### Subscripts

a	ambient
air	air
app	apparent
atm	atmospheric
b	bound water
c	continue
d	dispersed
f	freezing point
i	ice
s	solid
s	surface
sat	saturation
tw	total water
w	liquid water

### REFERENCES

- Bronfenbrener, L. and E. Korin. 1997. "Kinetic model for crystallization in porous media." *International Journal of Heat and Mass Transfer*, 40, No. 5, 1053-1059.
- Bronfenbrener, L. and E. Korin. 1999. "Two-phases zone formation conditions under freezing of porous media." *Journal of Crystal Growth*, 198/199, 89-95.
- Campañone, L. A., V. O. Salvadori and R. H. Mascheroni. 1998. "Modelling and simulation of heat and mass transfer during freezing and storage of unpacked foods". In *IIF-IIR - Commissions B1, C1 and C2* (Orsay), 180-197
- Chatterji, S. 1999a. "Aspects of the freezing process in a porous material-water system - Part 1. Freezing and the properties of water and ice." *Cement and Concrete Research*, 29, No. 4, 627-630.
- Chatterji, S. 1999b. "Aspects of the freezing process in a porous material-water system - Part 2. Freezing and properties of frozen porous materials." *Cement and Concrete Research*, 29, No. 5, 781-784.
- de Vries, D. A. 1958. "Simultaneous transfer of heat and moisture in porous media." *Transactions, American Geophysical Union*, 39, No. 5, 909-916.
- Lees, M. 1966. "A linear three-level difference scheme for quasilinear parabolic equation." *Mathematical and Computer Modelling*, 20, 516-522.
- Lucas, T., D. Flick, J. M. Chourot and A. L. Raoult-Wack. 2000. "Modeling and control of thawing phenomena in solute-impregnated frozen foods." *Journal of Food Engineering*, 45, No. 4, 209-218.
- Lucas, T., D. Flick and A. L. Raoult-Wack. 1999. "Mass and thermal behaviour of the food surface during immersion freezing." *Journal of Food Engineering*, 41, 23-32.
- Marcus, E. A. S. and D. A. Tarzia. 2000. "Explicit solution for freezing of humid porous half-space with a heat flux condition." *International Journal of Engineering Science*, 38, No. 15, 1651-1665.
- Mikhailov, M. D. 1976. "Exact solution for freezing of humid porous half-space." *International Journal of Heat and Mass Transfer*, 19, 651-655.
- Miyata, Y. 1998. "A thermodynamic study of liquid transportation in freezing porous media." *JSME International Journal - Series B (Fluids and thermal engineering)*, 41, No. 3, 601-609.
- Özişik, M. N. 1985. *Heat transfer - A basic approach*. McGRAW-HILL INTERNATIONAL EDITIONS, Singapore.
- Pham, Q. T. 1985. "A Fast, Unconditionally Stable Finite-Difference Scheme for Heat Conduction with Phase Change." *International Journal of Heat and Mass Transfer*, 28, No. 11, 2079-2084.
- Pham, Q. T. 1987. "Calculation of bound water in frozen food." *Journal of Food Science*, 52, No. 1, 210-212.
- Pham, Q. T. 2001. Modelling thermal processes: cooling and freezing. In *Food Process Modelling*, L. M. M. Tijskens, M. L. A. T. M. Hertog and B. M. Nicolai (Eds.), CRC Press, England, Cambridge, 312-339.
- Pham, Q. T. and J. Willix. 1984. "A model for food desiccation in frozen storage." *Journal of Food Science*, 49, 1275-1294.
- Radford, R. D., L. S. Herbert and D. A. Lovett. 1976. "Chilling of meat - A mathematical model for heat and mass transfer." *International Institute of Refrigeration. Bulletin Annexe*, 1976, No. 1, 323-330.
- Sakiyama, T., M. Akutsu, O. Miyawaki and T. Yano. 1999. "Effective thermal diffusivity of food gels impregnated with air bubbles." *Journal of Food Engineering*, 39, 323-328.
- Sasaki, A. 2000. "Transient heat characteristics of water-saturated porous media with freezing." *Heat Transfer-Asian Research*, 29, No. 4, 300-316.
- Singh, R. P. 1992. Heating and cooling processes for foods. In *Handbook of Food Engineering*, D. R. Heldman and D. B. Lund (Eds.), Marcel Dekker, INC. New York, 247-276.
- Song, M. and R. Viskanta. 2001. "Lateral freezing of an anisotropic porous medium saturated with an aqueous salt solution." *International Journal of Heat and Mass Transfer*, 44, No. 4, 733-751.
- van der Sluis, S. M. 1993. "Cooling and freezing simulation of bakery products". In *IIR Meeting Comm. B1, B2, D1, D2/3* (Palmerston North, November)
- Weaver, J. A. and R. Viskanta. 1986. "Freezing of liquid-saturated porous media." *Transactions of the ASME*, 108, No. August, 654-659.

# A STRUCTURED MULTI-FACTOR APPROACH TO INVESTIGATE THE EFFECTS OF FAT REDUCTION IN THE CREAM OF A BISCUIT

Eddie Schrevens  
Gerry De Rijck  
Hans Coppenolle

Faculty of Agricultural and Applied Biological Sciences  
Research Unit for Quality Management  
K. Universiteit Leuven  
Kasteelpark Arenberg 30, 3001 Heverlee, Belgium

Email: eddie.schrevens@agr.kuleuven.ac.be

Theo Neutelings

LU-Belgium, DANONE  
De Beukelaer-Pareinlaan 1, 2200 Herentals,  
Belgium

## KEYWORDS

Mixture experiments with process variables, optimization, fat reduction, aroma, emulsifier, food sciences.

## ABSTRACT

This research investigates the possibility to reduce the fat content in the cream of a cracker without a loss in quality (texture). The cream consists of 3 ingredients: cacao, sugar and fat. The effect of both an emulsifier and an aroma in compensating the fat reduction was investigated.

Using a unifactorial approach, reducing only the amount of fat in the cream, also changes the total amount of the cream and the proportions cacao, sugar and fat. In this approach, the experimental factors are mutually confounded. To avoid this correlation between the experimental factors, a multifactorial approach is used based on "mixture theory".

The properties of mixture systems are determined by the proportions of their components, rather than by their quantitative amounts. It is not possible to experiment with the composition of mixture systems in a classical orthogonal or in a unifactorial way. Mixture systems demand a specific design and analysis of the experiments.

The cream was considered as a 3 component mixture system consisting of the components cacao, sugar and fat. The emulsifier and the aroma were considered as process variables. Process variables are variables that are not mixture variables by may effect the properties of the mixture systems.

A {3,1} simplex lattice design in the mixture variables was combined with a 2<sup>2</sup> factorial design in the process variables, resulting in 12 treatments. The textural properties of the cream were measured with a penetrometer and analysed using specific mixture models.

## INTRODUCTION

The aim of this research is to investigate if it is possible to reduce the fat content in the cream of a biscuit from 32 to 27 % without quality loss. Reduction of the fat proportion involves an increase in the sugar and the cacao proportion. To keep the same high quality of the cream two components are added in very low proportions: aroma and emulsifier. Measurements of intrusion forces in time

(texture) are considered as response variables. In the original experiment also organoleptic properties are measured, these are omitted due to lack of space.

## MATERIAL AND METHODS

### Experimental design

The major components of the cream: cacao, sugar and fat can be considered as a 3 component mixture system (Figure 1). The operating composition 1 (12 % cacao, 56 % sugar, 32 % fat) is used in the cream production. The aim of the experiment is to reduce the fat proportion and add aromas and/or emulsifier to compensate for the quality loss.

The experimental design points 1, 2 and 3 form a {3,1} simplex lattice screening design (Figure 1, Table 1). This experimental design is D-optimal to fit a first degree canonical polynomial. This polynomial can be used to represent the response surface over the experimental region, situated between the three experimental design points.

Table 1: Proportions of the experimental design points in the mixture components

Mixture	Cacao	Sugar	Fat
1	0.12	0.56	0.32
2	0.17	0.56	0.27
3	0.12	0.61	0.27

To prevent high collinearity between the independent variables due to the small range of the emulsifier (0 – 1 %) and the aroma (0 – 0.2 %), these variables are considered as "process variables". Process variables are variables that are not mixture components, but may impact the blending properties of the mixtures. Considering the emulsifier and the aroma as process variables makes it possible to generate for these variables an orthogonal design (2<sup>2</sup> factorial design).

In a 2<sup>2</sup> factorial design 2 factors (variables) are investigated in two doses (levels). Each level of the first factor is combined with each level of the second factor, resulting in a total of 4 treatments (Table 2).

The combination of both experimental designs (Table 1 and Table 2) results in a total of 12 (3 x 4) treatments and

investigates a four dimensional experimental region, determined by 5 independent variables (Figure 2).

To investigate if it is possible to compensate for the quality loss due to the reduction of fat by adding aroma and/or emulsifier within the 4 dimensional experimental region, the 12 creams need to be prepared and all the response variables (texture, taste) need to be measured.

Table 2: Proportions of the experimental design points in the process variables

Exp Unit	Emulsifier	Aroma
1	0	0
2	0	0.002
3	0.01	0
4	0.01	0.002

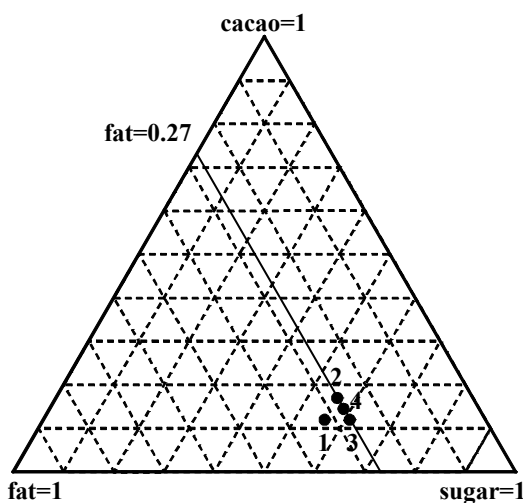


Figure 1: Experimental design in the cream components cacao, sugar and fat

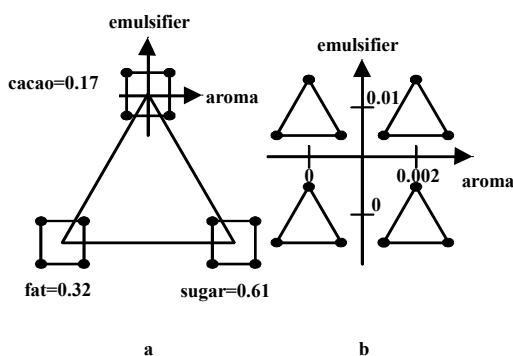


Figure 2: Combined experimental design of a 2<sup>2</sup> factorial design in emulsifier and aroma and a {3,1} simplex lattice design in cacao, sugar and fat. Factorial design nested in the mixture design (a). Mixture nested in factorial (b).

The 12 creams were prepared according to general practice and both textural and organoleptical measurements were carried out. The latter are not discussed in this paper.

The texture of the cream was measured 1 hour, 1 day and 1 week after preparation of the cream at a temperature of 22 °C. In this way, time can be considered as a process variable, extending the 4 dimensional experimental region to 5 dimensions. “Force 1” (penetrometer intrusion force) is considered as an objective measurement for the textural properties of the cream.

LU-DANONE prepared 7 times a cream with the same composition. The texture (force 1) of these creams was measured after 1 hour, 1 day and 1 week. These measurements are used as an error estimate for the preparation of the cream and the measurement of force 1 and are used to test if there is a significant difference in texture within the 5 dimensional experimental region.

## RESULTS

### Analysis of variance

Both the mixture components (Mix: fat, cacao and sugar), the emulsifier and time significantly effect the texture of the cream (Table 3). The investigated aroma doses did not significantly affect the texture of the cream.

There exist a significant interaction between the mixture components and emulsifier, the mixture components and aroma, emulsifier and aroma and emulsifier and time for the texture of the cream.

Table 3: Analysis of variance for the texture of the cream

Source	DF	Mean square	Pr > F
Mix	2	23175	<b>0.00002</b>
Emulsifier	1	1763584	<b>0.00000</b>
Aroma	1	1547	0.25529
Time	2	1101169	<b>0.00000</b>
Mix*emulsifier	2	58303	<b>0.00000</b>
Mix*aroma	2	8648	<b>0.00380</b>
Mix*time	4	1291	0.36261
Emulsifier*aroma	1	6188	<b>0.03038</b>
Emulsifier*time	2	516782	<b>0.00000</b>
Aroma*time	2	713	0.54043
Error	18	1120	

### Response surface regression

The texture of the creams is measured on 3 different times. The variable time can therefore be considered as a process variable, expanding the experimental region from 4 to 5 dimensions. To model the response of the combined experiment and the time, a combination is made of the interaction model in the three process variables emulsifier (z<sub>1</sub>), aroma (z<sub>2</sub>) and time (z<sub>3</sub>):

$$f(z) = \alpha_0 + \alpha_1 z_1 + \alpha_2 z_2 + \alpha_3 z_3 + \alpha_{12} z_1 z_2 + \alpha_{13} z_1 z_3 + \alpha_{23} z_2 z_3 + \alpha_{123} z_1 z_2 z_3$$

and the linear mixture model in the mixture components cacao (x<sub>1</sub>), sugar (x<sub>2</sub>) and fat (x<sub>3</sub>):

$$f(x) = \beta_1 x_1 + \beta_2 x_2 + \beta_3 x_3$$

This results in the following combined model:

$$f(x,z) = \gamma_0^{000} 100x_1 + \gamma_0^{000} 010x_2 + \gamma_0^{000} 001x_3 + (\gamma_0^{100} 100x_1 + \gamma_0^{100} 010x_2 + \gamma_0^{100} 001x_3) z_1 + (\gamma_0^{010} 100x_1 + \gamma_0^{010} 010x_2 + \gamma_0^{010} 001x_3) z_2 + (\gamma_0^{001} 100x_1 + \gamma_0^{001} 010x_2 + \gamma_0^{001} 001x_3) z_3 + (\gamma_0^{110} 100x_1 + \gamma_0^{110} 010x_2 + \gamma_0^{110} 001x_3) z_1 z_2 + (\gamma_0^{101} 100x_1 + \gamma_0^{101} 010x_2 + \gamma_0^{101} 001x_3) z_1 z_3 + (\gamma_0^{011} 100x_1 + \gamma_0^{011} 010x_2 + \gamma_0^{011} 001x_3) z_2 z_3 + (\gamma_0^{111} 100x_1 + \gamma_0^{111} 010x_2 + \gamma_0^{111} 001x_3) z_1 z_2 z_3$$

The complete combined model in pseudocomponent proportions was fitted to the data. This transformation reduces the negative effects of the multicollinearity between mixture components on the variance properties of the estimates. The following L-pseudocomponents transformations transform the weights of the mixture components in pseudocomponent proportions:

$$cacao = \frac{cacao' - 238}{100}$$

$$sugar = \frac{sugar' - 1000}{100}$$

$$fat = \frac{fat' - 500}{100}$$

with: cacao, sugar and fat: pseudocomponent proportions  
cacao', sugar' and fat': weight in kg

The complete combined model (Table 4) represents the data with an adjusted multiple correlation coefficient of 0.84. The variance inflation factors are the same for all variables and equal 7, sufficiently low for mixture experiments. In the complete combined model only the parameter estimates of the variables cacao, sugar, cacao\*time, sugar\*time and fat\*time are significantly different from zero. Replacing in this model cacao, sugar and fat by its pseudocomponent proportion, emulsifier, and aroma by its weight in gram and time by the time in hours, makes it possible to predict the texture for each cream composition and each point of time within the experimental region.

Using stepwise regression a reduced model with 8 terms is selected (Table 5), representing the results with an adjusted multiple correlation coefficient of 0.81.

The reduced model consists of the main effects cacao, sugar and fat, their interaction effects with time and the triple interactions sugar\*emulsifier\*time and fat\*emulsifier\*time. The emulsifier interacts antagonistically with sugar and time and with fat and time.

The reduced second degree model is used to represent the response surface over the experimental region. The complete experimental region is 5 dimensional (6 factors). Since aroma has no significant effect on the texture of the cream, this factor can be removed from the experimental design, reducing the experimental region to 4 dimensions.

Table 4: Regression statistics for the complete combined model

Variable	Parameter estimate	Prob > T	V.I.F.
Ca	536.69	<b>0.0215</b>	7.03
Su	563.57	<b>0.0168</b>	7.03
Fa	299.57	0.1661	7.03
ca*em	-34.56	0.2522	7.03
su*em	-25.85	0.3858	7.03
fa*em	-1.66	0.9549	7.03
ca*ar	-90.32	0.7821	7.03
su*ar	-123.43	0.7058	7.03
fa*ar	121.96	0.3091	7.03
ca*ti	4.97	<b>0.0336</b>	7.03
su*ti	4.76	<b>0.0404</b>	7.03
fa*ti	4.63	<b>0.0452</b>	7.03
ca*em*ar	17.52	0.7047	7.03
su*em*ar	16.06	0.7282	7.03
fa*em*ar	-11.25	0.8075	7.03
ca*em*ti	-0.43	0.1700	7.03
su*em*ti	-0.41	0.1832	7.03
fa*em*ti	-0.38	0.2201	7.03
ca*ar*ti	0.87	0.7930	7.03
su*ar*ti	0.07	0.9831	7.03
fa*ar*ti	-0.20	0.9527	7.03
ca*em*ar*ti	-0.10	0.8267	7.03
su*em*ar*ti	-0.03	0.9515	7.03

Table 5: Regression statistics for the reduced model

Variable	Parameter estimate	Prob > T	V.I.F.
Ca	362.68	<b>0.0027</b>	1.76
Su	414.89	<b>0.0008</b>	1.76
Fa	320.84	<b>0.0069</b>	1.76
ca*ti	2.99	<b>0.0125</b>	1.76
su*ti	5.42	<b>0.0006</b>	2.76
fa*ti	4.77	<b>0.0021</b>	2.76
su*em*ti	-0.55	<b>0.0029</b>	2.0
fa*em*ti	-0.40	<b>0.0256</b>	2.0

Figure 3 represents for 2 emulsifier and 3 times (major horizontal and vertical axis respectively) the response surface for cacao, sugar and fat. The right horizontal axis represents the sugar pseudocomponent proportion and the left horizontal axis represents the cacao pseudocomponent proportion. The pseudocomponent proportion of fat equals 1 minus the pseudocomponent proportion of cacao and sugar.

The major changes in force 1 are caused by time. Increasing time, increases force 1. Increasing the amount of emulsifier from 0 to 10 grams reduces force 1 and even more as time increases. If no emulsifier is added to the cream, force 1 increases as the sugar proportion increases. If 10 gram of emulsifier is present, the highest force 1 is reached at a low sugar and fat proportion and a high cacao proportion.

## CONCLUSIONS

The combination of a {3,1} simplex lattice design in the mixture components cacao, sugar and fat and a  $2^2$  factorial design in the process variables emulsifier and aroma resulted in 12 treatments (creams). The textural properties (intrusion force) of the 12 creams were investigated.

Both the cacao, the sugar, the fat and the emulsifier content of the cream effected its texture. A combined mixture model with 24 terms was fitted to the results and reduced to a model with 8 terms. This model was used to represent the response surface over the experimental region. Time had a strong positive effect, while emulsifier had a negative effect on force 1. If the cream contained no emulsifier the highest force 1 was found at a high sugar proportion. If the cream contained emulsifier, a high cacao proportion resulted in a high force 1.

## REFERENCES

- Belsley, D.A., Kuh, E. and Welsh, R.E., 1980. Regression diagnostics: identifying influential data and sources of collinearity. John Wiley and Sons, New York.
- Cornell, J.A., 1990. Experiments with mixtures. Designs, models and the analysis of mixture data. John Wiley and sons, New York.
- Crosier, R.B., 1984. Mixture experiments: geometry and pseudocomponents. *Technometrics* 26, 3:209-216.
- Gorman, J.W., 1970. Fitting equations to mixture data with restraints on the compositions. *J. Qual. Technol.* 2:186-194.
- Scheffé, H., 1958. Experiments with mixtures. *J. Roy. Stat. Soc. B* 20:344-360.

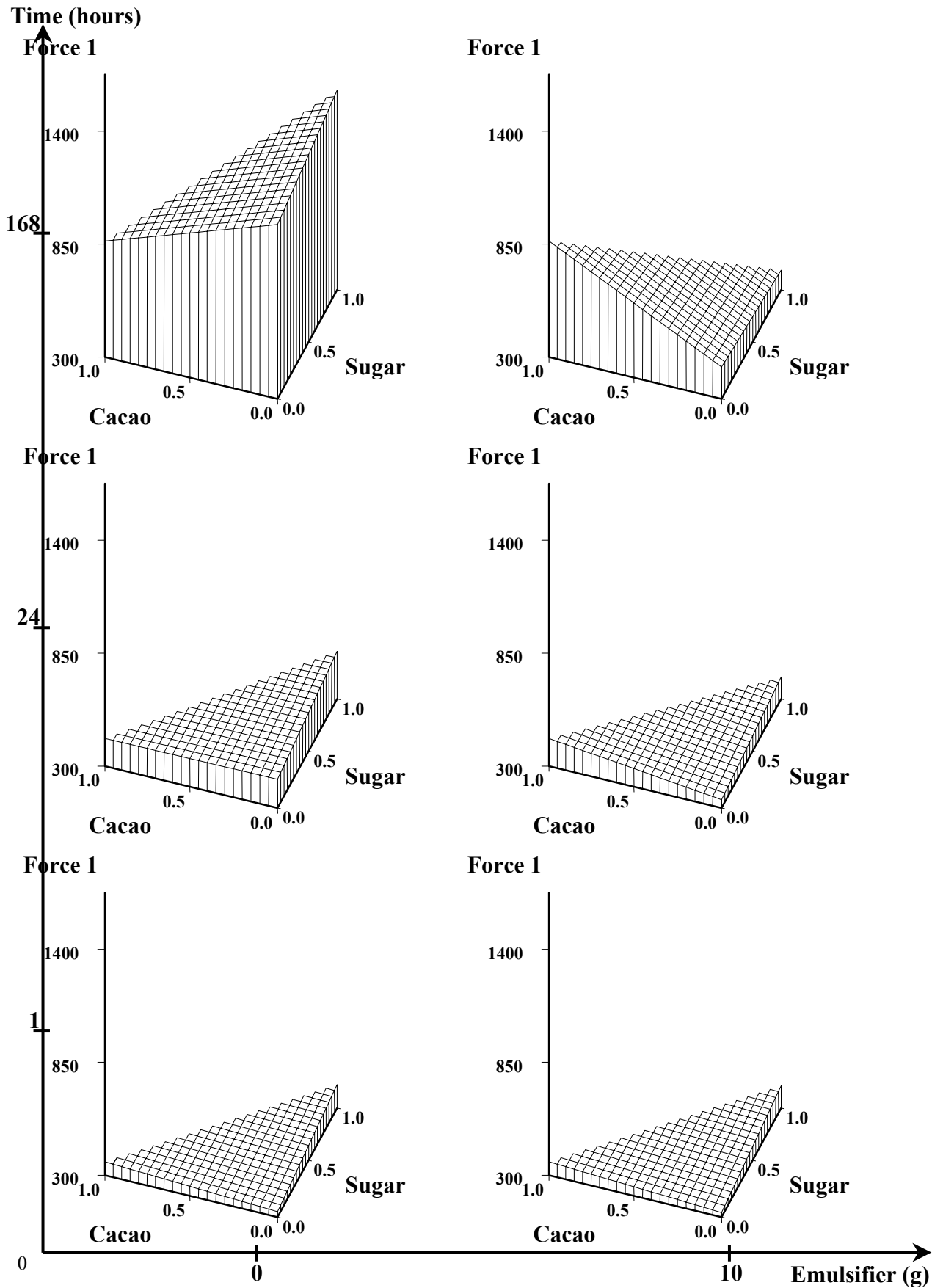


Figure 3: Texture (force 1) as a function of time and cream composition

# PROCESS OPTIMIZATION STRATEGIES TO DIMINISH VARIABILITY IN THE QUALITY OF DISCRET PACKAGED FOODS DURING THERMAL PROCESSING

Philippe Baucour, Kevin Cronin  
Department of Process Engineering  
University College Cork, Ireland  
E-mail: k.cronin@ucc.ie

## KEYWORDS

Temperature dispersion, Quality variability, Sterilization, Process design, Monte Carlo analysis.

## ABSTRACT

A distribution in food product thermal properties will produce a distribution in product temperature throughout a thermal process. This in turn will cause a permanent dispersion in product quality through the mechanism of the temperature sensitivity of product quality thermal degradation kinetics. To guarantee acceptable food safety, the slowest heating product must receive adequate thermal treatment, implying that the majority of the products are over-cooked. Strategies to ameliorate this problem are suggested by determining the optimum processing temperature to minimize the final quality dispersion. As an example, the batch sterilization of packaged foods is analyzed and described by a set of three partial differential equations for (i) the heat transfer, (ii) the quality change and (iii) the microbial reduction. In this case process optimization aims to reduce the final standard deviation in quality (without affecting the final safety) by optimizing schedules for the retort temperature.

## INTRODUCTION

For any food thermal process, it is not possible to obtain an identical temperature/time profile and hence a uniform final product temperature between items in the batch (Smout et al., 2001). A distribution in product initial temperature, variability in product thermal diffusivity together with random fluctuations in environmental processing parameters all contribute to dispersion in the product temperature, (Smout et al., 2000; Varga et al., 2000). Variability in product temperature will in turn produce variability in the levels of a number of product quality attributes, (Lund, 1978; Akterian et al., 1998). It is important to note that the variability in temperature between items in the batch which develops during a thermal process (for instance a heating or cooling schedule) is generally reversible as subsequent conditioning and controlled storage stages will promote temperature uniformity. However temperature dispersion combined with temperature sensitive irreversible quality changes will produce permanent variability in quality levels of the product.

The aim of this paper is to estimate the dispersion in product quality induced by a known variability in product thermal behavior. Variability in other contributing factors such as the quality reaction kinetics and the initial value of the quality attribute are ignored. Knowledge of the dispersion or range in a quality parameter enables the probability that extreme levels will or will not be exceeded to be assessed; this may be significant for customer acceptance. The change in food quality with time can be classified in terms of chemical changes, vitamin destruction, enzyme inactivation, color and taste change or desired structure. For this work a global quality parameter will be analyzed which is a measure of overall quality estimation of the product.

Once the dispersion in quality can be estimated, processing strategies to diminish this dispersion, whilst maintaining the mean quality level within an acceptable band, can be investigated. In particular the selection of the optimum processing temperature and processing time (collectively known as the processing schedule) to minimize quality variability is analyzed. This work examines the well known problem of the unwanted over-processing of most of the product units in a batch heating process to guarantee that the slowest heating unit receives adequate thermal treatment, from a new angle. It must be stated that relatively simple models of product temperature, safety and quality are employed because the focus is not the accurate determination of end points for these parameters but rather to identify their dependence on process settings as a basis for process design optimization. Furthermore while the sterilization of canned foods in a steam retort is selected to illustrate the concept, the intention is to present a more general framework that could be applied to a variety of thermal batch processes.

## THEORY

### TEMPERATURE / QUALITY / SAFETY MODELS

In general, theoretical prediction of the temperature at a given point in a packaged food during a heating process is difficult. Analytical solutions are only available for certain special cases. For a pure conductive heating model for a finite cylinder (like a can) the following differential equation can be applied:

$$\frac{\partial T}{\partial t} = \alpha \left( \frac{\partial^2 T}{\partial r^2} + \frac{1}{r} \frac{\partial T}{\partial r} + \frac{\partial^2 T}{\partial z^2} \right) \quad (1)$$

The model thus assumes no mass transfer (*i.e.* the package

container acts as an impermeable barrier) and heat flow is solely in the radial and axial directions. Furthermore assuming the can surface reaches the temperature ( $T_\infty$ ) of the surrounding medium (steam/hot water) the following boundary conditions will be appropriate:

$$\begin{aligned} T(r = R, z, t) &= T_\infty(t) \\ T(r, z = +\frac{H}{2}, t) &= T_\infty(t) \\ T(r, z = -\frac{H}{2}, t) &= T_\infty(t) \end{aligned} \quad (2)$$

$T$  is product temperature,  $r$  the coordinate in the radius direction,  $z$  the coordinate in the height direction.  $T(r, z, t)$  is the temperature at the position  $(r, z)$  at the instant  $t$ .  $T_i$  is initial product temperature and  $\alpha$  the thermal diffusivity. The dimensions of the can are  $R$  (radius) and  $H$  (height). In a pure conduction system as described by equation 1 the coldest point in the cylinder will be the centre of the can. This will be point of interest and henceforth product temperature is taken to be synonymous with centre temperature. Therefore the statement  $T(r = 0, z = 0, t)$  will be shorten in  $T(t)$  or  $T_\alpha(t)$  when its related to  $\alpha$ .

In equations 1 and 2 others parameters such as the product surface area, product thickness and surface heat transfer coefficient (assumed infinite in this case) are considered to be constant and time invariant. Depending on the exact formulation of the product thermal model, the thermal diffusivity,  $\alpha$  will represent the sensitivity to factors including the product thermal conductivity, specific heat capacity and density. Thus any random variability in these parameters will produce dispersion in the magnitude of the thermal diffusivity,  $\alpha$  and hence in the temperature of the products throughout processing.

If the mean,  $\mu_\alpha$  and standard deviation  $\sigma_\alpha$  in thermal diffusivity are known, appropriate estimates of the maximum and minimum magnitudes for the thermal diffusivity can then be assembled from ( $\alpha_{max/min} = \mu_\alpha \pm n\sigma_\alpha$ ).

Taking a value for  $n$  of 3 implies that approximately 99.7 % of the items will have a thermal diffusivity that lies within these limits assuming the underlying distribution is Normal.

Given the dispersion in temperature response, the subsequent dispersion in safety and quality can then be quantified. Note to distinguish the temperature of a product with a certain value of thermal diffusivity from another the temperature will be note as  $T_\alpha(t)$ .

Applying the D-z model of microbial destruction, the required processing time,  $t_p$  is related to the sterilization value ( $F$ ) by the following equation.

$$F = \int_0^{t_p} 10^{\frac{T_\alpha(t) - T_{ref}}{z}} dt \quad (3)$$

For a mathematical purpose equation 3 could be written as a differential equation.

$$\frac{dF}{dt} = 10^{\frac{T_\alpha(t) - T_{ref}}{z}} \quad (4)$$

Equation 3 or 4 must be solved numerically for each value of  $\alpha$  in order to ensure that each item can reach a minimum in  $F$  value (*i.e.*  $F_{min}$ ).

In general, the order of a quality reaction can vary depending upon the particular quality parameter under study. Nonetheless

according to both Zwietering and Hasting (1997) and Skjoldebrand and Ohlsson (1993) first order reaction kinetics can be used to describe the dominant quality changes:

$$\frac{dQ}{dt} = -kQ \quad (5)$$

$$\text{with } k = k_\infty e^{-\frac{E_a}{R_g T_\alpha(t)}} \quad (6)$$

where  $k$  is the reaction diffusivity and can be sensitive to product temperature, moisture content, quality property concentration, pH, etc. For this work  $k$  is restricted to a dependence on temperature alone and it will generally have a relationship with temperature described by the Arrhenius formula

$E_a$  is termed the activation energy of the particular quality reaction and is a measure of the temperature sensitivity of the reaction.  $R_g$  is the gas constant and  $T_\alpha(t)$  is absolute product temperature, measured in Kelvin. The term  $k_\infty$  is a pre-exponential factor and quantifies the magnitude of the reaction rate independent of temperature.

## MODEL PARAMETERS

For the simulation, all the products were taken to have an identical initial temperature  $T_i$  of 40°C and the processing temperature  $T_\infty$  is investigated within a range from 50°C to 200°C. The physical, thermal and quality properties of the product are chosen to represent those of an average food product, (Hallstrom et al., 1988). The mean value for thermal diffusivity,  $\mu_\alpha$  is  $1.6 \times 10^{-7} \text{m}^2 \cdot \text{s}^{-1}$  and this variable is taken to be described by a Normal distribution, truncated at the  $\pm 3\sigma$  limits, with a coefficient of variation ( $CV$ ) of 10% ( $CV = \sigma_\alpha / \mu_\alpha = 0.1$ ). These values are in line with literature values quoted for food variability with the coefficients of variation being in the region of 10%. The dimensions of the pack are a radius ( $R$ ) of 37.5 mm and height ( $H$ ) of 108 mm. In the safety model,  $T_{ref}$  is 121.1°C,  $z$  is 10°C and  $F_{min}$  is 3 minutes (*i.e.* 180 seconds) which correspond to the standard values for sterilization. The quality kinetic parameters are chosen representatively to be a  $k_\infty$  of  $1.36 \times 10^{-8} \text{s}^{-1}$  and the activation energy  $E_a$  is 86 KJ.Kmol<sup>-1</sup>. These values should be considered as typical values of quality parameters.

## PROCESS OPTIMIZATION

The aim is to diminish the range in product quality at the end of the sterilization process, without affecting the safety of the process, by the optimum choice of magnitudes of the processing parameters. The range in product quality at the end of the heating stage arises from the dispersion in product temperature that in turn is as a result of the variability in the thermal diffusivity. From equation 5 it can be seen that the level of quality at the end of the heating cycle for a given product is a function of three quality kinetic parameters ( $Q_i$ ,  $k_\infty$  and  $E_a$ ) and four thermal process parameters ( $T_i$ ,  $T_\infty$ ,  $\alpha$  and  $t_p$ ). A particular quality reaction rate will fix the magnitudes of the quality parameters. Generally the initial product temperature  $T_i$  is set by an external constraint, *i.e.* the processing / storage regime that the product has received prior to sterilization. Potentially it is possible for the process designer to have some control over the thermal

diffusivity  $\alpha$ ; by adjusting either the surface heat transfer coefficient to the product and/or the product package dimensions,  $H$  and  $R$ . In many cases it is not possible to manipulate  $\alpha$  and this will be the situation here. This means that the thermal diffusivity of each product will be considered fixed and will only vary from one can to another following a normal distribution  $N(\mu_\alpha; \sigma_\alpha)$ .

Hence for this study only the processing temperature  $T_\infty$  will be considered to be adjustable within some acceptable range. Because a conduction heating thermal model is employed with negligible surface resistance, the surface of the food product will be at the temperature  $T_\infty$  and this imposes an upper limit on the possible range of processing temperature. Two separate cases will be analyzed.

- The first case is a single set-point schedule where  $T_\infty$  must remain at a single value throughout the process. Choosing a particular value for  $T_\infty$  will fix the duration, of the process  $t_p$  to achieve the minimum  $F$  value. An analysis will be performed on  $T_\infty$  to determine the best set  $(T_\infty; t_p)$  in terms of safety and final quality distribution. In this relatively straightforward case the criteria to be minimized is the quality range  $\Delta Q$  which is the absolute difference between the quality calculated with the minimum and maximum thermal diffusivity *i.e.*  $\Delta Q = Q_{\alpha_{min}} - Q_{\alpha_{max}}$ .
- The second case is analyzing a schedule where the processing temperature can take two distinct values ( $T_{\infty 1}$  and  $T_{\infty 2}$ ) over the processing time  $t_p$ . In theory this permits a processing schedule to be developed that allows both a minimum sterilization effect (set by food safety standards) and processing time (set by factory throughput requirements) to be independently satisfied. A processing temperature  $T_{\infty 1}$  will be applied for a duration  $t_1$  and a second processing temperature  $T_{\infty 2}$  applied for the remainder of the time. The piecewise function  $T_\infty(t)$  will be:

$$T_\infty(t) = \begin{cases} T_{\infty 1} & \text{if } 0 \leq t \leq t_1 \\ T_{\infty 2} & \text{if } t_1 < t \leq t_p \end{cases} \quad (7)$$

So in this case a set of  $(T_{\infty 1}; T_{\infty 2}; t_1)$  must be determined.

The mean quality  $\mu_Q$  or the standard deviation  $\sigma_Q$  in quality will be optimized *i.e.* a minimization of  $\sigma_Q$  or  $(1 - \mu_Q)$  with a set of constraints depending on the case. To take into account the dispersion in the thermal diffusivity, the optimization is performed with 30 values of  $\alpha$  picked within the normal distribution. When an optimum is found, an estimation of the final dispersion in temperature, quality and  $F$  values will be performed by using 500 values of  $\alpha$ . Table 1 lists the optimizations runs with the constraints in each case.

**Table 1:** Optimization runs with the associated constraints for 1 or 2 processing stages. Each run is designated by a number N°.

Stages	Criteria to minimized	Sampling	N°
1*	Quality range $\Delta Q$	3	1,2
2**	Mean quality $1 - \mu_Q$	30 / 500	3a, 3b
	Standard deviation $\sigma_Q$	30 / 500	4a, 4b

\* For one processing temperature the optimization is not necessary - a simple analysis of the final quality range will provide the best schedule time - temperature.

\*\*For 2 processing stages indices a and b correspond to the total processing time: a for  $t_p=84$  min and b for  $t_p=115$  min.

## RESULTS AND DISCUSSION

### OPTIMIZATION WITH ONE PROCESSING TEMPERATURE

In order to validate the numerical model, its output has been compared to the analytical solution of equation 1 for the case where the processing temperature is constant. A good agreement between the analytical and the numerical solution can be achieved with a 10x10 grid on the can. As an example a treatment at 127°C for 84 min. will lead to a maximum difference in temperature which is less than 1%.

Using a single set-point allows a reduction in the number of calculations. Applying the D-z model of microbial destruction, the required processing time ( $t_p$ ), can be found by considering the time needed for the slowest heating product (with the minimal thermal diffusivity constant  $\alpha_{min}$ ) to achieve the minimum necessary sterilization value,  $F_{min}$  that is appropriate for the particular food. This will ensure that all the items in the batch are adequately sterilized. Thus the safety constraint could be rewritten as a function of  $\alpha_{min}$  only. It will link the processing temperature to the processing time and delimit 2 areas and as is well known delimit two areas and an optimal path in the subspace  $(T_\infty; t_p)$ .

For a single processing temperature two sets of  $(T_\infty; t_p)$  were selected on the curve based the final quality predicted by equation 5. Figure 1 presents the relationships between the final quality and the processing temperature with 3 different values of diffusivities ( $\alpha_{min}, \mu_\alpha, \alpha_{max}$ ).

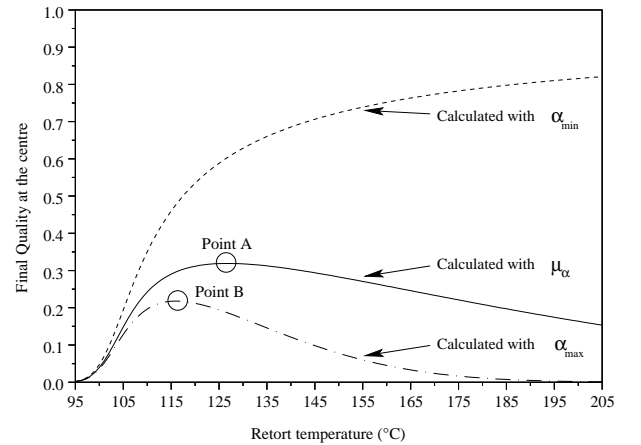


**Figure 1:** Final quality at the center of the can vs the processing temperature for 3 different diffusivities  $\alpha_{min}, \mu_\alpha, \alpha_{max}$ . Point A - Case N°1. Point B - Case N°2.

To illustrate the analysis two processing temperatures ( $T'_\infty$  and  $T''_\infty$ ) with the two corresponding process durations ( $t'_p$  and  $t''_p$ ) were selected in the investigated range. In each case, the required  $F_{min}$  is achieved at the end. The first arrangement (Case N°1) produces a maximum in quality for the mean diffusivity at the end of the process. The second schedule (Case N°2) gives a local minimum in the quality range  $\Delta Q$ .

**Table 2:** Optimization results presented in table 1. For cases 3 and 4 the temperature and quality profiles are shown on figure 2 and 3.

Case N°	$t_p$ (min.)	$T_{\infty 1}$ (°C)	$T_{\infty 2}$ (°C)	$t_1$ (min.)	$\mu_Q$ -	$\sigma_Q$ -
1	84	127	-	-	0.328	0.068
2	115	116	-	-	0.302	0.040
3a	84	118	140	46	0.346	0.078
3b	115	105	167	87	0.342	0.0714
4a	84	127	150	82	0.326	0.0677
4b	115	109	120	55	0.326	0.044

Table 2 presents the final quality distribution for the two possible schedules (Cases N°1 and N°2). The final mean quality is almost the same between the two schedules; 0.328 for a processing temperature of 127°C against 0.302 for 116°C. The higher temperature gives the better mean quality as is in accord with the *High Temperature - Short Time* processing philosophy. By contrast the lower temperature gives a much tighter distribution in quality; a range in quality of 26% for 116°C compared to 42% for 127°C. In other words a small reduction in mean product quality is more than compensated for by much improved control over dispersion in quality. The above analysis indicates that batch thermal processes may be more profitably optimised by considering the effect of processing conditions (*i.e.* temperature) on both mean and dispersion in quality rather than (as has been the case) considering the effect on mean quality only. So the influence of a variable product thermal diffusivity can lead to the adoption of slower schedule than the one generally selected via the standard sterilization rule *High Temperature - Short Time*. Ultimately the best schedule will depend on the costs incurred by the food manufacturer associated with a trade off between the mean and range in product quality.

### OPTIMIZATION WITH TWO PROCESSING TEMPERATURES

By selecting a schedule consisting of two sequential processing temperature and an intermediate time ( $T_{\infty 1}; T_{\infty 2}; t_1$ ), a reduction in the dispersion in  $Q$  at the end of the process compared to a single set point temperature may be possible to achieve (obviously whilst maintaining with the same safety level). From practical considerations each processing temperature will be chosen to lie within a range 50-200°C. In order to compare the two approaches (a schedule with one versus that with two temperatures) the total processing time,  $t_p$  will be given a value equal to 84 or 115 minutes.

Also to facilitate comparison, another constraint will be imposed on the final mean quality ( $\mu_Q$ ) at the centre of the can; *i.e.* it must not be less than the quality that can be achieved with only one processing temperature (*i.e.*  $\mu_Q \geq 0.328$ ). The optimisation software found that two combinations of  $T_{\infty 1}$  and  $T_{\infty 2}$  gave local maxima for quality parameters for each of the two process times. For all four schedules the pattern is that a low processing temperature followed by a higher temperature is best for quality (mean and dispersion) rather than the reverse. The best processing conditions, as predicted by the optimisation software, and the resultant mean and standard deviation in final product quality are given in table 2. The data is presented for two separate processes, having a total time of 84 min and and 115 min respectively and thus allows comparison with the corresponding single set-point schedules. Figures 4 and 5 compare the distribution in product quality given by the optimal schedules for the two step

process compared with the single point schedule (Table 2).

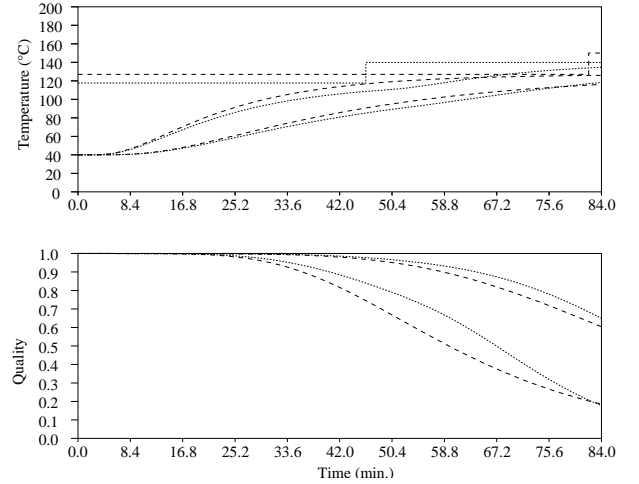


**Figure 2:** Temperature and Quality profiles determined after with two processing temperature (- - Case N°4a; ..... Case N°3a). For each schedule only the extreme values of the thermal diffusivity are represented ( $\alpha_{min}, \alpha_{max}$ ). The total processing time is 84 minutes.

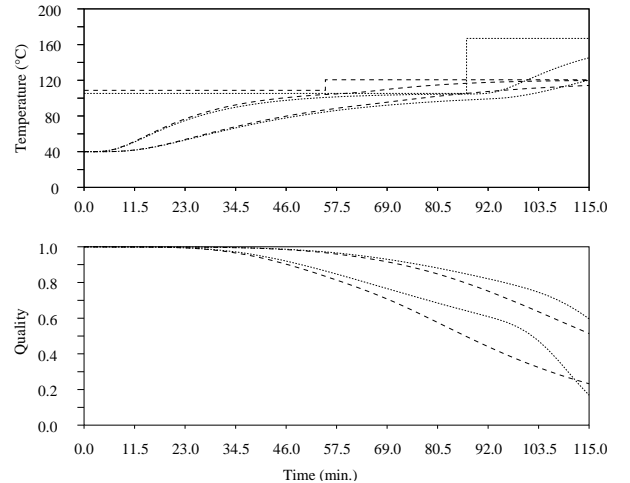


**Figure 3:** Temperature and Quality profiles determined after with two processing temperature (- - Case N°4b; ..... Case N°3b). For each schedule only the extreme values of the thermal diffusivity are represented ( $\alpha_{min}, \alpha_{max}$ ). The total processing time is 115 minutes.

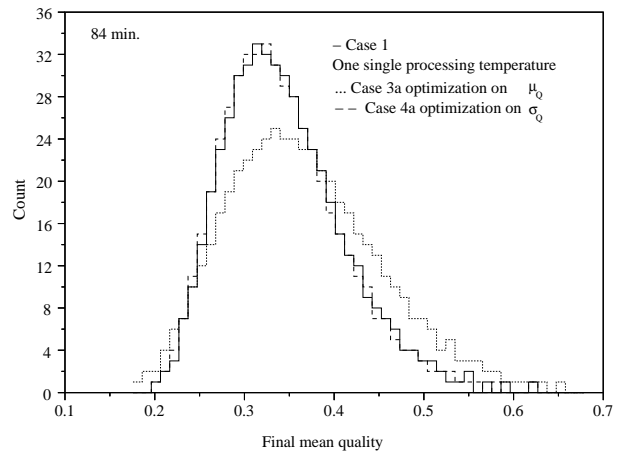


**Figure 4:** Optimization results. Compared distributions between cases 3a, 4a and the one determined with only one processing temperature. The total processing time is 84 minutes.

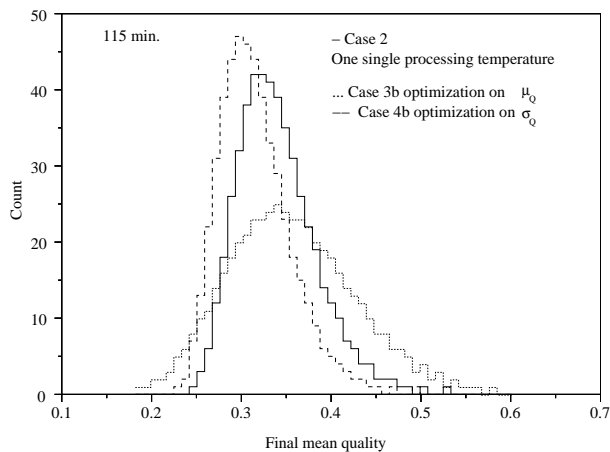


**Figure 5:** Optimization results. Compared distributions between cases 3b, 4b and the one determined with only one processing temperature. The total processing time is 115 minutes.

For a total processing time of 84 minutes there is a small improvement in the final mean quality (0.346 against 0.328) but a worse standard deviation (0.078 against 0.068) when comparing the two step schedule of 118°C / 140°C against the original single point schedule. The second two step schedule of 127°C / 150°C is very close to that of the single point schedule and matches the standard deviation but with a slightly worse mean value in quality (0.326 compared to 0.328). For the longer processing time of 115 minutes, both two step schedules give an improvement in mean quality when compared to the single set point schedule though at the expense of a slightly poorer standard deviation.

Overall then, these results indicate that a processing schedule consisting of two set points can only give a marginal improvement in final quality as compared to that achievable with a single set point. Choosing from the four two point schedules the best compromise between mean and standard deviation in quality is given by the 109°C for 55 minutes followed by 120°C for the remainder of the 115 minutes. The mean and standard deviation in quality (0.326 and 0.044) that would result from the adoption of this schedule are probably marginally preferable to the quality parameters that are available from the single set point schedules.

## CONCLUSIONS

A combination of tools to predict the temperature, quality and safety during a thermal processing have been developed. These tools have been combined with a Monte Carlo analysis to take into account the variability of the thermal diffusivity and an optimization routine to determine an acceptable processing schedule. As an example the sterilization process has been selected because it involves thermal processing combined with quality and safety issues. The schedules tested consist in constant processing temperatures for different period of time (1 or 2 stages). The optimization has been done in 3 steps:

1. For a single step process the optimization has been done via an analysis of the final quality range determined with the extremal possible values of the thermal diffusivities ( $\alpha_{min}$ ;  $\alpha_{max}$ ). for which it has been shown that adopting a

slower schedule ( $T_{\infty}=116^{\circ}\text{C}$ ,  $t_p=115$  min.) will give an acceptable final mean quality and a better standard deviation.

2. The 2<sup>nd</sup> step consists in an optimization of a 2 stages schedule with a 3 different values of the thermal diffusivity ( $\alpha_{min}$ ;  $\mu_{\alpha}$ ;  $\alpha_{max}$ ). The results show that none of the schedule selected are suitable for a variable thermal diffusivity.
3. Finally, an optimization which takes into account the variability has been performed. It has been shown that the gain in mean quality is almost negligible from an industrial point of view but a significant reduction of final dispersion is possible by adopting a 2 stages schedules. Once again a slower process provides the best result.

This framework could be implemented for any thermal process which involves a quality and / or a safety model. The main disadvantage consists in the use of a Monte Carlo analysis which is relatively easy to run and provides a good understanding of the statistical changes during the process. Unfortunately the Monte Carlo is computing time consuming and will not be suitable to extend the present study by crossing different sources of variability like the position, the processing temperature or the heat transfer coefficient.

## REFERENCES

- Akterian, S., Smout, C., Hendrickx, M., Tobback, P., 1998. Application of sensitivity functions for analysing the impact of temperature non-uniformity in batch sterilizers. *Journal of Food Engineering* 37 (1), 1–10.
- Hallstrom, B., Skjoldebrand, S., Tragardh, C., 1988. *Heat transfer and food products*. Elsevier Applied Science, London.
- Lund, D., 1978. Statistical analysis of thermal process calculations. *Food Technology* 3, 76–83.
- Skjoldebrand, C., Ohlsson, T., 1993. A computer simulation program for evaluation of the continuous heat treatment of particulate food products. Part 1: design. *Journal of Food Engineering* 20, 149–165.
- Smout, C., van Loey, A., Hendrickx, M., 2000. Non-uniformity of lethality in retort processes based on heat distribution and heat penetration data. *Journal of Food Engineering* 45 (2), 103–110.
- Smout, C., van Loey, A., Hendrickx, M., 2001. Role of temperature distribution studies in the evaluation and identification of processing conditions for static and rotary water cascading retorts. *Journal of Food Engineering* 48 (1), 61–68.
- Varga, S., Oliveira, J., Smout, C., Hendrickx, M., 2000. Modelling temperature variability in batch retorts and its impact on lethality distribution. *Journal of Food Engineering* 44 (3), 163–174.
- Zwietering, M., Hasting, A., 1997. Modelling the hygienic processing of foods - a global process overview. *Food and Bioproducts Processing* 75, 159–167.



# FLUIDS



# IMPINGEMENT COOLING OF SOLID CYLINDRICAL FOODS USING CFD

Eva E. M. Olsson  
Environment and Process  
Engineering  
SIK  
P.O. Box 5401  
SE-402 29 Göteborg  
Sweden  
eo@sik.se

Lilia M. Ahrné  
Environment and Process  
Engineering  
SIK  
P.O. Box 5401  
SE-402 29 Göteborg  
Sweden  
lia@sik.se

Christian Trägårdh  
Food Engineering, Centre for  
Chemistry and Chemical Engineering  
Lund University  
P.O. Box 124  
SE-221 00 Lund  
Sweden  
christian.tragardh@livstek.lth.se

## KEYWORDS

Impingement cooling, impinging air jet, heat transfer, Nusselt number, CFD, cylindrical food.

## ABSTRACT

Simulations of impingement cooling with a slot air jet in a semi-confinement area were performed using CFD (computational fluid dynamics). The surface heat transfer coefficient and the Nusselt number distribution on the cylindrical food product and on the underlying surface were studied. The dependency of Nusselt number on Reynolds number was determined under steady state condition. The Nusselt number increases with Reynolds number, which was varied between 23000 and 100000. The characteristics of the velocity distribution of the jet impinging on the cylinder in the computational domain were also determined.

## NOMENCLATURE

C	coefficient of correlation $Nu=CRe^m$
D	diameter of cylinder and width of jet (m)
Fr	Frössling number ( $Fr=Nu/Re^{0.5}$ )
h	heat transfer coefficient ( $W/(m^2K)$ )
H/D	nozzle-to-cylinder distance
k	thermal conductivity ( $W/(mK)$ )
m	exponent of Re in $Nu=CRe^m$
Nu	local Nusselt number ( $Nu=h*D/k$ )
$Nu_s$	Nusselt number in the stagnation point
Re	Reynolds number ( $Re=vD/\nu$ )
SST	shear stress transport
v	velocity (m/s)
x/D	distance from the jet stagnation point

## Greek symbols

$\theta$	angle on the cylinder
$\nu$	kinematic viscosity ( $m^2/s$ )

## INTRODUCTION

Cooling of pre-cooked solid foods is often the rate determining step in the process and therefore often a bottle neck in food production. With conventional chilling methods long chilling times are necessary to cool the

product to temperatures where growth of micro-organisms will not occur. Rapid chilling reduces the risk of microbiological growth, increases the product quality and the production capacity.

Impinging jets of air are widely used as an effective method to increase heat and mass transfer in widespread areas, such as cooling of electronics, drying of paper, cooling systems in gas turbines, anti-ice systems on aircrafts etc. In the food industry impingement jet systems is used for heating (Marcroft and Karwé 1999), drying (Moreira 2001) and freezing (Soto and Bórques 2001). The high turbulence characteristics enhance the heat transfer and therefore improve food quality.

Numerous studies, both experimental and numerical, of impingement heat transfer and flow characteristics have been reported in the literature. Most of the studies are concerned with the effect of Reynolds number, nozzle-to-surface distance, nozzle geometry, jet orientation, multiple jets, cross flow and impinging surface shape. Although many different jet characteristics have been considered a great majority of the impinging jet studies are on the flat plate (Baughn and Shimizu 1989; Yan et al. 1992). However, some papers are concerned with impinging jets on objects such as a curved surface (Lee et al. 1999), a cylinder (McDaniel and Webb 2000) and a cylindrical pedestal (Baughn et al. 1993).

Several reviews and summaries on impinging jet heat transfer can be found in the literature (Downs and James 1987; Jambunathan et al. 1992). Impingement in food processing has also been reviewed (Ovadia and Walker 1998).

Downs and James (1987) reviewed heat transfer characteristics of impinging jets with round and slot nozzles. Geometric and temperature effects, interference and crossflow, turbulence levels, incidence, surface curvature, externally applied factors, jet outlet conditions and non-uniformity of jet arrays were summarised. Jambunathan et al. (1992) reviewed experimental data for heat transfer rates on circular jet impinging on a flat plate. Jets of Reynolds number in the range of 5000-124000 and nozzle-to-plate surface distance in the range of 1.2-16 were considered.

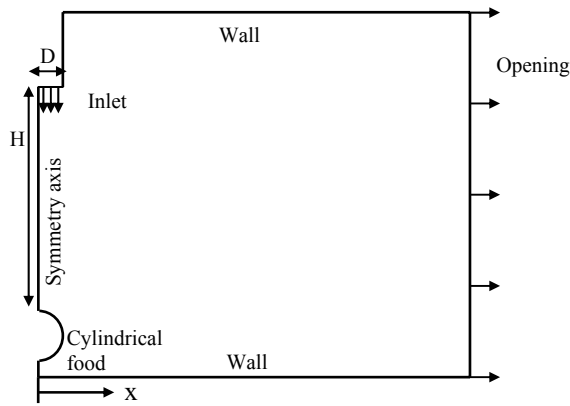


Figure 1. The computational domain.

In order to understand the heat transfer characteristics of impingement cooling of solid foods, the objective of this study is to determine the Nusselt number on the surface of the cylindrical food product and on the underlying plate for varying Reynolds numbers (23000-100000). The goal is also to determine the dependency of Nusselt number on Reynolds number, and to study the characteristics of the airflow from the slot air jet. The jet is impinging on a solid cylinder in two dimensions in a semi-confinement area.

## MATERIAL AND METHOD

Steady state simulations of a slot air jet impinging on a solid cylindrical food were performed using the CFD-software CFX 5.5 (AEA Technology).

The cylindrical food has a diameter of 35 mm and the slot air jet has a width of 35 mm. The depth is infinite. There is a symmetric boundary condition in the centre of the slot jet in the computational domain, see figure 1. The length of the domain is 30 cm, the height is 27.5 cm and the length of the nozzle is 5 cm. The food is “floating” 5 mm above the underlying surface due to computational difficulties. The nozzle-to-target distance ( $H/D$ ) is 4.

The air inflow has a temperature of  $2^{\circ}\text{C}$  and the operating pressure is 1 atm. The jet Reynolds number is varied between 23000 and 100000, i.e. a velocity of approx. 10 -

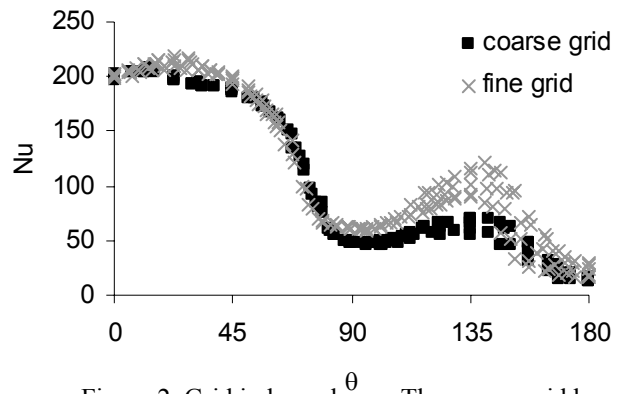


Figure 2. Grid independency. The coarse grid has approx. 250000 elements and the finer grid approx. 800000 elements,  $Re=50000$ .

40 m/s using the nozzle exit width as characteristic length. The initial temperature of the surface of the cylindrical food is  $35^{\circ}\text{C}$ . Using the ambient temperature (the jet exit temperature) and the surface temperature of the cylinder, the heat transfer coefficient and corresponding Nusselt number based on the jet width was then calculated.

The turbulence model used was the Shear Stress Transport model (SST) found in CFX 5.5. The SST model blends between a  $k-\omega$  model near the wall and a  $k-\epsilon$  model far away from the wall. The model uses a low Reynolds number model if the grid near a wall is very fine ( $y^+ < 11$ ) and a wall function beyond that (AEA Technology).

## RESULT AND DISCUSSION

### Grid independency

The computational domain, see figure 1, uses a tetrahedral mesh of approx. 250000 elements. In the boundary layers an inflated boundary is used with cumulative prisms from the cylinder,  $y^+=0.03-9.7$ . To make sure that the simulations are grid size independent a simulation was made with a finer mesh consisting of nearly 800000 elements. The finer grid had a similar shape of the distribution of local Nusselt number as the coarse grid, but especially at  $\theta=135^{\circ}$  the finer grid predicted a more pronounced secondary maximum, see figure 2. This could

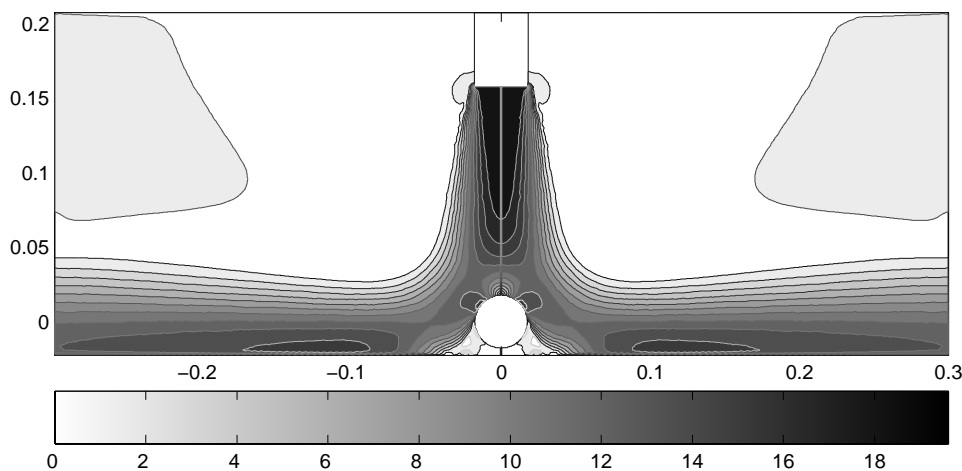


Figure 3. A contour plot of the velocity of a jet with Reynolds number of 50000 (reflected in the centre).

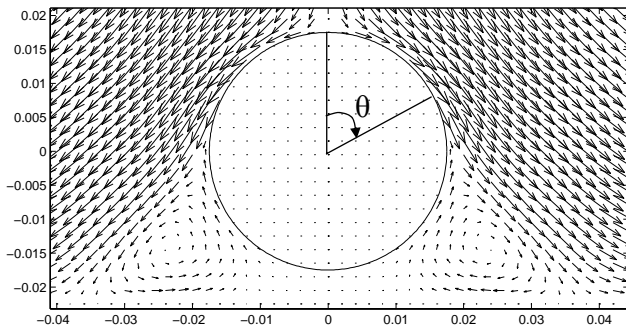


Figure 4. Flow pattern of the velocity near the vortex on the side of the impinging jet. Note: The vectors are resampled, the computational grid is not used.

be due to the difficulty in resolving the vortex behind the cylinder properly with a coarse grid. Another reason might be the location of the inner nodes at different dimensionless distances around the circumference of the cylinder.

### Flow characteristics

Figure 3 shows a contour plot of the velocity variation in the computational domain. The high velocity of the jet entrains air of lower velocity from the cavity and an initial mixing zone is created. Figure 4 shows the velocity vectors of the jet impinging on the cylindrical food. Flow separation occurs at about  $90^\circ$  on the cylinder and a vortex is created at the back ( $\theta=135^\circ$ ) of the cylinder. Just beyond the impingement region, the flow structure is significantly characterised by the strong curvature of the streamlines, see figure 6.

The impinging jet consists of two types of flow, one orthogonally that impinge on the surface and a parallel wall jet. At the top of the cylinder there is a stagnation point, where the jet impinge on the cylinder ( $\theta=0^\circ$ ). The heat transfer rate is high in the stagnation point, see figure 5 and 7. This is naturally a result of the flow predictions as well as how the analogy between momentum and heat transfer is formulated. Optimum nozzle-to-surface distance (H/D) coincides with the length of the potential core (Downs and James 1987). The potential core region for slot jets is  $H/D < 4-6$  (McDaniel and Webb 2000). The importance of the correct distance of nozzle-to-surface target (H/D) is

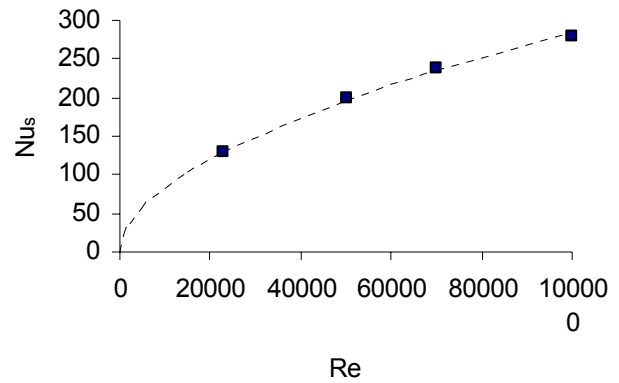


Figure 5. Nusselt number in the stagnation point as a function of Reynolds number. The fitted curve corresponds to  $Nu_s = 0.61 \cdot Re^{0.53}$ .

described in McDaniel and Webb (2000), along with the influence nozzle width has on the heat transfer rates.

### Stagnation point heat transfer

The Nusselt number in the stagnation point ( $Nu_s$ ) depends on the Reynolds number, see figure 5. For a fixed H/D distance the Nusselt number increases with Reynolds number. This result agrees fairly well with results of other authors on a flat plate (Baughn and Shimizu 1989; Yan et al. 1999). Baughn and Shimizu (1989) used a round impinging jet with a Reynolds number of 23750 and various H/D (2, 6, 10 and 14). Yan et al. (1999) used also a round impinging jet, a Reynolds number of 23000, 50000 and 70000 and an H/D distance of 2, 6 and 10. The Nusselt number is slightly lower (approx 10%) than on the flat plate. The result of Lee et al. (1999) indicates however that the  $Nu_s$  should be higher for jet impingement on a curved surface. Predicted values are strongly coupled to the features of the turbulence model. Each of the numerous turbulence models given in the literature has its own strengths and weakness both regarding prediction of the flow characteristics as well as for heat transfer.

A linear regression using the logarithms of  $Nu_s$  and Re is used to obtain the constant C and the exponent m in the relation  $Nu_s = C \cdot Re^m$  for H/D=4. The result is,  $C=0.61$  and  $m=0.53$ , i.e.  $Nu_s = 0.61 Re^{0.53}$ . The Frössling number ( $Fr = Nu_s / \sqrt{Re}$ ) in the stagnation point is 0.85-0.9.

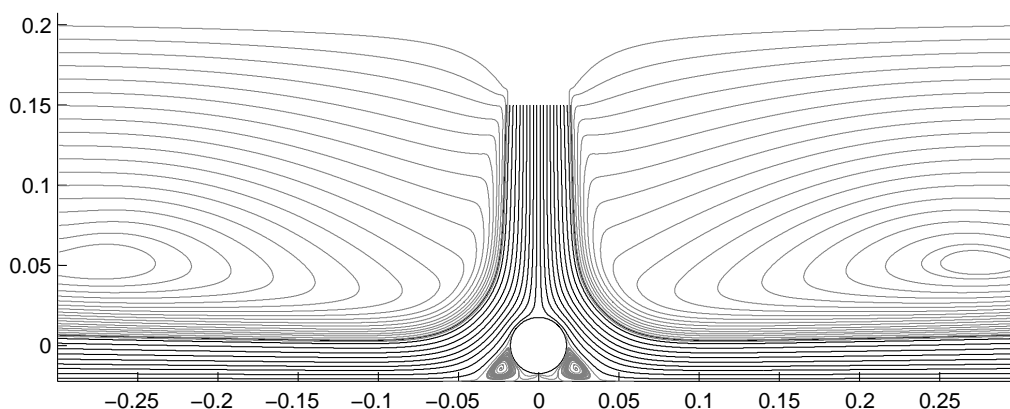


Figure 6. Streamlines of the velocity field,  $Re=50000$  (reflected in the centre).

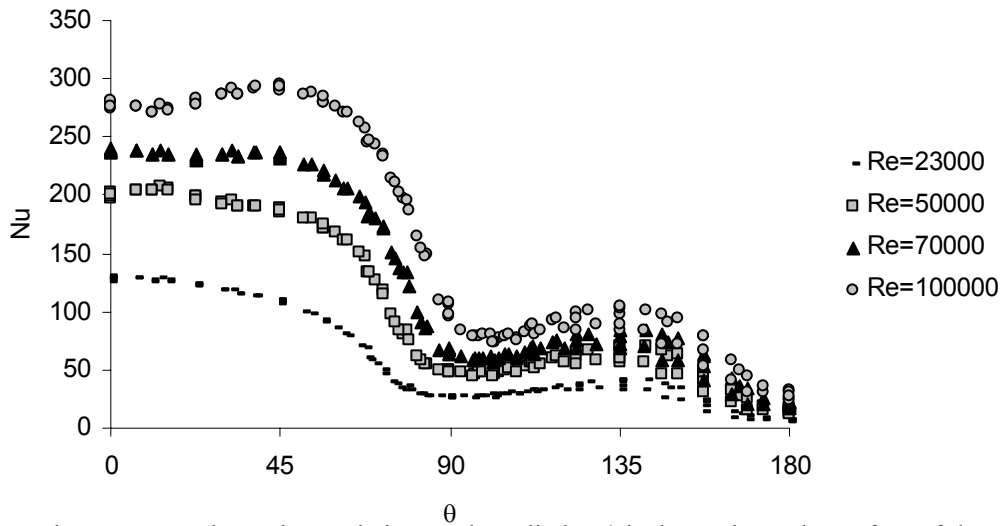


Figure 7. Nusselt number variation on the cylinder,  $\theta$  is the angle on the surface of the cylinder,  $\theta=0$  on top of the cylinder, for varying Reynolds number (23000-100000).

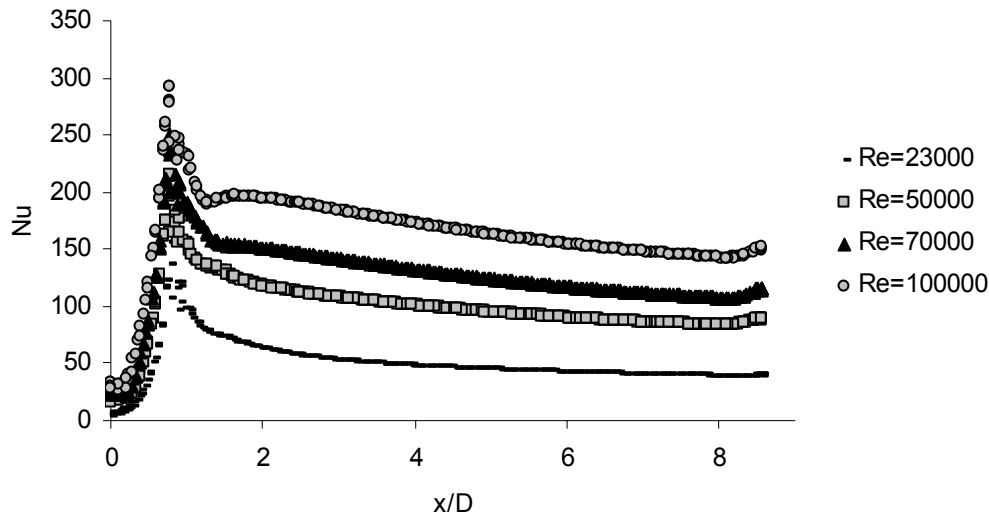


Figure 8. Nusselt number variation on the underlying surface, for varying Reynolds number (23000-100000).

### Nusselt number distribution on the cylinder

The Nusselt number varies on the surface of the cylinder, see figure 7. For Reynolds number of 23000, 50000 and 70000 the structure of the curve is identical, but different values of Nusselt number. The highest heat transfer is observed at the top of the cylinder. The Nusselt number on the upper half of the cylinder is slowly decreasing until approx.  $\theta \approx 50-55^\circ$ , where it decreases abruptly to a local minimum at  $\theta=90^\circ$ . The Nusselt number increases then to a local maximum at  $135^\circ$  and then down to zero at the back of the cylinder ( $\theta=180^\circ$ ).

For Reynolds number of 100000, the structure of the curve is similar to cases having lower Reynolds number, with exception of another local maximum at approx.  $45^\circ$ . A drastic reduction in boundary layer thickness at about this position, as the flow velocity increases, would be expected suggesting that this local maximum at about  $\theta=45^\circ$  may have some physical explanation.

The local minimum at  $\theta=90^\circ$  corresponds to the separation of flow at the edge of the cylinder and the local maximum at  $\theta=135^\circ$  corresponds to the creation of the wake behind the cylinder.

### Nusselt number distribution on the underlying surface

Figure 8 shows the distribution of the Nusselt number on the underlying surface ( $0 < x/D < 8.5$ ). The Reynolds number is varied between 23000 and 100000.

The Nusselt number is almost zero under the cylinder and increases to a peak value at  $x/D=0.5-1$ . This is in the same area where the maximum is on the cylinder. For  $x/D > 1$ , the Nusselt number decreases slowly. In comparison with results of Lee et al. (2000), the curve after  $x/D > 1$  agrees fairly well, but a round impinging jet on a flat surface is used as mention before. The result of Yan et al. (1992) is also comparable after about  $r/D=2$  where there is a maximum.

## CONCLUSIONS

The flow pattern from the jet impinging on the cylindrical food product, the Nusselt number distribution on the surface of the cylinder, the Nusselt number variation on the underlying surface and the Nusselt number dependency on the Reynolds number was studied using CFD simulations.

When the jet impinges on the cylinder, a stagnation point is created and the jet becomes a wall jet. A vortex is created on the side/below the cylinder.

The Nusselt number on the surface of the cylinder was estimated. The Nusselt number is highest in the stagnation point, indicating that the heat transfer rates are largest in the stagnation point. At the upper part of the cylinder ( $-50^\circ < \theta < 50^\circ$ ) the Nusselt number is approximately the same as in the stagnation point. On the side of the cylinder the Nusselt number drops rapidly to about one third of the Nusselt number in the stagnation point. The heat transfer increase slightly to a maximum at  $\theta \approx 135^\circ$ , it decreases then to zero on the back of the cylinder.

The distribution of Nusselt number on the underlying surface is almost zero below the cylinder, increasing abruptly to a peak value at  $x/D=0.5-1$  and then slowly decreases.

The stagnation point heat transfer was determined for various Reynolds numbers (23000, 50000, 70000 and 100000). The Nusselt number increases with Reynolds number as a function of  $Re^m$ . A linear regression gives the coefficients  $C=0.61$  and  $m=0.53$  (in  $Nu=CRe^m$ ) and the Frössling number is 0.85-0.9. It can be concluded that the heat transfer from the impinging jet is strongly dependent on Reynolds number, i.e. air velocity since ( $Re=vD/\nu$ ).

## FURTHER WORK

Further work on cooling of solid foods with impinging jets is planned. This paper is just the beginning of a Ph.D. project and it concludes the first steps of determining the heat transfer rates from impinging jets on solid foods.

In future work a more thorough investigation on heat transfer of impinging jets is planned, along with chilling times necessary to cool the food product to a certain temperature and the influence on texture of foods. Experiments for validation of the simulations are going to be performed in an impingement unit in a recent future.

## ACKNOWLEDGEMENTS

This work has been financed by the Swedish Knowledge Foundation and Lecora AB in Vadstena, Sweden.

## REFERENCES

AEA Technology "CFX 5.5 User manual."  
Baughn, J.; Mesbah, M.; and Yan, X. 1993 "Measurements of local heat transfer for an impinging jet on a cylindrical pedestal." *Turbulent Enhanced Heat Transfer ASME*, No. 239, 57-62

Baughn J. and Shimizu, S. 1989 "Heat transfer measurements from a surface with uniform heat flux and an impinging jet." *Journal of Heat Transfer*, No. 111, 1096-1098  
Downs, S.J. and James, E.H. 1987. "Jet impingement heat transfer - a literature survey." *The American Society of Mechanical Engineers*, 87-HT-35, 1-11  
Jambunathan, K.; Lai, E.; Moss, M.A.; and Button, B.L. 1992. "A review of heat transfer data for single circular jet impingement." *International Journal of Heat and Fluid Flow*, No. 13(2), 106-115  
Lee, D.H.; Chung, Y.S.; and Kim, M.G. 1999. "Technical Note Turbulent heat transfer from a convex hemispherical surface to a round impinging jet." *International Journal of Heat and Mass Transfer*, No. 42, 1147-1156  
Marcroft, H.E. and Karwé, M.V. 1999 "Flow field in a hot air jet impingement oven - part I: A single impinging jet." *Journal of Food Processing Preservation*, No. 23, 217-233  
McDaniel, C.S. and Webb, B.W. 2000 "Slot jet impinging heat transfer from circular cylinders." *International Journal of Heat and Mass Transfer*, No. 43, 1975-1985  
Moreira, R.G. 2001 "Impingement drying of foods using hot air and superheated steam." *Journal of Food Engineering*, No. 49, 291-295  
Ovadia, D.Z. and Walker, C.E. 1998. "Impingement in food processing." *Food Technology*, No. 52(4), 46-50  
Soto, V. and Bórquez, R. 2001 "Impingement jet freezing of biomaterials." *Food Control*, No. 12, 515-522  
Yan, X.; Baughn, J.W.; and Mesbah, M. 1992 "The effect of Reynolds number on the heat transfer distribution from a flat plate to an impinging jet." *Fundamental and Applied Heat Transfer Research for Gas Turbine Engines ASME*, No. 226, 1-7

## AUTHOR BIOGRAPHY

**EVA OLSSON** is an industrial Ph.D.-student at the Division of Food Engineering, Centre for Chemistry and Chemical Engineering, at Lund University, Sweden, working at the Dept. of Environmental and Process Engineering at SIK (The Swedish Institute for Food and Biotechnology). Her undergraduate education is from Chalmers University of Technology, Gothenburg, Sweden, where she finished her M.Sc. in Chemical Engineering with Engineering Physics in the end of year 2000.

**LILIA AHRNÉ** is research manager for Process Engineering at SIK. She graduated in Food Engineering in 1989 at Catholic University of Portugal, School of Biotechnology, and obtained her Ph.D. in Biotechnology, Food Science and Engineering in 1994. Her main areas of research are optimisation of food processes, considering heat and mass transfer and kinetics of quality changes during processing and storage.

**CHRISTIAN TRÄGÅRDH** is a professor and the head of the Division of Food Engineering, Lund Institute of Technology at Lund University, Sweden. In research, he is heading the Food Fluids Engineering Group. The core activities are experiments and modelling of dispersion, aggregation, coalescence and adhesion of molecules, particles, drops and bubbles and heat and mass transfer related to fluid flow. He is also theme manager in the Future Technologies for Food Production programme in Sweden, assisting prefect at the Centre for Chemistry and Chemical Engineering and educational leader for the Biotechnology programme at LTH.

# DETERMINING SHEAR DAMAGE OF MILK IN PROCESS EQUIPMENT

Jesper Sæderup Nielsen

Bo B. B. Jensen

Alan Friis

Food Process Engineering, BioCentrum-DTU

Building 221, DK-2800 Lyngby

Denmark

E-mail: jsn@biocentrum.dtu.dk

## KEYWORDS

Computational Fluid Dynamics, Milk Fat Globules, Process Modelling, Process Product interaction

## ABSTRACT

Shear rates may result in damage of milk fat globules depending on the actual process conditions. Using Computational Fluid Dynamics (CFD) to predict shear rates in process equipment, it is possible to set-up a food process model to simulate the fat globule damage in milk during processing. In extreme situations fat globule damage may become visible for consumers as insoluble fat lumps. Time, temperature and fat content are the three main factors influencing resistant towards shear damage of the fat globules. Result shows that the rate of fat globule damaged was increasing during shearing, and that they are most fragile in the temperature interval between 15 and 35°C. Cream containing 38 % fat was damaged at a lower shear rate compared to creams with lower fat content. Combining CFD simulations of flow fields in production equipments with results of flow describing parameters effect on food quality shows to be a powerful tool, which will extend our knowledge of producing good quality foods.

## INTRODUCTION

The quality of food products is determined by the raw material quality and the impact of the production processes involved. Previously the applied quality descriptors have largely been based on bulk parameters and thus lacking specific information on the influence of local occurrence of extreme process conditions in processing plants. Along with the use of continuous processing and design of still larger production facilities where pipe dimensions are on the increase the residence time distributions broadens and likewise the distributions of derived quality parameters. Hence investigations of local processing conditions and the characteristics of smaller fractions of a bulk can be of great importance when determining the quality of a food product. This paper introduces an approach where process parameters influencing the quality of milk products have been studied under controlled conditions in the laboratory. The distribution in physical characteristics is related to process models describing the flow of liquids through pipes. It is shown that the applied model can be used to predict how the process affects the quality distribution of the final product.

During processing, milk is exposed to shear rates of different magnitudes. Fat globules in milk are destabilised

when exposed to flow fields with a certain shear rate at a given temperature. The destabilisation is a consequence of fat globule deformation by shearing, and depends on fat globule size, conditions of the fat globule membrane and entrapped fat. Disruption of the fat globules may lead to agglomeration. In milk exposed to a harsh mechanical treatment i.e. high shear rates; agglomeration of fat globules could become visible to consumers as insoluble lumps of fat in the top of the milk container. This is a problem frequently occurring in e.g. organic whole milk, as this milk is not homogenised in Denmark.

In the dairy industry such knowledge has restricted milk velocities through pipes. These mean velocity recommendations have been applied to all pipe diameters disregarding that the maximum shear rate decreases with increasing pipe diameter at a given velocity. It has now been realised that this approach has its limitations, and the dairy industry has shown great interest in increasing the capacity of production lines by increasing the velocity. Hinrichs (1998) presented a model for milk and cream velocities in pipes, where fat globule damage is avoided. However, processing of milk is performed in other equipment than pipes e.g. bends, valves, pumps etc. Meaning that models based on fat globule damage in straight pipes are likely to over estimate the allowable velocities as shear rates are higher in complex equipments. This work aims at developing a model for predicting fat globule damage in milk during transport through complex equipment at different processing conditions. The model is based on data from measurements of fat globule damage in milk exposed to a known shear rates at different conditions. Computing shear fields in production equipment using Computational Fluid Dynamics (CFD) makes it possible to predict the total effect from the shear rates in production equipment on the milk fat globules. The process model is validated by experiments and is constructed to be applicable for scale-up to other production equipments where the shear rates are known only from CFD analysis. This article presents preliminary results, and illustrates the approach.

## MATERIAL AND METHODS

### Raw Materials

Pasteurised milk (3,5 % fat) and cream (38 % fat) bought locally was kept refrigerated until use. Required fat content in samples were achieved by gently mixing milk and cream.

**Shear Treatment**

The sample temperature was allowed ample time to equilibrate to the specified temperature. Samples were sheared in a Haake VT 500 viscometer (Thermo Haake, Germany) using the NV double cap cup and rotor. Temperatures were controlled during shearing by a Haake DC30-K10 water bath circulating water to the shear cell. After treatment, samples were cooled to 5°C and kept for fat globule damage measurements performed the same day.

**Fat Globule Damage Measurements**

Fat globule damage was measured by changes in fat globule size distribution measured with a Mastersizer 2000 fitted with a Hydro 2000 SM sample handling unit (Malvern Instruments Ltd., UK). Mean and 90 % fractal fat globule size was calculated with the Mastersizer 2000 software (version 4.00) using the general purpose model and a refractive index of 1,47 for milk fat. Measurements were performed at room temperature.

An increase in viscosity during shearing also indicates fat globule damage.

**CFD Simulation of Shear Fields**

Geometries for process equipment were implemented into the STAR-CD version 3.100b software package using the mesh generator in Prostar. The mesh was created as an unstructured mesh with hexahedral cells using couples to connect un-matching cell faces. For discretisation and modelling of turbulence the second order Central Difference scheme and the RNG k-ε model was used. The simulations are iterated until residuals below 10<sup>-6</sup> or constant residuals over a number of 200 iterations.

**RESULTS AND DISCUSSION**

At the present state of the project focus are on determining the process conditions that affect milk fat globules. This was done using a shear cell where predefined shear rates

were applied a sample with a controlled temperature. The apparent viscosity was recorded during the shear treatment, resulting in a viscosity increase (Figure 1) as fat globules agglomerates in the sample.

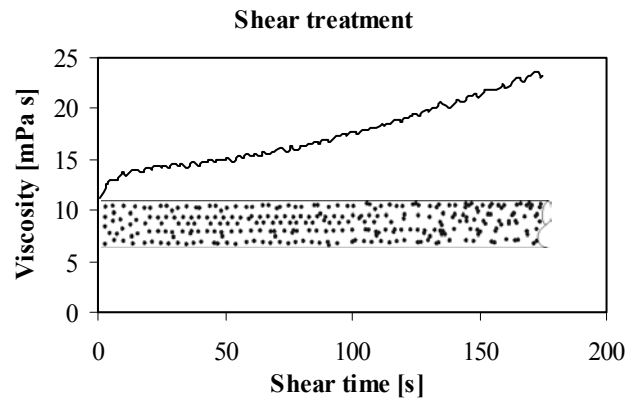


Figure 1: The increase in apparent viscosity of Cream (38 % fat) during Shearing at 20°C with a Shear Rate of 500 s<sup>-1</sup>. Enclosed drawing illustrates the ongoing Fat Globule Agglomeration occurring during Shearing

The viscosity incline during shearing seem to have three stages. During the first 10 seconds the viscosity increases rapidly, followed by a stage with slower increase. First stage is properly due to alignment of the fat globules and the second stage is due to an ongoing agglomeration. The change in fat globule size toward larger globules is probably accelerated by the agglomerated fat globules during shearing. The third stage is not shown in Figure 1, but a dramatic viscosity increase usually occurs followed by a decrease in viscosity. If the last stage occur, churned out fat is observed in the shear cell. Stability of fat globules is influenced by many factors. This project concentrates on determining the influence of temperature, time and fat content on the resistance of the fat globules to destabilise during shearing.

Figure 2 shows the size distribution, the calculated mean and 90 % fractal sizes of fat globules in cream samples

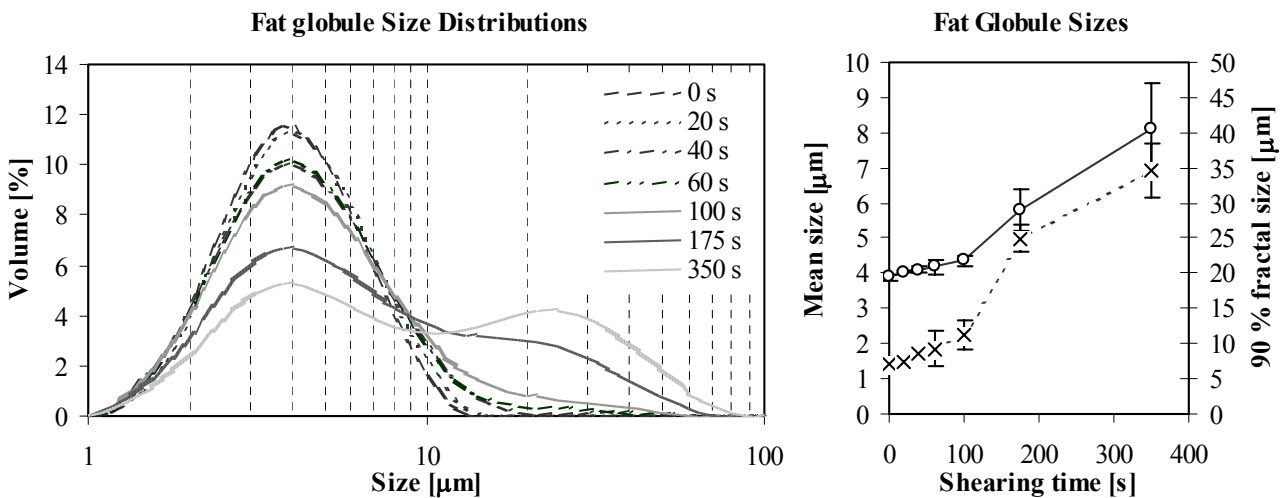


Figure 2: Left Graph shows the Size Distribution of Cream (38 % fat) Sheared at 500 s<sup>-1</sup> in 0, 20, 40, 60, 100, 175 and 350 seconds at 20°C. Right Graph shows the Calculated Mean Fat Globule Sizes and 90 % Fractal Sizes for the results

exposed to shearing at different length of time. The size distribution shows that during shearing the distribution was changed towards larger fat globules due to agglomeration. Exposed to the conditions applied in this experiment, the disruption of globules seems to occur at a constant rate in the first 100 seconds of shearing. Further shearing dramatically changed the size distribution, and fat lumps can be observed in the sample after shearing. Fat content in the samples has a large effect on the shear rates that the sample can withstand without being damaged (Foley et al. 1971; Hinrichs and Kessler 1997). When the fat content is increasing, the area where shear can evolve decreases, and the result is an increase in the shear that the surface of the globules exhibits resulting in an even greater risk of disruption. This is show for cream with 30 and 38 % fat in Figure 3.

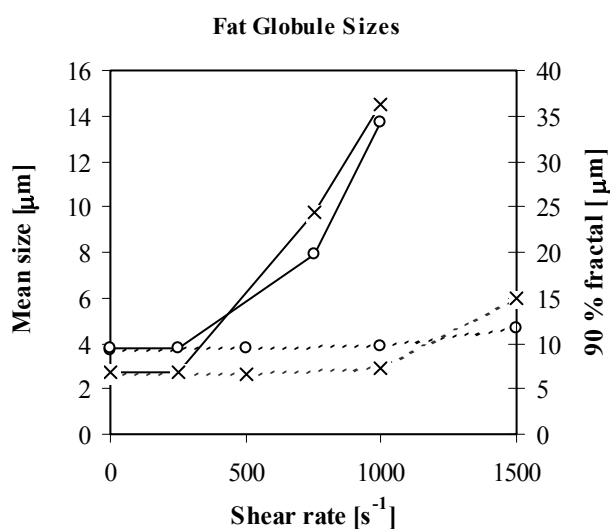


Figure 3: Mean (o) and 90 % Fractal (x) Fat Globule Sizes Measured in Cream Samples with 30 % fat (---) and 38 % fat (—) Sheared in 30 s at 20°C at the shown Shear Rates

Likewise temperatures have an effect on stability of the milk emulsion during processing (Schaller 1986; Lehmann 1988; Hinrichs 1994; Hinrichs 1998). As shown in Figure 4 fat globules are sensitive towards shearing in the temperature interval between 15 to 35°C. A critical amount of crystalline fat exist where fat globules is extremely sensitive to shearing. Therefore, designing process equipment should be done with the careful processing of milk products in mind when process temperatures are within the critical limits.

Shear rates in pipes with fully developed flow can easily be calculated from analytical or empirical formulas. Information on shear rates in complex geometries requires the use of computational tools like CFD or advanced experimental methods. The information is necessary to obtain data for shear rates for all types of equipment used in the dairy industry. Predicted shear rates can be validated by e.g. Laser Sheet Visualisation. The shear rate for cream flowing at 1.5 m s<sup>-1</sup> in a pipe with an internal diameter of 22,5 m s<sup>-1</sup>, gives a maximal shear rate of above 1000 s<sup>-1</sup> at the internal surface of the pipe.

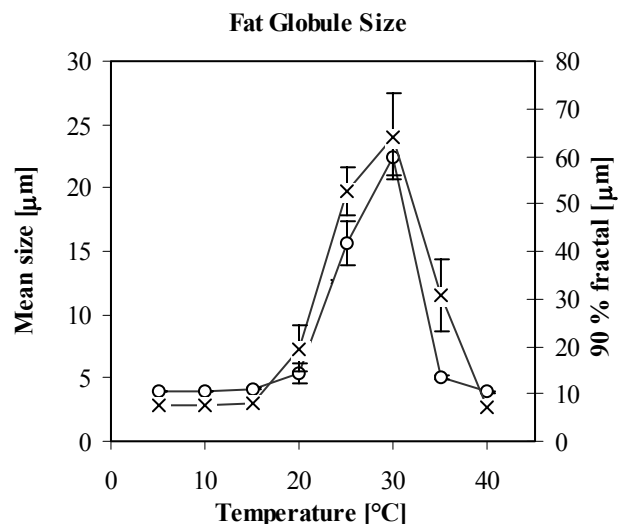


Figure 4: Mean (o) and 90 % Fractal (x) Fat Globule Sizes Measured in Cream (38 % fat) Sheared in 30 s with a constant Shear Rate of 750 s<sup>-1</sup>

Figure 5 shows predicted shear rates using CFD in a pipe bend and in the vicinity of a butterfly valve. The calculations were performed with cream flowing at an average velocity of 1,5 m/s, which is the typical flow rate used in the industry. Using CFD it is possible to estimate the time particles e.g. fat globules is located in different shear regions. To get a proper estimate the CFD simulations needs to be done with a large amount of particles to ensure that some particles enters the very often small areas of high shear rates that causes the larger fat globule damage. Such a calculation demands large computer power, and has not been performed in this project so far.

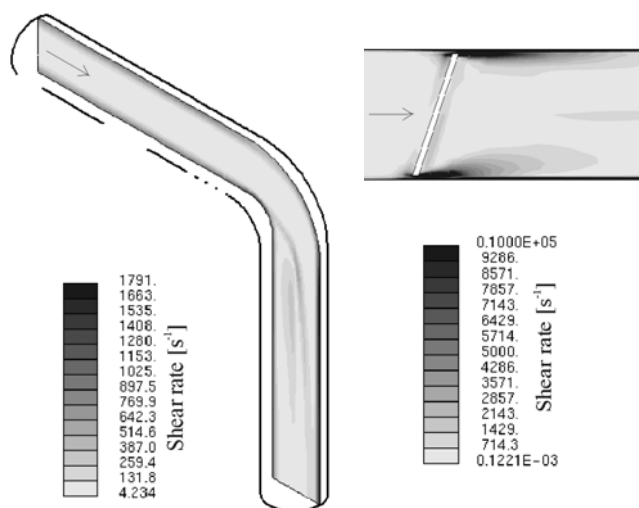


Figure 5: CFD Modelling of Shear Rates in the flow of Cream through a pipe Bend (left) and through a Butterfly Valve opened 10 % (right). The diameter is 22,5 mm and average Velocity of the Cream 1,5 m s<sup>-1</sup>. The Arrows show the Direction of Flow

## CONCLUSION

Combining CFD simulations on flow fields in production equipment with results of flow describing parameters effect

on food quality is shown to be a powerful tool, which will extend our knowledge of producing good quality foods. Based on the results presented above, it is clear that some degree of fat globule damage will occur in even simple processing equipment when processed in the sensitive temperature interval. From the illustration of shear rates around a slightly opened butterfly valve, it is seen that large pressure drops over a valve develop areas with extremely high shear rates. To prevent the problems that such high shear rates can cause, designers of equipment need to avoid unnecessary pressure build up in the production of equipment intended for use in dairy industries. This is done by correctly dimensioning process equipment and by controlling plant capacities by frequency-controlled pumps. Redesign of standard pipe bends towards giving a more uniform flow pattern, will also decrease total shear in production equipments.

#### FUTURE WORK

It is the ultimate goal of this project to set-up a validated process models capable of estimating fat globule damage in process equipment. From this model a process understanding can be extracted, which can be used to give recommendation for appropriate process conditions during manufacturing of milk products. Furthermore, it will be possible to set-up guidelines for design of process equipments. This project is running for another year, which is mainly going to be spent on model development.

#### ACKNOWLEDGEMENTS

We acknowledge financial support from the Danish Research Council and the Danish Dairy Board. Professor Jens Adler-Nissen and Associate Professor Jørgen Risum both BioCentrum-DTU for many fruitful discussions.

#### REFERENCES

- Foley, J., J. Brady, and P.J. Reynolds. 1971. "The influence of processing on the emulsion stability of cream." *Journal of the Society of Dairy Technology*, 24, 54-58.
- Hinrichs, J. 1994. "Grenzbelastung für Fettkügelchen." *Milchwirtschaftliche Berichte*, 121, 227-231.
- Hinrichs, J. and H.G. Kessler. 1997. "Fat content of milk and cream and effects on fat globule stability." *Journal of food science*, 62, 992-995.
- Hinrichs, J. 1998. "Flow rates for milk and cream in pipelines." *Milchwissenschaft*, 53, 139-143.
- Lehmann, H. 1988. "Rahm- und Fettkugelschädigung." *Deutsche Molkerei Zeitung*, 109, 671-673.
- Schaller, F. 1986. Fettschädigung bei der Milchbehandlung in Sammelstellen und Kaesereien." *Deutsche milchwirtschaft*, 37, 1406-1410.

#### AUTHORS BIOGRAPHY

**JESPER SÆDERUP NIELSEN** obtained his M.Sc. (Dairy Eng.) degree in 1999 from The Royal Veterinary and Agricultural University, Denmark. Before his studies he was employed two years in New Zealand working with design, manufacturing and start up of process equipment for the dairy industry e.g. membrane filtration plants, evaporators and spray driers. Presently he is working on his Ph.D. study about careful processing of milk products. Understanding how good food can be produced in large scale and teaching students technological aspects of food production, is the driving force behind his work. Email: jsn@biocentrum.dtu.dk

**ALAN FRIIS** is Associate Professor at BioCentrum-DTU and is heading the research in food process engineering. He holds a Ph.D. degree in the area of food processing from 1994 and obtained his M.Sc. (Mech. Eng.) degree in 1990 both at the Technical University of Denmark. The main research interests are: improvement of quality of industrially produced food products, catering, aspects of care in continuous processing of food products, modeling and simulation of food process operations, hygienic design of food processing equipment and rheology. Teaching activities are concentrated around aspects of food production. Email: af@biocentrum.dtu.dk

# ELABORATION OF TEXTURANT MODEL FLUIDS FOR FOOD INVESTIGATIONS

Romuald Guérin  
Guillaume Delaplace  
Gilles Ronse  
Jean-Claude Leuliet

Institut National de la Recherche Agronomique (I.N.R.A.)  
Laboratoire de Génie des Procédés et Technologie  
Alimentaire  
369, rue Jules Guesde, B.P. 39  
59651 Villeneuve d'Ascq cedex, France

Michel Lebouché  
LEMTA-CNRS UMR 7563

2 avenue de la forêt de Haye – BP 160 F-54501 Vandoeuvre-  
les-Nancy Cedex, France

## KEYWORDS

Texturant model fluids, gelatinization, melting, laboratory scale, pilot scale.

## ABSTRACT

In this paper, two texturant model fluids (gelatin or starch based products) have been elaborated for food investigations involving heat transfer process. These two model fluids based on mixtures of water, sucrose and gelatin or starch.

In this contribution, effect of sucrose content on melting temperatures of gelatin aqueous solutions and on gelatinization temperatures of starch aqueous solutions was investigated. Temperatures were obtained using Differential Scanning Calorimetry and dynamic viscoelasticity measurements.

It was clearly shown that increasing sucrose content raises both gelatinization temperatures of starch mixtures and melting temperatures of gelatin mixtures.

Finally, it was shown that preparation of the two texturant model fluids can be achieved in an industrial agitated vessel (34 litres).

## INTRODUCTION

Batch mixing of highly viscous fluids is widely used in the food and chemical industries. For these industries, the purpose of mixing operations could be quite different. For example, the requirement could be to ensure good homogeneity inside the vessel and/or to improve heat and mass transfer.

Efficiency of such operations is related to the geometry of mixing system and to the operating conditions. From a practical point of view, optimization of a mixing process in food industries still remains nowadays a difficult task. Indeed for these industries, most of the agitated fluids are complex (non-Newtonian) and properties of raw materials are greatly influenced by seasons. This causes additional difficulties to the process engineer to select the best operating conditions for the batch process.

In this case, model fluids with controlled and stable rheological properties are required.

Unfortunately, from a review of model fluids, it appears that most of them have been elaborated only for isothermal studies. One may mention gum solutions to simulate shear-thinning behaviour or glucose syrups to simulate Newtonian liquids. On the contrary, to the authors' knowledge, less model fluids have been proposed to simulate drastic changes in the texture which

appear during a heat transfer process like eggs, milk, starch or gelling agents based products in food industry. To fill this gap, an experimental program has been started in our laboratory. In particular, the aim was to obtain two texturant model fluids with specific rheological behaviour as shown in figure 1.

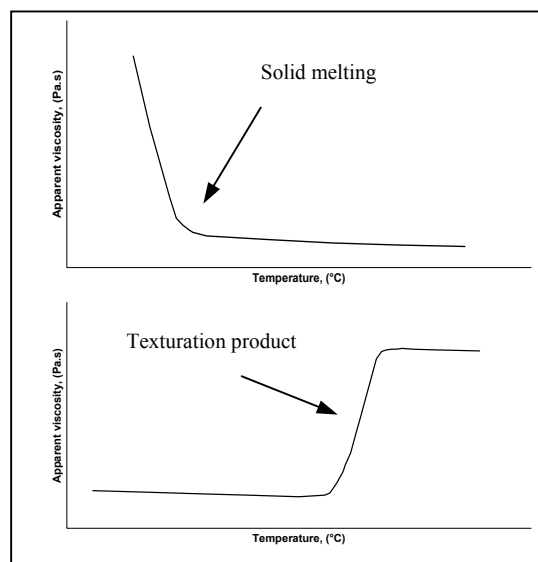


Figure 1. Evolution of apparent viscosity with temperature for the two model fluids elaborated in this study.

To obtain and select the required texturant products (Figure 1):

- first it was chosen to prepare gelatin and starch aqueous solutions containing various sucrose contents;
- then to follow evolution of apparent viscosity of these mixtures during heat treatment.

In this contribution, the effect of sucrose content on texturant properties of starch and gelatin mixtures, derived from this experimental program, was presented. In particular, dynamic rheological measurements and Differential Scanning Calorimetry results are reported and discussed. Finally, an additional trial will be presented concerning elaboration of model fluids at pilot scale.

## MATERIALS AND METHODS

### Preparation of model fluids.

Starch/sucrose and gelatin/sucrose aqueous solutions with various sucrose contents (0, 10, 20, 30, 40%, w/w) were prepared. A Waxy corn starch, a pig gelatin and a commercial sucrose (Beghin-Say firm) were used for this purpose. For all mixtures, the content of starch and of gelatin were fixed and equal respectively to 20% (w/w) and 5% (w/w). Solutions were achieved by dispersing starch/sucrose and gelatin/sucrose respectively at 30°C and at 60°C in distilled water. To increase the apparent viscosity of these solutions, a shear-thickening has been added. To avoid scatters of viscoelastic properties due to various time and thermal sample history (Michon and *al.*,1997), all products were vacuumed and maintained in a constant temperature at 4°C for 15 hours.

### Measurements of transition enthalpy and determination of representative gelatinization temperatures.

The gelatinization process of the starch suspension was measured by a DSC apparatus (SETARAM C80). Samples of about 5g were hermetically sealed in metal pans and placed on one side. The other, or reference, side held distilled water. The instrument heated both pans equally from 20 to 90°C at a rate of 0,1°C/min. Analysis of DSC thermograms of starch mixtures allow us to determine three representative temperatures of gelatinization:

- the onset temperature ( $\theta_0$ );
- the temperature of maximum differential heat flow (peak temperature,  $\theta_p$ );
- the termination temperature ( $\theta_t$ ).

The peak temperature was easily estimated, but onset and termination temperatures were generally not sharply defined. In this work, these temperatures were determined by the intersections between straight lines drawn through the base line and the sides of the DSC peak as proposed by Donovan (1979) (Figure 2). Finally, DSC thermograms were also used to determine the transition enthalpy. This was done by cutting out and weighting the area of peaks.

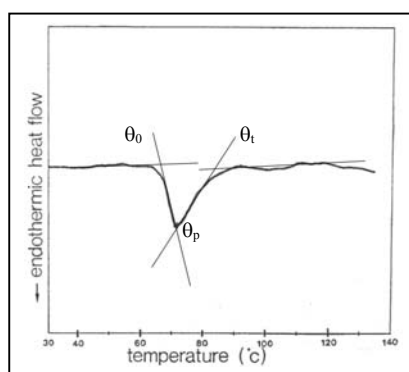


Figure 2. Determination of gelatinization temperatures for starch/sucrose aqueous solutions from DSC thermogram.

### Measurement of Dynamic Viscoelasticity.

Dynamic viscoelasticity measurements were performed in a cone plate system viscosimeter (Carrimed AR1000, TA

Instruments, UK - cone angle 2°, diameter 4 cm) to follow both the melting process of gelatin/sucrose solutions and the texturation process of starch/sucrose solutions during heat treatment. For that, an increasing temperature ramp varying from 10°C to 55°C for the gelatin solutions and from 30°C to 95°C for the starch solutions was applied at a rate of 1°C/min. In the same time, storage modulus ( $G'$ ), loss modulus ( $G''$ ) and  $\tan \delta$  ( $G''/G'$ ) were recorded. Note that liquid paraffin was used to minimize the water loss during the measurements. These trials were carried out in triplicate. For all runs, the strain and frequency were respectively set at 1% and 1Hz. Finally,  $G'$  curves versus temperature were analysed (intersection of tangents) in order to obtain representative melting ( $\theta_1, \theta_2, \theta_3$ ) or gelatinization ( $\theta_4, \theta_5$ ) temperatures (Figure 3).

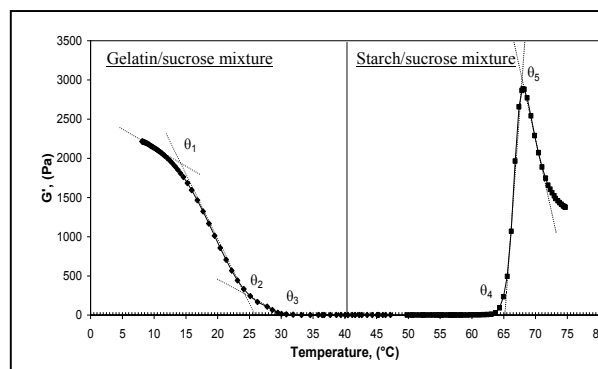


Figure 3. Examples of  $G'$  curve obtained for gelatin and starch aqueous solutions. Determination of representative temperatures for the two models fluids.

### Preparation of model fluids at pilot scale.

To establish the influence of mixer scale on texture of model fluids, it was decided to elaborate the product at two scales (a mixing tank of 34 litres equipped with a close clearance impeller and a jacketed vessel and a mixing system of 0,041 litres equipped with coaxial cylinders submerged in water bath) and to compare the evolution of their apparent viscosity during heat treatment. To carry out measurement in line of the apparent viscosity, the two mixing systems have been equipped with a torquemeter and a tachymeter. An increasing temperature ramp varying from 25°C to 95°C was performed at 1°C/min for the two mixing systems. Note that for the mixing equipment of 34 litres, it was difficult to maintain this rate at the end of the trial due to the operating conditions chosen. Indeed impeller rotational speed and wall temperature were fixed during all the heat transfer runs.

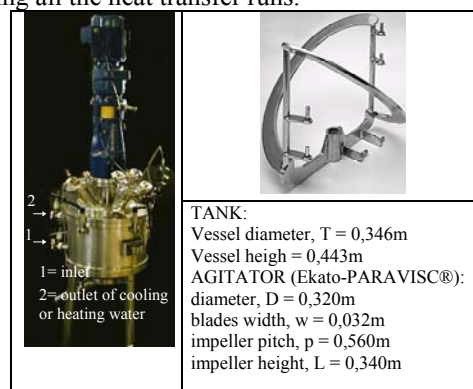


Figure 4. Pictures and geometrical parameters of the jacketed pilot mixing system used.

## RESULTS AND DISCUSSION

### *Gelatin/sucrose mixtures: Evolutions of texture obtained by dynamic viscoelasticity measurements.*

Figure 5 reports the results from dynamic viscosity measurements obtained for all gelatin solutions studied during the heating process. It appears that the storage ( $G'$ ) and loss ( $G''$ ) moduli sharply decrease while in the same time  $\tan \delta$  increases with temperature. These results prove that the gelatin melting process is induced by increasing temperature.

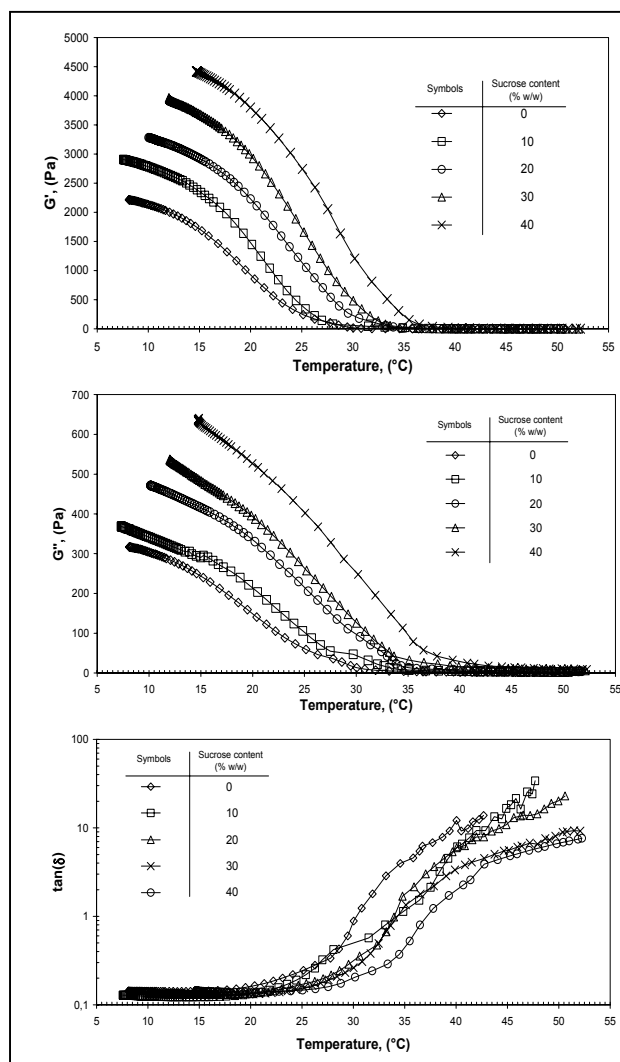


Figure 5. Change in rheological properties of gelatin/sucrose mixture with 0, 10, 20, 30 and 40% of sucrose during a heating from 10 to 55°C. Conditions: frequency, 1Hz; strain, 1%.

Table 1. Melting temperatures determined from  $G'$  curves for gelatin aqueous solutions with various sucrose contents.

Sucrose content (% w/w)	$\theta_1$ (°C)	$\theta_2$ (°C)	$\theta_3$ (°C)
0	13,4 +/- 0,4	23,2 +/- 0,3	30,7 +/- 0,7
10	16,5 +/- 1,0	26,2 +/- 1,0	33,2 +/- 0,7
20	18,6 +/- 0,5	28,9 +/- 0,6	34,7 +/- 0,6
30	19,7 +/- 0,6	29,4 +/- 1,2	37,0 +/- 0,5
40	23,3 +/- 1,0	31,8 +/- 0,7	38,8 +/- 0,3

Using method previously described (Figure 3), it was possible to obtain from  $G'$  curves representative melting temperatures. These temperatures ( $\theta_1, \theta_2, \theta_3$ ) are reported in table 1. Analysis of these data (Figure 6) shows clearly that gel-sol transition temperatures are influenced by sucrose contents. Indeed, for the range of sucrose contents investigated, we can note that melting temperatures of gelatin increase linearly with sucrose content.

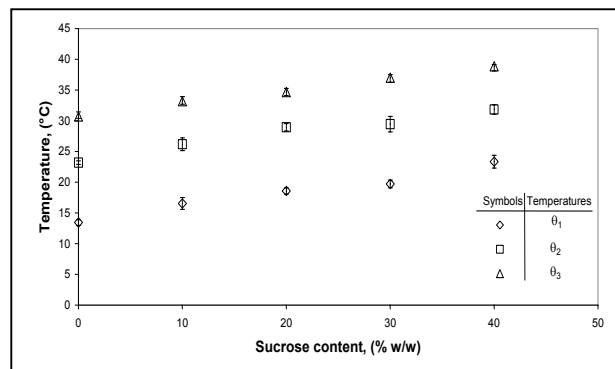


Figure 6. Effect of sucrose content on melting temperatures of a pig gelatin determined from  $G'$  curves. The bars represent standard deviation of three measurements.

### *Starch/sucrose mixtures: Evolutions of gelatinization temperatures obtained by DSC measurements.*

Figure 7 reports values of gelatinization temperatures and transition enthalpy obtained by DSC thermograms for the starch/sucrose solutions investigated.

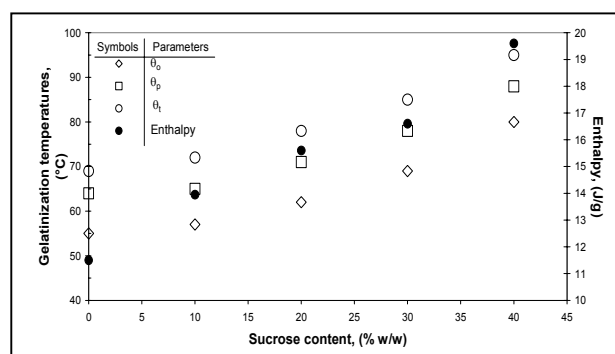


Figure 7. Effect of sucrose content on a corn starch gelatinization temperatures ( $\theta_o$ , the onset temperature;  $\theta_p$ , the peak temperature and  $\theta_t$ , the termination temperature).

We can note that both the representative gelatinization temperatures ( $\theta_o, \theta_p$  and  $\theta_t$ ) and values of transition enthalpy (from sol to gel) are influenced by sucrose content. For example, more than 20°C deviation was observed for peak temperature depending on sucrose content of starch mixtures. In the same time, transition enthalpy values vary more than 70%, depending on sucrose content.

These observations are in agreement with those obtained by other authors (Biliaderis and *al.*, 1980; Chinachoti and *al.*, 1990; Eliasson, 1980; Evans and Haisman, 1982 and Wootton and Bamunuarachchi, 1979) which underlined that gelatinization temperatures greatly depend on the environment of the starch granules.

**Starch/sucrose mixtures: Evolutions of texture determined by dynamic viscoelasticity measurements.**

Figure 8 illustrates the results from dynamic viscoelasticity measurements of starch solutions during heating.

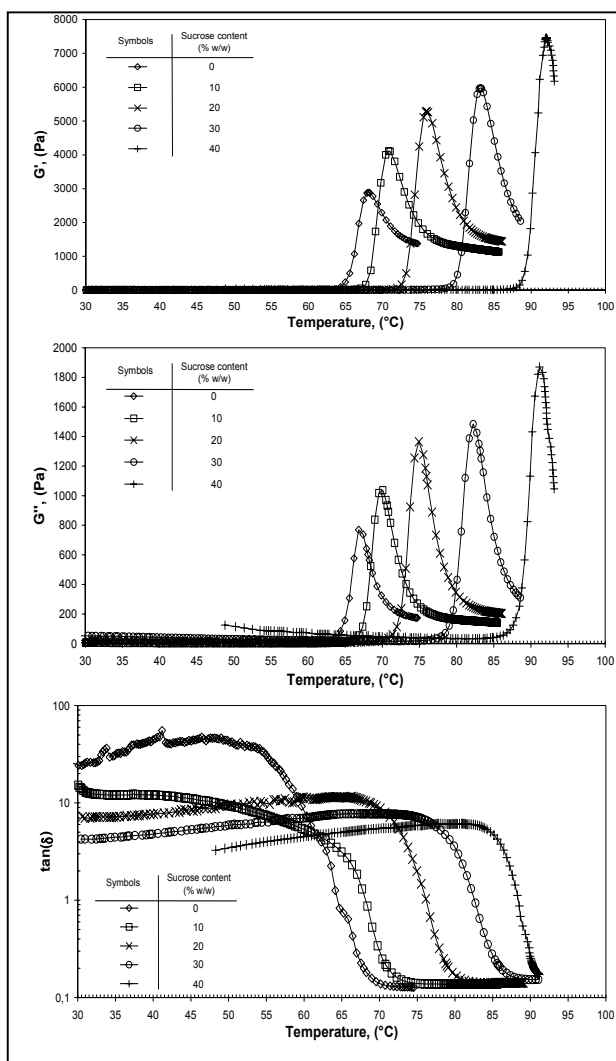


Figure 8. Evolution of storage modulus ( $G'$ ), loss modulus ( $G''$ ) and  $\tan \delta$  with temperature (30 – 95°C) for various aqueous solutions of starch with various sucrose contents: 0, 10, 20, 30 and 40%. Operating conditions: frequency, 1Hz; strain, 1%.

The storage ( $G'$ ) and loss ( $G''$ ) moduli sharply increased with temperature and reached a maximum value which may be attributed to the closely packed network of swollen starch granules (Eliasson, 1986; Hsu and *al.*, 2000; Lii and *al.*, 1985). In the same time,  $\tan \delta$  sharply decreases with temperature. From the rheological point of view, this decrease corresponded to a sol-to-gel transition (Hsu and *al.*, 2000).

With further increase in temperature,  $G'$  and  $G''$  decreased indicating that the gel structure was destroyed during prolonged heating. This destruction was probably due to the melting of the crystalline region remaining in the swollen starch granules (Eliasson, 1986). Representative temperatures,  $\theta_4$  and  $\theta_5$ , obtained from  $G'$  curves and reported in table 2.

Table 2. Gelatinization temperatures of starch/sucrose mixtures versus sucrose content determined from  $G'$  curves.

Sucrose content (% w/w)	$\theta_4$ (°C)	$\theta_5$ (°C)
0	63,6 +/- 0,1	68,1 +/- 0,2
10	66,6 +/- 0,2	71,0 +/- 0,1
20	74,6 +/- 0,3	79,1 +/- 0,3
30	78,5 +/- 0,1	83,0 +/- 0,3
40	87,4 +/- 0,2	91,5 +/- 0,9

Results show that sucrose content influences gelatinization temperatures of starch aqueous solutions. Gelatinization temperatures increase with sucrose content. For instance, corn starch showed a range of gelatinization temperatures varying from 63,6°C to 68,1°C in pure water and 87,4-91,5°C for starch sample with 40% (w/w) of sucrose. These oscillation tests confirm reasonably well that starch gelatinization temperatures were influenced by changes in the environment of the starch granules (Figure 8). This observation was in agreement with various authors (Chang and Liu, 1991; Evans and Haisman, 1982; Oosten, 1982; Singh and *al.*, 2002 and Wootton and Bamunuarachchi, 1980). This can be explain both by reducing the amount of water available to the granules and by adding high levels of hydrophilic solutes.

Figure 8 also shown that values of  $G'_{max}$  and  $G''_{max}$  increased with sucrose content. The  $G'$  peak was 2879 Pa for pure starch solution against 7447 Pa for starch solution with 40% w/w sucrose content. These observations clearly indicate that aqueous starch solution are more viscous with increasing sucrose content. This can be explained simply by the reduction of water content.

To compare DSC and dynamic viscoelasticity measurements, representative gelatinization temperatures of aqueous starch solutions have been plotted on Figure 9. We can note that there is a good agreement between the two set of values. Indeed,  $\theta_4$  determined from  $G'$  curves correpond to the peak temperature ( $\theta_p$ ) and  $\theta_5$  correspond to the termination temperature ( $\theta_t$ ). This indicates that the two experimental devices are accurate enough to detect both the beginning and the end of gelatinization process.

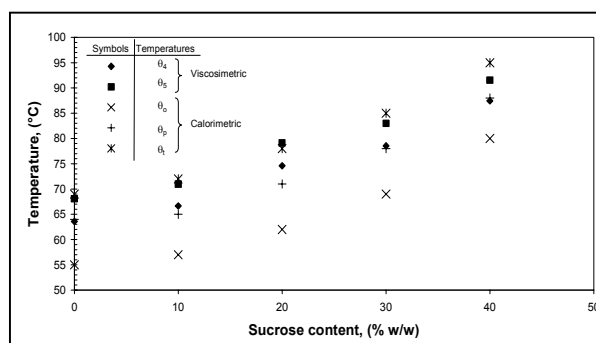


Figure 9. Gelatinization temperatures of aqueous solutions of starch with various sucrose contents determined by calorimetric ( $\theta_0$ ,  $\theta_p$  and  $\theta_t$ ) and viscosimetric ( $\theta_1$  and  $\theta_2$ ) methods.

### Preparation of model fluids at pilot scale.

Figures 10 and 11 show respectively the evolution of the apparent viscosity ( $\eta_a$ ) of starch/sucrose and gelatin/sucrose aqueous solutions obtained at laboratory and at pilot scale.

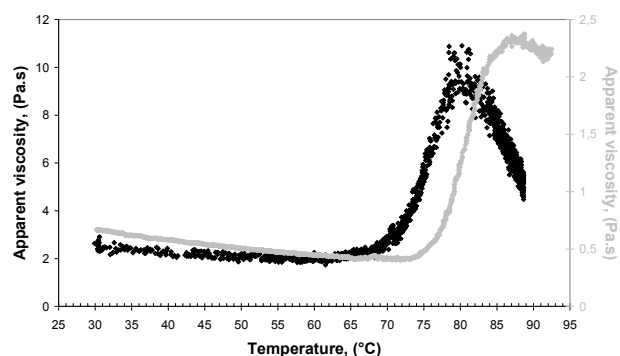


Figure 10. Evolution of the apparent viscosity for starch based texturant model fluid at the laboratory scale (grey symbols -  $\dot{\gamma} = 105\text{s}^{-1}$ ) and at the pilot scale (black symbols -  $\dot{\gamma} = 18\text{s}^{-1}$ ).

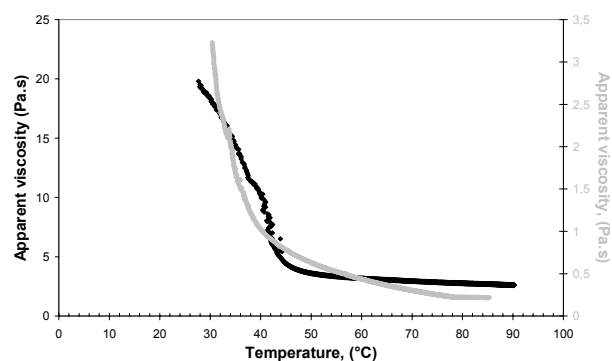


Figure 11. Evolution of the apparent viscosity for gelatin based texturant model fluid at the laboratory scale (grey symbols) and at the pilot scale (black symbols). Conditions:  $\dot{\gamma} = 105\text{ s}^{-1}$ , heating rate of  $1,0^\circ\text{C}/\text{min}$ .

These figures show that for the two scales there are similar drastic changes in the texture of the product caused by increasing temperature. These similar texturation processes at the two scales appear more clearly by comparing for the two mixing systems, activation energy of flow required for sol-to-gel or gel-to-sol transition in (Table 3).

Table 3. Activation energy of flow ( $E_{a_f}$ , kJ/mol) of models fluids at the laboratory scale (L) and at the pilot scale (P) (E – Relative error, %).

Starch based fluid			Gelatin based fluid		
$E_{a_f}$ (kJ/mol)			$E_{a_f}$ (kJ/mol)		
L	P	E (%)	L	P	E (%)
86,0	77,6	10,8	40,1	33,7	19,0

Indeed for the two scales, values of activation energy of flow are same order of magnitude which proves that similar texturation process (either gelatinization or melting) has been achieved.

Note that on Figure 10, there is a scatter between values of  $\eta_a$  versus temperature obtained at the two scales for starch/sucrose mixture. This may be explained by the different magnitude of average shear rate during heat treatment in the two mixing

systems. On the contrary, the deviation of apparent viscosity obtained for gelatin/sucrose mixtures (figure 11) can not be explained by different level of average shear rate but may be caused by various local shear rate distribution for the two mixing systems (Delaplace *et al.*, 2000).

### CONCLUSION

In this work, preparation of aqueous solutions of gelatin and starch with various sucrose contents have been carried out to elaborate and select two texturant model fluids for food investigations involving heat transfer process. Experimental measurements (DSC and dynamic viscoelasticity) with these solutions have allowed us to underline the effect of sucrose content on melting temperatures of gelatin and gelatinization temperatures of starch..

Finally, an additional trial have been performed to elaborate and follow apparent viscosity of these model fluids in line at industrial scale. Results obtained prove that it is feasible to elaborate such model fluids at this scale.

### BIBLIOGRAPHY

- Biliaderis C.G., Maurice T.J. and Vose J.R. 1980. "Starch gelatinization phenomena studied by differential scanning calorimetry". *J. Food Sci.*, 45, 1669-1674.
- Chang S.M. and Liu L.C. 1991. "Retrogradation of rice starches studied by Differential Scanning Calorimetry and influence of sugars, NaCl and Lipids". *J. Food Sci.*, 56, 564-566.
- Chinachoti P., Steinberg M.P. and Villota R. 1990. "A model for quantitating energy and degree of starch gelatinization based on water, sugar and salt contents". *J. Food Sci.*, 55, 543-546.
- Delaplace G., Torrez C., André C., Leuliet J.-C. and Fillaudeau L. 2000. "CFD simulation of foodstuff flows in an agitated vessel". 1<sup>st</sup> International Conference on simulation in food and Bioindustries, edited by Daniel Thiel, 179-186.
- Donovan J.W. 1979. "Phase transitions of the starch-water system". *Biopolymer*, 18, 263-275.
- Doublier J.-L. 1987. "A rheological comparison of wheat, maize, faba bean and smooth pea starches". *J. Cereal. Sci.*, 5, 247-262.
- Eliasson A.-C. 1980. "Effect of water content on the gelatinization of wheat starch". *Starch*, 32, 270-272.
- Eliasson A.-C. 1986. "Viscoelastic behaviour during the gelatinization of starch. I: Comparison of wheat, maize, potato and waxy barley starches". *J. Texture Studies*, 17, 253-265.
- Evans I.D. and Haisman D.R. 1982. "The effect of solutes on the gelatinization temperature range of potato starch". *Starch*, 34, 224-231.
- Hsu S., Lu S. and Huang C. 2000. "Viscoelastic changes of rice starch suspensions during gelatinization". *J. Food Sci.*, 65, 215-220.
- Lii C.Y., Shao Y.Y. and Tseng K.H. 1995. "Gelation Mechanism and rheological properties of rice starch". *Cereal Chem.*, Vol.72, 393-400.
- Michon C., Cuvelier G., Relkin P. and Launay B. 1997. "Influence of thermal history on the stability of gelatin gels". *Int. J. Biol. Macromolecules*, 259-264.
- Oosten B. 1982. "Tentative hypothesis to explain how electrolytes affect the gelatinization temperature of starches in water". *Starch*, 34, 233-239.
- Singh J., Singh N. and Saxena S.K. 2002. "Effect of fatty acids on the rheological properties of corn and potato starch". *J. Food Engin.* 52, 9-16.
- Wootton M. and Bamunuarachchi A. 1980. "Application of differential scanning calorimetry to starch gelatinization – III. Effects of sucrose and sodium chloride". *Starch*, 32, 126-129.

# DIMENSIONLESS ANALYSIS OF FLUID-TO-PARTICLE MASS TRANSFER COEFFICIENTS IN CONTINUOUS TUBE FLOW

Isabel Abreu  
Escola Superior de Biotecnologia  
Universidade Católica Portuguesa  
Rua Dr. António Bernardino de Almeida  
4200-072 Porto, Portugal  
E-mail: iabreu@morango.esb.ucp.pt

Fernanda Oliveira  
Department of Process Engineering  
University College Cork  
Cork, Ireland  
E-mail: f.oliveira@ucc.ie

## KEYWORDS

Fick's 2<sup>nd</sup> law, fluid-to-particle heat transfer coefficient, fluid-to-particle mass transfer coefficient, heat/mass transfer analogy.

## ABSTRACT

The selection of time-temperature conditions that maximize product quality while ensuring product safety in the aseptic processing of particulate fluid foods depends greatly on the ability to measure or predict fluid-to-particle heat transfer coefficients. Monitoring the temperature of a moving particle in two-phase flow without disturbing the flow conditions is however difficult, which hinders the determination of heat transfer coefficients. Mass transfer coefficients are often easier to determine experimentally. If correlations between Sherwood (Sh), Reynolds (Re) and Schmidt (Sc) numbers are developed, they might then be used to predict heat transfer coefficients, by the heat/mass transfer analogy, thereby replacing Sh and Sc numbers by Nusselt (Nu) and Prandtl (Pr) numbers, respectively. In this work fluid-to-particle mass transfer coefficients were determined in tube flow. Dimensionless correlations were developed and compared with published correlations for heat transfer, although the latter were developed for values of  $Pr_g$  much smaller than those of  $Sc_g$  determined in the present work. In general, those correlations overpredicted the Sh numbers, but a fair agreement was observed when using a correlation reported in literature that considers both the effect of translational and rotational relative particle-to-fluid velocities. These results show the potential of using heat/mass transfer analogies for estimating fluid-to particle heat transfer coefficients in continuous flow.

## INTRODUCTION

The estimation of fluid-to-particle heat transfer coefficients is one of the key aspects in the design and optimisation of continuous thermal processing of particulate fluid foods. Dimensional analysis is often used to correlate heat transfer coefficients with fluid properties, fluid velocity and particle geometry. Correlations have been reported in literature for fluid flow past single stationary spheres in a duct (Geankoplis 1983). In the continuous thermal processing of particulate fluid foods the particles flow freely with the fluid medium, and thus these correlations may not hold true. Ramaswamy and Zareifard (2000) reported that

information available in literature on fluid-to-particle heat transfer coefficients in continuous flow systems is scarce, often inconsistent and sometimes contradictory. Most of the equations found in literature are of the Frösling type. The major problem when measuring the fluid-to-particle heat transfer coefficient in a continuously flowing suspension of particles is the measurement of the particles' temperature without disturbing flow conditions (Sastry 1992). Fluid-to-particle mass transfer coefficients are in general easier to determine experimentally without disturbing the flow, and, by using the heat/mass transfer analogy, they may be converted to fluid-to-particle heat transfer coefficients.

The heat/mass transfer analogy relies on the similarity between the dimensionless relations that govern the thermal and the concentration boundary layers. If, for example, one has performed a set of mass transfer experiments to determine the form of a function that relates Sh with Re and Sc, for a particular surface geometry, the results should hold in convection heat transfer involving the same geometry, simply by replacing Sh with Nu and Sc with Pr, provided the range of dimensionless numbers is the same (Incropera and DeWitt 1996). Conversely, mass transfer coefficients may be estimated with correlations developed for heat transfer (e.g. as Califano and Calvelo 1983). The Chilton-Colburn analogy has proved useful for a number of situations (Chilton and Colburn 1934, Bird *et al.* 1960).

Noordsij and Rotte (1967) developed dimensionless correlations for predicting average mass transfer coefficients for rotating or vibrating spheres immersed in a liquid medium. They used different experimental conditions to ensure that mass transfer rate was controlled either by internal diffusion or external convection, which allowed for separate estimation of diffusivity (D) and mass transfer coefficient ( $K_c$ ). To the best of our knowledge, fluid-to-particle mass transfer in continuous flow has only been studied by Fu *et al.* (1998). They conducted experiments in vertical holding tubes of an aseptic processing system to determine fluid-to-particle mass transfer coefficients, and reported that the Sherwood number decreased with increasing residence time. Those results were then extended to predict heat transfer under similar conditions. The slight increase of fluid-to-particle heat transfer coefficient with decreasing particulate residence time suggested that fastest moving particles might not necessarily be the least sterilised.

The main objectives of this work were: (i) to measure mass transfer coefficients in continuous tube flow of a particulate fluid in a range of temperatures and flow rate, (ii) to use these data to develop dimensionless correlations to predict fluid-to-particle mass transfer coefficients, and (iii) to compare these correlations with others reported in literature for predicting fluid-to-particle heat transfer coefficients.

## MATERIAL AND METHODS

The mass transfer process studied was acetic acid uptake by agarose particles initially free of acid. Particles with different geometry (cubes and spheres) were tested. The carrier fluid was a carboxymethylcellulose solution (0.6%) containing acetic acid (0.2M). The experiments were conducted in a tubular continuous thermal processing unit under isothermal conditions.

### Agarose gel

An agarose gel was chosen as a model food because of its stability in acid at high temperatures, without shrinking or swelling. A 5%w/v agarose gel was prepared by adding agarose powder (N°05068, Fluka Chemika, Buchs, Switzerland) to deionised water held covered at 95 °C and stirred until it was transparent (about 45 min); the mixture was then poured into a mould and left to set. After gelation, detected by the white opacity, the gel was cut into  $10 \pm 0.1$  mm cubes. Agarose spheres with diameter in the range of approximately 6 to 9 mm were prepared by dropwise injection of the transparent agarose solution into an ice-cold mixture of toluene-chloroform-n-hexane (5:2:1, v/v/v), as described by Tahoun (1986). Excess solvent was removed by shortly shaking in 1,4-dioxane, followed by successive washing in deionised water. The cubes and spheres were stored at 4 °C in deionised water prior to use, for periods up to two weeks.

### The acidifying medium

Situations of interest to food processing usually involve low Reynolds number, since the carrier fluid often is a viscous solution. Moreover, these solutions usually have non-Newtonian behaviour. Carboxymethylcellulose (CMC) solutions are often used as model solutions, as they are non-Newtonian. CMC is also readily available and convenient for testing since it is stable, safe to use and clean (Campos *et al.* 1994). The 0.6% CMC solutions were prepared by adding slowly sodium carboxymethylcellulose (Hoechst AG – Tylose MHB 30000 yp<sup>TM</sup>) to water at 50 °C, with continuous stirring maintained for 3 days. Then, acetic acid (99+% pro analysis, Pronalab, Portugal) was added to the solution. The rheological characteristics of CMC solutions were determined using a controlled stress rheometer with cone-and-plate geometry (Carri-Med CS-50, Surrey, UK). Rheological measurements were performed at the beginning and at the end of each set of experiments at the same temperature, and no time dependence was found. Table 1 shows the rheological parameters at different temperatures. This table also includes the intrinsic viscosity ( $\mu_s$ ), evaluated

as the tangent of the shear stress versus shear rate curve, for zero shear stress.

Table 1: The Power Law Model Parameters and Intrinsic Viscosity of 0.6% CMC Solutions

T (°C)	K (Pa.s <sup>n</sup> )	n	$\mu_s$ (kg.m <sup>-1</sup> .s <sup>-1</sup> )
25	$0.54 \pm 0.02$	$0.613 \pm 0.003$	$0.150 \pm 0.004$
30	n.a.	n.a.	n.a.
35	$0.37 \pm 0.02$	$0.629 \pm 0.002$	$0.098 \pm 0.003$
40	$0.25 \pm 0.07$	$0.67 \pm 0.02$	$0.079 \pm 0.008$
45	$0.21 \pm 0.02$	$0.668 \pm 0.006$	$0.071 \pm 0.005$
50	$0.18 \pm 0.01$	$0.677 \pm 0.005$	$0.061 \pm 0.002$
55	$0.12 \pm 0.02$	$0.72 \pm 0.02$	$0.049 \pm 0.005$
65	$0.08 \pm 0.02$	$0.75 \pm 0.02$	$0.011 \pm 0.007$

n.a. – not available, for calculation purposes interpolated values ( $k = 0.44$  Pa.s<sup>n</sup>,  $n = 0.62$  and  $\mu_s = 0.12$  kg.m<sup>-1</sup>.s<sup>-1</sup>) were used.

The density of the acetic acid solutions was determined at different temperatures using a Mettler AM 100 balance and a density determination kit (Mettler ME-33340). Values ranged from 999.3 to 980.8 kg.m<sup>-3</sup> for temperatures between 25 and 65 °C. The density of the 5% agarose was  $1.02 \pm 0.01$  g.cm<sup>-3</sup>.

## The experiments

A continuous tubular processing system was used, designed by Pinheiro-Torres and Oliveira (1991), and built by ARSOPI, S. A. (Vale de Cambra, Portugal). This system includes a solid/liquid mixture feed tank, an alloy gear pump (Eco Gearchem, model no. ECO-G4-KCC-TTQ, Pulsafeeder, New York, USA), an electromagnetic flowmeter (flow transmitter Model PD340, from Process-Data) a three way valve to introduce the agarose particles, a visualization section and a tubular thermal processing unit with heating, holding and cooling sections (Figure 1). The inner tube of the heat exchangers, the holding tube and all the parts between the inlet and outlet have an internal diameter of 22 mm, and the total length is 30 m. The holding section has an upward inclination of 1 in/ft.

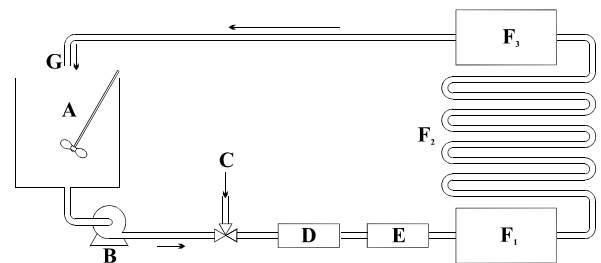


Figure 1: Schematic representation of the continuous tubular processing system.

A – stirred tank; B – pump; C – three way valve (inlet); D – visualization section; E – flowmeter; F<sub>1</sub>, F<sub>2</sub> and F<sub>3</sub> – heating, holding and cooling sections; G – outlet.

All the experiments were carried out isothermally, with a difference between the inlet and outlet lower than 1 °C. The

feeding tank is jacketed and was pre-heated and held at the selected temperature using steam. The acid solution was pumped from the tank to the unit and recirculated. Experiments were started after all the air was purged and the temperature stabilized. The agarose particles were pre-heated to the selected temperature. An agarose particle was introduced after the pump in the three-way valve, and later removed at the outlet, rinsed and immersed in a flask with deionised water. The particle's residence time was registered. The average acid concentration of the particles was measured by titration with standard 0.02M NaOH with an automatic titrator (Titralab<sup>TM</sup>), after dissolving the particle in 50 ml of hot water. Ten 10 particles were run, for each experiment, and a sample of the acid solution in the tank was taken to be titrated. The operating variables were: temperature (T); flow rate (Q); particle geometry and particle size ( $d_p$ ) (Table 2).

Table 2: Values of the Operating Variables

Particle geometry	$d_p$ (cm) *	T (°C)	Q (l.h <sup>-1</sup> )
cubes	1.24	25; 30; 35; 40; 45; 50; 55	120; 180; 240; 300; 360
spheres	0.63 to 0.69 0.83 to 0.90	25; 65	180; 360

\* for cubes  $d_p$  corresponds to the diameter of a sphere with the same volume.

## MATHEMATICAL CONSIDERATIONS

Joint estimation of D and  $K_c$  was avoided because of the high correlation coefficients between D and  $K_c$  (Azevedo *et al.* 1998)  $K_c$  values were estimated by non-linear regression, using the Simplex method (Nelder and Mead 1965) for minimization of the sum of the squares of the errors between experimental data and the values predicted by the solution of Fick's 2<sup>nd</sup> law (Crank 1975) subject to the appropriate boundary conditions (uniform initial concentration, symmetry condition and a convection boundary condition). A Fortran program was specially written for this purpose. The D values used in these calculations were estimated using data from earlier experiments where the carrier fluid was water, so that the external resistance to mass transfer was negligible (parameters for the Arrhenius dependence of D on temperature:  $E_a$  (activation energy)=  $24 \pm 1$  kJ.mol<sup>-1</sup>;  $D = 1.88 \times 10^{-9} \pm 0.03 \times 10^{-9}$  m<sup>2</sup>.s<sup>-1</sup> at T = 45 °C).

Analysis of variance and non-linear regression for developing dimensionless correlations were performed using the R program (R 1.1.1, A Language and Environment Copyright 2000). For cubes,  $K_c$  was estimated for each group of 10 particles used in a given experiment; for spheres  $K_c$  values were estimated for each particle separately, as they did not have exactly the same diameter. Sh was then calculated (Equation (1)) and correlated with the relevant generalized dimensionless numbers,  $Re_g$  and  $Sc_g$  (Equations (2) and (3)).

$$Sh = \frac{K_c d_p}{D_f} \quad (1)$$

$$Sc_g = \frac{k \left( \frac{3n+1}{n} \right)^n 2^{n-3}}{\rho_f D_f \left( \frac{\nu}{d_p} \right)^{1-n}} \quad (2)$$

$$Re_g = \frac{8 \rho_f \nu_f^2 \frac{n}{d_p}}{2^n k \left( \frac{3n+1}{n} \right)^n} \quad (3)$$

where k and n are the constants of the power law model,  $\rho$  is the density,  $\nu$  is the viscosity, and the subscripts f and p stand, respectively, for fluid and particle.

A single correlation was developed for cubes and spheres. A weight of 10 was attributed to the mass uptake data regarding cubes, as in this case each Sh corresponds to the average of 10 particles.

## RESULTS AND DISCUSSION

### Fluid-to-particle mass transfer coefficients

The generalized Reynolds numbers based on the tube diameter ranged from 12.5 to 163 for cubes, and from 21.9 to 221 for spheres, meaning that the regime flow for undisturbed liquid flow was laminar. Fluid-to-particle mass transfer coefficients ranged from  $0.55 \times 10^{-5}$  to  $2.14 \times 10^{-5}$  m.s<sup>-2</sup>, increasing both with temperature and flow rate, as expected. Figure 2 shows the results for cubes (the surface represents the dimensionless correlation).

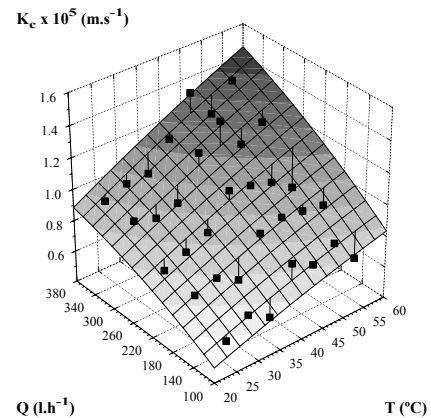


Figure 2: Effect of Flow Rate and Temperature on Fluid-to-particle Mass Transfer Coefficients during Continuous Flow of Agarose Cube Particles in an Acetic Acid Solution Carrier.

The analysis of variance (at 95% significance level) confirmed the influence of temperature and flow rate on  $K_c$  and showed no significant interactive effect of these two operating variables for particles with cube geometry, whereas for spheres the effect of temperature was more

pronounced at high flow rates; the diameter of the particles had no significant effect. The precision of  $K_c$  estimates was found to be independent of temperature and flow rate. Biot numbers ( $Bi=K_c d_p/D_p$ ) ranged from 15 to 47 for cubes and from 11 to 62 for spheres, increasing with increasing flow rate and decreasing with increasing temperature, showing that the diffusion coefficient of the acid in the gel is more sensitive to temperature than the external mass transfer coefficient. Experimental data were more scattered for spheres than for cubes, particularly at 25 °C, owing to the smaller size of the particles and consequently lower acid uptake.

### Dimensional analysis

A Frösling type correlation assuming the theoretical value of 2 for Sh in static conditions (i.e.  $Re_g=0$ ) yielded good fits to the experimental data ( $R^2=0.91$ ):

$$Sh = 2 + (0.03 \pm 0.01) Re_g^{(0.46 \pm 0.05)} Sc_g^{(0.62 \pm 0.04)} \Psi^{(0.02 \pm 0.30)} \quad (4)$$

where  $\Psi$  is the particle sphericity (1 for spheres and cube edge/diameter of a sphere with the same volume for cubes). Figure 3 shows the good agreement between experimental and predicted values and Table 3 summarises the ranges of dimensionless numbers used in this work.

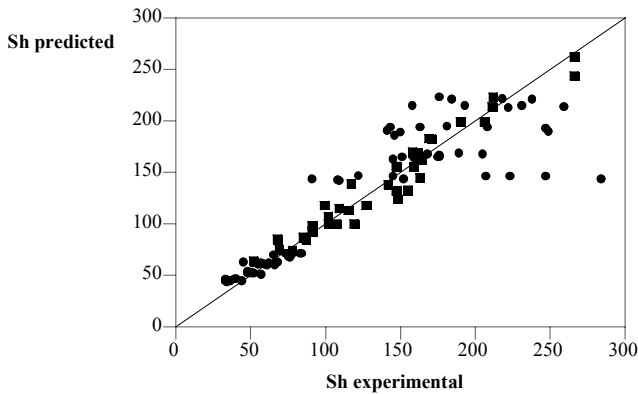


Figure 3: Prediction of Sh by Dimensional Analysis (Equation (4))

Table 3: Range of the dimensionless numbers in the conditions tested

Dimensionless number	Particle geometry	
	cubes	spheres
$Re_g$	8.8 - 108	10.3 - 114
$Sc_g$	18,744 - 293,654	9,197 - 221,666
Sh	52 - 266	33 - 284
$Ar^*$	2.09 - 4.90	0.66 - 54.7
$Fr^*$	0.036 - 0.321	0.080 - 0.321

\*  $Ar$  - Arquimedes number;  $Fr$  - Froude number

The exponent of  $Re_g$  is not statistically different from 0.5, the theoretical value for laminar flow over a horizontal surface and the most common figure in published studies, whereas  $Sc_g$  is higher than the theoretical value for the same

situation (0.33). The exponent of  $\Psi$  is not statistically different from zero, probably owing to insufficient experimental data (two sphericity factors only were evaluated). However, the inclusion of this factor clearly improved the fit.

### Comparison with correlations for heat transfer

Correlations reported on heat transfer studies cover similar ranges of  $Re_g$ , yet  $Pr_g$  values are much lower than the  $Sc_g$  values measured in our work. When comparing our results with those correlations, it was found that they tend to overpredict Sh. A fair agreement was however observed when using a published correlation that considers both the effect of translational and rotational relative particle-to-fluid velocities on the fluid-to-particle heat transfer coefficient in flow in a straight tube (Baptista *et al.* 1997b). Using the heat/mass transfer analogy, this equation can be written as:

$$Sh = 2.0 + 0.025 \times Sc_s^{1/3} \times Gr^{1/2} + 0.64 \times Re_{gvr}^{0.59} \times Sc_{gvr}^{0.28} + 0.17 \times Re_{g\omega}^{0.71} \times Sc_{g\omega}^{0.42} \times (d_p / d_t)^{0.28} \quad (5)$$

This correlation was developed for  $7 < Re_g < 284$  and  $144 < Pr_g < 1,755$ . The particles linear and rotational velocities were estimated with dimensionless correlations reported by Baptista *et al.* (1997a). These correlations were developed for  $62 < Re_g < 4,734$ ,  $7.6 < Ar < 4.34 \times 10^5$ ,  $0.035 < Fr < 2.29$ ,  $0.065 < \alpha < 0.425$  and  $0.216 < d_p/d_t < 0.649$ . Thus, the range of  $Re_g$ ,  $Ar$  and  $\alpha$  do not cover the values found in our work. Furthermore, while Equation (5) refers to experiments carried out in a straight tube, we have worked with a continuous thermal processing unit that includes a number of bends. Despite all these limitations, equation (6) yielded predictions of the same order of magnitude, with better results for cubes, probably due to the better quality of the experimental data for this geometry (Figures 4 and 5).

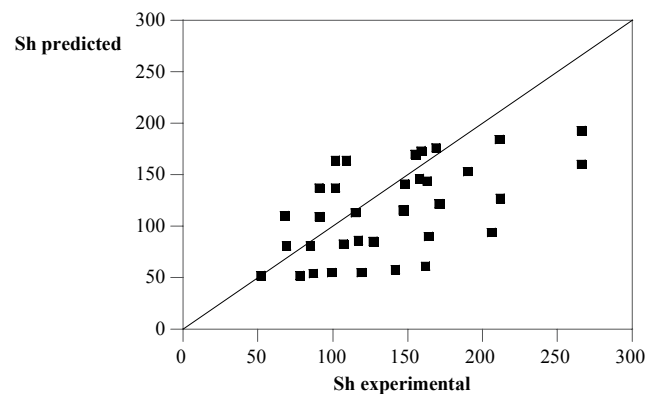


Figure 4: Prediction of Sh for cubes using the Correlation reported by Baptista *et al.* (1997b) (Equation (5)).

### CONCLUSIONS

Dimensionless correlations were developed to predict Sh, and thus fluid-to particle mass transfer coefficients, as a function of  $Re_g$  and  $Sc_g$  during flow of particulate fluids. A published correlation for heat transfer was found to predict

Sh values within the same order of magnitude of those determined in this work, in spite of having been determined in experimental conditions and ranges of dimensionless numbers quite different from those used in our study. This shows the potential of using the heat/mass transfer analogy to estimate fluid-to-particle heat transfer coefficients from correlations developed in mass transfer studies, which would allow to overcome the hassle in measuring particle temperature in continuous flow. More studies should be performed in a wider range of conditions and both heat and mass fluid-to-particle transfer coefficients should be measured, to further assess this approach.

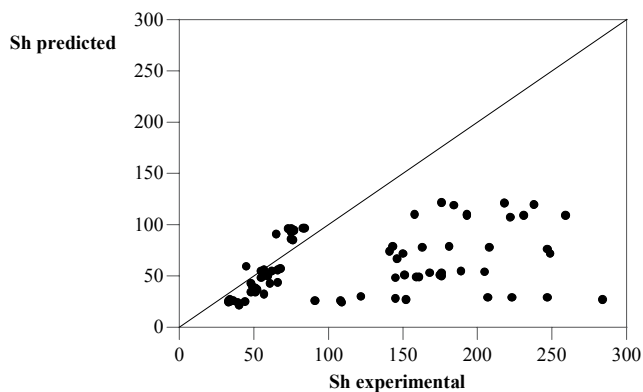


Figure 4: Prediction of Sh for spheres using the Correlation reported by Baptista *et al.* (1997b) (Equation (5)).

## ACKNOWLEDGEMENTS

The author Isabel Abreu is grateful to Fundação Calouste Gulbenkian for financial support.

## REFERENCES

- Azevedo, I.C.A.; Oliveira, F.A.R. and Drumond, M.C. 1998. "A study on the accuracy and precision of external mass transfer and diffusion coefficients jointly estimated from pseudo-experimental simulated data." *Mathematics and Computing in Simulation*, 48 (1), 11-22.
- Baptista, P.N.; Oliveira, F.A.R.; Oliveira, J.C. and Sastry, S.K. 1997a. "Dimensionless Analysis of the flow of spherical particles in two phase flow in straight tubes." *Journal of Food Engineering*, 31, 125-136.
- Baptista, P.N.; Oliveira, F.A.R.; Oliveira, J.C. and Sastry, S.K. 1997b. "The effect of translational and rotational relative velocity components on fluid-to-particle heat transfer coefficients in continuous tube flow." *Food Research International*, 30 (1), 21-27.
- Bird, R.B.; Stewart, W.E. and Lightfoot, E.N. 1960. *Transport phenomena*. John Wiley & Sons, Inc., New York, USA.
- Califano, A.N. and Calvelo, A. 1983. "Heat and Mass Transfer During the Warm Water Blanching of Potatoes." *Journal of Food Science*, 48, 220-225.
- Campos, D.T.; Steffe, J.F. and Ofoli, R.Y. 1994. "Statistical method to evaluate the critical Reynolds number for pseudoplastic fluids in tubes." *Journal of Food Engineering*, 23 (1), 21-32.
- Chilton, T.H. and Colburn, A.P. 1934. "Mass transfer (absorption) coefficients." *Industrial and Engineering Chemistry*, 26 (11), 1183-1187.

- Crank, J. 1975. *The Mathematics of diffusion*. 2<sup>nd</sup> ed. Oxford University Press, London, England.
- Fu, W., Sue, Y. and Chang, K.L.B. 1998. "Distribution of liquid-solid heat transfer coefficient among suspended particles in vertical holding tubes of an aseptic processing system." *Journal of Food Science*, 63 (2), 189-191.
- Geankoplis, C.J. 1983. *Transport processes and unit operations*. 2<sup>nd</sup> ed. Allyn and Bacon, Inc., USA.
- Grabowski, S. and Ramaswamy, H.S. 1995. "Incipient carrier fluid velocity for particulate flow in a holding tube." *Journal of Food Engineering*, 24, 123-136.
- Incropera, F.P. and DeWitt, D.P. 1996. *Fundamentals of heat and mass transfer*. 4<sup>th</sup> ed. John Wiley & Sons, Inc., New York, USA.
- Nelder, J.A. and Mead, R. 1965. "A Simplex method for function minimization." *The Computer Journal*, 7, 308-313.
- Noordsij, P. and Rotte, J.W. 1967. "Mass transfer coefficients to a rotating and to a vibrating sphere." *Chemical Engineering Science*, 22, 1475-1481.
- Pinheiro-Torres, A.C. 1998. "Assessment of continuous thermal processing of liquid foods and its impact on process design." Ph.D. thesis, Escola Superior de Biotecnologia, Universidade Católica Portuguesa, Porto, Portugal.
- Ramaswamy, H.S. and Zareifard, M.R. 2000. "Evaluation of factors influencing tube-flow fluid-to-particle heat transfer coefficient using a calorimetric technique." *Journal of Food Engineering*, 45, 127-138.
- Sastry, S.K. 1992. "Modelling the continuous sterilisation of particulate foods." In *Mathematical modelling of food processing properties*, S. Thorne (Eds.). Elsevier Applied Science, Cambridge, Great Britain, 71-105.
- Tahoun, M.K. 1986. "Large agarose-lipase beads for the hydrolysis of triglycerides." *Food Chemistry*, 22, 297-303.
- Zitoun, K.B. and Sastry, S.K. 1994. "Determination of convective heat transfer coefficient between fluid and cubic particles in continuous tube flow using non-invasive experimental techniques." *Journal of Food Process Engineering*, 17, 209-228.

## AUTHORS BIOGRAPHY

**ISABEL ABREU** was born in Porto, Portugal and obtained an undergraduate degree in Chemical Engineering in 1990 at the Faculty of Engineering, University of Porto, Portugal. She has worked as a teaching assistant at the College of Biotechnology, Catholic University of Portugal, where she is also completing her PhD. Currently she is teaching assistant at University Fernando Pessoa, Porto, Portugal. Her research work focus on the application of statistical techniques to the optimisation of the estimation of mass transfer parameters.

**FERNANDA OLIVEIRA** was born in Viana do Castelo, Portugal, and obtained an undergraduate degree in Chemical Engineering in 1985 at the Faculty of Engineering, University of Porto, Portugal, and a PhD degree in Food Engineering in 1989 at University of Leeds, UK. She worked as Associate Professor and Associate Director at the College of Biotechnology, Catholic University of Portugal, as Associate Professor and Vice-President of the Inter-University Institute of Macau, China, and as Senior Consultant and Director of the Portuguese Society for Innovation (Porto, Portugal) before moving to Ireland, where she is currently Professor and Head of the Department of Process Engineering, at University College Cork.

# FLUID EXCHANGE FOR PREDICTING CLEANABILITY USING CFD

Bo Boye Busk Jensen  
Alan Friis  
Food Process Engineering, BioCentrum-DTU  
Build. 221, Soltofts Plads  
2800 Kgs. Lyngby  
Denmark  
E-mail: bbb@biocentrum.dtu.dk

## KEYWORDS

Computational Fluid Dynamics, Cleaning, Fluid Exchange, Computer Aided design.

## ABSTRACT

This work presents basic studies for future use of flow simulation tools in the area of hygienic design. By comparing traditional cleaning test results with state of the art Computational Fluid Dynamics (CFD) simulations, investigations are made to find a correlation between fluid exchange and cleanability. Previous work has shown that the wall shear stress alone is insufficient to predict the cleanability of components involving complex flow phenomena. This work is an extension, which covers the exchange of fluid from near wall zones yielding a qualitative correlation for cleanability. The exchange rate is predicted from transient CFD simulations by modelling two fluids with matching material properties. The investigation shows a direction for future work, as identification of a quantitative combination of wall shear stress and exchange rate is needed to provide a powerful tool for predicting cleanability using CFD.

## INTRODUCTION

As legislation on food processing equipment has been extended to include hygienic design during the recent decade (EHEDG 1993) manufacturers of food processing equipment have seen the importance of evaluating the hygienic state of equipment parts. Traditionally, comparing cleaning tests performed on the component of interest with the cleanability of a straight pipe produce a measure of the hygienic state of the component. This is implemented by the European Hygiene and Engineering Design Group (EHEDG) in their test method (EHEDG 1992). It is generally accepted that cleaning effects in closed process equipment is related to the mechanical action of the flow (Paulsson 1989). The relevant hydrodynamic parameters are not trivial to identify. However, Computational Fluid Dynamics (CFD) offers an attractive alternative to the traditional methods for predicting cleanability (Hall 1998). Using CFD requires increased knowledge of both quantitative and qualitative aspects of the hydrodynamic parameters controlling cleaning. Such knowledge offers equipment designers a tool for evaluating and increasing the hygienic quality of new components prior to prototype production for experimental testing.

In uni-axial flow wall shear stress has been identified as a measure of the required flow intensity for removal of material from surfaces (Duddridge et al. 1982). However, these findings cannot be transferred to true three-dimensional flow regimes in complex equipment (Jensen et al. 2001). Only straight pipes and ducts can be regarded as components with parallel flow as most other types of equipment contains zones with recirculating, stagnating or swirling flow. This leads us to investigate the influence of the fluid exchange rate from near-wall regions in the spherical shaped valve house (a Mix-proof valve) shown in Figure 1 and an upstand (displayed in Figure 2) to see if prediction of cleanability is possible from knowledge of fluid exchange or in a combination with wall shear stresses.

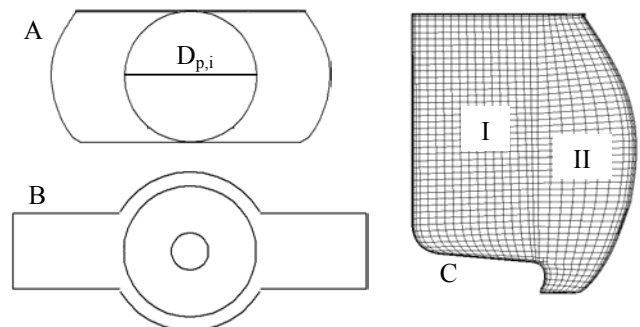


Figure 1: Spherical valve house seen from the end (A), the top (B) and the mesh seen from the end (C).

## THEORY

In addition to the wall shear stress, others (i.e. Graßhoff 1980) have postulated but not proven that the fluid exchange rate could be correlated to the degree of cleanability. Exchange of fluid serves as a transport mechanism, due to convection of detergent and heat from the main stream to the near wall region. These two components weaken the binding between deposit and surface, which allows a lower wall shear stress to remove the deposit (Eginton et al. 1998). In addition the exchange of fluid also transports the removed deposit away from the near wall regions enabling decontamination. The needs for transporting detergent and heat to surfaces are amplified as surfaces in areas of low fluid exchange very often are exposed to low wall shear stress because of recirculation zones of low fluid velocity.

## METHODS

Comparing cleaning test and CFD simulations on the components validates the influence of flow parameters on removal of deposit from surfaces. In this work cleaning trial results from an upstand geometry performed by Richardson et al. 2001 (Figure 2) and a sphere shaped valve house (Figure 1) are used for evaluating the influence of the exchange rate on the cleanability.

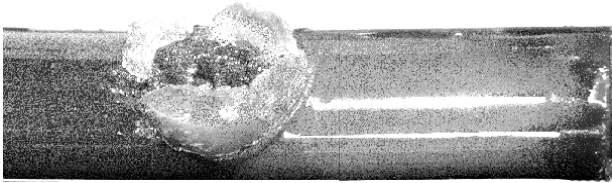


Figure 2: Cleaning trail result in upstand. Turbulent flow from left to right. Dark areas are cleaned zones and bright areas uncleaned zones (Richardson et al. 2001).

Exchange of fluid can be obtained from experimental methods such as conductive measurements (Graßhoff 1980) or by discrete sampling in the product stream, both yielding results on a macro scale level. An alternative is transient CFD simulations that provide a tool for prediction and visualization of the exchange of fluid on both micro- and macro scale levels. The method used for predicting the exchange of fluid involves two steps: 1) A steady state solution to predict the flow field in the geometry using appropriate properties of the CIP fluid of a predefined colour is carried out. 2) A transient simulation is restarted using the steady state solution as initial conditions. A new fluid with the same properties as the old one but with a different colour is used as inlet fluid from  $t = 0$  s and onwards. Stepping through time in small time steps gives the exchange of old with new fluid.

### Cleaning Tests on the Spherical Shaped Valve

The hygiene test used here and in the work of Richardson et al. 2000 is adapted from the guidelines of EHEDG 1992. The sterilized test piece and a reference pipe are soiled with a mixture of sour milk and *Bacillus stearothermophilus* spores. A gentle cleaning procedure is performed and cleanability is visualized by incubating the reference pipe and test piece in Shapton and Hindes agar (Shapton et al. 1963) for 20 hours at 58°C. As a standard the mean inlet velocity is set to 1.5 m/s. The results are visualized by a change from purple to yellowish agar due to a pH change as a result of fermentation by germinating spores still present on the surface (example seen in Figure 2). The sensibility of the test method requires two or more experiments to ensure that poor hygienic design exists in areas with discoloured agar. Jensen et al. 2001 found a critical wall shear stress for the above cleaning test on a 2B surface in a Radial Flowcell to approximately 3 Pa.

The tests performed on the sphere shaped valve house is performed with a decreased cleaning time to obtain

discolouration in the valve as the valve house otherwise is cleaned to such a degree that only very small areas of discoloured agar are seen. The critical wall shear stress in tests with decreased cleaning time is not affected significantly by the shorter CIP time.

### CFD Model of the Upstand

The upstand geometry is modelled using quadratic cells in an unstructured mesh with integral and arbitrary couplings between cells with unmatched faces. Both pipes are generated from the butterfly method (Figure 3).

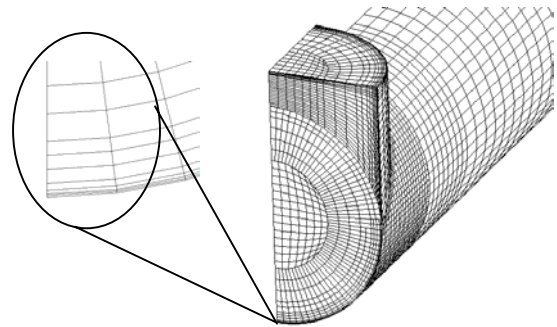


Figure 3: Mesh created to discretize the flow domain of the upstand.

Exploiting the geometric plane of symmetry, a model with 51,000 cells is created for one half of the upstand. The validity of the symmetry plane as a symmetry plane for the flow was tested (not shown) and shows only little difference in exchange rates. The mesh is created with a bow like shaped mesh of  $7 \times 7 \times 40$  (width  $\times$  height  $\times$  axial) cells in the core region and encircled by a  $5 \times 28 \times 40$  (radial  $\times$  tangential  $\times$  axial) celled cylindrical shaped mesh. The cells closest to the walls are refined radial to obtain  $y^+ \sim 5$  as recommended for the use of two-layer models (Figure 3). Cells part of an arbitrary couple is not refined. The upstand pipe positioned  $1.5 \cdot D$  to  $2.5 \cdot D$  downstream of the inlet consists of  $7 \times 7 \times 18$  box like and  $28 \times 5 \times 18$  cylindrical mesh and refinement is made of the near wall cells to  $y^+ \sim 5$ . 10 rows with double axial distance compared to the axial distance in the region of interest are added to the downstream side of the upstand to position the outlet boundary sufficiently far downstream. Following this refinement of the 36 rows centred around the upstand are axial refined once followed by an additional axial refinement of the 20 rows of the new mesh centre around the upstand. The latter of these refinements is only performed on the cells part of the outer region of the mesh in the pipe. Finally cells on the main pipe being part of an arbitrary couple with cells on the upstand are refined tangential once.

### CFD Model of the Spherical Valve House

A 2D patch (Figure 1) which consists of two areas (I and II) is created within the outline of the cross-section of the

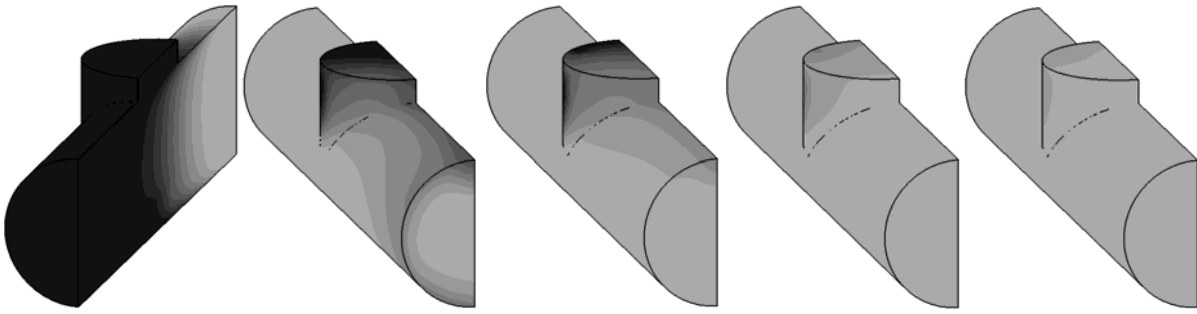


Figure 4: Predicted fluid exchange in an up-stand from CFD simulations. Grey fluid is introduced at time 0 s and gradually replaces the dark fluid. The pictures are shown at  $t = 0.05$  s, 0.2 s, 0.3 s, 0.8 s and 1.05 s (from left to right).

valve. When the patch is revolved 144 times around then centre axis region I and II consists of  $16 \times 144 \times 40$  cells and  $8 \times 144 \times 46$  cells respectively. The in- and outlet pipes are made as a butterfly mesh extended to  $1/2 \cdot D_{p,i}$  up- and downstream of the valve house (Figure 1). The pipes consist of a  $10 \times 10 \times 20$  celled quadratic mesh in the centre of the pipe encircled by a mesh of  $4 \times 40 \times 20$  cells. The outer layer of cells is refined once to obtain  $30 < y^+ < 100$  (limits for law of the wall treatment of the near wall region). The 8 layers of cells closest to the valve house is refined once in axial direction. Arbitrary couplings between the pipe and valve house are used at the interface. A total number 80,000 cells are obtained by this method.

Two-layer models as the one used in the sphere require  $y^+$  values in the range of 5. Therefore, radial refinement is made of all the near wall layer cells in the valve house to obtain  $y^+ \sim 5$ . Cells for refinement are identified from simulations using previous meshes. Near wall flow in the in- and outlet pipe is modelled by use of the “law of the wall” method that requires  $y^+ > 30$  and as a consequence a less number of cells. The total number of cells in the model with two-layer treatment of the near wall flow is 180,000.

## SIMULATION SET-UP

The simulations are performed using the finite volume based code Star-CD v. 3.100b. The Navier-Stokes equations set-up transport equations for momentum, energy and scalars by use of appropriate parameters (for more information see i.e. Versteeg et al. 1995). Spatial and temporal discretisation of the transport equations are performed using the second-order accurate Self Filtered Central Difference and Crank-Nicholson schemes respectively. Casey et al. 2000 showed the importance of choosing second-order discretisation for both dimensions of progress as numerical diffusion is significant in lower order schemes.

A time step of 0.005 s and 0.0005 s for the upstand and spherical shaped valve respectively is chosen to obtain Courant numbers below 100 to capture features of the flow. If the Courant number is too high, the risk of information convected across cells in the domain is large and thereby information from one cell is likely to be transferred across neighbouring cells. The time step used in the simulations of

the spherical shaped valve could have been the same as for the upstand without violating the Courant number of 100. However, with the mesh configuration and models chosen it was impossible to get a converged transient simulation at a time step of 0.005 s. A maximum number of 20 corrector steps are chosen to obtain a physical solution to the fluid exchange in the spherical shaped valve compared to only 10 in the upstand.

The RNG  $k-\varepsilon$  model with the two-layer model of Norris and Reynolds is used for turbulence modelling, with a dynamic estimation of the cells located within the near-wall layer (Rodi 1991) to describe the flow in the near wall region.

In both geometries the inlet conditions are described using the Dirichtlet method with a fully developed turbulent velocity profile at an average velocity of 1.5 m/s, turbulent kinetic energy of 5% and turbulent length scale of 1/10 of the inlet pipe diameter. The outlet is described as a pressure outlet with constant pressure on the boundary. Walls are prescribed with non-slip conditions and as hydraulic smooth.

## RESULTS

### Fluid Exchange in Upstand

In the short upstand investigated the flow is more complicated than in a longer upstand i.e.  $H/D = 0.5$ . A recirculation zone is seen in the longer upstand on a plane coinciding with the symmetry plane. As the space for this recirculation zone is reduced in the short upstand it is suppressed and almost non-existing. Instead a recirculation zone in the plane perpendicular to the axial direction is formed in the entire upstand and a recirculation zone is also seen in the horizontal plane. The effect of the non-existing recirculation zone is seen in the flow downstream of the upstand as it is pushed away from the wall producing a zone of low exchange rate (Figure 4). This is not seen in the long upstand, as the horizontal recirculation zone does not influence the main flow as much as in the short upstand. In the downstream zone exchange of fluid is approximately 3 and in the upstand 6 times slower than in the part affected by the bulk flow. Investigations of the magnitude of the wall shear stress (not presented) shows wall shear stress

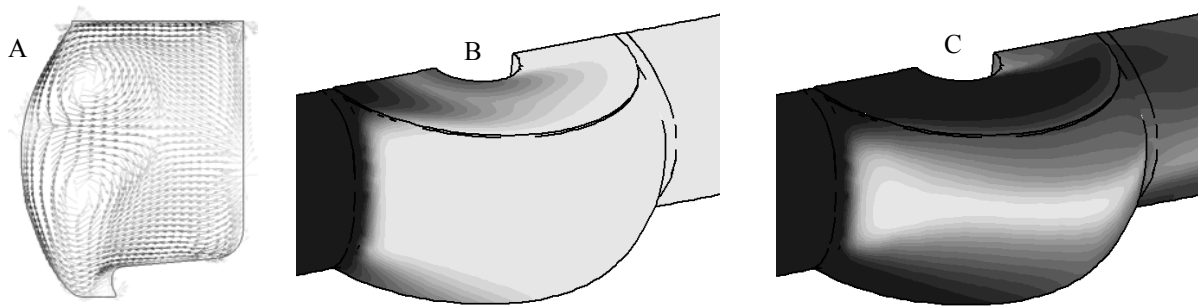


Figure 5: Vector plot of flow in spherical shaped valve seen from the inlet towards the outlet (A). The plane for visualisation is located perpendicular to the axial direction of the pipes and in the centre of the valve house. Fluid exchange at  $t = 0.13$  (B) and  $0.23$  s (C) are shown in the valve with flow from left to right.

below the critical value of 3 Pa in the upstand and in a thin streak downstream of the upstand. The zone of low exchange rate downstream of the upstand extends to more than  $1.5 \cdot D$  downstream of the upstand.

### Fluid Exchange in Sphere Shaped Valve

The flow pattern in a spherical valve house with in- and outlet located as shown in Figure 1 is very complex because of transition from a small circular cross sectional area to a larger of non-circular shape produces two swirl zones on top of each other in the zone seen closest to the outer surfaces (Figure 5). Near the cone the flow is almost unidirectional towards the outlet. These swirl zones have a large influence on the exchange of fluid from areas close to the outer walls. As new fluid enters the sphere most of it flows directly through the centre of the valve and towards the outlet pipe. Within 0.23 s most of the old fluid is exchanged in the main stream. As time progresses the old fluid is exchanged in the remaining part of the sphere. The zones with lowest exchange rate are near the equator of the sphere (light areas in figure 5 (C)) and especially in the area just next to the inlet. The total exchange takes 0.95 s. Wall shear stress is below 3 Pa in large zones on the surfaces (Figure 6). Only near the outlet pipe, close to the top and bottom and near the inlet, close to the bottom are wall shear stresses above 3 Pa (looking only at the outer surface of the valve).

### Cleaning of Upstand

The potential problems of cleanability in an upstand of  $H/D = 0.16$  with a mean inlet velocity of 1.5 m/s is seen in the upstand itself as expected (Figure 2). Upstream of the upstand the main pipe is cleaned to a degree where discoloration of the agar is not seen. On the contrary a great part of the pipe surface downstream and on the same side of the upstand is with attached spores. This zone is located from the upstand and until a downstream position of approximately  $1.5 \cdot D$ .

### Cleaning of Sphere Shaped Valve

Figure 6 illustrates cleaning results on one side of the sphere from a single cleaning procedure with decreased cleaning time. A common feature of the results is that discolouring is present just next to the inlet of the sphere. Further downstream the discoloured zone decreases in width towards the outlet. In one experiment the problem zone was present slightly below and in another slightly above the equator.



Figure 6: Illustration of results from cleaning trails with reduced cleaning time compared to the standard EHEDG test method. Black is uncleaned zones. Dotted lines mark the zones predicted as cleanable from a critical wall shear stress of 2.5 – 3 Pa.

Detailed information on the hygienic state in other parts of a sphere shaped valve house is under preparation for publication.

### DISCUSSION

Comparing cleaning results, CFD simulations and the critical wall shear stress shows that wall shear stress alone is insufficient for approximating problematic areas in the upstand and the spherical shaped valve used in this study. Areas with low wall shear stresses are cleaned (valve) and areas of high wall shear stress are not cleaned (upstand).

In the upstand zones with low exchange rate is shown as problematic areas. Especially in the downstream shadow

zone of the upstand problems with hygiene was seen. This was not expected from the wall shear stress but could be foreseen by investigations of the exchange rate. In this area the exchange rate is lower than in the main stream, while other areas in the upstand with the same wall shear stress as in the downstream problem zone was totally cleaned.

In the valve areas with wall shear stress below the critical value of 3 Pa is cleaned. The expected area of hygienic problems according to the wall shear stress is outlined in Figure 6 as the dotted lines and shows a large area around the equator expected to be uncleaned. Comparing Figure 6 to predicted exchange (Figure 5) shows that the zone of low exchange rate is decreased into a smaller and smaller zone just above the equator as time progresses. The areas cleaned having low wall shear stress, has a relative high exchange rate compared to the exchange in i.e. the upstand and other places in the valve with the same wall shear stress. From this, zones with low wall shear stress but clean can be explained by the relative low exchange time (below 0.3 s).

## CONCLUSION

Comparing the EHEDG tests to simulation results show that wall shear stress is insufficient to predict the outcome of the hygiene tests. Areas with wall shear stress lower than the critical value found experimentally using a Radial Flowcell could be cleaned and areas with higher wall shear stress not cleaned. It is shown that this can be explained from the rate of fluid exchange. With the gained knowledge of hydrodynamic cleaning effect it is possible to supplement i.e. the EHEDG test with CFD simulation. This allows manufacturers of food processing equipment to test different designs using CFD, which could lead to improved quality of the hygienic state of closed equipment in the future. To accomplish this, future work is needed to identify quantitative values for a combination of wall shear stress and fluid exchange to be present to achieve a satisfactory EHEDG test results.

## ACKNOWLEDGMENTS

The authors wish to thank Mr. Jens Folkmar Andersen and Mr. Preben Esbensen from Alfa Laval LKM a/s, Kolding, Denmark, Mr. Erik-Ole Jensen from Arla Foods Amba, Brabrand, Denmark and the Biotechnological Institute, Kolding, Denmark for their participations in fruitful discussions. The Centre for Hygienic Design and Cleaning of Food Process Equipment is acknowledged for the financial support of this work.

## REFERENCES

Casey, M. and T. Wintergerste. 2000. *ERCOFTAC Special Interest Group on "Quality and Trust in Industrial CFD - Best Practice Guide"*, ERCOFTAC, www.ercoftac.org, Hampshire

Duddridge, J.E., C.A. Kent, and J.F. Laws. 1982. "Effect of Surface shear stress on the Attachment of *Pseudomonas fluorescens* to Stainless Steel under Defined Flow

Conditions." *Biotechnology and Bioengineering*, 24, 153-164.

Eginton, P.J., J. Holah, D.G. Allison, P.S. Handley, and P. Gilbert. 1998. "Changes in the Strength of Attachment of Micro-organisms to Surfaces Following Treatment with Disinfectants and Cleansing Agents." *Letters in Applied Microbiology*, 27, 101-105.

EHEDG. 1992. "A Method for Assessing the In-place Cleanability of Food-processing Equipment." *Trends in Food Science & Technology*, 3, 325-328.

EHEDG. 1993. "The EC Machinery Directive and Food Processing Equipment." *Trends in Food Science & Technology*, 4, 153-154.

Graßhoff, A.V. 1980. "Untersuchungen zum Stromungsverhalten von Flüssigkeiten in zylindrischen Toträumen von Rohrleitungssystemen." *Die Kieler Milchwirtschaftlichen Forschungsberichte*, 32, 273-298.

Hall, J. 1998. "Computational Fluid Dynamics: A Tool for Hygienic Design." *Fouling and Cleaning in Food Processing*,

Jensen, B.B.B. and A. Friis. 2001. "Flow Parameters in Hygienic Design." in *The 32nd R3 Nordic Symposium*, Reklamproducenterne, Enköping, Sweden, 347-353.

Paulsson, B.-O. 1989. *Removal of Wall Deposits in Turbulent Pipe Flows*, Lund University - Department of Food Engineering,

Richardson, P.S., R.M. George, and R.D. Thorn. 2001. "Application of Computational Fluid Dynamics Simulation to the Modelling of Cleanability of Food Processing Equipment." in *Proceedings of the Eighth International Congress on engineering and Food (ICEF8)*, Technomic Publishing co., Lancaster Pennsylvania, 1854-1858.

Rodi, W. 1991. "Experience with Two-Layer Models Combining the k-e Model with a One-equation Model Near the Wall." *AIAA-91-0216*, 1-12.

Shapton, D.A. and W.R. Hindes. 1963. "The Standardisation of a spore Count Technique." *Chemistry and Industry*, 9, 230-234.

Versteeg, H.K. and W. Malalasekera. 1995. *An Introduction to Computational Fluid Dynamics - The finite Volume Method*, Longman Scientific & Technical, Essex, England

## AUTHOR BIOGRAPHY

**BO BOYE BUSK JENSEN** was born in Hou, Denmark and went to the Aalborg University, Department of Energy Technology, where he studied Mechanical Engineering in the area of energy consuming/producing machinery and fluid dynamics. He obtained his degree in 1998 after which he worked as a Research Assistant using Computational Fluid Dynamic at the same department as he graduated from. In 1999 he enrolled as a Ph.D. Student at BioCentrum-DTU, Technical University of Denmark working in the field of hygienic design using Computational Fluid Dynamics, which is still ongoing.

# SLIDING MESH METHOD TO SIMULATE FLOW OF HIGHLY VISCOUS FLUID IN STIRRED TANK AGITATED WITH HELICAL RIBBON IMPELLER.

Guillaume Delaplace  
Romuald Guérin  
Jean-Claude Leuliet

Institut National de la Recherche Agronomique  
Laboratoire de Génie des Procédés et Technologie Alimentaires  
369 rue Jules Guesde, B.P. 39,  
59651 Villeneuve d'Ascq Cédex, France  
E-mail: delapla@lille.inra.fr

Claude Torrez  
Christophe André

Hautes Etudes Industrielles (H.E.I.)  
Laboratoire de Génie des Procédés  
13 rue de Toul,  
59046 Lille Cedex, France  
E-mail: Claude.Torrez@hei.fr

## KEYWORDS

CFD, helical Ribbon agitator, laminar, particle tracks, sliding mesh

## ABSTRACT

In this paper, steady and unsteady particle tracks into a stirred tank was conducted by means of a commercial available fluid dynamic (CFD) software package (FLUENT).

A rounded bottom vessel equipped with an atypical helical ribbon impeller was used as mixing equipment and the viscous media was highly viscous fluids.

The reliability of the numerical procedure was demonstrated on the basis of a comparison of the numerical results with tracer experiments.

It is shown that using a sliding mesh technique, computational tools are able to predict accurately trajectory of a particle in the vessel.

Even if CPU times values are still high, these approaches are likely to have a significant impact in the close future to get an idea of mixing efficiency of various mixing systems.

## INTRODUCTION

Helical ribbon agitators have been widely used for mixing liquids of high viscosity. There are many experimental studies providing basic information of helical ribbon impeller concerning power consumption (Delaplace et Leuliet 2000) of agitators and /or mixing characteristics (Delaplace et al. 2000a) Unfortunately there were only few experimental works devoted to a detailed description of the hydrodynamics inside the vessel (Bourne et Butler 1969; Carreau et al. 1976; Soliman 1985)

From a practical point of view, this can be explained easily since there are not a lot of experimental techniques available for the local hydrodynamic characterization of flow pattern induced by such complex mixing systems.

On one hand, Pitot tubes or Hot-wire Anemometry are intrusive techniques (Mavros 2001).

On the other hand, Laser Doppler Velocimetry (LDV) and Particle Image Velocimetry (PIV), required the need for the fluid to be transparent. This is seldom the case in foodstuff industry. Moreover, even if real fluids are transparent, these techniques required a penetrating laser beam which are limited in such high viscosity fluids due to light diffusion (Aubin et al. 2000). Other inherent difficulties also explained the few experimental data. For instance, when blades of the close clearance impeller going by the laser beam, no experimental

data can be measured and consequently it is impossible to obtain the velocity profile at whole stage during a cycle (a cycle is the time taken for impeller to rotate one revolution).

This lack of information about the velocity field is very annoying since a detailed characterization of the three dimensional flow pattern inside the vessel is of vital importance to gain a better understanding of the state of the flow of the fluids and of the mechanisms responsible for homogenization and transport processes.

In this area, the perspective offered by advanced computational fluid dynamics (CFD) seems very interesting. The use of CFD for the investigation of mixing flow phenomena is not new and demonstrable benefits gained from its application have been obtained for classical agitators such as Rushton turbine (Ranade et Joshi 1990; Luo et al. 1994; Jaworski et al. 1997; Torrez and André 1998; Micalé et al. 1999; Ranade et al. 2001) and pitched blade turbine (Armenante et al. 1994; Jaworski et al. 2001; Aubin et al. 2001) in the turbulent flow regime. Development of unstructured and hybrid meshing techniques has allowed the representation of more complicated geometries often found in laminar flow mixing [anchor (Bertrand and al. 1996; Delaplace et al. 2000b), helical ribbon agitators with or without screw (Tanguy et al. 1992; Kaminoyama and Kamiwano 1994; Tanguy et al. 1997; De la Villéon et al. 1998; Delaplace et al. 2000c), helical screw impeller (Aubin et al. 2000)

Although the numerical knowledge of velocity field under laminar regime have represented an important step forward, these works is a shortcoming to investigate homogenisation process in agitated vessel.

Indeed, most of the particle tracks have been performed under steady flow. This means that the velocity field used by the software to compute the trajectory of a fluid element was not time-dependent but steady. Consequently, it is not possible to predict exactly particle track in the tank since fluctuations of velocity relative to the revolution of the impeller are disregarded. These modelling simplifications can be explained easily: the design of these agitators are not trivial and therefore correctly capturing the characteristic flow features require large amount of CPU times.

The aim of this paper is to show that, using a sliding mesh method and a commercial code (FLUENT 5.4 then FLUENT 6.0), succeeds in predicting the real trajectory of a fluid element subjected to laminar flow in a three dimensional mixing tank.

The reliability of the numerical unsteady particle tracks was compared with flow pattern visualization obtained by tracer experiments. For that, a colour indicator was injected in the transparent liquid and its flow was captured by a video camera.

## MATERIALS AND METHODS

### Mixing system

A sketch of the mixing system investigated is shown in Figure 1. The dimensions of the mixing system are also reported in Figure 1.

This non standard helical impeller has two particularities: firstly, it is equipped with an anchor at the bottom in order to avoid the formation of a stagnant zone; secondly the size of the pitch ratio  $p/d$  ( $p/d=1.7$ ) is greater than with a typical double helical ribbon mixer ( $0.5 < p/d < 1.2$ ). During all the experiments, the volume of agitated liquid was kept constant and equal to  $34 \cdot 10^{-3} \text{ m}^3$  which corresponds to a liquid depth,  $H_L$  of 0.409 m.

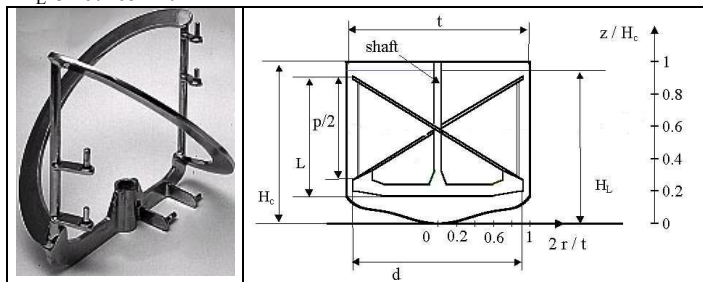


Figure 1. Picture of the agitator (PARAVISC®, Ekato) and scheme of the mixing system used. (vessel diameter,  $t=0.346$  m, impeller diameter,  $d=0.320$  m; blades width,  $w=0.032$  m, impeller pitch,  $p=0.560$  m; impeller height,  $L=0.340$  m, tank height,  $H_c=0.443$  m, Liquid height  $H_L=0.409$  m).

### Fluids

The Newtonian fluids used for tracer experiments were various mixtures of glucose syrup with various water contents. The Rheological properties and densities of these fluids were obtained at the same temperature as that encountered in the mixing equipment.

Numerical simulation of steady and unsteady particle tracks were carried out with Newtonian liquids. For these CFD simulations, viscosity and density of the agitated fluid were respectively set equal to 2.82 Pa.s and to 1380 kg/m<sup>3</sup>.

### Numerical simulations of steady and unsteady particle tracks

In this work, the trajectory of a fluid element subjected to laminar flow in an industrial agitated vessel equipped with an atypical helical ribbon impeller was computed numerically (particle track).

The trajectory of a fluid element has been computed using two approaches. The first one used a steady velocity field obtained by a rotating reference frame technique. For this case, particle track neglect velocity fluctuations due to the revolutions of the agitator blade. Consequently, the motion of the fluid element is only an approximation of real trajectory.

The second one used an unsteady velocity field obtained by a sliding mesh technique.

The numerical tools and procedure solution used by the commercial CFD finite volume software (FLUENT) to simulate the velocity field inside the vessel using a rotating reference have already been described in details (Delaplace et al. 2001b, 2001c). and will not be repeated in details here. Only specific details about the sliding mesh modelling options will be given.

The sliding mesh modelling approach involves two mesh regions, one (inner grid) attached to a rotating geometry (impeller) and one (outer grid) attached to stationary boundaries of the flow (tank walls). During the calculation, the cell zones slide (rotate) relative to one another along the grid interface in discrete steps. To compute the interface flux, the intersection between the interface zones is determined at each time step. In this study, the time step was equal to 0.2 seconds.

A view of the outer and inner grids used in this work are shown in Figure 2. The grid interface is located at the middle of the wall clearance.

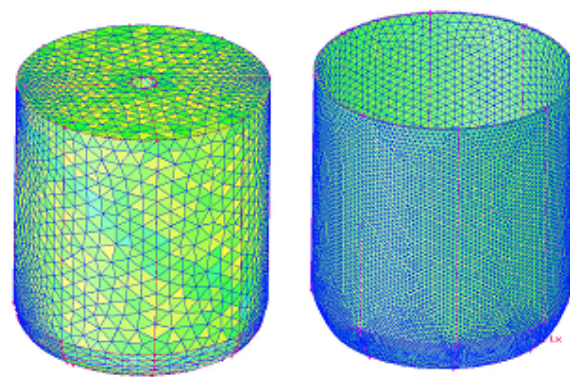


Figure 2: View of the grids used to discretize the domain. (left) Inner grid - (right) Outer grid

Note that to obtain a reasonable mesh size, it was decided to mesh the concentric zone around the shaft with hexahedral cells while regions close to the helical blades of the impeller consist of tetrahedral cells. (Figure 3)

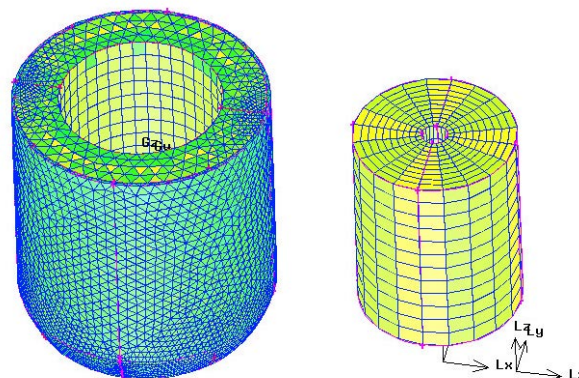


Figure 3: View of the cell types containing in the inner grids.

Actually, an unstructured mesh of 218,164 cells has been required to represent the whole mixing system (agitator + tank).

Note that the geometry of the mixing system used for simulation is very similar to the experimental equipment (figures 4 and 5). The rounded bottom of the vessel has been accurately duplicated (figure 5). Only additional parts of the impeller used to fix scrapers haven't been meshed

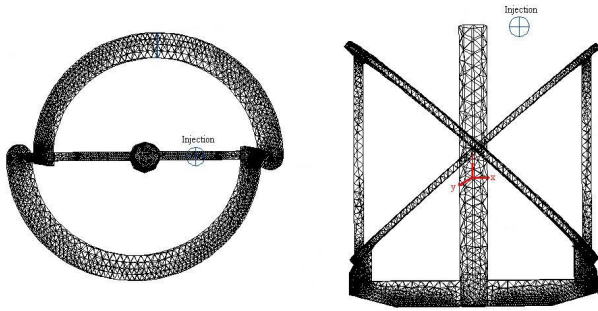


Figure 4. Mesh of the agitator [PARAVISC®, Ekato]. The initial position of the fluid element when using sliding mesh technique is also reported.



Figure 5. Mesh of the rounded bottom vessel studied.

The boundary conditions at the impeller shaft and at the vessel walls were those derived assuming the no-slip condition. At the free surface, the boundary conditions were modelling by requiring that there is no normal velocity and zero normal gradient for all variables.

Resolution of the algebraic equations was carried out using the Semi-Implicit algorithm Pressure Linked equation (SIMPLE) with a first order upwind discretisation scheme.

## RESULTS AND DISCUSSION

### Steady particle tracks

An example of trajectories results obtained for steady particle tracks with the close clearance agitator studied is presented in Figure 6 (N=35 rev/min,  $\mu = 2.8$  Pa.s).

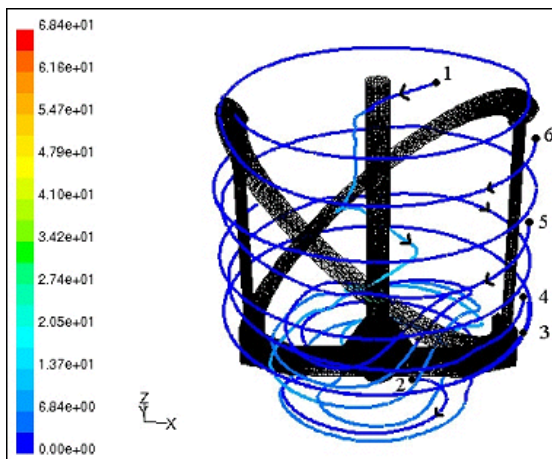


Figure 6: Particle traces (colored by residence time(seconds)) obtained numerically when steady flow simulation is performed.

For this test, various colors refers to various residence time. In this figure, six particles at various locations in the vessel were launched to obtain a view of the flow pattern in the vessel. These results agree in a certain extent with the experimental observations of tracer particles under same flow conditions. Indeed, rotating counter clockwise direction, it has been observed that tracer particles go down around the stirring shaft with an helical trajectory and subsequently go up along the vessel wall.

However, analysis of time to achieve a close loop (axial circulation time) are disagree with previous studies (Delaplace et al. 2000c). This may be explained by the fact that the velocity field used by the software to compute the trajectory of the fluid element are steady and consequently do not take into account velocity fluctuations due to impeller revolutions.

Unfortunately these data are required for accurate computation of fluid trajectory. Consequently, important errors are generated. For example, we can detect recycle zones which are not observed experimentally by recording flow of freely suspended particles. Consequently, such approach fails to predict precisely the trajectory of fluid element in the tank.

### Unsteady particle tracks

An example of a particle trajectory obtained using sliding mesh technique for the close clearance agitator studied is shown on Figure 7 (N=35 rev/min).

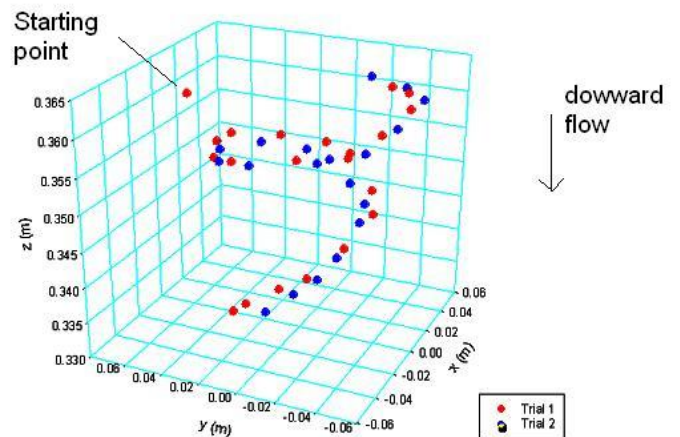


Figure 7: Particle trajectories obtained numerically when sliding mesh technique is performed.

Trials 1 and 2 refers to a similar injection which has been duplicated with two different computers. For the two simulations, tracer injection has been launched at the upper part of the vessel as shown in Figure 4.

As expected,, for the two computers, the trajectory of the fluid element are similar.

Note that on figure 7, only 4 seconds of the real mixing process has been simulated. This is explained by the large amount of CPU times required to achieve such simulations.

For instance, at the beginning (trial 1), the computations were performed on a Silicon Graphics computer with 300 MHz Octane R12000 processor and required more than 20 days of CPU times to simulate only 4 seconds of the real mixing process. For a Hp workstation X4000 computer with a 1.8 GHz P4 Xeon processor, CPU times decrease. 48 hours of CPU

times is required to simulate 4 seconds of real homogenisation process (trial 2).

Tracer experiments with a coloured fluid show that the computation of the fluid element trajectory is in agreement with those observed experimentally as indicated on figure 8.

Figure 8 was obtained when a colour indicator was injected in the transparent liquid and its flow was captured by a video camera. It appears that the red dye follow an helical trajectory along the shaft. This is also the case for numerical results (Figure 7).



Figure 8: Flow visualization in stirred vessel using a red colour tracer with similar rheological and physical properties than the viscous media.

Moreover, although it is too early to announce it (computations are not yet finished), it seems that there are less scatters between experimental and numerical particle tracks when unsteady velocity field is computed.

Taken by preliminary estimation of numerical average times taken by a fluid element to cross a given reference plane two times in the same direction (axial circulation time) seems in better concordance with experimental data.

## CONCLUSION

In this work, first a three-dimensional resolution of the flow equations in a mixing vessel has been conducted by CFD approach using two approaches : a sliding mesh and a rotating reference frame technique.

Then trajectory of a fluid element obtained by the two approaches (steady and unsteady flow field) have been computed and compared to those obtained by tracer experiments.

It has been shown that sliding mesh method succeeds in predicting the trajectory of a fluid element subjected to laminar flow in a three dimensional mixing tank. On the contrary, Steady particle tracks are not adapted for this close clearance impeller.

It is now clear that the science of mixing will benefit a lot from numerical simulation in a close future. Nevertheless, at the state of the art, it is indispensable that the amount of CPU times required for these simulations decreases.

## BIBLIOGRAPHY

- Armenante P.M., C-C. Chou and R.R. Hemrajani 1994. "Comparison Of Experimental And Numerical Fluid Velocity Distribution Profiles In A Unbaffled Mixing Vessel Provided With A Pitched-Blade Turbine." *I. Chem.E.Symp. Series* n°136, 349-362.
- Aubin J, Naude I, Bertrand J., Xuereb C. 2000. "Blending Of Newtonian And Shear-Thinning Fluid In A Tank Stirred With A Helical Screw Agitator." *Trans.I.Chem.E.*, Vol 78, Part A, 1105-1113.
- Aubin J., Mavros P., Fletcher D.F., Xuereb C., Bertrand J. 2001. "Effect Of Axial Agitator Configuration (Up Pumping, Down Pumping, Reverse Rotation) On Flow Patterns Generated In Stirred Vessels." *Proc. Trans.I.Chem.E.*, Part A, *Chem. Eng. Res. Des.* 79, A8, 845-856.
- Bertrand F., Tanguy P.A., Brito-de La Fuente E. 1996. "A New Perspective For The Mixing Of Yield Stress Fluids With Anchor Impellers." *Chem.Eng.Res. and Des.*, Vol 29, N°1, 51-58
- Bourne J.R., Butler H. 1969. "An Analysis Of The Flow Produced By Helical Ribbon Impellers." *Trans. Instn. Chem. Engrs.*, 47, 11-17.
- Carreau P.J., Patterson I., Yap C.Y. 1976. "Mixing Of Viscoelastic Fluids With Helical-Ribbon Agitators: Mixing Time And Flow Patterns." *The Can. J. of Chem. Eng.* 54, 135-142.
- De la Villéon J., Bertrand F., Tanguy P.A., Labrie R., Bousquet J., Lebouvier D. 1998. "Numerical Investigation Of Mixing Efficiency Of Helical Ribbons." *AIChE Journal*, Vol 44, N°4, 972-977.
- Delaplace G., J.C. Leuliet 2000. "Power Consumption of Helical Ribbon Impellers in Highly Viscous Liquids – A Review." *Entropie*, 227, 10-21.
- Delaplace G.; J.C. Leuliet and V. Relandeau. 2000a. "Circulation and mixing times for helical ribbon impellers - review and experiments." *Experiments in Fluids*; 28-2; 170-182.
- Delaplace G. , Torrez C., Gradeck M., Leuliet J.C. and C. André 2000b. "Flow Of Newtonian And Non-Newtonian Fluids In An Agitated Vessel Equipped With A Non-Standard Anchor Impeller " *Proc. 10th European Conference on Mixing, Delft, The Netherlands, H.E.A. Van den Akker and J.J. Derksen (editors)*, Elsevier Science B.V. , 321-328.
- Delaplace G., Torrez C., Andre C., Leuliet J.-C., Fillaudeau L 2000c. "CFD Simulation of Foodstuff Flows in an Agitated Vessel." *Proc. 1st International Conference on Simulation in Food and Bio Industries*, Nantes, France, Daniel Thiel (editors), Publication of the Society for Computer Simulation international: 289-291.
- Delaplace G. , Torrez C., C. André, J.C. Leuliet 2001a. "Tracer Experiments – a way to validate computational fluid dynamic simulations in an agitated vessel" *Proc. First International Congress and Second French Congress on tracers and tracing methods, Nancy, Vol 15, N°79* , 77-84.
- Delaplace G. , Torrez C., J.C. Leuliet, Belaubre N, C André 2001b. "Experimental and CFD simulation of heat transfer to highly viscous fluids in an agitated vessel equipped with a non standard helical ribbon impeller " *Chem. Eng. Res. and Des.* Vol 79: A8 , 2001, 927-937

- Jaworski Z., Dyster K.N., Moore I.P.T. Nienow A.W., Wyszynski M.L. 1997. "The Use of Angle Resolved LDA Data To Compare Two Differential Turbulence Models Applied To Sliding Mesh Cfd Flow Simulations In A Stirred Tank." *Récents Progrès En Génie Des Procédés*, Vol 11, N°51, 187-194
- Jaworski Z., Dyster K.N., Nienow A.W. 2001. "The Effect of Size, Location And Pumping Direction Of Pitched Blade Turbine Impellers On Flow Patterns LDA Measurements And CFD Predictions." *TransIChemE*, Part A, Chem. Eng. Res. Des. 79, A8,887-894.
- Kaminoyama M. and M. Kamiwano 1994. "Numerical analysis of reaction process of highly viscous liquids in a stirred vessel equipped with a double helical ribbon impeller." *IChemE.Symp. Series* n°136, 541
- Luo J.Y. R.I. Issa and A.D. Cosman 1994. "Prediction Of Impeller Induced Flows In Mixing Vessel Using Multiple Frames Of Reference." *IChemE.Symp. Series* n°136, 549-556
- Mavros. 2001. "Flow Visualization In Stirred Vessels A review of experimental Techniques, *Trans.I.Chem.E.*, Vol 79, Part A, 113-128.
- Micale G., Brucato A., Grisafi F., Ciofalo M. 1999. "Prediction of flow fields in a dual-Impeller Stirred vessel. " *AICHE J.*, vol 45, N°3, 446-464
- Ranade V.V., Joshi J.B. 1990. "Flow Generated By A Disc Turbine: Part II Mathematical Modelling And Comparison With Experimental Data." *TransIChemE*, Part A, Chem. Eng. Res. Des 68, A1, 34-50.
- Ranade V.V., Perrard M., Le Sauze N., Xuereb C., Bertrand J. 2001. "Influence of Gas Flow Rate on Structure of Trailing Vortices of Rushton Turbine: PIV Measurements and CFD Simulations." *TransIChemE*, Part A, Chem. Eng. Res. Des. 79, A8,957-964.
- Soliman M. G. 1985. "Agitation de fluides visqueux pseudoplastiques par un double ruban hélicoïdal. " Thèse de Docteur Ingénieur, INP Toulouse.
- Tanguy P.A., Lacroix R., Bertrand F., Choplin L., Brito-De La Fuente E. 1992. "Mixing Of Rheologically Complex Fluids With An Helical Ribbon-Screw Impeller: Experimental And 3D Numerical Studies.", *AICHE Symp. Ser. N°286*, Process Mixing-Chemical and biochemical Applications, G. Tattersson and R. Calabrese eds, 33-39
- Tanguy P.A., Thibault F, Brito-De La Fuente E., Espinosa-Solares T., Tecante A. 1997. "Mixing Performance induced By Coaxial Flat Blade –Helical Ribbon Impellers Rotating At Different Speeds " *Chem. Eng. Sci.*, Vol 52, N°11, 1733-1741.
- Torrez C. and André C 1998. "Power Consumption of a Rushton Turbine Mixing Viscous Newtonian and shear-thinning fluids: Comparison between experimental and numerical results" *Chem. Eng. Technol.* 21, 7, 15-20.

#### ACKNOWLEDGEMENTS

The authors are grateful to C. DELAHAYE and F. GAIGHER for their valuable work in obtaining some of the data presented here.



**SIMULATION**



# A DSS for forecasting the Performance Indicators in Food Industries

**Mahdi Movahedkhah**  
ENITIAA, Nantes, LARGECIA  
et Ecole Centrale de Paris  
Laboratoire de Productique – Logistique  
E-Mail : movahed@enitiaa-nantes.fr

**Daniel Thiel**  
E.N.I.T.I.A.A. Nantes, LARGECIA  
Rue de la Géraudière - BP 82225  
44322 Nantes Cedex 3 (France)  
E-Mail : thiel@enitiaa-nantes.fr

## SUMMARY:

The objective of this paper is to present the principle of an Interactive Decision Support System (DSS) applied to the management and the control of food production systems. A preliminary survey based on a systemic approach, enabled us to define the causal links between various industrial performance indicators. This first work permits us to conceptualize this empirical knowledge by an influence diagram and by a generic simulation model based on Forrester's System Dynamics Theory. The DSS which we propose, is composed by this continuous simulation model which extracts the data from a spreadsheet (or an EIS Executive Information System) which directly extracts its information from an ERP software (Enterprise Resource Planning).

The objective of this DSS is to forecast the evolution of the performance indicators and its originality, comparing to traditional statistical methods based on past chronological series, is to take into account the causal relationships between these indicators.

**KEYWORDS:** Performance Indicators, DSS, continuous simulation, System Dynamics, fresh food products.

## 1. INTRODUCTION

During the twenty last years, different transformations in the principles of the production organization in food industries, have been observed (cf. Treillon *et al.*, 1991 ; 1995 ; Nakhla, 1994 ; Lecomte *et al.*, 1996). This mutation was vital for a large number of companies and can be explained by the evolution of the markets and by an instability of the environment. The new production systems have often to react to different disturbances either external or internal to the firm (Jacot *et al.*, 1996). To implement new control systems, there have to adapt there performance measurement and forecasting tools. Our research focuses on this problematic and aims to propose the structure of a new decision support system (DSS) based on industrial performance indicators. In this research field, we have observed that no synthetic performance indicators have been find out according to these new production systems. The industrial performance concept is still often limited to a quantitative evaluation of the industrial productivity. By an accountancy point of view, the performance evaluation is thus often reduced to the control of individual performances of each resource of the firm. But we know today that other forms of performance were imposed in response to the evolutions of the technology and the environment of the

industrial firms. The performance cannot be only based on quantitative data, but also on more qualitative variables like for example, the delays and the production cycles times. According to many authors, this requires a "global" and "multi-criteria" approach, which is reflected as well on the performance control methods as on its evaluation tools (Ecosip, 1990) , (Lorino, 1991), (Kaplan & Norton, 1992). Thanks to an intensive survey in different firms, our research brought in light various explanatory factors of the performance and on the causal relationships which link the processes and the actions to the obtained results. We firstly present the results of this survey. From these empirical bases, we formalized a causal diagram showing the interrelationships between these performance indicators. This generic representation allowed us to build a continuous simulation model (flows-stocks model, cf. Forrester) which has been the heard of our DSS.

## 2. THE RESULTS OF THE SURVEY

A first interview-based inquiry was necessary to make easier the construction of a questionnaire concerning the structure of the production systems, their problematic at different time scales, their inputs-outputs and their behavior faced to uncertainty. This investigation was based on the system thinking paradigm (according to Forrester 1958 ; 1961 ; 1994 ; Richardson 1984 ; 1992). A cybernetic vision highlighted the regulation mechanisms of some industrial organizations faced to different fluctuations of their essential components (cf. their performance indicators). Nineteen firms have been asked. This study was limited to "simple" mechanisms easy to identify and was based on 1292 answers given by these 19 firms and corresponding to the decisions faced to dysfunctions of the food production systems.

### *Representation of the cybernetic mechanisms*

We qualitatively identified the most significant Indicators of Performance (IPs). From the different answers given by the managers, we analyzed the existence of some cybernetics control loops, we conceptualized an original knowledge of the industrial organizations causal working. In our sample, we have had three groups of food industries:

Group 1: dairy products manufacturers (like yogurts, cheeses,...)

Group 2: elaborated products manufacturers (like flat cooked, sausages,...)

Group 3: poultry cutting industries.

After an aggregation of the variables and a qualitative analysis of the loops, we have chosen the following variables as performance indicators:

#### Indicators of Performance :

- IP 1: Sales fluctuations
- IP 2: Quality of service or service rate
- IP 3: Internal Reliability rate
- IP 4: External Reliability rate
- IP 5: Information System Efficiency
- IP 6: Inventory Level rate
- IP 7: Real manufacturing costs

Now, we will describe the causal relationships which formalize the production systems behaviors observed in case of IP variations.

#### Consequences of customer orders fluctuations (IP1)

*In case of very urgent customer orders*



In the case of sales increasing in a sudden and instantaneous way (pulses), the systems are controlled in short term, by a re-scheduling of the orders in process and by overtime or temporary employment.

*In case of a sudden and permanent sales increase*



In the case of sales increasing in a sudden and permanent way (steps), the systems of the three groups, are controlled in the middle term, by temporary employment. Moreover, the group 1 uses frequently overtime, the group 2 personnel hiring and the group 3 personnel temporary employment.

*In case of occasional and very significant decreasing of sales*



In the case of occasional declining of the customer orders which implies a loading decrease, an active regulation (in the short term) is carried out by production anticipation.

*In case of sudden decreasing of sales*



In the case of sudden decreasing of the sales, only the response of the group 1 is significant : the solution is the regulation by production anticipation.

*In case of seasonal variations of the sales*



Seasonal variations in sales often involve the need of flexibility by following the sales profile.

*In case of random variations of the sales*



A random variation of the sales can involve flexibility by following the sales pattern. For the group 1, another solution consists in scheduling by priorities.

#### Consequences of the Quality of service variations (IP2)

*In case of non-delivered orders and frequent customers complaints (IP2a).*

The customers complaints for delivery problems, are often treated in the short term by a strict and more frequent production flow control ; for the group 1, by a management of the orders by priorities and for the groups 1 and 3, by a

preliminary negotiation between the sales managers and the scheduling managers.

*In case of too long manufacturing lead times (IP2a).*

The problem of the too long manufacturing delays for the group 2, can be solved by purchasing new manufacturing tools.

*In case of non-quality problems and customers complaints (IP2b).*

Customers complaints due to quality problems, can be reduced in short/middle terms, by increasing employees motivation and staff training. In the short term, a statistical quality control is often carried out. The groups 1 and 3 propose to improve the reliability of their production equipments.

#### Consequences of the variations of the internal reliability of production equipments (IP3)

*In case of fluctuating production capacities, productivity decreasing and absenteeism increasing (IP3a).*

The diminution of the production capacities can be caused by productivity decrease, an absenteeism increase or frequent stoppages of work. In these cases, an active regulation of the systems can be carried out by a rigorous analytic cost accounting, by automation of the production equipment, by the " re-motivation " and the responsibility of the personnel, by the re-organization of the tasks or by the implementation of flexible schedules in the middle term like by tighter and rigorous controls of the short-term activity.

*In case of work stoppages caused by strikes (IP3b).* The problem of the stoppages of work in the case of strike for the group 1, can be regularized by external subcontracting.

*In case of frequent dysfunctions of the production equipments (IP3c), the machines stoppages and too long set-up times (IP3b).*

Frequent dysfunctions in production due to machines breakdowns, are controlled in the middle term in an active way, by preventive maintenance and personnel training. Moreover for the groups 1 and 3, the long-term action will be done by new machines investment, automation or specialization of the factories by products. Nevertheless, the group 1 has in short-term, tendency to gather several customer of production orders.

#### Consequences of the variations of the external reliability rate (IP4)

*In case of deliveries problems with providers*

The implementation of an ERP or a JIT system can imply a reduction of the missed items in production. If there are too much missed items, some companies have diversified their providers or have increased their stock levels.

*In case of non-respect of the upstream workshops planning*

In this case, groups 1 and 2 often centralize the scheduling system and the group 3 sub-contracts its work.

**Consequences of the variations of the information system reliability (IP5)**

*In case of frequent dysfunctions of the orders and information transmissions*

In this case, the companies control the production systems in the medium term, by a revision, an improvement and by procedures automation.

**Consequences of the variations of the inventory levels (IP6)**

*In case of a too high level of stock of raw materials (IP6a) and finished products (IP6b).*

In these cases, a physical control will be done by a recurrent inspection of the inventories levels. A real time control of the production flows can also be ensured. In the long term, a "Just In Time" system can be implemented to reduce the stocks.

**Consequences of the real cost variations of the manufactured products (IP7)**

*In case of real costs increases*

The increase of the real manufacturing costs can be treated in an active way, by a reinforcement of controls of the material expenses, of the production rejections rate, and by analyzing the labor over-costs. Moreover, the group 3 sub-contracts in the middle term, a part of its production. In the same way, it develops automation or improves its cost control system.

**3. The structure of the generic model**

Of this preliminary analysis of the decision mechanisms, we propose to formalize this first qualitative knowledge by an influence diagram which shows the causal interactions between the characteristic variables of these systems. Figure 1 describes the causal diagram of our generic model. The glossary of the variables of the model is presented in table 1.

*Table 1 : Generic model variables listing*

Nominal capacity	Theoretical capacity of the production system.
Real capacity	Production capacity to answer to the commercial needs or following internal or external disturbances.
Coef. of working hour variation	Coefficient indicating the rate of overtime or temporary staff hiring.
Quality control	Rate representing the intensity of the quality control of the products.
Production flow Control	Rate representing the intensity of the quantitative and qualitative production controls.
Additional costs	This variable determines

	the additional costs caused by dysfunctions and various readjustments.
Supplying time	Delivery time of raw materials and components.
Readjustment time	Following manpower and capacity readjustments, this time corresponds to the response time of the organization for setting new solutions.
CLD PF	Consumption Limit Date of the fresh Finished Products.
RM Variations	This variable calculates the difference between the real stock of row materials (or components) and the desired inventory level
MPS Variations	This variable calculates the difference between the forecasts based on the MPS and the real sales.
Work-in-process	The production work-in-process.
Shipping FP	The flow of finished products sending to the customers.
Training	Rate measuring the intensity of the staff training.
Nominal motivation	Rate of the desired motivation level.
Real motivation	Real rate of motivation of the employees.
MPS	Master Production Schedule.
Information flow Quality	Quality of the orders and information transmission.
Overtime ratio	The maximum rate of overtime possible to realize in short time
Temporary staff ratio	Maximum rate of temporary staff which can be recruited in short term.
Rejections FP	Rejection rate of finished products caused by various factors of production and by products going beyond the dates of consumption.
Rupture RM and components	Average percentage of the raw material out-of-stock level.
Stock RM and components	Level of the raw material inventory
Objective stock MP and components	Level of the desired inventory of raw materials and components.

Stock FP	Real level of the stock of finished products.
Lot Size	The size of the production batches (political choice).
Rate provision	The raw materials rates supplying (political choice).
Scrap rate	The average material scrap rate.
Stoppages rate	The average machines breakdown rate.
DP Non-quality rate	The rates of non-conform Delivered Products.

Production rate	The manufacturing rate (political choice).
Service FP rate	The Finished Products customer service rate (varying from 0 to 1)
Variation of capacity	The coefficient of capacity variation.
Productivity variation	The coefficient of productivity variation.
Sales	This variable corresponds to the volume of the customer orders.

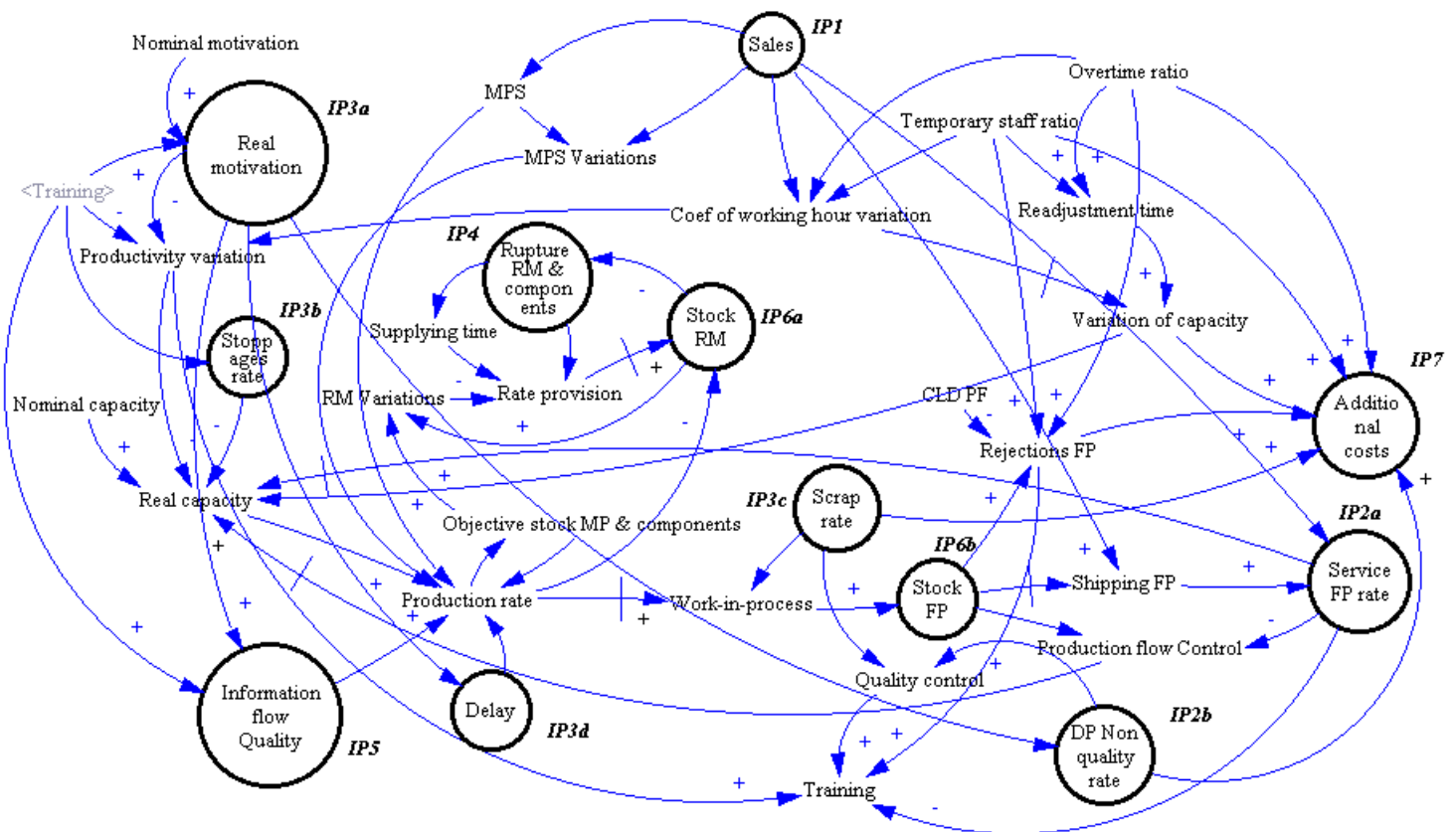


Figure 1. Influence diagram

The figure 1 can be interpreted in this following way : the nodes of the graph represent the variables, the arrows indicate the causal relations between these variables, the signs of the arrows correspond to the polarity of the causal relations : a sign (+) indicates a influence relation between two variables going in the same direction and the sign (-), in the opposite direction.

The double-arrows translate the delay effects corresponding to an exponential duration between the cause and effect (cf. Forrester, 1961). The encircled variables are the Performance Indicators and are numbered  $IP_i$  according to values of the index  $i$  described in the previous paragraph.

The diagram in the figure 1 clearly shows the causal interdependence between the different performance indicators, object of this research. This representation is a good qualitative base for behaviors analysis of the production systems after fluctuations of their IP.

After this first work, we develop a model represented by a Forrester's flow-stock diagram and transcribed it in a finite differences equations system.

#### 4. PROPOSAL OF A DSS

By implementing this continuous simulation model, different experimentations from various scenarios of fluctuations of the different indicators have be done according to a given

experimental plan. These simulations allowed us to study the stability of these systems faced to different perturbations. We will not present here the results of these simulations but we will show how to complete this first analysis by simulating an interactive neural network. This connectionist model was based on the previous influence diagram (see fig. 1) which formalized the causal relationships between the performance.

An influence diagram was built according to the systemic and cybernetics principles. It was essentially based, taking into account the complexity of the food production systems, on preliminary observations which highlighted the regulation and industrial management systems. From this first cognitive representation, we built a generic simulation model which will be the base of an operational Interactive Decision Support System (DSS). This support can simulate, starting from initial values performance indicators, the possible evolution of these same indicators.

More concretely, the production managers regularly controls the flows of production and the level of the indicators like the quality level, the stocks level, the returns rate, etc. These data have to be entered in the DSS which will simulate the evolution of these indicators from these initial conditions thanks to our system dynamics model. The logistic and production managers can then propose to modify some production policies after analyzing the causal structure of the model. The input data of the DSS will come from an Executive Information System (EIS) which directly imports its data from an ERP software (see figure 2).

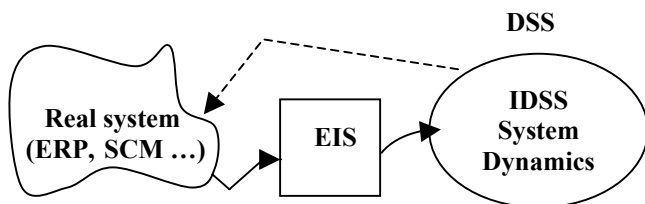


**Figure 2. Environment of the DSS**

This DSS which permits to make causal analysis showing the interdependence between the performance indicators, proves its benefit confronting to traditional statistical methods of search for correlation between variables. Indeed, these forecast methods based on the past values can only independently predict the evolution of each indicator.

However, in many companies, taking into account the significant number of performance indicators, the frequent question is : starting from the forecasts given by this statistical model, how to analyze the tendencies being able to be contradictory, between various performance indicators ? We also implemented a prototype of DSS which has been validated by two companies partners of our research.

This paper opens a new way for studying production system behaviors. The first simulation results of this connectionist model based on our system dynamics model, has permitted to underline trends which some industrial companies could meet in the proximity of these attractor states. The next step

of our research consists in validation of these models and attractors by comparison with real observations in different companies.

## 5. REFERENCES

- ECOSIP, 1990, *Gestion industrielle et mesure économique, approches et applications nouvelles*, éditions Economica.
- FORRESTER J.W., 1958, "Industrial Dynamics : A major breakthrough for decision makers", *Harvard Business Review*, 36, n°4., July-August, pp. 37-66.
- FORRESTER J.W., 1961, *Industrial Dynamics*, Cambridge, Massachusetts, MIT Press.
- FORRESTER J.W., 1994, "Policies, Decisions and Information Sources of modeling" in *Modeling for learning organizations*, Productivity Press, System Dynamics Series.
- JACOT J.H., MICAELLI J.P. (coordinateurs), 1996, *La performance économique en entreprise*, édition Hermès.
- KAPLAN R. S., NORTON D. P., 1992, *The balanced scorecard - measures that drive performance* Harvard Business Review, January-February, p 71-79.
- LECOMTE C., MAROLDA A., THIEL D., 1996 "La flexibilité industrielle dans la production et la logistique alimentaires : quelques réflexions », *Revue IAA*, octobre, p. 763-769.
- LORINO P., 1991, *Le contrôle de gestion stratégique : la gestion par les activités*, éditions Dunod.
- SIMON H.A., 1960, *The new science of management decisions*, Evanston, Harper and Row, New York, Publishers.
- NAKHLA, 1994, "Les systèmes de gestion de production assistée par ordinateur dans les industries agro-alimentaires", *Revue Française de Gestion Industrielle*, p. 267-285.
- RICHARDSON G.P., 1984, "Loop polarity, Loop dominance, and the concept of dominant polarity", *Proceedings of the 1984 International System Dynamics Conference*, Oslo, Norway.
- RICHARDSON G. P., 1992, *Feedback Thought in social Science and Systems Theory*, UPP, University of Pennsylvania Press.
- TREILLON R., 1991, "Agro-industrie et flux de production : quels systèmes de gestion ?", *Revue Française de Gestion Industrielle*, p. 318-338.
- TREILLON R., C. LECOMTE, 1995, "La gestion industrielle dans les entreprises alimentaires : perspectives et réalités", *Congrès International de Génie Industriel*, Montréal, p. 171-176.

## THANKS

This work is included in the framework of a public Contract 2000-2006 between the State and the Region "Pays de la Loire" and is supported by the French Ministry of Agriculture and Fisheries.

# EFFICIENT SIMULATION OF DIFFUSIONAL TRANSPORT IN COMPOSITE MATERIALS – APPLICATION TO THE IDENTIFICATION OF DISTRIBUTED DIFFUSION COEFFICIENT IN FOOD PACKAGING

Olivier Vitrac

Laboratory of biotechnology of polymer and food safety

INRA – UMR FARE

CPCB, Moulin de la Housse

51687 Reims cedex, France

E-mail: olivier.vitrac@lille.inra.fr

## KEYWORDS

chemical engineering, computer aided engineering, pseudospectral methods, parameter identification, image analysis

## ABSTRACT

In a first part, Chebyshev pseudo-spectrals methods were investigated for modeling diffusional transport through arbitrary structure including large jump in physico-chemical properties (diffusion coefficient, partition coefficient) such as those encountered in multilayer packaging materials. Stable and accurate results are obtained by incorporating Robin boundary conditions through a weak formulation of local transport equation. In a second part, the method combining spectral and multi-domain approach was used to derive a new numerical inverse procedure for retrieving unknown distributed diffusion coefficients from concentration history within structured samples. Finally, the whole method was tested to assess diffusion coefficients of a dye in a thin controlled 3 layers polymeric material. Reliable and consistent results were obtained for each uncoupled layer by combining approximations of spatial and time first derivatives on local Chebyshev basis through a variational formulation independent of unknown boundary and interface conditions.

## INTRODUCTION

Food packaging is nowadays an integrating part of food items and offers a large source of potential innovation for both food and packaging industries. As a result, new packaging materials are always more sophisticated and they are changed from passive and waste barriers into active, intelligent, recyclable and reusable materials. They are usually designed as composite materials including hierarchical organization by means of the assembling of multi-layers, multicomponents, nanostructure (e.g. dispersion, coatings, surface deposits or treatments...). From the technological point of view, the optimization of induced properties (e.g. barrier, selectivity, reactivity, retention) required an accurate control of diffusional transport through such complex structure. From the point of view of regulatory authorities and consumer, both modifications of the life cycle of food packaging and rapid diversification of formulations and combination of materials could potentially increase the risk of i) uncontrolled release of undesirable substances (additives, contaminants) or ii) higher reactivities

within food items (e.g. off-flavors, toxic substances). Consequently, there is considerable interest in the development of robust and efficient numerical methods for the prediction of cross mass transfer between i) food, ii) food packaging materials and iii) the surrounding, which takes into account the conditions of process, storage of both food and packaging. Such tools or methodologies would find immediate applications in diverse fields covering industrial, research and regulatory purposes. These include:

- problem 1) computer aided development of food packaging via simulation (forward problem),
- problem 2) numerical identification of mass transfer properties in complex configurations (i.e. structured materials) (inverse problem)

The purpose of this paper is to propose an enough general mathematical formulation of diffusional transport so as to handle efficiently both previous technological problems. The forward problem presents several difficulties associated with the numerical solution of partial differential equations (PDE) with i) a discontinuous initial condition, ii) large jumps in properties (e.g. diffusivities, solubilities) on small scales (e.g. thin layers, defects). Indeed, non-smooth solutions also called “multiscale solutions” would required high frequency information that is only tractable via fine/adaptative spatial discretization and/or optimal interpolation (Funaro 1991). Among various concurrent numerical strategies, pseudo-spectral (PS) techniques, so called “spectral domain decomposition”, appeared as one of the most natural to map with high accuracy an heterogeneous domain into “smoother” sub-regions and to formulate implicitly transport phenomena close to discontinuity as interfacial conditions (Boyd 2000). There are several further motives to use PS methods. One is that the extension of differentiation operators to 2D is competitive with tensor-product-based of 1D ones (Funaro 1991). The second is that PS methods can handle automatically and individually periodic discontinuities by means of a suitable choice of functions basis (i.e. Fourier series). The third is that they reduce the computation cost owing to sparse block matrix, scalable algorithms and possible replacement of matrix multiplication by FFT algorithm (for Fourier basis, but also for Chebyshev expansion, which is merely a Fourier cosine series). A last reason is that the calculated analytical form of the solution has meanings within both and frequency spaces, and makes it therefore possible to devise analogies between operators involved in numerical resolution of PDE and signal analysis, such as “filtering”, “homogenization», “aliasing” properties.

The paper is organized into three sections. First, we focus on devising a flexible and efficient PS technique for the 1-D diffusional transport within food packaging and at their interfaces with food. A general weak form of the PDE accounting for more common boundary conditions (BC) was formulated and used to derive a flexible multidomain version. The advocated mathematical formulation was an extension to  $M$  domains ( $M \geq 2$ ) of the one proposed by Faccioli *et al.* (1996) for the propagation of waves with absorbing BC, which presents analogy with partition BC. In order to decrease the computation cost, the Legendre grid was replaced by the Chebyshev-Gauss-Lobatto grid relevant for FFT algorithms. Possible variations within an element – but possibly discontinuous at elements interfaces – was assumed smooth and treated pseudospectrally by means of a special norm involving the variable property (Frutos and Muñoz-Sola 1995). Differentiation matrices were finally derived from stable algorithms provided by Weideman and Reddy (2000). The second section provides some numerical experiments of time dependent transport through multilayer materials, and are discussed regarding the accuracy and conditioning of operators. The third section proposes a fast numerical tool based on previous operators of interpolation and differentiation dedicated to the interpretation of 2D images of time dependent transport processes of marked molecules within food packaging. The case of tracer diffusion within a three-layer material is more particularly detailed.

## MATHEMATICAL FORMULATION OF THE FORWARD PROBLEM

Several schemes have been proposed for exploiting the structure of scale space where diffusional transport occurred. Most approaches need a very dense sampling of the hierarchical structure and are therefore computationally expensive. Bi-modal description including possible large-scale rough macrostructure and smooth microstructure would be a good compromise. Indeed, the microstructure contribution may be described by a set of space- and –time field variables and simulated by the phase field-method or assessed from a digitization of an experimental one (Zhu *et al.*, 2001). As a result, this coarse grained description leads to model diffusional transport through an arbitrary heterogeneous structure by a diffusion equation with a smooth variable diffusion coefficient and suitable boundaries conditions at the interfaces of macro-heterogeneities. In the case of a material with no microstructural evolution, the field variables are only function of spatial coordinates  $s$  and the diffusion coefficient is mapped for the entire calculation domain as  $D(s)$ .

### Transport equations through an arbitrary heterogeneous structure

According to the previous hypothesis and neglecting the interaction between diffusing species, the temporal diffusive transport process through the structure is finally written in a common form as:

$$\frac{\partial u(\mathbf{s}, t)}{\partial t} = \nabla \cdot D(\mathbf{s}) \nabla u(\mathbf{s}, t) \quad (1)$$

where  $u$  is the concentration in a particular diffusive species. The segregation of diffusing species at the boundary  $\partial\Omega$  between regions  $\Omega_A$  and  $\Omega_B$  (macroscopic heterogeneity) according to their affinity is described assuming sharply discontinuous Dirichlet and (possibly discontinuous) rate-limited Neumann constraints:

$$\begin{cases} u(\mathbf{s}, t)|_B^{\partial\Omega} = K_{AB} u(\mathbf{s}, t)|_A^{\partial\Omega} \\ D_B(\mathbf{s}, t) \nabla u(\mathbf{s}, t)|_B^{\partial\Omega} \cdot \bar{\mathbf{n}}_{\partial\Omega} = D_A(\mathbf{s}, t) \nabla u(\mathbf{s}, t)|_A^{\partial\Omega} \cdot \bar{\mathbf{n}}_{\partial\Omega} \end{cases} \quad (2)$$

where  $K_{AB}$  is the partition coefficient between structures A and B. In the case where B is a liquid, the set of equations (2) is replaced by a similar mechanism assuming the conservation of diffusive and convective fluxes, written as a Robin boundary condition:

$$-D_A(\mathbf{s}, t) \nabla u(\mathbf{s}, t)|_A^{\partial\Omega} \cdot \bar{\mathbf{n}}_{\partial\Omega} = h_m \left[ K_{AB} u(\mathbf{s}, t)|_A^{\partial\Omega} - u_B(t) \right] \quad (3)$$

where  $h_m$  is the convective mass transfer coefficient and  $\bar{\mathbf{n}}$  is the normal vector to  $\partial\Omega$ . Equation (3) requires an additional mass balance for the diffusive species in region  $\Omega_B$ . In case of a constant volume  $V_B$  and surface contact  $S_B$  for region  $\Omega_B$ , and without limiting hydrodynamic conditions (*i.e.* with uniform concentration in  $\Omega_B$ ), equation (3) can be conveniently replaced by an instantaneous and local mass balance at the boundary  $\partial\Omega$ :

$$-D_A(\mathbf{s}, t) \nabla u(\mathbf{s}, t)|_A^{\partial\Omega} \cdot \bar{\mathbf{n}}_{\partial\Omega} = \frac{V_B}{S_B} K_{AB} \frac{\partial u(\mathbf{s}, t)|_A^{\partial\Omega}}{\partial t} \quad (4)$$

### Macro-heterogeneities/structure splitting

In one dimension ( $s = [x \ 0 \ 0]$ ), the calculation domain was split into  $M$  ( $M \geq 2$ ) non-overlapping macro-elements  $\Omega_{i=1..M}$  (*i.e.* macro-heterogeneities or macro-structure), 2 external boundaries,  $\partial\Omega_1$  and  $\partial\Omega_M$ , and  $M-1$  internal interfaces, noted  $\gamma_{i=1..M-1}$  for the interface between  $\Omega_i$  and  $\Omega_{i+1}$  (with  $1 \leq i \leq M-1$ ). The way we include the discontinuous solution to equation (1) that are necessary in our multiscale approach is to consider a weak coupling between the solutions  $u_i$  to PDE (1) obtained on different subdomains. Since we do not need any of the difficult results concerning weak solutions, only the basic feature of variational approach is here outlined.

Let  $v=V(Y)$  be a smooth test function. If we multiply both sides of (1) by  $v$  and integrate over  $\Omega_1 \cup \dots \cup \Omega_i \cup \dots \cup \Omega_M$ , we obtain after integration by parts:

$$\begin{aligned} \sum_{i=1}^M \int_{\Omega_i} \frac{\partial u_i(t)}{\partial t} v \, dx &= \sum_{i=1}^M \int_{\Omega_i} \frac{\partial}{\partial x} \left( D_i \frac{\partial u_i(t)}{\partial x} \right) v \, dx \\ &= - \sum_{i=1}^M \int_{\Omega_i} D_i \frac{\partial u_i(t)}{\partial x} \frac{\partial v}{\partial x} \, dx - D_1 \frac{\partial u_1(t)}{\partial x} v \Big|_{\partial\Omega_1} + D_M \frac{\partial u_M(t)}{\partial x} v \Big|_{\partial\Omega_M} \\ &\quad + \sum_{i=1}^M D_i \frac{\partial u_i(t)}{\partial x} v \Big|_{\gamma_i} - D_{i+1} \frac{\partial u_{i+1}(t)}{\partial x} v \Big|_{\gamma_i} \end{aligned} \quad (5)$$

According to continuity of flux at interfaces  $\gamma_i$  imposed by (2) the last summation term vanishes. Moreover, by imposing (4) and an impervious/symmetry boundary layer ( $\partial u_i(t)/\partial x = 0$ ) respectively at  $\partial\Omega_1$  and  $\partial\Omega_M$ , we conclude that at each  $t$ , the set  $\{u_i\}_{1..M}$  satisfies the variational problem:

$$\sum_{i=1}^M \int_{\Omega_i} \frac{\prod_{j=1}^i K_j}{K_0} \frac{\partial w_i(t)}{\partial t} v dx = - \sum_{i=1}^M \int_{\Omega_i} \frac{\prod_{j=1}^i K_j}{K_0} D_i \frac{\partial w_i(t)}{\partial x} \frac{\partial v}{\partial x} dx - \frac{V_0}{S_0} \frac{\partial w_i(t)}{\partial t} \Big|_{\partial\Omega_i} v \Big|_{\partial\Omega_i}$$

$$w_i(t) \Big|_{\gamma_i} = w_{i+1}(t) \Big|_{\gamma_i} \quad i = 1..M-1 \quad (6)$$

where  $\{w_i\}_{i=1..M}$  is a piecewise solution (with same units of concentration) continuous at all interfaces  $\gamma_i$  and derived from mass transfer equilibrium considerations so that:

$$w_i(t) = \frac{u_i(t)}{\prod_{j=1}^i K_j} \quad (7)$$

Formally speaking, equation (6) has been obtained from (1) after taking at each time the variation respectively to all admissible functions  $v : \Omega_i \rightarrow \mathfrak{R}$ , which are precisely square (Lebesgue) integrable along their first derivative.

### Spectral approximation of local transport

In order to complete the discretization within each element (*i.e.* to account for local transport), one has to choose an approximation subspace with finite basis  $\{T_n\}_{n=0..N}$  for each  $w_i : \Omega_i \rightarrow \mathfrak{R}$  and a quadrature for the evaluation of the integrals in (6). If  $\{T_n\}_{n=0..N}$  are the Chebyshev polynomial of degree  $\leq N$  or its equivalent definition as weighted interpolant:  $w_N^{(i)}(x_n) = T_N(x_n)$  for a suitable set of collocation

points  $\{x_n\}_{n=0..N}$  on the canonical interval  $[-1, +1]$ ,  $\int_{-1}^1 w(x) dx$  can be approximated for any continuous function by the truncated series  $\sum_{n=0}^N w_N(x_n) \omega_n$ . The truncation error is in

particular zero for all  $w(x)$  which are polynomials of at most degree  $2N+1$  and  $2N-1$ , for respectively Gauss (G) and Gauss-Lobatto-Chebyshev (GLT) quadrature. Best performance for both interpolation and integration are achieved by choosing the latter relatively to the roots (GLT nodes) of  $(1-x^2)T_{N-1}(x_n)$  and their corresponding weights  $\omega_n$  (Boyd 1999). It follows that a finite version of equation (6) including a very high accurate second order differential operator can be provided:

$$\sum_{i=1}^M \left( k_i \frac{\partial w_N^{(i)}}{\partial t}, v_N \right)_N = - \sum_{i=1}^M \left( H^{(i)}, \frac{\partial v_N}{\partial x} \right)_N - \frac{V_0}{S_0} \frac{\partial w_N^{(i)}}{\partial t} \Big|_{\partial\Omega_i} v_N \Big|_{\partial\Omega_i} \quad (8)$$

with  $k_i = \prod_{j=1}^i K_j / K_0$ ,  $H^{(i)} = J_N^{(i)} \left( k_i D_i \frac{\partial w_N^{(i)}}{\partial x} \right)$ ,  $J_N^{(i)}$  the

Chebyshev interpolation operator at GLT nodes,  $(\varphi, \psi)_N$  the inner product defined by  $\int_{-1}^1 \varphi(x) \psi(x) dx \approx \sum_{n=0}^N \varphi(x_n) \psi(x_n) \omega_n$ .

The final linear system for the multidomain is obtained from an integration parts of the weighted residual form:

$$\sum_{i=1}^M \left( R_N^{(i)} w_N^{(i)}, v_N \right)_N, \quad \text{with} \quad R_N^{(i)} w_N^{(i)} = k_i \frac{\partial w_N^{(i)}}{\partial t} - \frac{\partial}{\partial x} \left( J_N^{(i)} k_i D_i \frac{\partial w_N^{(i)}}{\partial x} \right)$$

and by applying the Lagrangian polynomial basis constructed with GLT nodes as test functions  $v_N$ . Thus, a close set of equations is obtained:

a) *Internal equations*

$$R_N^{(i)} = 0 \quad \text{at} \quad x = \{x_n\}_{n=1..N-1} \quad (9)$$

b) *BC equations*

$$k_1 \left( D_1 \frac{\partial w_N^{(1)}}{\partial x} + \frac{V_0}{S_0} \frac{\partial w_N^{(1)}}{\partial t} \right) = \omega_0^{(1)} R_N^{(1)} w_N^{(1)} \quad \text{at} \quad x = x_0^{(1)} \quad (10)$$

$$k_M \left( D_1 \frac{\partial w_N^{(i)}}{\partial x} \right) = -\omega_N^{(M)} R_N^{(M)} w_N^{(M)} \quad \text{at} \quad x = x_N^{(M)} \quad (11)$$

c) *Interface conditions (IC)*

$$k_{i+1} D_{i+1} \frac{\partial w_N^{(i+1)}}{\partial x} - k_i D_i \frac{\partial w_N^{(i)}}{\partial x} = \omega_0^{(1)} R_N^{(1)} w_N^{(1)} + \omega_N^{(M)} R_N^{(M)} w_N^{(M)}$$

$$w_N^{(i)} = w_N^{(i+1)} \quad \text{at} \quad x = \{\gamma_i\}_{1 \leq i \leq M-1} \quad (12)$$

The main advantage of this variational approach over classical collocation lies in its higher accuracy, since it entails a linear combination between the PDE (1) and the physically consistent BC or IC.

### Time marching

The matrix assembling of (10)-(12) leads to an ordinary differential equation (ODE) in the usual form:  $M\dot{w} = Dw$ , where  $M$  is diagonal and  $D$  a sparse matrix with almost all real and negative eigenvalues. In practice,  $D$  contains diffusional transport information through not shape regular macro elements and with variable equivalent transport length or capacity. As a result,  $D$  is partially ill-conditioned with conditioning number typically between  $10^{15}$  and  $10^{19}$  and increasing with the order of the approximation. For economical and reliability reasons, only fully implicit schemes must be used to solve the ODE set for any initial condition :  $w(t=0) = w_0$ , such as backward differentiation formulas (BDF) or numerical differentiation formulas (NDF). Best results are obtained with a quasi-constant step size implementation of NDF up to order 5 (ode15s function of Matlab 6.x or from Matlab ODE suite). Due to the sparsity of  $D$ , this technique is highly competitive whatever the chosen BC even for large system (500x500) comparing with the introduction of the finite-element based preconditionner recently proposed by Shen *et al.* (2000).

It is worth to notice that BC (4) or Neumann BC coupled to an initial solution with zero gradient at the boundary must be initialized by including an external collocation point or by suitably modifying the initial solution (e.g. by replacing a constant profile with an Heaviside function).

### NUMERICAL EXPERIMENTS

Figure 1 provides three dimensionless examples of our PS method for the contamination propagation from one external layer to the others within a 4 layer material including large jumps in  $k_i$  and  $D_i$  values at each interface (and constant within each layer). Unidirectional and bidirectional transfer

are considered with different BC to illustrate the performance of the numerical scheme with respect to the partitioning and computation time. In particular, full impervious BC is a severe test to assess the simulation consistency regarding mass conservation laws. As an indication of the typical required CPU time, the whole figure 1 was generated on Matlab 6.1 within 2 s on a P4, 2.2 GHz.

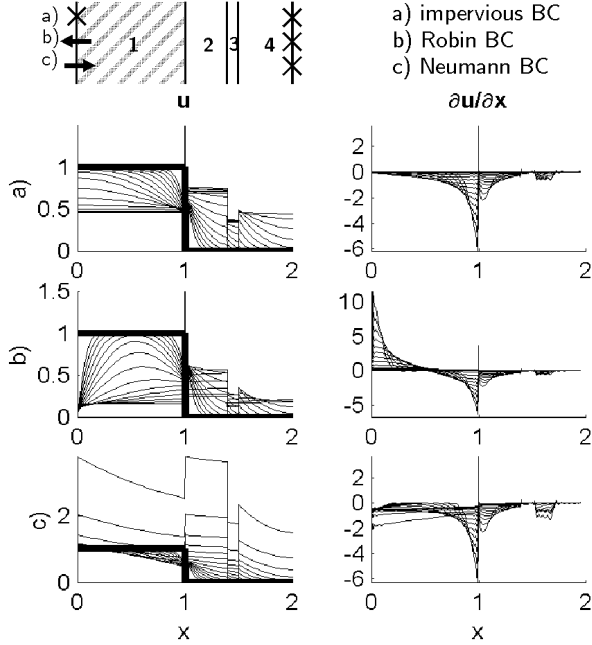


Figure 1: Numerical Experiments ( $M=4, N=30$ ) for Various BC.

## INVERSE PROBLEM: IDENTIFICATION OF DISTRIBUTED DIFFUSION COEFFICIENTS

### Typical example

In order to rapidly assess barrier properties of packaging composite (e.g. multilayer), the basic idea was to measure the migration through the whole structure of a non-volatile UV dye (2',5'-dimethoxyacetophenone, maximum absorbance at 330 nm) initially present in one layer. Versatility and robustness of the method require that diffusion properties may be retrieved from concentration profiles acquired for any of consecutive discrete times, in other words independently of the knowledge of initial conditions. Local dye concentrations were inferred from several microscopic observations (UV CCD camera model Hamatsu-C4742-95812E5 coupled with a UV microscope model Karl Zeiss -MPM800MCS) of a same cross-section area for different transmitting light wavelength (330 and 420 nm). In particular, the ratio  $\log_{10}(\max(I_{330})/I_{330})$  over  $\log_{10}(\max(I_{420})/I_{420})$  was shown to be directly related to the local dye concentration in common polyolefins and independent of surface irregularities, where  $I_\lambda$  is the 2D intensity image at the wavelength  $\lambda$ .

Figure 2 presents the 2D concentration results ( $1024 \times 1248$  pixels<sup>2</sup>) for 7 consecutive times (each 5 hours, after 4 days of migration at 40°C) within a  $M=3$  layer packaging ABC (thickness:  $155+60+85 \mu\text{m}$ ) coated with an epoxy resin, where A and B are a low density polyethylene (ldpe) and C a polypropylene (pp). The dye was initially only located in layer A and presented no significant partition effect between

pp and ldpe ( $k_{1,3}=1$ ). Moreover, it was assumed that i) significant dye transport occurred only along direction  $x$ , ii) boundary of A and C verified impervious conditions. Let  $\{J_N^{(i)}\}_{i=1..M}$  be an interpolant of  $D_i(x)$  in the coefficient form:

$$\sum_{i=0}^N a_n^{(i)} \phi_n^{(i)}$$

for some suitable basis functions  $\phi_n^{(i)}$ . The so-called inverse problem consists in finding

$$A = \{a_n^{(i)}\}_{i=1..M, n=0..N}$$

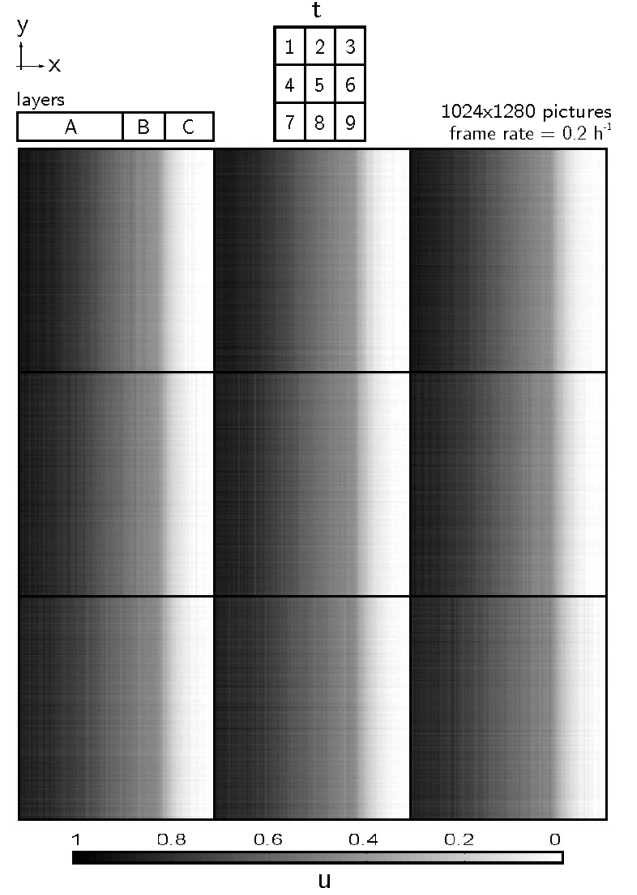


Figure 2: Variation of Local Concentration with time.

### Identification procedure

Equation (8) combined with a subdomain weak formulation leads to a natural approach for solving the latter problem. Indeed, since either  $w_i$  or  $u_i$  are assumed to be included within the coarse concentration picture series, noted  $Pxyt$ , matrix  $A$  remains the only unknown. By remarking that  $D_i$  values are independent between  $\Omega_i$  layers, "finding A" can be lumped into a common and direct (*i.e.* non iterative) minimization problem of mean weighted residuals (MWR). For a given  $\phi_n^{(i)}$  basis, MWR determines  $A$  by imposing for each  $\Omega_i$  ( $N+1$ ) conditions:

$$(v_j, R_N^{(i)} w_N^{(i)} [x, a_0..a_N])_{\Omega_i} = 0, \text{ for } j = 0..N \quad (13)$$

for some suitable "test functions"  $v_j(x)$  where the inner product  $(v, w)_{\Omega_i} = \int_{\Omega_i} \omega(x) v(x) w(x) dx$  for a given non-

negative weighted function  $\omega(x)$  and any  $v(x)$  and  $w(x)$ .

Equation (8) requires an accurate estimation of  $w(x)$  and its first derivatives in time and space from series  $Pxyt$ . Since

$P_{xyt}$  (1024×1280×7) contained noisy data along each dimension:  $x$  (subspace of diffusion path),  $y$  (redundant subspace) and  $t$  (temporal subspace),  $P_{xyt}$  was subsequently “statistically/likely” projected/collocated onto suitable subspaces. Firstly,  $P_{xyt}$  was factorized along in the frequency domain of  $y$  so as to reduce the whole computation cost and low pass filter crude data. The obtained 1024×40×7 analytical series  $P'_{xyt}$  was secondly interpolated in the  $L_2$  sense by  $M=3$  piece-wise Chebyshev polynomials ( $8 \leq N \leq 10$ ) respectively to each layer along  $x$ . Entailed BC (zero slope) and IC (continuity) were enforced owing to the introduction of corresponding constrains (relatively to Lagrange multipliers) in the assembled regularized least square problem. No condition on the first derivatives at interfaces were introduced since there are depending on the ratio of the unknown  $D_i$ . The obtained 48×7 coefficients were finally used to compute spectrally a 7<sup>th</sup> order centered approximation of  $\partial w(x)/\partial t$ .  $w(x)$  and  $\partial w(x)/\partial x$  were calculated for the same corresponding time.

### Reconstructed and identified results

Profiles of  $u(x)$ ,  $\partial u(x)/\partial x$ , and  $\partial u(x)/\partial t$  were *a priori* reconstructed with  $M=3$  and  $N=8$  (figure 3). As expected, the dye was smoothly distributed between A and B and a sharp change in  $u$  was detected between B and C. In one hand, the whole reconstruction procedure led to enough noise reduction to make both first time and spatial derivative almost as exploitable as the primitive signals  $u$ . On the other hand, enough high frequency along  $x$  remained in  $u$  to account for possible discontinuities between materials with different properties, such as ldpe and and pp (commonly one magnitude order). Close to external boundaries, zero gradient conditions regularized conveniently all profiles.

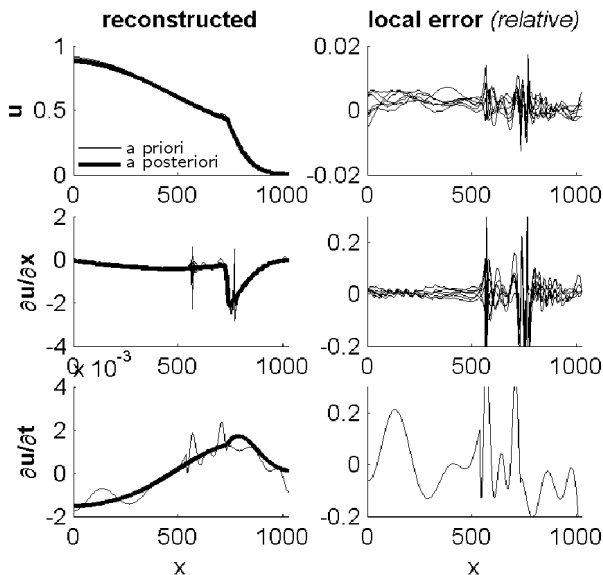


Figure 3: Reconstructed Profiles of  $u(x)$ ,  $\partial u(x)/\partial x$ , and  $\partial u(x)/\partial t$  from Concentration Images corresponding to figure 2 (*a priori* reconstruction) and from identified  $D_i$  Values (*a posteriori* reconstruction).

Because no significant variation of  $D_i$  was expected within each layer, the basis for  $D_i$  was reduced to an unique scalar

( $N=0$ ). As crude approximation, each  $D_i$  ( $i=1,2,3$ ) was identified from equation (13) with constant weight and  $v$  as “tent” or “hat” function. The latter made it possible to get an inner product formulation independent of boundary conditions. As a result, this approach yielded to consistent  $D$  estimation for layers A and C, with as expected  $D_C < D_A$ , but led to a difference between A and B up to one magnitude order, while same or at least similar values were needed. More robust estimation was achieved by using test functions, the first derivative of which decreased rapidly down to 0 close to interfaces, so as to reduce the influence of poor estimation of  $\partial u(x)/\partial x$  close to interfaces in (13). In the same manner, significant improvement (i.e.  $D_A \approx D_B$  and  $D_C/D_B \approx 12$  as expected) were obtained by choosing weighting functions, which take into account that regions were  $\partial u(x)/\partial x$  (or to some extent  $\partial u(x)/\partial t$ ) almost vanished did provide no pertinent information about the behavior of  $D$ .

It is clearly of interest to compare the *a posteriori* numerical solution, which can be calculated from identified diffusion coefficient, with the reconstructed measures, assuming reasonably a step initial profile. The comparison is analyzed as relative local error in figure 3. Errors in  $u$  was negligible whereas errors in  $\partial u(x)/\partial x$  and  $\partial u(x)/\partial t$  in the range of  $\pm 20\%$  were accordingly partially correlated and related to regions with weak signal or close to discontinuities. These results confirm the interest of our direct technique of identification that make it possible to assess and interpret accurately 7 concentration pictures in less than 30 s on a P4 2.2 GHz.

### CONCLUSION

The proposed pseudo-spectral method appears to provide accurate numerical results for both direct and inverse problems of diffusional transport within complex structure. Indeed, the multidomain approach combined with weak solutions allows effective and robust calculations in presence of strong jumps in transport properties. Further work appears desirable to validate both relative and absolute determination of diffusion coefficients in more general cases.

### REFERENCES

- Boyd, P. 2000. *Chebyshev and Fourier Spectral Methods*. 2ed. Dover Publications, Mineola, N.Y.
- Faccioli, E.; Maggio F.; Quarteroni A.; and A. Taghan. 1996. “Spectral-domain Decomposition Methods for the Solution of Acoustic and Elastic Wave Equations.” *Geophysics* 61, No.4, 1160-1174.
- Funaro, D. 1997. *Spectral Elements for Transport-Dominated Equations*. Springer-Verlag, Berlin.
- de Frutos, J. and R. Muñoz-Sola. 1995. “Chebyshev Pseudospectral Collocation for Parabolic Problems with non Constant Coefficients”. In *Proceedings of ICOSAHOM'95*, Houston.
- Shen, J.; Wang F.; and J. Xu. 2000. “A Finite Element Multigrid Preconditioner for Chebyshev-collocation Methods.” *Applied Numerical Mathematics* 33, 471-477.
- Weideman, J.A.C and S.C. Reddy. 2000. “A Matlab Differentiation Matrix Suite”. Technical report. <http://ucs.orst.edu/~weidemag/differ.html>.

# NUMERICAL SIMULATION OF THERMAL AND FLUIDDYNAMICAL TRANSPORT EFFECTS ON HIGH PRESSURE INDUCED INACTIVATION

Christoph Hartmann and Antonio Delgado  
Chair of Fluidmechanics and Process Control  
Technische Universität München  
Weihenstephaner Steig 23  
D-85350 Freising  
Germany  
E-mail: Christoph.Hartmann@wzw.tum.de

## KEYWORDS

High hydrostatic pressure, pressure induced inactivation, transport phenomena, thermo-fluid-dynamics, process non-uniformity

## ABSTRACT

The current paper deals with the effects of convective transport and heterogeneous heat transfer on high pressure induced inactivation. While the pressure within a high pressure chamber can be considered as spatially constant, the temperature, in general, is a heterogeneously distributed field quantity. In the present paper it is shown up to which extend thermal heterogeneities and convective transport lead to non-uniform inactivation results. As examples, the inactivation of *B.subtilis*  $\alpha$ -amylase dissolved in TRIS-buffer and the inactivation of *E.coli* suspended in a liquid similar to water in a model pressure chamber at pressures between 400 MPa and 500 MPa are considered. Aspects of the viscosity of the matrix as well as the heat transfer properties of the packaging material are considered. In both cases, significant process inhomogeneities can be determined.

## INTRODUCTION

The treatment food or food ingredients with high pressures between 100 MPa and 1000 MPa is always accompanied by an increase of the temperature in the treated volume. This is due to the change of the thermodynamic state of the system. Finite transport velocities of heat and suspended substances lead to the fact that temperature as well as substance concentration have to be considered as distributed balance quantities. In the present paper, the influence of hydrodynamic and thermodynamic transport on the process uniformity is investigated taking into account the above mentioned aspects.

The inactivation of a dissolved enzyme ( $\alpha$ -amylase) and of suspended micro-organisms (*E. coli*) in matrix liquids similar to water is simulated as a model process. During the high pressure processing a fluid flow develops which is interacting with the temperature field. Therefore, the inactivation takes place in a moving matrix and in transient thermal conditions.

## PROCESS MODEL

Two different configurations are considered. The first one, subsequently denoted as Process 1, represents the inactivation of *B.subtilis*  $\alpha$ -amylase dissolved in TRIS-buffer in a cylindrical high pressure chamber of approximately 0.8 L volume. The application of a pressure of 500 MPa at a temperature of 313 K is achieved by mass augmentation in the chamber, i. e. the solution is pumped directly into the chamber until the required pressure level is reached. The inlet velocity is chosen such that the level of 500 MPa is reached within a finite time interval of 25 sec. The pressure is held during 25 min. The pressure chamber is shown in figure 1. Its diameter and its height are 0.1 m leading to a volume of 0.8 litres. The grey shaded area represents a plane of axisymmetry. This plane will be used subsequently for graphical representation of field distributions.

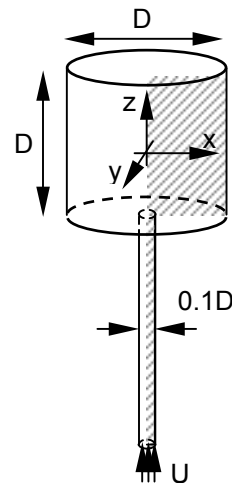


Fig. 1: Pressure chamber of process 1,  $D = 0.1$  m

The second process, subsequently denoted as Process 2, is an indirect one. This means, the processed samples are packed in containers which are placed in the chamber at distinct locations. The pressure is applied by mass increase of a liquid pressure medium leading to a compression of the medium, the package material and the contained suspension of *E. coli* in UHT milk. The pressure of 400 MPa is applied at a temperature of 303 K over 16 minutes. In process 2, the pressure application is assumed to be instantaneous, i. e. the

change of volume of the packages as well as the induced forced convection are neglected in order to circumvent numerical difficulties related to moving interfaces and fluid-structure interaction problems. The assumption is justified in the sense that the pressure increase phase is short compared to the pressure holding phase and forced convection is quickly dominated by natural convection (Hartmann, 2002 and Hartmann, 2002a). The geometry of the chamber is shown in figure 2. The volume amounts up to 6.3 litres. Again the grey shaded area represents the plane of graphical distribution of the field quantities.

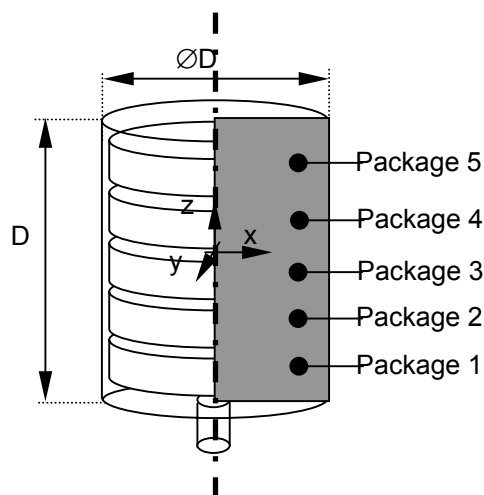


Fig. 2: Chamber for Process 2,  $D = 0.2$  m

## MODEL EQUATIONS

In order to simulate these processes, the basic equations of fluid dynamics, i. e. the continuity equation, the Navier-Stokes-equation, the energy equation and a balance equation for the activity of the suspended substances have to be solved. The latter contains a kinetic model for the inactivation, which is incorporated as a sink term in the equation. The kinetic model is taken from (Denys et al. 2000) for the enzyme and from (Hinrichs 2000) for the micro-organism.

An equation of state for water (Saul and Wagner 1989) valid in the considered pressure and temperature range is implemented as well as pressure and temperature dependent relations for the viscosity (Först et al. 2000) of water and the specific heat capacity.

These data are taken for both processes, since the specified liquids are similar to water and generic state data are not available for the considered range.

As thermal boundary condition constant temperature is prescribed at the housing. Fluid adhesion on the wall is assumed. In process 1, a constant velocity  $U$  is prescribed and a priori adapted such that the desired pressure increase within the compression phase is reached. In process 2, the pressure is set instantaneously to the desired value of 400 MPa leading to a temperature increase equal to that of a purely adiabatic process.

All liquids are supposed to be newtonian, compressible, and chemically inert. The flow is laminar. The assumptions and

modelling techniques have been validated by comparison to experimental data (Hartmann, 2002).

## METHODS

The finite volume method is used for the solution of the set of equations. Therefore, the commercial solver CFX-4 has been enhanced by own software extensions providing solution algorithms for the above-mentioned equations.

## RESULTS AND DISCUSSION

It can be shown, that the heterogeneity of the inactivation process depends strongly on the time scales of the hydrodynamic compensation, thermal compensation and the inactivation.

In process 1, significant heterogeneities can be observed for the case that the hydrodynamic compensation time scale is much smaller than the inactivation time scale and the thermal time scale is much larger than the inactivation time scale. Figure 3 shows the distribution of the relative activity (instant activity scaled with its initial value) of alpha-amylase obtained at the end of the high pressure process in a matrix fluid which of the viscosity is hundred times larger than that of water. The graphical representation shows a cross section through the pressure vessel (grey-shaded area in figure 1).

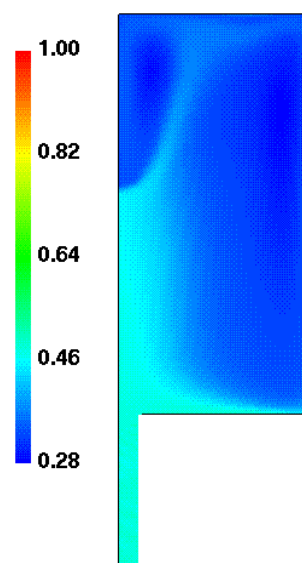


Fig. 3: Relative activity retention in a 0.8-litre volume after 1200 sec at 500 MPa and at 313 K

The activity retention is a distributed quantity that varies in the range between 28 % and 48 %. In the core zone and in the inlet, the highest activity retention can be observed while minimum values are obtained in the outer region of the chamber. This is due to the cumulative effect of thermal heterogeneities. In the core and at the inlet, the temperature is comparatively low due to forced convection of cold fluid into the chamber. The outer region is at a higher temperature due to compressive heating. Therefore, the

inactivation rate is higher in this region leading to a more efficient inactivation rate.

Furthermore, it has been observed that the inactivation leads to smaller values of the inactivation if the size of the chamber is increased (scale-up). This is due to the larger thermal compensation time scale leading to the effect that the inactivation is running at a higher average temperature.

Concerning process 2, the following results have been obtained. Again the process homogeneity depends strongly on the temperature decay time scales. An additional aspect enters into the discussion: the thickness and the thermal properties of the package material. Up to a certain extent the package material represents a heat barrier which provides almost homogeneous thermal conditions in all five packages. This is the case, when the package material is poly propylene at about 2 mm thickness. Figure 4 shows the average values of the colony forming units (cfu) per ml scaled by the initial concentration of  $10^8$  cfu per ml in each of the five packages at the end of the process.

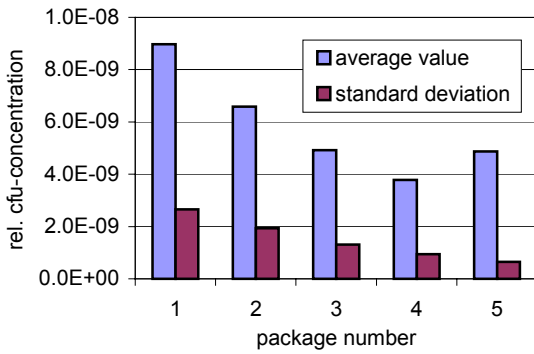


Fig. 4: CfU-concentration in 6.3 L-volume after 960 sec

It can be seen that an inactivation of at least eight orders of magnitude has been reached within the considered time period. In addition to this, the inactivation is maximum in package 4 and minimum in package 1. The standard deviation amounts up to 30 %, which can give rise to the assumption, that a significant process non-uniformity might exist in the present case. Nevertheless, spatial non-uniformities at such low concentrations of surviving cells are of minor importance. Therefore, the inactivation can be supposed to be highly efficient in this case.

Reducing the thickness to about 0.65 mm leads to thermal heterogeneities which induce a strongly heterogeneous inactivation result. Figure 5 shows the average values of the scaled cfu-concentration and their standard deviation for this case. The differences between the inactivation results obtained for the different packages are much more pronounced in the present case. They are larger than one order of magnitude. The standard deviation in the individual packages amounts up to 30 %. In this case, the non-uniformity between the individual packages is intensified by the non-uniformity within each package.

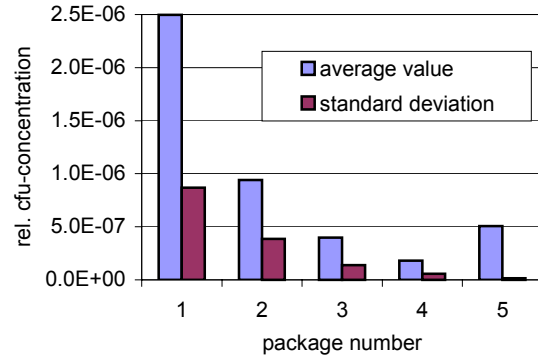


Fig. 5: CfU-concentration in 6.3 L-volume after 960 sec, improved heat transfer

The differences between the inactivation in the individual packages can be explained by the characteristics of the average temperatures in the packages shown in figure 6. The temperature rises up to 314 K during the adiabatic compression in all packages and then decreases to 305 K in package 1 and 307 K in package 4 within 960 sec. A temperature difference of about 2 K is established between package 1 and 4 after 220 sec and persists during the complete process. The temperature difference leads to an inactivation which runs at different rates in both packages, which yields the considerable difference in the cfu-concentration of more than one order of magnitude.

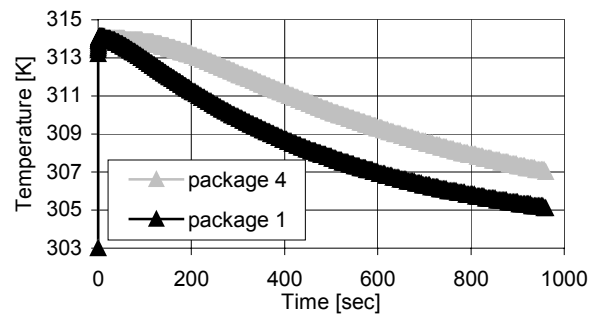


Fig. 6: Average temperature in packages 1 and 4 at reduced package material thickness

## CONCLUSION AND PERSPECTIVES

In the present analysis, thermally induced process heterogeneities are shown for two inactivation processes. It can be stated, that process heterogeneities have to be expected, when the fluid motion is of low intensity and heat conduction dominates thermal compensation. Furthermore, heat conduction has to be of the same time scale than the inactivation itself.

Furthermore, the package material represents a heat barrier which significantly influences thermal conditions of packed food. The more the material is insulating the more the temperature is homogeneous leading to a homogeneous inactivation in all packages.

Principal subject of further analysis is the modelling of the finite compression phase for configurations with packed

foods. Here, a special treatment of the moving package interface becomes necessary.

pressures up to 25000 MPa. J Phys Chem Ref Data 18:1537-1564.

## ACKNOWLEDGMENTS

This work has been partially supported by the Max-Buchner-Forschungsstiftung (Max-Buchner Science Foundation) within the project 2238 and by the German Science Foundation (DFG) within the project HA 2228/1.

## AUTHOR BIOGRAPHY

**CHRISTOPH HARTMANN** went to the Technische Hochschule Darmstadt, Germany, where he studied Mechanical Engineering. After a one year stay in the Ecole Centrale de Lyon, France, he obtained his diploma in 1992. He continued his studies preparing a PhD in Computational Fluid Dynamics within the Mechanics Department of the Technische Hochschule Darmstadt. He defended his PhD in 1996. After several month of post-doctoral activities he joined the Engineering Systems International (ESI) Company in 1997 as a research and development engineer for Finite-Element-Software (PAM-CRASH) for the simulation of occupants' safety in the automotive industry. In 1998, he joined the department of Fluid Dynamics and Process Control of the Technische Hochschule München as the head of the fluid dynamics research group. His global field of interest are interaction processes between thermofluidynamics and food- and biotechnology preferably solved by simulation techniques.

E-mail: Christoph.Hartmann@wzw.tum.de

http: www.wzw.tum.de/lfp

## REFERENCES

- Denys S, van Loey AM, Hendrickx ME. 2000. A modeling approach for evaluating process uniformity during batch high hydrostatic pressure processing: combination of a numerical heat transfer model and enzyme inactivation kinetics, *Innovative Food Science & Emerging Technologies* 1:5-19
- Först P, Werner F, Delgado A. 2000. The viscosity of water at high-pressures - especially at subzero degrees centigrade, *Rheologica Acta* 39:566-573
- Hartmann C. 2002. Numerical Simulation of Thermodynamic and Fluiddynamic Processes during the High Pressure Treatment of Fluid Food Systems, *Innovative Food Science and Emerging Technologies* 3 (1), pp. 11-18
- Hartmann C, Delgado A. 2002a. Numerical Simulation of Thermofluidynamics and Enzyme Inactivation in a Fluid Food System under High Hydrostatic Pressure, In: R. Hayashi (ed.), *Trends in High Pressure Bioscience and Biotechnology* (pp. 533-540), Elsevier, Amsterdam.
- Hartmann C, Delgado A. 2002b. Numerical Simulation of Convective and Diffusive Transport Effects on a High Pressure Induced Inactivation Process, accepted in *Biotechnology and Bioengineering*
- Hinrichs J. 2000. Ultrahochdruckbehandlung von Lebensmitteln mit Schwerpunkt Milch und Milchprodukte – Phänomene, Kinetik und Methodik -. *Fortschritt-Berichte VDI, Reihe 3, Nr. 656*, Düsseldorf: VDI
- Saul A, Wagner W. 1989. A fundamental equation for water covering the range from the melting line to 1273 K at

# A PETRI NET BASED SIMULATION APPROACH FOR EVALUATING BENEFITS OF TIME TEMPERATURE INDICATOR AND WIRELESS TECHNOLOGIES IN PERISHABLE GOODS RETAIL MANAGEMENT

Navneet Bhushan and Kishor Gummaraju  
Infosys Technologies Limited,  
Electronics City, Hosur Road,  
Bangalore –561229,  
India  
E-mail: Navneet\_bhushan@infy.com  
<http://www.infy.com>

## KETWORDS

Time Temperature Indicators, Petri Nets, Wireless LAN, Perishable Goods, Retail Management

## ABSTRACT

Effective management of perishable goods is a major problem faced by the retailers of perishable goods. Time-Temperature-Indicator (TTI) labels available today can indicate the remaining shelf life of these perishable products. This technology can change the way perishable goods inventory is managed today, from a *First-In-First-Out (FIFO)* and *Fixed Sell-By-Date* basis to *Least Shelf Life First Out (LSFO)*. In this paper a futuristic solution combining TTI and wireless technologies is proposed. Although the TTI and wireless based solution proposed in the paper is considered better, the benefits of the proposed solution have to be analyzed in quantitative terms. These have been analyzed using a Petri Net based approach for system simulation. The analysis shows that a retailer of perishable goods can reduce the losses suffered due to the expiry of perishable items before they can be sold, by more than 90% and increase the net profits by more than 10% in the test scenario. Thus we can conclude that adoption of the proposed system will benefit the retailer to a great extent.

## INTRODUCTION

The life of perishable products such as fruits, meat products, medicines and certain chemicals is a function of the product's characteristics and the environment in which the product is stored. An efficient cold chain is essential to ensure that the product remains fresh for the expected duration. However uncertainty in the cold chain, while the product is in transit to the retail store, adds to many complexities. The retailer could run the risk of selling an unsafe product to the consumer or might need to discard items that have perished before their expected date of expiry.

*Time-Temperature-Indicator (TTI) labels* (Taoukis et. al. 1998) available today can indicate the remaining shelf life of these perishable products. This technology could revolutionize the way in which perishable inventory is managed in the future. Inventory management would move from the current *First-In-First-Out (FIFO)* and *Fixed Sell-*

*By-Date* basis to *A Dynamic Shelf Life Based Inventory Management* or the *Least Shelf Life First Out (LSFO)* basis.

In this paper, we propose a solution to inventory, scheduling and supply chain management of perishable items combining the TTI and Wireless technologies. The proposed solution is compared with the existing situation, using a discrete event simulation methodology based on the Generalized Stochastic Petri Nets (GSPN).

In the next section we describe the existing system and proposed solution. Thereafter a brief introduction to Petri Nets and GSPN is provided. The GSPN based simulation approach, the results of the simulation, and an analysis of these results to evaluate the benefits of the proposed solution are described thereafter. Finally, conclusions and the scope for further work have been provided.

## SHELF LIFE BASED PERISHABLE INVENTORY MANAGEMENT

Every perishable item has a certain date before which it needs to be sold to the consumer. This date is computed assuming that the required cold chain is maintained. Any breakage in the cold chain, where the product is subjected to periods of higher temperature, would affect the longevity of the product. The current scenario in the life of a perishable good is shown in the figure below.

Retailers today are unable to determine the history of the "Time Temperature Exposure" of the product. This has the following business implications:

- The product purchased by the consumer could be unsafe although it is well within the sell-by-date.
- The product could perish in the warehouse itself, well before the printed sell-by-date. The product could have been pushed out to the store in time, had the warehouse been aware of the remaining shelf life.
- The product could also perish in the retail shelf, well before the printed sell-by-date, resulting in high shrink.
- It could be possible to retain some of the products longer on the shelf (even beyond the sell-by-date), if the cold chain was maintained very well. However, the retailer

(unaware of this) may markdown the price in an attempt to sell the product before the sell-by-date.

The ideal Inventory Management System would require the sell-by-date to be revised to reflect the actual shelf life of the product.

### The Opportunity

Time Temperature Integrators, are products, which are capable of measuring the life of temperature sensitive products. This is a small adhesive label consisting of an enzyme and a substrate filled ampoule separated by a breakable seal. Pressure on the ampoules breaks the seal and allows the two liquids to mix. This activates the time-temperature clock. The color of the label changes from green at the start to yellow at the end of the product life.

Any increase in temperature beyond the stipulated temperature would hasten the color change, indicating a reduction in life of the product. Since the process is cumulative in nature, it enables recording the entire history of temperature exposure. Thus the change in color, if captured, could help indicate the extent to which the shelf life of the product has been impacted and subsequent action to be taken.

### The Proposed Solution

The figure below shows the way in which the technology could be exploited to secure the benefits envisaged. The warehouse will manage the inventory based on the revised sell-by-date, which in turn is a function of the remaining life. In addition the warehouse will also use this information to provide a feedback to the vendor regarding possible mis-handling, resulting in shrink. This would enable the vendor and the transporter to better manage the cold chain. The retailer will manage the inventory based on the revised sell-by-date (recomputed at the retail receiving point). He will also establish decision support systems to determine the extent of markdown required to push the perishable product out before actual expiry.

Wireless technology could be deployed effectively as shown in figure 3 below, to enable capture of the present sell-by-date and the actual available shelf life while interfacing with the back-end store systems. Wireless Local Area Network (WLAN) is one technology that can create the infrastructure for enabling this system. The hand held device would need to read the TTI label as well as the sell-by-date on the barcode. It would further need to match the TTI indicator with the lookup tables for calculating the remaining shelf life. This would enable an informed decision to generate the appropriate label. A small portable printer could also generate the required labels with revised prices.

To analyze the benefits of the proposed solution vis-à-vis existing situation, a simulation study was carried out. The simulation is based on the well-established methodology of Petri Nets. In Section 4 we describe the PN based simulation model and results of the analysis. However, first we give a brief overview of Petri Nets in the next section.

## PETRI NETS

System studies require system representation and system analysis. To represent a system for its complete depiction and analysis many abstract methods (models) have been developed. Petri Nets (PN) is one of the most powerful formal models of Information flow. Concept of Petri Nets has its origin in work done by Carl Adam Petri in 1962. Since late 70's PNs have found increasing usage in design and analysis of a large number of systems (Ajmone and Chiola 1987; Ajmone et al. 1987; Bhushan 1997; Haas and Shelder 1989; Peterson 1977; Trivedi and Sun 2001).

A Petri Net is a particular type of digraph with an initial state called the initial marking,  $M_0$ . The underlying graph,  $N$ , of a PN is a directed weighted bipartite graph with two kinds of nodes, called places and transitions, where arcs are either from a place to a transition or a transition to a place. In graphical representation, places are drawn as circles and transitions as bars or boxes. Arcs are labeled with their weights (positive integers), where a  $k$ -weighted arc can be interpreted as the set of  $k$ -parallel arcs. A marking assigns a non-negative integer to each place. If the integer assigned to a place is  $j$  we say that the place has  $j$  tokens.

Formally a PN is defined as a 5 tuple  $PN = \{P, T, F, W, M_0\}$ , where,

$P = \{p_1, p_2, \dots, p_m\}$  is a finite set of places  
 $T = \{t_1, t_2, \dots, t_n\}$  is a finite set of transitions  
 $F \subseteq \{P \times T\} \cup \{T \times P\}$  is a set of arcs (flow relation)  
 $W: F \rightarrow \{0, 1, 2, 3, \dots\}$  is a weight function  
 $M_0: P \rightarrow \{0, 1, 2, 3, \dots\}$  is the initial marking  
 $P \cap T = \phi$ ;  $P \cup T \neq \phi$ .

The behavior of many systems can be described in terms of system states and their changes. In order to simulate the dynamic behavior of a system, a state or marking in a PN is changed according to the following transition (Firing) Rule:

- A transition  $t$  is said to be enabled if each input place  $p$  of  $t$  is marked with at least  $W(p, t)$  tokens, where,  $W(p, t)$  is the weight of the arc from  $p$  to  $t$ .
- An enabled transition may or may not fire (depending upon whether or not the event actually takes place)
- A firing of an enabled transition  $t$  removes  $W(p, t)$  tokens from each input place  $p$  of  $t$ , and adds  $W(t, p)$  tokens to each output place of  $t$ , where  $W(t, p)$  is the weight of arc from  $t$  to  $p$ .

Timed Transition Petri Net (TTPN) is a special class of PNs in which time is associated with each transition. These transition times may be deterministic or stochastic. Further PN Transitions may have a probability of firing associate with them. These are called Generalized Stochastic Petri Nets (GSPN).

In next section we describe how the representation capability of PNs can be used to simulate a system using the discrete event simulation methodology.

### System Simulation using Petri Nets

The simulation proceeds in the following steps:

- Modeling of the system (states and transitions) as a Timed Transition Petri Net (TTPN). In most of the cases the transition times are stochastic variables. Hence the TTPN becomes a GSPN (Generalized Stochastic Petri Net). The Petri Net has a set of places called sink or collector places where all the end states of the system are captured. These collector places are used to evaluate the system parameters of interest.
- Event driven Simulation of the Petri Net using Next-Event simulation approach. The firing of a transition representing the occurrence of an event involves removing as many number of tokens from the input places as specified by the arcs weights, and putting as many tokens in the output places as per the weights.
- Count the number of tokens in each of the collector places.
- Repeat the simulation till the desired confidence level and accuracy is achieved.
- The average number of tokens in the collector places is used for computing the relevant parameter, e.g., throughput, response time, etc.

The two situations described above are analyzed using a discrete event simulation methodology developed. The values of the parameters to describe the two scenarios are described in the Test Scenario below.

### THE PETRI NET BASED SIMULATION OF THE PERISHABLE GOODS RETAIL MANAGEMENT

The approach starts with modeling of the system under study as a Generalized Stochastic Petri Net (GSPN) and studying the dynamic state of the system as time progresses using the discrete event simulation methodology. For the purpose of evaluating the value of the proposed solution a simulation scenario as described below has been assumed.

#### The Simulation Scenario

- **The Demand:** In multiple Retail Stores there has been observed an average demand for 200 Boxes of Perishable Goods per day. Further this demand has been observed to follow a Poisson probability distribution, i.e., the inter arrival time between two demands is exponentially distributed with mean 200 boxes per day.
- **The Perishable Goods:** The Perishable Goods are labeled with Sell by Date at the Vendor Place. This Sell by Date is computed assuming average cold storage conditions on the way from the vendor to the store. There is no way at the retail store presently to find out the boxes that haven't met the average cold storage on the way. Therefore the

boxes having the least Sell by Date are picked in a FIFO manner.

- **The Vendor:** The vendor sends on an average 2000 boxes every 10th day. This is assuming that retail stores have a capability of storing 2000 boxes for 10 days after which the goods expire. These boxes are sent in 20 trucks each carrying 100 boxes. These trucks reach the respective stores on an average in 2 days starting from the vendor to the stores. On an average 10% of these trucks per 10 days do not meet the cold storage requirements. 10% actually exceed the cold storage required by Sell by Date. And 80% meet the cold conditions required by Sell by Date. Also, we assume that the goods not meeting the required cold conditions (we call them Category C) perish on an average in 2 days of reaching the retail outlets. The goods meeting the cold storage (Category B) perish on an average in 8 days of reaching the retail outlets. While goods exceeding the cold storage (Category A) perish on an average in 10 days of reaching the retail outlet.
- **Present Scenario:** There is no way presently to distinguish between the three categories at the retail outlets. Hence the Boxes are randomly picked (average 200 boxes per day) from Category A, Category B or Category C. This leads to possible customer dissatisfaction if they buy Category C and loss by the store if they sell Category A goods much before their actual Sell by Date.
- **Proposed Solution:** In the Proposed Solution because of TTI labels, it is possible to distinguish between the three categories and schedule their selling based on Least Shelf Life First Out (LSFO) scheduling

### PN MODEL OF THE SYSTEM

The GSPN corresponding to the system described above is shown in figure 4. There are five collector places in the GSPN shown above - *Requested*, *CategoryASold*, *CategoryBSold*, *CategoryCSold* and *TotalPerished*. Two input places called *BoxesWithVendor* and *DemandCreated* represent the number of boxes sent per day from the vendor to various stores and demand at the stores per day respectively. Dashed Circles represent the initial conditions. Tokens in these input places are zero. The bars represent the transitions indicating the occurrence of events. It should be noted that the arrowhead from place *BoxesWithVendor* to transition *BoxesSent* is filled circle. Similarly the arrowhead from the place *DemanCreated* to transition *Demand* is a filled circle. This represent that the condition to fire the transition is that the place should not have any tokens. Since, the input places do not have any tokens, the transition will keep on firing at the regular interval of time associated with the transitions.

The three layered bar indicates that this is a transition with stochastic firing time. The associated probability distribution with stochastic transitions is exponential. The single layer bars represent that the transitions have deterministic associated time periods. In the present case, the time period associated with these transitions is zero, i.e., the transitions are immediate. However, there can be an associate probability of firing of a particular transition. As the

transitions, *VeryWellMaintained*, *ColdChainMaintained* and *ColdChainNotMaintained* are three transitions with associated probabilities of 0.1, 0.8 and 0.1. This represent input variables where it is assumed that in 80% of the cases the cold chain is maintained as per the standard. Whereas, 10% of the cases the cold chain exceeds the required level, and in 10% cases the cold chain is not maintained.

### Simulation Results

The modeled system was simulated for 365 days (1 year) of operations. The results are shown in Table 1. These are at 95% confidence level and 5% error. The simulation time of a year was considered enough to take care of any fluctuations in the assumed scenario. Table 1 also shows the relative change in various parameters in the two cases. As can be seen there is a considerable increase in the sale of Category B Boxes in the proposed scenario (more than 25%). Category B goods sold as percentage of total goods sent also increases by 22%. Also the number of goods perished as percentage of total goods is decreased by more than 2.5 times.

Table 1: Simulation Results and Relative Change in Parameters

Parameters	Present Case (E)	Proposed Solution (N)	Relative Change (N/E)
Total Boxes Sent by Vendor (X)	69231	71224	1.029
Sold Category B (Y)	48972	61512	1.256
Sold Category C	5999	-	-
Sold Category A	6061	-	-
Perished (P)	220	87	0.395
Left (L)	7979	9625	1.206
% Category B sold (100 * Y/X)	70.7	86.4	1.222
% Perished (100 * P/X)	0.318	0.122	0.384
Category B Sales (% terms) have increased by 22%, perished goods have decreased by 60%.			

### Analysis of Simulation Results

As can be seen from the results in Table 1 above, the proposed solution decreases the amount of goods perished by 60% over the existing scenario. In addition it increases the sale of **Category B goods by 22%**, while there are **no Category C or Category A sales**.

Assuming the cost price of a box at the retail to be \$100 and selling price to be \$120, i.e., on each box \$20 profit is assumed. Also let the loss of customer goodwill for selling each category C box is (say) \$10. Further, assume the loss due to selling of each Category A Box to be \$5. Based on these assumptions Table 2 gives the benefits of the proposed solution over existing solution in Net Profit Terms for the assumed scenario. As can be seen that although the total number of boxes sold in the two cases is almost same, the

number of Category B boxes sold is much more in the proposed solution. This leads to the increase in net profit by 10%. *The total loss in \$ terms is down by more than 90% with the proposed system compared to the existing situation.* It must be stressed here that these results are for the assumed scenario within the ideal conditions defined.

Table 2: Detailed Analysis of the Simulation Results

Parameter	Present	Proposed	Change (%)
Boxes Sold (S)	61032 (Category A, B and C)	61512 (Category B only)	0.786
Revenue (S * \$ 120)	61032 * 120 = 7323840	61512 * 120 = 7381440	0.786
Profit (S * \$20) (P)	61032 * 20 = 1220640	61512 * 20 = 1230240	0.786
Loss Due to selling Category C (1)	5999 * \$10 = 59990	0	
Loss Due to Selling Category A (2)	6061 * \$5 = 30305	0	
Loss Due to Perished Boxes (3)	220 * \$100 = 22000	87 * \$100 = 8700	-60.455
Loss Due to <i>Loss in Profit</i> because of Perished Goods (4)	220 * \$20 = 4400	87 * \$20 = 1740	-60.455
Total Loss (L= 1+2+3+4)	116695	10440	-91.054
Net Profit (P -L)	1103945	1219800	10.495

### CONCLUSIONS

The proposed solution based on TTI technology to manage Perishable goods inventory will result in considerable savings. In the assumed scenario in this paper, the results indicate an increase in net profit of more than 10% and a reduction in loss of perishable goods by more than 90%. Hence we propose that the retail stores should seriously consider the proposed solutions to increase profits and decrease enormous amount of wastage that occurs due to the existing supply chain management of perishable goods.

### REFERENCES

Ajmone M. and G. Chiola. 1987. "On Petri Nets with Deterministic and Exponential Firing Times", *LNCS 266*, Springer Verlag.  
 Ajmone M., G. Chiola and A. Fumagalli. 1987. "An Accurate Performance Model of CSMa./CD Bus LAN", *LNCS 266*, Springer Verlag.

- Bhushan N. 1997. "Performance Evaluation of an Air Defence System Modelled as a Petri Net", *Proceedings of Symposium on Systems Analyses for Defence*, CASSA, Bangalore, India.
- Haas P.J. and G.S. Shelder, 1989. "Stochastic Petri Net Representation of Discrete Event Simulation", *IEEE Transactions on Software Engineering*, SE-15(4).
- Peterson J.L. 1977. "Petri Nets", *ACM Computing Surveys*, Vol. 9, No. 3.
- Taoukis P.S., M. Bili and M. Giannakourou. 1998, "Application of Shelf Life Modelling Of Chilled Salad Products to a TTI Based Distribution And Stock Rotation System", *International Symposium on Applications of Modelling as Innovative Technique in the Agri-Food Chain*. (Ed.) L.M.M. Tijskens and M.L.A.T.M. Hertog, NetherLands.
- Trivedi, K.S., and H. Sun. 2001. "Stochastic Petri Nets and Their Applications to Performance Analysis of Computer Networks", *Recent Developments in Operational Research*, (Eds) Agarwal M.L. and Sen K., Narosa Publishing House, New Delhi, India.

## BIOGRAPHIES

**NAVNEET BHUSHAN** is currently working with Software Engineering and Technologies Labs (SETLabs), Infosys Technologies Limited as Senior Research Associate. He holds two Masters degrees- one in Computer Science and

Engineering from Indian Institute of Technology (IIT), Madras, India and other in Software Science from Allahabad University, India. He has 12 years experience in research and software development related to strategic decision making, modeling & simulation, and networking. His research interests include Performance Evaluation, Mobile Computing, Software Engineering and Artificial Intelligence. His email id is [navneet\\_bhushan@infy.com](mailto:navneet_bhushan@infy.com).

**KISHOR GUMMARAJU** is a senior consultant with the Domain Competency Group (DCG) of Infosys Technologies Limited and has over eight years of professional experience in the areas of supply chain management, retail and finance across a range of industries such as Chemicals, FMCG and Foods. Kishor is a post-graduate in Management Studies from Indian Institute of Management (IIM), Lucknow. His interests include Performance Management in Supply Chains and Supply Chain Optimization. He may be reached at [kishor\\_gummaraju@infy.com](mailto:kishor_gummaraju@infy.com)

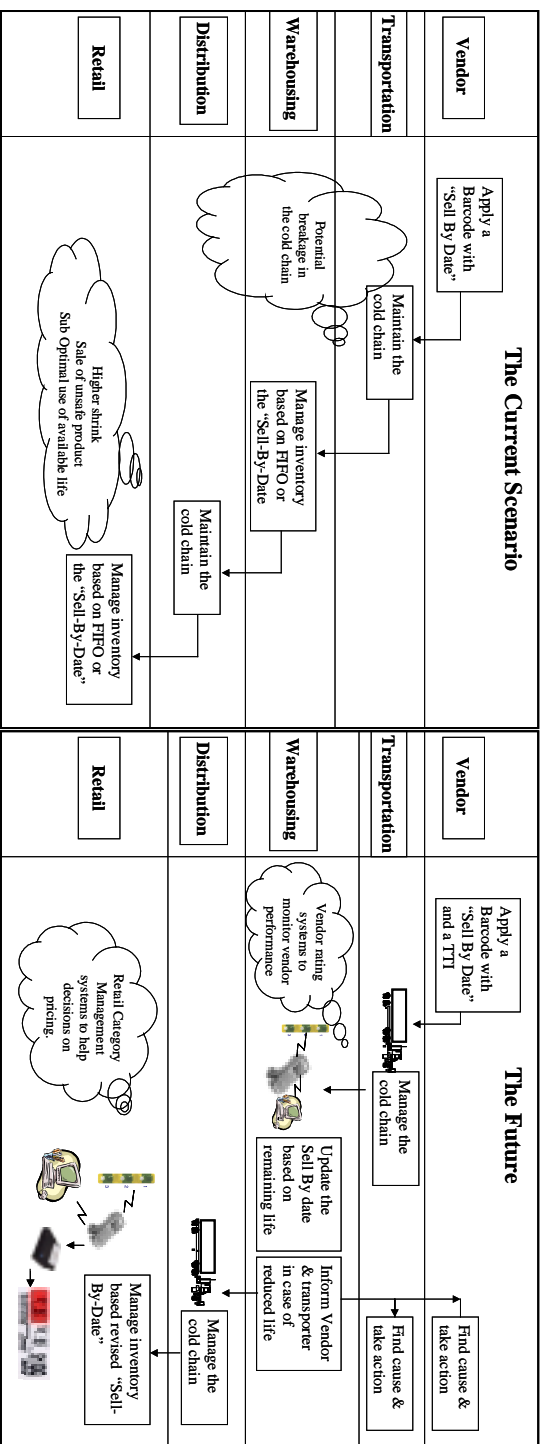


Figure 1: The Current Scenario in the Supply chain of Perishable Goods

Figure 2: The Futuristic Proposed Scenario

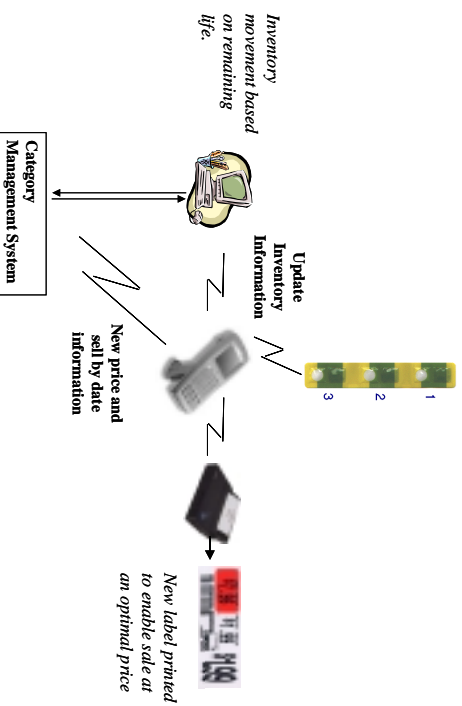


Figure 3: Integrating TTI and Wireless LAN Technologies

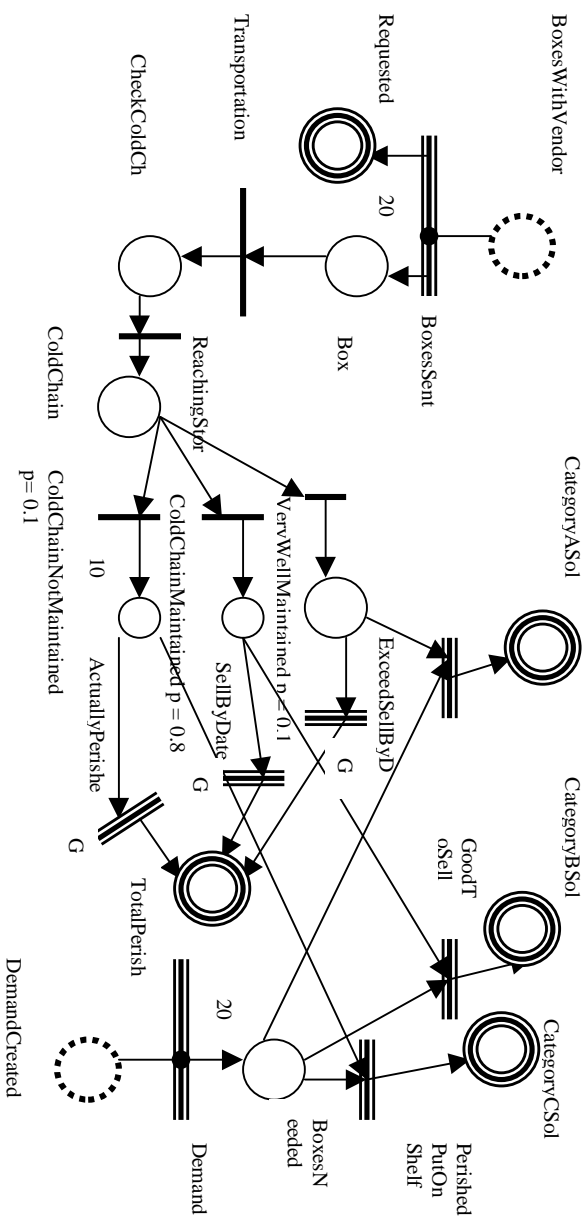


Figure 4: Petri Net Model of the Perishable Goods Supply Chain

# SIMULATION OF THERMAL FOOD PROCESSING WITH PHASE TRANSITIONS BY MEANS OF THE TNO DENSITY-ENTHALPY PHASE DIAGRAM

A.R.J. Arendsen and A.I. van Berkel  
TNO Environment, Energy and Process Innovation, Department of Energy Systems,  
P.O. Box 342, 7300 AH Apeldoorn, The Netherlands  
E-mail: A.R.J.Arendsen@mep.tno.nl

## KEYWORDS

Thermal food processing, phase transition, simulation, modelling, density-enthalpy phase diagram, Gibbs free energy minimization.

## ABSTRACT

To increase the accuracy, validity range, development speed and calculation speed of food models, TNO developed the TNO density-enthalpy phase diagram. This approach is based on the fact that density and enthalpy always suffice to define the current state of a product as long as thermodynamic equilibrium can be assumed. Density and enthalpy can be obtained from mass and energy balances. The use of the diagram is demonstrated by means of two examples of application. The first example consists of the heating of a closed system containing water and sugar. The second example describes vacuum freezing. Further research is concentrated on the implementation of the Finite Element Method in combination with the TNO density-enthalpy phase diagram to describe more complicated products. Validation will occur on the basis of sorption isotherms and freeze curves by means of Differential Scanning Calorimetry (DSC) measurements and ThermoGravimetric Analysis (TGA).

## INTRODUCTION

Most processes in the food industry involve adding and removing heat and/or moisture to and from the product. Common examples are pasteurisation, cooking, sterilisation, freezing and drying. During the past years TNO worked on the development of a PC-programme (BAKTIX and BERTIX) for the modelling of these processes (Wijnant-Timmerman 1998). This programme is currently used by the food industry and is used by TNO for industrial consultancy activities. This article describes a novel aspect of this modelling. A density-enthalpy phase diagram is used to increase the model accuracy, validity range and robustness when simulating thermal food processing with phase transitions. First, the common approach for modelling is discussed. Subsequently, the principle and the use of the TNO density-enthalpy

phase diagram is described. Finally, some examples of application are discussed.

## COMMON APPROACH

Food processes are usually characterised in terms of the development of pressure and temperature in time and/or position in the process. Naturally a physical/chemical model of such processes involves solving equations for temperature, pressure and concentration as a function of time. The simulation of food processing becomes more complicated when phase changes occur during the process. In that case pressure and temperature alone are no longer sufficient to describe the entire process. Additional variables such as the ice and vapour fractions are needed. Thus the simulation model must include additional equations for these new variables. Moreover the model must decide which model equations are appropriate at a given time during the simulation, for the phase changes usually occur only during a part of the entire process. The simulation of thermal food processing with phase changes is usually quite cumbersome due to this need to solve different sets of equations for different phases of the process. Switching from one set of equations to another can cause instability of the numerical solution procedure, especially when an iterative procedure is required. Furthermore, models to describe food processing with phase changes usually require a large amount of input parameters, such as specific heats of all the phases, latent heat of phase changes, and adsorption properties. Obtaining all these properties can be as much effort as developing the simulation model. In this article an alternative approach is discussed to overcome these problems.

## ALTERNATIVE APPROACH

In order to obtain a more robust simulation model for thermal processes with phase changes, an alternative approach is developed. This approach is based on the fact that density and enthalpy always suffice to define the current state of the product completely as long as thermodynamic equilibrium can be assumed. Thus if temperature, pressure and mass distribution over the

phases can be obtained as functions of density and enthalpy, the thermal food processing can be simulated by solving only one set of equations for the entire process, eliminating the need for switching between sets of equations. Moreover, all desired thermal properties needed for the calculation can be obtained as partial derivatives of these functions. Thus eliminating the need for sheer endless lists of input parameters.

Density and enthalpy can be obtained by solving mass and energy balances. A thermodynamic analysis is required for the resolution of temperature, pressure and mass distribution given density and enthalpy. In principle, the desired functions can be obtained through constrained minimization of the total Gibbs free energy as a function of temperature, pressure and mass distribution at given density and enthalpy. Due to the amount of variables and discontinuities of the density and enthalpy as functions of temperature pressure and vapour distribution, this minimization is cumbersome and time consuming. In fact, the aforementioned problem of different sets of variables for different stages of the process re-emerges here. TNO developed the density-enthalpy phase diagram to overcome these problems. By means of a density-enthalpy phase diagram it is directly possible to calculate the temperature, pressure and phase fractions given the density and enthalpy of the system.

### THE TNO DENSITY-ENTHALPY PHASE DIAGRAM FOR PURE WATER

The method of the density-enthalpy phase diagram is based on dividing the density-enthalpy plane into different zones. These zones correspond to the pure phase zones, phase transition lines and the triple points in the standard pressure-temperature phase diagram. The construction of the density enthalpy phase diagram is possible if the Gibbs free energy is known as a function of temperature and pressure. For water and steam (IAPWS 1996) or (IAPWS 1997) can be used, for ice (Hyland and Wexler 1983) is used. The boundaries of the different zones are relations between density and enthalpy. These boundaries are calculated based on the thermodynamic functions and can subsequently be used to determine directly in which zone the system currently is, given density and enthalpy. Figure 1 gives the boundaries of the different zones for pure water. The largest area in the diagram corresponds to liquid water in equilibrium with steam (G+L-area). This illustrates the fact that evaporation/condensation of water is accompanied by a large change in enthalpy and density. For example the boundary of the G+L-area with the G-area corresponds to the density as a function of the enthalpy of pure saturated steam.

Once the zone has been determined, calculating pressure, temperature and mass distribution is straightforward. Based upon thermodynamic equilibrium, only

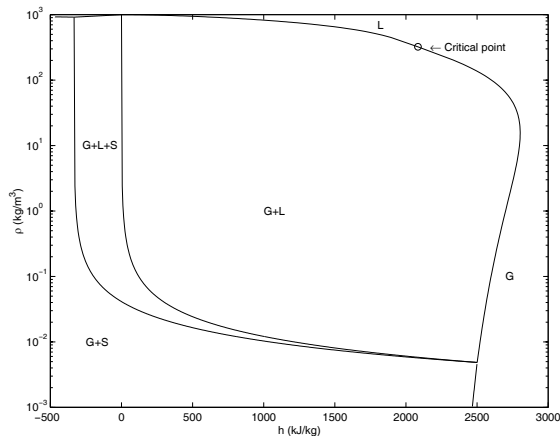


Figure 1: Boundaries of TNO density-enthalpy phase diagram for pure water; G : gas; L : liquid; S : solid

two variables need to be calculated, given density and enthalpy. In case of a single phase the variables are the temperature and pressure. In case of two phases the variables are the temperature or pressure and the fraction of one phase. Finally, in case of three phases the temperature and pressure are known and the variables are the fractions of two components. This procedure for calculating the equilibrium, as defined by minimum Gibbs energy, is very fast and robust.

Some results of the TNO density-enthalpy phase diagram of pure water are given in figures 2 until 5. By means of these figures it is possible to gather the temperature and mass fractions at different enthalpy and density. In principle, it is possible to observe the boundaries of figure 1 in these figures.

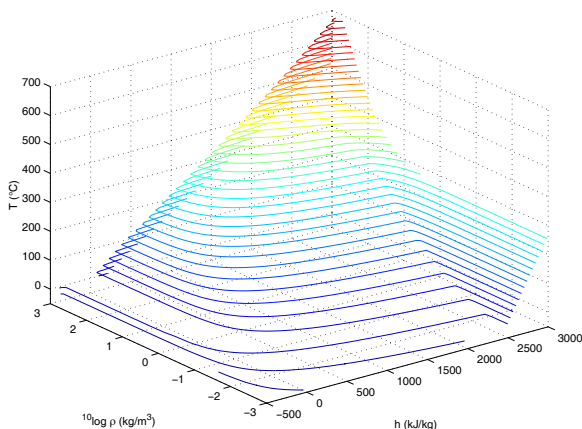


Figure 2: Temperature as function of density and enthalpy for pure water

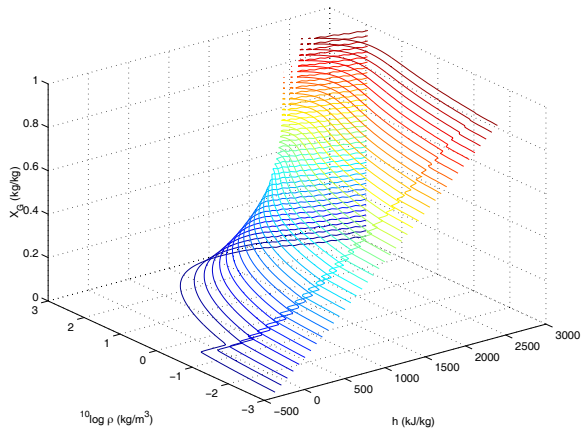


Figure 3: Gas mass fraction as function of density and enthalpy for pure water

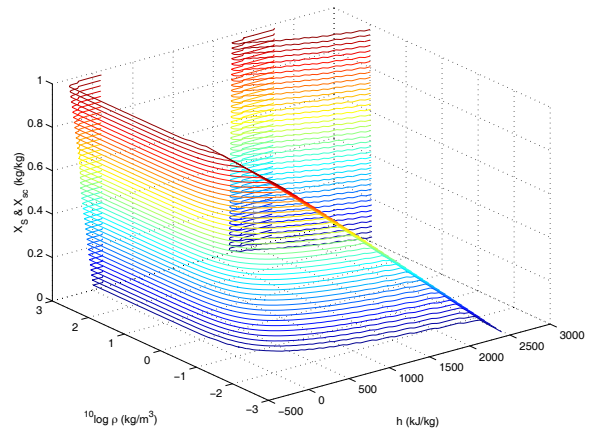


Figure 5: Solid and super critical mass fraction as function of density and enthalpy for pure water

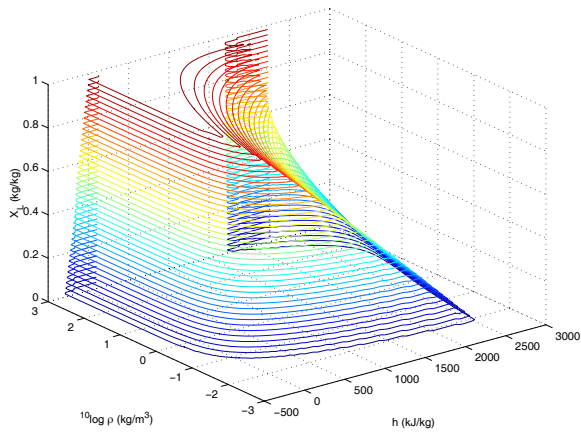


Figure 4: Liquid mass fraction as function of density and enthalpy for pure water

### THE TNO DENSITY-ENTHALPY PHASE DIAGRAM FOR FOOD

Food is usually modelled as a porous inert material, containing water and a solute. The water can exist as steam, fluid water and ice. The solute can exist in solution with water and as a solid. The interaction between water and solute causes elevation of the boiling point and depression of the freezing point. If the interaction is assumed to be ideal, knowledge of mole mass, solubility and enthalpy of the solute are sufficient to describe the whole system. For non-ideal systems, this information can be derived from sorption isotherms and/or freeze curves. The density axis of the diagram still corresponds to the water density, while the enthalpy axis corresponds to the enthalpy of the total product (water, solute and inert). Thus it can be assumed that the process allows the phases of the total product to be in ther-

mal equilibrium. Most processes in the food industry comply with this requirement. The boundaries between the areas in the diagram now depend on water density, enthalpy, moisture and inert content. Thus an infinite number of density-enthalpy diagrams can be conceived for food materials. A computer program can easily calculate the boundaries in the diagram depending on the composition. All thermodynamic properties of the total product, e.g. specific heat capacity and thermal expansion coefficient, follow naturally from the appropriate derivatives in the diagram.

### APPLICATION

Simple processes can easily be visualised on the diagram. The heating of a well-mixed canned product for instance is a straight horizontal line in the diagram. To simulate a process, the development of density and enthalpy in time must be calculated. For homogeneous products, this can be done through macroscopic mass and energy balances. For more complicated products the assumption of thermal equilibrium will only be valid locally. Thus a system of partial differential equations representing of mass and energy conversation in differential form must be solved to obtain density and enthalpy at every point in the product. These differential equations usually contain constants that depend on results of the diagram. The finite element method can be employed to solve these equations. The density enthalpy phase diagram is implemented as a Fortran subroutine. The input of this subroutine is the total water density, total enthalpy, mass fraction water (in all phases) and mass fraction solute in the product, which follow from the mass and energy balances. The output is the pressure and the temperature at equilibrium, the mass fractions steam, liquid water and ice, the mass fraction solid solute based on the total mass of solute, the mass fraction

solute in the solution and the mass fraction pure ice based on the total mass of ice. Two examples of application will be discussed in the following.

### Heating of a closed system

The first example consists of the heating of a closed system containing water and sugar. The solubility and melting enthalpy of the sugar and the effect of the sugar on the boiling and freezing point of the water are merged into the diagram. In consequence of the constant density, the heating of the system corresponds to a horizontal line in the diagram. To describe this system the following differential equations suffice:

$$V \frac{d\rho}{dt} = 0 \quad (1)$$

$$V \frac{d\left(\frac{\rho h}{X_w}\right)}{dt} = q \quad (2)$$

Where  $V$  ( $\text{m}^3$ ) is equal to the volume of the system,  $X_w$  ( $\text{kg}/\text{kg}$ ) is equal to the total water mass fraction and  $q$  ( $\text{W}$ ) is equal to the heat supply. The results are given in figure 6 and 7. The process starts at a temperature of  $-25^\circ\text{C}$ . At this temperature the water consists of ice in equilibrium with water vapour. The state of the sugar is solid. The ice consists of a fraction pure ice and a fraction ice mixed with solid sugar. Increasing the enthalpy results in a temperature and vapour pressure rise corresponding to the sublimation line. As a consequence the amount of ice decreases. When the eutectic temperature ( $-9.5^\circ\text{C}$ ) is reached the nonpure ice starts to melt. The solid sugar dissolves in the liquid water. During this process the temperature and vapour pressure remain constant. When all the solid sugar is dissolved the rest of the pure ice starts to melt, resulting in a dilution of the sugar solution. This dilution causes a reduction of the freezing point depression, resulting in a temperature rise until the initial freezing point. The whole process from the eutectic point until the initial freezing point takes place in a moving triple point in a standard  $P,T$  phase diagram. Further increase of the enthalpy results in evaporation of the liquid water and an increasing concentration of the sugar solution. This process decreases the water activity. When the maximum solubility of the sugar is reached, the sugar starts to solidify. Because of the relative small amount of water in the system, all the water is evaporated at a relatively low temperature. An increase in enthalpy results in a stronger increase of temperature, due to the lower heat capacity of water vapour. In the end the system consists of water vapour and solid sugar.

### Vacuum freezing

The second example consists of vacuum freezing of the same system as the first example. To describe this sys-

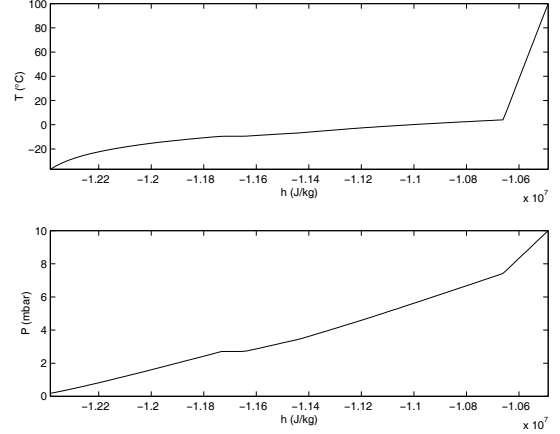


Figure 6: Temperature and pressure as function of enthalpy

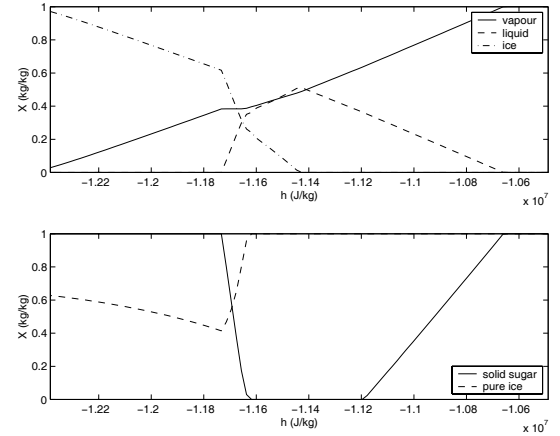


Figure 7: Mass fractions as function of enthalpy (vapour, liquid and ice fraction based on total amount water; solid sugar fraction based on total amount sugar; pure ice fraction based on total amount ice)

tem the following differential equations suffice:

$$V \frac{d\rho}{dt} = -\phi \quad (3)$$

$$V \frac{d\left(\frac{\rho h}{X_w}\right)}{dt} = -\phi h_g \quad (4)$$

Where  $\phi$  ( $\text{kg}/\text{s}$ ) is equal to the gas flow removed during vacuuming and  $h_g$  ( $\text{J}/\text{kg}$ ) is equal to the enthalpy of the removed gas. The results are given in figure 8 and 9. The process starts at a temperature around  $45^\circ\text{C}$ . Every time step a constant fraction of the present gas phase in the system is removed. This means that  $\phi$  is not constant. The temperature of the solution decreases due to the evaporation of water. At the initial freezing temperature pure ice starts to form until the

eutectic temperature is reached. The system stays at this temperature until all the water and sugar is solid. The temperature drops further due to the sublimation of the ice. At the end of the process 11.3% of the total amount of water has been removed.

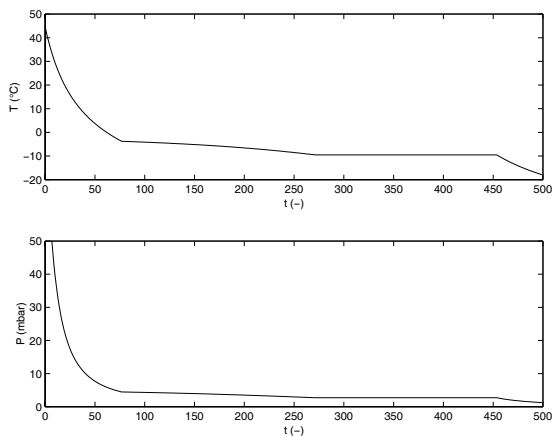


Figure 8: Temperature and pressure as function of time during vacuum freezing

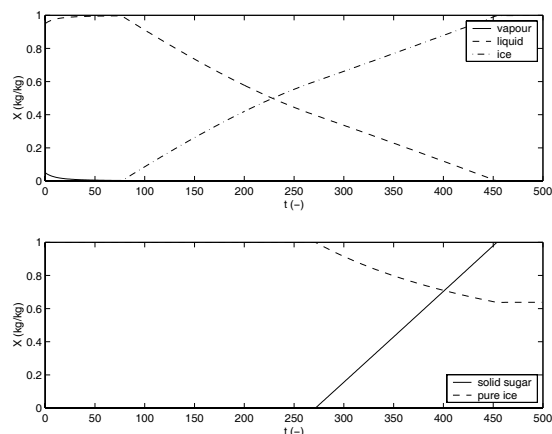


Figure 9: Mass fractions as function of time (vapour, liquid and ice fraction based on total amount water; solid sugar fraction based on total amount sugar; pure ice fraction based on total amount ice)

## CONCLUSIONS AND FURTHER RESEARCH

TNO developed a commercially available PC-programme (BAKTIX and BERTIX) for the simulation of thermal food processing with phase transitions. The use of the TNO density-enthalpy phase diagram increases the accuracy, validity range, development speed and calculation speed of these models. The application examples show that relatively complex systems can

be described by two differential equations only. These equations are independent of the existing phases in the system. The TNO density-enthalpy diagram has been implemented in the Finite Element Method to describe more complicated products. Now, it is possible to model food products with divers composition under broad conditions. In the near future these results will be published. Validation will occur on the basis of sorption isotherms and freeze curves by means of Differential Scanning Calorimetry (DCS) measurements and ThermoGravimetric Analysis (TGA).

## REFERENCES

- [1] Hyland, W. and A. Wexler. 1983. "Formulations for the thermodynamic properties of the saturated phases of H<sub>2</sub>O from 173.15 K to 473.15 K." *ASHRAE Transactions*, Vol. 89, No. 2A, 500-519.
- [2] IAPWS. 1996. *Release on the IAPWS Formulation 1995 for the Thermodynamic Properties of Ordinary Water Substance for General and Scientific Use*. IAPWS Secretariat, Fredericia, Denmark
- [3] IAPWS. 1997. *Release on the IAPWS Industrial Formulation 1997 for the Thermodynamic Properties of Water and Steam*. IAPWS Secretariat, Erlangen, Germany
- [4] Wijnant-Timmerman, S.I.; J.J.C. Veldkamp; R. van der Welle; and C.E. Krist-Spit. 1998. "Modelling of Sterilisation Process Leads to Process and Product Improvement." *Acta Hort.*, 476, ISHS, 205-212.

# Changing The Game: Systematic Innovation in Food Engineering Using TRIZ and Function Simulation Tools

Barry Winkless  
AMT Ireland, University College Cork,  
Tel: 00 353 (0) 87 9720544 Email: [winkfull@hotmail.com](mailto:winkfull@hotmail.com)

Darrell Mann  
University of Bath, UK  
Tel: +44 1225 826465 Email: [ensdlm@bath.ac.uk](mailto:ensdlm@bath.ac.uk)

Dr. Barry O'Connor  
AMT Ireland, University College Cork,  
Tel: 00 353 (0) 21 4902549 Email: [jboc@ucc.ie](mailto:jboc@ucc.ie)

*“Developing technological competence through process innovation is more than a shopping expedition for new equipment; it requires the systematic assessment, exploration and development of capabilities” Bessant (1994:57)*

## Introduction:

The following paper demonstrates the application of TRIZ (Theory of Inventive Problem Solving) in improving food processing technologies. The paper begins with a description of TRIZ and its five ‘pillars’. A functional simulation of a convection-based French fry process then follows. The TRIZ tools of Functional Analysis, Contradictions, and Technology Evolution are utilised within this analysis (using CREATRIZ™, a computer-based TRIZ application). The paper concludes with a description of viable concepts and improvements for the selected food process, and highlights a need for continued research in this area.

## TRIZ: The theory of Inventive Problem Solving

The Russian initiated Theory of Inventive Problem Solving, TRIZ, is a philosophy, a series of tools, methods and strategies developed through over 1500 person years of research and the study of over two million of the world’s most successful patents.

The key findings of TRIZ research are:-

- that all innovations emerge from the application of a very small number of inventive principles and strategies
- that technology evolution trends are highly predictable
- that the strongest solutions transform the unwanted or harmful elements of a system into useful resources.
- that the strongest solutions also actively seek out and destroy the conflicts and trade-offs most design practices assume to be fundamental.

TRIZ offers users access to the knowledge and experiences of the world’s finest inventive minds. It is

intended to complement and add structure to our natural creativity rather than replace it.

TRIZ is both simple and complex. To learn and gather a working knowledge of the whole structure will probably take six months. Some people are prepared to make this investment, and others are not. Those that are not can take comfort from the fact that they will be able to learn and realise significant benefit from just a short exposure to individual elements of the overall structure.

TRIZ is different to most other creativity aids, and quite appear a little

unnatural at first. The next section provides an overview of the major elements of TRIZ, before the paper moves on to examine the use of TRIZ to a pair of food industry related problems.

## THE FIVE PILLARS OF TRIZ

1500 person years of TRIZ research have produced a significant number of innovation tools and methods. Figure 1 illustrates the five main elements of TRIZ that distinguish it from other innovation and problem solving strategies.

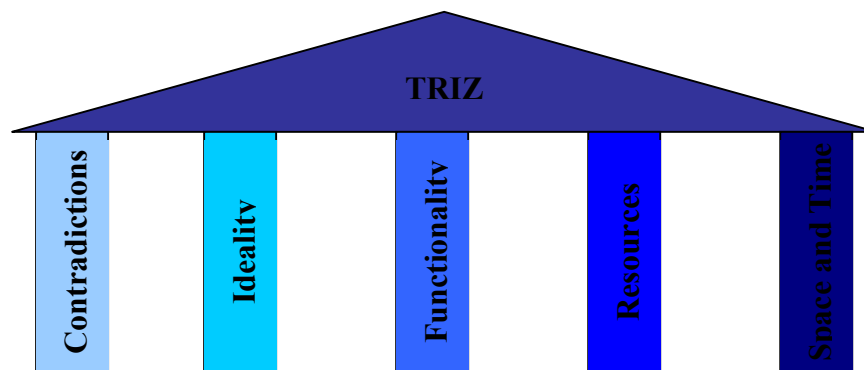


Figure 1: The five pillars of Triz:

### Contradictions

TRIZ researchers have identified the fact that the world's strongest solutions have emerged from situations in which the problem solver has successfully sought to avoid the conventional trade-offs that everyone else has taken for granted. More importantly they have offered systematic tools through which problem solvers can tap into and use the strategies employed by previous successes. The most commonly applied tool in this regard is the Contradiction Matrix – a 39x39 matrix containing the three or four most likely strategies for solving design problems involving the 1482 most common contradiction types. Probably the most important philosophical aspect of the

contradiction part of TRIZ is that, given there are ways of 'eliminating' contradictions', problem solvers should actively look for them.

### Ideality

While studying the patent database, TRIZ founder Genrich Altshuller identified a trend in which systems always evolve towards increasing 'ideality' and that this evolution process takes place through a series of evolutionary S-curve characteristics. A key finding of TRIZ is that the steps denoting a shift from one S-curve to the next are predictable. A number of underlying technology evolution trends consistent with the ideality concept have been identified during the course

of research on the global patent database. Used as a problem definition tool, the ideality part of TRIZ encourages problem solvers to break out of the traditional ‘start from the current situation’ type of thinking, and start instead from what is described as the Ideal Final Result (IFR). The simple definition of IFR is that the solution contains all of the benefits and none of the costs or ‘harms’ (environmental impact, adverse side-effects, etc). Although there are many instances where systems have been seen to evolve all the way to their Ideal Final Result, many have not. The method gets users to think about these situations by working back from the IFR to something which is practicably realisable. Generally speaking these solutions incorporate the concept of systems solving problems ‘by themselves’. The key word is ‘self’; things that achieve functions by themselves – self-cleaning, self-balancing, self-heating, self-aerating, etc – all represent, when incorporated in a true TRIZ fashion, very powerful and resource-efficient solutions.

### **Functionality**

Although the functionality aspects of TRIZ owe a significant debt to the pioneering work on Value Engineering, the method of defining and using functionality data is markedly different; sufficient at the very least to merit discussion as a distinct paradigm shift in thinking relative to traditional occidental thought processes. Three aspects are worthy of particular note:-

- 1) The idea that a system possesses a Main Useful Function (MUF) and that any system component which does not contribute towards the achievement of this function is ultimately

harmful. In a heat exchanger, for example, the MUF is to transfer heat to the working medium; everything else in the system is there solely because we don’t yet know how to achieve the MUF without the support of the ancillary components. (Systems may of course perform several additional useful functions according to the requirements of the customer.)

- 2) In traditional function mapping, the emphasis is very much on the establishment of positive functional relationships between components. TRIZ places considerable emphasis on plotting both the positive and the negative relationships contained in a system, and, more importantly, on using the function analysis as a means of identifying the contradictions, in-effective, excessive and harmful relationships in and around a system. Function and attribute analysis of systems thus becomes a very powerful problem definition tool.
- 3) Functionality is the common thread by which it becomes possible to share knowledge between widely differing industries. A motor car is a specific solution to the generic function ‘move people’, just as a washing powder is a specific solution to the generic function ‘remove solid object’. By classifying and arranging knowledge

by function, it becomes possible for manufacturers of washing powder to examine how other industries have achieved the same basic 'remove solid object' function. '*Solutions change, functions stay the same*' is a message forming a central thread in the TRIZ methodology: People want a hole not a drill.

### **Use Of Resources**

The Resources part of TRIZ relates to the unprecedented emphasis placed on the maximisation of use of everything contained within a system. In TRIZ terms, a resource is *anything in the system which is not being used to its maximum potential*. TRIZ demands an aggressive and seemingly relentless pursuit of things in (and around) a system which are not being used to their absolute maximum potential. Discovery of such resources then reveals opportunities through which the design of a system may be improved. In addition to this relentless pursuit of resources, TRIZ demands that the search for resources also take due account of negative as well as the traditionally positive resources in a system. Thus the pressures and forces we typically attempt to fight when we are designing systems, are actually resources. By way of an example of this 'turning lemons into lemonade' concept, TRIZ users often think of resonance as a resource. This is in direct contradiction to most Western practice, where resonance is commonly viewed as something to be avoided at all costs. TRIZ says that somewhere, somehow, resonance in a system can be used to beneficial effect. In effect, resonance is a potent force lever capable of amplifying small inputs into large outputs. Resonance is currently

being used to generate beneficial effects in a number of new product developments from vacuum cleaners, commercial bottle-washing systems, and in helping to empty vessels carrying powder-based substances more quickly.

### **Thinking in SPACE and TIME**

While not strictly speaking a TRIZ development, TRIZ researchers have also recognized the enormous importance of thinking about situations from all angles. TRIZ users are continuously changing their perspective on problems – zooming in to look at the fine details, zooming out to see the bigger picture, and thinking about how the situation is affected by changing time – whether that be nano-seconds or decades – in both the past and future. This is not a natural process for most people – our brains aren't wired that way – and so TRIZ contains tools to help in the process of thinking in TIME and SPACE.

All of these TRIZ pillars are brought together from a problem definition perspective during a function and attribute analysis (FAA) of a system. Several attempts have been made by TRIZ researchers and suppliers to integrate function analysis/value engineering techniques into TRIZ software-based problem definition processes. To date, these attempts have largely failed to deliver much by way of user benefit over non-software based methods. This has largely been due to the fact that software has been written to do little more than mimic the manual methods. In effect, the potentially enormous leverage to be gained by harnessing the power of the computer has remained largely untapped. Problem solvers have seen the consequences of this failure in three main areas:-

- 1) an inability to take adequate account of the **attributes** (for example, weight, volume, surface finish, corrosion resistance, etc) of a system component. The consequence of this is that main often key functional relationships are not identified in models.
- 2) an inability to take due account of the **time** issues surrounding a problem. The essential consequence of this is that the user does not have any value-adding means of defining how a functional model changes with time-based elements of the problem, and thus receives no guidance on how time-based problem solving strategies can be applied. This is particularly Important from the perspective of
- 3) a total failure of the software to **direct** a user from the function analysis model to the appropriate TRIZ solving tools.

The paper has employed the novel function analysis/value engineering modelling technique to be found in the CreaTRIZ™ problem management software. The new model has been designed to overcome each of the

above problems and to offer users powerful new ways of managing the complexity contained within the large majority of problem situations. The paper now examines application of the system to the first of two case studies:

### **1. Towards a better convection drier:**

The following case study focuses on the problems encountered in drying French fry potato chips without the extra addition of oil, in a high velocity convection cavity. Machine X consisted of an air blower, a heating element, a cavity, a filter a time-dependent release mechanism, and a sensor feedback system. The major problem with Machine X was the relatively frequent need to have it cleaned. Cleaning was also difficult due to the design of the inner cavity in which the fries were subjected to the high velocity convection stream. It was decided at an early stage that any changes should focus on improving the cleanliness of the machine and if possible require no addition of expensive or even cheap parts!

The first stage in the project involved a functional analysis, using CreaTriz software in order to ascertain the key problem areas. Figures 2 and 3, below, illustrates the functional analysis diagrams:

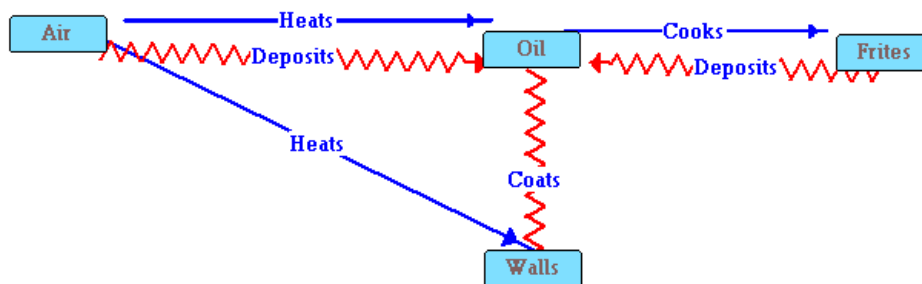


**Figure 2:** *Functional diagram A*



**Figure 3:** *Functional Diagram B:*

**Functionality: Harmful and Useful functions:**

What the function analysis makes clear is that the forced air within the system carries out both harmful and useful functions. Examination of the useful functions highlights the presence of 1) heating of the oil by the air, 2) heating of the fries, and 3) agitation of the fries in order to improve heat transfer and cooking properties. It also incurs harmful functions- predominantly the spraying of oil from the French Fries onto machine walls and the over agitation of chips (shown as an ‘excessive’ action) causing more widespread distribution of oil and potato crumb debris, which in turn increases the difficulty of cleaning the machine after use.

The temperature within the system obviously has the useful function of heating and cooking the fries, however there is also the harmful function of causing the oil to liquefy and again cause deposition of oil onto machine

surfaces. The oil itself carries out the useful function of improving heat transfer and mouth-feel of the chip but incurs the harmful function of being the major cause of dirt in the machine.

From a system analysis perspective, the functional analysis diagram can be used not only highlight the problems contained within the system, but also categorise them into different types in order to facilitate the selection of the most appropriate TRIZ (or other) tool to help tackle that problem. In this particular case, for example, the model highlights the existence of a number of contradictions in the system. As previously mentioned, the description of problems as contradictions is a powerful tool in TRIZ as it enables the engineer to extract powerful contradiction-breaking solutions from the most successful inventive solutions of others who have successfully overcome similar problems. The contradictions and suggested solutions for the fry-heating machine were identified as follows:

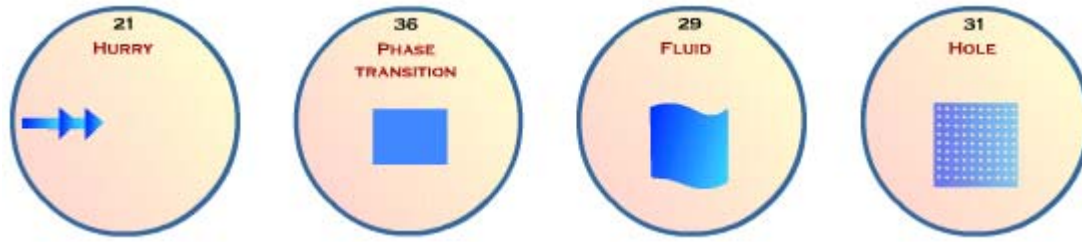


**Figure 4:** Possible Solutions to Hot air flow problems:

**Contradiction 1:** (with reference to the functional analysis diagrams)  
 Results for Improving Factor: Temperature (Hot Air is Heating the French Fries)

Where Worsening Factor is: Loss of substance (where the oil is being heated and therefore spraying from the French fries).  
 Results: Refer Figure: 1.2:

**Principle 21. Hurry**

A. Conduct an action at very high speed to eliminate harmful side-effects

- Use a high speed dentist's drill to avoid heating tissue
- Cut plastic faster than heat can propagate in the material, to avoid deforming the shape
- Break toffee with an impulsive blow from a hammer
- Drop forge
- Flash photography
- Super-critical shaft - run through resonant modes quickly

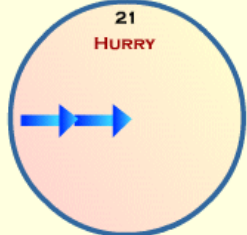


**Figure 5:** Principle 21-Hurrying

Many other patents, for example US Patent 5, 997, 938 '*process for preparing improved oven-finished French fries*' conduct French fry heating at very high temperatures over a very short time in order to minimise oil spray and potential damage to the French fry. Present cooking time in Machine X was 60 seconds and due to

the constraints placed upon design changes it was felt that such a drastic change would incur too many time and cost penalties whilst only offering small benefits to the system as a whole. Possible harmful effects from hurrying the process also included: the need for better containment, powerful heating mechanisms, better insulation.

**Principle 36. Phase transition**

A. Make use of phenomena taking place during phase transitions (e.g. volume changes, loss or absorption of heat, etc.)

- Latent heat effects in melting/boiling
- Water expands when frozen, unlike most other liquids.
- Heat pumps use the heat of vaporization and heat of condensation of a closed thermodynamic cycle to do useful work
- Volume expansion during water-to-steam transition
- Superconductivity

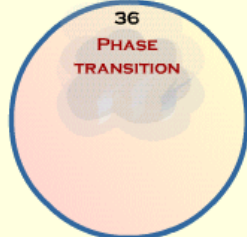


**Figure 6:** Principle 36-Phase transitions

The application of this principle to the solution of the problem may at first seem obscure however if focus turns to the French fry-oil could be added after the chip has been heated- the heat of the French fry (i.e. loss of heat of the French fry) could heat the oil to a certain extent and therefore increase the homemade/just fried taste and texture of the fry, as US Patent 6, 013, 296 *forced air convection oven*

*process for finishing French fries'* highlights- 'after cooking the fries are optionally coated with oil'. Alternatively focus could fall to the oil- the type used (sunflower oil at present) and how the temperature of the air affects the oil. Possible harmful effects from phase transitions: the need to add oil, expensive research into oils, different flavour profiles.

**Principle 29. Fluid**

**A. Use gases and liquids instead of solid parts or systems**

- Transition from mechanical to hydraulic or pneumatic systems
- Fluid clock
- Inflatable furniture/mattress/etc
- Gel filled shoe insole adapts to user
- Hovercraft
- Gas bearings



**Figure 7: Principle 29-Fluid**

Many convection-based patents use moisture within a heat stream (such as US 6229131, 6188045, and 5942142) in order to improve heat transfer to food products. For the purposes of Machine X, this is too major a change

and would involve costly redevelopment. Also texture and taste profiles differ from traditional or impingement ovens without moisture used in the process.

**Principle 31. Hole**

**A. Make an object porous or add porous elements**

- Drill holes in a structure to reduce the weight
- Cavity wall insulation
- Transpiration film cooled structures
- Foam metals
- Use sponge-like structures as fluid absorption media

**B. If an object is already porous, add something useful into the pores**

- Use a porous metal mesh to wick excess solder away from a joint
- Store hydrogen in the pores of a palladium sponge. (Fuel "tank" for the hydrogen car- much safer than storing hydrogen gas)
- Desiccant in polystyrene packing materials
- Medicated swabs/dressings

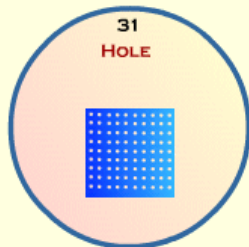


**Figure 8: Principle 31-Hole**

An interesting solution to the oil spray problem could be the introduction of small holes to the chip as a means to

hold the oil better in process. Research would have to be carried out in order to test the viability of this concept and

results may not be satisfactory. For the purposes of the Version 1 machine this may be moving away from an ideal solution.

**Contradiction 2:**

Results for improving factor: Force/Pressure: Agitation of chips increases heat exchange and overall heating effect.

Worsening factor: Duration of moving object (the chips are moving around too much and for too long).

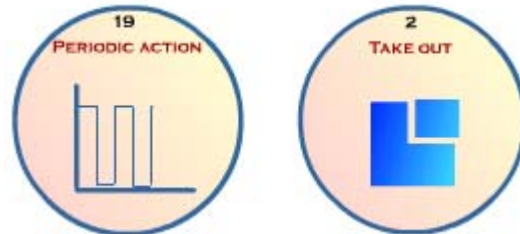


**Figure 9: Results for contradiction 2:**

One of the major problems within Machine X was the propagation of oil in the machine making it difficult to clean. Periodic action could solve this problem. By pulsating the air in the system, the French fries will not move around within the system as much as they would with a steady flow, nor will they cause as much oil build up at the filter. This is due mainly to the fact that pulsed air will not push the French Fries to such a great height. This solution in itself moves the machine towards a more ideal system because it will not add expense to the manufacture of the machine, and will negate to a large extent the need for an expensive filter. ‘Take Out’ highlights solutions that have been utilised in other French fry cooking patents, where a small cage or basket is used to contain the movement of the chips

. However a cage would probably only have a limited effect on oil spray within the system- cleaning would then also include the cage. ‘Take Out’ also highlights how the system could pulse air- the taking out of parts of the blower in order to create a pulsed air-flow. ‘Take Out’, could also refer to removing oil completely from the system..

The results of the TRIZ study focused development efforts on moving towards a more ideal system, i.e. the pulsing of the air, which in turn had the benefit of decreasing the size and cost of the filter. This solution is also in agreement with one of the TRIZ technology trends<sup>1</sup> which highlights a general trend towards pulsation as a more ideal system:

---

<sup>1</sup> Triz technology trends refer to a number of trends technological systems follow in the course of their development. Many of these trends were identified by Geinrich Alsthuller, creator of the Triz methodology.

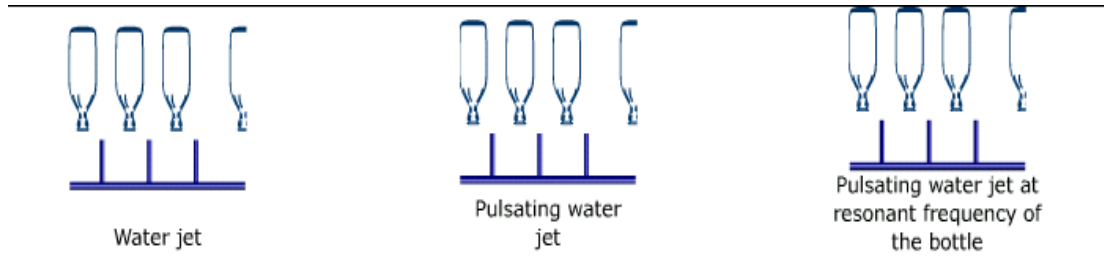


**Figure 10: From Jet to Pulsating Jet-One of the Triz technology trends**

## Conclusions

This case has demonstrated a small proportion of the capabilities of the TRIZ systematic innovation methodology. The simulation of systems through analysis of function is shown to offer new perspectives on both the management of complexity within systems, and the application of problem solving tools aimed at providing much stronger solutions than would emerge from traditional optimisation and trade-off design strategies.

Application of TRIZ to food engineering type issues – whether they be improvement of existing processes or conceptualisation of new products – is still at a relatively early stage of evolution. The opportunities for achieving tangible benefit in both areas are believed to be considerable.

# **BIOTECHNOLOGY**



# MODELISATION OF KILLER YEAST SYSTEMS: DETERMINATION OF MIXED CULTURE DYNAMICS WITH A SPECIFIC MEMBRANE BIOREACTOR

Sébastien Pommier  
Claire Albasi  
Pierre Strehaiano  
Marie-Line Delia.

Laboratoire de Génie Chimique, CNRS UMR 5503, Equipe Fermentations & Bioréacteurs.  
INP ENSIACET, 118 route de Narbonne, 31062 Toulouse Cedex, France.  
E-mail: Sebastien.Pommier@ensiacet.fr

## KEYWORDS

Killer Yeast, Mixed Culture Dynamics, Membrane Bioreactor, Fermentation Modeling.

## ABSTRACT

A reactor specifically designed to carry out studies of interacting populations was developed. Its basic principle consists in keeping both strains of the mixed culture separate by the way of a porous membrane, allowing substrates and metabolites to pass through. As the different strains grow separately, they can be sampled and analyzed distinctly. The culture medium is shared by both strains, so far as interactions between them occur as if they were mixed in the same vessel. The membrane bioreactor made it possible to carry out mixed killer/sensitive fermentations with a double physiological characterization of both strains and thus to compare a mathematical model for killer yeast interaction dynamics to reliable experimental data.

## INTRODUCTION

Many fermentation processes are carried out by various microorganisms, in particular those taking place under non-sterile conditions such as winemaking. Interactions between these microorganisms is a key parameter for the control of the bioreactions. One of the most famous examples of interactions between two microorganisms is the killer phenomenon. This phenomenon was described for the first time about 40 years ago (Bevan and Makover 1963). It occurs between yeast species sharing the same culture medium: one strain called "killer" has the property to excrete a toxin that affects another strain called "sensitive" by damaging its cell membrane and in the end killing it. This phenomenon can influence the quality of the final product as killer strains tend to become dominant and thus to set alcohol level and specific flavors.

In order to model, control, and optimize mixed fermentation processes involving killer interactions, it is necessary to be able to perform kinetic and physiological characterization of each of the protagonists. Modeling is mainly restrained by the lack of experimental data about mixed culture dynamics.

Actually, biomass quantification of each of the strains is hard to carry out, especially when microorganisms from the same species are involved. Though it is quite easy to estimate the global biomass concentration (by spectrophotometry, microscopic cell counting, etc.), the main difficulty is to differentiate one strain from another. Usual techniques required for such a differentiation are microscopic observations, agar plate counting and DNA analysis. These techniques are very fastidious and sometimes expensive. A specific membrane bioreactor made it possible to pick up new fundamental information for a better understanding and a modeling of the killer interaction and its consequences on population dynamics in *Saccharomyces cerevisiae* cultures.

## MATERIAL AND METHODS

### The New Membrane Tool

The experimental membrane bioreactor was designed in order to make it easier to get instantaneous information about each of the microorganisms involved in two-strain mixed fermentations. The two strains grow separately but share the same culture medium. Therefore it is composed of two jars interconnected by a hollow fiber-membrane module, immersed in the liquid of one of the jars (see Figure 1). Fibers are U-shaped and they are hold together in their upper part with an epoxy resin. The bundle is contained in a stainless steel receptacle.

The pore size of the membrane fibers (0,1  $\mu\text{m}$ ) allows metabolites and substrates to pass through while keeping each of the microorganisms separate. Medium flow and mixing between the two jars are induced by alternatively applying pressure into the headspace of each vessel. Level control by conductivity probes drives electrovalves defining the medium way of circulation. An extra benefit of the alternate flow is the control of fouling by backflushing.

The main constraint of the bioreactor validity is that dynamics are governed by the reaction rates and not by the mixing rates. The device performances have been checked by comparison with classical fermentation methods (Salgado Manjarrez et al. 2000). Neither problem due to mixing times nor incident linked to fouling has been noticed.

## Numerical Method

Smoothing of measured populations was established by spline functions (Reinsch 1967) in order to estimate the specific growth rate  $\mu = \frac{1}{X} \frac{dX}{dt}$ .

The proposed mathematical model was solved by an explicit Runge-Kutta formula, and parameter identification was obtained using a simplex method developed on Matlab™.

## RESULTS AND DISCUSSION

The physiological characterization of each strain was performed thanks to the membrane bioreactor and to the separation between the sensitive and killer cells. It was then possible to assess the mixed culture growth kinetics and in the end to compare a mathematical model to reliable experimental data.

### Physiological Characterization of Yeast Cells

The physiological characterization of the yeasts growing in the mixed culture (dead cells or viable cells) is fundamental for chasing the killer effect. Two methods were tested : intracellular ATP measurements and methylene blue staining.

As only viable cells contain ATP, it is possible to numerate viable cells directly from intracellular ATP measurements. This analytical method begins to be widespread and can be automated in plant-scale fermentation processes.

The traditional method for the assessment of yeast viability is methylene blue staining and numeration in a Thoma counting chamber. This technique is cheaper, but not appropriate for on-line measurements.

A good correlation between intracellular ATP concentration and viable population measured by methylene blue staining was established for each of the yeast strains (Figures 2 and 3). One can notice the ATP level per cell is 3 times higher in the killer strain K1 than in the sensitive strain S6.

According to these observations, methylene blue staining was chosen for the physiological characterization of the yeasts in the mixed culture further described. Thus both viable and dead cells were counted from a single observation through a counting chamber.

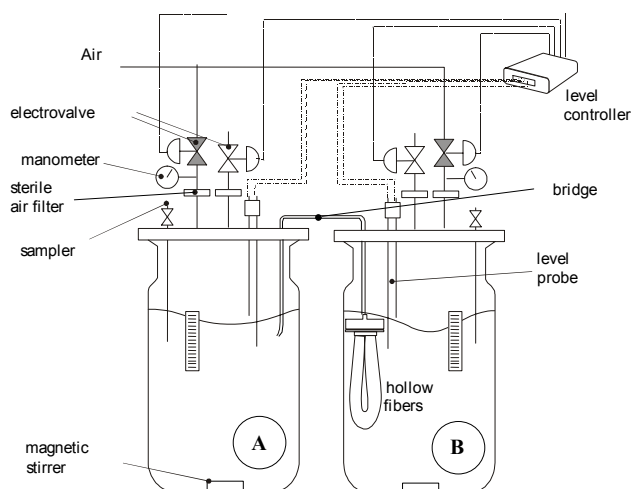


Figure 1 : Membrane Bioreactor Scheme

### Cultures

Commercial yeast strains *Saccharomyces cerevisiae* K1 (killer strain) and *Saccharomyces cerevisiae* S6 (sensitive strain), both obtained from Lallemand Inc™, were used. Mixed fermentations were carried out in the previously described membrane bioreactor.

A synthetic culture medium was used (Strehaiano 1984). Glucose was the carbon source, and ammonium sulfate the nitrogen source. Temperature level was set to 25°C, which is optimal for the involved toxin activity. Inoculation of each strain was performed in the separated vessels of the device. Total fermentation volume was 4 liters.

Population estimation was carried out through O.D. (620 nm, Anthelie™ Advanced Spectrophotometer) and cell numeration with a Thoma counting chamber.

Methylene blue staining was used for the estimation of yeast viability.

Mixed cultures were carried out with an initial ratio of 10% killer cells for a total seeding at 3.3 million viable cells per milliliter referred to the total working volume (4 L).

### ATP Measurements

Intracellular ATP measurements have been performed, in order to characterize biomass physiological state. ATP quantification was assessed through bioluminescence.

A luciferine-luciferase enzymatic complex is used to react with free ATP in the samples. Light emission by the ATP/luciferin-luciferase reaction is measured through a luminometer (LUCY C8 life). Yeast cells are hydrolyzed (Biofax A, Yelen™) before adding the enzymatic complex.

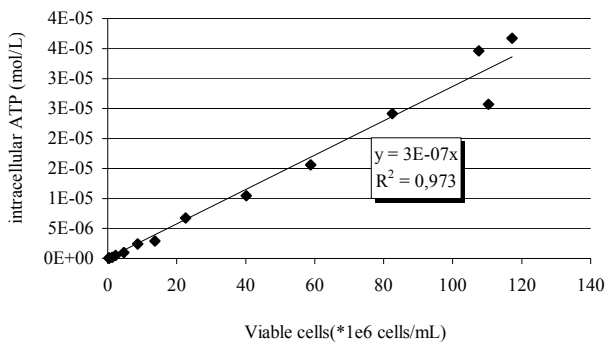


Figure 2 : : Relation between viable cell counting (Thoma chamber) and intracellular ATP concentration for *S.cerevisiae* K1

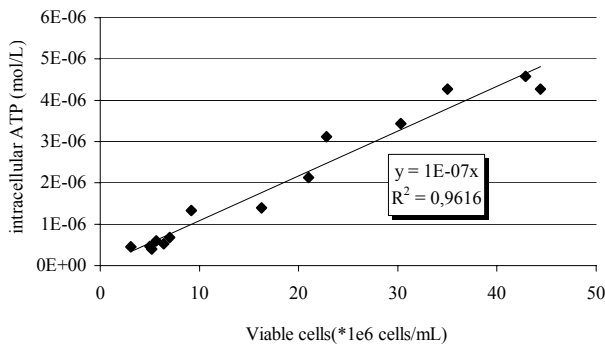


Figure 3 : Relation between viable cell counting (Thoma chamber) and intracellular ATP concentration for *S.cerevisiae* S6

### Mixed Culture Growth Kinetics

Microbial growth kinetics of each strain of the mixed culture was established by simple analytical methods thanks to the separation between killer yeasts and the sensitive ones.

Figure 4 shows the evolution of the killer and sensitive populations in the mixed culture.

Estimation of biomass viability for each strain by methylene blue coloration made it possible to determine the killing effect kinetics. The device made it possible to perform an accurate analysis of the ratio of viable and dead cells for each population all along the fermentation. The biomass evolution underlined a break in the sensitive strain growth, as the killer population quickly became dominant (Figure 5).

In the first 10 hours of the mixed culture, sensitive cells grew at maximum viability level, and the killer/sensitive ratio remained almost constant. During this period, both strains grew just as if they were separate, without any lethal interaction. After about 12 hours, the viability of the sensitive cells began to decline. Less than 15 hours later,

most of the sensitive population was characterized as dead. The end of the fermentation was performed by the single killer strain.

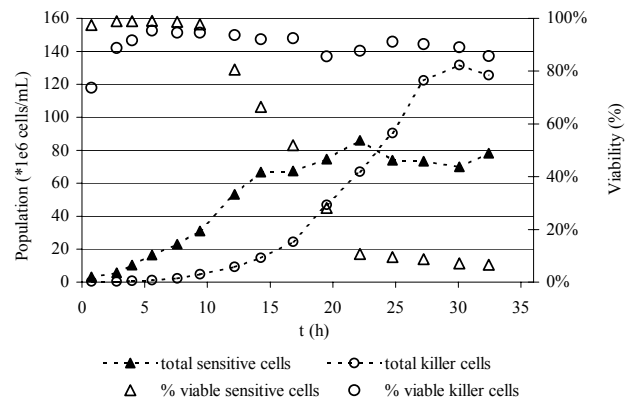


Figure 4 : Evolution of total cells population and percentage of viable cells for both sensitive and killer strains growing in the mixed culture.

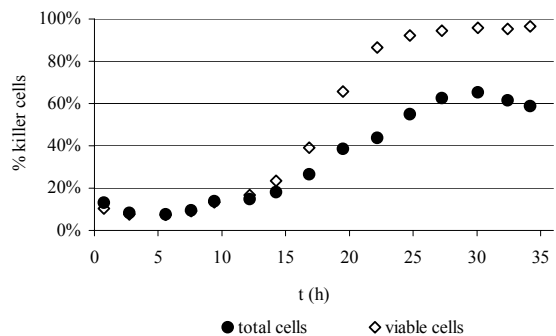


Figure 5 : Evolution of killer/sensitive proportion in the mixed culture

The killer toxin involved in the observed phenomenon is a protein which has been identified as a glycoprotein of about 16 kDa (Pfeiffer and Radler 1984). The pore size of the porous membrane of the bioreactor (0,1  $\mu\text{m}$ ) makes it possible for such molecules to pass through. The death of the sensitive cells in one of the vessels was due to the action of the  $K_2$  toxin, that was produced by the killer yeasts in the other vessel, but which concentration was homogenous in the whole reactor volume.

### Modeling

A mathematical model expressing the dynamic characteristics of killer/sensitive yeast mixed cultures was proposed (Ramon-Portugal et al. 1997, Alfenore 1999). It is

based on the quantification of the medium culture killer toxicity. The physiological state of both killer and sensitive cells is considered, thus biomass is segregated into 4 variables: viable killer cells ( $X_{v,k}$ ), viable sensitive cells ( $X_{v,s}$ ), dead killer cells ( $X_{d,k}$ ), and dead sensitive cells ( $X_{d,s}$ ).

An expression of the growth rate ( $r_{v,k}$ ;  $r_{v,s}$ ) and of the death rate ( $r_{d,k}$ ;  $r_{d,s}$ ) is given for each of the strains, as expressed in Equations (1), (2), (3), and (4) below. The terms  $\mu_{d,k}$  and  $\mu_{d,s}$  stand for “natural” death rate of killer and sensitive cells. The growth rate is supposed to be limited by inhibition, and is expressed by a logistic-like expression. The variable  $I$  is standing for an unidentified inhibitor, which is common to both killer and sensitive strains.

$$r_{v,k} = \mu_{\max,k} \cdot X_{v,k} \cdot (1 - A_k \cdot I) \quad (1)$$

$$r_{v,s} = \mu_{\max,s} \cdot X_{v,s} \cdot (1 - A_s \cdot I) \quad (2)$$

$$r_{d,k} = \mu_{d,k} \cdot X_{v,k} \quad (3)$$

$$r_{d,s} = \mu_{d,s} \cdot X_{v,s} + K \cdot X_{v,s} \cdot T \quad (4)$$

The death rate of the sensitive strain is divided into two terms : natural death and death caused by the killer effect, which is linked to the medium toxicity ( $T$ ). The toxin production  $r_{P_T}$  was shown to be proportional to the growth rate of the killer strain (Ramon-Portugal et al. 1994) as expressed in Equation (5). The toxin consumption rate,  $r_{C_T}$ , due to adsorption on sensitive cells, is supposed to be almost instantaneous and proportional to both toxicity and viable sensitive population (Equation (6)).

$$r_{P_T} = \alpha \cdot r_{v,k} \quad (5)$$

$$r_{C_T} = -W \cdot X_{v,s} \cdot T \quad (6)$$

Inhibitor  $I$  is assumed to be produced during both killer and sensitive yeast growth, with a production rate given by Equation (7) :

$$r_I = a \cdot (r_{v,k} + r_{v,s}) \quad (7)$$

The dynamic evolution of each of the six variables of the model is given by Equations (8) to (13) :

$$\frac{dX_{v,k}}{dt} = r_{v,k} - r_{d,k} \quad (8)$$

$$\frac{dX_{v,s}}{dt} = r_{v,s} - r_{d,s} \quad (9)$$

$$\frac{dX_{d,k}}{dt} = r_{d,k} \quad (10)$$

$$\frac{dX_{d,s}}{dt} = r_{d,s} \quad (11)$$

$$\frac{dT}{dt} = r_{P_T} - r_{C_T} \quad (12)$$

$$\frac{dI}{dt} = r_I \quad (13)$$

The new device made it possible to obtain the evolution of both killer and sensitive strain growing together in the mixed culture, as well as a their physiological characterization (viable or dead) by methylene blue staining or/and ATP measurements. The collected data were confronted to the model.

Experimental values of  $X_{v,k}$ ,  $X_{d,k}$ ,  $X_{v,s}$ , and  $X_{d,s}$  were used for the identification of parameters in Equations (1), (2), (3), (4). Variables  $T$  and  $I$  cannot be experimentally measured, thus parameters  $\alpha$ , and  $a$  in Equations (5) and (7) have been arbitrary set to 1. Any changes in this value only induces a proportional factor in  $T$  and  $I$  evaluation.

As shown in Figures 6 and 7, the proposed mathematical expressions properly fit experimental data.

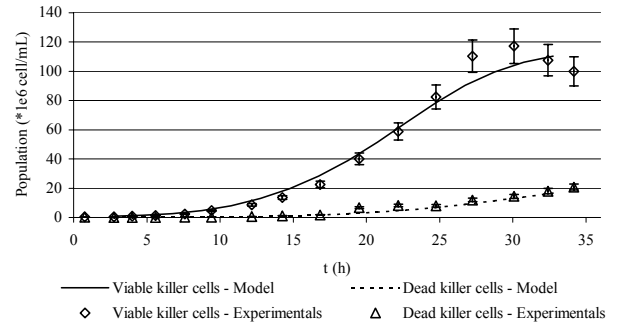


Figure 6 : killer strain growth kinetics in mixed culture

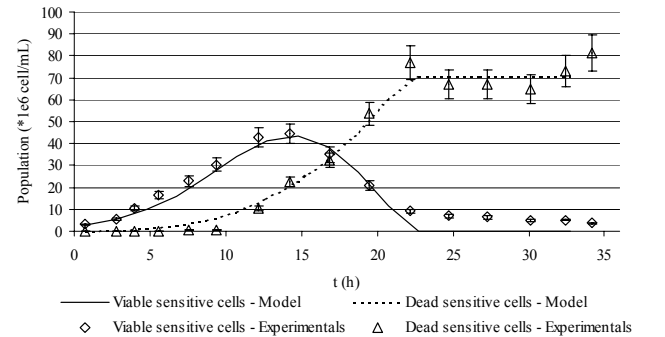


Figure 7 : sensitive strain growth kinetics in mixed culture

This curve fitting is however incomplete for a good appreciation and a possible improvement of the model. Mixed fermentations with different initial conditions must be studied in order to check whether the model can be predictive or not.

## CONCLUSION

A new experimental device has been used in order to get fundamental data for the modeling of mixed cultures including killer interactions. Biomass segregation thanks to a porous membrane made it possible to characterize the physiological state of both strains of the co-culture. This characterization was performed through two different techniques: methylene blue staining and ATP measurements. The results showed these methods were matching.

An existing mathematical model was confronted to collected data. This confrontation validated the proposed mathematical expressions for the description of the killer phenomenon.

Further experiments have to be carried out in order to confront the model to different starting conditions. The model can also be improved, especially by introducing pH and temperature factors as they happen to be crucial for toxin activity.

## REFERENCES

- Alfenore, S. 1999. "Interaction du type killer chez *Saccharomyces cerevisiae*. Etudes physiologiques et cinétiques. Quantification et modélisation". Thèse, Institut National Polytechnique de Toulouse, FRA.
- Bevan, E.A. and M. Makover. 1963. "The physiological basis of the killer character in yeast". *Genetics Today. XI<sup>th</sup> International Congress of Genetics*. Geers S.G. Editor. Pergamon Press, Oxford. 1, 202-203.
- Pfeiffer, P. and F. Radler. 1984. "Comparison of the killer toxin of several yeast and the purification of a toxin of type K2". *Arch. Microbiol.* 137, 357-361.
- Ramon-Portugal, F.; M.L. Delia-Dupuy; G. Schneider; and P. Strehaiano 1994. "Yeast killer activity: a quantitative study". *Biotechnol. Techniques*, 8, 797-804
- Ramon-Portugal, F.; M.L. Delia-Dupuy; H. Pingaud, G.A. Carrillo-Leroux; and J-P. Riba 1997. "Kinetics study and mathematical modelling of killer and sensitive *Saccharomyces cerevisiae* strains growing in mixed culture". *Bioprocess Engineering*, 17, 375-381
- Reinsch, C.-H. 1967. "Smoothing by spline functions". *Numerische Mathematik*, 10, 177-183
- Salgado Manjarrez, E.; C. Albasi; and J-P. Riba. 2000. "A two-reservoir, hollow-fiber bioreactor for the study of mixed-population dynamics: design aspects and validation of the approach". *Biotechnol. Bioeng.*, 69(4), 401-408
- Strehaiano, P. 1984. "Phénomènes d'inhibition en fermentation alcoolique". Thèse Dr ès Sciences, Institut National Polytechnique de Toulouse, FRA.

## NOMENCLATURE

$a$	Inhibitor production constant	$(g.cell^{-1})$
$A$	Braking factor for logistic-like expression	$(L.g^{-1})$
$I$	Growth inhibitor	$(g.L^{-1})$
$K$	Toxin lethal action constant	$(L.g^{-1}.h)$
$t$	Time	$(h)$
$T$	Toxin concentration	$(g.L^{-1})$
$W$	Toxin consumption constant	$(L.cell^{-1}.h)$
$X$	Yeast population	$(cell.mL^{-1})$
$\alpha$	Toxin production constant	$(g.cell^{-1})$
$\mu_{max}$	Maximum specific growth rate	$(h^{-1})$
$\mu_d$	Specific natural death rate	$(h^{-1})$

### Subscripts

$k$	killer
$s$	sensitive
$v$	viable
$d$	dead

## AUTHOR BIOGRAPHY

**SEBASTIEN POMMIER** was born in Tulle, France and went to the Institut National Polytechnique de Toulouse where he studied Chemical Engineering at ENSIGC. He is a PhD student in the Laboratoire de Génie Chimique in Toulouse. His work is focused on experimental study and modeling of interactions in yeast mixed cultures.

# A NEW APPROACH FOR THE ENZYMATIC ACTIVITY TEMPERATURE DEPENDENCY MODELLING. APPLICATION TO THE BEER MASHING PROCESS

Cédric Brandam

Xuân-Mi Meyer

Pierre Strehaiano

Laboratoire de Génie Chimique

(LGC UMR - CNRS 5503),

BP 1301, 5 Rue Paulin Talabot

31106 TOULOUSE (France)

Email: [Cedric.Brandam@ensiacet.fr](mailto:Cedric.Brandam@ensiacet.fr)

Hervé Pingaud

Centre de Génie Industriel

Ecole des Mines d'Albi Carmaux

Campus Jarlard - Route de Teillet

81013 Albi CT Cedex 09 (France)

Jacques Proth

TEPRAL, Brasseries Kronenbourg

68 route d'Oberhausbergen

67037 Strasbourg (France)

## KEYWORDS

Enzymatic activity, Modelling, Amylases, Mashing.

## ABSTRACT

This paper deals with a new approach for the enzymatic activity temperature dependency modelling. The global enzymatic activity is modelled by the contribution of two terms: thermal denaturation function of couple time-temperature and specific activity only temperature dependant. The approach and the modelling has been applied with success to the beer mashing process.

Measurements on pilot-plant experiments have been realised to determine the thermal denaturation during mashing for  $\alpha$ -amylase,  $\beta$ -amylase and  $\beta$ -glucanase. Specific activities temperature dependency of these enzymes have been obtained on laboratory experiments.

## INTRODUCTION

Enzymes are protein compounds whose biological function is to catalyse reactions occurring in organisms (Wallach,1997). Their action is based on the more or less specific recognition between an enzyme region (active site) and the molecule concerned by the catalysed transformation (substrate). Many parameters can affect this recognition ability and so increase or decrease the enzyme action. More than the enzyme concentration, difficult and rarely determined, it is important to quantify this recognition ability. The notion of enzymatic activity was then introduced and defined as the speed at which a reaction catalysed by the enzyme is realised.

Temperature is one of the most important parameter influencing enzymatic activity. It has a double effect : on one hand, it increases the reaction rate by providing the energy necessary to overcome the activation barrier of the reaction, on the other hand, it acts on the tri-dimensional structure of enzymes, leading to the denaturation and the deactivation of these proteins. These two antagonist effects result in an optimal temperature for the enzymatic activity as shown on figure 1.

Moreover, time also contributes to the enzyme denaturation. Modelling the enzymatic activity in a non

isothermal reactive medium must take into account both effects of temperature and the effect of time. Yet, classical enzyme activity measurements, as done in brewery, do not always enable to characterise all these effects.

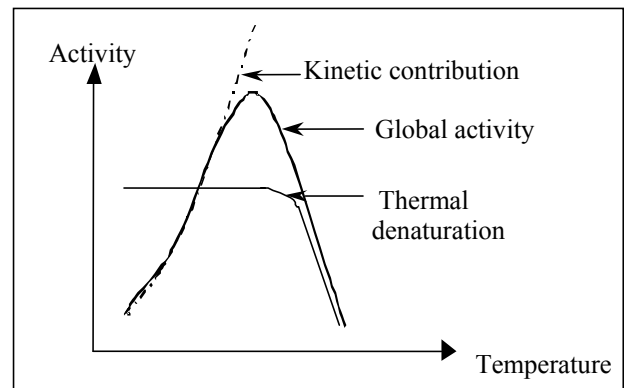


Figure 1: Temperature Influence on Enzymatic Activity

Several enzymes are involved in brewing and more particularly in mashing. During this step, malt endogenous enzymes catalyse the hydrolysis reactions of the malt compounds (starch,  $\beta$ -glucans and proteins). Final beer characteristics (organoleptic quality and ethanol content) are greatly dependent of mashing insofar as it determines the wort composition before fermentation. Mastering the enzymatic activity is an essential step to further model the production of fermentable carbohydrates, dextrans and  $\beta$ -glucans during mashing and to improve the control of this process. As far as mashing is concerned, the most important enzymes are the  $\alpha$ - and  $\beta$ -amylases involved in the starch hydrolysis into fermentable carbohydrates and dextrans, the  $\beta$ -glucanases which catalyse  $\beta$ -glucan hydrolysis into residual  $\beta$ -glucan chains and the proteases necessary for the protein hydrolysis into free amino acids and peptides. As each enzyme reacts differently to temperature, mashing must be performed according to a temperature diagram drawn up to favour each enzyme optimal temperature range. Therefore, it is essential to have a good knowledge of the temperature dependency of the activity of each involved enzyme.

In the brewing literature, the measurement method of specific substrate consumption at a reference temperature is always used to evaluate enzymatic activity evolutions during mashing (Moll et al., 1981; Marc et al., 1983; Muller, 1990; Koljonen et al., 1995). For instance, in breweries,  $\alpha$ -amylase activity is evaluated by measuring the consumption of a specific substrate (azurine-crosslinked amylose) at 40°C, in pH 5.6 buffer, during 20min (MEGAZYME method). The values obtained performing this method compare the residual activity of different samples at a reference temperature. They can be considered as a relative activity measurement and are interesting to determine and compare malt initial enzymatic potential when the grains are in the same initial conditions. But this method is not well adapted to follow activity evolutions when temperatures vary (as during mashing), because it only takes into account the thermal denaturation contribution. Until now, no authors have reported global enzymatic activity values corresponding to mashing processing conditions though it is the most interesting measure to determine the optimal mashing temperature policy.

To cover this lack, a new approach is proposed to determine and model the global enzyme activity. It is illustrated on  $\alpha$ -,  $\beta$ -amylase and  $\beta$ -glucanase activity in a mashing tank.

## ENZYME ACTIVITY MEASUREMENT

The two temperature contributions involved in the global activity are determined separately.

### Enzyme denaturation

To measure enzyme denaturation during mashing, mashes were realised in the 100 litre microbrewery of TEPRAL Research (KRONENBOURG breweries research center). All experiments were done with the same raw material: malt from Scarlett variety. 20kg of malt were mixed with 70kg of water. Ten experiments have been realised with different temperature policies.

Samples were withdrawn at the beginning and the end of each temperature rest. They were rapidly cooled at 4°C in carbo-ice to stop enzymatic activities and then centrifuged for 12 min at 4000g. Sample enzymatic activity is then measured in liquid phase by the Megazyme methods, based on specific coloured substrate consumption. These methods measure enzyme activities at a reference temperature: 30°C for  $\beta$ -amylases and  $\beta$ -glucanases and 40°C for  $\alpha$ -amylases. The experimental relative error for each enzyme denaturation method has been determined to be about 7%.

### Temperature kinetic contribution

From the same active enzyme quantity, isothermal laboratory experiments have been carried out at temperatures ranging between 30 and 75°C. The initial

speed of specific substrate consumption for enzymes gives the specific activity with respect to the temperature.

## MODEL

### Enzyme denaturation

Thermal denaturation kinetic is determined at a reference temperature and it is usually represented by a first order rate process:

$$r_{dE}(T_{ref}) = \left( \frac{d[E]}{dt} \right)_{T_{ref}} = k_{dE} \cdot \exp\left(-\frac{E_{dE}}{RT}\right)[E] \quad (1)$$

$r_{dE}(T_{ref})$  is the denaturation rate (U/kg.s),  $[E]$  is the active site concentration measured by Megazyme method (U/kg of maïsche),  $E_{dE}$  is the activation energy for the denaturation (J/mol),  $k_{dE}$  is the preexponential factor ( $s^{-1}$ ),  $T$  is the temperature (K) and  $R$  is the gas constant (8.31 J/mol.K).

### Temperature kinetic contribution

A relative specific activity  $a_s(T)$  has been defined as the ratio of the initial speed of specific substrate consumption  $v(T)$ , measured at the temperature  $T$ , on the initial speed measured at the reference temperature  $v(T_{ref})$ :

$$a_s(T) = \frac{v(T)}{v(T_{ref})} \quad (2)$$

Relative specific activity of sites, only temperature dependent, is modelled by polynomial laws.

### Global activity

The evolution rate of the global activity  $r_a(T)$  expressed in U/kg.s, can be represented by the product of thermal inactivation rate by the relative specific activity of these remaining sites at the mashing temperatures:

$$r_a(T) = r_{dE}(T_{ref}) * a_s(T) \quad (3)$$

So, the enzymatic activity can be globally represented by equation:

$$r_a(T) = -k_{dE} \cdot \exp\left(-\frac{E_{dE}}{RT}\right)[E] \times a_s(T) \quad (4)$$

This mathematic representation takes into account both temperature and time effects on the enzymatic activity.

## RESULTS and DISCUSSION

### Experimental results for denaturation

The experimental results of  $\alpha$ -amylase,  $\beta$ -amylase and  $\beta$ -glucanase denaturation for the classical four temperature rests mashing diagram are represented on figure 2.

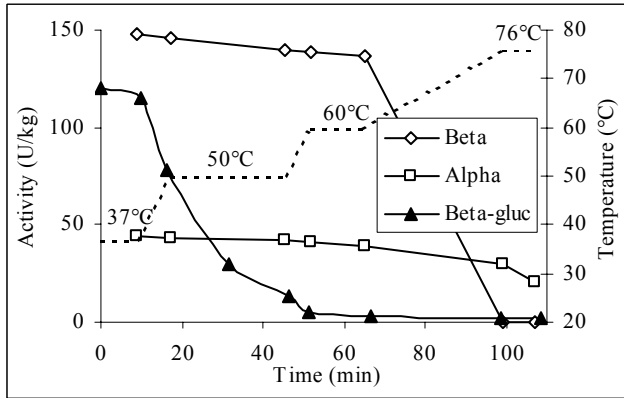


Figure 2:  $\alpha$ -amylase,  $\beta$ -amylase and  $\beta$ -glucanase Thermal Denaturation (measured by Megazyme method).

As long as the threshold temperature of denaturation is not reached, the enzymatic potential remains constant and, as the activities are measured at the reference temperature, the activities keep constant, even if temperature increases in the mashing tank. For instance, the denaturation threshold is about 50-60°C for  $\alpha$ -amylase and  $\beta$ -amylase and about 40°C for  $\beta$ -glucanase. Then, as soon as the denaturation temperature is exceeded, activities decrease rapidly for  $\beta$ -amylases and  $\beta$ -glucanases, slower for  $\alpha$ -amylases.

### Experimental results for the temperature kinetic contribution

On figure 3 are plotted the relative specific activities of the  $\alpha$ -amylase,  $\beta$ -amylase and  $\beta$ -glucanase versus temperature.

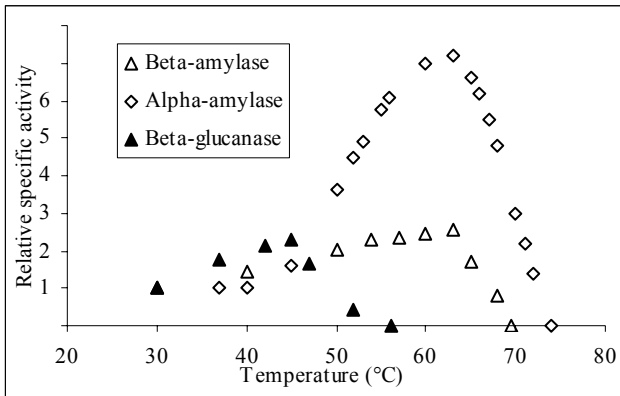


Figure 3:  $\alpha$ -amylase,  $\beta$ -amylase and  $\beta$ -glucanase Relative Specific Activity versus Temperature.

The relative specific activities reach a maximum before decreasing more or less rapidly according to the temperature sensitivity.  $\beta$ -glucanase are the most heat sensitive of the three enzymes and  $\alpha$ -amylase the less.

At 63°C, relative specific activity is 7 times higher than activity measured at 40°C for  $\alpha$ -amylases, and 2.5 times higher than the activity measured at 30°C for  $\beta$ -amylases. For  $\beta$ -glucanases, relative specific activity is the same between 30°C and 50°C, but it is 2.3 times higher at 45°C.

In table 1 are reported for each tested malt enzyme the denaturation threshold  $T_{denat}$ , the temperature corresponding to the maximal specific activity  $T_{max}$  and temperature beyond which no activity remains  $T_{dis}$ .

Table 1 : Characteristic Temperatures of malt  $\alpha$ -amylase,  $\beta$ -amylase and  $\beta$ -glucanase

	$T_{denat}$	$T_{max}$	$T_{dis}$
$\alpha$ -amylase	60°C	63°C	75°C
$\beta$ -amylase	55°C	63°C	70°C
$\beta$ -glucanase	40°C	45°C	55°C

### Global enzymatic activity

From these experimental values, global enzyme activity evolutions can be calculated by equation (4). Figure 4 shows the re-built values for a classical temperature diagram.

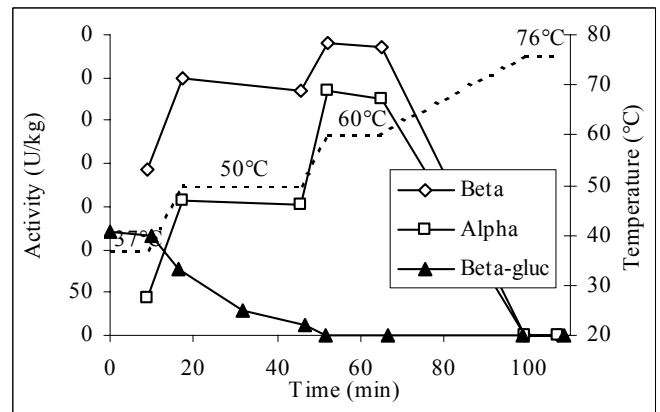


Figure 4:  $\alpha$ -amylase,  $\beta$ -amylase and  $\beta$ -glucanase Global Activity.

The importance of taking into account the temperature kinetic contribution term appears clearly by comparing figures 2 and 4. In one case (fig 2) the enzymatic activity remains constant between 50 and 60°C whereas it increases clearly if the thermal contribution is taken into account. The global amylase activity increases with the temperature until 60-63°C. The best efficiency is located between 60-63°C for amylases, between 37-45°C for  $\beta$ -glucanases.

### Model parameter estimation

Model parameters have been estimated by a least-square method from the experimental values collected from the ten experiments realised with different mashing diagrams. The obtained values are:

$$\underline{\alpha\text{-amylase}}: k_{d\alpha} = 6,94 \cdot 10^{30} s^{-1} \quad E_{d\alpha} = 224,2 \text{ kJ/mol}$$

$$\underline{\beta\text{-amylase}}: k_{d\beta} = 3,06 \cdot 10^{68} s^{-1} \quad E_{d\beta} = 460,1 \text{ kJ/mol}$$

$$\underline{\beta\text{-glucanase}}: k_{d\beta g} = 3,89 \cdot 10^{31} s^{-1} \quad E_{d\beta g} = 246,1 \text{ kJ/mol}$$

These parameter values are in accordance with the habitual bibliography values.

To model the temperature kinetic contribution, the relative specific activities were modelled by four polynomial laws for each enzyme (Temperature must be expressed in Kelvins in polynomes) :

*α-amylase:*

$$a_s = 1 \quad \text{for } T < 40^\circ\text{C}$$

$$a_s = -0,0011 T^3 + 1,091 T^2 - 352,9 T + 38008 \quad \text{for } 40^\circ\text{C} < T < 63^\circ\text{C}$$

$$a_s = -0,0253 T^2 + 16,553 T + 2702,1 \quad \text{for } 63^\circ\text{C} < T < 74^\circ\text{C}$$

$$a_s = 0 \quad \text{for } T > 74^\circ\text{C}$$

*β-amylase:*

$$a_s = 1 \quad \text{for } T < 37^\circ\text{C}$$

$$a_s = 0,0495 T - 13,993 \quad \text{for } 37^\circ\text{C} < T < 63^\circ\text{C}$$

$$a_s = -0,3829 T + 131,22 \quad \text{for } 63^\circ\text{C} < T < 70^\circ\text{C}$$

$$a_s = 0 \quad \text{for } T > 70^\circ\text{C}$$

*β-glucanase:*

$$a_s = 1 \quad \text{for } T < 30^\circ\text{C}$$

$$a_s = -0,0028 T^2 + 1,8566 T - 299,91 \quad \text{for } 30^\circ\text{C} < T < 45^\circ\text{C}$$

$$a_s = 0,015 T^2 - 9,9014 T + 1636,3 \quad \text{for } 45^\circ\text{C} < T < 56^\circ\text{C}$$

$$a_s = 0 \quad \text{for } T > 56^\circ\text{C}$$

Global *α-amylase* and *β-amylase* activity calculated values are compared to the experimental values on figure 5. The mashing temperature diagrams is a classical mashing policy with three rests. On figure 6, the global *β-glucanase* activity is represented for a four rests temperature diagrams.

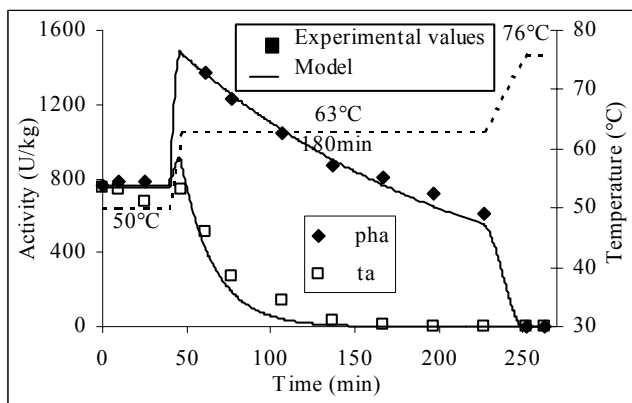


**Figure 5:** Comparison of *α-amylase* and *β-amylase* global activity experimental values and model prediction for a three rests mashing temperature policy (50°C – 63°C – 76°C)

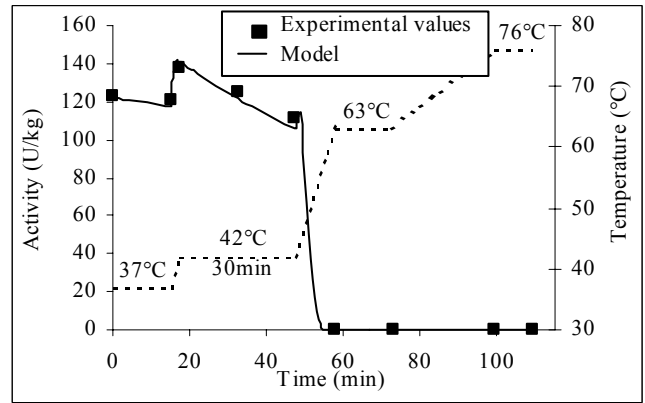


**Figure 6:** Comparison of *β-glucanase* global activity experimental values and model prediction for a four rests mashing temperature policy (37°C – 42°C – 63°C – 76°C)

The tested mashing diagrams cover all the usual temperature mashing scale. The representation of the *α-amylase*, *β-amylase* and *β-glucanase* activities by the model is good for all experiments.

### Model validation

The model was applied to the mashing of malts different from the one used for the parameter estimation. Figures 7a and 7b show the good agreement between model and experiment for these new experiments and so validate the model.

### Kinetic rate of enzymatic catalysed reaction

Our works questioned the way to model the enzymatic activity evolution back. Until now, kinetics of enzymatic reactions introduced activation energies and pre-exponential factor to represent temperature effect on the production rates:

$$r = k \cdot \exp\left(\frac{-E}{RT}\right) [\text{enzyme}] [\text{substrate}]$$

With our model, the temperature effect is already taken into account in the enzymatic activity modelling. Then, the enzymatic reaction rate can be simply written:

$$r = k \cdot [\text{enzyme}] [\text{substrate}]$$

The kinetic of products need to identify only one kinetic parameter, not temperature dependant. The identification problem is so easier. This is a very interesting advantage to model the real enzymatic activity at each times and temperatures of mashing.

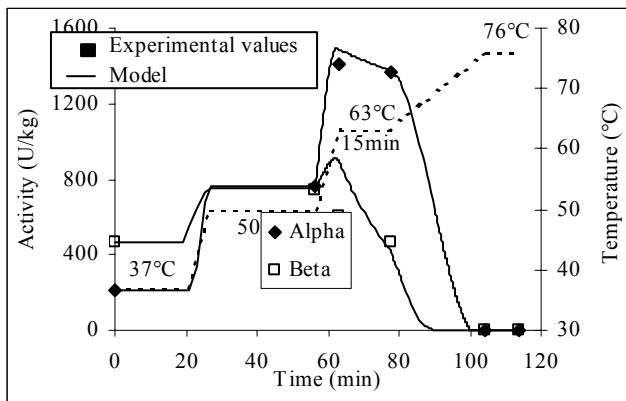


Figure 7a: Model validation for  $\alpha$ -amylase and  $\beta$ -amylase. Comparison between model and experiment values for a mashing realised with an other malt.

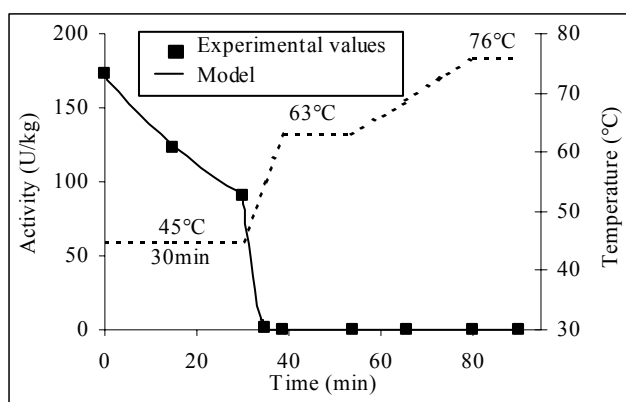


Figure 7b: Model validation for  $\beta$ -glucanase. Comparison between model and experiment values for a mashing realised with an other malt.

## CONCLUSIONS

The classical way to measure enzymatic activity is not sufficient to characterize its temperature dependency. The original modelling of global amylase activities presented in this paper takes into account not only the denaturation term but also the kinetic contribution influencing enzymatic activity and enable to determine the global enzymatic activity at effective mashing temperatures. This approach will allow to determine the optimal temperature policy to apply during mashing to obtain the best enzyme efficiency and to reach the wort specification necessary to get a reliable beer organoleptic quality.

## REFERENCES

- Brandam C., Meyer X.M., Proth J., Strehaiano P., Pingaud H. 2002. "A new reaction scheme for the starch hydrolysis and temperature policy influence during mashing". *Food Science and Biotechnology*, Vol.11, No.1, 40-47.
- Koljonen T., Hämäläinen J.J., Sjöholm K., Pietilä K. 1995. "A model for the prediction of fermentable sugar

concentrations during mashing". *Journal of Food Engineering*, 26, 329-350.

- Marc A., Engasser J.M. 1983. "A kinetic model of starch hydrolysis by alpha- and beta-amylase during mashing". *Biotechnology and Bioengineering*, Vol.XXV, 481-496.
- Moll M., Flayeux R., Lipus G., Marc A. 1981. "Biochemistry of mashing". *MBAA technical quarterly*, 18, 166-173
- Muller R.E. 1990. "The effects of mashing temperature and mash thickness on wort carbohydrate composition". *Journal of the Institute of Brewing*, 97, pp.85-92
- Wallach J. 1997. "Les enzymes". Coll.128, Nathan University

# A new strategy for production of *Saccharomyces* biomass by fed-batch cultures

**Audrey Serra,**  
**Patricia Taillandier,**  
**Pierre Strehaiano,**  
*Laboratoire de Génie Chimique*  
*UMR 5503, INP-ENSIACET,*  
*118 route de Narbonne,*  
*31062 Toulouse Cedex, France*  
[audrey.serra@ensiacet.fr](mailto:audrey.serra@ensiacet.fr)

**Isabelle Masneuf**  
*Enita*  
*Cours du général de Gaulle,*  
*BP 201, 33175 Gradignan cedex*  
[i-masneuf@enitab.fr](mailto:i-masneuf@enitab.fr)

**Jean François Laffort**  
*Laffort Œnologie,*  
*7 rue Franc Sanson,*  
*BP 17, 33015 Bordeaux, France*  
[www.laffort.fr](http://www.laffort.fr)

## KEYWORDS

Production, fed-batch, yeast biomass, optimization

## ABSTRACT

For some industrial uses (baking, wine-making, brewing) great amounts of yeast viable biomass are needed. Due to the Crabtree effect which *Saccharomyces cerevisiae* are sensitive to, cultures with excess oxygen supply and glucose limitation are generally carried out in order to get a maximal biomass yield of 0,5 g/g. To achieve such conditions, fed-batch cultures are usually run. In order to optimise aerobic fed batch cultures of glucose-sensitive yeasts with regard to productivity and cell yield, it is necessary to use a feed-back feeding control devices. The most efficient one is based on the Respiratory Quotient (RQ) measurement using fermentor exhaust gas stream.

The objective of this work was the establishment of a general model of sugar feeding rates for the production of different *S. cerevisiae* wine strains, under different conditions. This glucose feeding rate was first obtained experimentally for one typical strain before being validated with others. An average glucose feeding profile was established as grams of sugar versus time. This mathematical expression modelled the glucose feeding kinetics to obtain an optimal biomass production. In the second step, this profile was extrapolated successfully to others strains, without used the RQ measurement.

The advantage of this work is double. First, the profile allows the biomass production of the yeast strain *Saccharomyces cerevisiae* for any volume of fermentor and any sugar concentration in the feeding medium. Second, thanks to this model the yeast biomass production can be achieved without the RQ on-line measurement so, with a simpler device.

## INTRODUCTION

In biological experiments, a response of a cell culture has to be analysed in relation to the environment. There is an exchange between the environment and the cells, and environmental parameters may influence their physiology. An important factor in studies dealing with the regulation of metabolism is the nutritional limitation which may change the metabolism of the cells drastically. The regulation of the process is so strictly connected to this regulation of metabolism.

During growth of *Saccharomyces cerevisiae* in a batch culture under aerobic conditions with glucose as sole energy and carbon source, ethanol is always released into the culture medium as a by-product. This fact leads to a fall in biomass yield. However, if the yeast is cultivated in a chemostat at low dilution rates, a strictly oxidative metabolism can be observed ; this state results in exclusive formation of biomass and carbon dioxide. When the dilution rate is increased (i.e. the glucose concentration) up to a particular critical value, the yeast metabolism becomes fermentative and ethanol appears in the medium because of the catabolic repression by glucose. So, when the glucose concentration is high, even with excess oxygen, some yeasts consume the glucose mainly by the fermentative way. This phenomenon is known as Crabtree effect (Fiechter et al., 1981) and these yeasts are called glucose-sensitive yeasts.

For some industrial uses (baking, wine-making, brewing) great amounts of yeast viable biomass are needed. So, due to the Crabtree effect which *Saccharomyces cerevisiae* are sensitive to, aerobic cultures with glucose limitation are generally carried out in order to get a maximal biomass yield of 0,5 g/g.

To achieve such conditions, fed-batch cultures are usually run thus permitting the circumvention of the problem of aerobic fermentation due to the glucose effect (Yamane and Shimizu, 1984). In order to optimise aerobic fed batch cultures of glucose-sensitive yeasts with regard to productivity and cell

yield, it is necessary to use a feed-back feeding control devices. The most efficient one is based on the Respiratory Quotient (RQ) measurement using fermentor exhaust gas stream (Aiba et al., 1976 ; Cooney et al., 1977). Thus, the yeast always undergoes a respiratory metabolism and none ethanol is accumulated.

The objective of this work was the establishment of a general model of sugar feeding rates for the production of different *S. cerevisiae* wine strains and different *Saccharomyces* species which are Crabtree positive. This glucose feeding rate was first obtained experimentally for one typical strain before being validated and extrapolated with others.

## MATERIAL AND METHODS

### Yeast strain.

Three strains of *Saccharomyces cerevisiae* was used in this work : 71 B (Lallemand, Montreal, Canada), VLC3 and L5 (Laffort Oenologie, Bordeaux, France).

### Culture media.

It was a synthetic medium containing [mg.(g glucose)<sup>-1</sup>] : ammonium sulfate, 300 ; KH<sub>2</sub>PO<sub>4</sub>, 140 ; CaCl<sub>2</sub>.2H<sub>2</sub>O, 5 ; NaCl, 10 ; MgCl<sub>2</sub>.6H<sub>2</sub>O, 120 ; Yeast Extract (Oxoid) 20. Ammonium sulfate and the other products of the medium were separately heat-sterilized (121°C, 20 min) to avoid Maillard reaction, then mixed and added of 0.2 mL.(g glucose)<sup>-1</sup> of each sterile vitamins and minerals solution which had the following composition [mg.L<sup>-1</sup>] : “vitamins solution” : biotin, 3 ; calcium pantothenate, 40 ; inositol, 250 ; pyridoxine HCl, 50 ; thiamine HCl, 100 ; “minerals solution” : FeSO<sub>4</sub>.7H<sub>2</sub>O, 556 ; ZnSO<sub>4</sub>.7H<sub>2</sub>O, 576 ; CuSO<sub>4</sub>.5H<sub>2</sub>O, 14 ; Na<sub>2</sub>MoO<sub>4</sub>.2H<sub>2</sub>O, 50 ; CoCl<sub>2</sub>.6H<sub>2</sub>O, 50 ; MnSO<sub>4</sub>.H<sub>2</sub>O, 338 ; H<sub>2</sub>SO<sub>4</sub>, 10 drops. This synthetic medium was established by Aranda Barradas (1999). The use of a defined media makes it possible to study the influence of the process conditions on the yeast physiological state independently of variations due to the medium composition. However, the culture on the synthetic medium has been compared to a culture on molasses medium, which is used in the industrial process, and we obtained same results for the growth kinetics and the yield (data not shown). So the synthetic medium has been validated.

### Culture conditions.

Precultures were grown to stationary phase in shake-flasks cultures on synthetic medium (glucose 50 g.L<sup>-1</sup>), at 30°C, 250 rpm. These cultures were used to inoculate batch cultivation. This step was used to form a sufficient quantity of fresh biomass for the fed-batch cultivation. The fed batch cultures were conducted in two bioreactors of 4 (Inceltech Series 210, Toulouse, France) and 14 working volume liter (Applikon Z8 1315 M607, Schiedan, Holland), equipped with a condenser to avoid loss by evaporation during the culture. The reactor was aerated with sterile air. The dissolved O<sub>2</sub> concentration was monitored with an O<sub>2</sub> electrode (model 34 10 3003, Ingold (Mettler Toledo AG, Suisse)) and remained automatically above 20% of air saturation by varying the

stirring rate. The pH was kept constant at 5.0 ± 0.1 by automatic addition of 1 M NaOH with a pH controller (Inceltech LH PPV3, Toulouse, France or Applikon Biocontroller ADI 1030, Schiedan, Holland). The temperature was kept constant at 30°C.

### Gas analysis.

Gas analysis was performed on-line with a Servomex type 4100 analyser (Servomex, Crowborough, England). The exhaust gas was cooled in a condenser, dried with a Hygrostop (Environnement S.A., France) and subjected to gas analysis in a paramagnetic O<sub>2</sub> and infrared CO<sub>2</sub> gas analyzer sampling every 5 min along the fed batch culture. The gas analyzer was calibrated with air and nitrogen and a mixture of 5% CO<sub>2</sub> and 95% synthetic air.

### Feeding of reactor.

The on-line calculation of RQ was made automatically by a program using the data given by the exhaust gas analysis. The reactor was feeding by a peristaltic pump (Minipuls 3, Gilson, Villiers-Le-Bel, France), which the flow rate was adjusted according to either the RQ value or the program value. To maintain a strictly respiratory metabolism, the RQ value had to be equal to 1, for the studied yeast strains. By this way, the glucose was completely transformed in biomass (strictly oxidative metabolism).

### Biomass evaluation.

Three methods were used to estimate the active biomass in the cultures : cell count / viability, optical density and dry weight.

#### *Cell count / viability.*

If needed cell suspensions were diluted to a maximal concentration of 50 x 10<sup>6</sup> cell.mL<sup>-1</sup> in distilled water. Methylene blue solution (0.1 g methylene blue in 1 liter sodium tricitrate 2%) was added volume to volume to the culture sample. Microscopic count was carried out 10 minutes later, magnification × 400, using a Thoma hematory-meter.

#### *Optical density.*

Samples were poured in 1 cm optical length spectrometric tubs from Alliance Concept. Absorbance of yeast suspensions was measured with Secoman Anthelic Advanced (Toulouse, France) spectrophotometer, at 620 nm wavelength. A linear regression between absorbance and biomass concentration is observed for absorbance range of 0.1 to 0.8. For higher values, samples were diluted with distilled water. We define optical density as the red absorbance multiplied by dilution factor.

#### *Dry weight.*

For measuring the biomass concentration, 10 mL of culture sample were centrifuged, washed twice with distilled water to eliminate particles of medium culture and then dried by a humidity analyzer (Precisa HA60, Suisse). Figure 1 shows the linear regression of biomass concentration versus optical density.

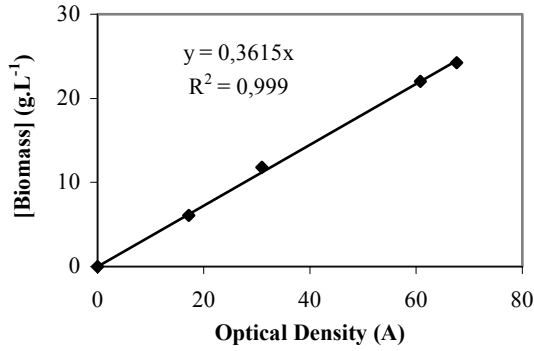


**Figure 1.** Linear regression between biomass concentration and optical density for *S. cerevisiae* L5 growth on synthetic medium.

### Determination of glucose and ethanol.

Glucose was determined with an enzymatic glucose analyzer (YSI 2700 Select, Yellow Springs, Ohio, USA). Ethanol was analyzed by gas chromatography (Chrompack 437A, Delf, The Netherlands). Prior to injection, the cells were removed by centrifugation and a known amount of isopropanol 1% solution was added as internal standard. The column was Chrompack Poraplot Q wide-bore (0.53 mm × 25 m), the injector and detector temperatures were 200°C and the vector gas was nitrogen (8 mL.min<sup>-1</sup>).

## RESULTS AND DISCUSSION

### Establishment of a general model of sugar feeding rate.

The first step was the production of the wine strain *S. cerevisiae* 71B by fed-batch cultures regulated by RQ on-line measurement. The experiment has been repeated several times. These cultures were conducted in the 4 L bioreactor with an initial volume of 1.5 L at 7.5 g.L<sup>-1</sup> of biomass. Two examples are showed on figure 2.

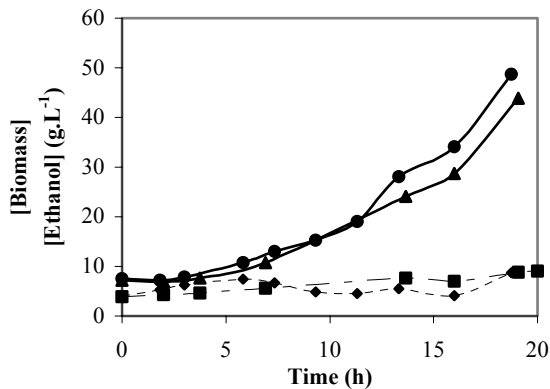


**Figure 2.** Evolvement of biomass (●,▲) and ethanol (■,◆) concentration during two fed-batch cultures regulated by RQ measurement.

The behaviour was the same for the two cultures. The biomass was accumulated until 45 g.L<sup>-1</sup> and 49 g.L<sup>-1</sup> for 350 g consumed glucose. We obtained a maximal yield (0.5 g biomass / g sugar) and a great final concentration of cells (2.6×10<sup>9</sup> cells per mL, with a viability superior to 97%). The

ethanol present in the medium was formed in majority during the batch culture. During the fed batch culture the ethanol concentration did not increased, indicating that little ethanol was produced. So, for these cultures, we obtained an optimal production.

The feeding of reactor profile is presented on figure 3. The feeding flow had increased exponentially and we established an average glucose feeding profile as grams of sugar versus time. Experimental data are represented as symbols and the curve is a polynomial regression obtained with the “Statlets” software, expressed by the equation (1) :

$$\text{Sugar} = 0.371 + 1.857 \times t + 0.799 \times t^2 - 0.086 \times t^3 + 0.005 \times t^4 \quad (1)$$

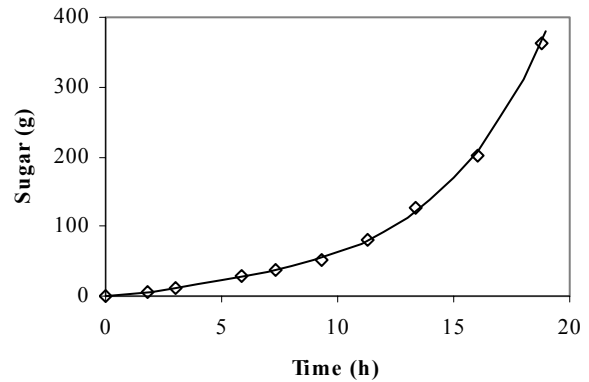


**Figure 3.** Feeding of glucose during a 4 L fed batch culture.

This mathematical expression modelled the glucose feeding kinetics to obtain an optimal biomass production for the strain *Saccharomyces cerevisiae* and a feeding volume of 2.5 L. This optimal biomass can be obtained since an oxydative pathway is followed all along the growth. The model takes into account the oxygen demand for growth. With this relation, it is easy to determine the feeding flow according to the volume of reactor and the sugar concentration of the alimentation medium.

### Model validation.

In the second step, this profile was validated with the production of an other strain (VLC3) in the same conditions (volume, sugar quantity), but without used the RQ measurement. The feeding of reactor was controlled by an informatic program which calculated the flow rate each five minutes, according to the equation (1). The theoretical and experimental flow profiles were showed on figure 4.

The feeding of the reactor was done as planned by the previous polynomial regression. The results of this culture are presented in the table 1. The sugar concentration was measured in the reactor, so not consumed by the yeasts.

The residual sugar concentration in the reactor was very weak, indicating that the yeasts have consumed all the carbon source. So, the sugar feeding according to the model was not in excess and fitted the growth of this strain.

The final biomass concentration appeared lower than previously, but in fact, the final volume was more important, due to the pH regulation. Therefore, we obtained a good production of biomass, with a yield of 0.485 g biomass / g sugar consumed and an excellent viability of cells. The growth of cells was not limited by the sugar feeding.

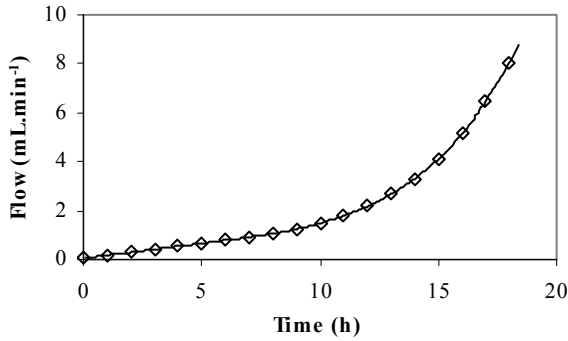


**Figure 4.** Theoretical ( $\diamond$ ) and experimental (—) flow of feeding for the fed batch culture of VLC3 without RQ measurement.

**Table 1.** Biomass production during a fed batch culture controlled by the model of sugar feeding rate.

	Initial time	Final time
[Biomass] ( $\text{g.L}^{-1}$ )	6.84	38.32
Cells number ( $\cdot 10^6/\text{mL}$ )	330	2530
Viability (%)	97.2	98.1
Sugar (g)	0	0.068
Volume (L)	1.5	4.7

The productions of biomass, with and without the RQ measurement, were very similar for the two strains (productivity of 2.3 and 2.25  $\text{g.L}^{-1}.\text{h}^{-1}$ , respectively). The exponential profile allowed to get optimal growth. So, we could validate the model of sugar feeding rate established for a fed batch culture of a *Saccharomyces cerevisiae* yeast strain with a medium feeding of 2.5 L.

#### Model extrapolation.

In the last step, we used this model to produce others yeasts strains, without RQ measurement and with an other volume of bioreactor.

The fed batch culture was conducted in the 14 L bioreactor with the yeast L5. In this experiment, we changed the volume of reactor but not the growth characteristic, because we used a *Saccharomyces cerevisiae* strain like previously. Like the specific growth rate was the same for all strain *Saccharomyces cerevisiae*, the feeding sugar profile could be obtained by a translation of the volume. Previously, the initial volume was 1.5 L and the feeding volume was 2.5 L, now, these volumes were, respectively, 6 L and 8 L. The results of the culture were presented on figure 5, for the comparison of the two flow profiles and on table 2.

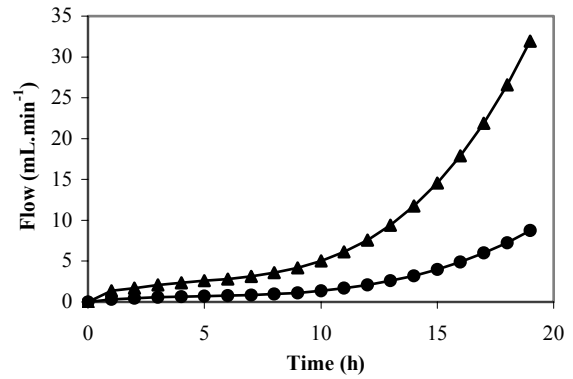


**Figure 5.** Feeding flow profiles for the 14 L ( $\blacktriangle$ ) and the 4 L ( $\bullet$ ) fed batch cultures.

**Table 2.** Biomass production during the 14 L fed batch culture.

	Initial time	Final time
[Biomass] ( $\text{g.L}^{-1}$ )	6.11	24.2
Cells number ( $\cdot 10^6/\text{mL}$ )	250	1139
Viability (%)	99.7	98.5
Volume (L)	6.8	11

In this experiment, the maximal volume was not reached. The culture was limited by the oxygen transfer and the foam formation, so only 2.8 L of medium was bring in the fermentor. The production was stopped after 12 hours instead of 18 hours, at half of exponential phase. Therefore, the quantity of biomass produced was lower, but, in fact, as the sugar quantity bring was lower too, the yield was good (0.505 g biomass / g sugar consumed) and the productivity almost the same ( $2.1 \text{ g.L}^{-1}.\text{h}^{-1}$ ).

For evaluate the quality of the production, the biomass formed was dried like Active Dried Yeasts (A.D.Y. ). We obtained 220 g of dried yeast with  $19.3 \times 10^9$  viable cells per g of dried yeast. This quantity allows to inoculate 10 to 12 hL of musts. Some experiments in flasks showed a good fermentation of sugar by the biomass produced (data not presented), indicating a high quality for the production.

#### CONCLUSION

In this work, we have determined a model of sugar feeding rate for the biomass production. The advantage of this work is double. First, the profile allows the biomass production of the yeast strain *Saccharomyces cerevisiae* for any volume of fermentor and any sugar concentration in the feeding medium. So we have a good flexibility of the correlation. This profile enables an optimal conversion of sugar in biomass. In fact, we obtained a productivity of 2.1-2.3  $\text{g.L}^{-1}.\text{h}^{-1}$  and in industrial process, the usually value is 2  $\text{g.L}^{-1}.\text{h}^{-1}$ . These results were achieved if the best conditions culture were present, in particular, if the culture was not limited by aeration.

Second, thanks to this model the yeast biomass production can be achieved without the RQ on-line measurement so, with a simpler device. Like this, the production is easier.

We are now testing it for others *Saccharomyces* species with a correcting factor according the specific growth rate of each wine strain. These strains must have the same metabolic characteristics, i.e., the yeast must be Crabtree-sensitive.

## REFERENCES

- Aiba S. ; Nagai S. ; Nishizawa Y. ; “Fed batch culture of *Saccharomyces cerevisiae*: a perspective of computer control to enhance the productivity in baker's yeast cultivation”, *Biotechnology and Bioengineering*, 1976, 18, 1001-1016.
- Aranda Barradas J.S. 1999. “*Production de biomasse levurienne : influence du procédé sur les potentialités fermentaires des levures*”, Thèse Institut National Polytechnique de Toulouse, France.
- Cooney C.L. ; Wang H.Y. ; Wang D.I.C. ; “Computer-aided material balancing for prediction of fermentation parameters”, *Biotechnology and Bioengineering*, 1977, 19, 55-67.
- Fiechter A. ; Fuhrmann G.F. ; Kappeli O. ; “Regulation of glucose metabolism in growing yeast cells”, *Advanced in microbiology and physiology*, 1981, 22, 123-183.
- Yamane T. ; Shimizu S. ; « Fed-batch techniques in microbial processes », *Advanced in biochemical engineering and biotechnology*, 1984, 30, 147-194.

## AUTHOR BIOGRAPHY

**AUDREY SERRA** was born in Nice (East-South of France) in 1978. In 2000, she obtained a diploma of process engineer, with a specialisation in biotechnology. Now, she is doing a PhD thesis in the Laboratoire de Génie Chimique, in the team “Fermentations et Bioréacteurs” (Toulouse, France). The aim of her work is the production of wine yeast biomass to be used as starters.

# OPTIMAL DYNAMIC EXPERIMENT DESIGN FOR ESTIMATION OF MICROBIAL GROWTH KINETICS AT SUB-OPTIMAL TEMPERATURES: MODES OF IMPLEMENTATION

Bernaerts, K. and Van Impe, J.F.

BioTeC-Bioprocess Technology and Control

Katholieke Universiteit Leuven

W. De Croylaan 46, B-3001 Leuven, Belgium

Tel. +32-16-32.19.47 Fax. +32-16-32.19.60

E-mail: jan.vanimpe@agr.kuleuven.ac.be

## KEYWORDS

optimal experiment design, dynamic conditions, predictive microbiology, bioreactors, constrained design, advanced data processing.

## ABSTRACT

Application of *optimal experiment design for parameter estimation* enhances the informative character of experiments in view of maximising the parameter estimation quality. In this work, dynamic temperature inputs are applied to optimally estimate two kinetic parameters describing the temperature-dependence of the specific growth rate of micro-organisms. Validity of the model structure is constrained to (i) the sub-optimal growth temperature range, and to (ii) relatively small temperature gradients. This paper presents different ways to deal with these model validity constraints during optimal experiment design.

## INTRODUCTION

Within mathematical modelling exercises, experimental data generation, model structure characterisation, parameter estimation and model validation make up the major –though closely intertwined– steps. Experimental data can largely contribute to the effectiveness (and efficiency) of model structure selection and parameter estimation. Assuming the model structure is perfectly known, the remaining parameter estimation problem can reasonably benefit from the application of optimal experiment design techniques for parameter estimation. Practical parameter identifiability requires *persistently exciting* inputs yielding observations that contain enough *information* such that the model parameters can be estimated uniquely and with the greatest statistical confidence, i.e., the estimated values approach the true parameter values and carry a minimum variance.

In this work, optimal dynamic input design for parameter estimation is applied in the field of predictive microbiology. This research discipline aims at modelling the outgrowth, inactivation or survival of pathogenic and spoilage micro-organisms in food products that are characterised by various product properties and exposed to various processing, distribution or storage conditions (see, e.g., Whiting and Buchanan, 1994). These models aid in food safety management systems and risk assessment studies which makes that their (predictive) quality is of great importance.

Nowadays, great –but not always efficient– effort is spent on the determination of kinetic parameters (appearing in so-called secondary models) which relate microbial dynamics to environmental influences. The classical approach comprises a labor-intensive and time-consuming data generation step. At different levels of the environmental factor(s) under study, microbial growth is monitored. Subsequently, the relationship between treatment combinations and microbial kinetics is identified. Instead of applying *static* experiments, optimally designed *dynamic* conditions may engender a maximum information within a minimum number of experiments. In Bernaerts *et al.* (2000), *time-varying* temperature profiles are designed for optimal estimation of the Square Root model parameters based upon (a single set of) cell density measurements. The so-called Square Root model is known as a prototype model describing the influence of sub-optimal growth temperatures on the maximum specific growth rate of micro-organisms (Ratkowsky *et al.*, 1982). It can be shown that structural parameter identifiability requests for dynamic temperature conditions. Amongst different input parameterisations, an optimised *step input* encompassing an abrupt temperature shift spanning the complete sub-optimal growth temperature domain proves to be most informative. Experimental validation using *Escherichia coli* K12 (MG1655), however, reveals a transient distur-

bance of the exponential growth regime by this large and sudden temperature increase (Bernaerts *et al.*, 2002). This delayed response (intermediate *lag* phase) violates the model validity –implicitly presumed during optimal experiment design– and thus has implications towards optimal design, parameter estimation and their efficiency.

At this point, three strategies complying with this transient growth behaviour yet striving for optimal parameter estimation can be put forward.

(i) The *model* structure is *adapted* to accurately describe the intermediate lag phase induced by the large temperature jump.

(ii) The optimal design is recalculated based on the original model yet *constraining* the admissible temperature shifts to explicitly guarantee model validity.

(iii) Available experimental data are subjected to advanced data processing.

## DESIGN PROBLEM AND METHODOLOGY

In general, optimal experiment design for parameter estimation relies on the minimisation or maximisation of some scalar function of the *Fisher information matrix*. Under the assumption of uncorrelated normal random errors with zero-mean and constant variance, the inverse of this matrix defines the parameter variance-covariance matrix (see, e.g., Walter and Pronzato, 1997).

In this particular study, the modified *E*-criterion is considered for optimal design of a dynamic temperature input  $[T(t)]$  which yields cell density data  $[n(t)]$  enabling efficient estimation of the Square Root model parameters, i.e.,  $\mathbf{p} = [b \ T_{min}]^T$ . This criterion produces designs aiming at circular contours of the identification cost within the parameter space  $(b, T_{min})$ . In other words, the cost surface is *shaped* such that an optimisation algorithm can easily find unique parameter values during parameter estimation. Concurrently, the diameter of the confidence contours corresponding with the optimal design may be minimised as well. The design problem can be mathematically formulated as

$$\min_{\text{admissible } T(t), t \in [0, t_f]} [\Lambda(\mathbf{F}(t, \mathbf{p}^\circ))] \quad (1)$$

with  $\Lambda(\mathbf{F}(t, \mathbf{p}^\circ))$  the condition number of the Fisher information matrix  $\mathbf{F}$  evaluated at the *nominal* parameter vector  $\mathbf{p}^\circ \triangleq [b^\circ \ T_{min}^\circ]^T$ . The Fisher information matrix  $\mathbf{F}$  is defined as follows:

$$\mathbf{F}(t, \mathbf{p}^\circ) \triangleq \int_0^{t_f} \left( \frac{\partial n}{\partial \mathbf{p}} \Big|_{\mathbf{p}=\mathbf{p}^\circ} \right) \cdot \left( \frac{\partial n}{\partial \mathbf{p}} \Big|_{\mathbf{p}=\mathbf{p}^\circ} \right)^T dt \quad (2)$$

where  $n(t)$  denotes the model output which is given by

the following set of differential equations:

$$\begin{aligned} \frac{dn}{dt} &= \frac{Q(t)}{1 + Q(t)} \cdot \underbrace{[b \cdot (T(t) - T_{min})]^2}_{\mu_{max}(T(t))} \cdot [1 - \exp(n(t) - n_{max})] \\ \frac{dQ}{dt} &= \underbrace{[b \cdot (T(t) - T_{min})]^2}_{\mu_{max}(T(t))} \cdot Q(t). \end{aligned} \quad (3)$$

In (3),  $n(t)$  denotes the natural logarithm of the cell density  $[\ln(\text{CFU}/\text{mL})]$ ,  $n_{max}$  is the natural logarithm of the maximum population density, and  $Q(t)$  is a measure for the physiological state of the cells [-], the initial value of which affects the lag time after inoculation. The maximum specific growth rate  $\mu_{max}$  [ $\text{h}^{-1}$ ] is a (square root) function of the temperature with  $b$  [ $^\circ\text{C}^{-1} \cdot \text{h}^{-1/2}$ ] a regression coefficient, and  $T_{min}$  [ $^\circ\text{C}$ ] the (theoretical) minimum temperature for growth. The maximum cell density can be assumed temperature-independent within the temperature region of interest. Note that in this model –combination of the growth model of Baranyi and Roberts (1994) and the Square Root model of Ratkowsky *et al.* (1982)–, it is assumed that the maximum specific growth rate  $\mu_{max}$  *instantaneously* adapts to the (possibly time-varying) temperature.

The sensitivity vector  $\partial n / \partial \mathbf{p}$  is scaled with respect to the (nominal) model parameters and the (nominal) model output, yielding *fully relative sensitivity functions* (Munack, 1989). The scaling of the sensitivity functions by the model parameters takes into account the significant difference in order of magnitude between the Square Root model parameters. Dividing by the nominal output ( $n^\circ(t)$ ) tends to equalise the weight of small and large cell density counts within the Fisher information matrix. Apart from these weighting factors, no further weighting is needed for this single output case. The sensitivity functions are calculated by numerical integration of the associated differential equations. Nominal model parameters ( $\mathbf{p}^\circ$ ) represent an initial guess for the unknown Square Root model parameters. Due to the model non-linearity, the Fisher information matrix depends on the unknown model parameters themselves which makes the resulting designs only *locally* valid. Realistic values for the nominal parameters of *E. coli* K12 (MG1655) (grown aerobically in Brain Heart infusion broth at pH 7.55), initial states and other model parameters are:  $b^\circ = 5.261 \times 10^{-2} \text{ } ^\circ\text{C}^{-1} \cdot \text{h}^{-1/2}$ ,  $T_{min}^\circ = 8.689 \text{ } ^\circ\text{C}$ ,  $n(0) = \ln(10^3)$ ,  $Q(0) = 200$  (no initial lag),  $n_{max} = \ln(3 \times 10^9)$  (Bernaerts *et al.*, 2002). The minimisation of  $\Lambda(\mathbf{F}(\mathbf{p}^\circ))$  is established by optimal choice of the degrees of freedom of the parameterised temperature input ( $\triangleq T(t)$ ). Here, temperature step inputs containing the following degrees of freedom: the initial temperature  $T_1$  [ $^\circ\text{C}$ ], the time of the temperature step  $t_{\text{shift}}$  [h], and the final temperature  $T_2$  [ $^\circ\text{C}$ ]. General constraints are the lower and upper temperature bound of the sub-optimal growth temperature region, i.e.,  $[T_{\text{low}}, T_{\text{high}}]$ .

Optimisation of a step function according to the aforementioned design strategy converges to a large temperature jump from the lower to the upper boundary of the sub-optimal growth temperature range. Experimental implementation yields colony counts ( $n(t)$ ) exhibiting an *intermediate* lag phase (Bernaerts *et al.*, 2002).

## MODES OF IMPLEMENTATION

To cope with this intermediate lag, interventions take place at the level of the model structure, the design, and the experimental implementation and data processing.

### Model adaptation

In general, microbial lag is observed at inoculation ( $t = 0$ ) and can be appointed to the biochemical adaptation of cells to the new environmental conditions. In (3), the *initial* lag phase is modelled by the *adjustment function*

$$\alpha(t) \triangleq \frac{Q(t)}{1 + Q(t)} \quad \text{with} \quad \frac{dQ}{dt} = \mu_{max} \cdot Q(t).$$

Assuming that  $Q(t = 0)$  is small, the adjustment function will be smaller than one causing the specific growth rate of the population to be smaller than the (actual) maximum specific growth rate. As time proceeds,  $Q(t)$  increases exponentially, and  $\alpha(t)$  will tend to one. At that point, the population starts exponential growth ( $\mu = \mu_{max}$ ). Obviously, the variable  $Q(t)$  loses any biological interpretation from this point on. Once  $\alpha(t)$  is approximately equal to one, a change in the actual environment (causing a change in  $\mu_{max}$ ) cannot evoke an additional lag phase in the growth curve.

To introduce an intermediate lag within the exponential growth phase,  $Q(t)$  is re-initialised to a small value at the time of the temperature shift  $t_{shift}$ . This results in an additional degree of freedom in the fitting procedure. Doing so, the experimental data can be described well (i.e., low mean sum of squared errors and no trend in the residuals) which also yields adequate estimates for the Square Root model parameters (see below).

### Constrained input designs

Dynamic temperature inputs are (re-)parameterised and constrained in view of model validity (i.e., no intermediate lag induction). When defining admissible temperature inputs, a trade-off between the optimality of the experiment design (in terms of the value of the design criterion) on the one hand, and model validity on the other, needs to be made. To avoid intermediate lag, the temperature change  $\Delta T$  must be limited to (*at most*)  $5^\circ\text{C}$  (based on experimental knowledge). Doing so, the simple step profile including a single temperature shift cannot induce sufficient information to allow accurate estimation of the Square Root model parameters (see,

e.g., Bernaerts *et al.*, 2002). When the domain of admissible temperature inputs is extended to include  $T(t)$  inputs encompassing several temperature –but amplitude limited– steps, it can be seen that the information content can be significantly increased by introduction of a series of (*small*) incremental temperature shifts (see, e.g., Bernaerts *et al.*, 2002).

Based upon practical feasibility limitations and the informative character of larger temperature changes, a sequence of three temperature shifts of  $5^\circ\text{C}$ , is selected.

### Advanced data processing

The starting point of this *novel* approach is to maintain the original problem formulation (without any adaptation/constraint at the level of the model structure nor at the level of the temperature input). Available experimental data are then subjected to advanced data processing. Key idea is that segments of (on themselves) non-informative (static) data are concatenated such that optimally computed informative data are obtained.

Optimised step temperature inputs based on the modified *E*-criterion (1) are *all* characterised by  $T_1 = T_{low}$  and  $T_2 = T_{high}$ . Instead of performing a dynamic experiment, the experimental plan consists of two static experiments, one at either temperature level. The temperature levels are now fixed, and the remaining degree of freedom, i.e.,  $t_{shift}$ , can be optimised. In contrast with previous computations, initial conditions and other model parameters are here chosen in perfect agreement with the experimental observations. Based upon the resulting information, the computed *optimal* dynamic experiment is (re-)constructed through concatenation of (informative) data windows from the static growth curves. The methodology is explained in full detail in Van Impe and Bernaerts (2002).

## RESULTS AND DISCUSSION

Modes of implementation are validated for *E. coli* K12 (MG1655). Material and methods are described in, e.g. Bernaerts *et al.* (2002). Figure 1 summarises the experimental data, the identified model, as well as the confidence on the estimated model parameters. For full details reference is made to Bernaerts (2002).

### Model adaptation

Using the additional fitting parameter  $Q(t_{shift})$  yields a good description of the dynamic growth data as well as satisfactory confidence levels on the parameter estimates (see Figure 1, left column).

Yet, the modelling methodology becomes reasonably impractical within the more general framework of growth modelling and prediction making under changing temperatures as the intermediate lag phenomena are insufficiently characterised at present. Moreover, the inter-

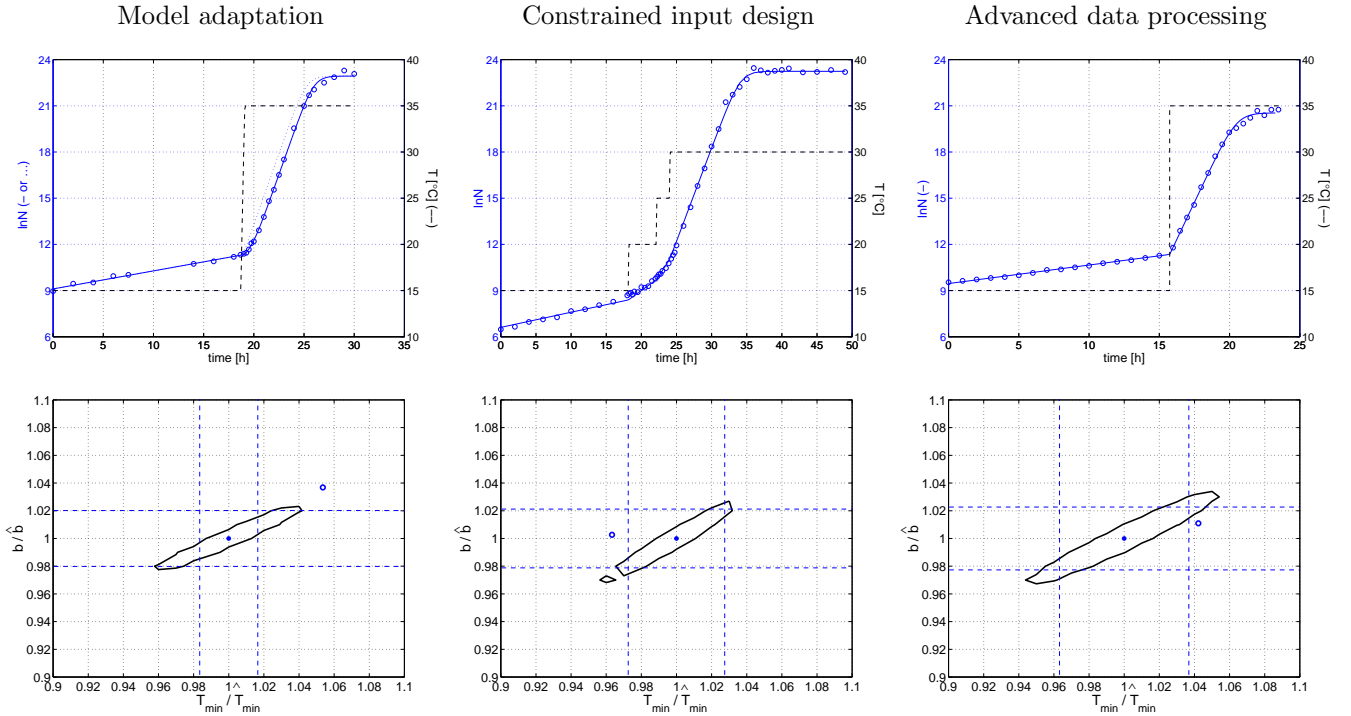


Figure 1: Upper plots: Cell density data of *E. coli* K12 (MG1655) (o) corresponding with the *optimally designed*  $T(t)$ -conditions (---). In case of advanced data processing, these data result from appropriate concatenation of windowed static data. The full line depicts the fitted growth model (3). In case of intermediate lag,  $Q(t)$  is re-initialised at  $t = t_{\text{shift}}$ . Lower plots: Joint confidence region on  $\hat{b}$  and  $\hat{T}_{min}$  (at 99% confidence level) (Bates and Watts, 1988). The dashed lines delimit the 95% *individual* confidence interval on  $\hat{b}$  and  $\hat{T}_{min}$ . The circle (o) depicts  $p^o$ .

mediate lag cannot be accounted for in the computed optimal experiment designs for parameter estimation. The proposed model adaptation remains a pragmatic solution. A *founded* model structure adjustment would represent a study on its own.

### Constrained input designs

Putting *constraints* on the abrupt temperature shift drastically reduces the information content when relying on temperature inputs with a single step. Inclusion of a *series* of small temperature shifts can augment the information content significantly. As few as three limited –yet optimally designed– temperature steps yield acceptable parameter estimation results. This is illustrated in Figure 1 (middle column). The experimental data reveal that the temperature input does not violate model validity (no lagged growth) and suffices to enable (reasonably) accurate estimation of the Square Root model parameters.

Despite the more involved experimental implementation, the time-varying temperature yields an excellent validation test for the applicability of the growth model under (more realistic) dynamic temperature conditions.

### Advanced data processing

The optimal design framework –without additional constraints– is retained but the data generation and data processing step are modified. Realisation of this procedure (see Figure 1, right column) yields accurate parameter estimates as expected from the theoretical optimal experiment design (Van Impe and Bernaerts, 2002).

Although looking rather artificial, the methodology can be justified by the original goal, i.e., exploring the effectiveness of (theoretical) optimal experiment design for practical parameter identification. The imposed temperature input encompasses an instantaneous temperature change at  $t_{\text{shift}}$  which is usually not feasible in practice (due to, e.g., limited heating capacity). In comparison to the preceding methods, model validity under time-varying temperatures is not put to trial. Moreover, the model remains not valid under the simulated temperature profile. Such temperature step would induce an intermediate lag (see above).

The data windowing technique provides an attractive alternative to deal with (circumvent) intermediate lag phenomena. Static experiments can be easily generated using common laboratory equipment. The optimisation

of  $T(t)$  and subsequent data processing step can be easily implemented into a userfriendly software program.

## CONCLUSIONS

Large temperature jumps initiate intermediate lag and thus cause model validity problems when considering the proposed growth model. Because the model structure is assumed correct within the framework of optimal experiment design for parameter estimation, the lag phenomenon should be dealt with in one or another way. Different solutions coping with this model validity limitation have been put forward. Overall, the extracted parameter estimation accuracy is in all cases highly acceptable. The selection of either approach will depend on user-specific preferences, *a priori* knowledge on the micro-organism, and objectives.

## ACKNOWLEDGEMENTS

This research is supported by the Research Council of the Katholieke Universiteit Leuven as part of projects OT/99/24 and IDO/00/008, the Institute for the Promotion of Innovation by Science and Technology (IWT), the Fund for Scientific Research - Flanders (FWO) as part of project G.0213.02, the Belgian Program on Interuniversity Poles of Attraction and the Second Multiannual Scientific Support Plan for a Sustainable Development Policy, initiated by the Belgian State, Prime Minister's Office for Science, Technology and Culture. The scientific responsibility is assumed by its authors.

## REFERENCES

- Baranyi, J. and T.A. Roberts (1994). A dynamic approach to predicting bacterial growth in food. *Int. J. Food Microbiol.* **23**, 277–294.
- Bates, D.M. and D.G. Watts (1988). *Nonlinear regression analysis and its applications*. John Wiley and Sons, Inc.. New York.
- Bernaerts, K. (2002). *Dynamic experiment design and validation in predictive microbiology: optimal estimation of two-parameter microbial growth kinetics as function of temperature*. Phd Thesis 519. Department of Food and Microbial Technology, Faculty of Agricultural and Applied Biological Sciences. Katholieke Universiteit Leuven.
- Bernaerts, K., K.J. Versyck and J.F. Van Impe (2000). On the design of optimal dynamic experiments for parameter estimation of a ratkowsky-type growth kinetics at suboptimal temperatures. *Int. J. Food Microbiol.* **54(1-2)**, 27–38.
- Bernaerts, K., R.D. Servaes, S. Kooyman, K.J. Versyck and J.F. Van Impe (2002). Optimal temperature input design for estimation of the Square Root model parameters: parameter accuracy and model validity restrictions. *Int. J. Food Microbiol., Special issue* **73(2-3)**, 147–159.
- Munack, A. (1989). Optimal feeding strategy for identification of Monod-type models by fed-batch experiments. In: *Computer applications in fermentation technology, modelling and control of biotechnological processes* (N.M. Fish, R.I. Fox and N.F. Thornhill, Eds.). pp. 195–204. Elsevier. Amsterdam.
- Ratkowsky, D.A., J. Olley, T.A. McMeekin and A. Ball (1982). Relationship between temperature and growth rate of bacterial cultures. *J. Bacteriol.* **149**, 1–5.
- Van Impe, J.F. and K. Bernaerts (2002). (*submitted*).
- Walter, E. and L. Pronzato (1997). *Identification of parametric models from experimental data*. Springer. Masson.
- Whiting, R.C. and R.L. Buchanan (1994). Microbial modeling. *Food Technol.* **48(6)**, 113–120.

## BIOGRAPHY

KRISTEL BERNAERTS was born in Bonheiden, Belgium, in 1974. She received her Master's degree Engineering in Chemistry and Biochemistry with specialisation in industrial microbiology from the Katholieke Universiteit Leuven in 1997. Since 1997, she is working as a research assistant at BioTeC - Bioprocess Technology and Control, K.U.Leuven. She received a doctorate in applied biological sciences from the Katholieke Universiteit Leuven in 2002. Her main research interests are in the field of predictive microbiology, more particularly, the design of optimal experiments aiming at accurate model building.

JAN F. VAN IMPE was born in Varsenare, Belgium, in 1965. He received his master's degree in electrical and mechanical engineering from the University of Ghent in 1988, and a doctorate in applied sciences from the Katholieke Universiteit Leuven in 1993 (ESAT Laboratory). Thereafter, he joined the Department of Food and Microbial Technology of the same university (since 1995 as an associate professor). Since 2001, he is professor at the Department of Chemical Engineering. During that period he started the BioTeC research group, which has nowadays about 20 members. He teaches courses in system analysis, bioreactor engineering, and process engineering and control. His research interests are mainly in nonlinear systems and identification, nonlinear and adaptive control, and its applications in model-based optimization and control of (bio-)chemical conversion processes. He has (co-)authored about 250 papers in these areas. In 1995 he received the Barco Award of the Fund for Scientific Research, in 1996 he was laureate of the Belgian Royal Academy, and in 1997 he was awarded the KIWANIS prize of the KULEuven Research Council. In 2002 he became a member of the board of the EUCA, the European Union Control Association.

# **AUTHOR LISTING**



## AUTHOR LISTING

Abreu I. ....	141	Gummaraju K. ....	173
Agioux L. ....	99	Hamdami N. ....	109
Ahrné L.M. ....	127	Hartmann C. ....	169
Albasi C. ....	197	Herlihy D. ....	65
André C. ....	151		
Arendsen A.R.J. ....	180	Ioannou I. ....	99
Arnold S. ....	86		
		Jensen B.B.B. ....	132/146
Baucour P. ....	119		
Becker T. ....	86	Kurz T. ....	86
Bernaerts K. ....	212		
Bhushan N. ....	173	Laffort J.-F. ....	207
Brandam C. ....	202	Le Bail A. ....	109
Brecht J.K. ....	35	Lebouché M. ....	136
Butler F. ....	18	Leuliet J.-C. ....	136/151
		Lian G. ....	75
Carney E. ....	18	Luna R. ....	35
Chevallereau V. ....	99		
Coppenolle H. ....	22/114	Mallikarjunan P. ....	91
Corrieu G. ....	99	Mann D. ....	185
Cronin K. ....	81/119	Martin D.R. ....	75
Cummins E. ....	18	Masneuf I. ....	207
		Massonnet G. ....	31
Darius P.L. ....	31	Mauris G. ....	99
de Jong P. ....	13/45	Melrose J.R. ....	75
De Rijck G. ....	114	Meyer X.M. ....	202
Delaplace G. ....	136/151	Mitzscherling M. ....	86
Delgado A. ....	86/169	Montañez J.C. ....	35
Delia M.-L. ....	197	Monteau J.-Y. ....	109
Demir A.D. ....	81	Movahedkhah M. ....	159
Downing C.J. ....	50/55	Murnleitner E. ....	86
Duffy G. ....	18		
		Nally P. ....	18
Eder H.H. ....	5	Neutelings T. ....	114
		Nielsen J.S. ....	132
Fellner M. ....	86		
Fernandez P. ....	35	O'Connor B. ....	103/185
Fonseca S.C. ....	35	O'Brien S. ....	18
Frias J.M. ....	35	O'Connor B. ....	65
Friis A. ....	132/146	O'Dwyer A. ....	60
		Oliveira F.A.R. ....	35/141
Griffin B. ....	50	Olsson E.E.M. ....	127
Guérin R. ....	136/151		

## AUTHOR LISTING

O'Mahony T.....	55	Strehaiano P. ....	197/202/207
Perrot N. ....	99	Taillandier P.....	207
Pingaud H.....	202	Thiel D. ....	159
Pommier S. ....	197	Torrez C. ....	151
Portier K.M.....	31	Trägårdh C. ....	127
Proth J.....	202	Trystram G. ....	99
Riverol C. ....	103	van Berkel A.I. ....	180
Ronse G. ....	136	van de Wiel J.....	45
Roudot A.-C. ....	27	van der Knaap H.C.M. ....	31
Schrevens E. ....	22/31/114	Van Impe J.F. ....	212
Serra A.....	207	Verschueren M.....	13/45
Sheridan J. ....	18	Vissers M.M.M. ....	13/45
Sheridan P. ....	91	Vitrac O.....	164
Shilton N. ....	91	Weerts A.H.....	75
Smit E. ....	13/45	Winkless B. ....	185
Straatsma H. ....	13/45		